P63 and Cleft Lip: Expanding the P63 Network

A thesis submitted to the University of Manchester for the degree of Doctor of Philosophy in the Faculty of Medical and Human Sciences.

2015

Robert James Tyrer Sullivan

School of Dentistry

Contents

Title 1

Contents 2

List of figures 10

List of tables 12

List of abbreviations 14

Nomenclature 16

Abstract 17

Declaration 18

Copyright 18

Acknowledgements 19

Chapter 1 - Introduction 20

1.1 Human facial development 20

1.1.1 Development of the upper lip and primary palate 20

1.1.2 Secondary palate development 22

1.2 Abnormal facial development 23

1.2.1 Classifications of clefts 25

1.2.2 The incidence of orofacial clefts 26

1.2.3 Non-syndromic clefts 26

1.2.4 Syndromic clefts 29

1.3 Researching orofacial development 32

1.3.1 Model systems: using the mouse as a model organism 32

1.3.2 Mouse upper lip and primary palate development 33

1.3.3 Secondary palate development 34

1.4 Molecular control of lip development 37

1.4.1 Bone morphogenetic protein signalling 37

1.4.2 Sonic hedgehog signalling 40

1.4.3 Platelet-derived growth factor signalling 42

1.4.4 Fibroblast growth factor signalling 46

1.4.5 Wingless signalling 48

1.4.6 Other molecular controls of upper lip morphogenesis 52

1.4.7 Mechanisms of orofacial fusion 55

1.5 *TP63* 61

1.5.1 *TP63* - An introduction 61

1.5.2 Human syndromes resulting from *TP63* mutation 63

1.5.3 Ectrodactyly-ectodermal-dysplasia-clefting syndrome 65

1.5.4 Ankyloblepharon-ectodermal-dysplasia-clefting syndrome 65

1.5.5 The role of P63 - the *Trp63*$^{-/-}$ mouse 66

1.5.6 *TP63* and *IRF6* 70

1.5.7 P63 targets in the upper lip development 72

1.5.8 Other molecular targets of P63 74

1.6 Aims and Objectives 80

Chapter 2 - Materials and Methods 81

2.1 Mice 81

2.1.1 *Trp63* genotyping 81

2.2 Dissection and processing of embryos 82

2.2.1 Mouse breeding and embryo dissection 82

2.3 Chromatin immunoprecipitation 82

2.3.1 Chromatin extraction 82

2.3.2 ChIP 83

2.3.3 Purification and qPCR 83

2.4 Expression analysis 84

2.4.1 RNA extraction 84

2.4.2 cDNA synthesis 84

2.4.3 Quantitative PCR (qPCR) 85

2.5 Whole mount *in situ* hybridisation 85

2.5.1 Riboprobe preparation 85

2.5.2 Plasmid template ligation 85

2.5.3 DH5α cells transformations, blue/white selection 86

2.5.4 Generation of riboprobes 86

2.5.5 Probe hybridisation 87

2.5.6 Embryo processing 87

2.5.7 Antibody detection 88

2.6 Sanger sequencing 88

Chapter 3 - Identification of potential P63 target genes 89

3.1 Introduction 89

3.2 Materials and Methods 94

3.2.1 E11.5 ChIP-Seq 94

3.2.2 ChIP-qPCR validation and establishment of the MVS 94

3.2.3 E11.5 and E12.5 microarray analysis 94

3.2.4 Quantitative PCR (qPCR) 94

3.2.5 Gene ontology analysis 95

3.2.6 Other bioinformatics analysis 95

3.1 Results 96

3.3.1 E11.5 ChIP-Seq analysis 96

3.3.1.2 ChIP-Seq whole genome intersection 96

3.3.1.3 Identifying functional trends within the E11.5 ChIP-Seq 96

3.3.1.4 Conservation of P63 binding sites between E11.5 and E14 100

3.3.1.5 P63 co-localisation with P300 103

3.3.2 Identifying targets of P63 regulation 103

3.3.2.1 E11.5 microarray 103

3.3.2.2 Identifying functional trends within the E11.5 microarray 103

3.3.2.3 E12.5 microarray 111

3.3.2.4 Identifying genes common between E11.5 and E12.5 microarrays 111

3.3.2.5 Identifying functional trends within the E12.5 microarray 111

3.3.2.6 Real-time qPCR validation of the E12.5 microarray at E11.5 119

3.3.3 E11.5 ChIP-Seq to E12.5 microarray intersection 119

3.3.3.1 Gene ontology varies with maximum intersection distance 120

3.3.3.2 Identifying functional trends within the intersected data set 120

3.3.3.3 Identifying functional groups for further investigation 123

3.4 Discussion 127

3.4.1 Identification of E11.5 facial processes specific P63 binding sites 127

3.4.2 A subset of P63 binding sites lack the P63 binding motif 129

3.4.3 Limitations of the current ChIP-Seq and microarray analysis 131

3.4.4 P300 co-localises with a subset of P63 binding motifs 134

3.4.5 ChIP-Seq and microarray analysis identified enrichment within Wnt-related genes 136

3.4.6 ChIP-Seq and microarray analysis identified enrichment within Fgf-related genes 139

3.4.7 ChIP-Seq and microarray analysis identified enrichment within adhesion-related genes 141

3.5 Summary and further work 145

Chapter 4 - P63 regulates expression of Wnt and Fgf signalling components 149

4.1 Introduction 149

4.2 Materials and Methods 151

4.2.1 Embryos dissections and processing 151

4.2.2 nCounter analysis 151

4.2.3 Expression analysis 151

4.2.4 ChIP-Seq annotation 151

4.2.5 Analysis of Canonical Wnt signalling in *Trp63*$^{-/-}$ embryos 151

4.2.6 LiCl induction of Canonical Wnt signalling 152

4.3 Results 153

4.3.1 nCounter analysis identified Wnt genes for prioritisation 153

4.3.2 P63 signalling is required for correct expression of *Wnt4* during lip morphogenesis 153

4.3.3 P63 signalling is required for correct expression of *Wnt3* during lip morphogenesis 159

4.3.4 P63 signalling is required for correct expression of *Wnt9b* during lip morphogenesis 162

4.3.5 Loss of P63 signalling results in the down-regulation of *Shh* 164

4.3.6 P63 signalling is required for correct expression of *Lrp6* during lip morphogenesis 166

4.3.7 P63 signalling is required for correct expression of *Fzd10* during lip morphogenesis 169

4.3.8 P63 signalling is required for correct expression of *Grhl3* during lip morphogenesis 172

4.3.9 P63 signalling is required for correct expression of *Lef1* during lip morphogenesis 176

4.3.10 P63 signalling is required for correct expression of *Pax6* during lip morphogenesis 179

4.3.11 P63 signalling is required for correct expression of *Sox2* during lip morphogenesis 179

4.3.12 Loss of P63 regulation results in misregulation of multiple members of the Wnt signalling network 185

4.3.12.1 *Wnt2b* 185

4.3.12.2 *Wnt3a* 185

4.3.12.3 *Wnt7a* 186

4.3.12.4 *Wnt7b* 187

4.3.12.5 *Wnt10b* 187

4.3.12.6 *Wnt11* 188

4.3.12.7 *Sfrp1* 188

4.3.12.8 *Krm2* 189

4.3.12.9 *Fzd4* 189

4.3.13 Loss of P63 regulation does not affect expression of *Spry1* 191

4.3.14 Loss of P63 regulation results in the up-regulation of *Spry2* 194

4.3.15 Loss of P63 signalling results in misregulation of multiple members of the Fgf signalling network 197

4.3.16 P63 is required for correct canonical Wnt signalling during upper lip morphogenesis 199

4.3.17 Induction of the Wnt canonical pathway fails to rescue the cleft phenotype of Trp63-/- embryos 200

4.4 Discussion 203

4.4.1.1 *Wnt2b* 203

4.4.1.2 *Wnt11* 204

4.4.1.3 *Wnt4* 205

4.4.1.4 *Wnt7a* 206

4.4.1.5 *Wnt9b* 207

4.4.1.6 *Krm2* 208

4.4.1.7 *Pax6* 209

4.4.1.8 *Fzd10* 210

4.4.1.9 *Sfrp1* and *Shh* 212

4.4.1.10 *Sox2* 212

4.4.1.11 Fgf-related genes 213

4.4.2 Human mutations of *LRP6* cause tooth agenesis and orofacial clefting 214

4.4.3 Canonical Wnt signalling is disrupted in *Trp63*$^{-/-}$ facial processes 216

4.5 Conclusions and Summary 220

Chapter 5 - Discussion and further work 223

5.1 A data set of P63 binding sites and putative target genes was generated 223

5.2 P63 regulates Wnt signalling during upper lip morphogenesis 228

5.3 A putative P63/Wnt feedback regulatory loop 229

5.4 Canonical Wnt signalling is attenuated in E11.5 *Trp63*$^{-/-}$ facial processes 231

5.5 P63 inhibits the expression of differentiation factors during upper lip morphogenesis 232

5.6 P63 regulates multiple members of the Fgf signalling pathway during upper lip morphogenesis 232

5.7 Further characterisation of identified P63 binding sites 233

5.8 Summary 234

Chapter 6 - Summary and Conclusions 235

6.1 P63 regulates Wnt and Fgf signalling during upper lip morphogenesis 235

6.2 conclusion 239

Chapter 7 - References 240

Appendix 1 264

Appendix 2 266

Appendix 3 267

Appendix 4 **CD-Rom**

Word count: 78,977

List of figures

Figure 1.1	Developmental stages of the upper lip	**21**
Figure 1.2	Development of the lip and palate	**24**
Figure 1.3	Classification of orofacial clefts	**27**
Figure 1.4	Developmental stages of the mouse upper lip	**35**
Figure 1.5	Haematoxylin and eosin-stained coronal sections of mouse secondary palate	**36**
Figure 1.6	An overview of Wnt signalling	**49**
Figure 1.7	Structure of *TP63*	**62**
Figure 1.8	Phenotype to genotype correlations of mutations within *TP63*	**64**
Figure 1.9	Bilateral cleft lip observed in *Trp63*$^{-/-}$ *mice*	**68**
Figure 3.1	Chromatin immunoprecipitation work flow	**90**
Figure 3.2	Dissection of E11.5 facial processes	**92**
Figure 3.3	A two tiered research approach	**93**
Figure 3.4	ChIP-qPCR validation of ChIP-Seq targets	**97**
Figure 3.5	ChIP-Seq analysis of wildtype E11.5 facial processes identified 10209 putative P63 binding sites	**98**
Figure 3.6	Whole genome intersection of E11.5 ChIP-Seq	**99**
Figure 3.7	E11.5 microarray PCA analysis	**104**
Figure 3.8	E12.5 microarray PCA analysis	**110**
Figure 3.9	qPCR validation of E12.5 microarray	**118**
Figure 4.1	*Wnt4* is a target of P63 signalling	**157**
Figure 4.2	Whole mount *in Situ* hybridisation analysis of *Wnt4*	**158**
Figure 4.3	*Wnt3* is a target of P63 signalling	**160**
Figure 4.4	Whole mount *in Situ* hybridisation analysis of *Wnt3*	**161**
Figure 4.5	*Wnt9b* is a target of P63 signalling	**163**
Figure 4.6	*Shh* is a target of P63 signalling	**165**
Figure 4.7	*Lrp6* is a target of P63 signalling	**167**
Figure 4.8	Whole mount *in Situ* hybridisation analysis of *Lrp6*	**168**
Figure 4.9	*Fzd10* is a target of P63 signalling	**170**

Figure 4.10	Whole mount *in Situ* hybridisation analysis of *Fzd10*	**171**
Figure 4.11	*Grhl3* is a target of P63 signalling	**174**
Figure 4.12	Whole mount *in Situ* hybridisation analysis of *Grhl3*	**175**
Figure 4.13	*Lef1* is a target of P63 signalling	**177**
Figure 4.14	Whole mount *in Situ* hybridisation analysis of *Lef1*	**178**
Figure 4.15	*Pax6* is a target of P63 signalling	**180**
Figure 4.16	Whole mount *in Situ* hybridisation analysis of *Pax6*	**181**
Figure 4.17	*Sox2* is a target of P63 signalling	**183**
Figure 4.18	Whole mount *in Situ* hybridisation analysis of *Sox2*	**184**
Figure 4.19	ChIP-qPCR and qPCR analysis of Wnt-related genes	**190**
Figure 4.20	*Spry1* is not a target of P63 signalling	**192**
Figure 4.21	Whole mount *in Situ* hybridisation analysis of *Spry1*	**193**
Figure 4.22	*Spry2* is a target of P63 signalling	**195**
Figure 4.23	Whole mount *in Situ* hybridisation analysis of *Spry2*	**196**
Figure 4.24	ChIP-qPCR and qPCR analysis of Fgf-related genes	**198**
Figure 4.25	Canonical Wnt signalling is disrupted in *Trp63*$^{-/-}$ embryos	**201**
Figure 4.26	Induction of Wnt signalling via lithium chloride fails to induce a phenotypic change in *Trp63*$^{-/-}$ embryos	**202**
Figure 5.1	Chromatin conformation capture (3C)	**227**
Figure 5.2	P63 regulates multiple members of the Wnt signalling pathway	**230**

List of Tables

Table 1.1	Human CL/P syndromes and their causative genes	**31**
Table 3.1	Results of the serial intersection of E11.5 ChIP-Seq data set against the mouse whole genome	**99**
Table 3.2	Gene ontology analysis of the E11.5 ChIP-Seq against mouse whole genome using GREAT analysis	**101**
Table 3.3	Summary of intersected P63 binding sites between the E11.5 and E14 P63 ChIP-Seq data sets	**102**
Table 3.4A	Summary of intersected P63 binding sites between the E11.5 and identified P300 candidate facial enhancer sites	**102**
Table 3.4B	Summary of intersected P63 binding sites between the E11.5 ChIP-Seq and validated P300 facial enhancer sites	**102**
Table 3.4C	Co-ordinates of the fourteen P63 binding sites found to overlap with validated P300 facial enhancer sites	**102**
Table 3.5	Differentially regulated genes between E11.5 *Trp63*$^{+/+}$ and *Trp63*$^{-/-}$ facial processes	**104**
Table 3.6	E11.5 (P= 0.005) DAVID functional analysis	**105**
Table 3.7	DAVID analysis of E11.5 up & down-regulated genes (p= 0.05)	**106**
Table 3.8	DAVID analysis of E11.5 down-regulated genes (P= 0.05)	**108**
Table 3.9	DAVID analysis of E11.5 up-regulated genes (p= 0.05)	**109**
Table 3.10	Differentially regulated genes between E12.5 *Trp63*$^{+/+}$ and *Trp63*$^{-/-}$ facial processes	**110**
Table 3.11	Identification of genes differentially expressed within the E11.5 and E12.5 microarrays	**112**
Table 3.12	The 14 E11.5 p= 0.005 genes common to the E12.5 microarray	**112**
Table 3.13	DAVID functional analysis of E12.5 microarray up/down-regulated genes (p= 0.005)	**113**
Table 3.14	KEGG pathway analysis of E12.5 up/down-regulated genes (p= 0.005)	**114**
Table 3.15	DAVID functional analysis of E12.5 microarray down-regulated genes (p= 0.005)	**115**
Table 3.16	DAVID functional analysis of E12.5 microarray up-regulated genes (p= 0.005)	**117**
Table 3.17	Variation in intersected genes vs. maximum distance	**121**
Table 3.18	Variation in GREAT analysis vs. maximum intersection distance	**121**
Table 3.19	Gene ontology analysis of the E11.5 ChIP-Seq/ E12.5	**122**

	microarray intersected data set	
Table 3.20	Target genes for further investigation	**124**
Table 3.20	Target genes for further investigation	**125**
Table 3.20	Target genes for further investigation	**126**
Table 4.1	Wnt, Fgf and adhesion-related genes selected for nCounter analysis	**154**
Table 4.2	Genes displaying significant differential expression by nCounter (p= 0.05)	**155**

List of abbreviations

3C	Chromatin confirmation capture
4C	Circularised chromatin conformation capture
5C	Carbon-copy chromosome conformation capture
AARRS	Awadi/Raas-Rothschild/Schinzel Phocomelia syndrome
ADULT	Acro-dermato-ungual-lacrimal-tooth
AEC	Ankyloblepharon-ectodermal-dysplasia-clefting
AER	Apical epidermal ridge
BMP	Bone morphogenetic protein
CCFSE	Carboxyfluorescein
CDMP	Cartilage-derived morphogenic proteins
ChIP	Chromatin immunoprecipitation
ChIP-qPCR	Chromatin immunoprecipitation quantitative polymerase chain reaction
ChIP-Seq	Chromatin immunoprecipitation followed by deep sequencing
CL	Cleft lip
CL-	Cleft lip negative
CL/P	Cleft lip/palate
CL+	Cleft lip positive
CLPED1	Cleft lip and palate-ectodermal dysplasia
CP	Cleft palate
DBD	DNA-binding domain
Dc	*Dancer*
DEPC	Diethykpyrocarbonate
DIG	Digoxygenin
DPP	Decapentaplegic
DTT	Dithiothreitol
ECM	Extracellular matrix
ED	Ectodermal dysplasia
EDC	Epithelial differentiation complex
EEC	Ectrodactyly-ectodermal-dysplasia-clefting
EMT	Epithelial to mesenchymal transformation
FGFR	Fibroblast growth factor receptor
GDF	Growth and differentiation factors
GO	Gene ontology
GWAS	Genome wide association study
HH	Hedgehog
Hi-C	Chromatin capture Hi-C
HILS	heat-inactivated lamb serum
HSP	Heat shock protein
ISO	Oligomerization domain
KO	Knockout
LB	Liquid broth
LMS	Limb-mammary syndrome
LNP	Lateral nasal process
LRP	Low density lipoprotein receptors

MANP	Mandibular process
MEE	Medial edge epithelium
MES	Medial epithelial seam
MNP	Medial nasal process
MVS	Minimum validation score
MXP	Maxillary process
NSCL/P	Non-syndromic cleft lip/palate
OP	Osteogenic proteins
p63BS	P63-binding site
PBS	Phosphate buffer solution
PBST	Phosphate buffer solution tween
PCA	Principle component analysis
PCR	Polymerase chain reaction
PDGF	Platelet-derived growth factor
PERP	*P53 apoptosis effector-related to PMP-22*
PFA	Paraformaldehyde
PPS	Popliteal pterygium syndrome
qPCR	Quantitative polymerase chain reaction
R26R	*Rosa-loxP-stop-LacZ*
RTS	Rubinstein-Taybi syndrome
SAM	Sterile-α-motif
SHFM	Split hand/foot malformation
SHFM1-BS	Split hand/foot malformation binding site
Shh	Sonic hedgehog
SNP	Single nucleotide polymorphism
TAD	Transactivation domain
Tgfβ	Transforming growth factor beta
TID	Transcription-inhibition domain
TRF	Transcriptional repression factors
TSS	Transcriptional start site
Tw	*Twirler*
VWS	van der Woude syndrome
WISH	Whole mount *in situ* hybridisation
Wnt	Wingless
WT	Wildtype
Xt^{bph}	*Extra-toes*

Nomenclature

For the purpose of this thesis, standard HUGO genetic nomenclature was used (http://www.genenames.org). All references to genes are italicised. Human and chick genes are written fully in uppercase. Mouse genes are written with the first letter capitalised followed by lowercase. All proteins are written non-italicised with the first letter capitalised and following letters lowercase.

For *TP63*, the human gene is written as *TP63* and mouse gene *Trp63*. Proteins are referred to as P63.

The University of Manchester

ABSTRACT

Submitted by Robert James Tyrer Sullivan for the degree of PhD Basic Dental Sciences (Stem Cell Biology) and entitled, “P63 and Cleft Lip: Expanding the P63 Network”

2015

Cleft lip and palate is a developmental abnormality which affects 1 in 500 live births resulting in considerable morbidity for the affected individual and their families and providing an economic burden to the state. Human mutations in *TP63* have been shown to induce at least five developmental syndromes which are characterised by the presence of orofacial clefting, malformed limbs and defects in ectoderm-derived tissues. Mouse models of *Trp63* knockout display phenotypes similar to the clinical manifestation of *TP63* human mutations. To date the majority of orofacial P63-related research has focussed on secondary palate development, as such the role of P63 during upper lip development remains poorly characterised.

Upper lip development is similar between mouse and human. The medial nasal, lateral nasal and maxillary processes form as outgrowths of the frontonasal prominence. Directed growth of the facial processes results in their epithelial contact and adhesion. At the site of epithelial contact a double epithelial seam is formed, which must be degenerated to allow mesenchymal confluence across the upper lip. *Trp63* has been shown to be expressed within the epithelia of the facial processes throughout upper lip development, with expression detected during process outgrowth, contact and adhesion. Down-regulation of *Trp63* expression within the epithelial seams is followed by seam degeneration and upper lip fusion. Furthermore, the cleft lip and palate phenotype of *TP63*-related conditions suggests P63 plays a key role in upper lip morphogenesis. Previous studies have identified P63 target genes using high throughput methods. However, P63 functions in a tissue specific manner and so the applicability of these studies to upper lip development is hampered by their choice of model tissue.

The aim of this study was therefore to identify targets of P63-regulation in upper lip development using stage appropriate tissue. High throughput methods were used to identify sites of P63 binding and genes misregulated in *Trp63*$^{-/-}$ mouse facial processes. Via characterisation of putative target genes a novel role for P63 in the regulation of Wnt and Fgf signalling during upper lip morphogenesis was identified. It is therefore suggested that during upper lip morphogenesis P63 regulates the expression of multiple members of the Wnt and Fgf signalling family to maintain the proliferative and differentiation potential of the facial processes. Furthermore regulation of Wnt and Fgf signalling provides a mechanism by which P63 may regulate epithelial to mesenchymal signalling.

This project has identified potential novel targets of P63 regulation during upper lip development, in addition to providing a novel mechanism of P63 regulation of wider relevance to the embryological development of multiple tissues.

Declaration

No portion of the work referred to in the thesis has been submitted in support of an application for another degree or qualification of this or any other university or other institute of learning.

Robert J. T. Sullivan

Copyright statement

Acknowledgements

Initial thanks must go to my supervisors Dr. Jill Dixon and Prof. Mike Dixon whose patience, tutorship and encouragement have been integral to the completion of this PhD. Furthermore the eternal patience shown during the writing of this thesis with the proof-reading and advice offered must be acknowledged. Additional thanks go to the past and present members of the Dixon lab whose friendships and help have been a constant source of support and made the lab a happy and fun place to work. Special thanks must go to Nigel Hammond and Rose Richardson who helped throughout this PhD with friendship, advice and technical tutorship.

I would like to thank the BBSRC for funding this PhD and the University of Manchester for providing an excellent work environment.

Thanks must go to the collaborators of the Dixon lab including the Zhou and Selleri labs whose kindly provided their ChIP-Seq facilities and generated the *Trp63;BAT-Gal* mice used in this project.

Completion of this PhD would not have been possible without the constant love and support of my family. The daily phone calls to my parents Andrew and Helen provided a vital lifeline over the last few months of writing, without which I would surely have failed. Their support has been unconditional and without their ceaseless encouragement and my mother's insistence on "action-plans" I could not have achieved my goals.

Finally thanks must go to my long suffering partner Natalie whose love and support made this PhD possible. Her endless patience and tolerance of the late nights and early mornings are truly the attributes of a saint. I could not have done this without you. Thank you.

1.0 Introduction

1.1 Human facial development

1.1.1 Development of the upper lip and primary palate

Human orofacial development begins during the fourth week of gestation. Expansion of the forebrain pushes the overlying ectoderm forward, coupled with the migration of neural crest cells from the forebrain and midbrain, this creates the frontonasal prominence (Hinrichsen, 1985; Jiang *et al*. 2006). The frontonasal prominence consists of a core of mesoderm cells covered in a layer of ectoderm (Figure 1.1 A). Further expansion of the midbrain and newly formed frontonasal prominence causes an inferior invagination, the stomodeum, which acts as a precursor of the mouth (Hinrichsen, 1985; Som & Naidich, 2013a). Thickening of the ectoderm causes invaginations to form a pair of swellings, the nasal placodes (Iizuka, 1973; Jiang *et al*. 2006). The nasal placodes then deepen due to further growth within both the surface ectoderm and core mesoderm at the edges of the placodes (Figure 1.1 A) (Yoon *et al*. 2000; Som & Naidich, 2013a).

During the fifth week of development further growth of the nasal placodes results in formation of the paired facial processes; the lateral nasal processes and the medial nasal processes (Figure 1.1 B) (Hinrichsen, 1985; Yoon *et al*. 2000; Som & Naidich, 2013a). The paired maxillary and mandibular processes are formed by growth within the first branchial arch (Warbrick, 1960; Iizuka, 1973). The maxillary processes lie lateral to the stomodeum while the mandibular processes are below (Figure: 1.1 B). The mandibular processes expand rapidly towards the midline until they contact one another, adhere and fuse (Warbrick, 1960). Expansion within the medial and lateral nasal processes causes elongation of the nasal placode as well as causing the nasal placodes to extend rostrally into the stomodeum (Jiang *et al*. 2006; Yoon *et al*. 2000; Som & Naidich, 2013a). The nasal pits are moved medially through the directed growth of the maxillary processes towards the midline and shaped through the ventrolateral expansion of the medial nasal processes, changing the nasal pits into nasal slits (Warbrick, 1960; Iizuka, 1973; Som & Naidich, 2013a).

Following the re-shaping of the nasal pits into slits, growth of the maxillary processes towards the midline causes their medial edges to approach the medial nasal processes (Figure 1.1 C) (Iizuka, 1973; Jiang *et al*. 2006; Som & Naidich, 2013a).The bucconasal groove is formed at the future site of contact between the medial nasal and maxillary processes.

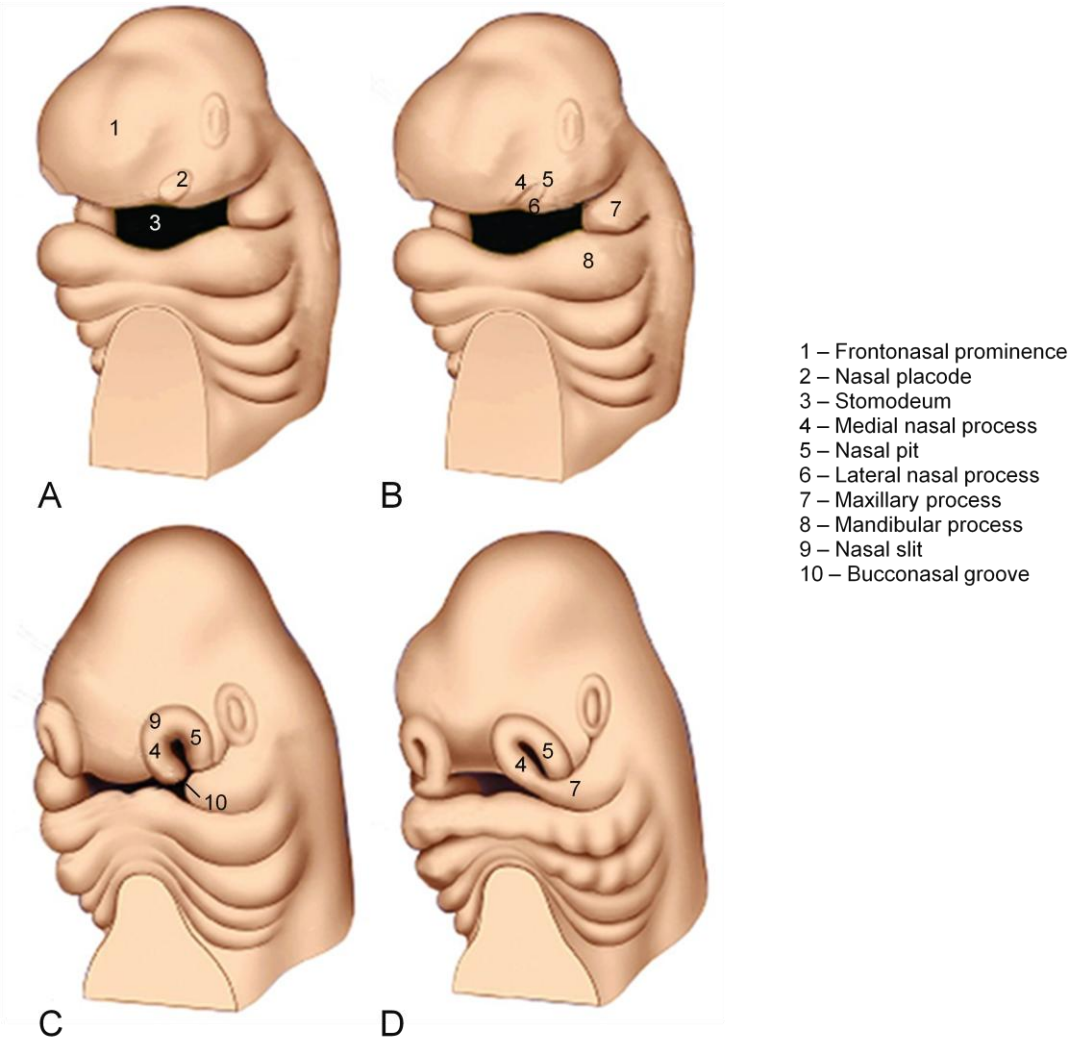

Figure 1.1: Developmental stages of the upper lip. (**A**) During the fourth week of human gestation neural crest cell migration forms the frontonasal prominence. Thickening within the ectoderm of the frontonasal prominence produces the nasal placodes. (**B**) Directed growth within the nasal placodes forms a nasal pit and gives rise to the medial nasal and lateral nasal processes superior to the maxillary and mandibular processes formed from the first branchial arch. Further growth within the lateral nasal processes, medial nasal processes and maxillary processes causes deepening of the nasal pits, converting them into nasal slits. (**C**) The medial nasal and maxillary processes contact each other at the bucconasal groove. (**D**) The site of contact between the medial nasal and maxillary processes forms a double layered epithelial seam, which undergoes degeneration resulting in the fusion of the facial processes. (Figure adapted from Som & Naidich, 2013).

Further growth in both the medial nasal and maxillary processes results in their contact across the bucconasal groove, the two sets of paired processes then adhere to one another and undergo fusion (Figure 1.1 D) (Iizuka, 1973; Hinrichsen, 1985; Yoon *et al*. 2000; Thomason *et al*. 2008; Som & Naidich, 2013a). The anterior region of the bucconasal groove undergoes complete fusion, while the posterior region is closed through the growth of an epithelial layer, known as the bucconasal membrane (Som & Naidich, 2013a). Closure of the bucconasal groove will result in the separation of the nasal cavity from the oral cavity, however, this process will only be complete with the growth of the primary palate (Diewert, 1983; Som & Naidich, 2013a).

During the sixth week of gestation, the medial nasal processes thicken causing their medial edges to contact and adhere. Following adherence the processes fuse to form the intermaxillary segment which contributes to the primary palate (Hinrichsen, 1985). Fusion of the medial nasal processes occurs posteriorly to anteriorly (Hinrichsen, 1985). Fusion between the lateral nasal processes and maxillary processes will form the lateral nose and borders of the nostrils, while the medial nasal and maxillary processes will form the upper lip and jaw (Figure 1.2) (Warbrick, 1960; Som & Naidich, 2013a). The nasolacrimal groove is formed at the junction between the maxillary and lateral nasal processes, extending from the developing eye towards the lower nose (Som & Naidich, 2013a). Growth within the nasolacrimal groove forms the nasolacrimal duct and the lacrimal sac (Som & Naidich, 2013a). During the sixth week of gestation the nasolacrimal groove is closed through fusion of the lateral nasal and maxillary processes forming the side of the nose and the cheek (Figure 1.2) (Dixon *et al*. 2011; Som & Naidich, 2013a).

The philtrum and columella are formed during the seventh week of gestation through the fusion of the medial nasal processes medially and the growth and expansion of the maxillary processes (Warbrick, 1960; Hinrichsen, 1985). Fusion of the medial nasal processes pushes the frontonasal processes superiorly and posteriorly (Warbrick, 1960; Dixon *et al*. 2011; Som & Naidich, 2013a). The intermaxillary segment extends into the oral cavity where it will contribute to the anterior palate segment and fuse with the secondary palate (Diewert, 1983; Hinrichsen, 1985).

1.1.2 Secondary palate development

Secondary palate development occurs in concert with development of the upper lip and primary palate (Yoon *et al*. 2000; Jiang *et al*. 2006). During the sixth week of development, the intermaxillary process extends posteriorly into the oral cavity to form the primary palate which will later give rise to the premaxilla and will encompass the four upper incisor teeth (Som & Naidich, 2013b). Directed growth within the maxillary prominences results in the bilateral outgrowth of the paired palatal shelves consisting of periderm and basal epithelium covering a mesenchymal core (Diewert, 1983; Jiang, *et al*. 2006). Following outgrowth, the palatal shelves extend vertically downwards lateral to the tongue (Yoon *et al*. 2000; Jiang *et*

al. 2006; Marazita *et al*. 2012). The palatal shelves continue to grow downwards until the seventh week of gestation, when continued growth of the maxilla and mandible pulls the tongue downwards away from the primary palate (Yoon *et al*. 2000; Som & Naidich, 2013b). Movement of the tongue facilitates the re-orientation of the palatal shelves into a horizontal position superior to the tongue (Figure 1.2D).

Once elevated above the tongue, the palatal shelves grow towards the midline of the oral cavity driven by proliferation within the mesenchymal core of each process. Continued mesenchymal proliferation results in contact between the epithelia covering the medial edges of the palatal shelves (Figure 1.2E) (Jiang *et al*. 2006; Thomason *et al*. 2010; Som & Naidich, 2013b). Subsequently, the medial edge epithelia of the apposed palatal shelves adhere and fuse to form the medial epithelial seam (MES). Between the seventh and eighth weeks of gestation the MES is removed to allow mesenchymal confluence across the palatal shelves (Moxham, 2003). The secondary palate then fuses anteriorly with the primary palate and dorsally with the nasal septum (Figure 1.2F). Fusion of the primary and secondary palates separates the oral and nasal cavities, with the surface epithelial cells on the oral surface differentiating into stratified squamous epithelium and cells on the nasal surface differentiating into columnar ciliated epithelium (Diewert, 1983; Moxham, 2003; Som & Naidich, 2013b). Following fusion of the secondary palate, ossification occurs, proceeding posteriorly. The primary palate and anterior regions of the secondary palate undergo ossification to form the hard palate (Yoon *et al*. 2000; Som & Naidich, 2013b). The posterior segments of the secondary palate do not undergo ossification, instead they extend posteriorly fusing with the nasal septum to form the soft palate (Yoon *et al*. 2000; Som & Naidich, 2013b).

1.2 Abnormal facial development

Correct orofacial development relies upon a discrete sequence of events which must be completed in both the correct temporal and spatial fashion to facilitate the formation of the upper lip and palate (Warbrick, 1960). A number of steps are key to correct development: neural crest cells must migrate to populate the frontonasal prominence and branchial arches; directed proliferation within the frontonasal prominence and facial processes must occur; adequate tissue movement must be achieved to shape the morphology of the facial regions; multiple epithelial adhesions must occur followed by removal of epithelial seams to complete facial fusion (Warbrick, 1960; Jiang *et al*. 2006). The delay or disruption of any of these events can result in craniofacial abnormalities (Mossey *et* al. 2009; Jiang *et al*. 2006). Of the craniofacial abnormalities, the most common forms are the orofacial clefts which arise as a result of incomplete or disrupted formation of the upper lip and primary palate and the secondary palate (Mossey *et al*. 2009).

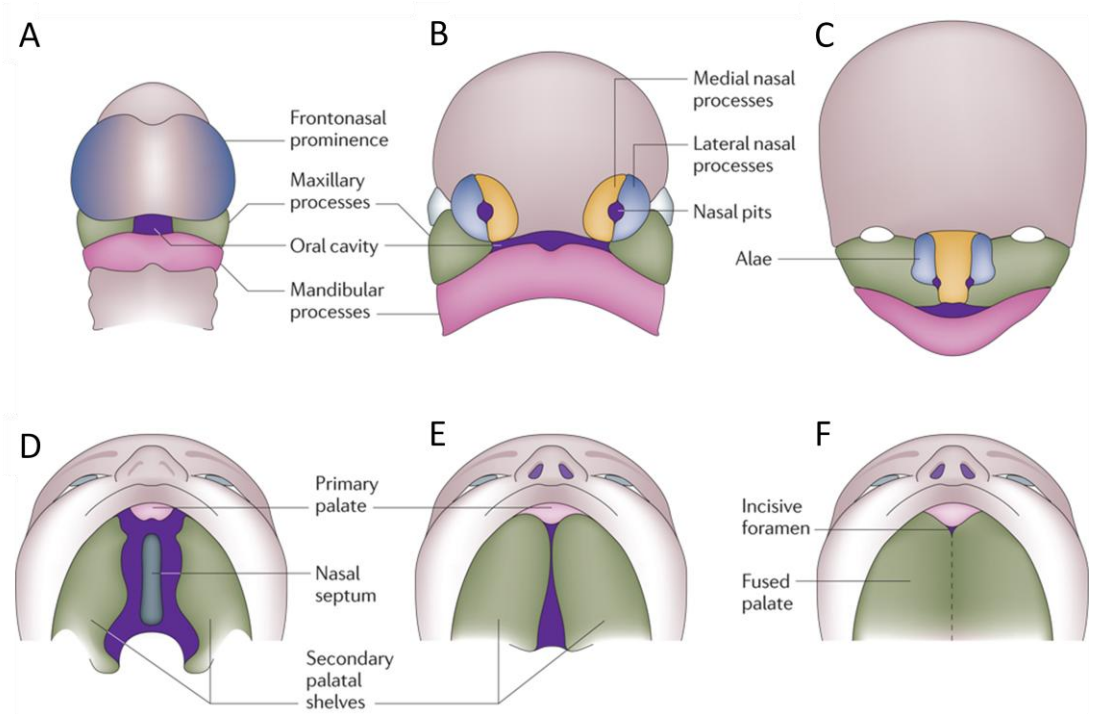

Figure 1.2: Development of the lip and palate. (**A**) Growth within the frontonasal prominence results in the formation of the medial nasal and lateral nasal processes. (B) Directed growth of the medial nasal, lateral nasal and maxillary processes results in their contact and adherence to one another, followed ultimately by fusion. (**C**) Maxillary processes contribute to the cheeks and upper lip of the face, while the medial nasal processes contribute to the upper lip and the lateral nasal processes form the alae of the nose. (**D**) During the sixth week of gestation the palatal shelves are formed as a pair of bilateral outgrowths from the maxillary prominences, while the primary palate is formed from the intermaxillary segment extending posteriorly into the oral cavity. (**E**) The palatal shelves initially grow vertically downwards flanking the tongue, before elevating into a horizontal position. Once elevated the palatal shelves extend medially where they contact and adhere to one another medially and the primary palate anteriorly. (**F**) At the site of contact between the palatal shelves, a double layer epithelial seam is formed, the medial epithelial seam which degenerates to allow formation of a confluent mesenchymal layer and midline fusion of the palate. The secondary palate further fuses with the primary palate anteriorly and the nasal septum dorsally. (Figure adapted from Dixon *et al*. 2011).

The presence of an orofacial cleft can result in a number of secondary pathologies. Affected individuals are known to display increased morbidity including increased risks of cancers, seizures and defects in dental and auditory development (Christensen *et al*. 2004). Furthermore affected individuals are susceptible to behavioural problems such as alcoholism and depression (Christensen & Mortensen, 2002; Mossey *et al*. 2009). Post cleft repair, affected individuals commonly display defects in dental and speech development as well as otologic complications such as chronic otitis media, tympanic membrane perforation and cholesteatoma (Shkoukani *et al*. 2014). Studies have identified a link between those affected by clefts and abnormalities of the brain, with males showing an increased risk of abnormalities and an apparent correlation between severity of cleft and the degree to which the brain is affected (Nopoulos *et al*. 2007). Indeed, research has shown that affected individuals display shorter life spans which may be due to the increased risk of psychological disorders and an increased risk of some cancers recorded in affected females (Christensen & Mortensen, 2002; Bille *et al*. 2005; Vieira, 2008).

Due to the variation seen in cleft phenotypes as well as the number of associated pathologies correction of orofacial clefts requires a multidisciplinary approach. The high prevalence of orofacial clefts means that multiple protocols for lifetime care have been established requiring the cooperation of oral maxillofacial surgeons, plastic surgeons, paediatricians, speech pathologists, audiologists, social workers and psychologists (Shkoukani *et al*. 2014).The requirement of such multidisciplinary care results in affected individuals providing a significant economic burden on either the state, if public healthcare is available, or their families (Wehby & Cassell. 2009; Alkire *et al*. 2011; Shkoukani *et al*. 2014). With the wide ranging implications of an orofacial cleft on both the affected individual and the state itself, it is clear that further research into the genetic and environmental causes of these conditions is important with the ultimate aim of prevention of clefting.

1.2.1 Classifications of clefts

Orofacial clefts are broadly divided into two subgroups based upon the structures affected (Figure 1.3). Cleft lip (CL) arises through a failure in the formation of the upper lip and primary palate (Mossey *et al*. 2009). CL may be caused through failure of any of the facial processes to adhere correctly and fuse to each other, for example the midline fusion between the medial nasal processes to form the intermaxillary segment, or the resolution of the nasolacrimal or bucconasal grooves (Mossey *et al*. 2009; Som & Naidich, 2013a). The intermaxillary segment contributes to the formation of the secondary palate. Therefore the presence of a CL may induce a cleft palate. Clefts may therefore be classified as cleft lip with/without cleft palate (CL/P) (Wang *et al*. 2014). The second main classification of orofacial clefts are cleft palate (CP) or cleft palate only (CPO) where only the secondary palate is affected. In these cases an orofacial cleft is a result of the failure of the palatal shelves to adhere correctly and fuse above the tongue (Mossey *et al*. 2009). The co-segregation of CL/P and CPO, or “mixed clefting”, within a single pedigree is a rare

occurrence suggesting they are genetically and etiologically distinct conditions (Neilson *et al*. 2002). Furthermore, studies of monozygotic twins suggest a 60% rate of concordance in the presence of an orofacial cleft suggesting the interaction of both genetic and environmental influences (Kimani *et al*. 2010). However, monozygotic twins display a higher rate of concordance of cleft lip and palate compare with dizygotic twins suggesting a strong genetic element (Grosen *et al*. 2011).

Clefts can be said to be either complete or incomplete, Wang and colleagues note that there is ambiguity in the accurate classification of clefts due to personal interpretations of what constitutes a complete cleft. It is suggested that the simplest definition of whether a cleft is complete or incomplete is whether a cleft extends into the nostril (Elsahy, 1973; Wang *et al*. 2014). Clefts can be further subcategorised dependent on which side of the facial midline they affect. Cleft lip may be classified as either unilateral or bilateral dependent on whether they affect one or both sides of the facial midline, with research suggesting that unilateral cleft lip more commonly affects the left side (Gundlach & Maus, 2006; Dixon *et al*. 2011; Mossey & Modell, 2012). The final classification of clefts is dependent on whether they are syndromic or non-syndromic (Wang *et al*. 2014).

1.2.2 The birth prevalence of orofacial clefts

Orofacial clefts are one of the most common developmental defects with the global incidence estimated to be between 1 in 500-2500 live births; however this is known to vary due to both geographic location and ethnicity (Mossey & Modell, 2012; Tanaka *et al*. 2012; Yu *et al*. 2014). CL/P is generally more common than CP, however this has been found to vary in some populations, for example CP is seen with a significantly higher frequency in Finnish populations (Diewert & Wang, 1992; Jugessur & Murray, 2005; Vieira *et al*. 2005; Jiang *et al*. 2006; Kling *et al*. 2014; Matthews *et al*. 2014). Several studies have identified a higher incidence of CL in males than females (Gundlach & Maus, 2006; Brydon *et al*. 2014; Kling *et al*. 2014; Matthews *et al*. 2014; Sangwa *et al*. 2014).

1.2.3 Non-syndromic clefts

The most common forms of CL/P and CP are those which occur in the absence of additional anomalies and are classified as non-syndromic or isolated cleft lip and palate (NSCL/P) which account for 70% of CLP and 50% of CP cases (Jugessur *et al*. 2009; Leslie & Marazita, 2013). While NSCL/P account for the majority of facial clefting, the details of how these clefts arise remain obscure in most cases. It is thought that NSCL/P is the result of a complex interplay of multiple genes and environmental factors, thus posing a significant challenge in the elucidation of the underlying mechanisms (Vieira *et al*. 2005). *IRF6* for example, is known to be directly associated with syndromic forms of clefting through van der Woude syndrome (VWS) and popliteal pterygium syndrome (PPS) (Kondo *et al*. 2002).

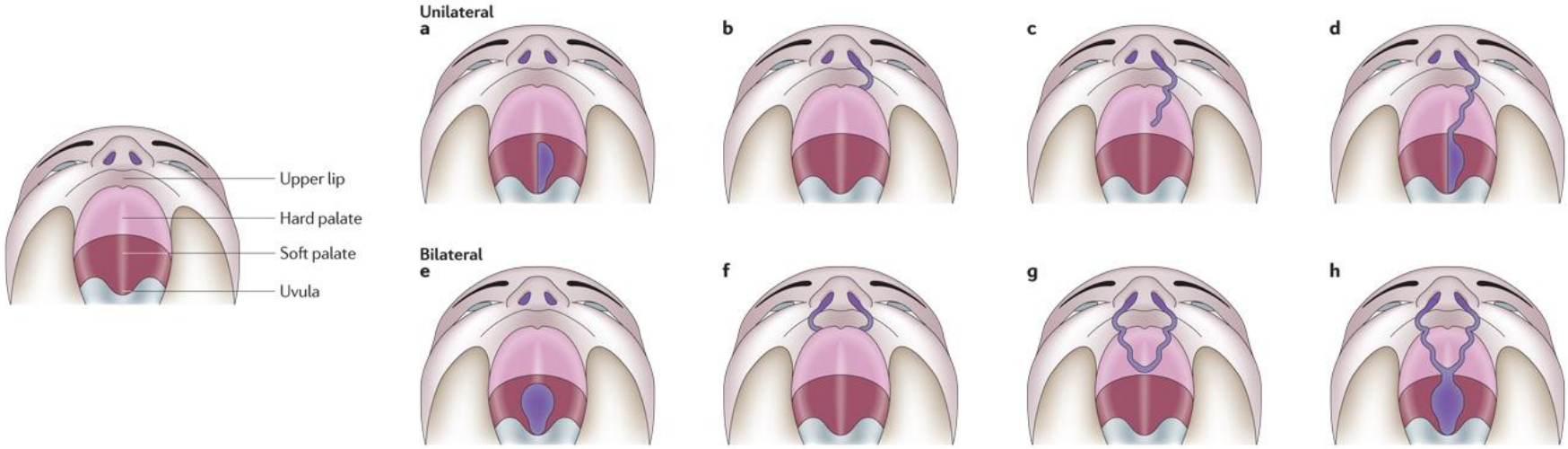

Figure 1.3:Classification of orofacial clefts. Orofacial clefts are broadly divided into those which affect the upper lip and primary palate with/ without the secondary palate (CL/P) and those which affect the secondary palate only (CP). Clefts are further subdivided based on whether they affect one, unilateral, (**a**-**d**), or both, bilateral, (**e**-**h**) sides of the facial midline. Additionally CL/P can be classified as either complete (**b-d** & **f-h**) or incomplete (**a** & **e**), dependent on if the cleft extends into the nostril. (**a**) unilateral incomplete cleft palate, (b) unilateral complete cleft lip, (**c**) unilateral complete cleft lip and soft palate, (**d**) unilateral complete cleft lip and palate, (**e**) bilateral incomplete cleft palate, (**f**) bilateral complete cleft lip and (**g**) bilateral complete cleft lip and soft palate and (**h**) bilateral complete cleft lip and palate (Figure adapted from Dixon *et al*. 2011).

Furthermore a single nucleotide polymorphism (rs646961, G>A), linked to an increased risk of NSCL was found to disrupt the binding of AP-2α to an enhancer site upstream of *IRF6* (Kondo *et al*. 2002; Rahimov *et al*. 2008; Zucchero *et al*. 2004; Leslie & Marazita, 2014).

The advancement of genetic techniques as well as the increased frequency and accuracy of patient records has allowed a number of causative mutations for NSCL/P to be investigated. A number of techniques are now employed to identify possible risk variants in NSCL/P including, linkage analysis, characterisation of genomic rearrangements, candidate gene approaches which makes use of existing knowledge to identify genes for investigation, and genome wide association studies (GWAS) to identify candidate genes or loci in an unbiased fashion (Beaty *et al*. 2010; Dixon *et al*. 2011; Leslie & Marazita. 2014). The use of genetic techniques has identified multiple genetic causes of NSCL/P including, *AXIN2*, a negative regulator of the Wnt signalling pathway (Menezes *et al*. 2009), interactions between *IRF6* and *TGFA* (Letra *et al*. 2012), *P63* (Berdón-Zapata *et al.* 2004; Leoyklang *at al.* 2006), *MSX1* (Lidral *et al*. 1998) and *PVRL1* (Sözen *et al*. 2001).

GWAS studies have identified multiple loci associated with NSCL/P (Setó-Salvia & Stanier, 2014). The most significant loci identified is a 64 kb region located at chromosome 8q24.21. The marker rs987525 was found to be highly significant, with three SNPs at this locus achieving genome-wide significance (Birnbaum *et al*. 2009; Grant *et al*. 2009). 8q24 is a gene desert with no known genes identified (Birnbaum *et al*. 2009; Grant *et al*. 2009). The nearest genes are *MYC*, *PVT1* and *GSDMC* (Birnbaum *et al*. 2009). It was therefore suggested that 8q24 contains regulatory elements whose disruption contributes to NSCLP (Birnbaum *et al*. 2009). The association between rs987525 and NSCLP has been further confirmed through additional studies across multiple ethnicities (Beaty *et al*. 2013; Aldhorae *et al*. 2014). In addition studies have identified associations in regions including chromosome 1q22.1 (within *ABCA4*), 1q32 (including *IFR6*), 1q36 (within *PAX7*), 2p21 (within *THADA*), 3p11 (3 kb downstream of *EPHA3*), 3q12 (including *COL8A1* and *FILIP1L*), 8q21, 8q24, 9q22 (including *FOXE1* and *HEMGN*), 10q25.3 (within *VAX1*), 13q31.1 (adjacent to *SPRY2*), 15q22 (20 kb upstream of *TPM1*), 16p13 (adjacent to *CREBBP* and *ADCY9*), 17q13 (within *NTN1*), 17q22 (including *NOG*) and 20q12 (within *MAFB*) (Moreno *et al*. 2009; Beaty *et al*. 2010; Mangold *et al.* 2010; Ludwig *et al*. 2012; Sun *et al*. 2015).

In addition to genetic techniques, observational studies have identified a putative link between environmental factors and NSCL/P. Maternal intake of folic acid, both before and during the first 12 weeks of pregnancy, reduces the risk of neural tube defects and NSCL/P, with Kelly and colleagues identifying a 4.36-fold higher risk of CLP in mothers who did not take folic acid supplements (Li *et al*. 2012; Kelly *et al*. 2012). Interestingly, while this finding is supported in other cohort studies, other studies have produced conflicting data. De-Regil and colleagues identified a significant reduction in neural tube defects in those taking folic acid supplements, but the study failed to achieve significant results in relation to prevention of CLP (De-Regil *et al*. 2010). Furthermore, while a subset of studies identified a reduced

risk of CLP resulting from folic acid supplementation no benefit has been found from intake of folic acid intake in regards to CP (Boyles *et al*. 2008; Li *et al*. 2012). The putative link between folic acid and clefting was strengthened with the association of two gene polymorphisms *MTHFD1* 1958 G -> A and *MTHFR* 677 C -> T, which encode folic acid enzymes, as maternal risk factors for both CLP and CP (Boyles *et al*. 2008; Mills *et al*. 2009).

Prenatal maternal smoking has been associated with an increased incidence of orofacial clefts, with some studies suggesting that smoking may contribute to 4% of orofacial clefts and 12% of bilateral CLP (Little *et al*. 2004a; Little *et al*. 2004b; Honein *et al*. 2007; Mossey *et al*. 2007; Hackshaw *et al*. 2011). Hackshaw and colleagues conducted analysis of 38 studies examining the risk associated with smoking and CLP, finding 13 to show a significant correlation and six to display a dose-response relationship (Hackshaw *et al*. 2011). Other environmental factors associated with the risk of CL/P include parental exposure to anticonvulsants or retinoids, irregular alcohol consumption and maternal exposure to illness during pregnancy (Dixon *et al*. 2011; Leslie & Marazita, 2014).

1.2.4 Syndromic clefts

CL/P is classified as syndromic where an orofacial cleft is present in addition to other physical or cognitive abnormalities (Leslie & Marazita, 2014). In contrast to non-syndromic clefts, a large number of syndromic clefts are caused by the mutation of a single genetic locus (Leslie & Marazita, 2014). To date over 487 syndromes have been found which feature a cleft as a phenotype (Venkatesh, 2009). Investigation of syndromic clefts has provided valuable insights into the genetic mechanisms underlying the pathogenesis of CLP and the normal developmental processes of craniofacial morphogenesis. Due to the observable mode of mendelian inheritance of syndromic clefts, the genetic cause of 75% of these clefts is now known, the most common being VWS which accounts for approximately 2% of all CL/P cases (Leslie & Marazita, 2014).

VWS is characterised by pits in the lower lip, CL/P and hypodontia (Van der Woude, 1954). VWS displays both intra- and interfamilial variations in the clinical phenotype of affected individuals (Martelli-Junior *et al.* 2007). Through the study of monozygotic twins discordant for VWS, mutations within the transcription factor *interferon regulatory factor 6* (*IRF6*) were identified (Kondo *et al*. 2007). The group identified a single nonsense mutation within exon 4 of *IRF6* in the affected twin and equivalent mutations were found in 45 additional unrelated affected families as well as families affected by PPS, thus identifying *IRF6* mutations as the cause of both conditions (Kondo *et al*. 2002). Characterising the location of mutations of VWS or PPS affected individuals identified clustering within the DNA-binding domain and protein interaction domain of *IRF6*. Identified mutations include: missense mutations Val18Met, Pro39Ala and Arg84Cys; nonsense mutations Tyr23X and Gln68X and frameshift mutations Met1Ile and Ala2Val (Kondo *et al*. 2002). Furthermore mutations within *IRF6* were

found to display a phenotype-genotype correlation, with mutations causing PPS confined to the residues which directly contacted DNA within the DNA binding domain, while VWS mutations were shown to be spread between both domains (Kondo *et al*. 2002).

Mutations in *WNT3* in humans are known to cause Tetra-Amelia syndrome (Niemann *et al*. 2004). Tetra-Amelia syndrome is characterised by profound abnormalities of the limbs, facial regions and urogenital areas. Common features of Tetra-Amelia syndrome include; CL/P, gastroschisis, agenesis of the left kidney, spleen, uterine malformations and abnomalies of the vagina and anus (Neimann *et al*. 2004). Rarely patients affected by Tetra-Amelia can display a complete absence of all four limbs (Niemann *et al*. 2004). Some studies into the association between *WNT3* and NSCLP have failed to achieve significance in Chinese populations, while others do suggest an association (Chiquet *et al*. 2008; Mostowska *et al*. 2012; Xin *et al*. 2013). The identification of the causes of syndromic CL/P has been integral to the identification of key stages of orofacial development. As such a number of genes have now been identified as the causal factor in human conditions as seen in table 1.1.

Syndrome	Causative Gene	Clefting observed	Reference
van der Woude	*IRF6*	CL/P	Kondo *et al*. 2002
PPS	*IRF6*	CL/P	Kondo *et al*. 2002
Tetra-amelia syndrome	*WNT3*	CL/P	Niemann *et al*. 2004
Ectrodactyly-ectodermal-dysplasia-clefting	*TP63*	CL/P	Celli *et al*. 1999
Opitz syndrome	*MID1*	CL/P	Quaderi *et al*. 1997
Gorlin's syndrome	*PTCH1*	CL/P	Johnson *et al*. 1996
Kallman syndrome	*FGFR1*	CL/P	Kim *et al*. 2005
Muenke syndrome	*FGFR3*	CL/P	Agochukwu *et al*. 2012
Cleft lip/palate-ectodermal dysplasia	*PVRL1*	CL/P	Suzuki *et al*. 2000
Bartsocas-Papas	*RIPK4*	CL/P	Mitchell *et al*. 2012
Holoprosencephaly	*SHH*	CL/P	Roessler *et al*. 1996
Holoprosencephaly	*GLI2*	CL/P	Roessler *et al*. 1996
DiGeorge	*TBX1*	CP	Packman & Brook, 2003
Ankyloblepharon-ectodermal dysplasia-clefting	*TP63*	CL/P	McGrath *et al*. 2001
Oro-facial-digital	*GLI3*	CL/P	Johnston *et al*. 2010
Siderius X-linked mental retardation	*PHF8*	CL/P	Laumonnier *et al*. 2005
Pierre Robin	*SOX9*	CP	Benko *et al*. 2009
Treacher Collins	*TCOF1*	CP	The Treacher Collins Syndrome Collaborative Group, 1996
Miller syndrome	*DHODH*	CP	Ng *et al*. 2010
Isolated cleft palate	*SATB2*	CP	Fitzpatrick *et al*. 2003

Table 1.1 Human CL/P syndromes and their causative genes. (Adapted from Dixon *et al*. 2011)

1.3 Researching orofacial development

Due to the highly visible impact of orofacial defects on affected individuals, a great deal of research has been conducted into development of the orofacial regions and the pathologies of orofacial clefts. The complexity of orofacial development coupled with contribution of both genetic and environmental influences has resulted in a broad spectrum of techniques being employed. Previous work such as that of Warbrick identified the processes of orofacial development using human embryos. Through histological sectioning of human embryos Warbrick helped to clarify the stages involved in development of the nasal cavity and upper lip (Warbrick, 1960). However, owing to the availability of genetic manipulation and established genetic backgrounds, the majority of craniofacial research is now conducted using animal models (Bokhoven & Brunner, 2002).

1.3.1 Model systems: using the mouse as a model organism

To date a number of animal models have been used to investigate orofacial development. The most common model organism for orofacial development is the mouse. Mice provide an excellent model system for orofacial research for a number of reasons. Facial development in mice involves a conserved series of events that are highly similar to those observed in humans (Gritli-Linde, 2008). The use of mice is aided by their rapid gestation times and low maintenance cost. Furthermore, the development of multiple tools allowing manipulation of the mouse genome to produce models of orofacial defects, has allowed research to be conducted into both the genetic and environmental components of orofacial development (Juriloff *et al*. 2001; Gong *et al*. 2000).

In addition to mice, chicks provide an excellent model system due to the accessibility of the orofacial regions during development (Couly *et al.* 1992; Mossey *et al.* 2009). Chick embryos are accessible during gestation allowing the addition of growth factors through bead implantation assays (Kawakami *et al*. 2014). Development of the orofacial regions in chick displays subtle differences to that of mammals (Jiang *et al*. 2006). In contrast to mammalian development, the medial nasal, lateral nasal and maxillary processes adopt a square configuration (Yee & Abbott, 1978). Further differences arise in the composition of the medial nasal processes. In mammalian development the medial nasal processes develop as paired outgrowths of the frontonasal mass isolated by a midline fissure (Jiang *et al*. 2006). In contrast the medial nasal processes in chick develop as elevations of the frontal prominence separated by a shallow median groove (Yee & Abbott, 1978). The difference between chick and mammalian development means that mice provide a superior model for research pertaining to human development.

1.3.2 Mouse upper lip and primary palate development

Development of the primary palate begins at embryonic day (E) 9.5 when two populations of neural crest cells migrate from regions within the midbrain and forebrain to the midfacial region (Jiang *et al*. 2006). Enlargement of the forebrain pushing the ectoderm forward and laterally and neural crest migration produces the facial primordia: the frontonasal mass, the maxilla and the mandible (Richman & Crosby, 1990; Som & Naidich, 2013a). Each process consists of a core of mesoderm and neural crest cells covered with an epithelial layer (Couly *et al*. 1992; Johnston & Bronsky, 1995; Jiang *et al*. 2006). The frontonasal process, the paired maxillary and the paired mandibular processes are formed from the facial primordia (Gritli-Linde, 2008). Neural crest cells from the midbrain contribute to the formation of the lateral nasal processes, while cells from the forebrain form the medial nasal processes (Som & Naidich, 2013a).

The lower lip, mandible and the anterior segment of the tongue are formed through the fusion, at the medial ends, of the bilateral mandibular processes (Jugessur & Murray, 2005; Jiang *et al*. 2006). At E10 nasal placodes, formed from the frontonasal process, undergo invagination as a result of thickening of the surface ectoderm (Figure 1.4 A,B,F&G) (Johnston & Bronsky, 1995). Further growth of the frontonasal process around the nasal placodes results in formation of the nasal pits and the paired lateral and medial nasal processes (Figure 1.4 C&H) (Jin *et al*. 2012). Development of the telencephalic vesicles induces a paired configuration between the processes (Jiang *et al*. 2006).

At E10.5 rapid growth of the mesenchyme in the maxillary processes results in medial movement of the nasal pits. The medial nasal processes grow ventrolaterally, which shapes the nasal pits into dorsal pointed slits (Figure 1.4 D&I). At this stage the upper lip consists of maxillary processes laterally, the medial nasal processes medially and the lateral nasal processes between them (Jiang *et al*. 2006).

The medial and lateral nasal processes contact and begin to fuse, while the maxillary processes lie below the lateral nasal processes. At the point of contact between the processes a double epithelial layer is formed. This epithelial seam is known as the nasal fin and must be removed to allow mesenchymal confluence (Diewert & Wang, 1992; Jiang *et al*. 2006; Gritli-Linde, 2008). At E11 the lateral nasal processes are pushed rostrally by the rapid growth of the maxillary and medial nasal processes. This results in the distal ends of the maxillary and medial nasal processes coming into direct contact. The processes adhere and begin to fuse as a second epithelial seam is formed which must also be removed (Johnston & Bronsky, 1995). The contact and fusion of the maxillary and medial nasal processes is not reliant upon the prior adherence and fusion of the medial and lateral nasal processes (Jiang *et al*. 2006).

The upper lip is formed from tissue derived from both the medial nasal and maxillary processes. The lateral nasal processes contribute to the walls of the nasal alae (Gritli-Linde, 2008). Following successful fusion, the medial groove between the medial nasal processes remains. At E11.5-E12 rapid growth of the maxillary processes pushes the nasal pits and medial nasal processes mediofrontally (Figure 1.4 E&J) (Hinrichsen, 1985). Meanwhile the continued growth and confluence of the medial nasal and maxillary mesenchyme results in the medial groove becoming shallow and smooth (Johnston & Bronsky, 1995; Jiang *et al*. 2006). These morphogenic changes coupled with complete fusion between the medial and lateral nasal processes convert the nasal pits to nasal chambers and ducts (Jiang *et al*. 2006).

The nostrils are converted to small slits and their lower edge is remodelled due to the fusion between the medial nasal and maxillary processes (Jiang *et al*. 2006). By E12.5 both epithelial seams at the site of process fusion have been degenerated allowing mesenchymal confluence (Diewert & Wang, 1992; Jugessur & Murray, 2005). The nasal chambers are moved medially and the medial groove filled while the intermaxillary segment extends into the oral cavity to form the anterior palate segment and subsequently fuse with the secondary palate (Diewert & Wang, 1992; Jiang *et al*. 2006).

1.3.3 Secondary palate development

Secondary palate development begins at approximately E11 with the outgrowth of paired bilateral processes, the palatal shelves, from the paired maxillary processes. Between E12.5-E14 the shelves grow vertically downwards (Figure 1.5 A) on either side of the tongue until early E14. Downwards growth of the mandible causes the tongue to drop allowing a mechanical flipping of the palatal shelves into the horizontal position superior to the tongue (Figure 1.5 B&C) (Wilkie & Morris-Kay, 2001; Moxham, 2003; Gritli-Linde, 2007; Mossey *et al*. 2009; Zhu *et al*. 2012). Once elevated, mesenchymal proliferation extends the palatal shelves medially (Figure 1.5 C) (Ito *et al*. 2003; Zhu *et al*. 2012).

By E14.5, the palatal shelves have contacted and adhered to each other, resulting in the formation of the medial epithelial seam (MES) (Figure 1.5 D). Palatogenesis requires degeneration of the MES and mesenchymal confluence (Gritli-Linde, 2007; Mossey *et al*. 2009; Warner *et al*. 2009). Fusion of the palatal shelves is completed by E15 (Figure 1.5 E&F). The secondary palate then fuses anteriorly with the primary palate and the nasal septum dorsally. Following fusion of the primary and secondary palates, ossification occurs, initially within the primary palate before extending into the secondary palate. Ossification of the anterior palatal processes forms the hard palate, while the posterior palatal processes do not undergo ossification (Gritli-Linde, 2007; Som & Naidich, 2013b). The posterior palatal processes extend into the nasal septum to form the soft palate (Som & Naidich, 2013b).

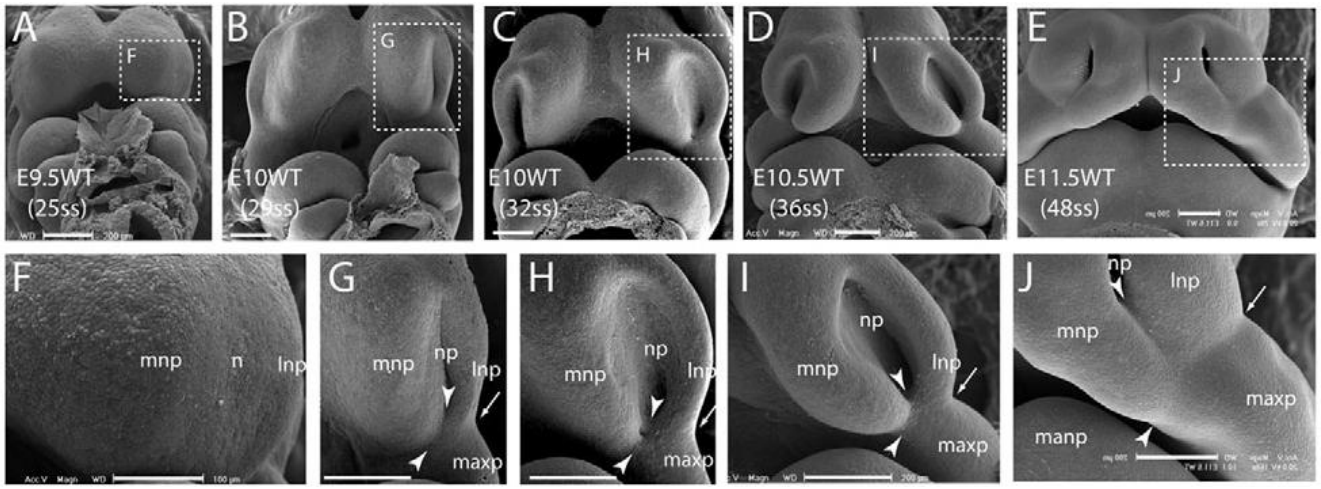

Figure 1.4: Developmental stages of the mouse upper lip. Images show frontal views of the developing mouse facial regions from E9.5-E11.5. (**B**&**G**) The medial nasal and lateral nasal processes are formed through thickening of the surface ectoderm and invagination produces the nasal pits. (**C**&**H**) Nasal pits are moved medially due to growth of the mesenchyme of the maxillary processes. (**D**&**I**) Ventrolateral growth of the medial nasal processes shapes the nasal pits into slits and contact is made between the lateral and medial nasal processes. (**E**&**J**) Rapid growth of the medial nasal and maxillary processes results in contact between the two. Contact between both the lateral and medial nasal processes and the medial nasal processes and maxillary processes results in the formation of an epithelial seam at the site of contact, which must be degraded to allow fusion. Scale bars A-E - 200µm and F-J - 500µm. Arrows denote the site of fusion between the facial processes. mnp – medial nasal process, n – nasal placode, lnp – lateral nasal process, maxp – maxillary process, manp – mandibular process. (Adapted with permission from Development - Song *et al*. 2009).

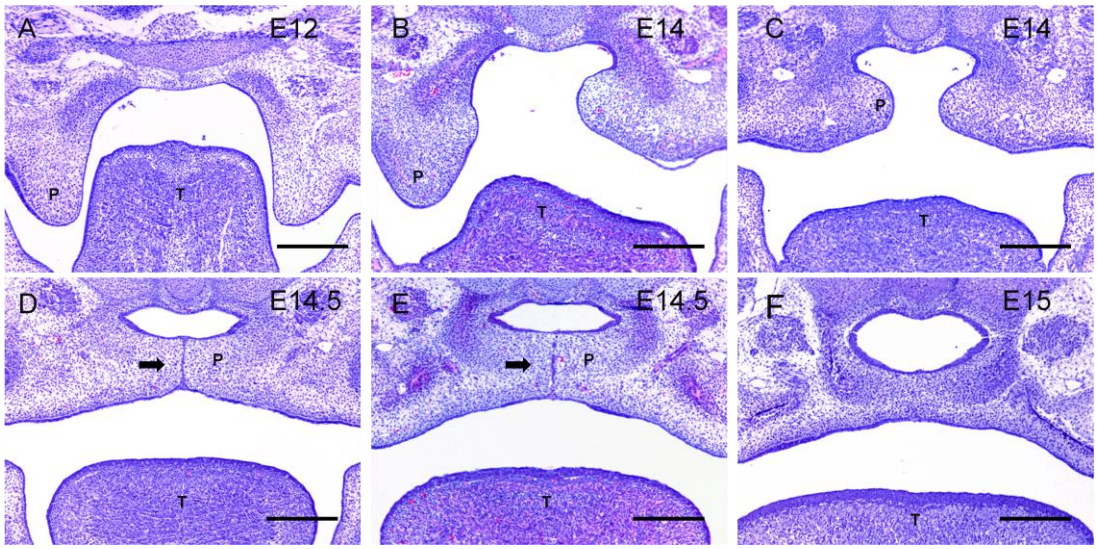

Figure 1.5: Haematoxylin and eosin-stained coronal sections of mouse secondary palate development. (**A**) Between E11-E14 the palatal shelves grow vertically downwards flanking the tongue. (**B**-**C**) At E14 the palatal shelves elevate into the horizontal orientation superior to the tongue and extend towards the midline above the tongue. (**D**) At E14.5, the apposing palatal shelves contact and adhere at the medial edge epithelia forming the transient medial epithelial seam (arrowed). (**E**-**F**) Fusion of the secondary palate occurs through the progressive degeneration of the medial epithelial seam. Fusion of the palatal shelves is completed by E15 through the complete degeneration of the medial epithelial seam allowing mesenchymal confluence and the separation of the oronasal space into the oral and nasal cavities. P – palatal shelves, T - tongue. Scale bars: 3 µm.

The developmental stages of primary and secondary palate development display morphogenic overlap suggesting similarities in their molecular controls. Research into the removal of the MES in the secondary palate has suggested three hypotheses, periderm cell migration, apoptosis or epithelial to mesenchymal transformation (EMT) (Moxham, 2003; Jugessur & Murray, 2005; Gritli-Linde, 2007; Warner *et al*. 2009). To date, no consensus has been reached.

1.4 Molecular control of lip development

Development of the orofacial regions requires the complex interplay of multiple biological processes. The process of upper lip morphogenesis requires the outgrowth of the facial processes, directed proliferation to shape the facial processes and successful contact, adherence and ultimately fusion of the medial nasal, lateral nasal and maxillary processes (Warbrick, 1960). Through the identification of the mutations underlying syndromic forms of CL/P and attempts to elucidate the etiological causes of NSCL/P, some of the molecular and environmental factors which contribute to the various stages of lip morphogenesis have been identified (Murray, 2002, Leslie & Marazita, 2014). While the molecular events during development of the secondary palate have been investigated extensively, control of lip development remains poorly characterised.

1.4.1 Bone morphogenetic protein signalling

The bone morphogenetic protein (Bmp) signalling network consists of a group of secreted signalling proteins of the transforming growth factor beta (Tgfβ) super family which bind to cell surface receptor serine/ threonine kinases to induce intracellular signalling (Jiang *et al*. 2006; Parada & Chai, 2012). Roles for Bmp signalling have been found in the development of almost all organs of the vertebrate body (Sieber *et al*. 2009). Ligands for Bmp signalling are divided into Bmps, osteogenic proteins (Op), cartilage-derived morphogenic proteins (Cdmp) or growth and differentiation factors (Gdf) and then further subdivided into five groups based upon sequence similarity known as: the decapentaplegic (Dpp) subfamily consisting of Bmp2 and Bmp4; the 60A subfamily consisting of Bmp5, Bmp6, Bmp7 and Bmp8; Bmp3 and Bmp3b are classified as a subfamily; Gdf5, Gdf6 and Gdf7 make up an additional family and Nodal and Lefty are further classified as a distinct subfamily (Nie *et al*. 2006; Parada & Chai, 2012).

The Bmp family has been characterised extensively with over twenty known members identified (Nie *et al*. 2006). Bmp ligands function predominantly through association with Bmp receptors, which in turn phosphorylate and activate transcriptional co-activators Smads (Parada & Chai, 2012). Bmp receptors are divided into type I and type II receptors, which display variation in their affinity for Bmp ligands (Nie *et al*. 2006). Type I receptors include Alk2, Alk3 and Alk6 and display high affinity for Bmp ligands, while type II receptors consist of BmprII, ActrIIa and ActrIIb. Type II receptors display reduced affinity for Bmp ligands compared with type I (Nie *et al*. 2006; Parada & Chai, 2012). Binding of Bmp ligands to Bmp

receptors triggers the Bmp signalling cascade with type II receptors able to phosphorylate type I receptors which in turn phosphorylate Smads (Parada & Chai, 2012). Smad1, Smad5 and Smad8 are directly phosphorylated by type I receptors which allows heterodimerisation with Smad4 and translocation to the nucleus to induce transcription (Nie *et al*. 2006). In addition to the Smad co-activators, Smad6 and Smad7 function as inhibitors of the Bmp signalling cascade (Nie *et al*. 2006). Bmp induction is also thought to induce a number of signalling pathways including the Mapk, Pi3 kinase, Pkc and Msx pathways (Nie *et al*. 2006; Parada & Chai, 2012).

Bmp ligands are expressed in the facial primordia and the Bmp signalling cascade is active during upper lip development (Liu *et al*. 2005). Work in chick embryos identified the expression of *BMP4* localised to the epithelium of the facial processes during their outgrowth (Francis-West *et al*. 1994). The group identified discrete patterns of *BMP4* and *BMP2* expression, initially in the epithelium of the medial nasal, lateral nasal and maxillary processes, followed by expression within the distal mesenchyme. Once expression of *BMP4* was established within mesenchymal cells, there was a marked reduction in expression within the previously *BMP4*-positive epithelium (Francis-West *et al*. 1994; Jiang *et al*. 2008). Francis-West and colleagues suggested that *BMP4* may play a role in the outgrowth of the facial processes as well as in epithelial to mesenchymal signalling (Francis-West *et al*. 1994).

Epithelial expression of *BMP2*, *BMP4* and *BMP7* within the facial processes was required for up-regulation of *MSX1* and *MSX2* within the mesenchyme. Expression of *MSX1* and *MSX2* induced proliferation and outgrowth of the facial processes (Barlow & Francis-West, 1997; Ashique *et al*. 2002). Mouse models of *Msx1* knockout display cleft palate. However, ectopic expression of *Bmp4* can rescue the cleft phenotype, suggesting *Bmp4* is a downstream target of *Msx1* (Zhang *et al*. 2002).

BMP7 and *BMP4* are expressed within the epithelium at the site of fusion between facial processes in chick (Francis-West *et al*. 1994; Ashique *et al*. 2002). The Bmp antagonist Noggin was shown to be involved in regulating Bmp signalling between the epithelium and mesenchyme with both expansion and reduction of Bmp signalling resulting in orofacial deformities due to lack of proliferation or apoptosis (Ashique *et al*. 2002). Furthermore the expression of *FGF8* and *SHH* within the epithelium of the facial processes was found to be under the control of Bmp signalling. Loss of Bmp regulation resulted in increased *FGF8* and *SHH* expression within the epithelium of facial processes which had contacted one another. Fgf and Shh signalling act to promote cell survival and prevent the epithelial apoptosis required for fusion of the facial processes (Ashique *et al*. 2002). The work of Richman's group highlights the molecular crosstalk that occurs during facial development (Ashique *et al*. 2002; Nie *et al*. 2006).

The role of Bmp4 in avian facial development has been recapitulated in mice (Gong & Guo, 2003; Liu *et al*. 2005). Research into the role of Bmp4 in mammalian lip development was initially hampered due to the embryonic lethal nature of *Bmp4* knockouts, which occurs prior to facial development. However, the development of conditional *Bmp4* knockout mice has shown that removal of *Bmp4* expression during lip development induces isolated CL (Liu *et al*. 2005). Liu and colleagues generated a *Bmp4* conditional knockout through *Bmp4*^{floxneo} which contained LoxP sites flanking exon 4 (Liu *et al*. 2004). Generation of *Nestin cre;Bmp4*$^{null/flox}$ resulted in excision of exon 4 and a loss of *Bmp4* expression in E10.5 and E12.5 embryos (Liu *et al*. 2005). *Bmp4* conditional knockouts, display a complete bilateral CL at E12.5, before undergoing spontaneous correction to display a unilateral isolated CL at E14.5 (Liu *et al*. 2005).

The expression of *Bmp4* has been found to be similar between mouse and chick, with *BMP4* expressed within the epithelium of the facial processes prior to fusion, and within the mesenchyme post fusion (Ashique *et al*. 2002; Gong & Guo, 2003). Gong and Guo suggest that *Bmp4* expression may demarcate cells within the epithelium of the lateral nasal and medial nasal processes which are destined to adhere and fuse (Gong & Guo, 2003). Furthermore it is suggested that Bmp4 may regulate apoptosis within the epithelial seam during fusion of the medial nasal and lateral nasal, as previously shown in chick (Ashique *et al*. 2002; Gong & Guo, 2003).

Bmpr1a (*Alk3*) encodes a type I Bmp receptor required for successful development of the upper lip and primary palate and the secondary palate (Liu *et al*. 2005). In a similar fashion to *Bmp4*, *Bmpr1a* knockout is early embryonic lethal in mice (Liu *et al*. 2005; Nie *et al*. 2006). Loss of *Bmpr1a* expression results in bilateral CL through premature apoptosis within the epithelium of the medial nasal processes and increased apoptosis in the mesenchyme (Liu *et al*. 2005; Nie *et al*. 2006). Loss of Bpr1a disrupted the expression of *Fgf8* within the mesenchyme of the medial nasal processes which is thought to contribute to the apoptosis observed. In addition to *Fgf8*, expression of *P63* and *Pitx1* was shown to be disrupted (Liu *et al*. 2005).

Similar to *Bmpr1a*, mouse knockouts for the type I BMP receptor *Alk2* display embryonic lethality (Dudas *et al* 2004; Liu *et al*. 2005). Conditional knockouts for *Alk2* display CP but fail to display defects in the upper lip or primary palate (Dudas *et al*. 2004). The diversity of phenotypes displayed by Bmp knockouts and their suggested roles during development further illustrates the complexity of orofacial development as well as highlighting the similarities and differences in regulation of lip and palate development (Parada & Chai, 2013; Nie *et al*. 2006).

1.4.2 Sonic hedgehog signalling

Members of the sonic hedgehog (Shh) signalling network are involved in growth, patterning and morphogenesis of multiple regions and organs during embryonic development (Ingham & McMahon, 2001). Expression of Shh signalling pathway components including *Shh*, *Ptch1*, *Smo* and *Gli1* has been observed during lip development (Jiang *et al*. 2008; Metzis *et al*. 2013). Shh functions through binding of the Shh ligand to the cell surface receptor Ptch1 (Taipale *et al*. 2002). Ptch1 regulates the intracellular ratio of active to inactive Smo (Taipale *et al*. 2002). Upon binding by Shh, Ptch1 repression of Smo is lost increasing the concentration of active Smo (Taipale *et al*. 2002). Smo proteolytically cleaves the transcription factors Gli1, Gli2, and Gli3 (Wang *et al*. 2000). Therefore binding by Shh to Ptch1 relieves repression of Smo which in turn cleaves Gli factors to active forms, thus allowing the inhibition or activation of downstream targets of Shh signalling (Wang *et al*. 2000; Jiang *et al*. 2006).

The most characterised member of the Hh signalling family is *Shh* which has been found to be highly conserved across multiple species (Katoh & Katoh, 2005). Studies of *Shh* expression have identified roles in embryonic structures such as the notochord, the floorplate of the neural tube, posterior margin of tetrapod limb buds, and the facial regions (Chiang *et al*. 1996). Analysis of mouse *Shh* knockouts identified defects in multiple tissues including; defects of the cephalic regions, lack of fore and hindlimb structures, and profound defects in facial morphology including loss of the eyes, nose, and orofacial structures (Chiang *et al*. 1996). Mutations in *SHH* in humans have been shown to be a cause of holoprosencephaly (Nanni *et al*. 1999). *SHH* mutations display a range of phenotypes including, midline defects, anophthalmia or cyclopia, ocular hypertelorism, complete or incomplete CL/P, the absence of a mature nose and the absence of the olfactory nerves or corpus callosum (Belloni *et al*. 1996; Roessler *et al*. 1996; Hu & Helms, 1999). Furthermore defects within *SHH* display a distinct genotype to phenotype correlation, with severity directly related to the degree to which the *SHH* gene is affected, with patients displaying translocations of *SHH* afflicted with milder phenotypes than those with deletions (Belloni *et al*. 1996).

Due to the severe phenotype of the *Shh* knockout mouse (loss of all facial structures) identification of the role of *Shh* in facial development has relied upon other models (Chiang *et al*. 1996). Use of the chick allowed the role that Shh plays during facial morphogenesis to be dissected. During the outgrowth of the facial processes, *SHH* is expressed within the surface ectoderm (Hu & Helms, 1999). By removing the *SHH*-positive ectoderm, Hu and Helms found that loss of Shh resulted in a lack of expression of the Shh receptor protein Ptch1 (Hu & Helms, 1999). Furthermore, loss of *SHH* expression from the frontonasal prominence or the maxillary processes resulted in a loss of symmetrical growth and lack of proliferation within the mesenchyme (Hu & Helms, 1999).

Inhibition of *SHH* expression in chick through the use of a blocking antibody showed that ectodermal expression was required for fusion of the facial processes (Hu & Helms, 1999; Jiang *et al*. 2006). Furthermore, over-expression of *SHH* in the frontonasal process and maxillary processes results in up-regulation of *PTCH1, GLI1* and *BMP2* leading to expansion of the mesenchyme due to increased proliferation. Ultimately, inappropriate proliferation results in widening of the midfacial regions which caused CP and in some cases the formation of additional structures resembling extra beaks (Hu & Helms, 1999). The work of Hu and Helms demonstrated that *SHH* expression must be kept within appropriate levels as either increased or decreased Shh results in abnormal facial development.

Ptch is the membrane receptor for Shh and is known to be expressed within the mesenchyme of developing facial processes. Mutations in *PTCH* in humans are associated with Gorlin syndrome as well as being associated with familial and sporadic forms of clefting (Johnson *et al*. 1996; Metzis *et al*. 2013). Gorlin syndrome, also known as basal cell nevus syndrome, is characterised by polydactyly, syndactyly, spina bifida, developmental abnormalities of the ribs and craniofacial regions (Johnson *et al*. 1996). A study into the possible association between *PTCH* mutations and NSCLP was able to identify linkage, but could not elucidate the direct molecular causes (Mansilla *et al*. 2007).

Murray's group identified a number of novel mutations in their subject groups located within the extracellular loops of Ptch, which are thought to be required for Shh binding (Mansilla *et al*. 2007). However, the mutations Pro295Ser, Ser827Gly and Asp436Asn were present in both affected and control individuals suggesting that the presence of these mutations alone were not the cause of CL/P. It was therefore suggested that there may be a threshold for loss of Ptch function which must be overcome to induce an orofacial phenotype. Ptch has been shown to induce proliferation and apoptosis, with over-expression of Ptch inducing apoptosis of cells required for the closure of the lip or palate during development (Mansilla *et al*. 2007).

Mouse models homozygous for *Ptch1* knockout are not viable, displaying embryonic lethality between E9.0 and E10.5, i.e. prior to lip development (Goodrich *et al*. 1997). *Ptch1* knockout mice display a phenotype similar to that of $Shh^{-/-}$ embryos, with a failure to close the neural tube, expansion of the hindbrain and spinal cord and abnormal heart development which is thought to be the cause of lethality, therefore a conditional knockout is the only viable option for the study of *Ptch1*-related lip morphogenesis (Goodrich *et al*. 1997; Metzi *et al*. 2013).

Loss of *Ptch1* resulted in expansion of Shh signalling in the developing medial nasal, lateral nasal and maxillary processes, with expression of *Gli1* greatly increased (Metzi *et al*. 2013). *Ptch1* expression was localised to the neural crest-derived mesenchyme. Furthermore, a midline gap between the paired medial nasal processes was seen which was suggested to be due to defects in the invagination of the nasal pits (Metzi *et al*. 2013). Analysis of *Fgfr1*, *Fgfr2*, *Fgf8* and *Spry1* expression showed that Fgf signalling was perturbed in *Ptch1*-

deficient embryos, with full deletion of Fgf expression within the epithelium suggesting that Shh signalling is required for Fgf expression during lip morphogenesis (Metzi *et al*. 2013). Administration of Fgf8 was able to affect a partial rescue (Metzi *et al*. 2013). Bmp signalling has also been shown to regulate Fgf signalling at this key stage of lip development further highlighting the extent of molecular crosstalk present (Ashique *et al*. 2002; Jiang *et al*. 2006; Metzi *et al*. 2013).

Analysis of *Ptch1* expression in a conditional knockout of *Smo* showed a marked reduction in the facial processes suggesting that Hh signalling is able to self-regulate during lip morphogenesis (Jeong *et al*. 2004). Loss of *Foxc2*, *Foxd1*, *Foxf1* and *Foxf2* was observed in the *Smo*$^{-/-}$ embryos suggesting that they are positively regulated by Shh signalling during lip development and act as downstream effectors (Jeong *et al*. 2004). Loss of *Smo* resulted in increased levels of apoptosis between E9.5 to E10 followed by reduced proliferation at E11.5 further confirming previous findings for the roles of Shh signalling in facial development (Hu & Helms, 1999; Jeong *et al*. 2004; Jiang *et al*. 2006; Metzi *et al*. 2013). Truncations in *Foxc2* and silent mutations in *Foxf2* have previously been shown to be involved in craniofacial development, however mutations in both are more commonly linked to CP rather than CL (Bahuau *et al*. 2002; Jeong *et al*. 2004; Jochumsen *et al*. 2008).

Activation of the Shh signalling pathway ultimately results in the proteolytic cleavage of Gli1, Gli2 and Gli3 to an active form (Wang *et al*. 2000; Jiang *et al*. 2006). With the prevalence of clefting phenotypes observed in deficiencies of *Shh* and *Ptch1* it would be logical to assume that as effectors of Shh signalling, deficiencies in *Gli* expression would result in a clefting phenotype (Hu & Helms, 1999; Jiang *et al*. 2006; Metzi *et al*. 2013). Mutations in *Gli*3 result in a clefting phenotype with *Gli3*$^{-/-}$ embryos displaying a cleft palate through over expression of *Fgf8* (Aoto *et al*. 2002). In contrast, *Gli1*$^{-/-}$ mice have been shown to be phenotypically normal (Park *et al*. 2000; Drakopoulou *et al*. 2010). Mutations in *GLI2* in humans are linked to CL/P as well as polydactyly, branchial arch anomalies and semi-lobar holoprosencephaly (Bertolancini *et al*. 2012). It is significant to note that models featuring compound deletions of *Gli1*, *Gli2* and/or *Gli3* display increasingly severe phenotypes, suggesting they play both redundant and individual roles (Mo *et al*. 1997; Motoyama *et al*. 1998; Park *et al*. 2000).

1.4.3 Platelet-derived growth factor signalling

The family of platelet-derived growth factor (Pdgf) signalling factors consists of ligands and receptor proteins, originally identified due to their role in proliferation in arterial smooth muscle cells (Ross *et al*. 1974). Characterisation of Pdgf function has identified multiple roles including proliferation, cell survival, cell migration and the deposition of extracellular matrix (ECM), and tissue remodelling factors (Hoch & Soriano, 2003). The Pdgf family currently consists of four ligands, Pdgfa, Pdgfb, Pdgfc and Pdgfd, which form homodimers able to bind two receptor tyrosine kinases, Pdgfrα and Pdgfrβ which further form both homo- and heterodimers (Heldin & Westermark, 1999; Hoch & Soriano, 2003). Ligands are further

subdivided based upon their secretion and activation process, Pdgfa and Pdgfb may be activated via proteolytic cleavage intracellularly and secreted in their active form, while Pdgfc and Pdgfd are secreted in the inactive form and later undergo activation via cleavage of their N-terminal (Hock & Soriano, 2003). Pdgfa and Pdgfb can also be secreted in their inactive form for subsequent cleavage (Heldin & Westermark, 1999).

Pdgf signalling is triggered through the binding of the Pdgf ligands to the cell surface receptors. Once bound, Pdgfrs form dimers resulting in the activation of their tyrosine kinase domains, which autophosphorylate the receptors (Hock & Soriano, 2003). Phosphorylation of Pdgfrs allows the recruitment of a diverse spectrum of intracellular signalling molecules, allowing Pdgfrs to induce multiple signalling cascades (Heldin & Westermark, 1999; Hock & Soriano, 2003). Activation of Pdgf signalling is able to induce the action of numerous signalling molecules including; the PI 3-kinase family, the Src tyrosine kinase family, Ras via Grb2, Sos and Gap, a tyrosine phosphatise Shp-2 and members of the Stat family of transcription factors (Heldin & Westermark, 1999). Recent work by the Soriano lab examined signalling network induction following activation of the Pdgf and Fgf signalling pathways (Vasudevan *et al*. 2015). Using E13.5 mouse embryonic palatal mesenchyme (MEPM) cells, Vasudevan and colleagues conducted RNA Seq on cells one and four hours post induction of Pdgf and Fgf signalling through ligand administration and compared the transcriptional response (Vasudevan *et al*. 2015).

Initial analysis of transcriptional induction suggested Fgf signalling activation triggered a greater response than Pdgf signalling with Fgf signalling inducing 159 genes, while Pdgf signalling induced 40. However the Pdgf-induced genes consisted of a subset of Fgf-induced genes (Vasudevan *et al*. 2015). Furthermore, genes common to both signalling networks including *Ap-1*, *Fos*, *Jun* and *Egr1-4* were found to be up-regulated to a greater degree via Fgf signalling. RNA-Seq four hours post induction identified divergence in the signalling networks, with Fgf signalling favouring Mek dependent signalling to induce proliferation and Pdgf signalling inducing differentiation through Pi3k dependent pathways (Vasudevan *et al*. 2015). In addition, the authors noted that induction of Fgf and Pdgf signalling networks resulted in compensatory activation of additional pathways. Inhibition of pErk downstream of both Fgf and Pdgf signalling caused pJnk induction, while inhibition of Pi3k caused increased pErk activation, but only downstream of Fgf signalling (Vasudevan *et al*. 2015). This study is highly important as it underlies the complexity of signalling networks during development. Furthermore, the authors noted that the transcriptional response to induction was dependent upon multiple factors including signal intensity, number of receptor proteins and crosstalk between multiple signalling networks modulating the signalling cascade (Vasudevan *et al*. 2015). The study further highlights the need to dissect the hierarchy of signalling networks active in facial development.

Mouse knockouts for members of the Pdgf family often exhibit severe phenotypes including embryonic lethality, therefore investigation of Pdgf function has been largely characterised

through the use of conditional knockouts and mouse mutants (Levéen *et al*. 1994; Heldin & Westermark, 1999; Fruttiger *et al*. 1999; Xu *et al*. 2005). Analysis of *Patch* mutant mice which feature a deletion including the *PDGFRα* gene, found that mice homozygous for the *Patch* mutation displayed cleft face (Grüneberg & Truslove, 1960). Deletion of *Pdgfrα* is embryonic lethal with mice surviving until E13. *Pdgfrα*$^{-/-}$ embryos displayed multiple abnormalities, with defects in neural tube closure, skeletal defects of the ribs and sternum, cleft face and extensive haemorrhaging which is thought to be the cause of lethality (Soriano, 1997). Cleft face was suggested to be due to increased rates of apoptosis in the migrating neural crest cells, which form the proliferating core mesenchyme in the facial primordia (Couly *et al*. 1992; Soriano, 1997). *Pdgfrβ*-deficient embryos do not display orofacial clefting, however when deleted in concert with a *Pdgfrα* conditional knockout, loss of Pdgfrβ exacerbated the *Pdgfrα*$^{-/-}$ phenotype as well as inducing cleft palate (Richarte *et al*. 2007).

Characterisation of *PDGFRα* expression during chick embryogenesis showed expression within the developing face between E9.5–E12.5 (Orr-Urtreger *et al*. 1992). *PDGFRα* was found to be expressed within the mesenchyme of both the medial nasal and lateral nasal processes at E10.5, with expression within the lateral nasal processes reducing by E11.5 (Orr-Urtreger *et al*. 1992; He & Soriano, 2013). Recent studies have characterised the role that Pdgfrα signalling plays in the development of the medial nasal processes (He & Soriano, 2013). Soriano's group generated a conditional knockout mouse for *Pdgfrα* (*Pdgfrα*^{cko}) targeted to the neural crest cells (He & Soriano, 2013). *Pdgfrα*^{cko} were neonatal lethal displaying skeletal defects of the basisphenoid, alisphenoid and pterygoid bones as well as facial clefts (He & Soriano, 2013).

Loss of Pdgfrα resulted in a significant midline facial cleft between the medial nasal processess. Furthermore morphological analysis of E13.5 *Pdgfrα*^{cko} embryos showed that the philtrum and primary palate were absent (He & Soriano, 2013). Pdgf signalling is known to function via a number of signalling pathways and previous work has shown that PI3K signalling is the major effector of Pdgfrα in craniofacial development (Heldin & Westermark, 1999; He & Soriano, 2013). It was suggested that the cleft face phenotype is directly caused through a lack of proliferation within both the frontonasal prominence prior to nasal placode invagination and the medial nasal processes post invagination. Comparisons between rates of proliferation between the lateral nasal and medial nasal processes identified a significant reduction in the medial nasal processes between wildtype and *Pdgfrα*^{cko}, but the lateral nasal processes was unaffected (He & Soriano, 2013). This finding is of particular importance as it suggests that there may be individual genetic controls governing the development of each facial process. It is known that populations of neural crest cells from the midbrain give rise to the lateral nasal processes while cells from the forebrain contribute to the medial nasal processes however variations in their molecular controls are uncharacterised (Som & Naidich, 2013a).

The genes *Alx3* and *Alx4* have been shown to be required for the outgrowth of the nasal processes, with *Alx3*$^{-/-}$;*Alx4*$^{-/-}$ mice exhibiting a cleft face similar to that of *Pdgfrα*^{cko} (Beverdam *et al*. 2001). Analysis of *Alx3* and *Alx4* expression in *Pdgfrα*^{cko} medial nasal processes showed a reduction in *Alx3* but not *Alx4* expression, though it is unclear whether *Alx3* is a direct target of Pdgf signalling (He & Soriano, 2013). Furthermore, He and Soriano confirmed that Pdgfrα signals via Pi3k signalling, through analysis of Pi3k deficient mice. Administration of Pdgfa, a ligand for Pdgfrα was able to induce proliferation in control cells but not Pi3k deficient cells suggesting that Pi3k lies downstream of Pdgfrα signalling (He & Soriano, 2013). In addition a reduction in the GTP-binding protein Rac1, which is a member of the Rho family of small GTPases, was observed in the medial nasal processes (He & Soriano, 2013). Rac1 has previously been shown to play a role in neural crest cell migration with *Rac1*$^{-/-}$ mice displaying midline facial clefts (Thomas *et al*. 2011). It was suggested that Rac1 further acted as a target of Pdgf signalling in regulating cell migration and proliferation (He & Soriano, 2013).

Lineage tracing of neural crest cells migrating from the forebrain to the frontonasal prominence and subsequently the medial nasal processes, identified reductions in the number of migrating cells resulting in fewer neural crest cells populating the medial nasal process mesenchyme (He & Soriano, 2013). It was suggested that Pdgfrα functioned to directly regulate neural crest cell migration through chemotaxis, which is in keeping with previous research into Pdgf signalling and neural crest cell migration (Richarte *et al*. 2007; Smith & Tallquist, 2010; He & Soriano, 2013). Additionally, defects were identified in cell morphology with cells being smaller and producing fewer lamellipodia which are required for cell mobility (He & Soriano, 2013). It was therefore suggested that Pdgfrα further regulated neural crest cell migration through motility, a function in keeping with previous studies identifying Pdgfs ability to alter ECM composition (Gnessi *et al*. 1993; Hoch & Soriano, 2003; He & Soriano, 2013). It has previously been shown that Pdgfa regulates *Mmp-2* in the *Patch* mutant mouse (Robbins *et* al. 1999). It was suggested that a loss of Pdgfa is linked to a loss of *Mmp-2* expression which contributes to the cleft phenotype observed through reduced cellular motility, however it was unclear if this was via direct regulation or a secondary effect (Robbins *et al*. 1999). Additional studies have suggested other members of the Pdgf family can induce expression of multiple Mmp genes (Hoch & Soriano, 2003; Wågsäter *et al*. 2009).

In addition to *Pdgfrα*, mutations in other members of the Pdgf family have been found to induce orofacial clefting phenotypes. *Pdgfc*-deficient mice are neonatal lethal displaying a CP phenotype in addition to subcutaneous edema and blistering (Ding *et al*. 2004). Studies have suggested that Pdgfc is involved in regulating proliferation within the palatal shelves and may be itself regulated via the retinoic acid pathway (Han *et al*. 2006). Furthermore mutations in humans in *PDGFC* have been linked to the incidence of NSCL/P in studies of

Chinese patients (Wu *et al*. 2012). Compound homozygous mice for *Pdgfa* and *Pdgfc* deficiency recapitulated the phenotype of the *Pdfgrα*$^{-/-}$ (Ding *et al*. 2004).

1.4.4 Fibroblast growth factor signalling

The Fgf signalling family in vertebrates currently consists of 22 family members acting as ligands to four receptors known as the Fgfrs (fibroblast growth factor receptor) (Dorey & Amaya, 2010). The majority of Fgf ligands function as secreted signalling molecules which bind to and activate Fgfrs on the cell surface, however Fgf11, Fgf12, Fgf13 and Fgf14 are unable to activate Fgfr signalling and are thought to play an intracellular role in mediating Fgf signalling (Krejci *et al*. 2009). Receptors for Fgf signalling consist of a family of receptor tyrosine kinases encoded by four genes *Fgfr1*, *Fgfr2*, *Fgfr3* and *Fgfr4* displaying a common general structure (Johnson *et al*. 1991; Zhang *et al*. 1999). Fgf signalling is induced when an Fgf ligand binds, in combination with heparin sulphate, to the extracellular domain of Fgfrs forming a 2:2:2 Fgf:Fgfr:heparin dimer (Ornitz, 2000; Dorey & Amaya, 2010). Upon ligand binding, the resulting Fgfr dimer undergoes autophosphorylation allowing the recruitment of downstream signalling molecules, including members of the Ras/Erk pathway, Akt pathway or protein kinase C pathway (Dorey & Amaya, 2010). Fgf signalling has been associated with multiple roles during embryogenesis including proliferation, cellular migration, regulating cellular differentiation and left/ right axis specification (Dorey & Amaya, 2010).

Analysis of the expression profiles of multiple members of the Fgf family in mice identified expression of *Fgf2*, *Fgf8*, *Fgf9*, *Fgf10*, *Fgf15*, *Fgf17* and *Fgf18* in the surface ectoderm of the medial nasal processes at E10.5 and E11.5 (Bachler & Neubüser, 2001). Furthermore, three Fgf receptors were found to be expressed throughout facial development in chick (Wilke *et al*. 1997; Matovinovic & Richman, 1997). *FGFR1* has been shown to be expressed ubiquitously throughout the epithelium of chick embryos in all tissues including the facial processes (Wilke *et al*. 1997). At later stages of development *FGFR1* is expressed in the lateral edges of the frontonasal mass, the site of contact between the frontonasal mass, lateral nasal and maxillary processes, suggesting that it may play a role in their fusion (Wilke *et al*. 1997).

Prior to migration of the neural crest cells *FGFR2* and *FGFR3* are expressed throughout the neural tube in both overlapping and distinct domains, however following neural crest cell migration and outgrowth of the facial processes, *FGFR2* and *FGFR3* are found to be expressed throughout the mesenchyme of the frontonasal mass and the superior aspects of the lateral nasal processes (Wilke *et al.* 1997; Matovinovic & Richman, 1997). Furthermore it has been shown that the epithelium is required to induce mesenchymal *FGFR2* expression in the frontonasal mass further supporting the notion that epithelial to mesenchymal signalling is integral to correct lip development (Matovinovic & Richman, 1997). The role of Fgfr signalling in lip development is further strengthened through association of CL/P in

humans with Kallmann and Muenke syndromes, which are caused by mutations in the *FGFR1* and *FGFR3* genes respectively (Kim *et al*. 2005; Agochukwu *et al*. 2012).

Further studies into the disruption of Fgfrs have found that Fgf signalling within the mesenchyme is required to maintain the proliferative potential of cells during outgrowth of the facial processes (Szabo-Rogers *et al*. 2008). This finding is further supported through the presence of cleft lip in chick embryos where a repressor of Fgf downstream signalling, *SPRY2*, is over-expressed (Goodnough *et al*. 2007). Over-expression of *SPRY2* during outgrowth of the facial processes resulted in reduced proliferation causing an arrest in frontonasal, maxillary and mandibular processes outgrowth (Goodnough *et al*. 2007). However, over expression prior to process outgrowth was not inhibitory to proliferation of neural crest cells, suggesting that the effects of Fgf signalling are stage specific (Goodnough *et al*. 2007).

Between E9.5 and E11.5, the Fgf ligand *Fgf8* has been shown to be broadly expressed within the midfacial ectoderm initially, followed by distinct expression within the ectoderm at the edge of the nasal pit and medial nasal processes (Bachler & Neubüser, 2001). Due to the multiple roles Fgf signalling plays during development, study of Fgf8 function in facial development was initially hampered due to $Fgf8^{-/-}$ mice exhibiting embryonic lethality with embryos failing to progress past gastrulation (Sun *et al*. 1999). Therefore, a compound heterozygous mutant mouse strain termed $Fgf8^{neo/-}$ which are hypomorphic for *Fgf8* was generated (Abu-Issa *et al*. 2002).

Analysis of $Fgf8^{neo/-}$ mice identified multiple defects in craniofacial and cardiovascular development. Pharyngeal arches, which give rise to structures such as the jaw, were found to be greatly reduced in size (Abu-Issa *et al*. 2002). Proliferation was found to be unaffected in $Fgf8^{neo/-}$ pharyngeal arches. However, TUNEL assays identified an overlap between loss of *Fgf8* expression and increased levels of apoptosis as seen in *Bmp4* knockout mice (Abu-Issa *et al*. 2002; Ashique *et al*. 2002). It was suggested that the cause of craniofacial defects in $Fgf8^{neo/-}$ mice was due to increased apoptosis in the migrating neural crest cells, providing evidence that *Fgf8* is required for neural crest cell survival during facial development (Abu-Issa *et al*. 2002). Furthermore, studies making use a *Fgf8;Nes-cre* mouse model, where *Fgf8* was deficient in the mesenchyme of the branchial arches, identified an identical phenotype where the abnormal phenotype resulted from increased apoptosis of neural crest-derived mesenchyme (Trumpp *et al*. 1999). Analysis of transcription factors involved in development of the pharyngeal arches and frontonasal process, *Dlx2, Msx1, Gli1* and *Tbx1*, showed significant down-regulation (Abu-Issa *et al*. 2002). Firnberg and Neubüser showed that ectopic expression of *FGF8* in chick nasal mesenchyme induced the expression of *TBX2*, *ERM*, *PEA3* and *PAX3*, suggesting these genes may be downstream mediators of *FGF8* (Firnberg & Neubüser, 2002).

Griffin and colleagues generated multiple hypomorphic and null mutants to vary the dosage of *Fgf8*. The combination of genotypes generated mouse models for approximately 20% (*Fgf8*$^{Null/Neo}$), 40% (*Fgf8*$^{Neo/Neo}$), 50% (*Fgf8*$^{+/null}$) or 70% (*Fgf8*$^{+/Neo}$) of wildtype levels of *Fgf8* (Griffin *et al*. 2013). Comparisons between strains showed a scale of facial deformity that increased in an *Fgf8*-dependant manner with *Fgf8*$^{Null/Neo}$ embryos displaying significant defects in the frontonasal prominence and medial nasal processes resulting in midline clefts and cleft face (Griffin *et al*. 2013). It was suggested a threshold for *Fgf8* loss must be exceeded to induce an abnormal phenotype with mice with 50-70% *Fgf8* expression appearing phenotypically normal while reductions to 40-20% of wildtype expression resulted in hypoplasia within the nasal capsule and changes in polarity and orientation of the nasal capsule (Griffin *et al*. 2013). Furthermore changes in the expression of the genes *Satb2*, *Spry1*, *Pea3*, *Tbx3*, *Msx1* and *Msx2* were observed in the mesenchyme and *Bmp4*, *Six1*, *Pitx1*, *Dlx5* and *Raldh3* in the epithelium of the frontonasal prominence in E10-E10.5 *Fgf8*$^{null/neo}$ embryos (Griffin *et al*. 2013).These results suggest that Fgf signalling functions in a dosage-dependent manner during orofacial development.

Recent studies have identified an association between mutations in *FGF8* with holoprosencephaly and NSCL/P (Riley *et al*. 2007; Rosenfeld *et al*. 2010; McCabe *et al*. 2011). A *Tfap2α* mouse model showed that by modifying *Fgf8* dosage, the CL/P phenotype of *Tfap2α*$^{-/-}$ may be partially rescued (Green *et al*. 2014). *Tfap2α*$^{neo/null}$ mice display bilateral CL/P due to hypomorphic expression of *Tfap2α*. Bilateral CL was caused by over expression of *Fgf8* at the lambdoidal (λ) junction, preventing apoptosis and fusion of the facial processes (Green *et al*. 2014). Partial rescue of the clefting phenotype was achieved through crossing the *Tfap2α*$^{neo/null}$ mice with *Fgf8*$^{+/-}$ to create compound heterozygotes. Modulating *Fgf8* dosage induced a phenotypic effect, however rescued embryos still displayed a unilateral CL. It was suggested that in addition to correct Fgf dosage, the morphometric state of the facial processes is also key to correct development, further highlighting the complexity of the genetic and mechanical interactions required for successful facial development (Green *et al*. 2014).

1.4.5 Wingless signalling

Wingless (Wnt) signalling was first discovered in 1987 in mouse, with the identification of *Int-1* (*Wnt1*) as a homologue of the Drosophila developmental patterning gene *wingless* (*wg*) (Rijsewijk *et al*. 1987). Subsequently multiple Wnt genes and their receptors have been identified and their roles in development elucidated. Wnt signalling has been shown to play roles in multiple processes during vertebrate development including; regulating adhesion, maintaining stem cell identity, regulating proliferation via induction or inhibition or acting as a morphogen (Cadigan & Peifer, 2009; Archbold *et al*. 2012). The Wnt signalling family consists of a number of secreted glycoproteins which bind to cell surface receptors

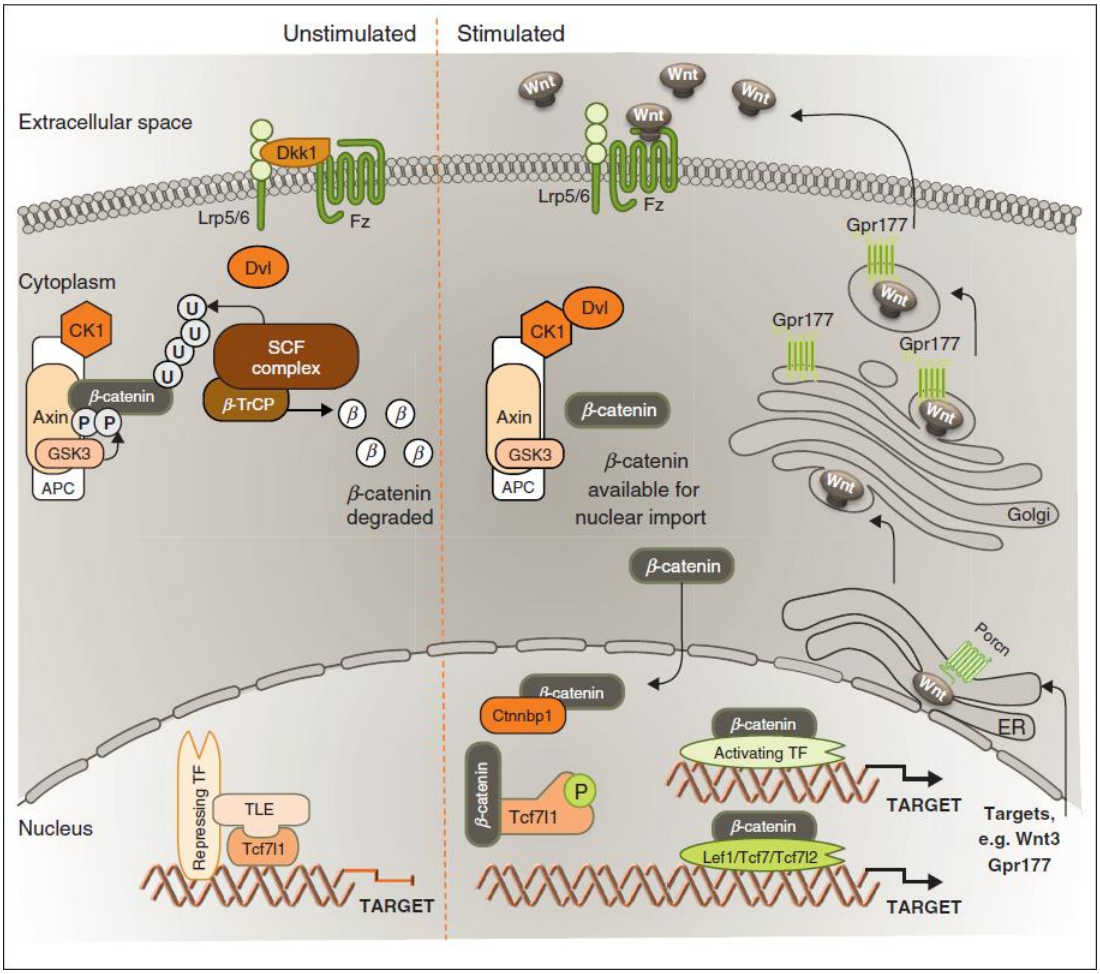

Figure 1.6: An overview of Wnt signalling. Wnt signaling is unstimulated (left) in the presence of an inhibitor such as Dkk1 or in the absence of a Wnt ligand such as Wnt3. In the unstimulated form, β-catenin is targeted for proteasomal degredation via phosphorylatation (P) by the Ck1/ Axin/ Gsk3/ Apc complex and polyubiquitylation (U) by the Scf/β-Trcp complex. Wnt target gene transcription is inhibited by Tcf7l1 and Tle co-repressors. Wnt signaling is stimulated (right) through the binding of a Wnt ligand to the Lrp5/6 and Fzd co-receptors. Through a cytoplasmic signaling cascade, inhibition of β-catenin is lost allowing nuclear translocation. Nuclear β-catenin relieves repression of the Wnt effectors Lef1 and Tcf allowing transcription of target genes. Ctnnbp1 can bind to β-catenin to inhibit its activator function (Adapted from Arkell *et al*. 2013).

consisting of Frizzled (Fzd) receptor proteins and low density lipoprotein receptor-related protein 5 or 6 (Lrp5 and Lrp6) (Figure 1.6) (Archbold *et al*. 2012).

Wnt signalling functions through multiple pathways, however the most characterised method is the canonical β-catenin signalling pathway (Jiang *et al*. 2006). At normal levels β-catenin is localised at the plasma membrane associated with cadherins and α-catenin where it co-ordinates the structure of the actin cytoskeleton (Widelitz, 2005). Cellular β-catenin is maintained through constant degradation. Serines 29, 33, 37 and 45 and threonine 41 are phosphorylated to target β-catenin for ubiquitin-dependent proteasomal degradation, however should phosphorylation of β-catenin be obstructed cellular levels can increase (Widelitz, 2005). Increased levels of β-catenin result in nuclear translocation and interaction with Wnt effectors, the Tcf/Lef transcription factors (Jiang *et al*. 2006). Disruption of the β-catenin pathway in chick facial development via *DKK-1* resulted in craniofacial abnormalities (Kawakami *et al*. 2014).

Dkk1 is a secreted Wnt inhibitor which is able to bind to the Wnt co-receptor Lrp6 (Mao *et al*. 2001). Mouse models in which Dkk1 function is ablated display striking defects in brain development, forelimb malformation and a complete absence of the anterior head structures (Mukhopadhyay *et al*. 2001). In chick, implantation of Dkk1 soaked beads into the mesenchyme of the maxillary processes as they were undergoing fusion resulted in a loss of β-catenin. Loss of β-catenin at this key stage of lip morphogenesis resulted in bone defects of the upper lip and CP (Kawakami *et al*. 2014). Administrating LiCl, an inducer of canonical Wnt signalling, rescued the phenotype confirming that the defects were caused by a loss of β-catenin. Furthermore, inhibition of β-catenin in the mesenchyme post lip fusion failed to generate a phenotype suggesting that correct temporal regulation of β-catenin is key to lip development (Kawakami *et al*. 2014). Loss of canonical Wnt signalling resulted in reduced expression of *LHX8*, *MSX1* and *MSX2*, potent inducers of proliferation, and a lack of proliferation contributed to the phenotype observed (Kawakami *et al*. 2014).

WNT3 is a member of the Wnt family of ligands and its expression and function through craniofacial development has been well characterised (Niemann *et al*. 2004; Geetha-loganathan *et al*. 2009). *Wnt3* plays an integral role during the early stages of embryonic development, with mouse knockouts failing to generate a primitive streak and displaying embryonic lethality post E10 (Liu *et al*. 1999). Analysis of *Wnt3* expression during craniofacial development shows discrete expression of *Wnt3* in the surface ectoderm of the medial nasal, lateral nasal and maxillary processes between E10 and E11 with expression highly localised to the point of contact between the facial processes (Ferretti *et al*. 2011). A recent study by Ferretti and colleagues into the role of *Pbx* genes in craniofacial development identified *Wnt3* and *Wnt9b* as direct signalling targets of Pbx1 and Pbx2 (Ferretti *et al*. 2011). Compound heterozygous mice for *Pbx1*$^{-/-}$;*Pbx2*$^{+/-}$ and *Pbx1*$^{-/-}$;*Pbx3*$^{+/-}$ display a fully penetrant bilateral or unilateral CL/P suggesting that *Pbx1* is required for craniofacial morphogenesis while *Pbx2* and *Pbx3* collaborate in gene regulation at sites of

co-expression (Ferretti *et al*. 2011). Loss of *Pbx* expression in the developing facial processes causes a reduction of *Wnt3* expression within the surface epithelium of the medial nasal, lateral nasal and maxillary processes (Ferretti *et al*. 2011). Furthermore, analysis of the intragenic region between *Wnt3* and *Wnt9b* identified five putative Pbx-Prep binding sites, two of which were shown to be bound during lip development confirming *Wnt3* and *Wnt9b* as direct targets of Pbx regulation (Ferretti *et al*. 2011).

Wnt9b has been shown to be expressed within the surface ectoderm of the medial nasal, lateral nasal and maxillary processes during lip development in both mouse and chick (Geetha-Loganathan *et al*. 2009; Ferretti *et al*. 2011). *Wnt9b* mouse knockouts are neonatal lethal displaying abnormalities of the kidneys and CL/P palate suggesting it is involved in craniofacial development (Carroll *et al.* 2005). The role of *Wnt9b* in craniofacial development is further confirmed through its association with the clefting phenotype of A/WySn mice (Carroll *et al*. 2005; Juriloff *et al*. 2006). The A/WySn mouse model commonly exhibits a CL/P with variable penetrance (Juriloff & Harris, 2004). A/WySn mice are a member of the A/~ strain family of mouse models for multifactorial NSCLP, with CL/P in A/WySn mice associated with mutations within two loci, *Clf1* on chromosome 11 and *Clf2* on chromosome 13 (Juriloff & Harris, 2004). A complementation study identified *Wnt9b* as the cause of CL/P in A/WySn mice (Juriloff *et al*. 2006).

A recent study identified *Wnt9b* as a downstream target of Pbx signalling in the facial processes; in addition the study suggested that *Wnt9b* is required for induction of *Fgf8* (Ferretti *et al*. 2011). E10.5-E11 *Wnt9b* knockout and $Pbx1^{-/-};Pbx2^{+/-}$ compound heterozygous mice displayed a reduction in *Fgf8* expression within the nasal and oral ectoderm of the medial nasal, lateral nasal and maxillary processes at the lambdoidal junction (Ferretti *et al*. 2011). It was suggested *Wnt9b* functions downstream of *Pbx* in a signalling cascade to regulate *Fgf8* expression (Ferretti *et al*. 2011). Subsequent studies have shown that Fgf signalling is perturbed in the developing facial processes of $Wnt9b^{-/-}$ embryos (Jin *et al*. 2012). It has been shown that loss of *Wnt9b* expression within the lateral nasal, medial nasal and maxillary processes results in a reduction in the ectodermal expression of *Fgf8*, *Fgf10* and *Fgf17* (Jin *et al*. 2012). Loss of ectodermal *Fgf8*, *Fgf10* and *Fgf17* expression results in a lack of proliferation within the mesenchyme of the medial nasal and maxillary processes (Jin *et al*. 2012). These findings suggested that Wnt signalling regulates Fgf during lip morphogenesis. Furthermore, Shh signalling, which plays a role in Fgf regulation, has been shown to regulate Wnt expression during facial development highlighting the complexity of craniofacial morphogenesis (Jin *et al*. 2012; Metzi *et al*. 2013; Kurosaka *et al*. 2014).

Wnt signalling functions through the binding of a Wnt ligand to co-receptors Lrp6/5 and Fzd receptors (Arkell *et al*. 2013). *Lrp6-KO* (knockout) mice at E13.5 displayed dramatic defects including bilateral cleft lip and hypoplasia of the upper lip. At E16.5, a fully penetrant CL/P was present while the anterior primary palate was absent and the maxillary and mandibular

structures were hypoplastic (Song *et al*. 2009). Immunohistochemical analysis showed active β-catenin was present within the epithelia and mesenchyme of E10.5 medial nasal processes, however was markedly reduced compared with wildtype littermates (Song *et al*. 2009). Furthermore, expression of the Wnt effectors *Lef1* and *Tcf4* was found to be significantly down-regulated in *Lrp6* deficient primordia (Song *et al*. 2009).

BrdU and TUNEL assays of E10.5 *Lrp6-KO* medial nasal and lateral nasal processes showed that proliferation was significantly reduced within the mutant mesenchyme, but epithelial proliferation was comparable to wildtype (Song *et al*. 2009). In addition, at E10.5 apoptosis was comparable between mutant and wildtype facial primordia. At E11.5 apoptotic cells were observed throughout the epithelial seam of wildtype embryos, but were absent from mutants. It was unclear however, if the reduction in apoptosis was a direct result of *Lrp6* knockout, or the result of failed facial process fusion (Song *et al*. 2009). Analysis of genes key to facial development showed a significant down-regulation of *Msx1*, *Msx2*, *Sostdc1* and *Wnt3*, while *Fgf8*, *Bmp4* and *Wnt9b* were comparable to wildtype and *Raldh3* was up-regulated (Song *et al*. 2009). Furthermore, Tcf/Lef sites were identified in the promoters of *Msx1* and *Msx2* suggesting they are direct targets of Wnt signalling (Song *et al*. 2009). The authors therefore suggested that Lrp6 is a key mediator of Wnt signalling during upper lip morphogenesis and Wnt/β-catenin signalling is able to induce expression of *Msx1* and *Msx2* in a Bmp independent manner (Song *et al*. 2009).

Use of a *TOPGAL* reporter, a reporter construct activated by *Tcf/Lef* function, showed canonical WNT signalling is active during lip morphogenesis (Lan *et al*. 2006). In E11-E12.5 embryos intense *TOPGAL* staining was observed around the within the distal regions of the medial nasal and lateral nasal processes and throughout the maxillary processes. Additional staining was detected surrounding the lambdoidal junction suggesting that canonical Wnt signalling plays a role in lip fusion (Lan *et al*. 2006).

1.4.6 Other molecular controls of upper lip morphogenesis

In addition to the signalling networks above, many other genes have been shown to be involved in lip development, with over 300 human mendelian syndromes identified which feature CL/P as a phenotype (Jiang *et al*. 2006). In contrast to humans where CL/P is common, mouse models of CL/P are rare, with few demonstrating fully penetrant cleft lip (Jiang *et al*. 2006). The *Dancer* mouse was identified by Deol & Lane as a mouse model for CL/P caused by a spontaneous mutation in *Dc* (Deol & Lane, 1966). *Dancer* mice display a number of phenotypic abnormalities including malformation of the inner ear, behavioural abnormalities and when homozygous for the *Dc* mutation neonatal lethality and highly penetrant bilateral CL/P (Deol & Lane, 1966). To identify the causative mutation in *Dancer* mice, Bush and colleagues undertook a process of intraspecific backcross mapping, identifying eleven mice which localised the *Dc* mutation within a 1-cM region between markers *D19Mit32* and *FosL1* (Bush *et al*. 2004).

90 genes were found to be present between *D19mit32* and *FosL1* including *Tbx10*. Tbx family members, *TBX1* and *TBX22*, have previously been associated with Di-George Syndrome and X-linked cleft palate with ankyloglossia respectively (Bush *et al*. 2004). *D19UR2*, a microsatellite sequence within the 5' region of *Tbx10* displayed strong linkage with *Dc* (Bush *et al*. 2004). Analysis of the *Tbx10* gene in *Dancer* mutants identified a 3.3 kb translocation of the *P23* gene within the first exon of *Tbx10* resulting in ectopic expression during E9.5-E12.5 (Bush *et al*. 2004). Ectopic *Tbx10* expression was suggested to induce CL/P through over-expression or inhibition of target genes required during craniofacial development. *Tbx10* may antagonise the function of other T-box factors including *Tbx1*, *Tbx15*, *Tbx18* and *Tbx22* which display homology in their DNA binding domain and are expressed in overlapping domains during craniofacial development (Bush *et al*. 2004). Furthermore, sequencing of individuals with isolated CL/P has suggested a possible association between *Tbx10* mutations and NSCL/P in humans. 10 individuals displaying CL/P were found to carry an Arg354Gln mutation, however the mutation was found in six control samples (Vieira *et al*. 2005). It is therefore unclear if the *Tbx10* Arg354Gln mutation contributes to the incidence of NSCL/P (Vieira *et al*. 2005).

Twirler mice display a highly similar phenotype to that of *Dancer* mice including, "waltzing behaviour", abnormalities of the inner ear and when homozygous for the *Tw* mutation, neonatal lethality and CL/P (Lyon, 1958; Deol & Lane, 1966). In addition heterozygous *Twirler* mice often become obese (Gong *et al* 2000). A recent study suggested the *Twirler* phenotype is caused by a single nucleotide substitution within exon 1 of *Zeb1* disrupting a binding site for the Myb family of regulatory proteins (Kurima *et al*. 2011). Furthermore, knockin mice for the *Zeb1* mutation c.58+181G>A recapitulated the *Twirler* phenotype. qPCR and western blots of whole head extracts of *Tw/Tw* mice showed increased levels of *Zeb1* transcript and protein levels compared to wildtype (Kurima *et al*. 2011). It was therefore suggested the *Twirler* mutation is hypermorphic or neomorphic to *Zeb1* expression within the ear (Kurima *et al*. 2011). While the study did not directly address the CL/P phenotype *Zeb1* knockout mice display CL/P suggesting it may be a candidate gene in the *Twirler* mouse orofacial phenotype (Kurima *et al*. 2011; Takagi *et al*. 1998).

In contrast to the *Twirler* and *Dancer* mice, *Brachyphalangy* mice were generated through neutron irradiation experiments (Johnson, 1969). The phenotypes of both heterozygous and homozygous *Brachyphalangy* mice were found to be distinguishable from, but highly similar to *Extra-toes* (Xt^{bph}) mice, suggesting the mutations were allelic (Johnson, 1969). Mice homozygous for Xt^{bph} displayed embryonic lethality and oedema (Johnson, 1969). Mice carrying the Xt^{bph} mutation exhibit a number of phenotypes including limb abnormalities, abnormal development of the sternum and associated structures, facial blebbing and the presence of a CL/P post E16 (Johnson, 1969). Analysis of *Extra-toes* mice through linkage analysis identified a deletion within an intron of *Gli3*, however the exact function of this region is currently unknown (Vortkamp *et al*. 1992). Furthermore *Extra-toes* is identified as

being homologous to the human condition Greig cephalopolysyndactyly syndrome, which can feature craniofacial defects as part of the phenotype (Vortkamp *et al*. 1992; Patel *et al*. 2014). The genetic variation between *Xt* and Xt^{bph} has yet to be identified and the direct genetic consequences of these mutations are still unknown.

The *Legless* mouse model was generated through the insertion of a transgene *Pht1-1* which includes the Drosophila heat shock gene *Hsp70* and a herpesvirus thymidine kinase gene (McNeish *et al*. 1988). *Legless* mice display abnormal forelimbs which lack digits, failure of hindlimb development, brain abnormalities and facial anomalies which include partially penetrant CL/P (40%) (McNeish *et al*. 1988). Mice heterozygous for the transgene are phenotypically normal, while homozygotes display a range of pathologies which result in neonatal lethality (McNeish *et al*. 1988). The hindlimbs phenotype observed is very rare in mouse models, and the combination of facial and limb defects suggests that the insertion of *Pht1-1* has disrupted a gene integral to development, the combination of phenotypes observed is reminiscent of $Trp63^{-/-}$ mice which also display profound defects of the fore and hindlimbs and CL/P (McNeish *et al*. 1988; Mills *et al*. 1999; Yang *et al*. 1999). The genetic cause of the *Legless* phenotypes remains unknown, however investigations into the site of transgene insertion identified two strongly linked sites on chr12, *lgl* and *iv*. It was therefore suggested that the *Legless* phenotype was caused through the disruption of multiple loci (Singh *et al*. 1991).

Sp8 is a member of the Sp family of zinc finger transcription factors and was a candidate gene for disruption in the *Legless* mutant mouse (Bell *et al*. 2003). At E10.5 expression of *Sp8* was localised to the epithelium of the medial nasal and lateral nasal processes and absent from the mesenchyme (Bell *et al*. 2003; Kasberg *et al*. 2013). *Sp8* knockout mice displayed defects of the limbs, neural tube and craniofacial regions (Bell *et al*. 2003). Facial development was abolished in $Sp8^{-/-}$ embryos with mice displaying cleft face at E14.5. Furthermore, analysis of individual facial regions showed that while maxillary processes were normal size, they failed to develop normally and the medial nasal and lateral nasal processes were significantly smaller than wildtype and failed to undergo any fusion events (Kasberg *et al*. 2013). The facial clefting phenotype observed was suggested to be caused through reduced proliferation and increased rates of apoptosis within the neural crest-derived mesenchyme of the facial processes (Kasberg *et al*. 2013). Furthermore, disruption of both Fgf and Shh signalling was observed with a loss of expression of *Fgf8* and *Fgf17* within the epithelium of the facial processes. Reduced *Gli3* expression was observed, and thought to be a consequence of elevated Shh signalling. A partial rescue of the facial cleft phenotype was achieved through inhibition of Shh signalling, however a CL/P remained, suggesting that *Sp8* and *Shh* play complementary roles during lip development (Kasberg *et al*. 2013).

In contrast to mouse models, CL/P is more common in humans. Identification of the causative mutations in NSCLP can be used as cues as to genes which play a role in

orofacial development. SNPs in *CDH1* (E-cadherin), a gene known to be involved in adhesion and adherens junctions, have recently been identified as being associated with the risk of NSCLP in multiple populations (Frebourg *et al*. 2006; Letra *et al*. 2009; Hozyasz *et al*. 2014). Expression of *CDH1* is detected within the frontonasal prominence during weeks 4 and 5 of human gestation, and within the lateral nasal and medial nasal processes during week 6 (Frebourg *et al*. 2006). Furthermore, the mutation c.531+2T->A was found to induce abherrant splicing, causing CL/P and hereditary gastric cancer (Frebourg *et al*. 2006). E-cadherin is known to interact with Nectin-1 the product of the gene *PVRL1* in the formation of adherens junctions (Tachibana *et al*. 2000). Mutations in *PVRL1* are known to cause the condition cleft lip/palate-ectodermal dysplasia syndrome as well as being associated with an increased incidence of NSCLP (Suzuki *et al*. 2000; Sözen *et al*. 2009; Kohli & Kohli, 2012). Furthermore, during secondary palate development, *PVRL1* is expressed within the MEE suggesting it plays a role in adhesion of the palatal shelves (Suzuki *et al*. 2000).

Retinoic acid is a metabolite of vitamin A that has been shown to be required for correct craniofacial development (Jiang *et al*. 2006). Overexposure to retinoic acid has been shown to induce retinoic acid embryopathy, a condition which includes craniofacial abnormalities (Lammer *et al*. 1985). The retinoic acid receptor family consists of three genes *RARA*, *RARB* and *RARG* which encode three retinoic acid receptors Rarα, Rarβ and Rarγ, which form heterodimers with retinoid X receptors Rxrα, Rxrβ and Rxrγ (Yamaguchi *et al*. 1998; Dollé, 2009). Further splicing of *RAR* genes produces a number of isoforms for each receptor (Lohnes *et al*. 1994). Expression of all *RAR* genes is detected in the developing facial processes, with *Rarb* expressed within the mesenchyme and discrete regions of the olfactory epithelium (Dollé *et al*. 1990; Dollé, 2009). Lohnes and colleagues generated multiple conditional mouse knockout models for *Rara*, *Rarb* and *Rarg* isoforms to investigate their individual functions. Gross analysis of *Rara* and *Rarg* knockouts displayed multiple defects, including defects of the limbs, growth retardation, abnormal brain development, skeletal abnormalities and malformation of the craniofacial regions with midfacial clefts and abnormal nasal development (Lohnes *et al*. 1994). *Rar* knockouts displayed a high rate of embryonic lethality highlighting their integral function to multiple stages of development. Furthermore multiple knockouts, including $Rar\alpha1^{-/-};Rar\alpha2^{+/-};Rar\gamma^{-/-}$ and $Rar\alpha^{-/-};Rar\gamma^{-/-}$, displayed craniofacial abnormalities with compound nulls displaying the most severe cases. It was therefore suggested that while individual *Rar* genes *Rara* and *Rarg* are integral to lip development, there is also functional overlap between the family members (Lohnes *et al*. 1994).

1.4.7 Mechanisms of orofacial fusion

During the development of the orofacial regions, epithelial seems are generated at the site of contact between the medial nasal, lateral nasal and maxillary processes and between the apposing palatal shelves (Som & Naidich, 2013a; Som & Naidich, 2013b). If these epithelial

seams are not degenerated facial development is ablated resulting in an orofacial cleft (Jiang *et al*. 2006). Due to the pivotal role of seam degeneration in orofacial development, the mechanisms of orofacial fusion have been extensively characterised, with three mechanisms suggested: epithelial-mesenchymal transformation, apoptosis and periderm migration (Jiang *et al*. 2006). The precise mechanisms by which epithelial seams are degenerated in facial development still remain unknown (Jiang *et al*. 2006).

Epithelial-mesenchymal transformation (EMT) has been suggested to play a role in the embryonic development of multiple tissues in addition to wound healing and tumour metastasis (Kang & Svoboda, 2005). The role of EMT in the development of the facial processes is a contentious issue. EMT has been suggested as the mechanism by which the epithelial seams present during upper lip morphogenesis are removed (Sun *et al*. 2000). Chick embryos have been used to investigate fusion between the maxillary processes and medial nasal processes (Sun *et al*. 2000). Carboxyfluorescein (CCFSE) labelling and transmission electron microscopy was used to label the epithelia of chick embryos allowing tracing of epithelial cells at the site of fusion (Sun *et al*. 2000). Following adhesion of the facial processes, CCFSE-positive cells were observed in the epithelial seam extending filopodia to contact surrounding mesenchymal cells. Spaces between epithelial cells within the seam were observed before mitosis occurred resulting in transformation to mesenchymal cells. Mesenchymal cells derived from epithelial cells appeared morphologically comparable to existing mesenchyme (Sun *et al*. 2000). Mesenchymal staining for CCFSE was observed, however CCFSE levels may have diminished due to poor initial uptake via the *in ovo* injection delivery method (Sun *et al*. 2000). Furthermore no TUNEL staining was seen in cells of the epithelial seam during or post seam degradation, however some staining was seen prior to fusion confined to the periderm (Sun *et al*. 2000).

Other studies found no evidence of EMT within the degenerating nasal fin, the point of fusion between the medial nasal and lateral nasal processesf (Gaare & Langman, 1977). Serial sectioning of the nasal fin during degeneration in mice identified multiple epithelial cells undergoing cell death via condensation-fragmentation. Previous studies suggested that mitochondrial swelling was a marker for condensation-fragmentation, however Gaare and Langman suggested mitochondria of the MES cells was comparable to healthy cells (Gaare & Langman, 1977). It was suggested that epithelial cells of the nasal fin remain viable with only a small number displaying cell death (Gaare & Langman, 1977). Cells of the epithelial seam did not remain in the mesenchyme, suggesting that they migrated to the persisting epithelial layers. Furthermore phagocytosis of apoptotic cells by both epithelial and mesenchymal cells was observed, which may explain the CCFSE-positive cells seen post-fusion in previous studies (Gaare & Langman, 1997; Sun *et al*. 2000).

The CL/Fr mouse strain has been shown to display a genetic predisposition to CL/P (Millicovsky & Johnston, 1981). It was suggested that failure of epithelial cells to undergo EMT within the nasal fin was the cause of clefting within CL/Fr mice (Nakazawa *et al*. 2008).

Expression of E-cadherin and Vimentin, markers of epithelial and mesenchymal cells respectively, was examined during fusion of the facial processes at E11.5. Expression was analysed within the mesenchymal bridge, a junction which is formed as the epithelial seam undergoes degeneration and the mesenchyme of the medial nasal processes and lateral nasal processes mix (Nakazawa *et al*. 2008). At E11.5 in cleft lip negative embryos (CL-), E-cadherin was present demarking the epithelial cells of the seam. Epithelial cells transformed into spindle-like cells expressing vimetin (Nakazawa *et al*. 2008). In contrast, in cleft lip-positive embryos (CL+) E-cadherin expression was maintained and transformation to vimetin-expressing cells was lost (Nakazawa *et al*. 2008). Nakazawa and colleagues suggested that the lack of EMT results in seam persistence and CL, however the lack of lineage tracing of the cells undermines these claims as it cannot be ascertained if the vimetin-positive cells which replace E-cadherin positive cells in CL- embryos are transformed epithelial cells or neighbouring mesenchymal cells which have migrated into the mesenchymal bridge. Furthermore, TUNEL assays showed epithelial cells within the nasal fin were TUNEL-positive in CL- embryos, suggesting they underwent apoptosis (Nakazawa *et al*. 2008). In contrast, epithelial cells of the nasal fin in CL+ embryos were TUNEL-negative (Nakazawa *et al*. 2008).

Jiang and colleagues investigated the role of apoptosis during fusion of the facial processes as part of their review of lip development. Caspase-3, an early marker for cells destined to undergo apoptosis was found to be highly expressed within cells of the nasal fin (Jiang *et al*. 2006). Jiang's group suggested therefore that apoptosis is key to seam degeneration (Jiang *et al*. 2006).

The role of EMT and apoptosis has been more comprehensively investigated in secondary palate development compared with upper lip and primary palate. One of the first studies to suggest EMT in palatal development was that of Fitchett and Hay, who analysed MES degeneration in the rat (Fitchett & Hay, 1989). MES cells were described as healthy during seam degradation and it was suggested degeneration was caused by reduced epithelial proliferation compared to the surrounding mesenchyme. The epithelial seam broke into islands of epithelium, followed by conversion to mesenchymal cells (Fitchett & Hay, 1989). Furthermore, MES cells failed to display apoptosis, instead expressing vimentin, suggesting EMT had occurred (Fitchett & Hay, 1989).

Follow up studies used lineage tracing techniques to identify the fate of MES cells (Shuler *et al*. 1992; Griffith & Hay, 1992). Shuler's group investigated EMT through incorporation of the dye DiI (1,1-dioctadecyl1-3-3-3',3'-tetramethylindocarbocyanine per-chlorate) into the plasma membrane of epithelial cells (Shuler *et al*. 1992). Keratin immunostaining was used to distinguish epithelial and mesenchymal cells. Prior to palatal shelf contact, both DiI and keratin were co-localised throughout the MEE and absent from the palatal mesenchyme. Following adhesion, keratin expression in the MES was lost while DiI fluorescence remained. Furthermore, once fusion was complete DiI remained detectable within the

mesenchyme and appeared to demark the site of the degenerated MES (Shuler *et al*. 1992). Shuler and colleagues concluded that the transfer of DiI into the mesenchyme was the result of EMT (Shuler *et al*. 1992).

In contrast Griffith and Hay used CCFSE to label palatal epithelium (Griffith & Hay, 1992). Lineage tracing showed CCFSE staining within the epithelia and absent from the mesenchyme prior to fusion. Following adherence, CCFSE was detected in the MES. Post fusion, CCFSE fluorescence was detected in the mesenchyme (Griffith & Hay, 1992). It was therefore suggested that MES cells underwent EMT resulting in CCFSE presence within the mesenchyme. Furthermore, Griffith and Hay showed that individually cultured palatal shelves failed to undergo EMT suggesting that adhesion of the MEE is required to induce EMT (Griffith & Hay, 1992).

The role of apoptosis in MES degeneration has been investigated through the use of TUNEL assays (Martínez-Álvarez *et al*. 2000). Prior to palatal shelf adhesion, few TUNEL-positive cells were found in palatal epithelia. TUNEL labelling was seen in cells of the MEE immediately prior to contact and adhesion, furthermore multiple cells within the degenerating MES were found to be TUNEL-positive (Martínez-Álvarez *et al*. 2000). The presence of TUNEL-positive cells in the MES suggested apoptosis plays a role seam degeneration, however not all cells of the MES were TUNEL-positive (Martínez-Álvarez *et al*. 2000).

TUNEL assays were complemented with lineage tracing assays using a retroviral vector CXL carrying a *LacZ* reporter construct (Martínez-Álvarez *et al*. 2000). *LacZ* expression was seen throughout the epithelium both prior to and following palatal shelf adherence and absent from the mesenchyme (Martínez-Álvarez *et al*. 2000). *LacZ* was detected in mesenchymal cells at the site of the degenerated MES (Shuler *et al*. 1992; Griffith & Hay, 1992; Martínez-Álvarez *et al*. 2000). Furthermore, morphological and TUNEL analysis of *LacZ*-positive mesenchymal cells indicated they were non-apoptotic and indistinguishable from surrounding mesenchymal cells, it was therefore suggested these cells underwent EMT (Martínez-Álvarez *et al*. 2000). Staining for the macrophage marker, F4/80, was observed at the MES suggesting macrophages were present. In addition, phagocytosis of dying MES cells was seen both during and post-degeneration (Shuler *et al*. 1992; Griffith & Hay, 1992; Martínez-Álvarez *et al*. 2000). It has been suggested the presence of labels such as DiI and CCFSE in the mesenchyme could be the result of uptake of dying cells via phagocytosis (Martínez-Álvarez *et al*. 2000; Jiang *et al*. 2006). Martínez-Álvarez and colleagues suggested that both apoptosis and EMT play roles in MES degeneration (Martínez-Álvarez *et al*. 2000).

A similar study used palate cultures which included the nasal region of the head (Cuervo & Covarrubias, 2004). The authors noted that isolated palatal shelf cultures fused 24hrs later than cultures including the nasal region. It was suggested inclusion of the nasal region more closely represented *in vivo* conditions and that variation in fusion time affected the reliability

of results obtained. Cuervo and Covarrubias used a similar sytem to Martínez-Álvarez's group through epithelial infection with a *LacZ* carrying viral vector, however they used an adenovirus-based vector system as the retroviral vector used by Martínez-Álvarez *et al*. requires the addition of serum to induce proliferation which may introduce artefacts to the results (Martínez-Álvarez *et al*. 2000; Cuervo & Covarrubias, 2004). *LacZ* and CCFSE-staining allowed lineage tracing of MES cells. Prior to fusion no *LacZ*- or CCFSE-positive cells were detected within the mesenchyme. Furthermore, during and post-fusion any cells within the mesenchyme expressing epithelial reporters were TUNEL-positive (Cuervo & Covarrubias, 2004). Cuervo and Covarrubias failed to identify any evidence of EMT in their model and instead suggested apoptosis is the major regulator of MES degeneration (Cuervo & Covarrubias, 2004). However other studies found that cultured palatal shelves fused successfully in the presence of apoptosis inhibitors caspase -1 and -3, suggesting apoptosis is not the only factor involved in MES degeneration (Takahara *et al*. 2004)

Using *ShhGFPCre* and *Krt14;Cre* transgenic mice Vaziri Sani and colleagues investigated the role of EMT during palatal fusion (Vaziri Sani *et al*. 2005). *Cre* transgenic mice were crossed with *Rosa-loxP-stop-LacZ* reporter mice (*R26R*) resulting in cre-recombination and activation of the reporter, allowing the fate of MES cells to be traced *in vivo* (Vaziri Sani *et al*. 2005). *LacZ* staining between E15-E18.5 identified cells of MES as *LacZ* positive. In addition, as MES degeneration proceeded, the number of cells positive for *LacZ* decreased, until at E18.5 no *LacZ* expression was detected within the fused mesenchyme (Vaziri Sani *et al*. 2005). The absence of *LacZ* within the mesenchyme, coupled with the use of two mouse strains and the irreversible nature of the reporter system used, provided strong evidence that EMT does not contribute to MES degeneration (Vaziri Sani *et al*. 2005).

In contrast, the recent work of Jin & Ding, who used a similar *R26R/K14-Cre* mouse suggested that EMT was observed during MES degeneration (Jin & Ding, 2006). Lineage tracing showed the presence of β-gal-positive epithelial cells within the MES following adhesion. Post seam degeneration, β-gal-positive mesenchymal cells were detected at E15.5. It was therefore suggested that MES cells had undergone EMT (Jin & Ding, 2006). However previous studies have observed palatal fusion up until E18.5, where β-gal staining was lost from the mesenchyme (Vaziri Sani *et al*. 2005). Furthermore, no TUNEL assays were conducted on the β-gal-positive mesenchymal cells and so it is unknown if they were undergoing apoptosis (Jin & Ding, 2006).

The periderm migration model of MES degeneration was originally proposed from the work of Carette and Ferguson who observed the migrations of epithelial cells of the MES to form epithelial triangles, but did not realise they were detecting periderm (Carette & Ferguson, 1992). Confocal laser scanning microscopy of *in vitro* DiI labelled palatal shelf epithelia allowed the movement of MEE cells during seam degeneration to be followed. Following MES degeneration, no DiI-positive cells were observed within the mesenchyme suggesting MES epithelia neither underwent apoptosis or EMT (Carette & Ferguson, 1992).

Furthermore epithelial triangles were observed at the oral and nasal aspects of the palate. It was therefore suggested that MES degeneration was achieved through the migration of epithelial cells and subsequent assimilation into the nasal and oral epithelia (Carette & Ferguson, 1992).

Subsequent studies into the role of apoptosis during MES degeneration showed high levels of TUNEL-positive cells with the MES (Cuervo & Covarrubias, 2004). CCFSE labelling of MEE periderm allowed lineage tracing during palatal shelf contact, adhesion and fusion. Following palatal shelf adhesion, CCFSE-positive cells were present throughout the MES (Cuervo & Covarrubius, 2004). However as fusion proceeded, an accumulation of labelled cells was seen at the apex of the MES consisting of epithelial triangle cells, before undergoing apoptosis. It was therefore suggested periderm cells migrate away from the MES during seam degeneration but do not intergrate into the nasal and oral epithelia, instead undergoing cell death as confirmed by TUNEL staining (Cuervo & Covarrubius, 2004). Furthermore inhibition of cell migration with cytochalasin D prevented the formation of epithelial triangles and palatal adhesion. It is therefore suggested that the migration of periderm from the MEE and their subsequent apoptosis is required for MES degeneration (Cuervo & Covarrubius, 2004).

Through the use of *Rosa26*-C57BL/6 chimeric palate cultures Jin and Ding further investigated the role of cell migration during secondary palate fusion (Jin & Ding, 2006). A *K14-Cre* transgenic line was crossed onto the *R26R* background, placing expression of Cre recombinase under the control of a *K14* promoter and enhancer, a well characterised marker of epithelium, allowing lineage tracing of the MEE through a LacZ reporter (Jin & Ding, 2006). Chimeric cultures of *R26/K14-Cre* and C57BL/6 palatal shelves displayed migration of *R26* β-gal-positive MEE cells into C57BL/6 β-gal negative nasal epithelium during fusion (Jing & Ding, 2006). Furthermore lineage tracing showed MES cells migrated posteriorly along the anterior posterior axis and nasally along the nasal-oral axis. It is notable that migration was observed exclusively in the nasal direction along the nasal-oral axis, as previous studies have identified migration and epithelial triangle formation at both the oral and nasal aspects (Carette & Ferguson, 1992; Jin & Ding, 2006). It was therefore suggested that MEE migration is required for correct MES degeneration.

The respective roles of EMT, cell migration and apoptosis within degeneration of the epithelial seams during lip development and the MES of palate development remain contentious. Studies have produced compelling evidence for each hypotheses and it is clear that our current knowledge of seam degeneration is incomplete.

1.5 *TP63*

1.5.1 *TP63* – An introduction

TP63 is a member of the Tp53 family of transcription factors (Yang *et al*. 1998). *TP53*, a homolog of *TP63,* has been characterised extensively due to its role as a tumour suppressor and has been found to be mutated in more than 50% of cancers (Bokhoven & Brunner. 2002). Loss of P53 regulation during tumour development has been shown to enhance the progression of cancers through a lack of cellular differentiation, increased genetic instability, and increased metastatic potential (Bieging *et al*. 2014). It is known that members of the Tp53 family have both distinct and overlapping cellular roles (Bieging *et al*. 2014). It is interesting to note that although *TP53* was characterised prior to *TP63* or *TP73*, recent biochemical modelling studies, analysing the individual functional domains of each protein suggest that *TP63* and *TP73* are the ancestral genes with *TP53* having arisen as the results of a genomic duplication (Dötsch *et al*. 2010).

The *TP63* gene is located on human chromosome 3q27-q29 and is comprised of 15 exons (Yang *et al*. 1998). *TP63* was first characterised via structural homology to *TP53* and the newly discovered *TP73* (Kaghad *et al*. 1997; Yang *et al*. 1998). Multiple isoforms of P63 were characterised and the localisation of P63 in several tissues including human foreskin, cervix, vaginal epithelium, urothelium and prostate was characterised through immunohistochemistry (Yang *et al*. 1998). Functional overlap between P63 and P53 was observed, with P63 displaying the ability to bind to and activate P53 response elements as well as displaying the ability to negatively regulate the actions of P53 and other P63 isoforms (Yang *et al*. 1998; Serber *et al*. 2002).

P63 displays a high degree of conservation within its structural domains with other members of the *TP53* family (Yang *et al*. 1998; Dötsch *et al*. 2010). Three domains are conserved across the *TP53* family members: the DNA-binding domain (DBD); the transactivation domain (TAD); and the oligomerization domain (ISO). Furthermore, P63 and P73 contain two additional mofits, a sterile α-motif (SAM) and a transcription-inhibition domain (TID), which are not present in P53 (Figure 1.7) (Serber *et al*. 2002; Dötsch *et al*. 2010).

TP63 encodes multiple isoforms due to both variable promoter use and alternative splicing. P63 isoforms are broadly classified into two subgroups based upon the differential use of promoter sites at the start of exon one and exon three (Bokhoven *et al*. 2011). Isoforms which make use of the first promoter site contain the TA domain and so are termed TAp63 isoforms while those using the second promoter site lack the TA domain and are termed ΔNp63 isoforms (Yang *et al*. 1998). Further promoter sites are present both upstream of and within exon one, which together with the TA and ΔN isoforms produce a high degree of variability in the protein products of *P63* (Bokhoven & Brunner, 2002).

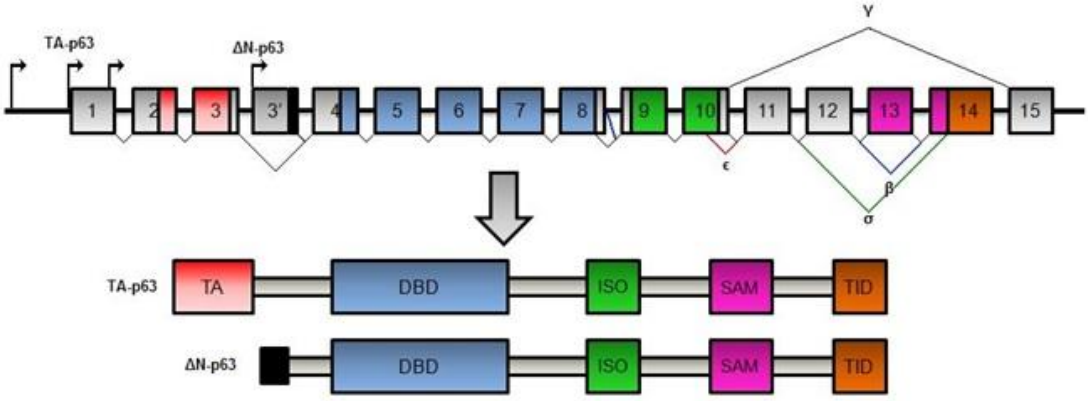

Figure 1.7: Structure of *TP63.* *TP63* consists of 15 exons. Isoforms containing the transactivation domain are transcribed using the promoter site in exon 1. ΔNP63 isoforms are transcribed using the promoter in exon 3. Variable splicing of the carboxyl terminus results in a high degree of variance producing further isoforms termed: α, β, γ, ε or δ. All isoforms contain the DNA binding (DBD) and oligermerization (ISO) domains. Exons two and three code for a transactivation domain (TA), four to eight encode the DBD, nine and ten the ISO, thirteen and fourteen a sterile alpha motif (SAM) which is involved in protein-protein interaction and exon fourteen also contributes to a trans inhibitory domain (TID). Exon colour demarks contribution to protein structure (adapted from Bokhoven *et al.* 2011).

The DBD and ISO domains are common across all P63 isoforms, however variable splicing patterns affecting the carboxyl terminus introduces variation in protein structure (Mangiulli *et al*. 2009). Isoforms are characterised based on the splicing pattern observed termed α, β, γ, ε or δ. The α isoforms of P63 contain both the SAM and TID domains, while the β, γ, ε and δ isoforms have variable C termini but all lack the SAM and TID domains (Figure 1.7) (Yang *et al*. 1998; Manguilli *et al*. 2009; Koster, 2010; Bokhoven *et al*. 2011). P63 isoforms containing the TID display a dominant negative effect towards TA isoforms. The TID was able to bind to three hydrophobic side chains within the TA domain responsible for transactivation (Serber *et al*. 2002).

ΔNp63 isoforms have been shown to retain transactivational activity. A second TA domain was shown to be created within exons 11 and 12 of the carboxyl terminus through variable splicing (Ghioni *et al*. 2002; Helton *et al*. 2006; Guerrini *et al*. 2011). Ghioni and colleagues investigated the activation potential of the primary and secondary TA domains. The ability of both TA domains to induce gene expression using verified P53-regulated promoters of *MDM2* and *P21* suggested a functional overlap in their target genes (Ghioni *et al*. 2002). In addition ΔNp63α-exclusive induction of *GADD45* was observed, suggesting the TA domains display a degree of functional separation (Ghioni *et al*. 2002). It was suggested the second TA domain is required for the activation of pro-apoptosis genes (Ghioni *et al*. 2002).

Structural analysis of members of the P53 family has identified conservation in the structure of the DBD, with P63 able to bind to and regulate P53 response elements (Serber *et al*. 2002). Further characterisation of P63-specific binding sites has identified the consensus sequence of the P63 binding motif, which displays 60% conservation with the P53 binding motif (El-Deiry *et al*. 1992; Ortt & Sinha, 2008). It is suggested that P63 binds to a 22 bp full response element (5'AAA**CATG**TTTTAAAA**CATG**TTT3') consisting of two CATG cores with A/T rich flanking regions (Ortt & Sinha, 2008; Chen *et al*. 2011). Furthermore it was shown P63 was able to bind to a half site consisting of (5'AAACATGTTT3') so it is unsurprising that it is estimated there are over 1 million putative P63 binding sites within the human genome (Chen *et al*. 2011; Sethi *et al*. 2014).

1.5.2 Human syndromes resulting from *TP63* mutation

Human *TP63* mutations exert an autosomal dominant effect resulting in five developmental conditions: ectrodactyly-ectodermal-dysplasia-clefting (EEC) syndrome; ankyloblepharon-ectodermal-dysplasia-clefting (AEC) syndrome; acro-dermato-ungual-lacrimal-tooth (ADULT) syndrome; limb-mammary syndrome (LMS) and non-syndromic split hand/foot malformation (SHFM) (Brunner *et al*. 2002b; Steele *et al*. 2005; Rinne *et al*. 2007; Koster, 2010; Bokhoven *et al*. 2011). Similar to *IRF6*, mutations in *TP63* display a phenotype to genotype correlation, with mutations occurring within the DNA binding domain causing EEC and within the SAM domain causing AEC (Figure 1.8) (Kondo *et al*. 2002; Ghioni *et al*. 2002; Berdón-Zapata *et al*. 2004; Browne *et al*. 2011; Iorio *et al*. 2011).

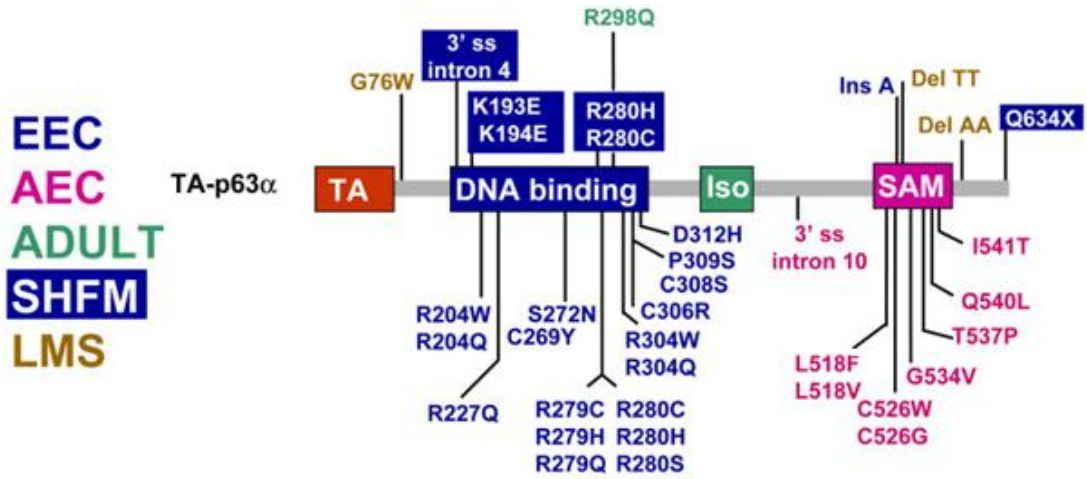

Figure 1.8: Phenotype to geneotype correlations of mutations within *TP63.* Mutations within *TP63* give rise to mutiple conditions. Clustering of EEC causing mutations are seen within the DNA binding domain, while mutations within the sterile α motif (SAM) cause AEC. EEC, ectrodactyly-ectodermal dysplasia clefting; AEC, ankyloblepharon-ectodermal dysplasia-clefting; ADULT, acro-dermato-ungual-lacrimal-tooth; SHFM, split hand/foot malformation; LMS, limb-mammary syndrome. (Figure adapted from Brunner *et al*. 2002).

1.5.3 Ectrodactyly-ectodermal-dysplasia-clefting syndrome

EEC is the most common of the conditions caused by *P63* mutations and displays an autosomal dominant mode of inheritance with variable penetrance (Roelfsema & Cobben. 1996; Iorio *et al*. 2011). EEC is primarily classified via orofacial clefts and its effects on ectoderm-derived tissues. Tissues affected include: the epidermis, hair, teeth, nails and exocrine glands. Furthermore, EEC often results in urogenital abnormalities and conductive hearing loss (Bokhoven & Brunner, 2002; Rinne *et al*. 2007; Koster, 2010; Chiu *et al*. 2011). Studies have identified consanguineous individuals with identical *TP63* mutations which display distinct manifestations of EEC suggesting the input of multiple genetic pathways (Roelfsema & Cobben, 1996; Berdón-Zapata *et al.* 2004). Berdón-Zapata and colleagues identified an affected mother and daughter who both carried the Arg204Trp mutation. While both individuals carried the same mutation, the daughter presented a more severe phenotype with bilateral CL/P, ectodermal dysplasia and complete ectrodactyly of the hands and feet (Berdón-Zapata *et al*. 2004).

Research into the causes of EEC has identified the most common sites of mutation in *TP63* including Arg204, Arg227, Arg279, Arg280 and Arg304 (Bokhoven & Brunner, 2002). Further characterisation of affected codons identified mutations in regions associated with protein – DNA interactions with Arg304 interacting with the DNA backbone and Arg279 thought to insert into the minor groove of DNA required for specific DNA recognition (Celli *et al*. 1999). It is thought that mutations within these residues abolish the function of the DBD through direct disruption of binding, or by preventing the correct folding of the DBD (Cho *et al*. 1994; Celli *et al*. 1999). However recent studies found that mutations within both the DBD and SAM domains resulted in increased stability of the P63 protein, and suggested the dominant negative phenotype was caused through a misregulation of a currently unknown *TP63* regulatory mechanism (Browne *et al*. 2011).

1.5.4 Ankyloblepharon-ectodermal-dysplasia-clefting syndrome

AEC, Hay-Wells and Rapp-Hodgkin syndromes were initially classified as individual conditions; however due to the phenotypic overlap present, some studies suggested they should be viewed as a spectrum of the same condition (Cambiaghi *et al*. 1994; Steele *et al*. 2005). AEC is phenotypically similar to EEC in that it features orofacial clefts and ectodermal dysplasia, however dysplasias are often more severe in AEC. Common features of AEC include: dermatitis of the scalp accompanied by recurring infections, syndactyly and craniofacial abnormalities (Berdón-Zapata *et al*. 2004; Steele *et al*. 2005). The defining feature of AEC is the presence of ankyloblepharon, a developmental defect affecting the eyes, resulting in congenital fusion of the eyelids (Bokhoven *et al*. 2002: Berdón-Zapata *et al*. 2004; Steele *et al*. 2005).

In contrast to EEC, AEC is more commonly associated with mutations within the SAM domain of P63 (Berdón-Zapata *et al*. 2004; Kantaputra *et al*. 2011; Browne *et al*. 2011). The SAM domain is highly conserved with P73 and features a small five helix bundle with a hydrophobic core (Chi *el al*. 1999; Sathyamurthy *et al*. 2011). Modelling of AEC mutations found that they occurred within key residues of the SAM domain, for example Leu553 which is located within the hydrophic core. It was found that mutations within the SAM domain may disrupt the hydrophic core of the domain or surface structures thus destabilising the domain and inhibiting wildtype function (Sathyamurthy *et al*. 2011). Furthermore, P63 isoforms with SAM mutations were able to bind and inhibit transcriptional activity of wildtype ΔNp63α, suggesting this as an explanation for the dominant negative effect of the mutations (Browne *et al*. 2011).

1.5.5 The role of P63 – the *Trp63*$^{-/-}$ mouse

The roles of P63 in mammalian development were characterised through the simultaneous work of Bradley and McKeon in 1999. Both groups identified the function of P63 using an *in vivo* mouse model in which P63 function was abrogated (Mills *et al*. 1999; Yang *et al*. 1999). Heterozygous mice displayed a wildtype phenotype while *Trp63*$^{-/-}$ mice recapitulated the phenotypes of human *TP63* mutations including orofacial clefting, ectodermal dysplasia and limb abnormalities (Figure 1.9) (Mills *et al*. 1999: Yang *et al*. 1999).

Trp63$^{-/-}$ mice display profound abnormalities of the limbs, with the absence of hindlimbs and deformed forelimbs which are abnormally shaped and reduced in size compared with their wildtype littermates (Mills *et al*. 1999). ΔNp63α was suggested to be the predominantly expressed isoform during both limb morphogenesis and development of the epithelium (Yang *et al*. 1999; Laurikkala *et al*. 2006). Extensive expression of *Trp63* was identified in the apical ectodermal ridge (AEC) of wildtype developing limb buds, a region absent in *Trp63*$^{-/-}$ embryos (Mills *et al*. 1999; Yang *et al*. 1999). Analysis of *Fgf-8* and *Msx-1*, markers for limb outgrowth, showed significant down-regulation in *Trp63*$^{-/-}$ embryos compared to wildtype littermates. Coupled with the failure to correctly stratify the AEC, the results suggested that a loss of P63 disrupted ectoderm – mesenchymal signalling thereby disrupting the proliferative potential of the underlying mesenchyme required for limb outgrowth (Mills *et al*. 1999; Yang *et al*. 1999).

Trp63$^{-/-}$ neonates perish shortly after birth; they display a thin, shiny epithelium with the cause of neonatal lethality thought to be desiccation (Yang *et al*. 1999; Mills *et al*. 1999). Histological analysis the skin of *Trp63*$^{-/-}$ neonates identified an absence of normal epidermal structure with mice covered with a single layer of flattened cells and the absence of hair follicles (Mills *et al*. 1999; Yang *et al*. 1999). Analysis of markers for epithelial differentiation showed an absence of Keratin-14 (Krt14) and Keratin-1 (Krt1). Furthermore, markers of both early and terminal epithelial differentiation, Keratin-10 (Krt10), Filaggrin and Loricrin were

absent (Mills *et al*. 1999). It was therefore suggested that P63 is required for the commitment of cells to the stratified epithelial lineages (Mills *et al*. 1999).

McKeon's group identified expression of the terminal differentiation markers Locricrin and Filaggrin in clusters of abnormal epithelial cells of *Trp63*$^{-/-}$ mice. These findings suggested that the embryonic epidermis of *Trp63*$^{-/-}$ mice commits to squamous lineage and undergoes the process of differentiation (Yang *et al*. 1999). Furthermore the finding that the differentiated cells were positive for TUNEL labelling, suggested they undergo a process of differentiation and cell death normally associated with epidermal tissue (Yang *et al*. 1999). It was therefore suggested that P63 functions to maintain the regenerative potential of epithelial stem cells in both the epithelia, limb-bud AER and other ectoderm-derived tissues (Yang *et al*. 1999).

The different methods utilised in the generation of the two *Trp63* mutant mouse-lines are thought to have resulted in subtle differences between the strains (Wolff *et al*. 2009). McKeon's mouse is considered a true knockout due to the removal of exons 6-8, found in the DBD of both TA and ΔN isoforms (thus removing all P63 proteins) (Yang *et al*. 1999; Wolff *et al*. 2009). Bradley's group generated a mutant line *Brdm2*, which disrupted *Trp63* from exon 10 onwards (Mills *et al*. 1999; Wolff *et al*. 2009). Research has shown mice homozygous for the *Brdm2* insertion expressed P63γ isoforms close to wild-type levels (Wolff *et al*. 2009). It was suggested the differences in P63 ablation between the two models accounts for the identified differences between the strains and caution must be used in drawing conclusions about total P63 function from studies where the *Brdm2* mouse was used (Wolff *et al*. 2009). Appropriate model selection in P63 research is therefore critical to the validity and applicability of data generated.

The characterisation of *Trp63*$^{-/-}$ mice identified abnormalities in development of the ectoderm derived structures, including teeth and hair follicles (Mills *et al*. 1999; Yang *et al*. 1999). To further investigate the molecular effects of P63 on development of these structures Laurikkala and colleagues made use of the *Trp63* mutant mouse model to characterise the expression profile of *Trp63* and putative target genes during embryogenesis (Laurikkala *et al*. 2006). The group confirmed the finding of Mills and Yang that ΔNp63α isoforms were the predominantly expressed form of *Trp63* during development with TA isoforms accounting for only 1% of *Trp63* expression in E13 skin samples (Mills *et al.* 1999; Yang *et al*. 1999; Laurikkala *et al*. 2006). Functions of P63 isoforms are highly specific with different isoforms unable to compensate for a reduction in their counterparts (Wolff *et al*. 2009).

Laurikkala and colleagues assessed the expression of 29 putative P63 target genes in the epithelium of dental placodes and follicles. The expression of *Fgf-8* was found to be unchanged in both the ectoderm of the first branchial arches and dental lamina (Laurikkala *et al*. 2006). Previous studies identified a loss of *Fgf-8* in the AER, the apparent conflict in whether *Fgf-8* is a P63 target may be due to tissue specific gene regulation (Laurikkala *et al*.

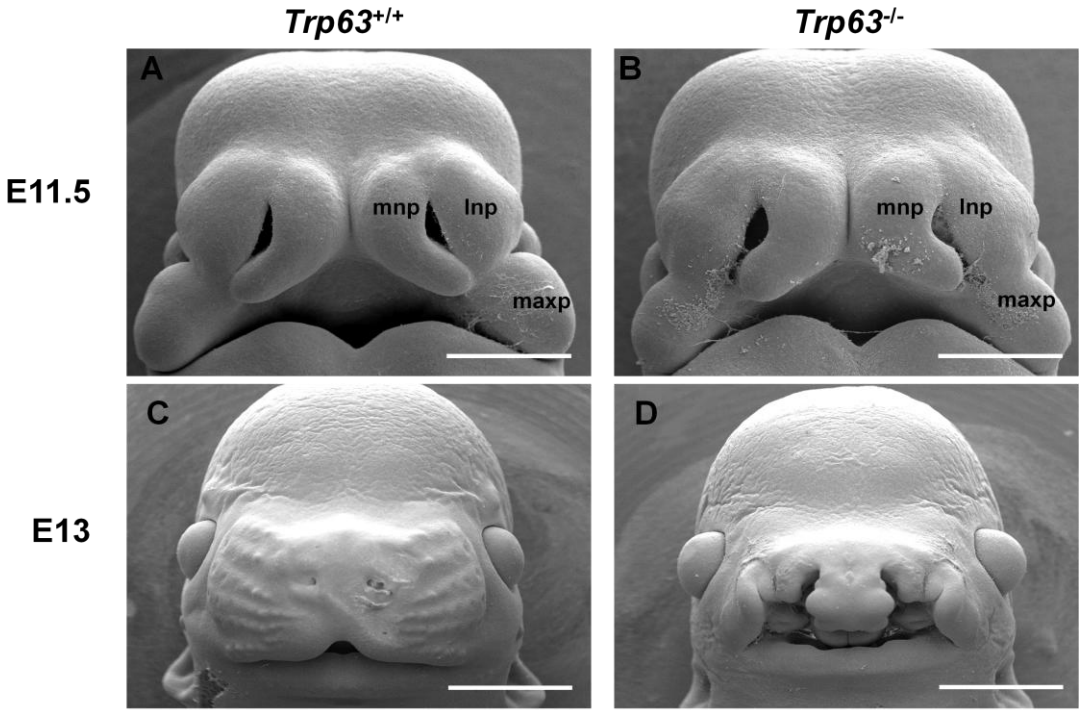

Figure 1.9: Bilateral cleft lip observed in *Trp63*$^{-/-}$ mice. Frontal images of *Trp63*$^{+/+}$ and *Trp63*$^{-/-}$ embryos. (**A-B**) Bilateral cleft lip is first apparent in *Trp63*$^{-/-}$ embryos at E11.5 where the medial nasal, lateral nasal and maxillary processes fail to contact and adhere to one another. (**C-D**) E13 lack of correct contact and adherence results in a fully penetrant bilateral cleft lip. mnp- medial nasal process, lnp- lateral nasal process, maxp- maxillary process, scale bars A-B: 500 µm, C-D 1 mm. (Figure adapted from Thomason *et al*. 2008).

2006; Mills *et al*. 1999; Yang *et al*. 1999). Furthermore the study suggested that *Bmp7*, *Fgfr2b*, *Jag1* and *Notch1* are downstream molecular targets of P63 while Bmp2, Bmp7 and Fgf10 were inducers of *Trp63* expression (Laurikkala *et al*. 2006).

In addition to *Trp63*$^{-/-}$ mice, recent studies have generated mouse models carrying human *TP63* mutations and knockouts for specific P63 isoforms (Lindahl *et al*. 2013; Romano *et al*. 2012). Through site directed mutagenesis, Mills' group generated a *Trp63* mouse model (Trp63^{R279H}) carrying the p.Arg318His mutation which corresponds to the human *TP63* p.Arg279His mutation which causes EEC (Lindahl *et al*. 2013). Mutant mouse generation using a pTV*p63*^{floxN} construct generated three *Trp63* model strains: *Trp63*^{R279HN}, which contained a flox neomycin cassette; *Trp63*^{R279H}, in which the neomycin cassette was excised by cre-recombination and *Trp63*^{Am3} in which exons encoding the DBD were absent, thus mimicking *Trp63*$^{-/-}$ models (Mills *et al*. 2002; Lindahl *et al*. 2013).

While both *Trp63*^{R279HN} and *Trp63*^{R279H} carried the Arg318His mutation, *Trp63*$^{R279HN/+}$ embryos displayed the greatest phenotypic overlap with human manifestations of EEC, with embryos displaying 18 % lethality, CP, anomalies of the distal limbs, defective tooth morphogenesis, dystrophic nails and alopecia (Lindahl *et al*. 2013). Furthermore, neonatal skin analysis showed up-regulation of the ∆Np63α,β and γ isoforms with western blot analysis showing accumulation of P63 in the epidermis. To determine if TAp63 functions as a modifier of EEC, *Trp63*^{R279H} strains were crossed into a TAp63 null background, *Trp63*^{TA} (Lindahl *et al*. 2013). *Trp63*$^{TA-/-}$ embryos failed to display cleft palate, suggesting that loss of TAp63 isoforms alone was insufficient to induce cleft palate. Furthermore, *Trp63*$^{R279HN/TA-}$, *Trp63*$^{R279H/TA-}$ and *Trp63*$^{Am3/TA-}$ all displayed a marked increase in the incidence of and severity of cleft palate. It was therefore suggested that the EEC phenotype was not solely caused by the Arg279His mutation but also by a loss of wildtype TAp63 isoforms (Lindahl *et al*. 2013). Further morphological analysis of compound heterozygous limbs, showed only *Trp63*$^{R279H/TA-}$ embryos displayed an increased incidence of limb defects (Lindahl *et al*. 2013). The *Trp63*$^{R279H/TA-}$ mouse model therefore provides a powerful tool for the analysis of EEC.

In addition to modelling *TP63* mutations, the Sinha and Mills' groups have generated *Trp63* mouse models featuring selective removal of TAp63 and ∆Np63 isoforms respectively (Guo *et al*. 2009; Romano *et al*. 2012). Mills and colleagues generated a *Trp63*^{TA} conditional null mouse model using *loxP* sites flanking exons 2 and 3 and crossing mice with *CMV-Cre* transgenic mice (Guo *et al*. 2009). Analysis of TAp63 conditional knockouts showed that TAp63 isoforms are required to induce Ras-induced senescence. Furthermore, a loss of TAp63 isoforms results in increased proliferation in mouse embryonic fibroblasts (Guo *et al*. 2009). In contrast to Mills' group, Sinha and colleagues generated a ∆Np63 null model through replacement of exon 3 with *GFP* (Romano *et al*. 2012). Homozygous ∆*Np63*$^{gfp/gfp}$ embryos recapitulate the phenotype of *Trp63*$^{-/-}$ embryos exhibiting neonatal lethality, truncated forelimbs and the absence of hindlimbs and defects of the ectoderm-derived

tissues (Romano *et al*. 2012). The severity of the Δ*Np63*$^{gfp/gfp}$ mouse phenotype contrasts greatly with *Trp63*^{TA} mice and further confirms the importance of ΔNp63 isoforms in development (Guo *et al*. 2009; Romano *et al*. 2012). Additionally, comparative use of the Δ*Np63*$^{gfp/gfp}$ and *Trp63*^{TA} mouse lines could provide a powerful research tool in further dissecting the P63 signalling network.

1.5.6 *TP63* and *IRF6*

Mutations in *IRF6* are known to be one of the leading causes of syndromic orofacial clefting, with mutations in exons 3, 4, 7 and 9 identified as contributing to both VWS and PPS (Kondo *et al*. 2002; Butali *et al*. 2014). A link between P63 and *IRF6* regulation was initially proposed by Kondo and colleagues based upon phenotypic overlaps between *TP63*- and *IRF6*-related conditions. *TP63*- and *IRF6*-related conditions were both found to present mixed clefting phenotypes within families, a rare phenomenon in syndromic orofacial clefts (Kondo *et al*. 2002).

In a similar manner to *TP63*-related conditions, there is a phenotypic overlap between the conditions caused by *IRF6* mutations (Kondo *et al*. 2002). Both PPS and VWS commonly feature lip pits and orofacial clefts as a part of the phenotype (Blanton *et al*. 2005). Other features of these conditions include dental, ectodermal and genital abnormalities (Kondo *et al*. 2002). Association between *IRF6* and P63 and their joint role in palatogenesis was suggested based on the observations that their temporal-spatial expression patterns during embryogenesis are highly similar with both genes being highly expressed within the cells of the basal epithelium (Kondo *et al*. 2002; Thomason *et al*. 2010). *Irf6* is highly expressed between E14.5- E15 during secondary palate formation, with some expression overlapping with*Trp63*. *Irf6* expression is detected in the MEE of the palatal shelves during their extension phase with expression persisting in the MES while *Trp63* expression decreases (Kondo *et al*. 2002; Thomason *et al*. 2010; Moretti *et al*. 2010).

It was previously known that disruption of an AP-2α binding site within an *IRF6* enhancer site, *MCS9.7,* is associated with cleft lip (Rahimov *et al*. 2008). In addition, recent work by the Dixon group identified P63 binding at an enhancer region 10 kb upstream from the transcriptional start site of *Irf6* shown to overlap with *MCS9.7* (Rahimov *et al*. 2008; Thomason *et al*. 2010). Furthermore, the Dixon group showed ΔNp63α was able to bind and activate the enhancer element (Thomason *et al*. 2010). Together these results could suggest that P63 and AP2α may co-localise at *MCS9.7* in the regulation of *Irf6* (Rahimov *et al*. 2008; Thomason *et al*. 2010). It has been suggested that the relationship between *P63* and *IRF6* during secondary palate development functions as an autonomous negative regulatory loop, which down-regulates proliferation within the MES and up-regulates differentiation during MES degeneration (Moretti *et al*. 2010).

During development of the secondary palate, the ΔNp63α isoform is expressed, which induces proliferation and prevents differentiation within the extending palatal shelves (Thomason *et al*. 2010). *IRF6* has been shown to be a direct target of P63 binding within developing palatal shelves and is up-regulated by ΔNp63 (Moretti *et al*. 2010; Thomason *et al*. 2010). Analysis of *Irf6* expression in primary mouse keratinocytes showed that *Irf6* was positively regulated by ΔNp63 isoforms but not TAp63 isoforms (Moretti *et al*. 2010). Furthermore the up-regulation of *Irf6* induced proteasome-dependent degradation of ΔNp63, thus reducing the proliferation potential of the epidermal cells and allowing differentiation (Moretti *et al*. 2010).

Thomason and colleagues (2010) further investigated the relationship between *Trp63* and *Irf6* making use of mice carrying a knock-in of the PPS-causing *IRF6* mutation Arg84Cys. Compound heterozygous mice for $Trp63^{+/-}Irf6^{+/R84C}$ displayed a persistent periderm layer along the MES which prevented adequate adhesion between the palatal shelves resulting in cleft palate. In contrast to $Trp63^{+/-}Irf6^{+/R84C}$ embryos, $Trp63^{+/-}$ and $Irf6^{+/R84C}$ single heterozygotes were phenotypically normal, indicating disruption of both genes was required to induce a disease phenotype. These findings indicated a direct genetic interaction between the two genes (Thomason *et al*. 2010).

Analysis of common mutations within both *Irf6* and *Trp63*, indicated that mutations within *Trp63* made P63 resistant to proteasome-mediated degradation, while mutations within *Irf6* resulted in a failure to down-regulate *Trp63* expression (Thomason *et al*. 2010). It was suggested that *Trp63* mutations, Arg279His and Arg304Trp, and *IRF6* mutation, Arg84Cys, induced a biochemical imbalance causing a disease phenotype. These findings confirm that conservation of the *Trp63 Irf6* relationship is key to correct secondary palate development (Moretti *et al*. 2010; Thomason *et al*. 2010).

It is thought that *TP63* is also an anti-apoptotic factor at least in part by up-regulating the expression of anti-apoptotic factors including heat shock protein 70 (*HSP70*) and down-regulating pro-apoptotic genes such as *IGFBP*-3, *P21* and *P53* (Barbieri *et al.* 2005; Wu *et al.* 2005; Hau *et al*. 2011). Down-regulation of ΔNp63α within the MES is followed by a combination of cellular differentiation and apoptosis, which is thought to contribute to its degeneration (Bokhoven & Brunner, 2002; Jugessur & Murray, 2005). In this way, P63 and *Irf6* interact in the development of the secondary palate, through controlling cellular proliferation, apoptosis and differentiation and it is clear that correct *Irf6* expression is reliant upon P63 (Thomason *et al*. 2010). Furthermore the overlap in gene function and temporal expression suggests P63 and IRF6 operate in similar regulatory pathways which could explain the great similarities in the conditions they cause (Thomason *et al*. 2010; Moretti *et al*. 2010).

1.5.7 P63 targets in the upper lip development

Correct orofacial development requires a precise set of sequential developmental stages to be completed to ensure formation of the orofacial structures. In both the development of the primary palate/upper lip and the secondary palate a number of morphogenetic events occur which show high degrees of overlap (Jiang *et al.* 2006). Key to the formation of both tissues is the outgrowth of processes derived from a neural crest and mesenchymal core surrounded by an epithelial layer (Jiang *et al.* 2006; Mossey *et al*. 2009; Jin *et al*. 2012).

The role of P63 in regulating cell cycle has now been characterised extensively, with many studies examining P63's role in maintaining the proliferative potential in stem cells (Candi *et al*. 2007; Iorio *et al*. 2011). Previous studies have shown that *Trp63* is expressed within the basal epithelial layer of the medial and lateral nasal processes and the developing palatal shelves (Thomason *et al*. 2008). The expression of *Trp63* is also highly localised to the point of fusion between the developing facial processes in the upper lip. In the secondary palate a similar localisation is seen, with P63 being required for extension of the palatal shelves (Thomason *et al*. 2010). These observations would suggest that similar molecular controls operate in the development of the upper lip and secondary palate.

A recent study by Thomason and colleagues extensively characterised *Trp63*$^{-/-}$ embryos and identified a number of potential targets of P63 (Thomason *et al*. 2008). At E11.5 *Trp63*$^{-/-}$ mice displayed a fully penetrant CL/P with the medial nasal processes failing to contact the lateral nasal processes and displaying a more rounded appearance compared with wildtype littermates. Histological analysis of the medial nasal, lateral nasal and maxillary processes of *Trp63*$^{-/-}$ embryos showed they were abnormally shaped and smaller than wildtype littermates (Thomason *et al*. 2008). CL/P arose as a result of a loss of signalling between the mesenchyme and ectoderm, resulting in increased levels of apoptosis and reduced rates of proliferation. Thomason and colleagues identified rounded irregular cells sloughing away from the surface epithelium of the E11.5 medial nasal, lateral nasal and maxillary processes. The irregular cells were Caspase-3-positive, suggesting they underwent inappropriate cell death, however, no cell death was seen within the mesenchyme of the facial processes (Thomason *et al*. 2008). BrdU assays failed to display a difference in proliferation between E10.5 *Trp63*$^{-/-}$ facial processes and wildtype littermates; however the authors noted that total cell counts were significantly lower in the null facial processes. Furthermore at E11.5 regions of the medial nasal, lateral nasal and maxillary processes were found to display a significant reduction in proliferation compared to wildtype (Thomason *et al*. 2008).

The misregulation of apoptosis and proliferation was linked to the expression of components of Bmp, Fgf and Shh signalling networks. Specifically, *Bmp4* was up-regulated in the caudal regions of *Trp63*$^{-/-}$ lateral nasal processes and the anterior regions of the maxillary processes at E10.5. The authors suggested that absence of P63 resulted in up-regulation of *Bmp4* and increased levels of apoptosis (Thomason *et al*. 2008). In addition to *Bmp4*

expansion, expression of *Msx1* was up-regulated in the medial nasal and maxillary prcoesses of *Trp63*$^{-/-}$ embryos (Thomason *et al*. 2008). It has previously been found that the expression of the genes *Msx1* and *Msx2* is regulated through the action of BMP signalling and that abnormal Msx regulation results in CL/P (Jezewski *et al.* 2003; Chishti *et al.* 2006; Song *et al*. 2009). Studies suggest that *Msx1* is involved in inhibiting early cellular differentiation during facial process outgrowth, and misregulation results in a lack of appropriate growth (Jezewski *et al*. 2003). By regulating *Bmp4* expression, P63 also acts indirectly to regulate the expression of *Msx1* and *Msx2*.

In addition to *Bmp4* regulation, other potential targets of P63 include *Fgf8*. (Section 1.4.4) (Petiot *et al*. 2003; Laurikkala *et al.* 2006; Riley *et al*. 2006). Expression of the *Fgf8*-target gene *Barx1* was down-regulated in the anterior regions of *Trp63*$^{-/-}$ maxillary processes (Thomason *et al*. 2008). Furthermore, loss of proliferation in the facial processes of *Trp63*$^{-/-}$ embryos correlated with the loss of *Fgf8* expression, suggesting that P63 up-regulates the expression of *Fgf8* to induce proliferation (Riley *et al.* 2006; Thomason *et al*. 2008).

The association between Fgf signalling and P63 has been further investigated by the work of the Missero group who generated a mouse line carrying the human AEC mutation, Leu514Phe (Ferone *et al*. 2012). The study identified a highly specific function for P63 in regulating expression of both *Fgfr2* and *Fgfr3* within primary mouse keratinocytes and embryonic skin. The loss of regulation caused by the Leu514Phe mutation resulted in decreased ectodermal proliferation during development. Furthermore the group identified a novel function of P63 in controlling progenitor cell expansion, previously only found in *Fgfr2b*$^{-/-}$ mouse lines (Petiot *et al*. 2003; Ferone *et al*. 2012). The study further confirms the regulation of Fgf signalling by P63 during development and identifies the loss of progenitor cell expansion as a possible contributor to the unique phenotype of AEC syndrome (Ferone *et al*. 2012).

The Shh signalling pathway consists of the signalling molecule Shh, which binds to the cell surface receptor Ptch1 resulting in a loss of inhibition of the protein Smo (Section 1.4.2). The result of this is the up-regulation of genes involved in driving proliferation, a key process in palatal development (Jiang *et al*. 2006). It was found that in *Trp63*$^{-/-}$ embryos*, Shh* was down-regulated in the medial nasal processes and was absent from the maxillary processes during embryogenesis. This interaction is thought to be involved in inducing proliferation (Thomason *et al*. 2008). Previous studies have shown a link between the expression of *Trp63* and the induction of *Shh* expression, with *Trp63* isoforms binding to the *Shh* promoter (Caserta *et al*. 2006).

During the development of the lip, the lateral nasal, medial nasal and maxillary prcoesses converge and adhere resulting in the formation of an epithelial seam which must be degraded in order to allow fusion, the λ junction (Ferretti *et al*. 2011). A pathway recently identified as playing a role in the normal degeneration of this seam is the Wnt signalling

pathway. Mutations within the Wnt pathway have previously been shown to induce cleft lip and palate resulting from misregulation of *Bmp4*, which in turn regulates the expression of *Msx1* and *Msx2* (Song *et al.* 2009).

A recent study showed loss of *Pbx1*, *Pbx2* and *Pbx3* disrupted Wnt signalling and the expression of both *Irf6* and *Trp63*. It was suggested Wnt signalling lies upstream of *Trp63*, which ultimately regulates *Irf6* expression for correct λ seam degeneration (Section 1.4.5) (Ferretti *et al.* 2011). Previous studies have shown that apoptosis is required for degenerating the λ junction (Jiang *et al*. 2006; Song *et al*. 2009). In the absence of *Pbx1, Pbx2* and *Pbx3*, a lack of apoptosis was observed within the λ junction, resulting in a fully penetrant cleft lip and palate (Ferretti *et al*. 2011).

The work of Kurosaka and colleagues further characterised the interaction of P63 and *Irf6* as well as highlighting some of the networks involved in the regulation of P63 signalling during orofacial development (Kurosaka *et al*. 2014). Through the use of mouse models for disruptions of *Shh*, Kurosaka's group identified modified P63/ Irf6 signalling within the λ junction (Kurosaka *et al*. 2014). Modification of Shh signalling resulted in a disruption of canonical Wnt signalling, which in turn affects the P63 *Irf6* signalling pathway to induce CL/P (Ferretti *et al*. 2011; Kurosaka *et al*. 2014).

1.5.8 Other molecular targets of P63

Additional targets of P63 include a *P53* associated gene, *P53 apoptosis effector-related to PMP-22* (*Perp*) (Chung *et al*. 2011). Previous studies found that the expression levels of *Perp* were regulated by *TP63* isoforms. *Perp* expression was shown to be required for epithelial integrity through cellular adhesion and homeostasis (Ihrie *et al*. 2005). A recent study found that the DNA binding protein Satb2 is a co-regulator of *Perp* with *P63*. It was shown that common mutations in AEC and EEC affected the ability of *P63* to associate with *SATB2* in different ways and thus altered *Perp* regulation. This was suggested as a reason for the varied phenotype seen between AEC and EEC (Ihrie *et al.* 2005; Chung *et al*. 2011).

Further investigations into the cause of variation in the phenotypes of *TP63*-related conditions have identified possible mechanisms for how P63 regulates target genes. Previous studies have suggested a direct association between P63 and the genes *Dlx5/Dlx6*, due to co-localisation within cells of the limb bud AER (Lacono *et al*. 2008). P63 was shown to bind to the *Dlx5/Dlx6* promoters, with Luciferase reporter assays showing ΔNp63 isoforms were able to induce transcription (Lacono *et al*. 2008). In contrast TAp63 isoforms failed to activate *Dlx5/Dlx6* transcription. Further analysis using expression vectors incorporating Lys193Glu, Lys194Glu, Arg279His, Cys306Arg and Leu518Phe, common human *Trp63* mutations, showed all the mutations, excluding Leu518Phe, reduced P63 induction of *Dlx5/Dlx6* (Lacono *et al*. 2008). Lacono and colleagues noted that the variable effect of *Trp63* mutations on *Dlx5/ Dlx6* induction could explain the variance in *TP63*-related

conditions, with Leu518Phe mutations causing AEC, which does not present limb defects (Lacono *et al*. 2008).

Furthermore, expression analysis of *Dlx5* and *Dlx6* in *Trp63*$^{EEC/EEC}$ embryos showed both genes were significantly down-regulated in mutant limb buds with *in situ* hybridisation showing a marked reduction of *Dlx5* expression in the AER of E10 embryos (Lacono *et al*. 2008). Expression analysis of *Trp63* in compound *Dlx5*$^{-/-}$;*Dlx6*$^{-/-}$ mice was comparable to wildtype littermates, suggesting that *Dlx5*/*Dlx6* do not regulate *Trp63* expression. *Trp63*$^{EEC/+}$ and *Dlx5*$^{-/-}$;*Dlx6*$^{+/-}$ mice do not display limb abnormalities (Celli *et al*. 1999; Lacono *et al*. 2008). However when crossed to generate *Trp63*$^{EEC/+}$;*Dlx5*$^{-/-}$;*Dlx6*$^{+/-}$ compound heterozygotes, embryos displayed severe ectrodactyly suggesting correct P63-*Dlx* regulation is required for limb development (Lacono *et al*. 2008).

P63-*Dlx* regulation was further investigated by the Zhou and Von Bokhoven groups, who performed genome-wide DNA-binding profiling by chromatin immunoprecipitation followed by deep sequencing (ChIP Seq) to identify possible targets of P63 regulation (Kouwenhoven *et al*. 2010). In excess of 11,000 putative P63 binding sites were identified in cultures of adult human primary keratinocytes from the skin, with 94 % containing the characterised P63 binding motif. Analysis of the prospective binding sites identified a significant co-localisation of Ap1, Bach1 and Bach2 binding motifs, known to be binding sites for C-jun and C-fos (Kouwenhoven *et al.* 2010). A P63 binding site, SHFM1-BS1 was identified, that was associated directly with regulating *DLX5/DLX6* expression and suggested to be an enhancer site. Patients with deletions which spanned the SHFM1-BS1 site were found to display SHFM (Kouwenhoven *et al*. 2010).

In contrast to Lacono's group, the Zhou and Von Bokhoven groups failed to detect P63 binding at *DLX5/DLX6* promoters (Lacono *et al*. 2008; Kouwenhoven *et al*. 2010). Using chromosome conformation capture, it was suggested a looping mechanism would allow P63 to regulate the expression of *DLX5/DLX6* by binding at SHFM1-BS1, suggesting P63 is able to regulate gene expression at distances greater than 250 kb (Kouwenhoven *et al*. 2010). Furthermore, specific expression controlled by SHFM1-BS1 was absent from craniofacial development, suggesting that the mechanism of P63 regulation of *DLX5/DLX6* is tissue specific (Kouwenhoven *et al*. 2010).

Further to the work of Von Bokhoven and Zhou and colleagues, McDade's group identified 7574 prospective P63 binding sites within human keratinocytes derived from foreskin. McDade and colleagues showed that 85% of peaks contained the P63 binding motif (McDade *et al*. 2012). 15% of binding sites did not feature the P63 binding motif, which may be indicative of either a secondary and currently uncharacterised binding motif, or P63 binding via an associated protein (McDade *et al*. 2012). McDade's group provided further evidence for the conservation of function between P53 family members by intersecting their data set with two P53 ChIP-Seq data sets. Through this approach the group were able to

demonstrate that approximately 1000 of their 7500 binding sites were shared between P53 and P63, with ChIP-qPCR confirming P53 was unable to bind to the P63-specific sites (McDade *et al*. 2012). Gene ontology analysis was completed, identifying peaks within 25 kb of genes associated with CP. Validation of peaks proximal to 41 CP genes was completed using ChIP qPCR of human foreskin keratinocytes and showed eight binding sites displayed positive enrichment by P63 (McDade *et al*. 2012). Intersection of the data set with two array data sets from murine keratinocytes and MCF10A basal breast epithelial cells showed 10 genes previously associated with cleft palate, including *IRF6*, *FGFR2* and *PVRL1*, to be differentially regulated in P63 depleted human keratinocytes (McDade *et al*. 2012).

Motif analysis of the P63 motif-negative binding sites identified enrichment for AP2α sites. The group therefore further characterised the association between P63 and AP-2, showing that P63 was able to co-localise with Tfap2a (AP-2α) and Tfap2c, with P63 being required for Tfap2a recruitment. 16% of sites identified in the study were bound by both P63 and Tfap2a (McDade *et al*. 2012). Gene ontology analysis showed enrichment for processes including cell adhesion, development of the epidermis/ ectoderm and regulation of cell death and proliferation which are processes involved with formation of the upper lip and primary palate (Jiang *et al*. 2006; McDade *et al*. 2012).

Both the Zhou and McDade groups adopted a highly effective method of identifying prospective targets of P63 regulation, using a combination of ChIP-Seq and expression data (Kouwenhoven *et al*. 2010; McDade *et al*. 2012). However, as exemplified by SHFM1-BS1 which is active in limb development but not orofacial development, the functional relevance of these studies is undermined by their choice of tissue. For example the McDade group sought to investigate cleft palate genes using neonatal foreskin (McDade *et al*. 2012). Due to the tissue specificity of P63 regulation, it is clear that selection of stage appropriate tissue is key to experimental design.

P63 has been found to play a direct role in chromatin remodelling (Fessing *et al*. 2011; Mardaryev *et al*. 2014). *Satb1*, a gene responsible for chromatin remodelling, has been identified as a direct target of P63 regulation (Fessing *et al*. 2011). A P63 binding site was identified approximately 1500 bp upstream from the *Satb1* TSS and shown to display P63 binding during development of the epidermis of embryonic mice. Satb1 was co-expressed with P63 in the nuclei of basal epithelial cells and depletion of P63 produced a significant reduction of Satb1 expression (Fessing *et al*. 2011). Furthermore ectopic expression of *Satb1* within *Trp63*$^{-/-}$ skin was able to partially rescue the mutant phenotype, while further ablation of *Satb1* exacerbated it (Fessing *et al*. 2011). It was suggested that during epithelial development, the induction of *Satb1* by P63 induces chromatin remodelling within the epithelial differentiation complex (EDC) allowing expression of differentiation-linked target genes. In *Trp63*$^{-/-}$ samples, the lack of *Satb1* expression resulted in chromatin compression, thus preventing gene expression (Fessing *et al*. 2011). This association has not been identified within orofacial development.

The role of P63 in chromatin remodelling has been further characterised through the identification of the gene *Brg1* as a direct transcriptional target of P63 (Mardaryev *et al*. 2014). In a similar manner to *Satb1*, *Brg1* was found to be significantly down-regulated in the epidermis of *Trp63*$^{-/-}$ embryos (Fessing *et al*. 2011; Mardaryev *et al*. 2014). Furthermore a P63 binding motif was identified within exon 1 of *Brg1* and was found to be enriched by P63 in the epidermis of E16.5 embryos (Mardaryev *et al*. 2014).

It was suggested P63 acts to induce expression of *Brg1* which acts in a similar manner to Satb1 in chromatin remodelling (Fessing *et al*. 2011; Mardaryev. 2014). Furthermore a reduction in *Brg1* expression within *Trp63*$^{-/-}$ epidermis results in movement of the EDC to the periphery of the nucleus, suggesting that P63 functions through Brg1 to translocate the EDC to the nuclear interior to induce the expression of genes required for successful differentiation (Mardaryev *et al*. 2014). Together these findings suggest a key role for P63 in chromatin remodelling as well as providing a putative mechanism of pathology for human P63-linked conditions.

Recent work by the Dixon group into the role of P63 regulation in secondary palate development identified *Grhl3* and *Sfn* as direct targets of P63 (Mitchell *et al*. manuscript in preparation). The group adopted a similar method to the McDade and Zhou groups using a combination of ChIP-Seq and expression data to identify target genes (Kouwenhoven *et al*. 2010; McDade *et al*. 2012; Mitchell *et al.* manuscript in preparation). Gene ontology analysis identified enrichment for adhesion related genes including *Col7a1*, *Grhl3*, *Sfn*, *Fermt1* and *Plec1*. *Col7a1* encodes an extracellular matrix protein involved in the adhesion of the epidermis and dermis (Burgeson, 1993; Mitchell *et al*. manuscript in preparation). Human mutations within *COL7A1* cause dystrophic epidermyolysis bullosa which is characterised by nail dystrophy, blistering and mutilation of the extremities, failure to thrive and premature demise (Dang & Murrell, 2008). qPCR analysis of *Col7a1* expression showed significant down-regulation in E14.0 *Trp63*$^{-/-}$ compared with wildtype. Furthermore, immunohistochemistry on E14.0 and E17.5 skin showed a marked reduction in *Col7a1* expression along the basement membrane of the epithelium, with *Col7a1* absent in E17.5 *Trp63*$^{-/-}$ skin (Mitchell *et al*. manuscript in preparation). Luciferase reporter assays showed ΔNp63α strongly activated transcription of the P63 binding site proximal to *Col7a1* which suggested it was a direct target of P63 regulation (Mitchell *et al*. manuscript in preparation).

In addition to regulating *Col7a1* expression during skin development, Mitchell and colleagues identified P63 regulation of periderm and basal epithelia adhesion during secondary palate development (Mitchell *et al*. manuscript in preparation). Immunohistochemical analysis of proteins involved in desomosome and adherens junction formation showed a marked reduction in protein levels in E14 *Trp63*$^{-/-}$ palatal shelves compared with wildtype. In wildtype samples, desmosomal proteins Plakoglobin and Keratin 5 were found localised to the basal epithelium/ periderm boundary. Comparisons to *Trp63*$^{-/-}$ embryos revealed a marked reduction in protein levels with staining absent at the apical

border of basal cells (Mitchell *et al*. manuscript in preparation). The adherens junction protein Nectin-1 displayed a similar expression pattern. Nectin-1 was localised to the basal epithelia/ periderm boundary and markedly reduced in *Trp63*$^{-/-}$ embryos. Furthermore, the group analysed the expression pattern of Nectin-4, an adherens junction protein which had not been identified as a potential P63 target gene. Nectin-4 expression was comparable between *Trp63*$^{-/-}$ and wildtype palatal shelves (Mitchell *et al*. manuscript in preparation). It was therefore suggested that P63 regulates periderm adhesion during secondary palate development and loss of this regulation may contribute to the CP phenotype seen in *TP63*-related conditions.

Carroll and colleagues further investigated the role of P63 regulation in adhesion, using the human breast epithelial cell line, MCF-10A, which predominantly express the ∆Np63α isoform (Carroll *et al*. 2006). Specific knockdown of P63 isoforms using shRNAs showed that ablation of all P63 isoforms, or P63α isoforms induced a marked phenotypic effect. Cells adopted a round morphology, detatched from the plate and underwent apoptosis (Carroll *et al*. 2006). In contrast, cells in which TAp63 isoforms were ablated were comparable to controls, suggesting loss of adhesion was ∆Np63 specific (Carroll *et al*. 2006). Expression profiling of cells in which ∆Np63α or ∆Np63γ were ectopically expressed showed up-regulation of genes involved in adhesion including Integrins, Extracellular matrix components, Cadherins and Catenins (Carroll *et al*. 2006). Furthermore, ChIP-qPCR showed P63 was bound to P53 response elements adjacent to *ITGα3*, *β4*, *α5* and *α6* and *LAMININ-γ2* with Luciferase reporter assays showing ∆Np63α strongly activated the *ITGβ4* binding site. It was therefore suggested *ITGβ4* was a direct target of P63 regulation in MCF-10A cells (Carroll *et al*. 2006). Expression analysis conducted on mammary epithelial cells from *Trp63* conditional knockout mice and human foreskin keratinocytes in which P63 was ablated, identified a similar down-regulation of adhesion genes in the absence of P63 to MCF-10A cells (Carroll *et al*. 2006). Together these results suggested that ∆Np63α regulation is essential for expression of adhesion genes including *ITGβ4* (Carroll *et al*. 2006).

In addition to integrins, P63 has previously been shown to regulate the expression of *Cldn1* and *Cldn4* (Lopardo *et al*. 2008; Kubo *et al*. 2014). Claudins are one of the three principle components of tight junctions, which seal the intercellular space in epithelial and endothelial cellular sheets and are integral to the barrier function of the epidermis (Tsukita & Furuse, 2000; Furuse *et al*. 2002). Both *Trp63*$^{-/-}$ and *Cldn1*$^{-/-}$ mice display severe skin abnormalities and are neonatal lethal due to dessication (Mills *et al*. 1999; Yang *et al*. 1999; Lopardo *et al*. 2008). Due to the phenotypic overlap between *Trp63*$^{-/-}$ and *Cldn1*$^{-/-}$ mice, Lopardo and colleagues examined the expression of *Cldn1*, *3* and *10* in primary mouse keratinocytes in which ∆Np63 isoforms were selectively ablated through siRNA (Lopardo *et al*. 2008). Expression of *Cldn1*, *3* and *10* were found to be significantly down-regulated in ∆Np63-ablated cells (Lopardo *et al*. 2008). Furthermore, ChIP-qPCR analysis identified two binding

sites within the *Cldn1* promoter, R1 and R2, which displayed P63 binding. Luciferase reporter assays showed ∆Np63α activation of reporter constructs containing R1 and R2, suggesting *Cldn1* was a direct target of P63 regulation (Lopardo *et al*. 2008).

Analysis of *CLDN1* expression in skin biopsies from an AEC patient carrying the mutation Ile537Thr, showed a marked reduction in *CLDN1* expression within the affected individual, with expression absent from the basal and suprabasal layers compared to wildtype (Lopardo *et al*. 2008). In addition, Luciferase reporter assays using cells co-transfected for human AEC mutations AEC518 and AEC540 showed the mutations reduced P63's activation of *Cldn1*. Taken together these results suggested that P63 directly regulates the expression of *CLDN1* in human skin, and a loss of *CLDN1* expression in the skin of AEC patients may contribute to the fragile skin phenotype observed (Lopardo *et al*. 2008).

Analysis of *CLDN4* expression in human keratinocytes showed P63 and *CLDN4* expression was mutually exclusive, with Cldn4 present within the granular layer, while ∆Np63 was detected throughout the basal to spinous layers (Kubo *et al*. 2014). Due to the exclusion of CLDN4 expression from P63-positive regions, the group suggested ∆Np63 negatively regulated *CLDN4*. Expression analysis of *CLDN4* in HaCaT keratinocytes depleted for ∆Np63 through RNAi showed a significant up-regulation of *CLND4* (Kubo *et al*. 2014). Furthermore, administration of poly I:C, a synthetic ligand of the ∆Np63 repressor TLR3, resulted in up-regulation of *CLDN4* (Kubo *et al*. 2014). Kubo and colleagues therefore suggested that ∆Np63 negatively regulates the expression of *CLDN4* in human keratinocytes (Kubo *et al*. 2014).

P63 is involved in the embryonic development of both the primary and secondary palate, therefore research into this gene has aided in determining the sequence of events in palatal formation as well as elucidating the molecular controls involved (Bokhoven *et al*. 2002). Furthermore as a transcription factor, studies of P63 targets within the developing palate reveal further molecular elements required for correct embryonic palatal development, as well as suggesting molecular components in other developmental systems which involve P63 (Thomason *et al*. 2010; Moretti *et al*. 2010; Kouwenhoven *et al.* 2010; Browne *et al*. 2011).

1.6 Aims and objectives

The majority of research into P63's role in orofacial development has focussed on secondary palate development. As such our knowledge of P63 function and transcriptional targets during upper lip and primary palate morphogenesis remains poor. This project provides further expansion of the P63 signalling network as well as identifying direct targets of P63 regulation in upper lip morphogenesis.

Null embryos display a fully penetrant bilateral cleft lip and palate. To identify prospective targets of P63 regulation a combination of ChIP-Seq and expression data will be used to identify genes differentially expressed between *Trp63*$^{-/-}$ and wildtype facial processes with a P63 binding site nearby. To prioritise genes for further investigation, gene ontology will be used to identify functional trends within the data (Chapter 3).

Having identified prospective target genes, computational methods will be used to detect P63 binding motifs proximal to target genes. Each binding site will be further evaluated using ChIP-qPCR to determine if P63 binding is present during upper lip morphogenesis. To determine if target genes are misregulated by P63, expression will be quantified using qPCR and the expression profile of each target gene in facial development characterised using whole mount *in situ* hybridisation in *Trp63*$^{-/-}$ and *Trp63*$^{+/+}$ embryos (Chapter 4).

Chapter 2 – Materials and Methods

All reagents were purchased from Sigma-Aldrich, Thermo-Fisher Scientific or BDH unless otherwise stated. Micro-centrifugation steps were conducted at 13,000 rpm at room temperature unless otherwise stated.

2.1 Mice

All mice were housed in the accredited animal facilities at the University of Manchester. All procedures were approved by the University of Manchester Ethical Review Committee and are licensed under the Animal (Scientific Procedures) Act 1986, issued by the Home Office, Her Majesty's Government, London, United Kingdom.

2.1.1 *Trp63* genotyping

Ear punching was used for mouse identification and genotyping. A single ear punch or tissue sample was removed from each pup or embryo for *Trp63* genotyping. Tissue was incubated in 1x PCR (10 mM Tris-HCl, pH 8.3, 50 mM KCl, 1.5 mM $MgCl_2$, and 0.1% gelatine) buffer containing 2.5 mg/ml of Proteinase-K overnight at 55°C. Samples were shaken vigorously to disrupt digested tissue and micro-centrifuged for five minutes. PCR was completed using 3 µl of supernatant.

Forward primers 5'-GGT GCT TTG AGG CCC GGA TC-3' and 5'-GAA AGC GAA GGA GCA AAG CTG-3' were used in conjunction with the reverse primer 5'-TTC TCA GAT GGT ACC GCT CC-3'. Primers generated an amplicon of approximately 600 bp for wildtype mice and 450 bp for the targeted allele.

PCR reactions were completed in a total volume of 25 µl containing 50 pmol each of the forward and reverse primers, 3 µl of DNA, 200 µm of each dNTP (dATP, dCTP, dGTP and dTTP) and 1x PCR buffer. Control reactions were performed simultaneously, the positive control consisted of an appropriate DNA sample and the negative control contained dH_2O in place of DNA. Reactions were completed in a 0.5 ml Eppendorf tube. A hot start reaction was performed using a Verity 60 well thermal cycler (Applied Biosystems). Samples were denatured at 96 °C for 10 minutes and cooled and held at the annealing temperature of 60 °C. 0.75 units of *Taq* DNA polymerase (Invitrogen) were added to each sample. PCR consisted of 30 cycles of: DNA denaturation at 94 °C for 30 seconds, primer annealing at 60 °C for 30 seconds and primer extension at 72 °C for 30 seconds. A final extension step was performed at 72 °C for ten minutes. Post PCR, products were separated by gel electrophoresis on a 3% agarose gel containing 0.5 µg/ml of Ethidium Bromide. Products were visualised using a UV light transilluminator (Uvitec). 1 kb DNA ladder was used as a size standard.

2.2 Dissection and processing of embryos

All dissection equipment was sterilised in 70% ethanol and solutions were autoclaved and then chilled to 4 °C.

2.2.1 Mouse breeding and embryo dissection

Wildtype CD1 embryos were provided by the animal facilities at the University of Manchester. *Trp63*$^{-/-}$ embryos on a BALB/c background were obtained by heterozygous overnight time-matings. Pregnancy was assessed the following morning through the presence of a vaginal plug considered to be embryonic day (E) 0.5. At the required embryonic age, mice were sacrificed via Schedule 1 cervical dislocation and embryos dissected into sterile, ice-cold phosphate buffered saline (PBS). Subsequent processing was dependent on upon procedural requirement and will be discussed in reference to individual protocols. For morphological analysis embryos were fixed in Bouin's fixative for 24 hours at 4 °C. For ChIP protocols facial processes were dissected into sterile, ice-cold PBS and pooled into a single 1.5 ml Eppendorf tube. Facial processes were cross-linked in 1% formaldehyde at 4 °C for 23 minutes. Fixation was stopped through the addition of glycine 0.125 M and incubated for 5 minutes at 4 °C. Samples were washed twice for 5 minutes in PBS at 4°C, before PBS was removed and samples were frozen on dry ice. Samples were stored at -80 °C. Facial processes for RNA extraction were placed in individual, sterile 1.5 ml Eppendorf tubes, snap frozen in liquid nitrogen and stored at -80 °C. Embryos for whole mount *in situ* hybridisation were dissected into individual 2.0 ml Eppendorf tubes and fixed overnight at 4 °C in 4% paraformaldehyde (PBS). The following morning embryos were washed twice for 5 minutes in PBS. Embryos were dehydrated through 5 minute washes of serial dilutions of methanol in PBS (25%, 50%, 75% and 100%) before being stored at -20 °C overnight in 100% methanol.

Embryos for whole mount *in situ* hybridisation were bleached through five hour incubation in 5% hydrogen peroxide (100% methanol). Following bleaching embryos were washed three times for five minutes in 100% methanol and stored at -20 °C.

2.3 Chromatin Immunoprecipitation

2.3.1 Chromatin extraction

Samples were suspended in ice cold PBS and homogenised using an Ultra-Turrax Homogeniser and centrifuged at 4,500 rpm for 5 minutes at 4 °C. Supernatant was removed and samples were incubated in PIPES buffer (5 mM PIPES pH 8.0, 85 mM KCl, 0.5% NP40, 1mM PMSF, 1x PICS) at 4 °C for 10 minutes. Following centrifugation at 4,500 rpm for 5 minutes at 4 °C, the supernatant was removed and the pellet was resuspended in SDS lysis buffer (50 mM Tris-HCl pH 8.1, 10 mM EDTA, pH 8.0, 1% SDS, 1x PICS) and incubated at 4 °C for 20 minutes to 2 hours. Following lysis, chromatin was sonicated using a Sonics

Vibracell with seven 10 second pulses set to an amplitude of 40. Following the final sonication, a 20 µl aliquot was taken to verify appropriate sonication. Samples were centrifuged for 10 minutes at 4 °C and the supernatant transferred to a clean Eppendorf and stored at -70 °C.

The 20 µl aliquots were combined with TE buffer and NaCl 0.25 M, vortexed and incubated at 65 °C overnight. The following morning RNase A (1 mg/ml) was added to each aliquot and incubated at 37 °C for 30 minutes. Samples were purified using the Qiagen PCR clean-up kit (Qiagen) and eluted in dH_2O. Samples were separated through gel electrophoresis on a 1.5% agarose gel containing 0.5 µg/ml of Ethidium Bromide and visualised using a UV light transilluminator (Uvitec). 1 kb DNA ladder was used as a size standard and samples sizes were assessed for adequate sonication.

2.3.2 ChIP

Sonicated chromatin was diluted 1:10 in ChIP dilution buffer (10% BSA) and 10% removed and stored at -20 °C for use as input. Chromatin was pre-washed with Protein A-Agarose beads (SC-2001; Santa Cruz) at 4 °C for 2 hours. Chromatin was centrifuged at 4000 rpm for 5 minutes at 4 °C and the supernatant retrieved. 2 µg of α isoform-specific P63 antibody (H129; Santa Cruz) was added and samples were incubated overnight at 4 °C. The following morning antibody-bound chromatin was recovered using protein A-agarose beads (Santa Cruz) and incubated for 4 °C for 2 hours. Chromatin was centrifuged at 4000 rpm at 4 °C for 5 minutes, the supernatant was removed and the resin washed with low salt buffer (0.1% SDS, 1% Triton X-100, 2 mM EDTA pH8.0, 20 mM Tris-HCl pH8.1, 167 mM NaCl). Chromatin was washed additionally with low salt buffer, followed by a single high salt buffer (0.1% SDS, 1% Triton X-100, 2 mM EDTA pH 8.0, 20 mM Tris-HCl, 500 mM NaCl) wash and two washes each of LiCl buffer (0.25 M LiCl, 1% NP40, 1% DOC, 1 mM EDTA pH 8.0, 10 mM Tris-HCl pH 8.1) and TE (0.1 M Tris, 1 mM EDTA). Between washes samples were centrifuged for 5 minutes at 4000 rpm at 4 °C and the supernatant removed.

Following the final wash, the supernatant was removed and the resin resuspended in 2% SDS in TE. Samples were incubated at room temperature with agitation for 30 minutes before being centrifuged at 13,000 rpm at room temperature for 10 minutes. The supernatant was retrieved and 25 mM NaCl was added to both ChIP-chromatin and the input sample. Samples were then incubated at 65 °C overnight.

2.3.3 Purification and qPCR

2 µg of proteinase k was added to the input and ChIP samples and incubated at 45 °C for 1 hour. All samples were then purified using the Qiagen PCR clean-up kit (Qiagen) and eluted in dH_2O. The input sample was diluted 1:10 prior to qPCR, while ChIP material was used neat. 5 µl of each sample was used for qPCR. For each putative binding region, primers were designed using Primer 3 (http://primer3.ut.ee/). Where possible primers were designed

to a maximum size of 20 bp with a GC content of 50% to produce a melting temperature of 60 °C. Primers were designed to produce an amplicon of 90-150 bp. Full details of all ChIP-qPCR primers can be found in Appendix 1. For each qPCR reaction, 2 µl of 5 pmol of forward and reverse primer was added to an optical 96 well plate (Applied Biosystems). qPCR reactions were performed in a Step One machine (Applied Biosystems) using Power SYBR Green PCR master Mix (Life Technologies) according to the manufacturer's protocol in a 25 µl reaction volume. PCR protocol consisted of 40 cycles of: DNA denaturation at 95 °C for 20 seconds, primer annealing at 60 °C for 20 seconds and primer extension at 72 °C for 20 seconds. For each primer set a meltcurve was generated to confirm target specificity. Each putative target region was interrogated in triplicate across biological replicates. A previously verified P63 binding site approximately 24 kb upstream of *Pvrl1* was used as a positive control while a region within exon 2 of *Myoglobin*, where P63 does not bind, was used as a negative control. ChIP efficiency of candidate binding sites was calculated using percentage of immunoprecipitated DNA against input chromatin. P63 occupancy was calculated relative to *Myoglobin* through the $2^{\Delta\Delta CT}$ method and significance was assessed using the Student's T-test (Livak & Schmittgen, 2001).

2.4 Expression analysis

Where possible all glassware was baked over night at 180 °C, all solutions were pre-treated with diethylpyrocarbonate (DEPC) and sterilised by autoclaving.

2.4.1 RNA extraction

Facial processes were dissected as described in section 2.2.1. RNA isolation was performed using the Qiagen RNeasy kit according to the manufacturer's protocol and eluted in 30 µl dH_2O. Purity and concentration of isolated RNA was determined using a Nanodrop 2000 spectrophotometer (Thermo Scientific) and stored at -80 °C.

2.4.2 cDNA synthesis

To prevent genomic DNA contamination, 2.5 µg of RNA samples were treated with 6 Units of DNase I (Roche) in 1x DNase buffer (Roche) in a total volume of 20 µl. Samples were incubated at 37 °C for 30 minutes, before DNase I was denatured through administration of 1 mM EGTA and incubation at 65 °C for 10 minutes. 100 ng of random primers (Invitrogen) were added and samples were incubated at 70 °C for 10 minutes. RT mastermix (8 µl 5x first strand buffer, 4 µl 0.1 M DTT, 4 µl of 100 ng/µl dNTP and 0.5 µl of RNAsin (Invitrogen) was added to each sample and incubated at 37 °C for 2 minutes. Prior to addition of the reverse transcriptase, a 2 µl aliquot was taken to serve as a negative control. MMLV reverse transcriptase (Invitrogen) was added to the samples according to the manufacturer's protocol and samples and controls were incubated at 37 °C for 1 hour. The presence of cDNA was confirmed through PCR as described in section 2.1.1 using an annealing temperature of 55 °C. PCR was conducted using generated cDNA and negative controls

using exon spanning β-actin primers. Products were separated using gel electrophoresis on a 2% agarose gel containing 0.5 µg/ml Ethidium Bromide and visualised using a UV light transilluminator (Uvitec). 1 kb DNA ladder was used as a size standard. Having confirmed the presence of cDNA in samples and absence from controls, cDNA was diluted to the required concentrations and stored at -20 °C.

2.4.3 Quantitative real-time PCR (qPCR)

Primers were designed for target genes using Primer 3 (http://primer3.ut.ee/). Primers were designed to produce an amplicon of 90-150 bp and where possible, to cross exon-exon boundaries to prevent genomic contamination. Prior to use, primers were tested on serial dilutions of cDNA to generate a standard curve and calculate primer efficiency. Once tested, qPCR was conducted as previously described in section 2.3.3. Genes were tested using cDNA generated from E11.5 *Trp63*$^{+/+}$ and *Trp63*$^{-/-}$ facial processes in triplicate across five biological replicates. cDNA was normalised relative to the house keeping gene *β-actin* and changes in gene expression calculated via the $2^{\Delta\Delta CT}$ method. Statistical significance was assessed using the Mann Whitney U test. All primer sequences used can be found in Appendix 2.

2.5 Whole mount *in situ* hybridisation

Prior to use, sense probes were generated and tested.

2.5.1 Riboprobe preparation

Primers for riboprobe generation were designed using Primer 3 (http://primer3.ut.ee/). Primers were designed to produce an amplicon of 450-1000 bp and where possible to cross exon-exon boundaries. Once designed, primers were modified to include either RNA polymerase recognition sites, or restriction enzyme site. Probes were generated by two methods, through bacterial amplification and by PCR amplification. Primer sequences for all probes generated can be found in Appendix 3.

Probe templates were generated via PCR as previously described (Section 2.1.1) using an annealing temperature of 55 °C. Products were separated using gel electrophoresis on a 1.5% agarose gel containing 0.5 µg/ml Ethidium Bromide. 1 kb ladder was used as a size standard. Bands of the appropriate size were gel extracted using the Qiagen gel extraction kit (Qiagen) according to the manufacturer's protocol and eluted in dH_2O. PCR templates were stored at -20 °C.

2.5.2 Plasmid template ligation

The pBlueScript II expression vector was used for bacterial amplification (Agilent Technologies). Plasmids and inserts were digested with an appropriate restriction enzyme and purified using a QIAquick PCR purification kit (Qiagen) according to the manufacturer's

protocol. Purified insert and vector were combined in a 1:3 (vector: insert) ratio in a 0.5 ml Eppendorf. Mixes were heated to 45 °C for 5 minutes before cooling on ice for 5 minutes. Reaction volume was made up to 10 µl with 0.5 µl of T4 DNA ligase to a final concentration of 1x ligation buffer and 1 mM rATP. Samples were incubated overnight at room temperature before adding 90 µl dH_2O. Samples were stored at -20 °C.

2.5.3 DH5α cell transformations, using blue/white selection

Ligated plasmid was incubated with 50 µl of *E. Coli* DH5α competent cells (Invitrogen). Reaction mixes were incubated on ice for 45 minutes before heat shocking at 42 °C for 90 seconds. Samples were returned to ice and made up to 1 ml with LB (1% Tryptone, 0.5% Yeast Extract, 1% NaCl). Bacterial cultures were incubated at 37 °C for 1 hour with agitation (250 rpm). After incubation, 100 µl of bacterial culture was plated onto LB plates containing 50 µg/ml of ampicillin and 100 µl X-gal and incubated overnight at 37 °C. The following morning white colonies were selected and incubated in 10 ml LB containing 50 µg/ml ampicillin. Cultures were incubated overnight at 37 °C. The following morning plasmids were extracted using a QIAprep spin miniprep kit (Qiagen) according to the manufacturer's instructions. 1 µg of plasmid was digested with the appropriate restriction enzyme and the products separated using gel electrophoresis on a 1.5% agarose gel containing 0.5 µg/ml Ethidium Bromide. Bands were visualised using a UV light transilluminator (Uvitec) and 1 kb DNA ladder was used as a size standard. Having confirmed insert size, plasmid DNA was sequenced to confirm insert identity as described in 2.6. Following confirmation of insert identity, 40 µg of plasmid containing insert was linearised through restriction digest with the appropriate restriction enzyme and the products separated through gel electrophoresis. The DNA band of appropriate size was extracted using the QIAquick gel extraction kit (Qiagen) according to the manufacturer's protocol. Linearised plasmid was eluted in dH_2O and diluted to a stock concentration of 1 µg/µl. Linearised plasmid was stored at -20 °C.

2.5.4 Generation of riboprobes

For anti-sense probe generation, the following 25 µl reaction mix was utilised: 1x transcription buffer (Promega), 10 mM dithiothreitol (DTT) (Promega), 1x digoxigenin-UTP RNA labelling mix (Roche), 1.5 µg linearised plasmid/PCR probe template, 40 units of the appropriate T3 or T7 RNA polymerase (Promega) and made to volume with dH_2O. Samples were incubated at 37 °C for 2 hours. A control aliquot was taken and the remaining reaction was treated with 20 units of DNase I and incubated at 37 °C for 45 minutes. Following incubation a sample aliquot was taken and separated simultaneously with the control aliquot through gel electrophoresis on a 1.5% agarose gel containing 0.5 µg/ml Ethidium Bromide. Bands were visualised using a UV light transilluminator to confirm insert presence and the digestion of the DNA template/plasmid DNA. Probe was precipitated through the addition of 70 µl dH_2O, 10 µl 4 M LiCl, 8 µl 0.2 M EDTA and 250 µl 100% EtOH and incubation at -80 °C overnight. The following morning probes were centrifuged at 13,000 rpm for 20 minutes

at 4 °C and the supernatant discarded. Pellets were washed with 70% EtOH and centrifuged at 13,000 rpm for 5 minutes at 4 °C. EtOH was removed and pellets were air-dried for 10 minutes at room temperature before re-suspension in 100 µl DEPC-dH_2O. Probes were stored at -80 °C.

2.5.5 Probe hybridisation

Where possible all glassware was baked over night at 180 °C and solutions were pre-treated with diethylpyrocarbonate (DEPC) and sterilised by autoclaving. Embryos were genotyped according to section 2.1.1. Each target gene was interrogated in triplicate, with each experiment consisting of a single *Trp63*$^{+/+}$ and *Trp63*$^{-/-}$ embryo processed simultaneously in a single 2 ml Eppendorf. An appropriate volume of each solution was used to ensure adequate embryo coverage. All washes were completed for 5 minutes at room temperature unless otherwise stated.

Embryos were rehydrated through sequential washes of a descending methanol/PBST series (100%, 75%, 50%, 25%, PBST). Once rehydrated embryos were washed twice with PBST before incubation for 15 minutes in 10 µg/ml Proteinase K (PBST) (Roche Diagnostics). Proteinase K digestion was halted through two washes of 2mg/ml glycine (PBST) and two washes of PBST. Embryos were re-fixed through 20 minute incubation with 0.2% glutaradehyde (4% PFA/ PBS) at room temperature. Once fixed samples were washed twice with PBST and prehybridised for 1 hour at 60 °C in hybridisation mix (50% formamide, 5x SSC pH 5.0, 50µg/ml heparin, 1% SDS). Following pre-hybridisation, embryos were incubated in fresh hybridisation mix and 2 µl of probe. Embryos were hybridised for 2 days at 60 °C.

2.5.6 Embryo processing

Samples were washed twice in solution 1 (50% formamide, 5x SSC pH 5.0, 1% SDS) for 30 minutes at 60 °C, followed by a single wash for 10 minutes at 60 °C in a 1:1 mix of solution 1 and solution 2. Embryos were further washed twice in solution 2 (0.5M NaCl, 10 mM Tris HCl pH 7.5, 0.1% Tween 20) for 30 minutes at 37 °C and twice in solution 3 (50% formamide, 2x SSC pH 5.0) for 30 minutes at 60 °C. Embryos were then pre-blocked in 10% heat-inactivated lamb serum (HILS) in TBST with 2 mM levamisole for 90 minutes at room temperature.

Antibody solution was generated as such. 0.009 g of embryo powder was suspended in 1.5 ml TBST and heated at 70 °C for 30 minutes. The solution was cooled on ice and HILS (10%) and 3 µl (0.75 Units/µl) antidigoxygenin antibody coupled to alkaline phosphatase (Roche Diagnostics) were added. The solution was incubated for 1 hour on ice before being centrifuged for 10 minutes. The supernatant was removed and used to make the following antibody solution (10% levamisole, 25% supernatant, 10% HILS).

Blocking HILS was removed from samples and embryos were incubated over night at 4 °C in antibody solution. The following morning embryos were initially washed three times with 2 mM levamisole (TBST) for 5 minutes followed by a further five washes of 2 mM levamisole (TBST) for 1 hour each. Embryos were then stored at 4 °C overnight.

2.5.7 Antibody detection

Embryos were incubated in the detection agent BM purple alkaline phosphatase substrate (Roche Diagnostics) at 4 °C until the desired level of staining was achieved. Once developed to the required extent, embryos were repeatedly washed in TBST at 4 °C. For long term storage, embryos were re-fixed in 4% PFA (TBST). Embryos were photographed using a Leica DMRB photomicroscope using Leica digital photographic software.

2.6 Sanger sequencing

For insert sequencing the following 10 µl reaction mixture was utilised: 500 ŋg of DNA was incubated with 2 µl of Big Dye Terminator Ready Reaction Mix v3.1 (Applied Biosystems) and 1.6 pmol of primer. Samples were placed into a Verity 60 well thermal cycler (Applied Biosystems) and incubated through the following protocol: 96 °C for 4 minutes, 25 cycles of 96 °C for 30 seconds, 50 °C for 15 seconds and 60 °C for 4 minutes. Reactions were then diluted to 100 µl and precipitated in 10 µl 3 M sodium acetate pH 5.0, 200 µl 100% ethanol and 1 µl Glycoblue (Ambion). Reactions were vortexed and placed on ice for 30 minutes. Following incubation, reactions were centrifuged at 13,000 rpm for 15 minutes and the supernatant discarded. Pellets were washed with 70% ethanol and air-dried at room temperature for 10 minutes. Samples were transported to the University of Manchester DNA sequencing Facility, Faculty of Life Sciences. Chromatograms were analysed using Chromas software.

Chapter 3 Identification of potential P63 target genes

3.1 Introduction

The aim of this project was to identify novel targets of P63 regulation during the development of the upper lip and primary palate. The outcome of this research contributed both to expanding the current knowledge of the P63 signalling network and identifying genes which may play a role in the pathogenesis of cleft lip/palate in P63 related conditions. P63 functions as a transcription factor and has been demonstrated to both induce and repress transcription of target genes (Yang *et al*. 1998; Serber *et al*. 2002). Using model organisms of *Trp63* knockouts, the roles of P63 during development have begun to be unravelled (Thomason *et al*. 2006). Human mutations in *TP63* are known to induce conditions which commonly feature cleft lip and palate as a phenotype (Rinne *et al*. 2007). As such a great deal of research into P63 function has focused on its role in secondary palate development. In contrast however the role of P63 in upper lip and primary palate development remains largely unknown (Thomason *et al*. 2008; Ferretti *et al*. 2011). It is known that P63 is required for correct formation of the upper lip, with a loss of P63 signalling leading to a cleft lip phenotype in *Trp63*$^{-/-}$ mouse models (Mills *et al*. 1999; Yang *et al*. 1999). However, many of the transcriptional targets of P63 during lip morphogenesis remain unidentified.

The use of chromatin immunoprecipitation followed by deep sequencing (ChIP-Seq) provides a powerful tool for the *in vivo* determination of protein/ DNA interaction sites (Albert *et al*. 2007). The use of ChIP-Seq was first reported by Pugh's group in their investigation of nucleosomal elements within *Saccharomyces cerevisiae* (Albert *et al*. 2007). ChIP-Seq involves the extraction of chromatin from a chosen population of cells. DNA binding proteins are cross-linked to DNA before cells are disrupted by chemical or mechanical means (Figure 3.1A&B). Chromatin is fragmented and an antibody to the chosen target protein used to isolate bound sequences of DNA (Figure 3.1C) (Bailey *et al*. 2013). Bound fragments are then sequenced and computationally mapped against the genome (Figure 3.1D) (Bailey *et al*. 2013). The use of ChIP-Seq analyses allows the identification of the active binding sites of a chosen protein, on a genome wide scale. It therefore provides a powerful research tool in the study of transcription factor function. As such ChIP-Seq was used to identify P63 specific binding sites active during lip morphogenesis (Bailey *et al*. 2013).

Previous studies into the roles of P63 during development have made use of ChIP-Seq to high degrees of success (Kouwenhoven *et al*. 2010; McDade *et al*. 2012). Previous work by the McDade group identified in excess of 7500 P63 binding regions using ChIP-Seq on human neonatal foreskin (McDade *et al*. 2012). Gene ontology analysis of the identified sites showed enrichment for cleft palate genes (McDade *et al*. 2012). A similar study by the Zhou and Van Bokhoven groups identified in excess of 11,000 putative P63 binding sites using ChIP-Seq of adult human primary keratinocytes (Kouwenhoven *et al*. 2010). The group identified a P63 binding site SHFM1-BS1 which was shown to regulate *DLX5/DLX6* during

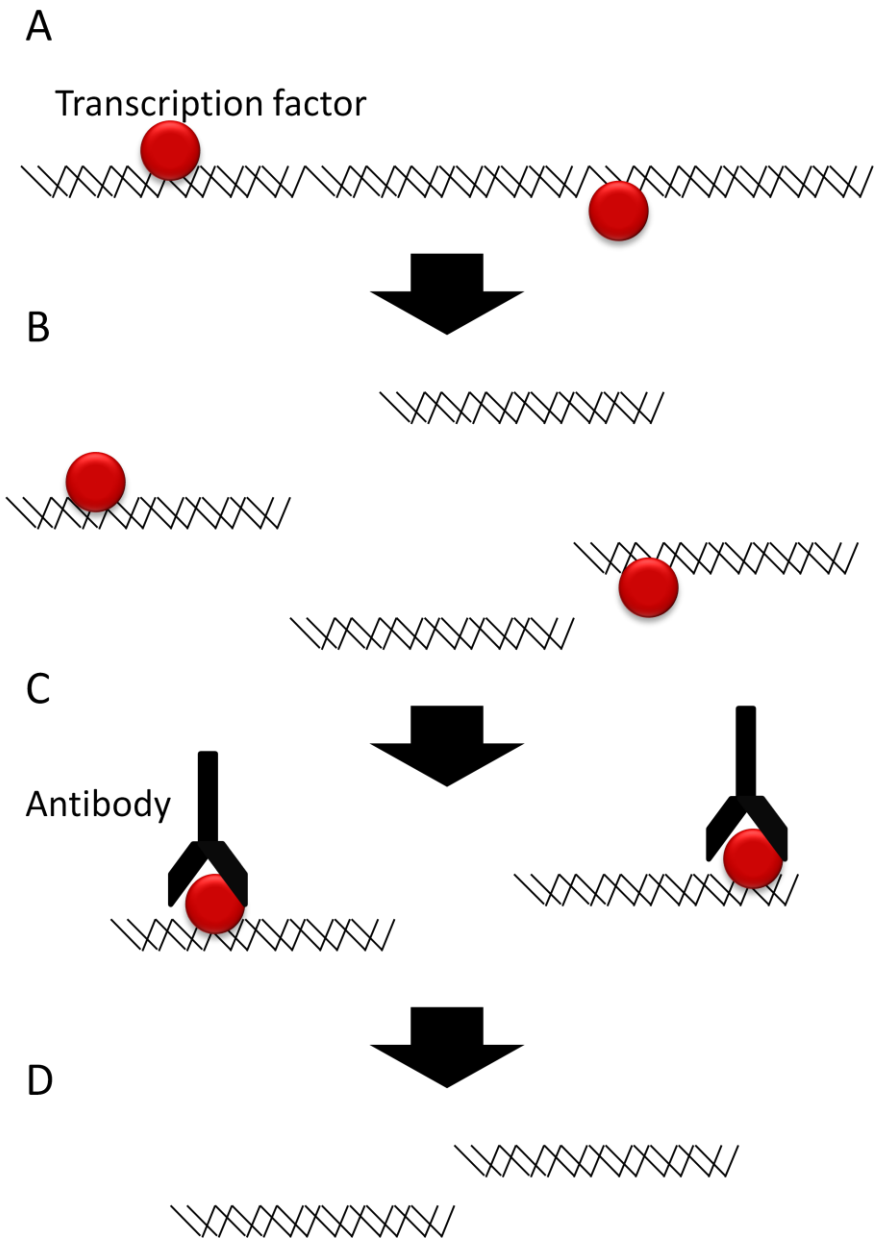

Figure 3.1 Chromatin immunoprecipitation work flow. (**A**) Proteins are cross-linked to DNA through incubation with formaldehyde. (**B**) Chromatin is extracted from cells and disrupted through chemical or mechanical means to generate fragments of the required size. (**C**) Antibodies specific for the protein of interest are used to isolate protein-bound fragments. (**D**) Isolated fragments are de-cross-linked to remove protein and antibodies. DNA is purified and can subsequently be used for sequencing or PCR analysis.

limb development, and deletions within this region contributed to the incidence of SHFM (Kouwenhoven *et al*. 2010). Furthermore in mouse models of *Trp63* knockout, *Dlx5*/*Dlx6* expression was found absent from the AER (Kouwenhoven *et al*. 2010). However *Dlx5*/*Dlx6* expression was found to be unaffected during orofacial development of *Trp63* knockout models suggesting that P63 regulation is tissue specific (Kouwenhoven *et al*. 2010). Genome wide scanning for the P63 binding motif in humans identified in excess of 1 million potential binding sites (Sethi *et al*. 2014). However both of the aforementioned studies identified P63 binding at a fraction of these sites (Kouwenhoven *et al*. 2010; McDade *et al*. 2012). Taken together these results underpin the requirement to use stage appropriate tissue to investigate P63 regulation. To this author's knowledge no studies have made use of ChIP-Seq on stage appropriate tissue to investigate the role of P63 in upper lip morphogenesis. It was therefore sought to characterise the transcriptional targets of P63 using ChIP-Seq techniques with tissue from E11.5 facial processes (Figure 3.2). E11.5 is a critical stage during lip morphogenesis due to the expansion of the facial processes in addition to the contact and adhesion of the medial nasal processes and lateral nasal processes (Jiang *et al*. 2006). Furthermore expression analysis has shown *Trp63* is widely expressed at E11.5 throughout the ectoderm of the facial processes (Thomason *et al*. 2008).

ChIP-Seq analyses of E11.5 facial processes identified in excess of 10,000 potential P63 binding sites, 83% of which were shown to contain the P63 specific binding motif. The presence of the P63 binding motif within the majority of identified sites served as validation that the data generated was accurate. The presence of a ChIP-Seq binding site is not directly indicative of biological activity. Furthermore, the quality of the data set generated is reliant upon antibody efficiency (Bailey *et al* 2013). Therefore an expression data set was generated from stage appropriate tissue from *Trp63*$^{+/+}$ and *Trp63*$^{-/-}$ facial processes. Microarray expression analysis was conducted on mRNA isolated from E11.5 and E12.5 facial processes, identifying in excess of 1400 genes as significantly differentially regulated ($p= 0.05$). Microarray data sets were validated using qPCR prior to data set intersections. Intersections between these data sets generated a list of differentially regulated genes proximal to putative binding sites.

DAVID and GREAT functional analysis of the generated data identified functional clustering within adhesion molecules, regulation of apoptosis, Wnt signalling, Fgf signalling and Shh signalling in addition to genes involved in cleft lip and cleft palate. A target gene list of 71 genes was generated based upon functional analysis of genes differentially regulated between *Trp63*$^{+/+}$ and *Trp63*$^{-/-}$ facial processes with a P63 peak within 150 kb of their transcriptional start site. A summary of the two-tiered approach adopted for this project can be seen in Figure 3.3.

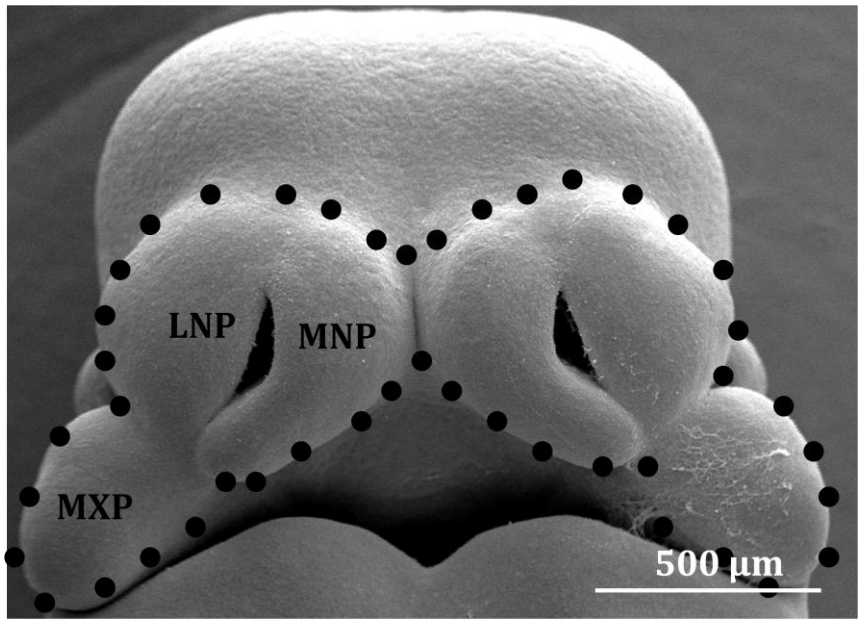

Figure 3.2 Dissection of E11.5 facial processes. Whole facial processes were dissected from E11.5 wildtype embryos. Incisions were made at the inferior aspects of the maxillary processes. Incisions were extended along the superior boundaries of the lateral nasal and medial nasal processes until facial processes were fully separated from embryos. LNP – lateral nasal processes, MNP – medial nasal processes, MXP – maxillary processes. Scale bar denotes 500 µm. (Adapted from Thomason *et al*. 2008).

Identification of P63 binding sites within E11.5 facial processes

ChIP-Seq – E11.5 facial processes

Detection of the P63 specific binding motif via P63 Scan

Gene ontology analysis via GREAT analysis

Identification of differentially regulated genes between *Trp63*$^{+/+}$ and *Trp63*$^{-/-}$ E11.5 and E12.5 facial processes

Microarray expressional analysis E11.5 & E12.5

Validation of results via Real-time PCR

Gene ontology analysis via DAVID functional annotation

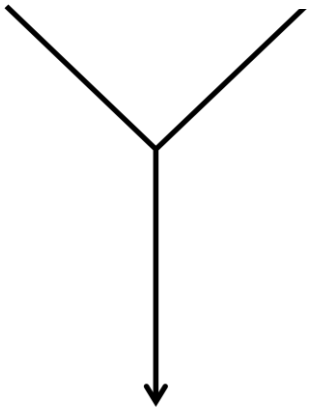

Identification of target genes for further investigation

Intersection of differentially regulated genes (P= 0.05) against P63 binding sites (≤150kb)

Gene ontology analysis via GREAT analysis

Target prioritisation based upon functional annotations

Figure 3.3 A two-tiered research approach. To identify targets of P63 regulation during lip morphogenesis, ChIP-Seq was used to determine sites of P63 binding in chromatin isolated from wildtype E11.5 facial processes. Identified peaks were validated using ChIP-qPCR and intersection against a previously validated E14 palatal shelf ChIP-Seq data set (Mitchell *et al*. 2014). To identify targets of P63 regulation, microarrays were completed on E11.5 and E12.5 *Trp63*$^{+/+}$ and *Trp63*$^{-/-}$ facial processes. Results of the microarray analysis were validated using qPCR. Gene ontology analysis was conducted on each data set, prior to intersection using GREAT and DAVID. Differentially regulated genes (p= 0.05) were intersected against the identified P63 binding sites with a maximum peak to TSS distance of 150 kb. Gene ontology analysis was then used in the prioritisation and generation of a target gene list (n= 71) for further investigation.

3.2 Materials and Methods

3.2.1 E11.5 ChIP-Seq

E11.5 facial processes from *CD1* wt embryos (n= 69) were dissected and processed as previously described (Chapter 2.3). ChIP reactions (n= 11) were completed and efficiencies assessed as previously described (Chapter 2.3.3). Following qPCR, ChIP samples were pooled and concentrated to 50 µl (3.6 ng/µl) and transported to the laboratory of Dr. J. H Zhou (UMC St Radboud, Nijmegen, Netherlands) for sequencing. Initial bioinformatic analysis was conducted by the Zhou group with ChIP-Seq peaks displayed on a custom UCSC tack (http://genome.ucsc.edu/cgi-bin/hgTracks?hgS_doOtherUser=submit&hgS_otherUserName=Jozhou&hgS_otherUserSessionName=mm9_palatal_shelves_201202) (July 2007 NCBI37/mm9).

3.2.2 ChIP-qPCR validation and establishment of the MVS

41 prospective P63 binding sites were selected for validation using ChIP-qPCR. E11.5 facial processes from *CD1* WT embryos were dissected and processed as previously described (Chapter 2.2.1). ChIP-reactions were completed as previously described (Chapter 2.3). ChIP efficiency of candidate binding sites was calculated using percentage of immunoprecipitated DNA against input chromatin. Occupancy used in ChIP experiments was calculated using ChIP efficiency of selected regions was calculated relative to the negative control, a region within exon 2 of *Myoglobin*, where P63 does not bind. Statistical significance was assessed using the Students T-test. For each candidate region, ChIP-qPCR was completed in triplicate across biological replicates. Primers for each region were designed using Primer3 (Koressaar & Remm, 2007; Untergrasser *et al*. 2012). Primers for candidate regions can be seen in Appendix 1.

3.2.3 E11.5 and E12.5 microarray analysis

Facial processes were dissected from *Trp63 BalbC* embryos of appropriate age (E11.5 – E12.5) for both *Trp63*$^{+/+}$ (n= 3) and *Trp63*$^{-/-}$ (n= 3). mRNA was isolated using the RNeasy minikit (Qiagen) according to the manufacturer's instructions. Two time points of lip morphogenesis were assessed, E11.5 during facial process fusion and E12.5, post fusion of the facial processes in *Trp63*$^{+/+}$ embryos. Isolated mRNA was sent to the University of Manchester Core Technology Facility for microarray analysis (Affymetrix Genechip Mouse Exon 1.0 ST Array). Initial Bioinformatics analysis was conducted by Dr. Leo Zeef (Faculty of Life Sciences, University of Manchester). Principle component analysis (PCA) was performed using the princomp function from the R package 'stats'.

3.2.4 Quantitative PCR (qPCR)

Facial processes were dissected from E11.5 *Trp63 BalbC* E11.5 embryos for *Trp63*$^{+/+}$ and *Trp63*$^{-/-}$ as previously described (Chapter 2.2.1). RNA was extracted as previously described

(3.2.3) and cDNA generated according to the manufacturer's instructions (Invitrogen). For each candidate gene (n= 16), qPCR was conducted as previously described (Chapter 2.4.3) in triplicate across five *Trp63*$^{+/+}$ *and Trp63*$^{-/-}$ biological replicates. cDNA was normalized relative to the house-keeping gene *β-actin*. Differences in relative transcript expression between *Trp63*$^{+/+}$ and *Trp63*$^{-/-}$ samples were calculated via the $2^{\Delta\Delta CT}$ method and statistical significance was assessed using the Mann Whitney U test. Primers were designed using Primer3 (Koressaar & Remm, 2007; Untergrasser *et al*. 2012). To further control for genomic contamination where possible primers were designed to cross exon-exon boundaries. Primers are listed in Appendix 2.

3.2.5 Gene ontology analysis

For ChIP-Seq gene ontology analysis, GREAT analysis was used (McLean *et al*. 2010). ChIP-Seq data was analysed using the Mouse: UCSC mm9 species assembly using either the entire genome as the expressional data set or the generated microarray data sets. Maximum peak to gene association distance was set at 150 kb for all analysis. Gene ontology analysis for microarray data sets was conducted using the DAVID bioinformatics resource (Huang *et al*. 2009a; Huang *et al*. 2009b). Candidate gene lists were uploaded to the DAVID webtool and analysed using the mouse whole genome as the background expressional data set. Analysis was conducted using default association settings.

3.2.6 Other bioinformatics analysis

Identification of genes common between microarrays was completed using the webtool "Compare two lists" (Whitehead Institute for Biomedical Research). Gene lists were compared using default settings. ChIP-Seq to expressional data set intersections were completed using the Galaxy/Centaurus RnaChipIntegrator tool (University of Manchester Bioinformatics Core Facility). Analysis was completed with a maximum distance from peak to TSS of 150 kb, identifying nearest gene to candidate peak. ChIP-Seq peak overlap between ChIP-Seq data sets was conducted using the Galaxy/Centaurus BED tools Count intervals in one file overlapping intervals in another file tool (University of Manchester Bioinformatics Core Facility). Analysis was conducted using default settings.

3.3 Results

3.3.1 E11.5 ChIP-Seq analysis

Facial processes were dissected from E11.5 *CD1* wild-type embryos and chromatin isolated. Following evaluation, 11 ChIP reactions were completed. Resultant chromatin was purified and library preparation completed before samples were transported to Nijmegen for ChIP-Seq. Initial peak calling using the MACS software version 1.3.7 was performed in Nijmegen. 41 randomly selected peaks were chosen for further interrogation using ChIP-qPCR to establish a minimum validation score (MVS). The 41 binding sites were validated using ChIP-qPCR in E11.5 facial processes dissected from *CD1* wild-type embryos.

For each binding site, an average occupancy relative to the negative control myoglobin was calculated using the $2^{\Delta\Delta CT}$ method. Binding sites were deemed to display positive enrichment with a relative occupancy greater than threefold that of the negative control myoglobin. Significance was calculated using the paired student's t-test. Of the 41 binding sites assayed, 39 displayed a relative occupancy greater than three-fold that of myoglobin ($P \leq 0.05$) (Figure 3.4). The 39 peaks which displayed positive enrichment were used to generate a MVS based upon their MACS scores. Applying the MVS of 58.19, 10,209 P63 binding sites were identified (Appendix 4). Peak calling analysis identifies the edges of protein binding locations, but not the precise site of protein DNA interaction (Zhang *et al*. 2008). Therefore the 10,209 binding sites were further interrogated using p63 scan software (Figure 3.5A). Each prospective binding site was scanned for the presence of the P63 specific binding motif (Figure 3.5B). Use of p63 scan showed 83.9% of identified binding sites contained the binding motif (Figure 3.5C).

3.3.1.2 ChIP-Seq whole genome intersection

ChIP-Seq data was intersected against the mouse genome to identify genomic coverage. Furthermore to determine optimal peak/gene distance for future analysis, intersections were completed with maximum peak distances of 25 kb, 50 kb, 75 kb, 100 kb, 125 kb and 150 kb (Table 3.1). ChIP-Seq peaks were intersected against the entire mouse genome using the galaxy RNAChIPIntegrator to identify the nearest transcript to each peak. At a maximum distance of 150 kb, 8131 transcripts were found proximal to P63 peaks. Furthermore 1177 peaks were found to overlap gene promoters (Figure 3.4). It is important to note that the presence of a P63 peak proximal to a gene does not imply biological activity. Therefore further analysis was completed incorporating P63 expression data.

3.3.1.3 Identifying functional trends within the E11.5 ChIP-Seq

To identify functional trends within the ChIP-Seq data set, GREAT was used to interrogate the data set. GREAT analysis was completed on the entire E11.5 ChIP-Seq data set using

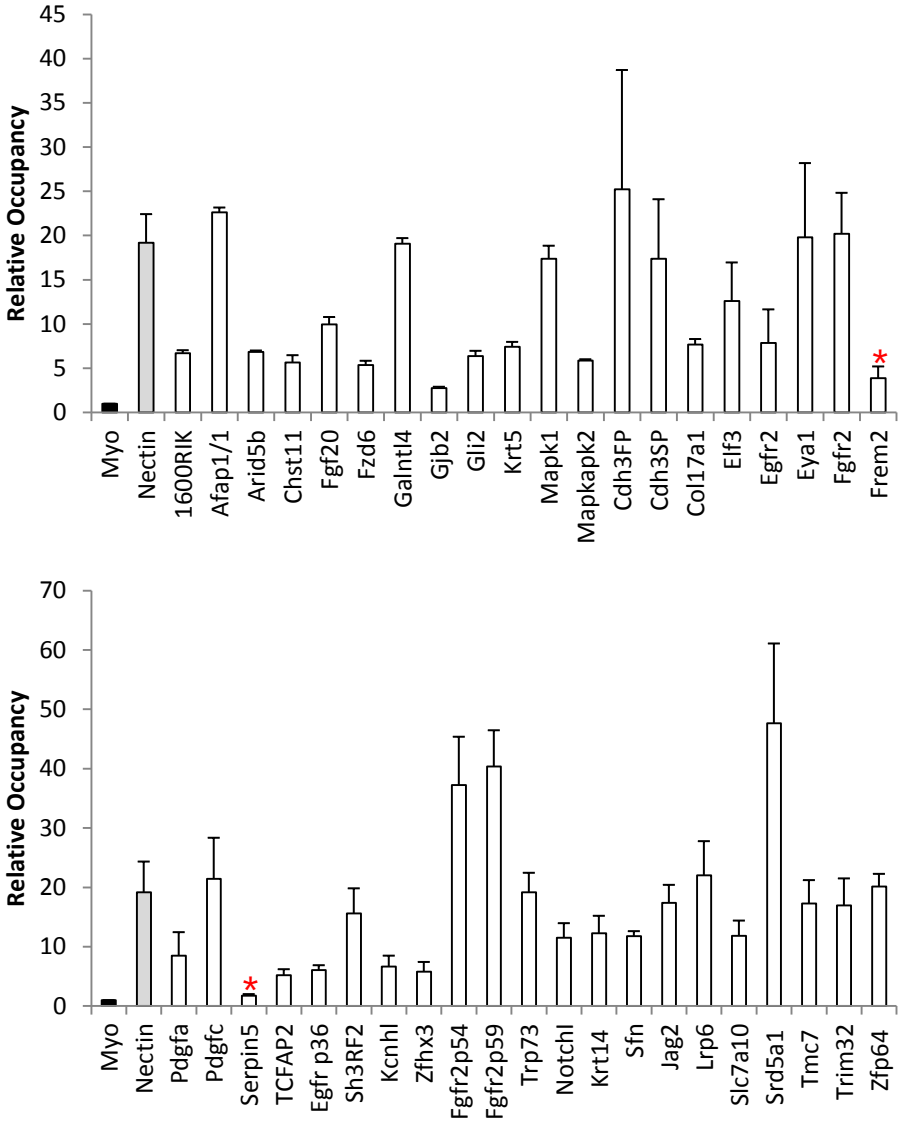

Figure 3.4 ChIP-qPCR validation of ChIP-Seq targets. ChIP-qPCR was conducted on 41 randomly selected potential P63 binding sites. Relative occupancy was calculated via the $2^{\Delta\Delta CT}$ method relative to the negative control *Myoglobin* (black). *Nectin1* (grey), a known P63 target, was used as a positive control. Binding sites with a relative occupancy greater than three-fold *Myoglobin* were deemed to display positive enrichment. Of the 41 sites, 39 displayed positive enrichment with sites proximal to *Frem2* and *Serpinb5* failing to show enrichment (marked). Error bars represent calculated standard error of the mean.

A

	Number of Peaks Identified
ChIP-Seq total	10209
P63-positive	8565

B

C

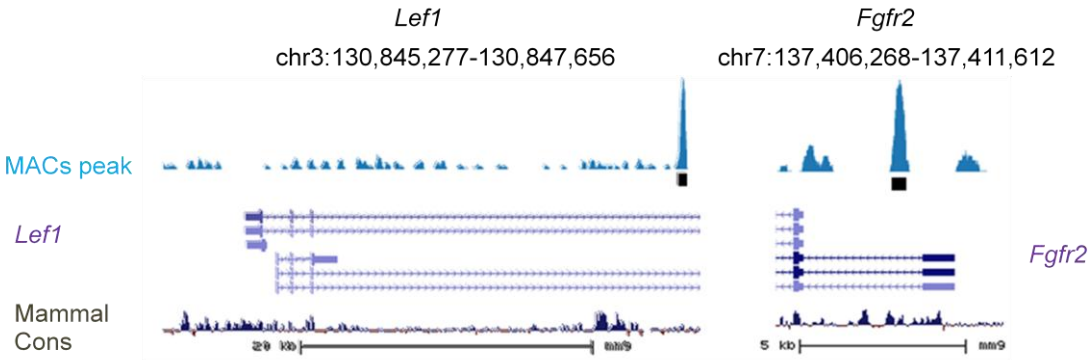

Figure 3.5 ChIP-Seq analysis of wildtype E11.5 facial processes identified 10209 putative P63 binding sites. (**A**) ChIP-Seq analysis identified a large number of putative P63 binding sites active during upper lip morphogenesis. Peak heights of 39 previously validated, positively enriched P63 binding sites were used to establish a minimum validation score of 58.19, identifying 10209 putative binding sites. (**B**) P63 Scan using the characterised P63 binding motif identified 8565 binding sites as P63 motif-positive and 1644 as P63 motif-negative. (**C**) The ChIP-Seq data set was visualised on a custom UCSC track, with peaks proximal to *Lef1* and *Fgfr2* identified.

Maximum Distance	Nearest TSS per peak (nearest 1)
25 kb	3972
50 kb	5643
75 kb	6672
100 kb	7353
125 kb	7790
150 kb	8131

Table 3.1 Results of the serial intersection of E11.5 ChIP-Seq data set against the mouse whole genome.

Number of intersected genes identified (nearest single gene per peak) at maximum peak distances of 25 kb to 150 kb.

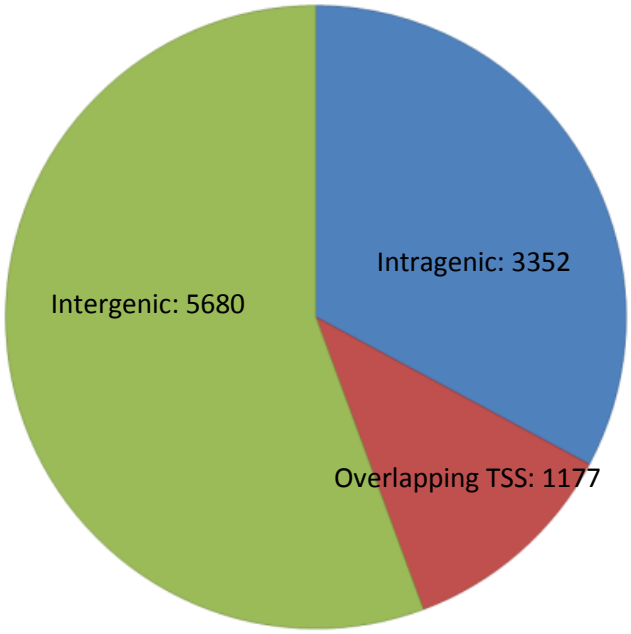

Figure 3.6 Whole genome intersection of E11.5 ChIP-Seq. To determine the optimal maximum peak to TSS intersection distance to use for further analysis, serial intersections were made of the ChIP-Seq data set against the mouse whole genome using the Galaxy/Centaurus RNAChIPIntergrator tool identifying nearest gene. Integration distance was increased by increments of 25 kb up to a maximum of 150 kb. At the maximum distance of 150 kb, 8131 peak to gene intersections were recorded with 1177 peaks shown to overlap with gene TSSs, 3352 were shown to be intragenic and the remaining 5680 intergenic. The maximum intersection distance of 150 kb was chosen to maximise genome coverage.

recommended settings with the mouse genome (mm9) as the expression background. GREAT analysis output includes multiple categories including GO molecular function, GO biological process, GO cellular component, mouse phenotype, human phenotype, disease ontology, MSigDB pathway, MGI expression and InterPro. A summary of GREAT analysis output can be seen in Table 3.2, for full GREAT analysis see Appendix 4. ChIP-Seq peaks were found proximal to 35% of all mouse genes. Therefore analysis at this level only identified broad trends within the data and further in-depth analysis was completed.

GO biological process analysis identified enrichment in multiple expected P63 processes. Enrichment was observed within functions including signal transduction by p53 class mediator, regulation of intrinsic apoptotic signalling, skin morphogenesis, limb bud formation, hair follicle morphogenesis and epidermis morphogenesis. Furthermore both human and mouse phenotype analysis identified enrichment within well characterised P63 functions including epidermis related terms including: thick epidermis, epidermal hyperplasia and abnormal epidermis stratum corneum morphology, abnormality of the toenails, fine hair, fragile nails and split foot (Rinne *et al*. 2007). Disease ontology analysis identified genes related to cleft lip and cleft palate as highly enriched within the data set. MSigDB pathway analysis identified enrichment within validated targets of TAp63 and ΔNp63 isoforms further increasing confidence within the data set.

In addition to expected P63 related functions, enrichment within Wnt signalling terms was observed. InterPro analysis identified enrichment within seven terms, two of which, Wnt and Wnt protein conserved site, were associated with Wnt signalling. GO molecular function identified frizzled binding as the most significantly enriched term. Furthermore enrichment for the terms non-canonical Wnt receptor signalling pathway, Wnt receptor signalling pathway involved in heart development and negative regulation of non-canonical Wnt receptor signalling pathway was observed.

3.3.1.4 Conservation of P63 binding sites between E11.5 and E14

P63 has been shown to be required for both upper lip morphogenesis and formation of the secondary palate (Mills *et al*. 1999; Yang *et al*. 1999). Therefore to investigate the validity of the E11.5 ChIP-Seq data, the data set was intersected with a previously generated, validated, unpublished P63 ChIP-Seq data set conducted on E14 palatal shelves (Table 3.3) (Mitchell *et al*. manuscript in preparation). A list of all intersected binding sites can be seen in Appendix 4. ChIP-Seq intersection was completed using the Galaxy BED interval analysis tool. Of the 6293 E14 ChIP-Seq peaks, 2621 were shown to be present within the E11.5 data set. Therefore 7633 of the E11.5 ChIP-Seq binding sites were found to be unique to E11.5 and absent at E14. These data suggested that P63 displays tissue specific activity. Furthermore the overlap of 25% of the E11.5 ChIP-Seq peaks with the E14 data set provided further evidence that the data set is accurate.

	Term Name	Binom Rank	Binom Raw P-Value	Binom FDR Q-Val	Binom Observed Region Hits
GO Molecular function	Frizzled binding	70	3.46495e-9	1.72406e-7	56
	ephrin receptor binding	93	3.13286e-7	1.17331e-5	44
	cadherin binding	95	4.98374e-7	1.82720e-5	37
	repressing transcription factor binding	100	8.99536e-7	3.13308e-5	54
GO Biological process	signal transduction by p53 class inhibitor	579	5.80024e-9	1.00738e-7	66
	regulation of intrinsic apoptosis signalling	455	3.43813e-11	7.59866e-10	89
	skin morphogenesis	509	4.73950e-10	9.36355e-9	64
	limb bud formation	590	8.39473e-9	1.43080e-7	34
GO Cellular Component	cell-cell adherens junction	63	5.02702e-11	9.62315e-10	77
	desmosome	80	4.68775e-8	7.06678e-7	34
	hemidesmosome	87	3.02374e-7	4.19153e-6	18
	lateral plasma membrane	98	1.46597e-6	1.80404e-5	43
Mouse Phenotype	epidermal hyperplasia	232	1.51338e-18	5.17224e-17	119
	thick epidermis	281	8.32028e-16	2.34774e-14	124
	eyelids open at birth	319	3.10731e-14	7.72346e-13	132
	abnormal hair follicle development	381	9.09526e-13	1.89282e-11	103
Human Phenotype	abnormality of the nail	16	2.18122e-24	8.31045e-22	248
	fine hair	82	4.74156e-13	3.52494e-11	71
	fragile nails	195	3.61614e-9	1.13046e-7	25
	abnormality of the supraorbital ridges	228	2.79744e-8	7.47948e-7	72
Disease Ontology	head and neck squamous cell carcinoma	108	5.52966e-18	1.13102e-16	188
	cleft lip	186	1.57071e-9	1.86543e-8	79
	cleft palate	188	2.06566e-9	2.42715e-8	71
	intraepithelial neoplasm	139	2.69333e-14	4.28026e-13	101
PANTHER pathway	p53 pathway	5	5.97081e-11	1.80318e-9	91
	p53 pathway feedback loops 2	6	3.62638e-9	9.12640e-8	60
MSigDB Pathway	Genes related to Wnt mediated signal transduction	5	7.04383e-16	1.85816e-13	127
	Validated transcriptional targets of TAp63 isoforms	6	2.94010e-15	6.46332e-13	77
	p73 transcription factor network	34	2.34404e-9	9.09350e-8	71
	Validated transcriptional targets of deltaNp63 isoforms	35	2.91356e-9	1.09800e-7	64
	Wnt signalling network	58	3.40386e-7	7.74084e-6	46
MGI expression detected	TS23_skin	319	1.43449e-32	4.21802e-31	291
	TS11_embryo ectoderm	385	8.33303e-28	2.03023e-26	246
	TS23_primary palate	2022	2.03734e-4	9.45115e-4	22
InterPro	Spectrin/alpha-actinin	20	1.00797e-8	4.81256e-6	54
	Spectrin repeat	27	2.53776e-8	8.97520e-6	45
	Wnt protein, conserved site	33	2.27104e-7	6.57156e-5	32
	Wnt	33	2.27104e-7	6.57156e-5	32

Table 3.2 Gene ontology analysis of the E11.5 ChIP-Seq against mouse whole genome using GREAT analysis.

GREAT analysis of E11.5 ChIP-Seq. The table lists identified term, Binom rank, raw Binom p-value, adjusted FDR q-value and number of peaks associated with each term.

ChIP-Seq data set	E11.5	E14
Total number of peaks	10209	6293
Number of overlapping peaks	2576	2621
Number of unique peaks	7633	3672

Table 3.3 Summary of intersected P63 binding sites between the E11.5 and E14 P63 ChIP-Seq data sets.

Data shows the total number of peaks with each data set, in addition to the number of common and unique peaks.

ChIP-Seq data set	E11.5	P300 candidate sites
Total number of peaks	10209	4399
Number of overlapping peaks	162	161
Number of unique peaks	10047	4328

Table 3.4A Summary of intersected P63 binding sites between the E11.5 ChIP-Seq and identified P300 candidate facial enhancer sites.

Data shows the total number of peaks with each data set, in addition to the number of common and unique peaks.

ChIP-Seq data set	E11.5	Validated P300 enhancers
Total number of peaks	10209	280
Number of overlapping peaks	14	14
Number of unique peaks	10195	266

Table 3.4C Co-ordinates of the fourteen P63 binding sites found to overlap with validated P300 facial enhancer sites.

Identified peak co-ordinates in the format of chromosome number, starting bp and end bp in reference to the Mouse: UCSC mm9 species assembly.

Chromosome	Start	End
chr1	1.95E+08	1.95E+08
chr1	1.95E+08	1.95E+08
chr1	1.95E+08	1.95E+08
chr19	60091465	60091888
chr3	33804239	33804801
chr3	86654017	86654596
chr3	1.22E+08	1.22E+08
chr4	64098275	64098962
chr5	1.12E+08	1.12E+08
chr6	72167876	72168424
chr6	98064202	98064696
chr8	93828039	93829134
chr8	94070495	94071230
chr8	1.11E+08	1.11E+08

Table 3.4B Summary of intersected P63 binding sites between the E11.5 ChIP-Seq and validated P300 facial enhancer sites.

Data shows the total number of peaks with each data set, in addition to the number of common and unique peaks.

3.3.1.5 P63 co-localisation with P300

Previously generated data (unpublished) within the Dixon lab suggested that P63 may co-localise with the transcriptional co-activator P300 at enhancer sites. To test this hypothesis, the E11.5 ChIP-Seq was intersected against a recently published P300 database (Table 3.4A&B) (Attanasio *et al.* 2013). Axel's group identified 4399 potential P300 enhancer sites in E11.5 facial processes with 280 validated using transgenic analysis (Attanasio *et al*. 2013). Intersections were completed using the Galaxy BED interval analysis tool. Of the 4399 P300 sites, 3.7% (n= 161) displayed potential co-localisation with P63. Furthermore of the 280 P300 sites positively validated, 5% (n= 14) were shown to display potential co-localisation (Table 3.4C). However of the potential P63 binding sites only 1.6% were P300-positive. It therefore remains unclear if P63 and P300 directly interact during lip morphogenesis. All P300 intersected sites can be seen in Appendix 4.

3.3.2 Identifying targets of P63 regulation

3.3.2.1 E11.5 microarray

Having identified sites of P63 interaction in E11.5 facial processes, we investigated the change in gene expression between *Trp63*$^{+/+}$ and *Trp63*$^{-/-}$ embryos. E11.5 facial processes (n= 6) were dissected and mRNA isolated. 47 genes were identified as being differentially expressed at high significance (p= 0.005) of which 22 were found to be up-regulated and 25 down-regulated. 735 genes were found to be significantly (p= 0.05) differentially expressed, of which 251 were found to be up-regulated and 484 were down-regulated. Genes displaying the greatest fold change can be seen in Table 3.5 and include *Alg3*, *Perp*, *Fermt1*, *Aim2*, *Ece2*, *Trim29* and *Jag2*. Of the 735 genes identified, 55 were olfactory associated genes and were removed prior to further analysis.

Principle component analysis was completed on the full E11.5 microarray data set (Figure 3.7). PCA analysis showed that while the *Trp63*$^{-/-}$ samples broadly clustered together, separation of *Trp63*$^{+/+}$ and *Trp63*$^{-/-}$ samples was sub-optimal with two of the *Trp63*$^{+/+}$ samples segregating with the nulls. The lack of clear segregation between *Trp63*$^{-/-}$/*Trp63*$^{+/+}$ samples may impact upon further analysis of the data set, reducing the relevance of the results obtained.

3.3.2.2 Identifying functional trends within the E11.5 microarray

To identify functional trends within the data set, gene ontology analysis was conducted using DAVID (Ver 6.7) (Huang *et al*. 2009a; Huang *et al*. 2009b). Initial analysis was conducted on the complete E11.5 (p= 0.005) data set, using default settings at medium stringency and mouse whole genome (mm9) as the expressional background (Table 3.6). 17 terms were enriched which segregated into 10 clusters. Terms associated with structural molecule

Gene Symbol	Chromosome	Fold-Change (wt vs. null)	p-value
Alg3	chr16	12.2659	6.90E-08
Perp	chr10	-3.84293	4.16E-06
Fermt1	chr2	-2.99993	3.60E-05
Aim2	chr1	3.09714	8.36E-05
Ece2	chr16	2.32253	0.0001
4930518C04Rik	chr14	2.05541	0.000302
Cbr2	chr11	-1.93372	0.000418
Trim29	chr9	-1.72185	0.000473
Olfr943	chr9	-2.17433	0.000741
Gm9919	chr10	-1.97541	0.000748

Table 3.5 Differentially regulated genes between E11.5 *Trp63*$^{+/+}$ and *Trp63*$^{-/-}$ facial processes.

The top 10 most significantly differentially regulated genes identified. Genes are identified by gene symbol, with chromosome, average fold change (wildtype vs. null) with up-regulated genes (green) and down-regulated genes (red) and associated p-value.

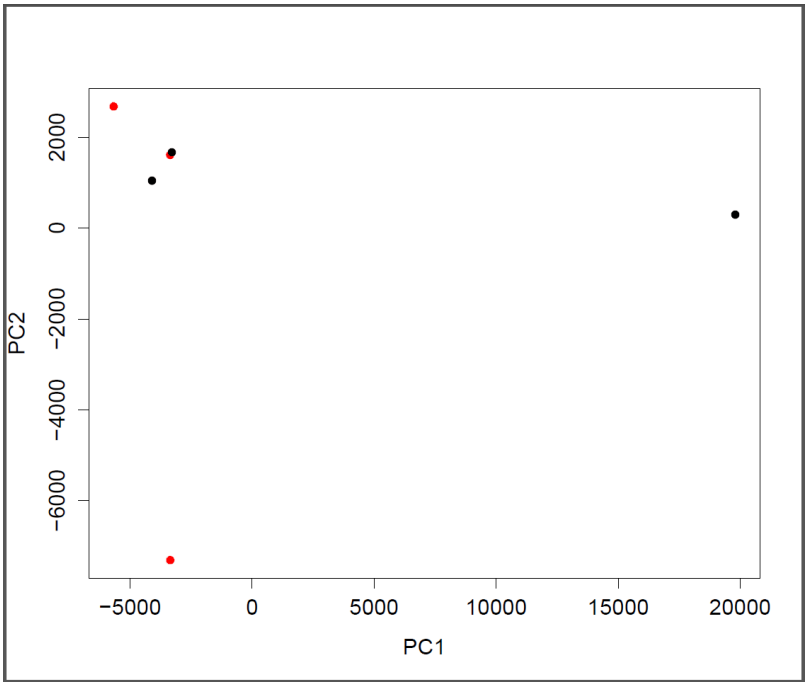

Figure 3.7 E11.5 microarray PCA analysis. PCA analysis failed to show clear segregation between wt and null samples, with clustering of WT (n= 2) and null (n= 2) samples observed based up both PC1 and PC2. Graph axes denote principle component 1 (PC1) and principle component 2 (PC2). Wildtype samples are black, nulls are red.

Category	Term	Count	p-Value
GOTERM_MF_FAT	GO:0005198~structural molecule activity	5	0.009333
GOTERM_CC_FAT	GO:0005887~integral to plasma membrane	5	0.022879
GOTERM_CC_FAT	GO:0031226~intrinsic to plasma membrane	5	0.025951
GOTERM_CC_FAT	GO:0070161~anchoring junction	3	0.026743
SP_PIR_KEYWORDS	nad	3	0.034613
GOTERM_CC_FAT	GO:0044459~plasma membrane part	8	0.044549
UP_SEQ_FEATURE	transmembrane region	13	0.046938
GOTERM_CC_FAT	GO:0005911~cell-cell junction	3	0.049789
GOTERM_MF_FAT	GO:0016620~oxidoreductase activity, acting on the aldehyde or oxo group of donors, NAD or NADP as acceptor	2	0.053202
GOTERM_CC_FAT	GO:0005886~plasma membrane	11	0.059435
GOTERM_CC_FAT	GO:0030054~cell junction	4	0.072403
SP_PIR_KEYWORDS	oxidoreductase	4	0.075852
GOTERM_MF_FAT	GO:0051287~NAD or NADH binding	2	0.079643
GOTERM_BP_FAT	GO:0007423~sensory organ development	3	0.080428
GOTERM_BP_FAT	GO:0007155~cell adhesion	4	0.082196
GOTERM_BP_FAT	GO:0022610~biological adhesion	4	0.082538
SP_PIR_KEYWORDS	transmembrane	14	0.091979

Table 3.6 E11.5 (p= 0.005) DAVID functional analysis.

Results show the 17 gene ontology terms identified within the E11.5 (p= 0.005) microarray data set ranked on p-value. Results are shown to include database/resource where terms originate (category), identified term, number of genes associated with the term and the modified Fisher Exact p-value, EASE score.

Category	Term	Count	p-Value
UP_SEQ_FEATURE	topological domain:Extracellular	79	2.30E-05
SP_PIR_KEYWORDS	disulfide bond	82	1.88E-04
SP_PIR_KEYWORDS	glycoprotein	110	2.81E-04
SP_PIR_KEYWORDS	membrane	156	3.13E-04
UP_SEQ_FEATURE	topological domain:Cytoplasmic	90	3.63E-04
GOTERM_BP_FAT	GO:0007155~cell adhesion	26	0.001018
GOTERM_BP_FAT	GO:0022610~biological adhesion	26	0.001049
UP_SEQ_FEATURE	transmembrane region	121	0.001124
UP_SEQ_FEATURE	disulfide bond	77	0.001167
SP_PIR_KEYWORDS	cell junction	20	0.001353
UP_SEQ_FEATURE	glycosylation site:N-linked (GlcNAc...)	103	0.001927
SP_PIR_KEYWORDS	glycolysis	6	0.002317
GOTERM_BP_FAT	GO:0016337~cell-cell adhesion	14	0.002871
GOTERM_BP_FAT	GO:0006096~glycolysis	6	0.003049
GOTERM_CC_FAT	GO:0030054~cell junction	22	0.004137
SP_PIR_KEYWORDS	cell adhesion	18	0.005336
GOTERM_BP_FAT	GO:0019320~hexose catabolic process	6	0.006302
GOTERM_BP_FAT	GO:0006007~glucose catabolic process	6	0.006302
GOTERM_BP_FAT	GO:0046365~monosaccharide catabolic process	6	0.007393
GOTERM_MF_FAT	GO:0022836~gated channel activity	14	0.007606
GOTERM_CC_FAT	GO:0005911~cell-cell junction	11	0.008338
KEGG_PATHWAY	mmu00010:Glycolysis / Gluconeogenesis	6	0.010932
SP_PIR_KEYWORDS	chromosomal protein	9	0.011295
GOTERM_BP_FAT	GO:0044275~cellular carbohydrate catabolic process	6	0.011444
GOTERM_MF_FAT	GO:0015267~channel activity	16	0.012015
GOTERM_MF_FAT	GO:0022803~passive transmembrane transporter activity	16	0.012015

Table 3.7 DAVID analysis of E11.5 up & down-regulated genes (p= 0.05).

Results show the top 25 gene ontology terms identified within the E11.5 (p= 0.05) microarray data set ranked on p-value. Results are shown to include database/resource where terms originate (Category), identified term, number of genes associated with the term and the modified Fisher Exact p-value, EASE score.

activity (n= 5, p= 0.009), integral to plasma membrane (n= 5, p= 0.023) and anchoring junction (n=3, p= 0.027) were identified as the most significantly enriched. Functional clustering was seen within terms associated with plasma membrane components (enrichment score = 1.45, p= 0.059), oxidation reduction (enrichment score: 1.16, p= 0.05), and cellular adhesion (enrichment score 1.05, p= 0.082).

Due to the relatively low number of results significant at P= 0.005, DAVID analysis was expanded to include results significant at p= 0.05 (Table 3.7). 146 Terms were enriched, with genes associated with glycoproteins (n= 110, p= 2^{-4}), membrane proteins (n= 156, p= 3^{-4}), cell adhesion (n = 26, p= 0.001), biological adhesion (n= 26, p= 0.001) and cell-cell adhesion (n=14, p= 0.005) displaying the greatest significance. 91 functional clusters were present within the data set and were ranked on enrichment score. Adhesion related genes (n = 84) displayed the greatest enrichment (enrichment score = 2.7). Functional clusters included plasma membrane associated genes (enrichment score= 2.7), glycoproteins (enrichment score = 1.78), genes associated with metabolic processes (enrichment score = 1.72), genes associated with ubiquitin-regulatory proteins (enrichment score = 1.47) and substrate binding proteins (enrichment score = 1.37). Furthermore KEGG pathway analysis identified enrichment for genes involved in glycolysis, ribosomes, neuroactive ligand-receptor interactions and hematopoietic cell lineage.

The data were further analysed to investigate what clusters existed in the up/down-regulated genes. Gene ontology analysis of down-regulated genes identified enrichment for 70 terms which segregated into 59 functional clusters (Table 3.8). The highest functional enrichment was observed within genes involved in glycolysis (n= 6, p= 2^{-4}), glucose catabolic process (n= 6, p= 5^{-4}), hexose catabolic process (n= 6, p= 5^{-4}), monosaccharide catabolic process (n= 6, p= 7^{-4}), cellular carbohydrate catabolic process (n=6, p= 0.001), epidermis development (n= 8, p= 0.001), alcohol catabolic process (n= 6, p= 0.002), ectoderm development (n= 8, p= 0.002), intermediate filament (n= 8, p= 0.003) and intermediate filament cytoskeleton (n= 8, p= 0.004). The functional cluster displaying the highest enrichment score included terms related to metabolic function (n= 70, enrichment score = 2.47).Further clustering was seen within terms related to cytoskeleton structure (enrichment score = 1.7), epithelial development (enrichment score = 1.39) and endoplasmic reticulum (enrichment score = 1.39). KEGG pathway analysis identified enrichment within the glycolysis pathway, ribosomal pathway, taste transduction and arachidonic acid metabolism.

Gene ontology analysis of up-regulated genes identified enrichment for 124 terms which segregated into 65 clusters (Table 3.9). In contrast to down-regulated genes, GO terms associated with adhesion and cell junctions displayed the greatest enrichment. Enriched terms included: cell adhesion (n= 17, p= 8^{-5}), biological adhesion (n= 17, p= 8^{-5}), cell-cell adhesion (n= 11, p= 8^{-5}), glycoprotein (n= 54, p= 2^{-4}), membrane proteins (n= 73, p= 5^{-4}), cell

Category	Term	Count	p-Value
SP_PIR_KEYWORDS	glycolysis	6	2.00E-04
GOTERM_BP_FAT	GO:0006096~glycolysis	6	2.69E-04
GOTERM_BP_FAT	GO:0019320~hexose catabolic process	6	5.91E-04
GOTERM_BP_FAT	GO:0006007~glucose catabolic process	6	5.91E-04
GOTERM_BP_FAT	GO:0046365~monosaccharide catabolic process	6	7.04E-04
GOTERM_BP_FAT	GO:0044275~cellular carbohydrate catabolic process	6	0.001141
GOTERM_BP_FAT	GO:0008544~epidermis development	8	0.001324
GOTERM_BP_FAT	GO:0046164~alcohol catabolic process	6	0.001636
UP_SEQ_FEATURE	topological domain:Extracellular	45	0.001784
GOTERM_BP_FAT	GO:0007398~ectoderm development	8	0.001892
SP_PIR_KEYWORDS	keratin	7	0.002941
GOTERM_CC_FAT	GO:0005882~intermediate filament	8	0.003328
GOTERM_CC_FAT	GO:0045111~intermediate filament cytoskeleton	8	0.003751
GOTERM_BP_FAT	GO:0016052~carbohydrate catabolic process	6	0.004288
GOTERM_CC_FAT	GO:0044432~endoplasmic reticulum part	10	0.005622
SP_PIR_KEYWORDS	disulfide bond	47	0.006346
INTERPRO	IPR002494:Keratin, high sulphur B2 protein	4	0.007285
KEGG_PATHWAY	mmu00010:Glycolysis / Gluconeogenesis	5	0.007491
PIR_SUPERFAMILY	PIRSF006060:amino acid transporter	3	0.008416
GOTERM_BP_FAT	GO:0006006~glucose metabolic process	7	0.010556
GOTERM_MF_FAT	GO:0016860~intramolecular oxidoreductase activity	4	0.011163
GOTERM_CC_FAT	GO:0045095~keratin filament	5	0.012754
UP_SEQ_FEATURE	topological domain:Cytoplasmic	50	0.014564
SP_PIR_KEYWORDS	Taste	4	0.016939
INTERPRO	IPR002293:Amino acid/polyamine transporter I	3	0.017631

Table 3.8 DAVID analysis of E11.5 down-regulated genes (p= 0.05).

Results show the top 25 gene ontology terms identified within the E11.5 (p= 0.05) down-regulated genes of the microarray data set ranked on p-value. Results are shown to include database/resource where terms originate (category), identified term, number of genes associated with the term and the modified Fisher Exact p-value, EASE score.

Category	Term	Count	p-Value
GOTERM_BP_FAT	GO:0007155~cell adhesion	17	8.12E-05
GOTERM_BP_FAT	GO:0022610~biological adhesion	17	8.30E-05
GOTERM_BP_FAT	GO:0016337~cell-cell adhesion	11	8.34E-05
SP_PIR_KEYWORDS	glycoprotein	54	2.65E-04
SP_PIR_KEYWORDS	membrane	73	5.20E-04
SP_PIR_KEYWORDS	cell adhesion	12	9.18E-04
SP_PIR_KEYWORDS	cell junction	12	0.00118
INTERPRO	IPR011705:BTB/Kelch-associated	5	0.001352
UP_SEQ_FEATURE	glycosylation site:N-linked (GlcNAc...)	51	0.001359
GOTERM_CC_FAT	GO:0030054~cell junction	13	0.00184
GOTERM_BP_FAT	GO:0051094~positive regulation of developmental process	8	0.004309
INTERPRO	IPR004031:PMP-22/EMP/MP20/Claudin	4	0.004957
GOTERM_BP_FAT	GO:0007156~homophilic cell adhesion	6	0.005125
GOTERM_BP_FAT	GO:0002089~lens morphogenesis in camera-type eye	3	0.005546
UP_SEQ_FEATURE	topological domain:Extracellular	34	0.005773
GOTERM_MF_FAT	GO:0030247~polysaccharide binding	6	0.006263
GOTERM_MF_FAT	GO:0001871~pattern binding	6	0.006263
SP_PIR_KEYWORDS	oxidation	3	0.006339
GOTERM_CC_FAT	GO:0005911~cell-cell junction	7	0.006413
GOTERM_BP_FAT	GO:0021871~forebrain regionalization	3	0.006514
GOTERM_BP_FAT	GO:0001525~angiogenesis	6	0.008723
INTERPRO	IPR013089:Kelch related	5	0.008806
UP_SEQ_FEATURE	topological domain:Cytoplasmic	40	0.009728
GOTERM_BP_FAT	GO:0048593~camera-type eye morphogenesis	4	0.010593
GOTERM_BP_FAT	GO:0048514~blood vessel morphogenesis	7	0.011505

Table 3.9 – DAVID analysis of E11.5 up-regulated genes (p= 0.05).

Results show the top 25 gene ontology terms identified within the E11.5 (p= 0.05) up-regulated genes of the microarray data set ranked on p-value. Results are shown to include database/resource where terms originate (Category), identified term, number of genes associated with the term and the modified Fisher Exact p-value, EASE score.

Gene Symbol	Chromosome	Fold-Change	p-value
Krt5	chr15	-14.841	1.57E-07
Fermt1	chr2	-4.06985	3.34E-07
Col17a1	chr19	-5.65079	3.51E-07
Krt14	chr11	-8.07407	4.06E-07
Gabrp	chr11	-5.91347	6.91E-07
Perp	chr10	-8.96205	8.04E-07
Trim29	chr9	-4.6218	1.43E-06
Prss8	chr7	2.20681	6.25E-06
Tnmd	chrX	-2.72945	6.67E-06
Kremen2	chr17	-3.13343	7.89E-06
Diras2	chr13	-3.12414	7.91E-06
Gjb2	chr14	2.61743	8.48E-06
Nts	chr10	-3.5301	8.75E-06
Edaradd	chr13	-2.46184	9.18E-06
Pkp2	chr16	2.23892	1.31E-05

Table 3.10 Differentially regulated genes between E12.5 *Trp63*$^{+/+}$ and *Trp63*$^{-/-}$ facial processes.

The top 15 most significantly differentially regulated genes identified. Genes are identified by gene symbol, with chromosome, average fold change (null vs. WT) with up-regulated genes (green) and down-regulated genes (red) and associated p-value.

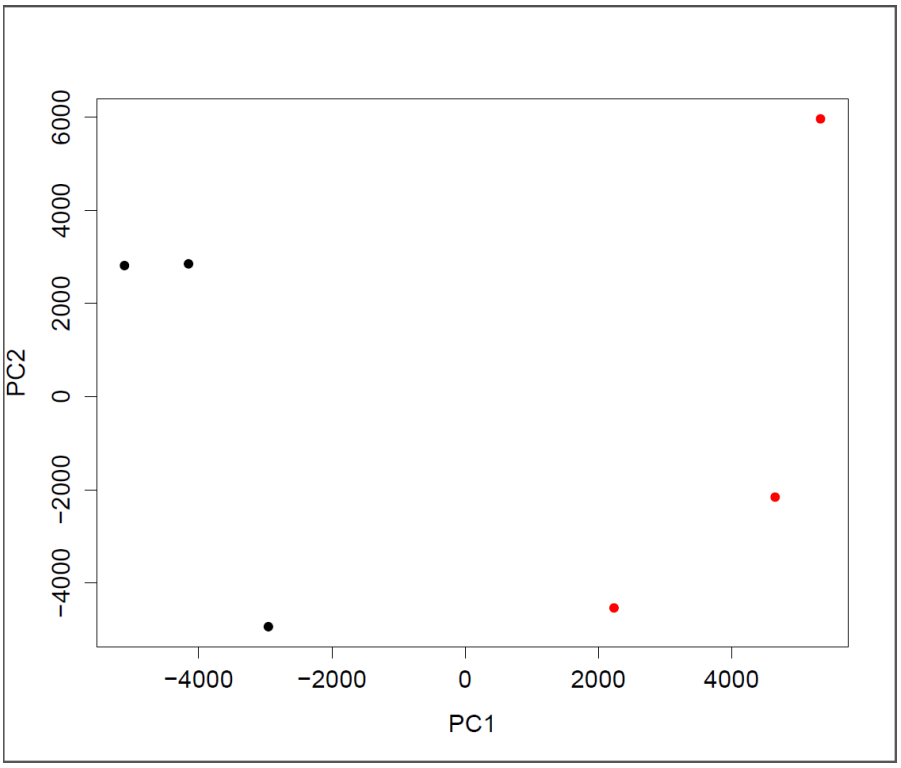

Figure 3.8 E12.5 microarray PCA analysis. PCA analysis showed clear segregation between WT and null samples, with two distinct clusters present based on both PC1 and PC2. One outlier was present within both the null and WT samples. Graph axes denote principle component 1 (PC1) and principle component 2 (PC2). Wildtype samples are black, nulls are red.

junctions (n= 12, p= 0.001), homophilic cell adhesion (n= 6), positive regulation of developmental process (n= 8), homophilic cell adhesion (n= 6, p= 0.005) and cell-cell junction (n= 7, p= 0.006). Positively regulated genes displayed functional clustering within terms associated with molecular adhesion (enrichment score = 2.46), glycoprotein and signalling peptides (enrichment score = 2.00) and membrane components (enrichment score = 1.91). KEGG pathway analysis identified enrichment for two pathways, cell adhesion molecules and sulphur metabolism.

3.3.2.3 E12.5 microarray

Due to the low number of statistically significant results obtained from the E11.5 microarray, it was decided to conduct a second microarray at a later time point. E12.5 facial processes (n= 6) were dissected from *Trp63*$^{+/+}$ and *Trp63*$^{-/-}$ embryos and mRNA isolated. In contrast to the E11.5 microarray, 464 genes were found to be variably expressed at high significance (p= 0.005) and 1431 were significant at p= 0.05. Of the 1431 variably expressed genes (p= 0.05), 818 were up-regulated and 613 down-regulated in the absence of P63. Genes displaying the greatest fold change at E12.5 can be seen in Table 3.10 and include *Krt5*, *Fermt1*, *Col17a1*, *Krt14*, *Gabrp*, *Perp* and *Trim29*.

PCA analysis was completed on the E12.5 data set (Figure 3.8). In contrast to the E11.5 PCA analysis there was a clear segregation of the *Trp63*$^{-/-}$ and *Trp63*$^{+/+}$ samples. Within both groups, one sample was found to be an outlier, however removal of these samples from analysis did not affect the number of genes differentially regulated. Therefore further analysis was completed using the complete data set. Furthermore, the clear segregation of samples present in the data suggested that the E12.5 microarray would provide a more accurate expression data set than the E11.5 data.

3.3.2.4 Identifying genes common between E11.5 and E12.5 microarrays

Prior to gene ontology analysis, the microarray data sets were intersected to identify genes common to each list. Microarray data sets were intersected using the webtool Compare Two Lists (Table 3.11). Comparisons at p= 0.05 identified only 100 genes common between the E11.5 and E12.5 microarrays, meaning that 635 genes (86%) of E11.5 genes were absent from the E12.5 data set. However intersection of the E11.5 high stringency (p= 0.005) genes showed that 14 of 47 genes (30%) were present in the E12.5 (p= 0.05) data set (Table 3.12). Furthermore 10 of the E11.5 high stringency targets were found to be common to the E12.5 high stringency data set (p= 0.005). It was therefore decided to refer to the E12.5 microarray for future analysis.

3.3.2.5 Identifying functional trends within the E12.5 microarray

Gene ontology analysis was completed on the E12.5 high stringency (p= 0.005) data set. Initial analysis was conducted on the full data set of 464 genes (Table 3.13). 680 terms were

	Microarray data set	
	E11.5	E12.5
No. Genes total (p= 0.005)	47	464
No. Unique genes (p= 0.005)	37	454
No. Genes in common (p= 0.005)	10	
No. Genes total (p= 0.05)	735	1431
No. Unique genes (p= 0.05)	635	1331
No. Genes in common (p= 0.05)	100	

Table 3.11 Identification of genes differentially expressed within the E11.5 and E12.5 microarrays.

Results show the number of total genes identified as differentially regulated at E11.5 and E12.5, the number of genes unique to each data set and the number of genes common to each data set at both p= 0.005 and p= 0.05.

Gene Symbol	Chromosome	E11.5 Fold change	E12.5 fold change
Aldh1a3	chr7	1.55005	2.04318
Bmp5	chr9	1.71992	1.20381
Cbr2	chr11	-1.93372	-1.57299
Ccdc80	chr16	1.57009	1.70598
Cldn8	chr16	1.98874	2.23828
Cryab	chr9	1.5767	1.97938
D4Bwg0951e	chr4	1.86966	1.43646
Fermt1	chr2	-2.99993	-4.06985
Jag2	chr12	-1.61447	-1.98663
Krt5	chr15	-1.87958	-14.841
Mrpl48	chr7	1.85623	1.40629
Perp	chr10	-3.84293	-8.96205
Taar7a	chr10	-1.15167	-1.67065
Trim29	chr9	-1.72185	-4.6218

Table 3.12 – The 14 E11.5 p= 0.005 genes common to the E12.5 microarray.

Results show the 14 genes found in common between the E11.5 (p= 0.005) data set and the E12.5 (p= 0.05) data set. Genes are denoted by gene symbol, chromosome number, and average fold change null vs. WT at E11.5 and E12.5.

Category	Term	Count	p-Value
SP_PIR_KEYWORDS	cell junction	46	5.53E-18
GOTERM_CC_FAT	GO:0030054~cell junction	49	2.31E-17
GOTERM_BP_FAT	GO:0030182~neuron differentiation	40	1.75E-13
GOTERM_CC_FAT	GO:0044459~plasma membrane part	88	8.46E-13
GOTERM_CC_FAT	GO:0005886~plasma membrane	128	1.23E-12
GOTERM_BP_FAT	GO:0007389~pattern specification process	32	3.53E-12
GOTERM_CC_FAT	GO:0005911~cell-cell junction	25	6.26E-12
GOTERM_BP_FAT	GO:0003002~regionalization	27	1.89E-11
SP_PIR_KEYWORDS	developmental protein	55	3.55E-11
GOTERM_CC_FAT	GO:0043296~apical junction complex	19	4.22E-11
GOTERM_CC_FAT	GO:0016327~apicolateral plasma membrane	19	5.94E-11
GOTERM_BP_FAT	GO:0030900~forebrain development	23	1.45E-10
GOTERM_MF_FAT	GO:0003700~transcription factor activity	50	6.24E-10
SP_PIR_KEYWORDS	glycoprotein	143	1.16E-09
GOTERM_MF_FAT	GO:0043565~sequence-specific DNA binding	40	2.35E-09
GOTERM_BP_FAT	GO:0060429~epithelium development	27	3.44E-09
GOTERM_BP_FAT	GO:0007409~axonogenesis	21	3.59E-09
GOTERM_BP_FAT	GO:0007423~sensory organ development	26	5.26E-09
GOTERM_BP_FAT	GO:0048812~neuron projection morphogenesis	21	1.36E-08
GOTERM_BP_FAT	GO:0030111~regulation of Wnt receptor signaling pathway	6	0.00259
SP_PIR_KEYWORDS	wnt signaling pathway	9	0.008964
GOTERM_BP_FAT	GO:0016055~Wnt receptor signaling pathway	9	0.015438
GOTERM_BP_FAT	GO:0030178~negative regulation of Wnt receptor signaling pathway	4	0.025581
KEGG_PATHWAY	mmu04310:Wnt signaling pathway	8	0.053414

Table 3.13 DAVID functional analysis of E12.5 microarray up/down-regulated genes (p= 0.005).

Results show gene ontology terms enriched within the E12.5 (p= 0.005) up/down-regulated genes of the microarray data set ranked on p-value. Results are shown to include database/resource where terms originate (Category), identified term, the number of genes associated with each term and the modified Fisher Exact p-value, EASE score.

Term	Count	p-Value
mmu05217:Basal cell carcinoma	10	3.35E-06
mmu04530:Tight junction	14	1.03E-05
mmu04670:Leukocyte transendothelial migration	12	7.47E-05
mmu04340:Hedgehog signaling pathway	8	2.00E-04
mmu04514:Cell adhesion molecules (CAMs)	12	7.22E-04
mmu05200:Pathways in cancer	18	9.85E-04
mmu04512:ECM-receptor interaction	8	0.002705
mmu05412:Arrhythmogenic right ventricular cardiomyopathy (ARVC)	7	0.007012
mmu04020:Calcium signaling pathway	10	0.029971
mmu04310:Wnt signaling pathway	8	0.053414
mmu05414:Dilated cardiomyopathy	6	0.058471
mmu04810:Regulation of actin cytoskeleton	10	0.059241
mmu04115:p53 signaling pathway	5	0.072048
mmu04916:Melanogenesis	6	0.077735
mmu04010:MAPK signaling pathway	11	0.080104

Table 3.14 KEGG pathway analysis of E12.5 up/down-regulated genes (p= 0.005).

Results show signalling pathways enriched within the E12.5 (p= 0.005) up/down regulated genes of the microarray data set ranked on p-Value. Results are shown to include identified pathway, number of genes associated with each pathway and the modified Fisher Exact p-Value, EASE score.

Category	Term	Count	p-Value
SP_PIR_KEYWORDS	glycoprotein	71	5.13E-10
GOTERM_BP_FAT	GO:0008544~epidermis development	13	2.48E-09
GOTERM_BP_FAT	GO:0007398~ectoderm development	13	5.06E-09
GOTERM_BP_FAT	GO:0060429~epithelium development	17	6.40E-09
GOTERM_BP_FAT	GO:0048729~tissue morphogenesis	16	8.16E-09
UP_SEQ_FEATURE	glycosylation site:N-linked (GlcNAc...)	68	1.12E-08
SP_PIR_KEYWORDS	signal	60	1.17E-08
UP_SEQ_FEATURE	signal peptide	60	6.36E-08
GOTERM_BP_FAT	GO:0002009~morphogenesis of an epithelium	13	9.70E-08
GOTERM_CC_FAT	GO:0070161~anchoring junction	11	3.72E-07
SP_PIR_KEYWORDS	Secreted	35	6.03E-07
GOTERM_CC_FAT	GO:0005886~plasma membrane	54	1.07E-06
KEGG_PATHWAY	mmu05217:Basal cell carcinoma	8	1.17E-06
GOTERM_CC_FAT	GO:0030057~desmosome	6	1.22E-06
GOTERM_BP_FAT	GO:0022612~gland morphogenesis	9	1.34E-06
GOTERM_BP_FAT	GO:0007155~cell adhesion	20	1.55E-06
GOTERM_BP_FAT	GO:0022610~biological adhesion	20	1.59E-06
GOTERM_CC_FAT	GO:0030054~cell junction	18	3.77E-06
GOTERM_CC_FAT	GO:0005576~extracellular region	37	3.82E-06
SP_PIR_KEYWORDS	wnt signaling pathway	6	0.005711
GOTERM_BP_FAT	GO:0016055~Wnt receptor signaling pathway	6	0.0082
KEGG_PATHWAY	mmu04310:Wnt signaling pathway	5	0.066235

Table 3.15 DAVID functional analysis of E12.5 microarray down-regulated genes (p= 0.005).

Results show gene ontology terms enriched within the E12.5 (p= 0.005) down-regulated genes of the microarray data set ranked on p-value. Results include databse/resource where terms originate (Category), identified term, the number of genes associated with each term and the modified Fisher Exact p-value, EASE score.

found to be enriched which segregated into 155 clusters. Enriched terms included cell junction (n= 46, p= 5^{-18}), neuron differentiation (n= 40, p= 1^{-13}), plasma membrane (n= 128, p= 1^{-12}), forebrain development (n= 23, p= 1^{-10}), transcriptional factor activity (n= 50, p= 6^{-10}), regulation of Wnt receptor signalling pathway (n= 6, p= 0.003), regulation of apoptosis (n= 27, p= 0.001) and cell-cell adhesion (n= 15, p= 0.002). Due to the large number of terms enriched within the data set, to identify potential trends functional annotation clustering was used. Clusters were observed in region specification (enrichment score = 8.71), neuron differentiation and cell morphogenesis (enrichment score = 7.42), cellular adhesion enrichment (enrichment score = 7.27), transcription factor activity (enrichment score = 4.76), regulation of HH signalling (enrichment score = 1.92) and regulation of Wnt signalling (enrichment score = 1.92). KEGG pathway analysis identified enrichment within seventeen pathways including: basal cell carcinoma (n= 10, p= 3^{-6}), tight junction formation (n= 14, p= 1^{-5}), HH signalling pathway (n= 8, p= 2^{-4}), calcium signalling pathway (n= 10, p= 0.03), and Wnt signalling pathway (n= 8, p= 0.05) (Table 3.14).

To determine whether the E12.5 microarray data should be separated into up and down regulated genes for future analysis, the p= 0.005 data set was further interrogated to identify trends within up/down regulated genes. Gene ontology analysis of down-regulated genes identified enrichment of 412 terms which segregated into 73 functional clusters (Table 3.15). Terms enriched included: glycoprotein (n= 71, p= 5^{-10}), epidermis development (n= 13, p= 2^{-9}), ectoderm development (n= 13, p= 5^{-9}), epithelium development (n= 17, p= 6^{-9}), secreted proteins (n= 35, p= 6^{-7}), cell adhesion (n= 20, p= 1^{-6}), Wnt receptor signalling (n= 6, p= 0.005) and regulation of apoptosis (n= 14, p= 0.002). Functional clustering was shown in functions including glycoprotein related terms (enrichment score = 6.58), adhesion (enrichment score = 5.31), plasma membrane components and junction formation (enrichment score = 4.28) and regulation of Wnt signalling (enrichment score = 1.52). KEGG pathway analysis identified enrichment for Hh signalling, calcium signalling, Wnt signalling and Notch signalling within the down-regulated genes.

Gene ontology analysis of up-regulated genes identified fewer enriched terms than down-regulated, identifying 342 terms which segregated into 95 functional clusters (Table 3.16). Enriched terms included those associated with cell junction formation (n= 31, p= 2^{-13}), forebrain development (n= 17, p= 4^{-9}), neuron differentiation (n= 26, p= 1^{-9}), transcription factor activity (n= 35, p= 1^{-8}) and plasma membrane components (n= 53, p= 3^{-8}). Functional clustering was seen in terms including those associated with neuron development (enrichment score = 5.45), cell junction formation (enrichment score = 5.3), pattern specification (enrichment score = 4.82) and cell motility (enrichment score = 3.26). Furthermore KEGG pathway analysis identified enrichment of four pathways including tight junction formation, leukocyte transendothelial migration, cell adhesion and nuclear receptors in lipid metabolism and toxicity.

Category	Term	Count	p-Value
SP_PIR_KEYWORDS	cell junction	31	2.46E-13
GOTERM_CC_FAT	GO:0030054~cell junction	31	9.14E-12
GOTERM_BP_FAT	GO:0030182~neuron differentiation	26	1.61E-09
GOTERM_MF_FAT	GO:0043565~sequence-specific DNA binding	30	4.06E-09
GOTERM_BP_FAT	GO:0030900~forebrain development	17	4.51E-09
GOTERM_BP_FAT	GO:0007423~sensory organ development	20	1.18E-08
GOTERM_MF_FAT	GO:0003700~transcription factor activity	35	1.37E-08
SP_PIR_KEYWORDS	Tight junction	11	2.26E-08
GOTERM_CC_FAT	GO:0044459~plasma membrane part	53	3.00E-08
GOTERM_CC_FAT	GO:0070160~occluding junction	11	1.54E-07
GOTERM_CC_FAT	GO:0005923~tight junction	11	1.54E-07
GOTERM_MF_FAT	GO:0030528~transcription regulator activity	43	1.59E-07
GOTERM_CC_FAT	GO:0005911~cell-cell junction	15	2.55E-07
GOTERM_CC_FAT	GO:0043296~apical junction complex	12	2.61E-07
GOTERM_BP_FAT	GO:0007389~pattern specification process	19	2.99E-07
GOTERM_CC_FAT	GO:0016327~apicolateral plasma membrane	12	3.20E-07
SP_PIR_KEYWORDS	dna-binding	47	3.89E-07
GOTERM_CC_FAT	GO:0005886~plasma membrane	74	4.01E-07
GOTERM_BP_FAT	GO:0007517~muscle organ development	15	4.38E-07
GOTERM_BP_FAT	GO:0030111~regulation of Wnt receptor signaling pathway	4	0.020763
GOTERM_BP_FAT	GO:0030178~negative regulation of Wnt receptor signaling pathway	3	0.058092

Table 3.16 DAVID functional analysis of E12.5 microarray up-regulated genes (p= 0.005).

Results show gene ontology terms enriched within the E12.5 (p= 0.005) up-regulated genes of the microarray data set ranked on p-value. Results include databse/resource where terms originate (Category), identified term, the number of genes associated with each term and the modified Fisher Exact p-value, EASE score.

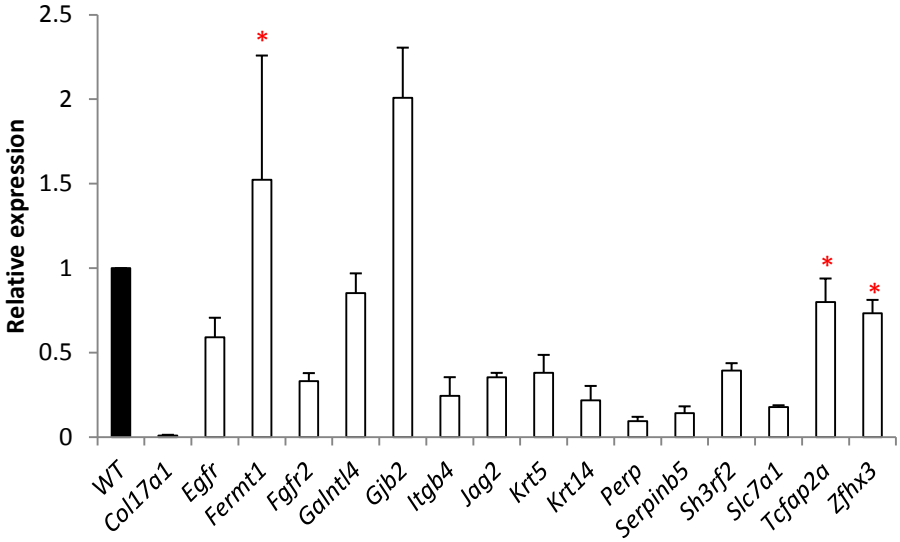

Figure 3.9 qPCR validation of E12.5 microarray. 16 differentially regulated (p= 0.05) genes identified within the E12.5 microarray were validated in E11.5 facial processes isolated from *Trp63*$^{+/+}$ and *Trp63*$^{-/-}$ embryos. Of the 16 genes assayed, 13 displayed a significant relative expression, with *Fermt1*, *Tcfap2a* and *Zfhx3* failing to achieve significance (*). cDNA was normalized relative to the house keeping gene β-actin. Differences in relative transcript expression were calculated using the $2^{\Delta\Delta CT}$ method and statistical significance assessed using the Mann Whitney U test. Error bars represent calculated standard error of the mean.

Gene ontology terms for both up/down-regulated genes of the E12.5 data set (p=0.005) were intersected. A total of 646 enriched terms were identified between them, with 107 terms common to both data sets. It was decided that due to the high degree of overlap and to reduce the risk of data-loss further analysis would be completed using the composite list of up and down-regulated genes. Furthermore comparisons between the gene ontology terms enriched between E12.5 p= 0.05 and p= 0.005 gene lists showed that 544 of a total 1136 terms were common to both lists. The E12.5 p=0.05 gene list was therefore selected for further analysis to increase the chance of identifying true P63 targets.

3.3.2.6 Real-time qPCR validation of the E12.5 microarray at E11.5

Prior to ChIP-Seq microarray intersection, the results of the E12.5 microarray were validated using real-time qPCR. Facial processes from *Trp63*$^{+/+}$ (n= 4) and *Trp63*$^{-/-}$ (n= 4) E11.5 embryos were dissected and cDNA generated. 16 significantly regulated genes (P= 0.05) were randomly selected and qPCR primers designed. The 16 selected genes included: *Col17a1*, *Egfr*, *Fermt1*, *Fgfr2*, *Galntl4*, *Gjb2*, *Itgfb4*, *Jag2*, *Krt5*, *Krt14*, *Perp*, *Serpinb5*, *Sh3rf2*, *Slc7a1*, *Tcfap2a* and *Zfhx3*. Real-time qPCR identified 13 of the 16 selected displayed significant differential expression (Figure 3.9), with *Fermt1*, *Tcfap2a* and *Zfhx3* failing to achieve significance with p-values of 17, 4, and 1 (Mann-Whitney U test). 81% of the genes validated displayed significant differential expression in accordance with the E12.5 microarray results, suggesting the data set could be used with confidence.

3.3.3 E11.5 ChIP-Seq to E12.5 microarray intersection

The presence of a ChIP-Seq peak proximal to a gene does not indicate biological activity, or that the gene is the target of P63-mediated regulation. Conversely differential expression by microarray cannot differentiate between a direct target of P63 transcriptional regulation and secondary effects due to misregulation of gene families or the abnormal morphogenic state of the tissue. Therefore the results of the E12.5 microarray and the E11.5 ChIP-Seq were intersected. The data sets were intersected using the galaxy RNAChIPIntergrator at 25 kb intervals at a maximum TSS to peak distance of 150 kb. At the maximum distance of 150 kb, 2655 peaks were shown to intersect with 1057 genes. To further identify which intersection to use for future analysis, the incremental increase in genes identified was calculated (Table 3.17). Incremental increase was shown to decrease conversely to increasing distance with the initial increase between 25 kb and 50 kb containing 210 genes and the final increase between 125 kb and 150 kb containing 51 genes. These data suggested that at 150 kb the maximum volume of relevant data was being identified.

Further analysis was conducted using the P300 data set. Both confirmed P300 enhancer sites and P300 candidate sites were intersected against the 150 kb intersected peaks. 52 peaks within the 150 kb data set were shown to overlap with P300 candidate sites and six

with confirmed P300 sites. The overlaps present within the data set may suggest P63 is binding at enhancer sites active during facial development.

3.3.3.1 Gene ontology varies with maximum intersection distance

Prior to full gene ontology analysis, it was investigated whether variation was present within the GO terms enriched at each maximum intersection distance. GREAT analysis was therefore conducted on each data set and the number of terms enriched for each subgroup compared (Table 3.18). It was hypothesised that the number of terms enriched in each subgroup would increase with maximum intersection distance. However this was not the case. A high degree of variation was seen within the subgroups with no distance displaying a clear over-enrichment of terms. However a peaking effect in the number of terms enriched was observed between 75 kb and 100 kb. It is important to note however that number of terms enriched is not a measure of accuracy within the data. The apparent reduction in terms from 100 kb+ may be due to the increased power available for analysis. Furthermore between all data sets, enrichment of terms related to adhesion, Wnt signalling and expected related phenotypes were observed. It was therefore decided to conduct full GREAT analysis at the maximum intersected distance to include the greatest number of binding sites and genes.

3.3.3.2 Identifying functional trends within the intersected data set

Having generated a data set of significantly differentially regulated genes featuring a P63 motif within 150 kb, functional trends within the data set were investigated. GREAT functional analysis was completed, a summary of enriched terms can be seen in Table 3.19, full GREAT results can be seen in Appendix 4. Ontology analysis of the 150 kb intersected data set revealed enrichment within multiple development related processes. Enriched terms included those related to skin development, epidermis development, apoptotic process involved in morphogenesis, face development and embryonic forelimb morphogenesis. Encouragingly terms related to both P63 and P53 function were enriched, including validated transcriptional targets of TAp63 isoforms, signal transduction by p53 class mediator, DNA damage response signal transduction by p53 class mediator and PANTHER pathway enrichment for the P53 pathway.

Human phenotype enrichment identified 241 terms, while mouse phenotype enrichment identified 955 terms. *TP63* related conditions in humans commonly feature ectodermal dysplasias, ankyloblepharon, ectrodactyly and cleft lip/palate as a phenotype (Rinne *et al*. 2007). In both human and mouse phenotype, terms related to eyelid morphology/ development, epidermis structure and abnormal limb structure were enriched. Furthermore disease ontology analysis identified terms related to cleft lip and cleft palate as highly enriched. It was encouraging to note that genes related to cleft lip displayed enrichment of higher significance ($P= 2.61^{-15}$) than CP ($P= 4.72^{-12}$).

Maximum TSS to peak distance	No. peaks present	No. genes identified	Incremental expansion of genes identified
25 kb	715	518	
50 kb	1228	728	210
75 kb	1649	854	126
100 kb	2023	945	91
125 kb	2333	1006	61
150 kb	2655	1057	51

Table 3.17 Variation in intersected genes vs. maximum distance.

Results show the maximum number of genes identified proximal to ChIP-Seq peaks (one per peak) varying with intersection distance. The E11.5 ChIP-Seq was intersected against the E12.5 microarray. Data displayed includes, maximum intersection distance, number of peaks intersected, number of genes identified and calculated serial increase in genes identified.

Maximum Peak distance	GO molecular function	GO biological process	GO cellular component	Mouse phenotype	Human phenotype	Disease ontology	PANTHER pathway	MSigDB pathway	MGI expression detected	InterPro analysis
25 kb	0	214	11	327	194	96	2	11	1125	0
50 kb	14	514	23	869	225	**200***	6	18	1614	2
75 kb	16	611	**24***	**1008***	202	171	**10***	**19***	1835	2
100 kb	**24***	**629***	22	949	**266***	165	8	16	**1977***	5
125 kb	23	622	19	971	**266***	166	9	17	1949	**9***
150 kb	22	543	19	955	241	143	8	11	1734	5

Table 3.18 Variation in GREAT analysis vs. maximum intersection distance.

Results show the number of enriched terms returned by GREAT analysis at sequential microarray to ChIP-Seq intersection distances. Data displayed includes, intersected distance with the number of terms enriched within each analysis pipeline. The greatest number of enriched terms identified across all distances for each analyses are denoted (*).

	Term Name	Binom Rank	Binom Raw p-Value	Binom FDR q-Val	Binom Observed Region Hits
GO Molecular function	sequence-specific DNA binding transcription factor activity	13	3.86849e-34	1.03646e-31	286
	nucleic acid binding transcription factor activity	14	5.72043e-34	1.42316e-31	286
	sequence-specific DNA binding	18	2.05525e-29	3.97692e-27	237
	frizzled binding	50	3.33257e-16	2.32147e-14	35
GO Biological process	system development	16	8.57670e-99	5.39046e-96	890
	biological adhesion	161	7.95034e-31	4.96575e-29	241
	regulation of Wnt receptor signalling pathway	254	4.10856e-21	1.62660e-19	97
	regulation of fibroblast growth factor receptor signalling pathway	359	1.38492e-14	3.87931e-13	32
GO Cellular Component	transcription factor complex	35	5.48857e-18	1.89120e-16	120
	Golgi membrane	41	7.45242e-16	2.19210e-14	133
	cell-cell junction	51	1.76094e-13	4.16411e-12	105
	basement membrane	82	6.90696e-7	1.01583e-5	39
Mouse Phenotype	preweaning lethality	4	5.56181e-104	1.10249e-100	919
	abnormal craniofacial morphology	15	1.31962e-61	6.97553e-59	405
	abnormal head morphology	22	4.75897e-58	1.71518e-55	334
	cleft lip	2111	8.69574e-4	3.26615e-3	13
Human Phenotype	Abnormality of the nail	5	5.85636e-50	7.14008e-47	145
	Abnormality of the skin	7	1.09574e-45	9.54232e-43	312
	Oral cleft	95	1.24391e-19	7.98201e-18	118
	Cleft upper lip	281	9.90850e-11	2.14954e-9	50
Disease Ontology	cancer	2	1.44014e-157	1.59064e-154	1252
	cleft lip	121	2.61018e-15	4.76519e-14	43
	cleft palate	145	4.72630e-12	7.20027e-11	35
	neuroectodermal tumour	29	1.89474e-47	1.44327e-45	357
PANTHER pathway	FGF signalling pathway	3	6.51766e-15	3.28055e-13	57
	Wnt signalling pathway	5	8.31197e-13	2.51022e-11	95
MSigDB Pathway	Validated transcriptional targets of TAp63 isoforms	2	3.51049e-20	2.31517e-17	43
	Genes related to Wnt-mediated signal transduction	7	4.38771e-13	8.26770e-11	50
	Hedgehog signaling pathway	14	5.05967e-11	4.76693e-9	35
	Tight junction	25	8.79021e-9	4.63771e-7	48
MGI expression detected	TS23_oral region	12	1.09309e-121	8.54434e-119	744
	TS23_upper lip	1546	1.41753e-7	8.60056e-7	59
	TS23_lower lip	1553	1.63148e-7	9.85403e-7	58
	TS24_hard palate	818	1.03594e-14	1.18791e-13	27
InterPro	Wnt	1	1.14321e-15	1.09165e-11	25
	Wnt protein, conserved site	1	1.14321e-15	1.09165e-11	25
	Basic-leucine zipper domain	6	5.96735e-14	9.49704e-11	33
	Pleckstrin homology-like domain	7	1.45812e-13	1.98909e-10	131

Table 3.19 Gene ontology analysis of the E11.5 ChIP-Seq/E12.5 microarray intersected data set.

GREAT analysis of E11.5 ChIP-Seq data set intersected against the E12.5 microarray. The table lists identified term, Binom rank, raw Binom p-value, adjusted FDR q-value and number of peaks associated with each term.

In addition to the expected P63 related terms enrichment was observed within Wnt related terms. Frizzled binding was highly enriched within GO molecular function (p= 3.33 x E^{-16}). Furthermore seven Wnt related terms were enriched including, Wnt signalling network, genes related to Wnt-mediated signal transduction, non-canonical Wnt receptor signalling pathway and positive regulation of canonical Wnt receptor signalling pathway. Furthermore InterPro analysis identified enrichment within Wnt and Wnt protein conserved site genes as the most significant results returned.

3.3.3.3 Identifying functional groups for further investigation

Due to the large volume of potential target genes, it was decided to prioritise genes for further interrogation based on functional annotation. Enrichment was seen within genes previously validated as targets of TAp63 isoforms (Table 3.19). Throughout the analysis process, the enrichment of the Wnt signalling family was prevalent. Identified Wnt genes included *Wnt3*, *Wnt3a*, *Wnt7a* and *Wnt7b*. A recent study into the removal of *Pbx* gene expression identified significant down-regulation of *Trp63* and *Irf6* (Ferretti *et al*. 2011). *Trp63* expression in *Pbx* mutant embryos was found to be regulated via the Wnt signalling network (Ferretti *et al*. 2011). Identified Wnt genes were therefore selected for further analysis.

In addition to Wnt signalling, enrichment was observed within genes associated with Fgf signalling and adhesion related genes. Misregulation of Fgf signalling has been shown to induce a clefting phenotype via abnormal proliferation and apoptosis (Abu-Issa *et al*. 2002; Goodnough *et al*. 2007). Furthermore members of the Fgf signalling family including *Fgf8*, *Fgfr2* and *Fgfr3* have previously been implicated as targets of P63 regulation (Laurikkala *et al*. 2006; Ferone *et al*. 2012; Sayan *et al*. 2010). A failure of palatal shelf adhesion due to the presence of a layer of abnormal periderm cells over the MEE has been shown to induce cleft palate in $Trp^{63+/-}/Irf6^{+/R84C}$ embryos (Thomason *et al*. 2010). Adhesion related genes including *Cldn1* have previously been identified as targets of P63 regulation (Lopardo *et al*. 2008). Therefore a target gene list of 71 genes was generated based on the ChIP-Seq, microarray intersection results and genes related to adhesion, Wnt and Fgf signalling (Table 3.20).

Gene Name	Gene Symbol	Chromosome	E11.5 Fold Change	E12.5 Fold Change	Number of P63 ≤150 kb
Rho GTPase Activating Protein 6	*Arhgap6*	X	-1.00985	1.26161	1
B-Cell CLL.Lymphoma 11b (Zinc Finger Protein)	*Bcl11b*	12	1.11934	-1.44528	2
BCL2-Related Ovarian killer	*Bok*	1	1.01322	-1.20366	2
CCAAT/Enhancer Binding Protein (C/EBP), Alpha	*Cebpa*	7	-1.04354	-1.30115	6
Claudin 1	*Cldn1*	16	-1.58267	-1.88238	2
Claudin 4	*Cldn4*	5	-1.01633	1.76711	2
Collagen, Type XVII, Alpha 1	*Col17a1*	19	-1.42285	-5.65079	5
Cytochrome P450, Family 26, Subfamily B, Polypeptide 1	*Cyp26b1*	6	1.01781	-1.48582	1
Epidermal Growth Factor Receptor	*Egfr*	11	1.00282	-1.37774	6
Engrailed Homeobox 1	*En1*	1	-1.02933	-1.63182	2
Fermitin Family Member 1	*Fermt1*	2	-2.99993	-4.06985	3
Fibroblast Growth Factor 9	*Fgf9*	14	1.19146	1.39984	4
Fibroblast Growth Factor Receptor 2	*Fgfr2*	7	-1.21794	-1.49156	9
Fibroblast Growth Factor Receptor 3	*Fgfr3*	5	-1.01625	-1.1952	1
Frizzled Class Receptor 10	*Fzd10*	5	1.00266	-1.75875	5
Frizzled Class Receptor 4	*Fzd4*	7	1.22514	1.46969	3
Growth Differentiation Factor 15	*Gdf15*	8	-1.10317	-1.32293	2
Gap Junction Protein, Beta 2, 26kDa	*Gjb2*	14	1.01163	2.61743	1
Gap Junction Protein, Beta 3, 26kDa	*Gjb3*	4	-1.07718	1.29536	1
Grainyhead-Like 3	*Grhl3*	4	-1.54766	-1.41187	6
Hes Family BHLH Transcription Factor 1	*Hes1*	16	1.02669	-1.18281	4
IKAROS Family Zinc Finger 2	*Ikzf2*	1	1.01956	1.48297	2
Integrin, Beta 4	*Itgb4*	11	-1.15721	-1.96874	4
Jagged 1	*Jag1*	2	1.00892	-1.48272	6

Table 3.20 Target genes for further investigation.

Data shown includes gene name, gene symbol, chromosome, E11.5 and E12.5 microarray fold change with negative fold changes (red) and positive fold changes (green) and the number of P63 peaks with 150 kb of the TSS.

Gene Name	Gene Symbol	Chromosome	E11.5 Fold Change	E12.5 Fold Change	Number of P63 ≤150 kb
Stratifin	*Sfn*	4	-1.27219	-1.52859	2
Secreted Frizzled-Related Protein 1	*Sfrp1*	8	1.04206	1.21746	2
Sonic Hedgehog	*Shh*	5	1.07316	-1.85367	3
Salt-Inducible Kinase 1	*Sik1*	17	-1.28005	-1.28191	8
SRY (Sex Determining Region Y)-Box 2	*Sox2*	3	1.2263	1.58959	1
SRY (Sex Determining Region Y)-Box 21	*Sox21*	14	-1.01567	-1.24419	4
SRY (Sex Determining Region Y)-Box 9	*Sox9*	11	1.01595	1.24083	1
Sprouty Homolog 1, Antagonist Of FGF Signalling (Drosophila)	*Spry1*	3	1.02942	1.21053	5
Sprouty Homolog 2 (Drosophila)	*Spry2*	14	1.16112	1.28369	3
Sulfatase 1	*Sulf1*	1	-1.04458	-1.20915	2
Transcription Factor AP-2 Alpha (Activating Enhancer Binding Protein 2 Alpha)	*Tcfap2a*	13	1.16301	1.19321	5
Transcription Factor AP-2 Gamma (Activating Enhancer Binding Protein 2 Gamma)	*Tcfap2c*	2	-1.05364	1.42106	7
Tumor Protein P73	*Trp73*	4	-1.07919	-1.76387	9
Vitamin D (1,25- Dihydroxyvitamin D3) Receptor	*Vdr*	15	1.35755	2.28243	4
Wingless- Type MMTV Integration Site Family, Member 10B	*Wnt10b*	15	-1.12509	-1.80646	2
Wingless- Type MMTV Integration Site Family, Member 11	*Wnt11*	7	-1.20284	1.5531	3
Wingless- Type MMTV Integration Site Family, Member 2B	*Wnt2b*	3	1.04533	-1.27926	2
Wingless- Type MMTV Integration Site Family, Member 3	*Wnt3*	11	-1.20852	-1.20977	4
Wingless- Type MMTV Integration Site Family, Member 3A	*Wnt3a*	11	-1.0995	-1.35572	5
Wingless- Type MMTV Integration Site Family, Member 4	*Wnt4*	4	-1.13897	-1.23423	5
Wingless- Type MMTV Integration Site Family, Member 7A	*Wnt7a*	6	1.0094	-1.52066	5
Wingless- Type MMTV Integration Site Family, Member 7B	*Wnt7b*	15	1.03001	-1.23596	2
Zinc Fingers And Homeoboxes 2	*Zhx2*	15	-1.11595	-1.20886	6

Table 3.20 Target genes for further investigation.

Data shown includes gene name, gene symbol, chromosome, E11.5 and E12.5 microarray fold change with negative fold changes (red) and positive fold changes (green) and the number of P63 peaks with 150 kb of the TSS.

Gene Name	Gene Symbol	Chromosome	E11.5 Fold Change	E12.5 Fold Change	Number of P63 ≤150 kb
Jun Proto-Oncogene	*Jun*	4	1.03096	1.32583	2
Lysine (K)-Specific Demethylase 2B	*Kdm2b*	5	-1.07909	1.19239	2
Kringle Containing Transmembrane Protein 2	*Kremen2*	17	-1.50909	-3.13343	1
Keratin 14, Type I	*Krt14*	11	-1.17283	-8.07407	4
LIM Domain Binding 2	*Ldb2*	5	-1.06167	-1.19488	2
Lymphoid Enhancer-Binding Factor 1	*Lef1*	3	-1.01603	-1.23498	6
Myelin Protein Zero	*Mpz*	1	1.05081	1.21827	2
Nerve Growth Factor Receptor	*Ngfr*	11	-1.05545	-1.49346	1
Orthodenticle Homeobox 2	*Otx2*	14	1.05422	1.70903	1
Paired Box 6	*Pax6*	2	1.11409	1.55038	1
PERP, TP53 Apoptosis Effector	*Perp*	10	-3.84293	-8.96205	3
Pleckstrin Homology-Like Domain, Family A, Member 3	*Phlda3*	1	-1.09481	-1.35397	3
Plakophilin 1	*Pkp1*	1	-1.15512	-2.95581	4
Plakophilin 3	*Pkp3*	7	-1.07117	-1.32567	6
Plectin	*Plec*	15	-1.04893	-1.2529	4
Pleckstrin Homology Domain containing, Family A Member 7	*Plekha7*	7	-1.10261	-1.23016	3
Periplakin	*Ppl*	16	-1.2539	-1.63628	1
Patched 2	*Ptch2*	4	-1.0106	-3.55362	1
Protein Tyrosin Phosphatase, Receptor Type, V, Pseudogene	*Ptprv*	1	-1.20332	-1.23258	4
Poliovirus Receptor-Related 1 (Herpesvirus Entry Mediator C)	*Pvrl1*	9	1.05604	-1.19627	6
Retinoblastoma 1	*Rb1*	14	-1.08933	-1.23802	9
Receptor-Interacting Serine-Threonin Kinase 4	*Ripk4*	16	-1.40492	-1.26021	4
Sema Domain, Immunoglobulin Domain (Ig), Short Basic Domain, Secreted, (Semaphorin) 3C	*Sema3c*	5	-1.07506	1.66364	3
Serpin Peptidase Inhibitor, Clade B (Ovalbumin), Member 5	*Serpinb5*	1	-1.12684	-1.33969	2

Table 3.20 Target genes for further investigation.

Data shown includes gene name, gene symbol, chromosome, E11.5 and E12.5 microarray fold change with negative fold changes (red) and positive fold changes (green) and the number of P63 peaks with 150 kb of the TSS.

3.4 Discussion

3.4.1 Identification of E11.5 facial process specific P63 binding sites

The aim of this project was to identify novel targets of P63 regulation during lip morphogenesis to further understand the P63 signalling network and the pathogenesis of *TP63*-related cleft lip and palate. To this aim a two-tiered methodology was adopted, to identify P63 binding sites, and genes which display differential regulation between *Trp63*$^{+/+}$ and *Trp63*$^{-/-}$ facial processes. ChIP-Seq peak calling using the MVS established using ChIP-qPCR identified 10,209 potential binding sites. 83.9% of which were shown to contain the P63 binding motif. As further validation of the ChIP-Seq data set was intersected against a previously generated P63 E14 palatal shelf ChIP-Seq data set (Mitchell *et al*. manuscript in preparation).

41.7% of the 6293 E14 peaks were shown to overlap with the E11.5 identified peaks (Mitchell *et al*. manuscript in preparation). In contrast with the E14 data set, the ChIP-Seq identified in excess of 10,000 genes with 7633 shown to be unique to the E11.5 data set. The presence of the 2576 overlapping binding sites within the data set is highly encouraging as it suggests reproducible sites of P63 binding have been identified. Furthermore P63 is known to be active during development of the upper lip and primary palate, and the subsequent development of the secondary palate (Thomason *et al*. 2008; Thomason *et al*. 2010). The processes of lip morphogenesis and secondary palate development display clear phenotypic overlaps, with the outgrowth of paired processes driven by mesenchymal proliferation, followed by process adhesion, formation of double epithelial seams and subsequent degeneration of the epithelial seams (Som & Naidich, 2013a; Som & Naidich 2013b; Jiang *et al*. 2006).

At E10.5 *Trp63* is expressed within the ectoderm of the medial nasal, lateral nasal and maxillary processes surrounding the nasal pits and the lambdoidal junction (Thomason *et al*. 2008). Immediately prior to fusion, *Trp63* expression is down-regulated at the site of contact between the maxillary, medial nasal and lateral nasal processes (Thomason *et al*. 2008). This expression profile is mirrored within secondary palate development. Between E12.5 to E14 *Trp63* is highly expressed throughout the ectoderm of the palatal shelves and within the medial edge epithelium (Gritli-Linde, 2010; Thomason *et al*. 2010). Following palatal shelf contact and adhesion, *Trp63* expression within the medial epithelial seam is down-regulated and is followed by palatal fusion (Thomason *et al*. 2010). Given the high degree of phenotypic similarity between development of the upper lip and secondary palate and *Trp63*'s expression throughout the facial processes and palatal shelves, it could be suggested that a subset of binding sites and genes would be common to both processes (Thomason *et al*. 2008; Thomason *et al*. 2010; Gritli-Linde, 2010).

Furthermore work by the Von Bokhoven and Zhou groups identified P63 binding sites active during lip morphogenesis (Kouwenhoven *et al*. 2010). A P63 binding site, SHFM1-BS1, was shown to be active during limb development in the regulation of *DLX5*/*DLX6* (Kouwenhoven *et al*. 2010). However SHFM1-BS1 regulation was shown to be absent during craniofacial development (Kouwenhoven *et al*. 2010). These results would suggest that P63 binding and regulation displays tissue and context specificity, therefore it is unsurprising that the majority of P63 binding sites identified are absent from the E14.5 data set (Kouwenhoven *et al*. 2010; Mitchell *et al*. manuscript in preparation).

To complement the ChIP-Seq data set, it was sought to identify genes differentially regulated between *Trp63*$^{+/+}$ and *Trp63*$^{-/-}$ facial processes. The initial microarray was completed using facial processes dissected from E11.5 embryos. At E11.5 contact is made between the lateral nasal, medial nasal and maxillary processes forming the lambdoidal junction (Jiang *et al*. 2006; Som & Naidich, 2013a). In wildtype embryos *Trp63* is expressed throughout the ectoderm of the facial processes, with expression present within the lambdoidal junction (Thomason *et al*. 2008). In contrast at E11.5 in *Trp63*$^{-/-}$ embryos, the medial nasal, lateral nasal and maxillary processes were found to be significantly smaller than wildtype littermates (Thomason *et al*. 2008). Furthermore no contact is made between the facial processes and the beginnings of a bilateral cleft lip were evident (Thomason *et al*. 2008). It was therefore hypothesised that conducting expression analysis at E11.5 would identify targets of P63 regulation.

However, microarray at E11.5 identified a low number of significantly differentially regulated genes, with 47 genes shown to be differentially regulated at p= 0.005 and 735 at p= 0.05. Further PCA analysis identified a poor degree of segregation between the *Trp63*$^{+/+}$ and *Trp63*$^{-/-}$ samples. It was hypothesised that at E11.5 the impact of the emerging bilateral CL was minimal. Cleft lip and palate first becomes apparent in *Trp63*$^{-/-}$ embryos at approximately E11.5 (Thomason *et al*. 2008). It was therefore concluded that the poor separation observed via PCA analysis was due to the impact of P63 depletion being reduced. Therefore a second microarray was completed at E12.5 where the phenotypic effects of P63 depletion would be greater. By E12.5 epithelia seams between the medial nasal and maxillary processes and the medial nasal and lateral nasal processes have both been degenerated allowing mesenchymal confluence (Johnston & Bronsky, 1995). In contrast to E11.5 embryos visual analysis of E12.5 *Trp63*$^{-/-}$ identified a fully penetrant bilateral cleft lip and palate. It was therefore hypothesised that greater phenotypic variation between the *Trp63*$^{+/+}$ and *Trp63*$^{-/-}$ would identify a greater number of potential P63-regulated genes.

Microarray analysis between facial processes isolated from E12.5 *Trp63*$^{+/+}$ and *Trp63*$^{-/-}$ embryos identified a greater number of differentially regulated genes, identifying 464 genes at p= 0.005 and 1461 genes at p= 0.05. Phenotypic analysis between the two microarray data sets was comparable, therefore it was decided to continue analysis using the E12.5 data set.

3.4.2 A subset of P63 binding sites lack the P63 binding motif

ChIP-Seq analysis of P63 binding during E11.5 lip morphogenesis identified in excess of 10,200 potential binding sites, however P63-Scan analysis revealed that approximately 17% of the binding sites do not contain the characterised P63 binding motif. There are therefore two possibilities to explain the binding of P63 at these sites, either P63 is directly binding to a currently unknown or uncharacterised binding motif, or P63 may be binding in conjunction with a co-factor.

Previous work by the McDade group used ChIP-Seq analysis within primary human neonatal foreskin to identify P63 binding sites (McDade *et al*. 2012). Motif discovery identified enrichment AP2alpha binding sites. Of the 7574 P63 binding sites identified, 2867 were shown to contain a TFAP2A binding motif proximal to the P63 motif (McDade *et al*. 2012). Luciferase reporter assays to determine if increasing levels of TFAP2A influenced P63's transcriptional regulation of an IRF6 enhancer failed to show a significant change in activation following addition of TFAP2A (McDade *et al*. 2012).

Comparative ChIP-qPCR on P63/TFAP2A-positive binding sites between *TP63* or *TFAP2A* depleted keratinocytes identified a significant reduction the binding of P63 in the absence of TFAP2A and in TFAP2A in the absence of P63 (McDade *et al*. 2012). These results would suggest that P63 and TFAP2A may co-regulate a subset of target genes. It is important to note that no TFAP2A binding motifs were found to overlap with P63 motifs (McDade *et al*. 2012). Furthermore no proteonomic analysis was conducted to determine if P63 is able to bind via TFAP2A (McDade *et al*. 2012). It is therefore unclear if Tfap2α co-localisation could enable P63 binding within the present data set in the absence of a P63 binding motif. Further investigation of Tfap2α as a potential co-regulator or binding partner of P63 would require proteonomic analysis beyond the scope of this project.

The transcriptional co-activator P300 has been shown to be able to directly bind to and acetylate members of the p53 family (Avantaggiati *et al*. 1997; MacPartlin *et al*. 2005). P300 is thought to contribute to the regulation of P53 levels through the ubiquitin-dependent protein degradation pathway (Grossman *et al*. 1998; Chan & Thangue. 2001). Binding of P300 to P53 was found to increase P53 stability and DNA binding activity (Gu & Roeder, 1997; Grossman *et al*. 1998). Furthermore P300 was found bound to the majority of cellular MDM2 and is thought to mediate the interaction of P53/MDM2 to control the native levels of P53 (Grossman *et al*. 1998).

In addition to regulating cellular levels of P53, binding of P53 to one of the C/H rich regions of P300 has been identified as a mechanism by which P53 participated in transcriptional regulation at a site lacking the characterised p53 binding motif (Aventaggiati *et al*. 1997). Due to the large degree of structural homology between P53 family members it may be possible that P63 behaves in a similar fashion (Serber *et al*. 2002; Dötsch *et al*. 2010).

Furthermore studies have shown that P300 was able to bind to the N-terminus of the TAp63γ isoform (MacPartlin *et al*. 2005). However it was shown that P300/P63 binding was TA isoform specific with ΔNp63γ failing to display binding (MacPartlin *et al*. 2005).

The predominantly expressed isoform of P63 active during E11.5 lip morphogenesis is the ΔNp63α isoform which, due to its modified N-terminus, would be unable to associate with P300 (Bokhoven & Brunner, 2002; MacPartlin *et al*. 2005). In addition to the low number of P300/P63 ChIP-Seq overlaps, taken together these results would suggest that P300 binding is not the major method of P63 binding at the P63 motif-negative peaks. Furthermore investigating a prospective P63/P300 DNA binding complex would require extensive proteonomic analysis investigation which is beyond the scope of this project.

The transcription factor Sox2 has previously been shown to both bind at overlapping genomic locations to P63 and has been shown to be able to directly interact with P63 (Watanabe *et al*. 2014). *Sox2*$^{-/-}$ embryos are not viable, with embryos failing to progress past E11 due to a failure to maintain pluripotent stem cells (Avilion *et al*. 2003). Furthermore *Sox2* has been shown to be expressed within the frontonasal prominence at E11.5 (Mandalos *et al*. 2014). Generation of conditional knockouts showed a reduction of *Sox2* expression during lip morphogenesis led to defective frontonasal process formation at E11.5 (Mandalos *et al*. 2014).

SOX2 was shown to be misregulated in squamous cell carcinomas, while ΔNp63α has been shown to be integral to tumour survival in head and neck squamous cell carcinoma (Rocco *et al*. 2006; Watanabe *et al*. 2014). Tandem affinity purification followed by liquid chromatography-tandem mass spectrometry identified P63 as a possible Sox2-interacting protein (Watanabe *et al*. 2014). Immunological pull down assays with an antibody against Sox2 contained P63 protein. In addition pull down assays in cell populations co-transfected with Sox2 and FLAG-tagged ΔNp63α with an anti-FLAG antibody retrieved Sox2 (Watanabe *et al*. 2014). Taken together these results would suggest a direct protein-protein interaction between P63 and Sox2 is possible.

P63 motif discovery analysis of Sox2 enriched sites identified P63 binding motifs directly adjacent to Sox2 sites enriched in squamous cell carcinoma cells (Watanabe *et al*. 2014). However analysis conducted in H9 cells failed to identify enrichment for P63 motifs in SOX2-occupied loci, suggesting the association may be specific to squamous epithelial cells (Watanabe *et al*. 2014). Research further showed that P63 and Sox2 collaborated in regulating the expression of *ETV4* (Watanabe *et al*. 2014). The potential interactions between P63 and Sox2 remain unclear. The study showed that P63 and Sox2 were able to co-localise, however sites were assayed on the basis of a P63 motif being present (Watanabe *et al*. 2014). It therefore remains unclear if protein interaction with Sox2 could account for P63 binding at P63 motif-negative peaks identified in this project.

In addition to potential binding with a co-factor, the putative lack of a P63 binding motif within 17% of identified peaks may be due to an error inherent within the programme P63 Scan. To this author's knowledge, three previous studies have completed P63 ChIP-Seq studies complimented with the use of P63 motif analysis (Kouwenhoven *et al*. 2010; McDade *et al*. 2012; Kouwenhoven *et al*. 2015). Within each of the listed studies a subset of identified P63 binding sites (10-15%) lacked the characterised P63 binding motif (Kouwenhoven *et al*. 2010; McDade *et al*. 2012; Kouwenhoven *et al*. 2015). The P63 Scan programme was adapted from the previously developed P53 Scan programme using a newly generated position weight matrix (PWM) of P63 binding sites (Kouwenhoven *et al*. 2010).

The original P53 Scan programme was developed using a PWM of characterised P53 binding sites using the presence of two palindromic consensus half-sites RRCWWGYYY (R= purine, W= A or T and Y= pyrimidine) separated by a median spacer of 0-13 bp to identify P53 binding sites (Smeenk *et al*. 2008). The P63 Scan programme operates on a similar algorithm using the characterised P63 motif (previously detailed in section 3.3.1 Figure 3.2B) with a 0 bp spacer element specified (Kouwenhoven *et al*. 2010). The efficacy of P63 Scan has been confirmed via the enrichment of P63 binding sites using ChIP-qPCR in this project and previous studies (Kouwenhoven *et al*. 2010). A possible weakness within the design of P63 Scan is that the programme exclusively identifies the 22 bp motif consisting of two half-sites with no spacer region (Kouwenhoven *et al*. 2010). However a previous study has shown that P63 is able to bind in the presence of a single half-site (Chen *et al*. 2011). It may therefore be the case that in the identified P63 motif-negative sites, a single half-site is present allowing P63 interactions and such sites were overlooked by the P63 Scan programme.

3.4.3 Limitations of the current ChIP-Seq and Microarray analysis

ChIP-Seq has provided a powerful tool for the analysis of transcription factor activity, allowing the high throughput *in vivo* determination of potential binding sites throughout a given genome (Albert *et al*. 2007). ChIP-Seq in this project identified 10,209 potential P63 binding sites allowing, in conjunction with expression arrays, the generation of a target list of 71 genes for further investigation. However it is important to assess the limitations of the methods adopted and any potential bias they may have introduced into the data set.

The validity of a ChIP-Seq data set is dependent upon the quality of the antibody utilized (Bailey *et al*. 2013). Throughout this project the P63 alpha H129 human polyclonal antibody was used, which is specific for α-isoforms of P63. However other P63 antibodies are available and have been used in similar studies previously (Kouwenhoven *et al*. 2010; McDade *et al*. 2012). Two previously completed P63 ChIP-Seq studies made use of the 4A4 pan-isoform antibody (Kouwenhoven *et al*. 2010; McDade *et al*. 2012) furthermore the Van Bokhoven and Zhou group made use of both the 4A4 and H129 antibodies in the generation of their data set (Kouwenhoven *et al*. 2010). A composite binding site list was generated by

intersection of the ChIP-Seq data sets with some discrepancies identified between antibody binding at some sites (Kouwenhoven *et al*. 2010). This study presented the first P63 ChIP-Seq data set generated from stage appropriate upper lip tissue. It is important to note that during lip E11 lip morphogenesis, the predominantly expressed isoform of P63 is ΔNp63α (Thomason *et al*. 2008). It could therefore be argued that use of the H129 antibody in isolation was appropriate to identify the targets of ΔNp63α regulation. However it is unclear whether complementation with the 4A4 antibody could have provided additional confidence in the data set or identified additional P63 binding motifs.

A pivotal stage in the ChIP-Seq analysis pipeline is peak calling (Diaz *et al*. 2012; Bailey et al. 2013). Peak calling in this project was completed using MACS (Zhang *et al*. 2008). It has been suggested that to maximise the efficiency of peak calling analysis, the comparative sequencing of a control sample is advised, such as that of the input sample (Kharchenko *et al*. 2008; Diaz *et al*. 2012; Bailey et al. 2013). This step was not included in this project, which could lead to an over-representation of false positive results within the data set (Bailey et al. 2013). However the MACS software package allows the analysis of ChIP-Seq data sets which lack a control sample using a MVS to filter identified binding sites (Zhang *et al*. 2008; Diaz *et al*. 2012). To mitigate the potential influence of false-positive results due to the lack of a control sample, an MVS was generated from validated P63 binding sites thus providing increased confidence in the data set. The lack of the control reference sample could explain the two binding sites which failed to display positive enrichment using ChIP-qPCR (Section 3.3.1) (Kharchenko *et al*. 2008; Bailey et al. 2013). The use of the MVS allowed further ChIP-Seq analysis to be completed with confidence, however it may be prudent in future work to complete an additional E11.5 ChIP-Seq experiment which incorporates an input control.

The presence of a ChIP-Seq peak proximal to a gene, while informative of protein/DNA interactions, does not suggest biological functionality in regulating the proximal gene. Therefore the ChIP-Seq data set was complemented via the use of microarrays to compare the expressional profile of the facial processes across *Trp63*$^{+/+}$ and *Trp63*$^{-/-}$ embryos. Two microarrays were completed on E11.5 and E12.5 facial processes, identifying 1431 genes as being significantly (p= 0.05) differentially regulated. For the purpose of this project the p-value was used as the measure of significance, however this method is contentious within microarray analysis (Aubert *et al*. 2004).

It has been suggested that to minimise the number of false positive results present within a microarray data set, further analysis should be conducted preferentially to q-value rather than p-value (Storey & Tibshirani, 2003). The p-value is calculated relative to the false positive rate (Storey & Tibshirani, 2003). It is therefore assumed that within a microarray data set, genes displaying differential regulation with a p-value ≤ 0.05 are those most likely to be truly positive results. In contrast, the q-value is calculated relative to the false discovery rate within a data set generated relative to p-value (Storey & Tibshirani, 2003). Therefore q-

value provides a far higher measure of potential significance by identifying the most significant genes present within a previously generated significant gene list (p= 0.05) (Storey & Tibshirani, 2003; Aubert *et al*. 2004).

In this project p-value was used to identify significant potential target genes for further investigation. However the use of p-value may have introduced false positive results into the data set. This may account for the three genes which failed to display significant differential expression using qPCR (Section 3.3.2.7). Use of the q-value in prioritisation of genes for further investigation would have reduced the number of significantly differentially regulated genes within the E12.5 microarray to 103 and within the E11.5 microarray to one. It could therefore be argued that continued analysis using the significant (q= 0.05) genes would have provided the most stringent gene list. However the potential impact of the use of p-value was partially mitigated via the intersection with the ChIP-Seq data set. Furthermore within the E11.5 microarray only one gene (*Alg3*) was shown to be significantly (q= 0.05) differentially regulated which, coupled with the PCA analysis, provided further evidence for the exclusion of the data set from further analysis.

Following the generation of ChIP-Seq and microarray data sets, identified peaks and genes were intersected to generate a data set of differentially regulated genes proximal to a P63 binding site. The galaxy RNAChIPIntergrator was used which allows the user to specify maximum TSS to peak distance. For the purpose of this project intersections were completed at serial distances increasing by increments of 25 kb to a maximum distance of 150 kb. Intersections were completed for nearest gene only. Of the 10,209 identified peaks, 1177 were found to overlap directly with the promoter of a gene. A maximum intersection distance of 150 kb was chosen for further analysis based upon comparisons between the increased numbers of genes identified against increasing genomic distance. However the maximum distance of 150 kb remains an arbitrary figure imposed upon the data set. It is important to consider the implications of imposing a maximum intersection distance upon such data analysis particularly in regards to P63 where the mechanism of gene regulation remains largely uncharacterised (Kouwenhoven *et al*. 2015).

Previous studies which have intersected P63 ChIP-Seq data against microarray data have made use of a cut-off distance of 25 kb (McDade *et al*. 2012). While this distance is smaller than the distance chosen for this study, it is important to note that P63 has been shown to regulate target gene expression at a diverse number of distances greater than 250 kb (Kouwenhoven *et al*. 2010; Watanabe *et al*. 2014; Mollo *et al*. 2015). Furthermore analysis of sites of P53 regulation have shown using chromosome conformation capture that P53 response elements were able to regulate gene expression at a distance greater than 400 kb (Melo *et al*. 2013). This therefore raised the possibility that potential gene to peak associations may be overlooked due to the choice of intersection distance. However difficulties arose during the analysis of the ChIP-Seq data due to the volume of identified

peaks. It was therefore decided that 150 kb was the optimal maximum distance for this study.

ChIP-Seq intersection was conducted to identify only the nearest gene. This method has previously been utilised in other studies where ChIP-Seq data was analysed (McDade *et al*. 2012; Léveillé *et al*. 2015). Nearest gene identification provided a simple method by which to identify potential genes for investigation (Bailey et al. 2013). However such an analysis method functions under the assumption that the gene most proximal to the peak is the most likely potential target of regulation. The method is therefore flawed in that it could potentially overlook any long distance regulation which may occur in deference of proximal genes. Furthermore a recent study identified a suggested chromatin looping mechanism by which P63 was able to regulate the expression of *DLX5/DLX6* during limb development at a distance greater than 250 kb (Kouwenhoven *et al*. 2010). While the potential impact of this analysis was lessened through the use of significantly differentially regulated genes only for the intersection, without a full knowledge of how P63 physically interacts with target genes, it is possible false positive or negative results could be generated. It may therefore prove prudent in future research to incorporate chromatin conformation capture, a technique which displays chromatin folding, to identify sites with greater confidence (Melo *et al*. 2013).

The final area of limitation identified within the analysis of this data set was the method of gene prioritisation. Intersection of the ChIP-Seq to microarray data sets generated a prospective gene list in excess of 800 genes. Therefore genes were prioritised based upon functional annotations. Functional annotation of the data sets identified enrichment for terms related to adhesion, cell signalling and the enrichment of Wnt, Fgf and Shh signalling. Previous studies conducted on P63 ChIP-Seq data sets used gene ontology to identify trends within the data sets (Kouwenhoven *et al*. 2010; McDade *et al*. 2012). While gene ontology provided an excellent tool for target gene identification, it is reliant upon the quality of curation (McLean *et al* 2010; Huang *et al*. 2008).

There is therefore the possibility that studies which have not been entered into the source database will be unavailable for analysis (Huang et al. 2008). Both DAVID and GREAT gene ontology tools are designed for use with large data sets, however difficulties can arise due to data volume. Due to the large number of peaks and genes identified within the study and the diverse number of ontology terms enriched it is possible that smaller degrees of functional clustering may be overlooked. For the purpose of this project, investigating the groups which display higher degrees of enrichment provided the greatest likelihood of *bona fide* P63 targets. However an argument could be made that investigating functional groups with a lower degree of enrichment could identify genes associated with functions novel to *Trp63*.

3.4.4 P300 co-localises with a subset of P63 binding motifs

Previously generated data from the Dixon lab group suggested that P300 may co-localise with P63 at a subset of potential P63 binding sites. Using a subset of candidate P300 facial enhancer sites and validated P300 enhancer sites, 161 binding sites were identified as displaying potential co-localisation. P300 is a histone acetyltransferase and transcriptional co-activator (Eckner *et al*. 1994). Previous research has shown that the P300 protein in humans contributes to the formation of the enhansosome and the initiation of transcription (Merika *et al*. 1998). Structural analysis of the P300 protein identified a core bromodomain in addition to three distinct cysteine/ histidine rich regions (Eckner *et al*. 1994). It has been suggested that these domains function to allow binding of multiple transcription factors (Eckner *et al*. 1994).

P300 has been shown to function in concert with the transcriptional co-activator Cbp, as scaffold proteins, and so they are commonly referred to in conjunction (Merika *et al*. 1998; Goodman & Smolik, 2000). Binding of multiple transcription factors to p300/Cbp is thought to allow the co-operation of signalling networks resulting in a rapid increase in transcription levels (Yao *et al*. 1998; He *et al*. 2012). The acetyltransferase activity of P300 is thought to contribute to transcriptional regulation through chromatin remodelling (Yao *et al*. 1998). Characterisations of P300/Cbp function have implicated roles cell cycle regulation in proliferation, apoptosis and differentiation (Chan & Thangue, 2001; Goodman & Smolik, 2000; Eckner *et al*. 1996).

Human mutations within *EP300* have been shown to cause Rubinstein-Taybi syndrome (RTS) which is a congenital condition which features growth and mental retardation as well as developmental defects of neural crest cell derived tissues (Roelfsema *et al*. 2005). Furthermore in rare cases affected individuals have been shown to display orofacial defects including cleft lip, cleft palate and dental abnormalities (Hennekam & Van Doorne, 1990). Mouse models of *P300* mutation display multiple defects including defects in neurulation, cell proliferation, heart developmental defects and embryonic lethality post E11.5 when *P300*$^{-/-}$ (Yao *et al*. 1998).

Due to the roles of P300/Cbp in transcription factor recruitment at enhancer sites, studies have sought to use P300 binding as a marker for potential enhancers (Blow *et al*. 2010; Attanasio *et al*. 2013). A recent study by Visel's group used ChIP-Seq conducted on chromatin extracted from E11.5 facial processes to identify potential facial enhancer sites (Attanasio *et al*. 2013). In excess of 4000 potential enhancer sites were identified. Of the 4000 potential enhancer sites, 205 were further investigated using the generation of transgenic *LacZ* reporter mice with 121 displaying reporter gene activity within the facial processes (Attanasio *et al*. 2013). Targeted deletions of three enhancers hs1431, hs746 and hs586 failed to generate an abnormal facial phenotype, however skeletal abnormalities were observed. Expression levels of presumptive target genes were shown to be reduced,

suggesting they were *bona fide* facial enhancer sites (Attanasio *et al*. 2013). Intersecting ChIP-Seq data against the P300 data set could provide an effective method of identifying enhancer sites present within the data, in addition P300 has been shown to be able to associate directly with P53 family members (Avantaggiati *et al*. 1997; Attanasio *et al*. 2013).

The presence of 161 P300 binding sites within the total P63 E11.5 ChIP-Seq data set is highly encouraging as it suggests that P63 binding at facial enhancer sites has been identified. Furthermore six validated facial enhancers were found to overlap with the ChIP-Seq data set post microarray intersection. While it would be interesting to further investigate the potential overlap between P63/P300 binding, the relatively low number of P63 binding sites identified as P300-positive was discouraging. The central aim of this project was to identify transcriptional targets of P63 regulation, it was therefore decided that further analysis of P300 interactions would not be completed as a priority.

3.4.5 ChIP-Seq and microarray analysis identified enrichment within Wnt-related genes

Consistently throughout the analysis pipeline, the Wnt signalling family was found to be over represented within both the ChIP-Seq and microarray data sets. The roles of Wnt signalling during upper lip morphogenesis have been characterised, however the individual function of members of the Wnt signalling family remain unresolved (Jiang *et al*. 2006). Multiple members of the Wnt family have been shown to be expressed throughout the facial processes at E11.5 including *Wnt4*, *Fzd1*, *Wnt3*, *Wnt3a* and *Wnt10b* (Summerhurst *et al*. 2008). Disruption of the Wnt signalling network during lip morphogenesis has been shown to result in craniofacial defects, with a loss of β-catenin resulting in bone defects of the upper lip and cleft palate (Kawakami *et al*. 2014). Furthermore a potential link between Wnt signalling and P63 was suggested via the analysis of *Pbx* knockout mouse models (Ferretti *et al*. 2011). A loss of *Pbx1* and *Pbx2* resulted in down-regulation of *Trp63* via *Wnt3* and *Wnt9b* (Ferretti *et al*. 2011). Due to their enrichment within the data set, a subset of Wnt genes was chosen for future analysis. It is therefore important to discuss their potential as putative P63 target genes.

ChIP-Seq microarray intersection identified two peaks 13608 bp and 74594 bp proximal to *Wnt3*. Mutations within *WNT3* in humans give rise to the condition Tetra-Amelia syndrome which is characterised by the absence of all four limbs in extreme cases (Niemann *et al*. 2004). Common phenotypes of Tetra-Amelia include abnormalities of the limbs, facial regions and urogenital regions (Niemann *et al*. 2004). Of interest for this study, Tetra-Amelia commonly features cleft lip and palate as a phenotype (Niemann *et al*. 2004). In addition, polymorphisms within *WNT3* have been shown to be significantly associated with the risk of NSCL/P (Mostowska *et al*. 2012). Human mutations in *TP63* commonly display limb defects in addition to cleft lip and palate as a phenotype (Rinne *et al*. 2007). The phenotypic overlap between *WNT3*- and *TP63*-associated conditions could suggest that they function within

shared signalling networks during development (Niemann *et al*. 2004; Rinne *et al*. 2007). Furthermore *Wnt3* has been shown to be expressed within the surface ectoderm of the medial nasal, lateral nasal and maxillary processes between E10 and E11.5, with expression highly localised to the lambdoidal junction (Ferretti *et al*. 2011). The significant down-regulation of *Wnt3* coupled with the identification of two putative binding sites and *Wnt3*'s expression profile during lip morphogenesis could suggest *Wnt3* is a transcriptional target of P63. It was therefore decided that *Wnt3* would be a high priority target for further investigation.

IRF6 is highly characterised target of P63 regulation, with the original association suggested due to the phenotypic overlap between VWS and *TP63*-related syndromes and the presentation of the rare phenotype of mixed clefting within families (Kondo *et al.* 2002). Mutations within *IRF6* in humans are responsible for approximately 70% of cases of VWS (Blanton *et al*. 2005). A recent study of VWS patients that were negative for mutation within *IRF6* identified coding mutations in the Wnt-related gene *GRHL3* (Peyrard-Janvid *et al*. 2014). Furthermore analysis of *Grhl3*-null embryos identified abnormalities within periderm development with 17% developing cleft palate, however cleft lip was not observed in mouse models and VWS patients with *GRHL3* mutations were more likely to display cleft palate than cleft lip (Peyrard-Janvid *et al*. 2014). Expression of *Grhl3* has been detected within the surface ectoderm and oral epithelium between E10.5 and E12.5, however expression during lip morphogenesis has not been comprehensively characterised (Auden *et al*. 2006; Gustavsson *et al*. 2007). *Grhl3* was found to be significantly down-regulated in microarray analysis and four putative P63 binding sites were identified ≤ 150 kb. Together these data could suggest *Grhl3* is regulated via P63 during lip morphogenesis and warranted further investigation.

Mutations within *TP63* in humans give rise to a number of conditions which feature cleft lip and palate as a phenotype, including SHFM (Sowińska-Seidler *et al*. 2014). To date at least six forms of SHFM have been characterised with mutations in *TP63* linked to autosomal dominant forms. A recent study identified mutations within *WNT10B* as the cause of an autosomal recessive form of SHFM within a consanguineous Pakistani family (Khan *et al*. 2012). WNT10B has been shown be involved in the development of multiple tissues including skin, bone and adipose tissue (Vertino *et al*. 2005; Wend *et al*. 2011). *Wnt10b* was found to be significantly down-regulated in *Trp63*$^{-/-}$ facial processes and two putative binding sites were identified ≤ 150 kb from the TSS. Furthermore expression of *Wnt10b* in secondary palate development closely resembles that of *Trp63* with expression highly localised to the epithelium of the palatal shelves and the medial epithelial seam prior to fusion (Warner *et al*. 2009; Thomason *et al*. 2010). *Wnt10b* expression was reduced within the medial epithelial seam immediately prior to fusion displaying further expressional overlap with *Trp63* (Warner *et al*. 2009; Thomason *et al*. 2010). These data could suggest that P63

regulates *Wnt10b* during upper lip morphogenesis, however comprehensive analysis of *Wnt10b* expression during lip morphogenesis remains to be completed.

It has previously been suggested Wnt genes display a degree of functional redundancy, allowing functional compensation in the event of expression loss (Song *et al*. 2009). Expression analysis of *Wnt10b*$^{-/-}$ myoblasts showed elevated levels of *Wnt7b* (Vertino *et al*. 2005). It was suggested that a loss of *Wnt10b* resulted in increased *Wnt7b* expression to compensate and maintain the differential potential of myoblasts (Vertino *et al*. 2005). *Wnt7b* has previously been shown to be involved in regulating the differentiation and proliferation of lung epithelium and contributed to the regulation of *Pdgfrα* and *Pdgfrβ* (Cohen *et al*. 2009). Investigation of potential markers for cleft lip and palate in Pyrenees shepherd dogs identified *Wnt7b* as a potential candidate gene, however linkage failed to achieve significance (Kemp *et al*. 2009). Furthermore expression of *Wnt7b* was detected within the epithelium of the facial processes at E11.5 in mouse embryos (Summerhurst *et al*. 2008). Discrete regions of *Wnt7b* expression was detected at the lambdoidal junction within the medial nasal, lateral nasal and maxillary processes with expression extending posteriorly along the lacrimal groove (Summerhurst *et al*. 2008). Two putative binding sites were identified proximal to *Wnt7b* and the potential overlap of expression of *Wnt7b* and *Trp63* may suggest its a transcriptional target of P63 and warrants further investigation (Summerhurst *et al*. 2008; Thomason *et al*. 2010).

Wnt signalling functions through the binding of a glycoprotein ligand, to Wnt receptor proteins including the *Frizzled* and *Low Density Lipoprotein Receptors* (Archbold *et al*. 2012). Binding induces a downstream signalling cascade resulting in transcriptional regulation (Archbold *et al*. 2012). *Fzd4* was found to be significantly up-regulated in the absence of P63 and three putative binding sites were identified ≤ 150 kb from the TSS of the *Fzd4* gene. In mouse, *Fzd4* has been shown to be expressed within the facial processes at E11.5. Expression was localised around the nasal pits predominantly within the medial nasal processes (Summerhurst *et al*. 2008). Furthermore expression analysis in chick identified expression within the epithelium and mesenchyme of the frontonasal mass and maxillary prominence (Geetha-Loganathan *et al*. 2009). Human mutations in *FZD4* have previously been associated with familial exudative vitreoretinopathy (FEVR), a hereditary ocular disorder characterised by degenerative vision loss, retinal detachment and subsequent blindness (Robitaille *et al.* 2002; Kondo *et al*. 2003). However a previous study has identified complex chromosomal rearrangements in a patient displaying exudative vitreoretinopathy, growth retardation and cleft palate (Li *et al*. 2006). Chromosomal rearrangements were found to induce *FZD4* haploinsufficiency, however additional deletions were present and it was unclear if *FZD4* deletions contributed to the clefting phenotype (Li *et al*. 2006).

Single nucleotide polymorphisms in the Wnt ligand *WNT3A* have previously been found to display significant association with the incidence of NSCLP (Yao *et al*. 2011; Mostowska *et al*. 2012). Within the present data set, *Wnt3a* was found to be significantly down-regulated in

Trp63$^{-/-}$ facial processes and five potential P63 binding sites were identified ≤ 150 kb from the TSS of the *Wnt3a* gene. While the previous association with NSCLP would suggest that *Wnt3a* would make an ideal candidate gene for P63 regulation, previous studies into *Wnt3a* expression during lip morphogenesis proved inconclusive (Geetha-Loganathan *et al*. 2009; Mostowska *et al*. 2012). Analysis of *Wnt3a* expression during chick facial development, failed to identify expression within the frontonasal prominence (Geetha-Loganathan *et al*. 2009). Furthermore expression within mouse facial processes at E11.5 was minimal (Summerhurst *et al*. 2008). The lack of *Wnt3a* expression within the facial processes could suggest that *Wnt3a* is not a target of P63 regulation, despite the fact that it was significantly differentially regulated within this data set. It may therefore be prudent to prioritise other target genes in preference to *Wnt3a*.

Previous research into the cleft lip phenotype of *Trp63*$^{-/-}$ embryos identified a significant reduction in size of the maxillary processes (Thomason *et al*. 2008). It was therefore suggested that a lack of proliferation within the maxillary processes contributed to the cleft lip phenotype observed (Thomason *et al*. 2008). At E11.5 expression of the Wnt effector *Lef1* was detected throughout the facial processes, but was shown to be highly concentrated within both the epithelium and mesenchyme of the maxillary processes (Mailleux *et al*. 2002). *Lrp6*$^{-/-}$ embryos display a similar bilateral clefting phenotype to *Trp63*$^{-/-}$ embryos with hypoplastic facial processes (Song *et al*. 2009). Additionally a reduction of *Lef1* expression was observed in the facial processes, however it was unclear whether this was causal or a consequence of reduced proliferation (Song *et al*. 2009). *Lef1* was found to significantly down-regulated within the present data set and six putative binding sites were identified ≤ 150 kb of the *Lef1* TSS. Due to the similarity in the phenotypes observed between *Trp63*$^{-/-}$ and *Lrp6*$^{-/-}$ embryos, a loss of P63 regulation of *Lef1* during lip morphogenesis may contribute to the hypoplasia observed within the facial processes.

Enrichment for the Wnt signalling network was consistent throughout all stages of analysis suggesting they may be *bona fide* targets of P63 regulation. Multiple Wnt genes have been shown to be expressed during upper lip morphogenesis and mutations within multiple Wnt genes have been linked to cleft lip and palate (Jiang *et al*. 2006; Summerhurst *et al*. 2008; Kemp *et al*. 2009; Yao *et al*. 2011; Khan *et al*. 2012). Furthermore the previous identification of *Wnt3*/*Wnt9b* regulation of *Trp63* is of particular interest as the present data could suggest a putative feedback regulation loop (Ferretti *et al*. 2011). It is clear that the Wnt signalling family warrants further investigation and classification.

3.4.6 ChIP-Seq and microarray analysis identified enrichment with Fgf related genes

Gene ontology analysis of the ChIP-Seq and microarray intersected data sets identified an enrichment of genes related to the Fgf signalling network. The roles of Fgf signalling during facial development have been extensively investigated, with the expression profiles of Fgf signalling molecules and their receptors characterised (Bachler & Neubüser, 2001).

Disruption of Fgf signalling during lip morphogenesis has been shown to induce a clefting phenotype due to proliferative and apoptotic defects (Abu-Issa *et al*. 2002; Goodnough *et al*. 2007). Previous studies have identified *Fgf8* and *Fgfr2b* as potential targets of P63 regulation (Laurikkala *et al*. 2006). A loss of *Trp63* expression within the limb bud apical epidermal ridge resulted in a loss of *Fgf8* expression, however no reduction of *Fgf8* was observed within the first branchial arches or dental lamina (Laurikkala *et al*. 2006). This could suggest that P63 *Fgf8* regulation was tissue specific (Laurikkala *et al*. 2006). Furthermore a loss of *Fgf8* expression was observed within the epithelium of the medial nasal, lateral nasal and maxillary processes in *Trp63*$^{-/-}$ embryos (Thomason *et al*. 2008). The enrichment of Fgf genes within this data set was therefore highly encouraging and may suggest P63 acts to regulate the expression of multiple Fgf genes.

Expression of the Fgf receptor genes *Fgfr2* and *Fgfr3* was found to be significantly down-regulated in the absence of P63. Nine putative P63 binding sites were identified proximal to *Fgfr2* and one proximal to *Fgfr3*. The association between P63 and *Fgfr2* and *Fgfr3* has previously been investigated by the Missero group (Ferone *et al*. 2012). The study showed P63 regulated the expression of *Fgfr2* and *Fgfr3* within primary mouse keratinocytes and embryonic skin. Of further interest, the group found the Leu514Phe (L514F) human mutation, a cause of the cleft lip and palate associated condition AEC, resulted in a loss of *Fgf* regulation (Ferone *et al*. 2012). These results could suggest that a loss of Fgf signalling contributes to the clefting phenotype observed in *TP63*-related conditions. Further studies in human cell lines derived from bladder cancers observed regulation of *FGFR3* by both TAp63 and ΔNp63 isoforms as well as isoforms of P73 (Sayan *et al*. 2010). Furthermore *FGFR2* and *FGFR3* have been shown to be expressed throughout the mesenchyme of the frontonasal mass and superior aspects of the lateral nasal processes in chick embryos (Matovinvic & Richman, 1997). Previous studies have shown that P63 can function in a tissue specific manner, it is therefore important to confirm if P63 regulation of *Fgfr2* and *Fgfr3* is active during lip morphogenesis (Kouwenhoven *et al*. 2010).

Spry proteins are able to function as either inhibitors or activators of RTK-dependent signalling pathways including Fgf signalling (Mason *et al*. 2006). *Spry1*$^{-/-}$ mouse embryos develop ureteric abnormalities with multiplex kidneys and multiple ureters (Basson *et al*. 2005). Generation of a conditional *Spry1* transgenic mouse model showed that over-expression of *Spry1* during neural crest migration resulted in profound facial defects including cleft face and cleft palate (Yang *et al*. 2010). Expression of *Spry1* in wildtype embryos identified expression with the fronotonasal prominence between E9.0 to E10.0 and prominently within the emerging medial nasal and lateral nasal processes (Yang *et al*. 2010).

Spry1 was found to be up-regulated in the absence of P63 and five putative P63 binding sites were identified ≤ 150 kb from the TSS of *Spry1*. These data could suggest that P63 functions to repress *Spry1* expression during lip morphogenesis and a loss of repression may contribute to the cleft phenotype observed in *Trp63*$^{-/-}$ embryos. The clefting phenotype

of *Spry1* transgenic embryos was more severe than *Trp63*$^{-/-}$embryos (Mills *et al*. 1999; Yang *et al*. 1999; Yang *et al*. 2010). The disparity between the two phenotypes could be due to the onset of *Spry1* misregulation with the *Spry1* transgenic displaying earlier disruption and as such developed a more severe phenotype (Yang *et al*. 2010). Due to the phenotypic overlap between *Trp63*$^{-/-}$ and *Spry1* transgenic embryos, coupled with the data generated by ChIP-Seq and microarray analysis, it could suggest that *Spry1* is a direct target of P63 regulation and warranted further investigation (Mills *et al*. 1999; Yang *et al*. 1999; Yang *et al*. 2010).

Spry proteins display functional redundancy displaying a high degree of structural conservation (Mason *et al*. 2006). In addition to *Spry1*, expression of *Spry2* was found to be up-regulated in *Trp63*$^{-/-}$ facial processes and three proximal P63 binding sites were identified. *Spry2*$^{-/-}$ embryos have been shown to display cleft lip and palate, furthermore analysis palatal cultured showed that cleft palate in *Spry2*$^{-/-}$ was due to elevated levels of mesenchymal proliferation (Welsh *et al*. 2007; Matsumura *et al*. 2010). At E11.5 *Spry2* expression was detected within the medial nasal, lateral nasal and maxillary processes epithelium and mesenchyme, with strong expression present within the lambdoidal junction (Welsh *et al*. 2007).

While the role of *Spry2* in palate development was further classified, the study did not investigate the effect of *Spry2*$^{-/-}$ on lip development (Welsh *et al*. 2007). Previous studies have shown a loss of *Spry2* expression resulted in cleft lip and palate, however in the present data set a loss of P63 resulted in increased expression (Welsh *et al*. 2007; Matsumura *et al*. 2010). It remains therefore unclear if *Spry2* is a target of P63 regulation and if abnormal *Spry2* expression contributes to the clefting phenotype observed.

The roles of Fgf genes in facial development are well characterised (Bachler & Neubüser, 2001). Coupled with the previous associations with P63-regulation, the enrichment of these genes within the data set is highly encouraging, adding further credence to the accuracy of the data (Laurikkala *et al*. 2006). Further investigation and characterisation of Fgf genes provides an exciting prospect, with the data indicating P63 may function to regulate multiple members of the signalling network, including ligands, receptors and antagonists.

3.4.7 ChIP-Seq and microarray analysis identified an enrichment of adhesion-related genes

In addition to enrichment within the Wnt and Fgf genes, enrichment was observed within a subset of genes related to biological adhesion. The role of P63 in regulating adhesion is well documented. *Trp63*$^{-/-}$ embryos are neonatal lethal, with a thin shiny epithelium which fails to provide appropriate barrier function leading to death via desiccation (Mills *et al*. 1999; Yang *et al*. 1999). Successful cellular adhesion is integral to upper lip morphogenesis with multiple adhesion events occurring, between the medial nasal and maxillary processes and subsequently the lateral nasal and maxillary processes (Warbrick, 1960; Hinrichsen, 1985).

The failure of the facial processes to adhere successfully can result in clefting (Mossey *et al*. 2012). The generation of *Trp63*$^{-/+}$/*Irf6*$^{+/R84C}$ embryos showed that the presence of a persistent periderm layer prevented the correct adhesion of the palatal shelves during secondary palate development resulting in cleft palate (Thomason *et al*. 2010).

Further work by the Trainor group recapitulated these findings in upper lip development, showing that a persistent periderm of the nasal processes in *Hhat*^{creface}*Ptch1*^{wiggable} embryos contributed to a failure of adhesion (Kurosaka *et al*. 2014). Together these findings underline the importance of adhesion during orofacial development. Furthermore recent work conducted by the Dixon and Missero groups identified enrichment within adhesion related genes in their E14 palatal shelf ChIP-Seq and microarray data sets (Mitchell *et al*. manuscript in preparation). It has been suggested that P63 and Irf6 cooperatively regulate periderm formation during palatal shelf outgrowth (Mitchell *et al*. manuscript in preparation). In addition it has been suggested P63 regulates the adhesion between periderm cells and the basal epithelium in the palatal shelves (Mitchell *et al.* manuscript in preparation). Due to the previous association of *Trp63* and adhesion, it is important to discuss the potential of P63 adhesion regulation in upper lip morphogenesis.

Cldn1 is a confirmed target of P63 regulation known to be required for epidermis formation (Lopardo *et al*. 2008). Claudins represent one of the three principle components of tight junctions, which are linked to occludins and the actin cytoskeleton by tight junction proteins (Tsukita & Furuse, 2000). Tight junctions function to seal the intercellular space in epithelial and endothelial cellular sheets and are integral to the barrier function of the epidermis (Tsukita & Furuse, 2000; Furuse *et al*. 2002). Models of *Cldn1* knockout display a skin phenotype highly similar to that of *Trp63*$^{-/-}$ embryos, with embryos displaying neonatal lethality due to desiccation caused by lack of barrier function of the epidermis (Furuse *et al*. 2002; Mills *et al*. 1999; Yang *et al*. 1999).

The Guerrini group were able to show P63 binding at two sites within the promoter of *Cldn1* (Lopardo *et al*. 2008). Furthermore *Cldn1* expression was shown to be reduced in mouse keratinocytes where *Trp63* was knocked-down (Lopardo *et al*. 2008). Further analysis of *CLDN1* expression within skin biopsies from AEC patients showed a significant down-regulation of *CLDN1* compared with wildtype, suggesting that misregulation of *CLDN1* contributes to the skin phenotype observed in *TP63*-related conditions (Lopardo *et al*. 2008). The presence of *Cldn1* within the present data set was therefore encouraging. However it was not possible to recapitulate the binding sites identified by the Guerrini group (Lorpardo *et al*. 2008). *Cldn1* was shown to be down-regulated in *Trp63*$^{-/-}$ facial processes and two putative binding sites were identified ≤ 150 kb from the *Cldn1* TSS. Current expression profiles of *Cldn1* during lip morphogenesis are unclear, therefore a comprehensive expression analysis in facial processes will need to be conducted (Magdaleno *et al*. 2006). However *Cldn1* has been shown to influence neural crest migration, which is a key precursor to the outgrowth of the facial processes (Jiang *et al*. 2006; Fishwick *et al*. 2012).

In contrast to *Cldn1*, *Cldn4* was shown to be up-regulated in *Trp63*$^{-/-}$ facial processes and two potential P63 binding sites were identified proximal to the TSS. Deletion of *CLDN4* in humans is linked to the incidence of Williams-Beuren syndrome, a neurodevelopmental disorder characterised by distinct facial features, mental retardation and cardiovascular complications (Paperna *et al*. 1998; Pérez Jurado, 2003). Williams-Beuren syndrome is caused by a heterozygous 1.5 Mb deletion at 7q11.23 encompassing 26-28 genes (Borralleras *et al*. 2015). Orofacial clefting is not considered to be a common phenotype of Williams-Beuren syndrome, however studies have identified patients displaying cleft palate (Blanco-Dávila & Olveda-Rodriguez, 2001; Domenico *et al*. 2013). To this author's knowledge cleft lip has not been reported as a phenotype of Williams-Beuren syndrome, however a clinical report on monozygotic twins with Williams-Beuren syndrome with cleft palate noted that their father had cleft lip (Pankau *et al*. 1993). Due to the number of genes deleted in Williams-Beuren syndrome, it is unknown if *CLDN4* plays a functional role in the pathogenesis of the condition (Borralleras *et al*. 2015). However the implication that *CLDN4* could be expressed during palatogenesis is encouraging.

Cldn4 has previously been identified as a putative target of P63 regulation (Kubo *et al*. 2014). Reductions in ΔNp63 expression in HaCaT keratinocytes resulted in up-regulation of *CLDN4* suggesting ΔNp63 acts to negatively regulate *CLDN4* (Kubo *et al*. 2014). However in the study by Ichimiya and colleagues, no ChIP-qPCR or comparable method was used to investigate P63 localisation at the *CLDN4* promoter, nor was motif discovery conducted (Kubo *et al*. 2014). The putative association between *CLDN4* therefore remains unconfirmed as no direct genomic interactions have been observed (Kubo *et al*. 2014). The present study could therefore identify potential P63 binding sites which regulate *Cldn4*.

The previously identified P63 target gene *Pvrl1* was shown to be down-regulated in *Trp63*$^{-/-}$ embryos and six putative binding sites identified within 150 kb of the TSS (Mollo *et al*. 2015). Polymorphisms in *PVRL1* have been associated with the incidence of NSCLP (Scapoli *et al*. 2006; Sözen *et al*. 2009). Furthermore mutations in *PVRL1* cause cleft lip and palate-ectodermal dysplasia (ED) syndrome (CLPED1), which is characterised by cleft lip and palate and defects of the ectoderm derived tissues (Suzuki *et al*. 2000; Yoshida *et al*. 2015). There is a substantial phenotypic overlap between the phenotypes of CLPED1 and the *TP63*-related conditions EEC and AEC (Suzuki *et al*. 2000; Rinne *et al*. 2007). It is therefore unsurprising that *PVRL1* has been shown to be a direct transcriptional target of P63 regulation (Mollo *et al*. 2015). Depletion of P63 in both human and mouse keratinocytes resulted in a significant down-regulation of *Pvrl1* (Mollo *et al*. 2015).

The group showed P63 enrichment at two sites within the first intron of *PVRL1*, termed p63BS1 and p63BS2 (Mollo *et al*. 2015). Further investigation using luciferase reporter assays showed that P63 binding at p63BS2 was inhibitory (Mollo *et al*. 2015). The presence of *Pvrl1* within the present data set is therefore highly encouraging, furthermore binding at p63BS2 was recapitulated in this data set however no binding was observed at p63BS1. The

absence of enrichment ofp63BS1 could suggest that site is not active during lip morphogenesis, furthermore Mollo and colleagues noted that P63 binding at p63BS1 was substantially lessened compared with p63BS2 (Mollo *et al*. 2015). Taken together these results would suggest that it is highly likely that P63 regulates *Pvrl1* expression during lip morphogenesis.

In addition to enrichment for genes related to tight junctions, *Gjb2* and *Gjb3*, genes which encode proteins integral to gap junctions were both found to be up-regulated in *Trp63*$^{-/-}$ facial processes. One putative P63 binding site was identified proximal to each gene. Gap junctions function to allow direct communication between adjacent cells through the diffusion of ions, metabolites and messenger proteins (Nickel & Forge, 2010). Mutations in *GJB2* and *GJB3* are well characterised, with mutations in both contributing to the incidence of non-syndromic deafness (Nickel & Forge, 2008). In addition mutations within *GJB3* have been shown to cause recessive eythrokeratodermia variabilis (EKV), characterised by transient red patches and localized or generalized hyperkeratosis (Richard *et al*. 1998; Gottfried *et al*. 2002).

There is a clear phenotypic overlap between the skin phenotype associated with *GJB3* mutations and the ectoderm dysplasias which characterise EEC and AEC (Bokhoven & Brunner, 2002; Rinne *et al*. 2007; Richard *et al*. 1998; Gottfried *et al*. 2002). Furthermore *TP63*-related conditions have been commonly shown to feature conductive hearing loss as a phenotype (Rinne *et al*. 2007). Should *GJB2* and *GJB3* be shown to be subject to P63-regulation, this could contribute to the explanation of the hearing loss phenotype. A study into the phenotypic variability of *GJB2* mutations in relation to hearing loss showed that mutations causing truncations in the connexion 26 protein resulted in a more severe hearing loss phenotype (Chan *et al*. 2010). In addition a subset of patients were shown to exhibit cleft lip and palate in addition to the hearing loss phenotype associated with *GJB2* mutations, however it is unclear if these clefts were a direct result of *GJB2* mutation (Chan *et al*. 2010).

The previous association between P63 and adhesion-related genes makes their enrichment within this data set highly encouraging (Mitchel *et al*. manuscript in preparation). Furthermore the recapitulation of a validated P63 binding site, p63BS2, within this data set gives further credence that an accurate and reliable database of potential P63 target genes has been produced (Mollo *et al*. 2015). The expression patterns of many of the genes identified including *Gjb2*, *Gjb3* and *Cldn4* have not been characterised within the facial processes during lip morphogenesis. These genes could therefore provide the opportunity to identify novel targets of P63 regulation within a tissue system in which they have not yet been characterised.

3.5 Summary and further work

Mutations in *TP63* in humans cause a number of conditions which feature cleft lip and palate as a phenotype (Rinne *et al*. 2007). To date the majority of P63 research has focussed on the role of P63 in secondary palate development, while the molecular interactions of upper lip morphogenesis remain largely uncharacterised (Thomason *et al*. 2008; Thomason *et al*. 2010; Ferretti *et al*. 2011; Mitchel *et al.* manuscript in preparation). Previous studies have completed ChIP-Seq assays on human primary keratinocytes isolated from skin and foreskin (Kouwenhoven *et al*. 2010; McDade *et al*. 2012). However the relevance of previous studies in relation to cleft lip research is limited through the choice of model tissue as P63 function has been shown to be tissue dependent (Kouwenhoven *et al*. 2010; McDade *et al*. 2012). This study reports, to this author's knowledge, the first P63 ChIP-Seq and microarray conducted on stage appropriate tissue for lip morphogenesis.

ChIP-Seq analysis identified a large number of potential P63 binding sites. In the absence of a control data set, a minimum validation score was generated based up on the ChIP-qPCR analysis of 41 random binding sites. ChIP-qPCR analysis showed 39 of 41 potential binding sites displayed significant (p= 0.05) positive enrichment (>3 fold the enrichment of *Myoglobin*). Applying the MVS to the ChIP-Seq data set identified 10209 potential binding sites. Motif discovery using P63 Scan identified 83.9% of peaks as P63 motif-positive. Previous P63 ChIP-Seq studies identified 10-15 % of identified binding sites as being P63 motif-negative (Kouwenhoven *et al*. 2010; McDade *et al*. 2012).

The lack of the characteristic P63 binding motif could be indicative of a currently uncharacterised binding motif, or binding via a chaperon protein. Previous studies which addressed the absence of the P63 binding motif identified an enrichment of Tfap2a binding sites (Kouwenhoven *et al*. 2015). Furthermore previous studies have shown that P63 is able to co-localise with proteins including Sox2, Ap2a and P300 (MacPartlin *et al*. 2005; McDade *et al*. 2012; Watanabe *et al*. 2014). In addition to potentially binding with a co-factor, a potential oversight within the P63 Scan programme may have been identified. The P63 Scan programme was originally adapted from P53 Scan (Kouwenhoven *et al*. 2010). The P63 scan programme identifies the characterised 22 bp motif consisting of two half-sites without a spacer element, however subsequent studies have shown P63 is able to bind to singular half-sites, which may be overlooked by P63 Scan (Kouwenhoven *et al*. 2010; Chen *et al*. 2011).

It is therefore unclear if the P63 motif-negative peaks indicate the action of a binding co-factor or a possible limitation of the P63 Scan programme. Future analysis of the ChIP-Seq data set could include further motif discovery to identify potential co-factors. In addition, it would prove highly informative to divide the data set into P63 motif-negative and P63 motif-positive peaks. Analysis of the P63-negative peaks in isolation for both motif discovery and gene ontology analysis could identify a subset of P63 target genes regulated exclusively in

partnership with co-factors. It is interesting to note that while a substantial number of P63 binding sites have been identified across both human and mouse model systems, the method of gene regulation by P63 is currently unknown (Kouwenhoven *et al*. 2010 ;McDade *et al*. 2012; Kouwenhoven *et al*. 2015). Further analysis of the P63 motif-negative peaks and any associated co-factors could provide further insights into how P63 regulates target genes.

Further validation of the ChIP-Seq data was achieved using the intersection against a previously generated and validated ChIP-Seq data set conducted on E14 palatal shelves (Mitchell *et al*. manuscript in preparation). 25% of identified E11.5 ChIP-Seq peaks were found to be present within the E14 data set. These results would suggest the data set generated is highly accurate. Furthermore previous studies have shown that P63 binding occurs in a tissue specific manner, it is therefore unsurprising that a large number of potential binding sites were unique to the E11.5 data set (Kouwenhoven *et al*. 2010). A further intersection against a data set of putative P300-positive facial enhancer sites identified a subset of 162 binding sites displaying potential co-localisation of P63 and P300 (Attanasio *et al*. 2013). Previous studies have shown that P300 is able to co-localise with P63 in the regulation of target genes (Avantaggiati *et al*. 1997). The co-localisation of P300 and P63 at these binding sites could imply they are enhancer sites active during upper lip morphogenesis, and further classification of these sites could prove highly informative (Blow *et al*. 2010). However it was decided it would not be possible within the confines of this project to further investigate potential interactions between P63 and P300 during upper lip morphogenesis.

To complement the ChIP-Seq data set microarray analysis was completed on facial processes isolated from E11.5 and E12.5 *Trp63*$^{+/+}$ and *Trp63*$^{-/-}$ embryos. Initial analysis was conducted on the E11.5 microarray, however a low number of differentially regulated genes were identified (n= 47 p= 0.005 and n= 735 p= 0.05). PCA analysis of the data set failed to show segregation between *Trp63*$^{+/+}$ and *Trp63*$^{-/-}$ samples. Therefore an additional microarray was conducted at E12.5 identifying a large number of differentially regulated genes (n= 464, p= 0.005 and n= 1431, p= 0.05). PCA analysis of the E12.5 microarray displayed segregation between the *Trp63*$^{+/+}$ and *Trp63*$^{-/-}$ samples. Comparisons between the E11.5 and E12.5 microarrays identified a high degree of overlap between the gene lists, with 32% of the E11.5 p= 0.005 genes present within the E12.5 data set. The results of the E12.5 microarray were validated using qPCR of 16 randomly selected genes in E11.5 *Trp63*$^{+/+}$ and *Trp63*$^{-/-}$ facial processes. 13 of the 16 selected genes displayed significant differential expression with *Fermt1*, *Tcfap2a* and *Zfhx3* failing to achieve significance. Based upon gene ontology analysis, it was decided to conduct further research using the entire p= 0.05 E12.5 microarray data set.

It was therefore attempted to identify *bona fide* targets of P63 regulation during upper lip morphogenesis using the intersection of the E11.5 ChIP-Seq and E12.5 microarray. Intersections were conducted at a maximum peak to TSS distance of 150 kb identifying

2655 binding sites potentially associated with 1057 genes. To further prioritise target genes for investigation, gene ontology analysis was conducted. DAVID functional analysis, which identifies functional clustering within a dataset of genes, identified enrichment within genes involved in the regulation of Wnt signalling, Fgf signalling and cellular adhesion. Therefore a gene list of 71 prospective target genes was generated for further analysis. The presence of a P63 binding site proximal to a differentially regulated gene does not signify biological activity.

Genes identified included *Wnt3*, *Grhl3*, *Fgfr2*, *Spry1*, *Spry2*, *Cldn1* and *Cldn4*. Multiple genes within the target data set have previously been implicated in orofacial clefting in both the syndromic or non-syndromic forms (Ferretti *et al*. 2011; Ferone *et al*. 2012; Khan *et al*. 2012; Peyard-Janvid *et al*. 2014). The presence of cleft lip with/without cleft palate-associated genes within the data set is highly encouraging, suggesting identified genes display functions appropriate for putative P63 target genes. The previously validated P63 target gene *Pvrl1* was found to be present within the data set (Mollo *et al*. 2015). Furthermore the validated P63 binding site p63BS2 was recapitulated in this data set (Mollo *et al*. 2015). The presence of p63BS2 within this data set is highly encouraging, suggesting a highly accurate and reproducible data set has been generated from which further analysis can be made.

Attempts have been made to identify the limitations of the analyses used and so limit the inclusion of false positive or negative results within the data. Identified limitations included the lack of an input ChIP-Seq data set for comparison, the use of p-value for the measurement of differential expression significance and potential limitations in the intersection protocol due to intersection distance and the restrictions of nearest gene identification (Aubert *et al*. 2004; Bailey et al. 2013; Kouwenhoven *et al*. 2015). Additional limitations were identified in the prioritisation of genes based on functional annotation, with the accuracy of such a method reliant on the quality of database curation and sufficient enrichment of associated terms (McLean *et al*. 2010; Huang et al. 2008). Attempts were made to mitigate the potential effects of these variables on the data set, via the establishment of the MVS. Furthermore the identification of false negative and positive results of the microarray will be mitigated using the intersection against the ChIP-Seq data set. It is therefore believed that a reliable and accurate data set has been generated, as reflected in the identified target genes.

Further analysis must be conducted for each prospective target gene. Each potential P63 binding site will be interrogated using the P63 Scan programme to verify the presence of a P63 binding motif. P63 binding will then be verified using ChIP-qPCR. Having confirmed P63 binding, genes will be further prioritised for investigation based upon Nanostring nCounter analysis. The novel technique of nCounter has been suggested to bridge the gap between the high throughput methodogy of microarrays with the accuracy of qPCR (Kulkarni, 2011; Richard *et al*. 2014). Genes will subsequently need to be further validated using qPCR to

confirm if they are differentially regulated between *Trp63*$^{+/+}$ and *Trp63*$^{-/-}$ embryos. Further expression analysis will be completed using whole mount *in situ* hybridisation to assess whether the expression profile of target genes is altered in *Trp63*$^{-/-}$ embryos. Using these methods it will be attempted to verify if target genes are *bona fide* targets of P63 regulation.

Validation of P63 binding and differential regulation between *Trp63*$^{+/+}$ and *Trp63*$^{-/-}$ embryos will provide strong evidence for the potential regulation of target genes. However as has previously been shown P63 is able to function at distances exceeding 150 kb (Kouwenhoven *et al*. 2010). Therefore to confirm peak to gene interactions it would be prudent to conduct chromatin capture Hi-C. Chromatin capture Hi-C is a novel technique which allows the biophysical properties of chromatin to be analysed to identify chromatin interactions, including enhancer to promoter interactions (Belton *et al*. 2012). Using the above methods it will be attempted to identify and validate targets of P63-regulation in upper lip morphogenesis.

4.0 P63 regulates expression of Wnt and Fgf signalling components

4.1 Introduction

As detailed in the previous chapter, a data set of potential P63 targets was generated using the intersection of a P63 ChIP-Seq data set conducted on E11.5 wildtype facial processes and a microarray completed on E12.5 *Trp63*$^{+/+}$ and *Trp63*$^{-/-}$ facial processes. Gene ontology analyses using DAVID functional analysis and GREAT analysis identified enrichment for genes involved in cell-cell adhesion, Fgf and Wnt signalling. A target gene list of 72 genes was therefore generated consisting of genes significantly differentially expressed between *Trp63*$^{-/-}$ E12.5 facial processes and wildtype controls, and featured a putative P63 binding site ≤150 kb of the target gene's TSS. Identified target genes were further characterised to determine if they were bona fide targets of P63 regulation during upper lip morphogenesis.

In order to confirm P63 binding at identified sites, ChIP-qPCR will be employed as previously described in Chapter 3. To assess if identified target genes are regulated by P63 in upper lip morphogenesis, expression quantification will be completed using Nanostring nCounter, followed by qPCR and whole mount *in situ* hybridisation (WISH). The nCounter system allows the simultaneous assay of up to 800 genes expression levels thus allowing rapid quantification of differential expression within a sample tissue (Kulkarni, 2011). It has been suggested that the nCounter system provides an accurate quantification of gene expression levels based on the abundance of mRNA. In contrast to classical expression assays, the nCounter system measures mRNA content of a sample without the conversion of mRNA to cDNA via reverse transcription or subsequent amplification of cDNA by PCR (Kulkarni, 2011).

For each target gene assayed by nCounter, custom probes are designed consisting of a unique colour barcode at the 5' end, a 35-50 bp target specific sequence and a biotin label at the 3' end allowing for probe retrieval and digital detection (Kulkami, 2011). Probes are hybridised in solution with sample mRNA before unbound probe is removed. Probe/target complexes can subsequently be aligned using the biotin label and the 5' barcode recorded. The expression level of an individual target gene is therefore assayed using recording the number of times the gene specific bar-code is present (Kulkami, 2011). Comparison against a control sample allows the determination of fold-change (Kulkami, 2011). The nCounter system has been utilised in multiple studies as an alternative to microarray and qPCR analysis and it has been suggested the nCounter system can provide an accuracy approaching that of qPCR (Northcott *et al.* 2012; Lovén *et al*. 2012; Kulkami, 2011).

While the nCounter system provides a rapid method for gene expression quantification, subtle changes in spatial expression may not be detected. To further characterise any putative P63 regulation of target genes, expression will be assayed using WISH between

Trp63$^{+/+}$ and *Trp63*$^{-/-}$ embryos. WISH involves the generation of a gene specific riboprobe which will permeate the tissue of experimental embryos and hybridise against native mRNA (Nieto *et al*. 1996). Digoxygenin labelled nucleotides are incorporated into the riboprobes, providing an immunological substrate for detection (Darnell *et al*. 2010). As such WISH can identify where genes are being actively expressed and comparisons between a test sample and control allow the identification of changes in expression levels and location (Nieto *et al*. 1996; Darnell *et al*. 2010). WISH samples can then be sectioned to provide greater detail of gene expression domains (Nieto *et al*. 1996).

Within the present chapter, nCounter was used to further prioritise target genes for investigation. A subset of 52 genes, consisting of adhesion, Wnt and Fgf-related genes, were assayed with 31 displaying significant differential expression between E11.5 *Trp63*$^{+/+}$ and *Trp63*$^{-/-}$ facial processes. It was therefore decided that genes related to Wnt and Fgf signalling activity would be further investigated using ChIP-qPCR, qPCR and WISH. Analyses identified the misregulation of multiple members of the Wnt and Fgf signalling families with expression changes both quantified using qPCR and characterised using WISH. Generation of *Trp63*$^{-/-}$*;BAT-Gal*$^{Tg/+}$ mice further revealed a reduction in canonical Wnt signalling throughout the medial nasal, lateral nasal and maxillary processes of *Trp63*$^{-/-}$ embryos.

Together the results obtained suggested P63 functions to regulate multiple members of the Wnt and Fgf signalling pathway during upper lip morphogenesis, identifying potential novel targets of P63 regulation.

4.2 Materials and Methods

4.2.1 Embryo dissection and processing

All embryos were dissected and processed as according to the protocol previous described (Chapter 2.2).

4.2.2 nCounter analysis

E11.5 *Trp63*$^{+/+}$ (n= 4) and *Trp63*$^{-/-}$ (n= 4) embryos were dissected and facial processes removed as according to the protocol previously described (Chapter 2.2). RNA was extracted as previously described (Chapter 2.4.1) and diluted to a concentration of 20 ng/µl. RNA was delivered to the University of Manchester Core Technologies Facility for nCounter analysis. 52 target genes were selected for nCounter analysis. Custom nCounter primers were designed for each target gene to incorporate a gene specific nCounter barcode. Analysis was completed on a Nanostring nCounter 100 well chip by the University of Manchester Core Technologies Facility.

4.2.3 Expression analyses

ChIP-qPCR, qPCR and WISH were conducted as previously described (Chapter 2.3, 2.4.3 & 2.5). All primers for ChIP-qPCR, qPCR and WISH and be found within Appendices 1-3.

4.2.4 ChIP-Seq annotation

As previously described ChIP-Seq data was displayed as a custom UCSC track (Chapter 3.2.1). Analysis of mammalian conservation was completed by eye using the UCSC mammalian conservation track. All peak co-ordinates are given in reference to the mouse UCSC July 2007 (NCBI37/mm9) genome.

Access to a recently generated H3k27ac, H3k4me3 and H3k27me3 database generated from E11.5 facial tissue and E13.5 and E14.5 palatal shelf tissue was generously provided by Dr. Niki Meerman (Dixon lab, Faculty of Life sciences, University of Manchester, Manchester, England). ChIP-Seq peaks were interrogated by eye for the presence of active markers of transcriptional regulation.

4.2.5 Analysis of Canonical Wnt signalling in *Trp63*$^{-/-}$ embryos

Trp63$^{+/-}$*;BAT-Gal*$^{Tg/+}$ crosses were completed in collaboration with the Selleri lab (Weill Cornell Medical College, New York). *BAT-Gal* mice were crossed onto the *BalbC* background for six generations prior to *Trp63* crosses. *Trp63*$^{+/-}$ mice were crossed with *BAT-Gal*$^{Tg/+}$ mice to produce compound heterozygous *Trp63*$^{-/+}$*;Bat-Gal*$^{Tg/+}$ mice. Compound heterozygotes were then crossed to generated *Trp63*$^{-/-}$*;BAT-Gal*$^{Tg/+}$ embryos. Matings were performed as described previously (Chapter 2.2.1). *LacZ* staining was performed as previously published (Maretto *et al*. 2003).

4.2.6 LiCl induction of Canonical Wnt signalling

A single cross of mice heterozygous for *Trp63*$^{-/+}$ was completed as previously described (Chapter 2.2.1). The pregnant dam was injected twice with 120 µl 150 mM LiCl at E8.5 and E9.5 via intraperitoneal injection. Embryos were collected and processed in Bouin's fixative as previously described (Chapter 2.2.1). Embryos were morphologically examined and photographed using a Leica DMRB photomicroscope using Leica digital photographic software. All embryos were photographed at the same magnification.

4.3 Results

4.3.1 nCounter analysis identified Wnt genes for prioritisation

A target gene list of 71 genes was previously generated from the intersection of the E11.5 ChIP-Seq and E12.5 microarray data sets. It was decided to initially investigate a subset of these genes. To prioritise genes for investigation the Nanostring nCounter system was used allowing the high throughput gene expression quantification of target genes between E11.5 *Trp63*$^{+/+}$ and *Trp63*$^{-/-}$ facial processes. Target gene selection was limited to 50 genes due to test chip limitations. In conjunction with a coinciding project, 52 target genes were selected for nCounter analysis. Selected genes can be seen in Table 4.1. nCounter analysis was completed using custom primer sets on mRNA isolated from *Trp63*$^{+/+}$ (n= 4) and *Trp63*$^{-/-}$ (n= 4) E11.5 facial processes. Analysis was conducted in triplicate across four biological replicates. For each gene a fold-change was calculated between *Trp63*$^{-/-}$ and *Trp63*$^{+/+}$. Significance was determined using the student's t-test. Of the 52 genes assayed, 31 were shown to display significant differential expression between *Trp63*$^{-/-}$ and *Trp63*$^{+/+}$ facial processes (P= 0.05), with 17 down-regulated and 14 genes up-regulated in null embryos (Table 4.2).

To further analyse the nCounter data set, results were intersected against the E11.5 and E12.5 microarrays. Fold-change comparisons against the E11.5 and E12.5 microarrays identified 25 instances where a discrepancy was present, with 14 discrepancies identified against the E12.5 microarray and 11 against the E11.5 data set. However when limiting the intersection against the significant differentially regulated genes, eight genes were shown to display discrepancies with two against the E12.5 data set and six against the E11.5 data set. These data suggested that the significant results from the nCounter analysis were accurate and should be investigated further. Due to the presence of discrepancies between the nCounter data set and E12.5 microarray, it was decided to conduct qPCR analysis of all targets in further analysis. Based on the results of the nCounter analysis, it was decided to initially prioritise Wnt and Fgf genes for further investigation.

4.3.2 P63 signalling is required for correct expression of *Wnt4* during lip morphogenesis

ChIP-Seq analysis identified five potential P63 binding sites proximal to *Wnt4* with peaks present at positions chr4: 136,743,061-136,743,083 Peak 1 (P1), 136,764,040-136,764,062 (P2), 136,827,753-136,827,775 (P3), 136,834,090-136,834,112 (P4) and 136,838,601-136,838,623 (P5) (mm9) (Figure 4.1A). P63 scan identified at least one P63 binding motif present within each of the potential binding sites. All binding sites were found to be conserved across mouse, rat, human, rhesus monkey, dog and horse with *Wnt4* P2, P4 and P5 displaying additional conservation across opossum and platypus. Further analysis of the

Gene Name			
Lef1	*Ppl*	*Jag1*	*Wnt3a*
Fzd10	*Phlda3*	*Bok*	*Wnt2b*
Perp	*Bcl11b*	*Sfrp1*	*Wnt11*
Grhl3	*Pax6*	*Ptprv*	*Shh*
Otx2	*Spry1*	*Hes1*	*Tcfap2a*
Wnt7b	*Fgfr3*	*Wnt7a*	*Gjb3*
Cebpa	*Sox2*	*Rb1*	*Arhgap6*
Plec	*Sox9*	*Fgf9*	*Sulf1*
Jun	*Wnt10b*	*Tcfap2c*	*Mpz*
Cyp26b1	*Ptch2*	*Wnt4*	*Spry2*
Wnt3	*Sik1*	*Cldn1*	*Ldb2*
Sema3c	*Vdr*	*Zhx2*	*Gdf15*
Ikzf2	*Fzd4*	*Ngfr*	*Kdm2b*

Table 4.1 Wnt, Fgf and adhesion-related genes selected for nCounter analysis.

52 genes related to Wnt, Fgf and adhesion were selected for nCounter expression analysis between mRNA isolated from *Trp63*$^{+/+}$ and *Trp63*$^{-/-}$ E11.5 facial processes.

		Microarray fold change					Microarray fold change		
Gene	**Fold Change Null vs. Wt**	**E11.5**	**E12.5**	**P value**	**Gene**	**Fold Change Null vs. Wt**	**E11.5**	**E12.5**	**p value**
Lef1	-2.49843	-1.01603	-1.19002	1.62E-06	***Pax6***	1.618689	1.11409	1.26364	0.004777
Fzd10	-2.22188	1.00266	-1.55822	1.77E-06	***Fgfr3***	-1.33488	-1.01625	-1.14058	0.00607
Perp	-7.30893	-3.84293	-5.75813	7.41E-06	***Ptch2***	-1.54335	-1.0106	-2.95709	0.006555
Wnt7b	-1.60016	1.03001	-1.15161	7.29E-05	***Sox2***	1.273219	-1.01567	1.6048	0.007494
Grhl3	-2.02066	-1.54766	-1.26609	0.000216	***Sik1***	-1.21763	-1.28005	-1.24288	0.008134
Otx2	1.669908	1.05422	1.68577	0.000329	***Wnt10b***	-4.90464	-1.12509	-1.684	0.008349
Plec	-1.39744	-1.04893	-1.08656	0.000445	***Bok***	1.25325	1.01322	-1.11879	0.015551
Cebpa	-2.003	-1.04354	-1.2682	0.0005	***Vdr***	3.066703	1.35755	2.42291	0.017172
Cyp26b1	-1.78746	1.01781	-1.35972	0.001163	***Jag1***	1.151214	1.00892	-1.4582	0.018354
Jun	1.398956	1.03096	1.34856	0.001174	***Fzd4***	1.314803	1.22514	1.54445	0.019044
Wnt3	-1.94288	-1.20852	-1.15505	0.001271	***Sox9***	1.136819	1.01595	1.27149	0.020746
Sema3c	1.367219	-1.07506	1.63429	0.001461	***Sfrp1***	1.163031	1.04206	1.12055	0.029181
Ppl	-2.53455	-1.2539	-1.56357	0.002705	***Ptprv***	-1.58202	-1.20332	-1.17293	0.031151
Bcl11b	-1.33317	1.11934	-1.41548	0.002802	***Spry1***	1.203362	1.02942	1.16815	0.040112
Ikzf2	1.418852	1.01956	1.37927	0.003439	***Hes1***	1.268527	1.02669	-1.11558	0.040741
Phlda3	-1.32904	-1.09481	-1.20888	0.004159					

Table 4.2 Genes displaying significant differential expression by nCounter (p= 0.05).

Results include the 31 genes identified as significantly differentially expressed between *Trp63*$^{+/+}$ and *Trp63*$^{-/-}$ E11.5 facial processes. Data includes gene name, nCounter calculated fold change, calculated fold change for the E11.5 and E12.5 microarrays and nCounter p-value.

Wnt4 binding sites identified potential overlaps with P4 with an E11.5 (facial) H3k4me1 site and H3k27ac site shown to be active at E11.5 (facial), E13.5 (palatal) and E14.5 (palatal). *Wnt4* P5 was shown to overlap with an identified H3k27me3 site active at E11.5 (facial), E13.5 (palatal) and E14.5 (palatal) and an H3k27ac site active at E14.5 (palatal). *Wnt4* P2 was also found to overlap with an H3k27ac site active in E11.5 facial tissue. The overlap between these sites and active H3k27me1, H3k27me3 and H3k27ac sites could suggest these binding sites are active in transcriptional regulation.

Therefore each binding site was validated using ChIP-qPCR to determine if P63 binding was present at E11.5. ChIP-qPCR analysis showed *Wnt4* P1, P3, P4 and P5 displayed significant positive enrichment for P63 binding (p= 0.05) with occupancies of 7.44, 8.49, 21.39 and 26.34 (Figure 4.1B). Binding site P2 failed to display positive enrichment with an occupancy of 0.91.

Having demonstrated P63 binding at putative sites proximal to *Wnt4*, expression was quantified between *Trp63*$^{+/+}$ and *Trp63*$^{-/-}$ embryos to determine if *Wnt4* expression was altered in P63 null embryos. qPCR analysis showed *Wnt4* expression was significantly down-regulated in *Trp63*$^{-/-}$ E11.5 facial processes compared with wildtype littermates with a relative expression of 0.48 compared to wildtype (p= 0.02) (Figure 4.1C).

Wnt4 expression was down-regulated in *Trp63*$^{-/-}$ facial processes. Therefore the expression profile of *Wnt4* was characterised in *Trp63*$^{+/+}$ and *Trp63*$^{-/-}$ embryos using WISH analysis. In *Trp63*$^{+/+}$ embryos expression was detected throughout the neural tube (Figure 4.2A). Within the facial process, expression was detected within the epithelium of the medial nasal and lateral nasal processes surrounding the nasal pit. Further expression was detected throughout the oral epithelium and the medial junction of the medial nasal processes (Figure 4.2C&E). Further expression was detected in the oral epithelium of the maxillary processes extending into the lambdoidal junction and within the lacrimal groove. Discrete expression of *Wnt4* was detected within the oral epithelium of the mandibular processes with diffuse expression present at the medial junction (Figure 4.2C).

In contrast to wildtype littermates, *Wnt4* expression in *Trp63*$^{-/-}$ embryos was markedly reduced. Expression surrounding the nasal pits was detected, however expression was reduced within the epithelium of the lateral nasal and medial nasal processes. Further expression within the nasal epithelium of the medial nasal processes appeared to have shifted posteriorly (Figure 4.2D). In addition expression within the oral epithelium and central junction of the medial nasal processes was dramatically reduced. Within the maxillary processes, *Wnt4* expression was completely absent from the lacrimal groove and almost completely absent from the oral epithelium and lambdoidal junction (Figure 4.2D&F). Furthermore expression within the oral epithelium of the mandibular processes was markedly reduced. *Wnt4* expression within the neural tube was comparable to wildtype

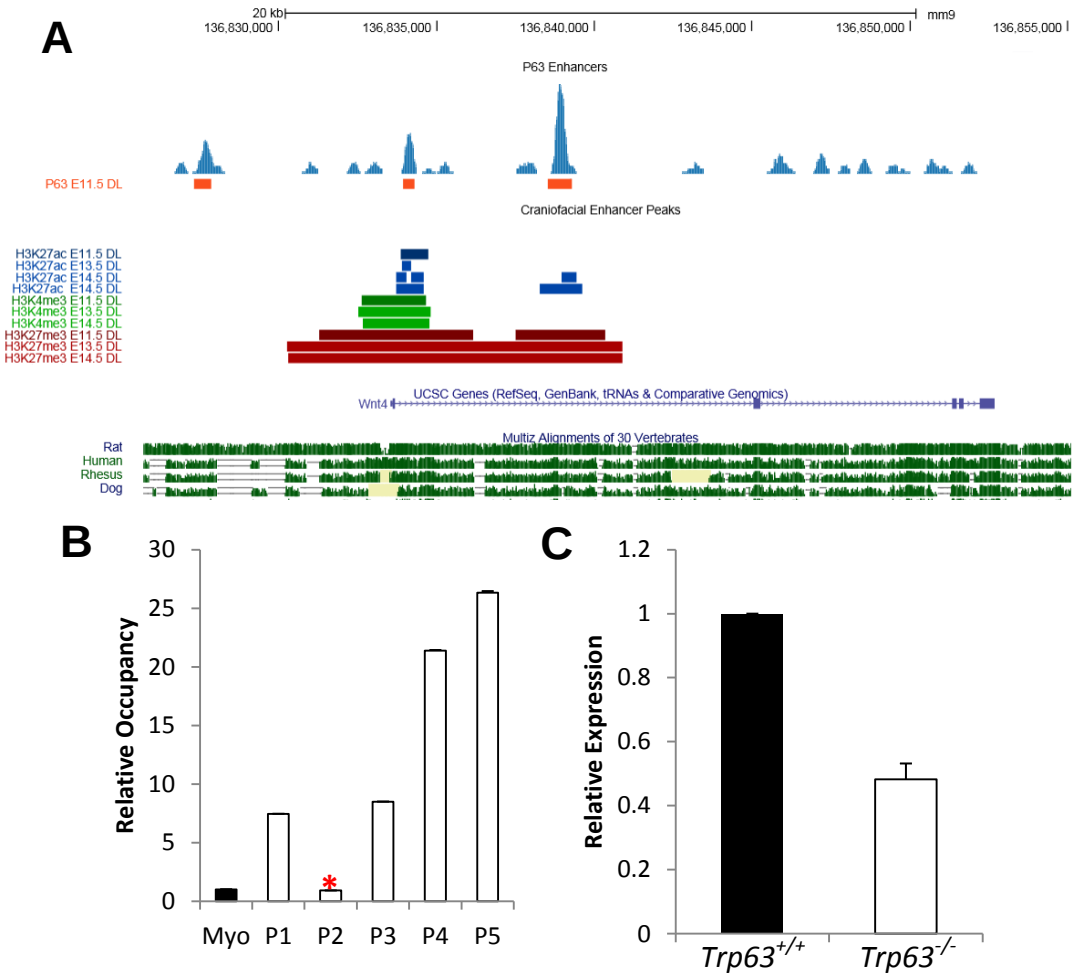

Figure 4.1 *Wnt4* is a target of P63 signalling. (**A**) ChIP-Seq/microarray intersection identified five potential P63 binding sites proximal to *Wnt4* (2 not shown). Peaks overlapped with markers of active transcriptional regulation including H3k27ac, H3k4me3 and H3k27me3 identified in E11.5 facial and E13.5 and E14.5 palatal tissue. Mammalian conservation is shown. (**B)** ChIP-qPCR was conducted on five putative P63 binding sites proximal to *Wnt4*. Relative chromatin occupancy was calculated relative to the negative control *Myoglobin* (black). Four out of five binding sites displayed positive enrichment by P63, with *Wnt4* P2 failing to display enrichment (*). (**C**) qPCR analysis of E11.5 *Trp63*$^{-/-}$ and WT facial processes identified a significant reduction in *Wnt4* expression relative to the house keeping gene *β-actin*. Error bars display standard error of the mean.

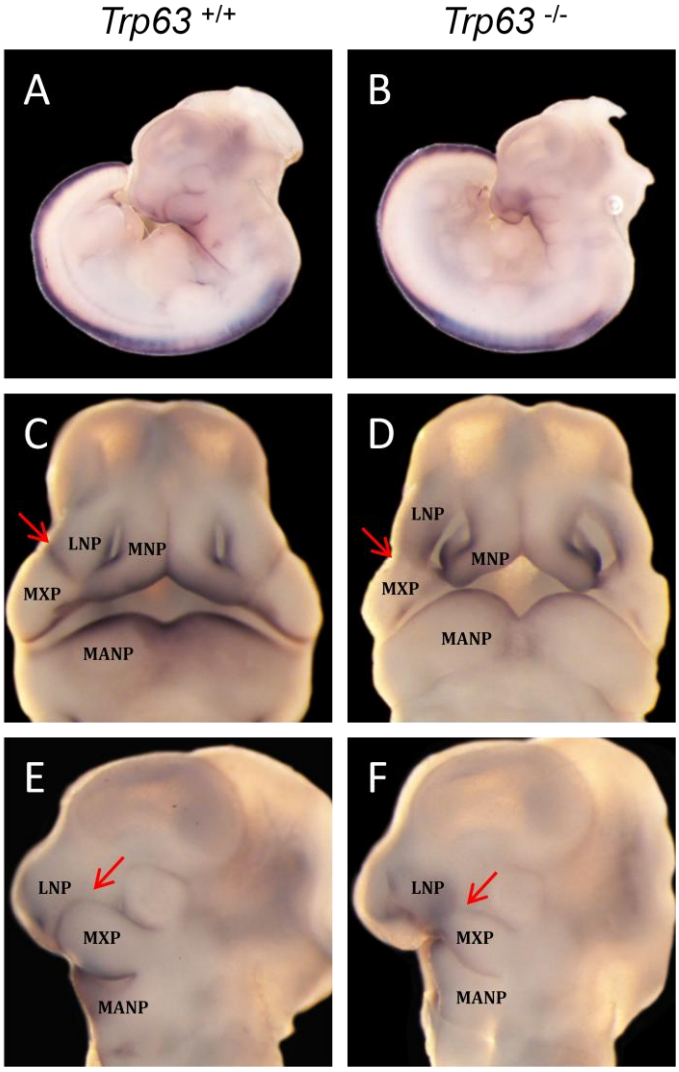

Figure 4.2 Whole mount *in situ* analysis of *Wnt4*. (**A**-**F**) WISH analysis of *Wnt4* between *Trp63*$^{+/+}$ and *Trp63*$^{-/-}$ E11.5 embryos. (**A**&**B**) *Wnt4* expression was comparable within the neural tube across WT and nulls. (**C**&**E**) In *Trp63*$^{+/+}$ embryos *Wnt4* expression was detected within the nasal epithelium of the medial nasal and lateral nasal processes. Further expression was detected throughout the oral epithelium of the medial nasal, maxillary and mandibular processes and within the lacrimal groove (arrowed) extending posteriorly towards the eye. (**D**&**F**) In *Trp63*$^{-/-}$ embryos, *Wnt4* expression was markedly reduced within the nasal epithelium of the lateral nasal processes and the oral epithelium of the maxillary and mandibular processes. The presence of comparable staining within the neural tube suggested loss of *Wnt4* expression in the facial processes was tissue specific. LNP- lateral nasal processes, MNP – medial nasal processes, MXP- maxillary processes, MANP- mandibular processes.

littermates suggesting the loss of *Wnt4* expression is specific to the facial processes (Figure 4.2A&B).Taken together these results show that correct P63 regulation is essential to *Wnt4* expression during E11.5 upper lip morphogenesis. Furthermore the positive enrichment by P63 within the identified binding sites, together with the overlap with active H3k4me1, H3k27me3 and H3k27ac sites suggested P63 could be active in gene regulation at these regions. The significant reduction in *Wnt4* expression in E11.5 *Trp63*$^{-/-}$ facial processes and the proximal binding of P63 to *Wnt4* could suggest P63 directly regulates *Wnt4* during upper lip morphogenesis.

4.3.3 P63 signalling is required for correct expression of *Wnt3* during lip morphogenesis

The misregulation of *Wnt3* has previously been demonstrated to result in the down-regulation of *Trp63* (Ferretti *et al*. 2011). *Wnt3* was identified as a gene of potential interest as being significantly down-regulated in *Trp63*$^{-/-}$ facial processes and by the presence of four P63 peaks ≤ 150 kb of the TSS. Potential binding sites were identified at positions chr11: 103,613,907-103,614,929 (P1), 103,702,894-103,702,916 (P2), 103,739,230-103,739,252 (P3) and 103,762,409-103,762,431 (P4) (mm9) (Figure 4.3A). P63 scan identified that all four peaks contained the P63 binding motif. Binding sites were found to show mammalian conservation between mouse, rat, human, rhesus monkey, dog and horse with *Wnt3* P2 and P3 showing additional conservation with opossum. Analysis for active transcriptional regulation markers showed an overlap between *Wnt3* P1 and an H3k27me3 site active at E11.5 (facial), E13.5 and E14.5 (palatal) tissue. Furthermore *Wnt3* P2 was shown to overlap with an H3k4me1 site active at E11.5 (facial) tissue. These results suggested P63 was binding at regions associated with transcriptional regulation.

Each binding site was assayed using ChIP-qPCR to determine if P63 binding was present during lip morphogenesis. Of the four binding sites, three were shown to display positive enrichment by P63 with *Wnt3* P1, P2 and P4 all displaying enrichments greater than 3 fold the negative control (Figure 4.3B). *Wnt3* P3 failed to display enrichment by P63 with a relative occupancy of 2.7. These results suggested that P63 does bind in proximity to *Wnt3* during upper lip morphogenesis.

Having confirmed P63 binding, the expression of *Wnt3* was quantified in *Trp63*$^{+/+}$ and *Trp63*$^{-/-}$ embryos. *Wnt3* expression was found to be significantly down-regulated in *Trp63*$^{-/-}$ embryos with a relative expression of 0.66 compared to wildtype (p= 0.02) (Figure 4.3C)

The expression profile of *Wnt3* was characterised using WISH analysis in E11.5 *Trp63*$^{+/+}$ and *Trp63*$^{-/-}$ embryos. In *Trp63*$^{+/+}$ embryos *Wnt3* was detected within the epithelium of the medial nasal, lateral nasal and maxillary processes (Figure 4.4A&C). Expression was highly localised to the inferior aspects of the nasal pits with expression present within the lambdoidal junction.

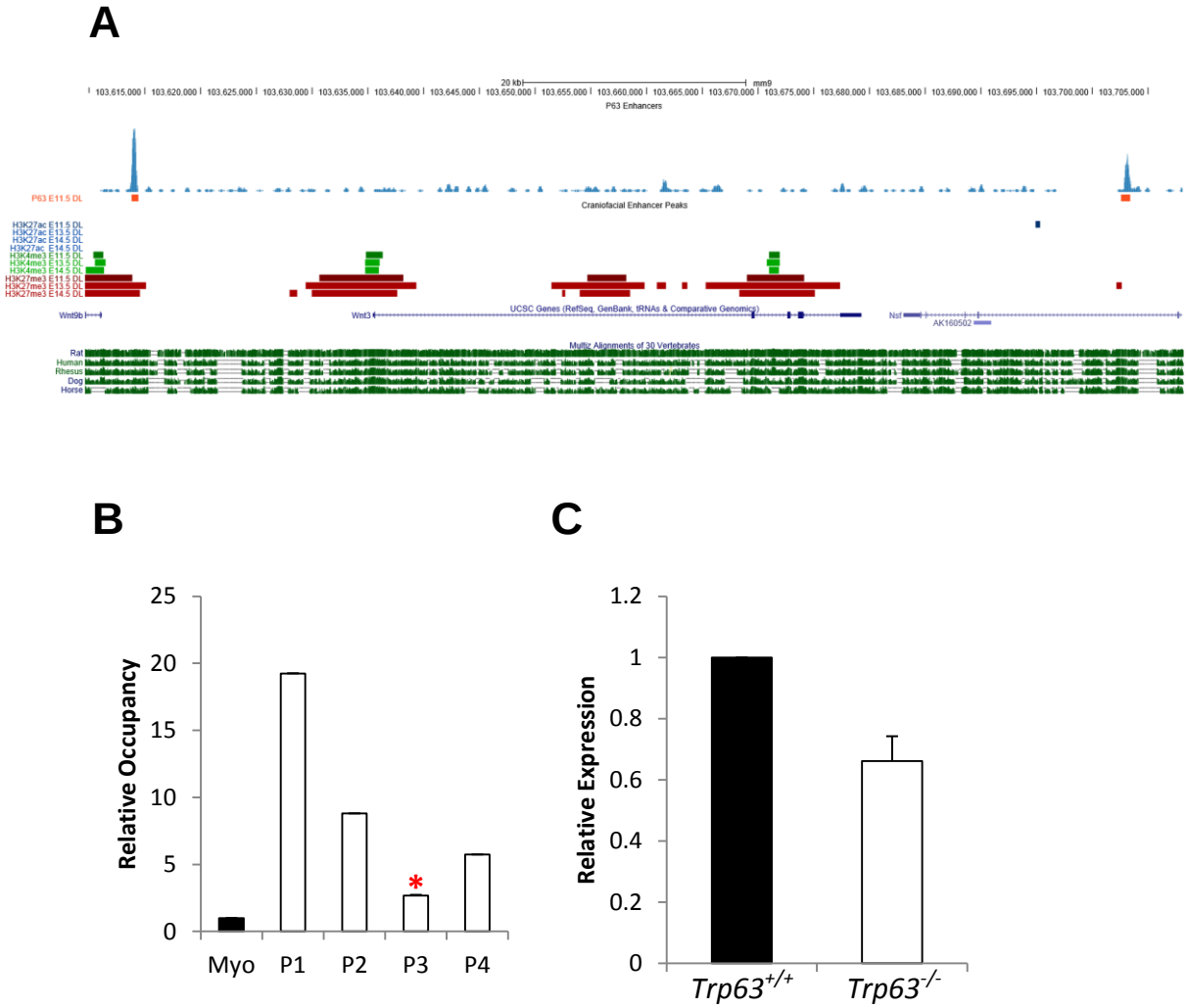

Figure 4.3 *Wnt3* is a target of P63 signalling. (**A**) ChIP-Seq/microarray intersection identified four potential P63 binding sites proximal to *Wnt3* (two not shown). Peaks overlapped with markers of active transcriptional regulation including H3k27me3 sites identified in E13.5 and E14.5 palatal tissue. Mammalian conservation is shown. (**B**) ChIP-qPCR was conducted on four putative P63 binding sites proximal to *Wnt3*. Relative chromatin occupancy was calculated relative to the negative control *Myoglobin* (black). Three out of four binding sites displayed positive enrichment by P63, with *Wnt3* P3 (*) failing to display enrichment. (**C**) qPCR analysis between E11.5 *Trp63*$^{-/-}$ and WT facial processes identified a significant reduction in *Wnt3* expression relative to the house keeping gene *β-actin*. Error bars display standard error of the mean.

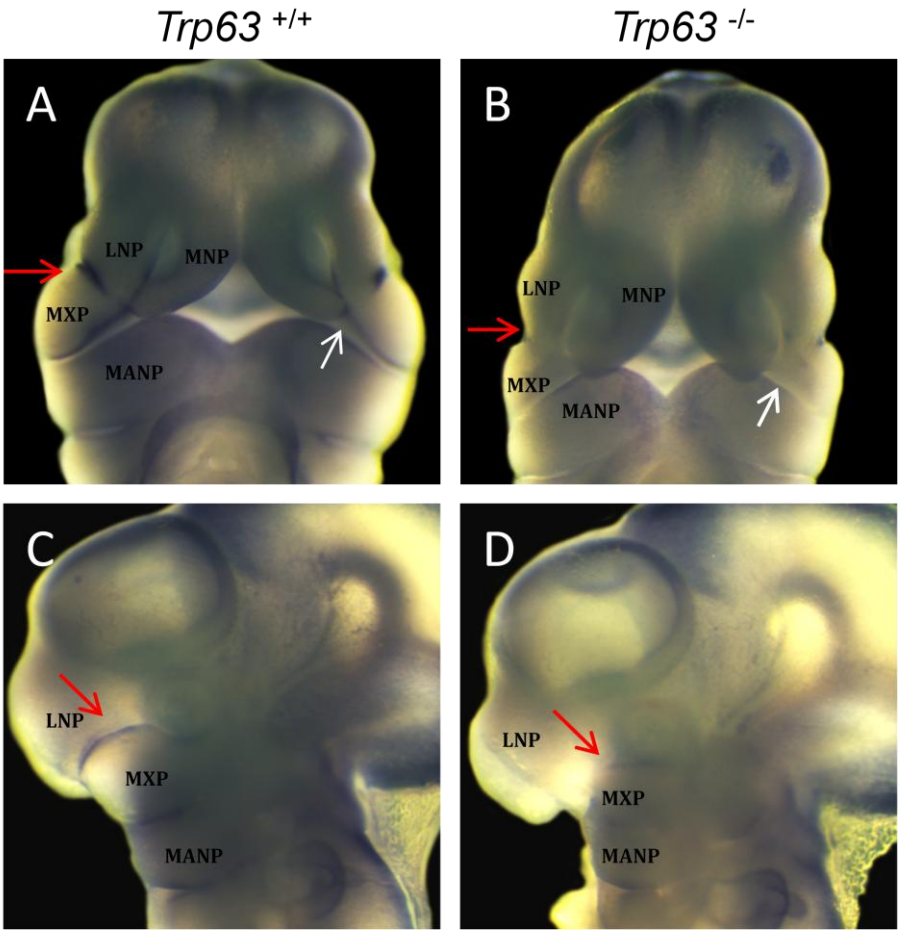

Figure 4.4 Whole mount *in situ* analysis of *wnt3.* (**A**-**D**) WISH analysis of *Wnt3* between *Trp63*$^{+/+}$ and *Trp63*$^{-/-}$ E11.5 embryos. (**A**&**C**) *Wnt3* expression was detected within the nasal epithelium of the medial nasal and lateral nasal processes. Further expression was detected throughout the oral epithelium of maxillary processes and within the lacrimal groove (arrowed - red) extending posteriorly towards the eye. Expression was detected within the epithelium of the lambdoidal junction (arrowed - white). (**B**&**D**) In *Trp63*$^{-/-}$ embryos, *Wnt3* expression was markedly reduced within the nasal epithelium of the medial nasal and lateral nasal processes. Expression within the lambdoidal junction was absent (arrowed – white) and expression within the lacrimal groove was markedly reduced. Furthermore *Wnt3* expression was absent from the oral epithelium of the maxillary processes. LNP- lateral nasal processes, MNP – medial nasal processes, MXP- maxillary processes, MANP- mandibular processes.

Furthermore expression was detected within the oral epithelium of the maxillary processes extending into the lambdoidal junction and posteriorly in the lacrimal groove (Figure 4.4B&D). Further expression was detected within the oral epithelium of the mandibular processes.

In contrast to wildtype littermates, expression of *Wnt3* was greatly reduced in *Trp63*$^{-/-}$ embryos (Figure 4.4B&D). The epithelial expression of *Wnt3* surrounding the nasal pits detected in *Trp63*$^{+/+}$ embryos was absent in null littermates. *Wnt3* expression was detected within the lacrimal groove, however it was found to be markedly reduced. Furthermore the expression of *Wnt3* within the oral epithelium of the maxillary processes was absent. Within the mandibular processes, *Wnt3* expression was absent within the oral epithelium. In contrast, expression of *Wnt3* appeared expanded at the medial junction between the mandibular processes, with diffuse expression observed.

Taken together these results would suggest that correct P63 regulation is required for *Wnt3* expression during E11.5 upper lip morphogenesis. P63 enrichment was observed for three binding sites ≤ 150 kb of *Wnt3* in E11.5 facial processes. Furthermore the overlap of *Wnt3* P2 and P3 with markers for transcriptional regulation could suggest identified sites are bona fide targets of P63 regulation during upper lip morphogenesis. With the marked reduction in *Wnt3* expression in *Trp63*$^{-/-}$ embryos, these results could suggest *Wnt3* is a direct target of P63 regulation in upper lip morphogenesis.

4.3.4 P63 signalling is required for correct expression of *Wnt9b* during lip morphogenesis

A previous study identified a loss of *Pbx1* and *Pbx2* resulted in down-regulation of *Trp63* and *Irf6* expression via Wnt3 and Wnt9b regulation (Ferretti *et al*. 2011). Furthermore *Wnt9b* knockout models display cleft lip and palate and abnormalities of the kidney (Carroll *et al.* 2005). A ChIP-Seq peak was identified between *Wnt3* and *Wnt9b* at Chr11:103,613,823-103,614,422 (mm9) (*Wnt3* P1) and P63 Scan identified a P63 binding motif was present (Figure 4.5A). *Wnt9b* was unchanged in *Trp63*$^{-/-}$ embryos with a fold change of -1.00288 however and result did not achieve significance (p value = 0.97). ChIP-Seq/microarray intersection therefore associated this binding site with *Wnt3* regulation. Due to the identified roles of *Wnt9b* in upper lip morphogenesis, *Wnt9b* was investigated as a potential P63 target gene (Ferretti *et al*. 2011). Enrichment of this site by P63 has previously been discussed (Section 4.3.3).

Having confirmed binding proximal to *Wnt9b*, expression levels of *Wnt9b* between *Trp63*$^{+/+}$ and *Trp63*$^{-/-}$ embryos were quantified. qPCR analysis at E11.5 indicated *Wnt9b* expression was down-regulated in *Trp63*$^{-/-}$ embryos with a relative expression of 0.68 to wildtype (p= 0.02) (Figure 4.5B). However the result failed to achieve significance (Mann Whitney U value

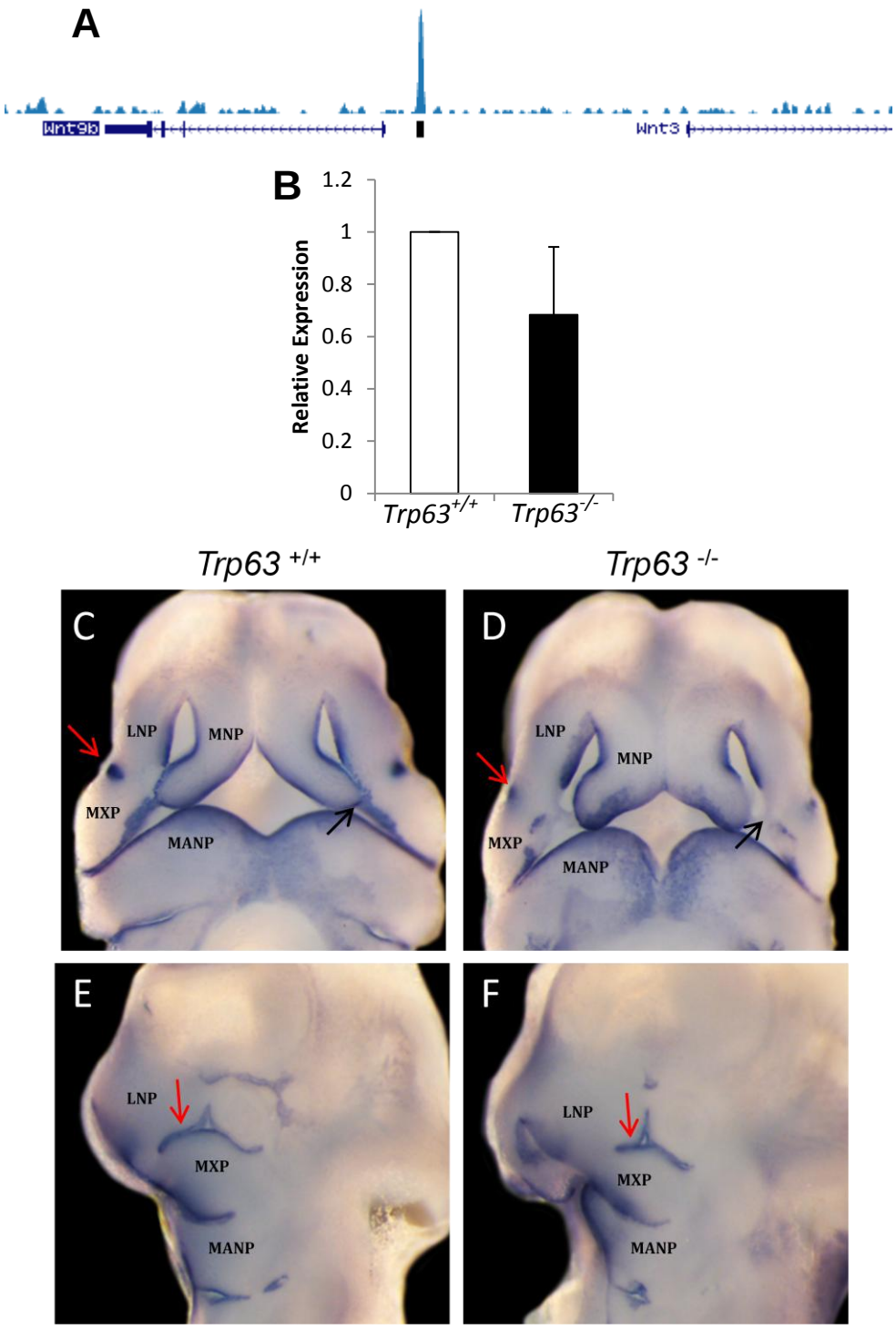

Figure 4.5 *Wnt9b* is a target of P63 signalling. (**A**) ChIP-Seq identified a P63 binding site between *Wnt3* and *Wnt9b* which was putatively associated with *Wnt3* through ChIP-Seq/microarray intersection (**B**) qPCR analysis between E11.5 *Trp63*$^{-/-}$ and WT facial processes identified a reduction in *Wnt9b* expression relative to the house keeping gene *β-actin*. However the result failed to achieve significance. Error bars display standard error of the mean. (**C**-**F**) WISH analysis of *Wnt9b* between *Trp63*$^{+/+}$ and *Trp63*$^{-/-}$ E11.5 embryos. (**C**&**E**) *Wnt9b* expression was detected within the nasal epithelium of the medial nasal and lateral nasal processes. Further expression was detected throughout the oral epithelium of the medial nasal, maxillary and mandibular processes and within the lacrimal groove (arrowed – red) extending posteriorly towards the eye. Expression was detected within the epithelium of the lambdoidal junction (arrowed - black) (**D**&**F**) In *Trp63*$^{-/-}$ embryos, *Wnt9b* expression appeared comparable to WT in the nasal epithelium of the lateral nasal and medial nasal processes and within the lacrimal groove (arrowed – red). Expression within the mandibular processes was comparable to WT. *Wnt9b* expression was markedly reduced within the oral epithelia of the maxillary processes and was absent from the lambdoidal junction (arrowed – black). LNP- lateral nasal processes, MNP – medial nasal processes, MXP- maxillary processes, MANP- mandibular processes.

= 4). Therefore the expression profile of *Wnt9b* in lip morphogenesis was characterised in *Trp63*$^{+/+}$ and *Trp63*$^{-/-}$ E11.5 embryos using WISH analysis. In *Trp63*$^{+/+}$, *Wnt9b* expression was detected within the surface epithelium of the medial nasal, lateral nasal and maxillary processes. Expression was localised to the border of the nasal pits and within the lambdoidal junction (Figure 4.5C). Furthermore expression was detected within the oral epithelium of the mandibular processes with diffuse expression present at the medial junction. Posteriorly expression was detected within the lacrimal groove and the epithelium of the optic cup (Figure 4.5E).

In contrast to wildtype littermates, expression of *Wnt9b* in *Trp63*$^{-/-}$ embryos was found to be significantly altered. Expression surrounding the nasal pits was comparable to wildtype, however the discrete expression detected in *Trp63*$^{+/+}$ embryos was disrupted with diffuse expression detected (Figure 4.5D). Expression within the maxillary processes was reduced with expression lost within the lambdoidal junction (Figure 4.5D). In contrast to the loss of expression observed in the medial nasal, lateral nasal and maxillary processes, expression of *Wnt9b* appeared expanded within the mandibular processes. Furthermore the expression within the lacrimal groove appeared comparable with wildtype littermates (Figure 4.5F). These results would suggest that correct P63 regulation is required for *Wnt9b* expression during upper lip morphogenesis.

4.3.5 Loss of P63 signalling results in the down-regulation of *Shh*

Previous studies have shown modulation of Shh signalling during facial process adhesion and fusion resulted in misregulation of Wnt signalling (Kurosaka *et al*. 2014). Expansion of Shh signalling resulted in down-regulation of Wnt expression and reductions in Shh signalling resulted in expansion of Wnt signalling (Kurosaka *et al*. 2014). Expression analysis of *Shh* using E11.5 nCounter and E12.5 microarray identified a significant down-regulation in *Trp63*$^{-/-}$ facial processes, with expression reduced by -1.26 and -1.85 compared with wildtype (p= 0.05) (Figure 4.6A). Therefore the expression profile of *Shh* was characterised in E11.5 *Trp63*$^{-/-}$ and *Trp63*$^{+/+}$ embryos using WISH analysis.

In *Trp63*$^{+/+}$ embryos discreet *Shh* expression was detected in the surface epithelium of the medial nasal, lateral nasal and maxillary processes at the lambdoidal junction (Figure 4.6B). Further expression was observed within the oral epithelium of the medial nasal processes and discrete expression was observed within the dorsal aspects of the limb buds (Figure 4.6B&E). In contrast to wildtype embryos, expression of *Shh* was markedly reduced in *Trp63*$^{-/-}$ embryos. While expression was detected at the lambdoidal junction, staining was less intense and the expression domain within the maxillary epithelium appeared reduced (Figure 4.6C). Expression within the medial aspects of the medial nasal processes appeared comparable. However, the discrete expression of *Shh* within the limb buds appeared disrupted with diffuse epithelial expression detected within the distal aspects (Figure 4.6F).

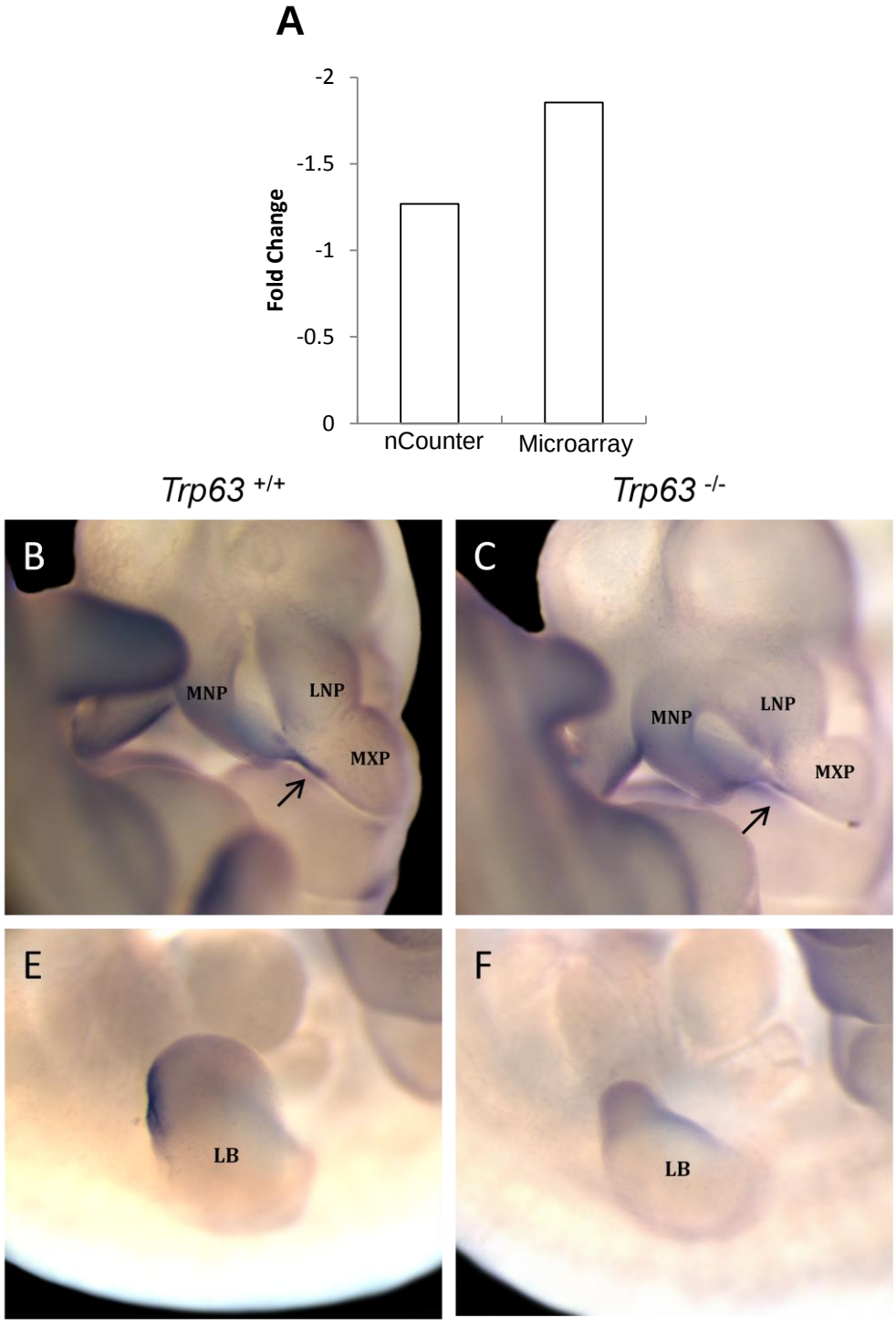

Figure 4.6 *Shh* is a target of P63 signalling. (**A**) Analysis of *Shh* expression in *Trp63*$^{-/-}$ and *Trp63*$^{+/+}$ facial processes showed *Shh* was down-regulated in P63 nulls at E11.5 by nCounter and E12.5 by microarray analyses. (**B**&**E**) WISH analysis of *Trp63*$^{+/+}$ E11.5 embryos identified expression of *Shh* was localised to epithelium of the lambdoidal junction (arrowed), the site of contact between the medial nasal, lateral nasal and maxillary processes. Expression of *Shh* was localised to the dorsal epithelium of the developing limb bud. (**C**&**F**) Loss of P63 signalling resulted in the down-regulation of *Shh* within the lambdoidal junction. *Shh* expression within the limb bud was reduced, with the discrete expression observed in WT lost. Diffuse expression was present within the distal aspects of the limb bud. LNP- lateral nasal processes, MNP – medial nasal processes, MXP- maxillary processes, LB – limb bud.

These results confirmed the findings of Thomason and colleagues, who identified a down-regulation of *Shh* within *Trp63*$^{-/-}$ E11.5 facial processes (Thomason *et al*. 2008). Furthermore, as it has previously been indicated Shh signalling negatively regulates Wnt signalling, it would be expected the reduction in *Shh* expression would result in up-regulation of Wnt signalling (Kurosaka *et al*. 2014). However in the presented data set, Wnt signalling was found to be reduced. These results suggest that in addition to Shh signalling, P63 signalling acts to regulate Wnt signalling during upper lip morphogenesis.

4.3.6 P63 signalling is required for correct expression of *Lrp6* during lip morphogenesis

A recent study implicated mutations in *LRP6* as contributing to the incidence of orofacial clefting identifying two unrelated individuals with oligodontia and isolated oligodontia (Ockeloen *et al*. 2015). Due to the link between Wnt signalling and upper lip morphogenesis *Lrp6* was investigated as a potential target of P63 regulation. ChIP-Seq analysis identified a P63 binding site within intron 7 of *Lrp6* with P63 scan identifying a P63 binding motif at position chr6:134,445,259-134,445,276 (mm9) (Figure 4.7A). The binding site was found to be conserved between rat, human, rhesus monkey, dog, horse and opossum. ChIP-qPCR analysis of the identified binding site displayed significant (p= 0.05) positive enrichment by P63 in E11.5 facial processes with a chromatin occupancy of 4.85 (Figure 4.7B). Having confirmed P63 binding proximal to *Lrp6* the expression of *Lrp6* was quantified in *Trp63*$^{-/-}$ and wildtype embryos. *Lrp6* failed to achieve significant differential expression on the E12.5 microarray with a fold-change of 1.02 (p-value = 0.73). qPCR analysis of *Lrp6* in E11.5 *Trp63*$^{-/-}$ facial processes displayed down-regulation, however the result was not significant with a relative expression of -0.79 to wildtype (Figure 4.7C). Therefore the expression of *Lrp6* was characterised during upper lip morphogenesis between E11.5 *Trp63*$^{+/+}$ and *Trp63*$^{-/-}$ embryos.

Lrp6 expression was investigated using WISH analysis at two stages, immediately after the fusion of the nasal processes (in wildtype) and slightly later in gestation when fusion was more established in *Trp63*$^{+/+}$ and *Trp63*$^{-/-}$ embryos. Throughout all analysis, *Lrp6* expression was mesenchymal. In *Trp63*$^{+/+}$ embryos at early E11.5 expression of *Lrp6* was detected throughout the mesenchyme of the medial nasal and lateral nasal processes and the mandibular processes (Figure 4.8A). Expression of *Lrp6* in *Trp63*$^{-/-}$ facial processes was comparable to wildtype littermates (Figure 4.8B). *Lrp6* expression was also examined in later-staged E11.5 embryos. In *Trp63*$^{+/+}$ embryos expression was detected within the mesenchyme of the medial nasal processes and within the lateral nasal processes proximal to the nasal slits (Figure 4.8C). Expression was found localised to the anterior regions of the medial nasal and lateral nasal processes (Figure 4.8C). Furthermore expression was detected within the inferior aspects of the maxillary processes with a region of high expression at the maxillary-mandibular boundary (Figure 4.8E).

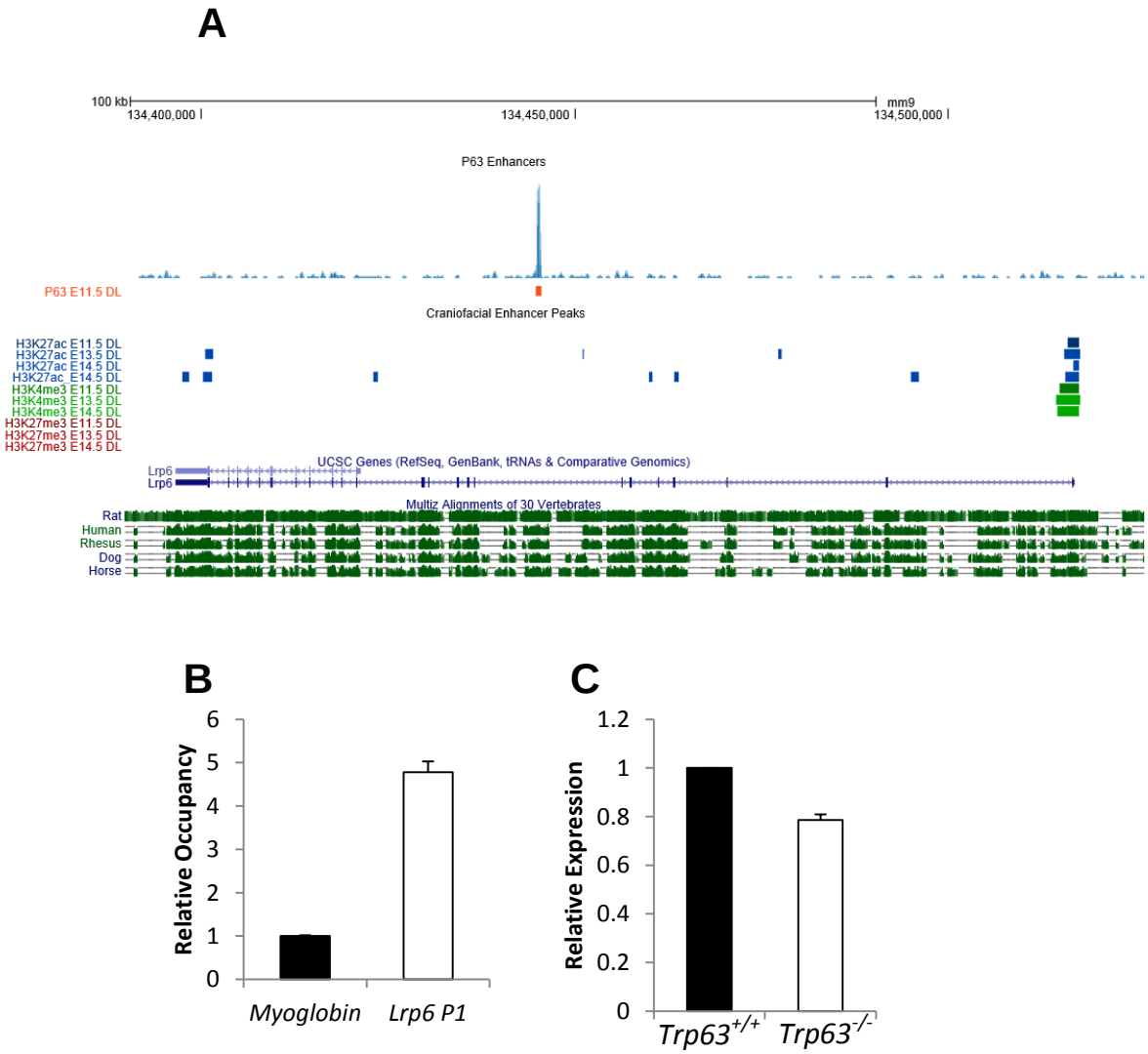

Figure 4.7 *Lrp6* is a target of P63 signalling. (**A**) ChIP-Sey/microarray intersection identified a putative P63 binding site proximal to *Lrp6*. *Lrp6* P1 did not overlap with any markers of transcriptional regulation. The binding site was conserved between mouse, rat, human, rhesus monkey, dog and horse. (**B**) ChIP-qPCR was conducted on a putative P63 binding site proximal to *Lrp6*. Relative chromatin occupancy was calculated relative to the negative control *Myoglobin* (black). *Lrp6* P1 displayed positive enrichment by P63 with a calculated occupancy ≥ 3-fold the negative control. (**C**) qPCR analysis between E11.5 *Trp63*$^{-/-}$ and WT facial processes identified a reduction in *Lrp6* expression relative to the house keeping gene *β-actin*. However the result failed to achieve significance. Error bars display standard error of the mean.

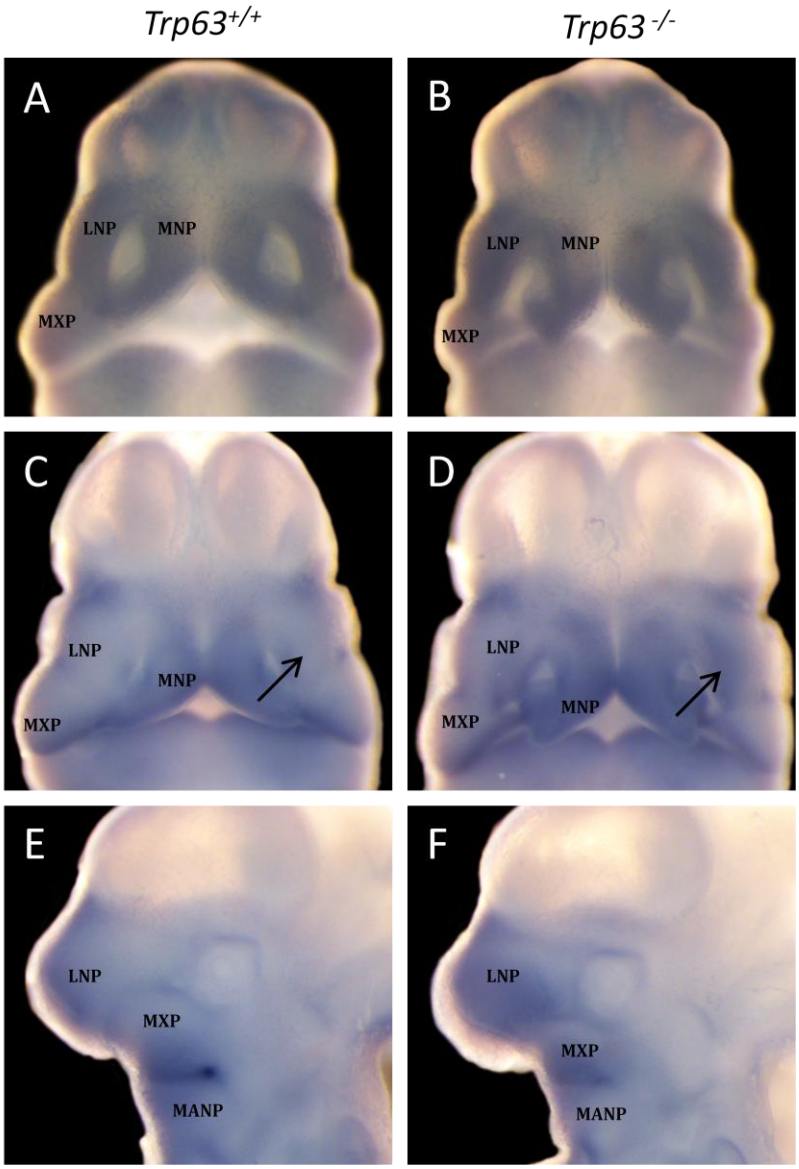

Figure 4.8 Whole mount *in situ* hybridisation analysis of *Lrp6.* (**A**-**B**) WISH analysis of *Lrp6* between *Trp63*$^{+/+}$ and *Trp63*$^{-/-}$ E11.5 embryos. (**C**-**F**) WISH of *Lrp6* between *Trp63*$^{+/+}$ and *Trp63*$^{-/-}$ late E11.5 embryos. (**A**) *Lrp6* expression was detected throughout the mesenchyme of the medial nasal, lateral nasal and maxillary processes. However *Lrp6* expression appeared excluded from the nasal and oral epithelium of the medial nasal, lateral nasal and maxillary processes. (**B**) In *Trp63*$^{-/-}$ embryos, *Lrp6* expression was indistinguishable from WT with expression present within the mesenchyme of the medial nasal, lateral nasal and maxillary processes. (**C**&**E**) Within late E11.5 WT embryos, *Lrp6* expression appeared absent from the mesenchyme of the lateral nasal processes, but was present within the medial nasal processes. Expression was still absent from the oral epithelium. Furthermore a spot of intense staining was observed at the boundary between the maxillary and mandibular processes. (**D**&**F**) In *Trp63*$^{-/-}$ embryos, expression of *Lrp6* within the medial nasal processes was comparable to WT, however expression within the lateral nasal processes appeared expanded (arrowed). In contrast, the intense spot of staining observed at the maxillary-mandibular boundary appeared reduced. LNP- lateral nasal processes, MNP – medial nasal processes, MXP- maxillary processes, MANP- mandibular processes.

In contrast to wildtype littermates, *Lrp6* expression within the late E11.5 *Trp63*$^{-/-}$ embryos appeared to be expanded within the mesenchyme of the lateral nasal processes (Figure 4.8D). Expression was shown to be expanded posteriorly within the lateral nasal processes. In contrast to the medial nasal and lateral nasal processes, expression of *Lrp6* within the maxillary processes appeared comparable to wildtype littermates, however the high expression observed at the maxillary mandibular boundary appeared reduced (Figure 4.8F). These results would suggest that *Lrp6* expression is modified in *Trp63*$^{-/-}$ E11.5 facial processes. However *Lrp6* expression appeared to be absent from the epithelium of the facial processes where *Trp63* is exclusively expressed (Thomason *et al*. 2010). The lack of overlap between expression of *Trp63* and *Lrp6* would suggest that *Lrp6* is not a direct target of P63 regulation upper during lip morphogenesis.

4.3.7 P63 signalling is required for correct expression of *Fzd10* during lip morphogenesis

ChIP-Seq/microarray intersection identified five potential P63 binding sites proximal to *Fzd10* in E11.5 facial processes and P63 scan showed all identified peaks contained at least one P63 binding motif. Motifs were identified at positions Chr5: 129,051,247-129,051,266 (P1), 129,076,220-129,076,239 (P2), 129,078,315-129,078,334 (P3), 129,126,087-129,126,106 (P4) and 129,155,375-129,155,395 (P5) (mm9) (Figure 4.9A). Investigation for mammalian conservation of the identified motifs showed *Fzd10* P1 and P3 were not conserved beyond mouse and rat. *Fzd10* P2, P4 and P5 were found to be conserved across mouse, rat, human and rhesus monkey with P4 showing additional conservation across dog and horse. Furthermore *Fzd10* P2 and P4 were shown to overlap with transcriptional regulation markers active in E11.5 facial tissue with P2 overlapping with H3k4me1 and P4 overlapping with H3k4me1 and H3k27ac. Further regulatory overlap was observed by *Fzd10* P3 which overlapped with an H3k27ac site active in E14.5 palatal tissue.

The presence of markers for transcriptional regulation overlapping *Fzd10* P2 and P4 was highly encouraging, suggesting these sites are active in gene regulation. P63 binding at putative binding sites was therefore assessed in E11.5 facial processes using ChIP-qPCR. ChIP-qPCR showed four of five binding sites displayed significant positive enrichment by P63 greater than three-fold the negative control (p= 0.05) (Figure 4.9B). *Fzd10* P1 failed to display positive enrichment with an occupancy of 1.85. *Fzd10* P2, P3, P4 and P5 displayed occupancies of 8.23, 10.27, 34.94 and 3.98. These results confirmed P63 does bind proximal to *Fzd10* during E11.5 upper lip morphogenesis. In addition, the presence of active regulation markers could suggest that P63 is participating in transcriptional regulation at these sites.

Having confirmed P63 binding proximal to *Fzd10* the expression of *Fzd10* was quantified in E11.5 *Trp63*$^{+/+}$ and *Trp63*$^{-/-}$ facial processes. *Fzd10* expression was found to be significantly down-regulated in both the E12.5 microarray with a fold-change of -1.76 and the E11.5

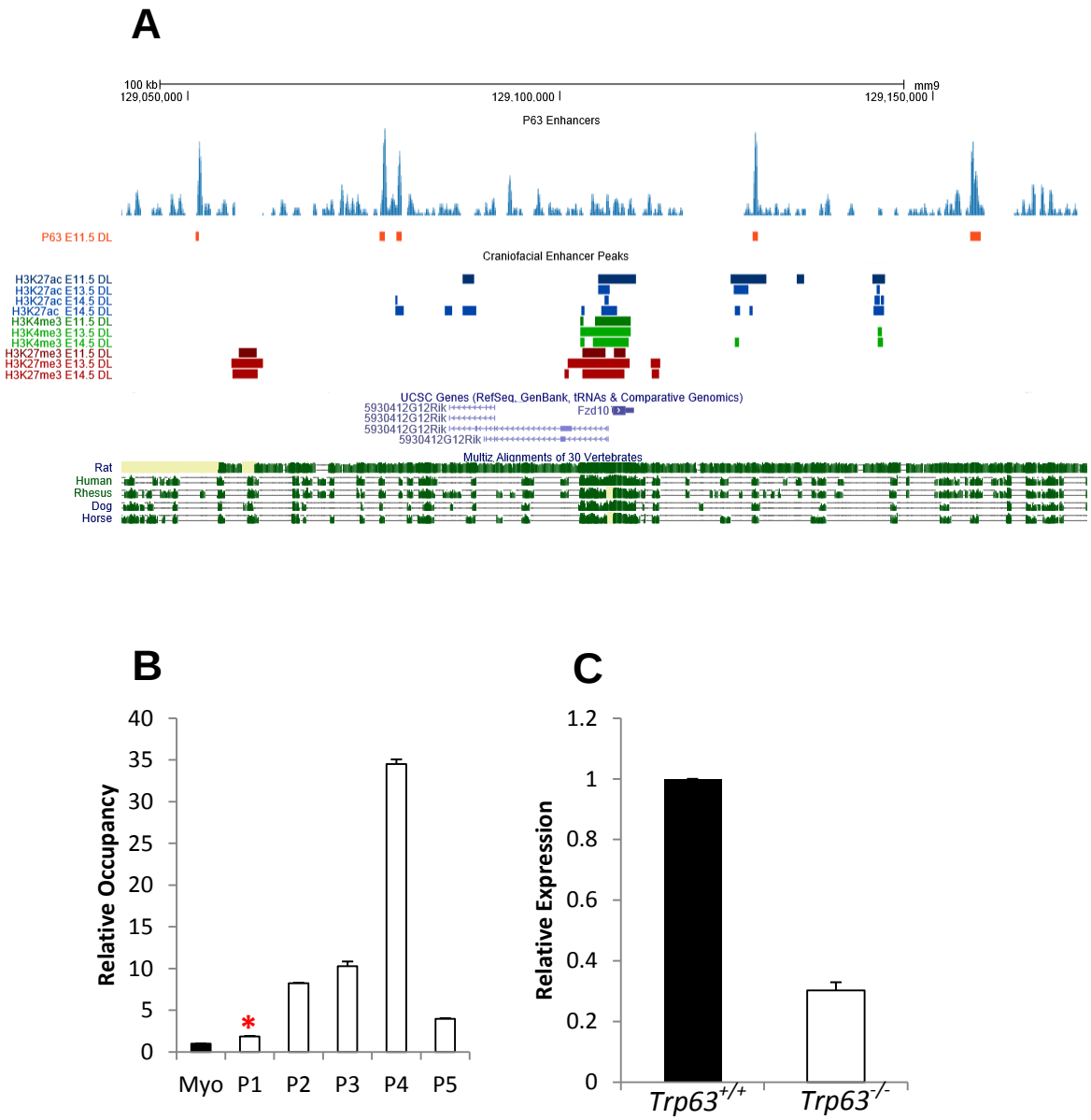

Figure 4.9 *Fzd10* is a target of P63 signalling. (**A**) ChIP-Seq/microarray intersection identified five potential P63 binding sites proximal to *Fzd10*. Peaks were shown to overlap with active markers of transcriptional regulation including H3k4me1 and H3k27ac sites active in E11.5 facial tissue. Mammalian conservation is shown. (**B**) ChIP-qPCR was conducted on five putative P63 binding sites proximal to *Fzd10*. Relative chromatin occupancy was calculated relative to the negative control *Myoglobin* (black). Four out of five binding sites displayed significant positive enrichment by P63 (p= 0.05), with *Fzd10* P1 (*) failing to display enrichment. (**C**) qPCR analysis between E11.5 *Trp63*$^{-/-}$ and WT facial processes identified a significant reduction in *Fzd10* expression relative to the house keeping gene *β-actin* (p= 0.05). Error bars display standard error of the mean.

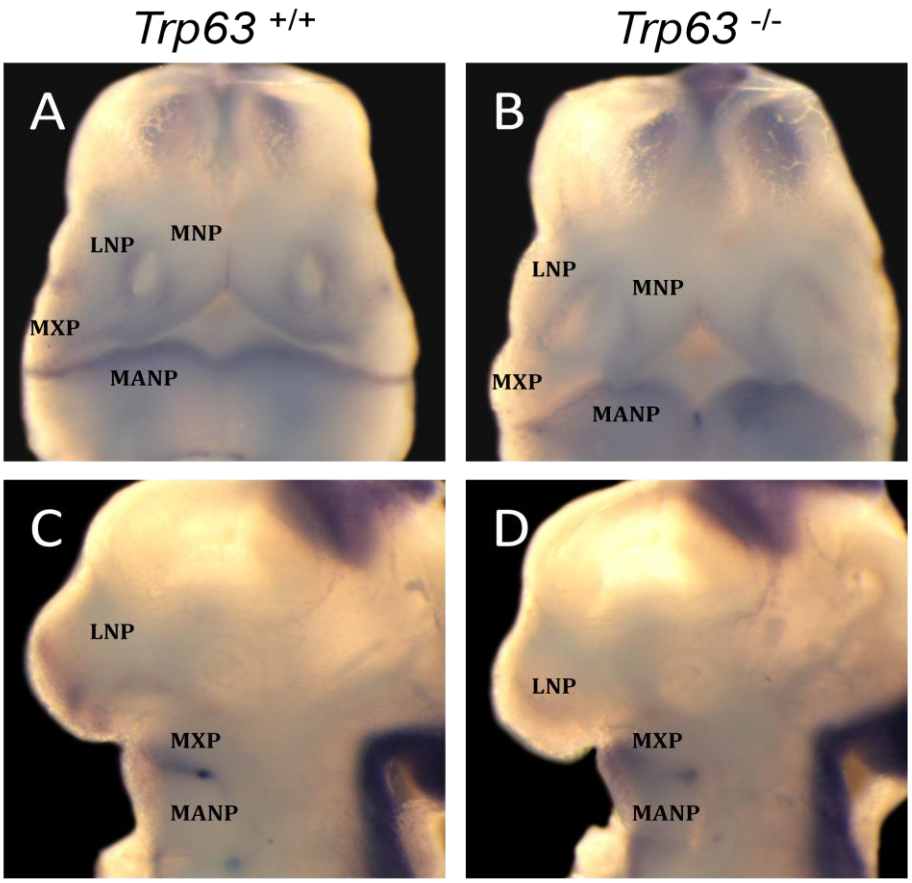

Figure 4.10 Whole mount *in situ* analysis of *Fzd10*. (**A**-**D**) WISH analysis of *Fzd10* between *Trp63*$^{+/+}$ and *Trp63*$^{-/-}$ E11.5 embryos. (**A**&**C**) In *Trp63*$^{+/+}$ embryos, *Fzd10* expression was detected within the nasal epithelium of the medial nasal and lateral nasal processes. Further expression was detected throughout the oral aspects of the medial nasal, maxillary and mandibular processes. In a similar manner to *Lrp6,* a spot of intense staining was observed at the maxillary-mandibular boundary (**B**&**D**) in *Trp63*$^{-/-}$ embryos, *Fzd10* expression was reduced within the nasal epithelium of the lateral nasal processes and appeared absent from the oral aspects of the maxillary processes. Expression of *Fzd10* was comparable to WT within the medial nasal processes. Furthermore, the spot of intense staining at the maxillary-mandibular boundary displayed reduced intensity. LNP- lateral nasal processes, MNP – medial nasal processes, MXP- maxillary processes, MANP- mandibular processes.

nCounter with a fold-change of -2.22 (p= 0.05). Therefore *Fzd10* expression was investigated using qPCR analysis of E11.5 *Trp63*$^{+/+}$ and *Trp63*$^{-/-}$ facial tissue. qPCR analysis identified a significant down-regulation of *Fzd10* in *Trp63*$^{-/-}$ facial processes compared with wildtype littermates, with relative expression of 0.30 compared to wildtype (p= 0.02) (Figure 4.9C).

Having quantified the down-regulation of *Fzd10* in E11.5 *Trp63*$^{-/-}$ facial processes, the expression pattern in *Trp63*$^{-/-}$ and wildtype littermates was characterised using WISH analysis. In E11.5 *Trp63*$^{+/+}$ embryos *Fzd10* expression was detected within the epithelium of the medial nasal and lateral nasal processes surrounding the nasal pits. Further expression was detected at the medial junction between the medial nasal processes (Figure 4.10A). Expression was detected within the oral aspects of the medial nasal and maxillary processes, however it appeared absent from the oral epithelium. Further expression was detected within the oral aspects of the mandibular processes. In a similar pattern to *Lrp6*, intense staining was observed at a small region at the boundary between the maxillary and mandibular processes (Figure 4.10C).

In contrast to wildtype littermates, expression of *Fzd10* in *Trp63*$^{-/-}$ embryos appeared reduced. While *Fzd10* expression was detected within the nasal epithelium of the medial nasal and lateral nasal processes, staining appeared less intense (Figure 4.10B). In addition staining appeared reduced at the junction of the medial nasal processes and appeared absent from the maxillary processes. Expression within the mandibular processes appeared expanded with a region of intense staining observed at the medial junction. Furthermore the intense staining seen at the maxillary-mandibular boundary appeared reduced compared to wildtype littermates (Figure 4.10D).

Taken together these results would suggest that correct P63 regulation is required for *Fzd10* expression during E11.5 upper lip morphogenesis. Furthermore the overlap in expression between *Trp63* and *Fzd10* within the nasal epithelium, together with the confirmed binding of P63 proximal to *Fzd10* could implicate *Fzd10* as a direct target of P63 regulation.

4.3.8 P63 signalling is required for correct expression of *Grhl3* during lip morphogenesis

ChIP-Seq and microarray analysis identified *Grhl3* as a potential target of P63 regulation. ChIP-Seq identified six peaks proximal to *Grhl3* with P63 scan identifying at least one P63 binding motif within each peak. P63 binding motifs were identified at positions Chr4: 135,074,797-135,074,816 (P1), 135,129,153-135,129,172 (P2), 135,153,720-135,153,739 (P3), 135,301,339-135,301,358 (P4), 135,302,371-135,302,390 (P5) and 135,336,322-135,336,341 (P6) (mm9) (Figure 4.11A). Investigation of mammalian conservation showed *Grhl3* P2 and P4 were conserved between mouse and rat. In addition, *Grhl3* P1 was found to be conserved between mouse, rat, human, rhesus monkey, dog, horse and opossum.

Furthermore *Grhl3* P2, P3 and P4 were found to overlap with active regulation markers. *Grhl3* P2 was found to overlap with transcriptional regulation markers H3k4me1, H3k27ac and H3k27me3 found to be active in E11.5 facial tissue and E13.5 and E14.5 palatal tissue. *Grhl3* P3 and P4 were found to overlap with H3k27ac sites active in E13.5 and E14.5 palatal tissue. The presence of active markers of regulation beneath identified P63 binding sites was highly encouraging, suggesting that P63 may be active in gene regulation at these sites.

To confirm if P63 binding was present at the identified motifs in wildtype E11.5 facial processes, binding sites were investigated using ChIP-qPCR. ChIP-qPCR showed five of the six binding sites displayed significant positive enrichment by P63 (p= 0.05) greater than three-fold the negative control *Myoglobin* (Figure 4.11B). *Grhl3* P1, P2, P3, P5 and P6 all displayed positive enrichment with calculated occupancies of 8.30, 13.77, 7.91, 4.19 and 3.13. *Grhl3* P4 failed to display positive enrichment with a calculated occupancy of 2.74 (p= 0.05). Having confirmed P63 binding proximal to *Grhl3* the expression of *Grhl3* was quantified between E11.5 *Trp63*$^{+/+}$ and *Trp63*$^{-/-}$ facial processes. qPCR analysis showed *Grhl3* was significantly down-regulated in *Trp63*$^{-/-}$ facial processes with a relative expression of 0.44 compared with wildtype littermates (Figure 4.11C).

The expression profile of *Grhl3* was characterised in E11.5 *Trp63*$^{+/+}$ and *Trp63*$^{-/-}$ embryos using WISH analysis. In E11.5 *Trp63*$^{+/+}$ embryos *Grhl3* expression was detected in the nasal epithelium of the medial nasal and lateral nasal processes surrounding the nasal pit (Figure 4.12A). Further expression was detected at the lambdoidal junction at the boundary between the medial nasal, lateral nasal and maxillary processes. Expression within the maxillary processes was detected within the oral epithelium, the lacrimal groove and at maxillary-mandibular boundary (Figure 4.12C). In contrast to wildtype littermates, *Grhl3* expression within *Trp63*$^{-/-}$ embryos was markedly reduced (Figure 4.12B). While expression within the nasal epithelium could be detected, it appeared reduced, with expression within the lateral nasal processes most affected. Expression at the lambdoidal junction appeared absent. Furthermore expression within the lacrimal groove and the maxillary- mandibular boundary was absent (Figure 4.12D).

Taken together these results would suggest that correct regulation by P63 is required for expression of *Grhl3* during upper lip morphogenesis. Furthermore the confirmation of bound P63 binding sites overlapping with markers of active transcriptional regulation and the marked reduction in *Grhl3* expression in *Trp63*$^{-/-}$ embryos could suggest that *Grhl3* is a direct target of P63.

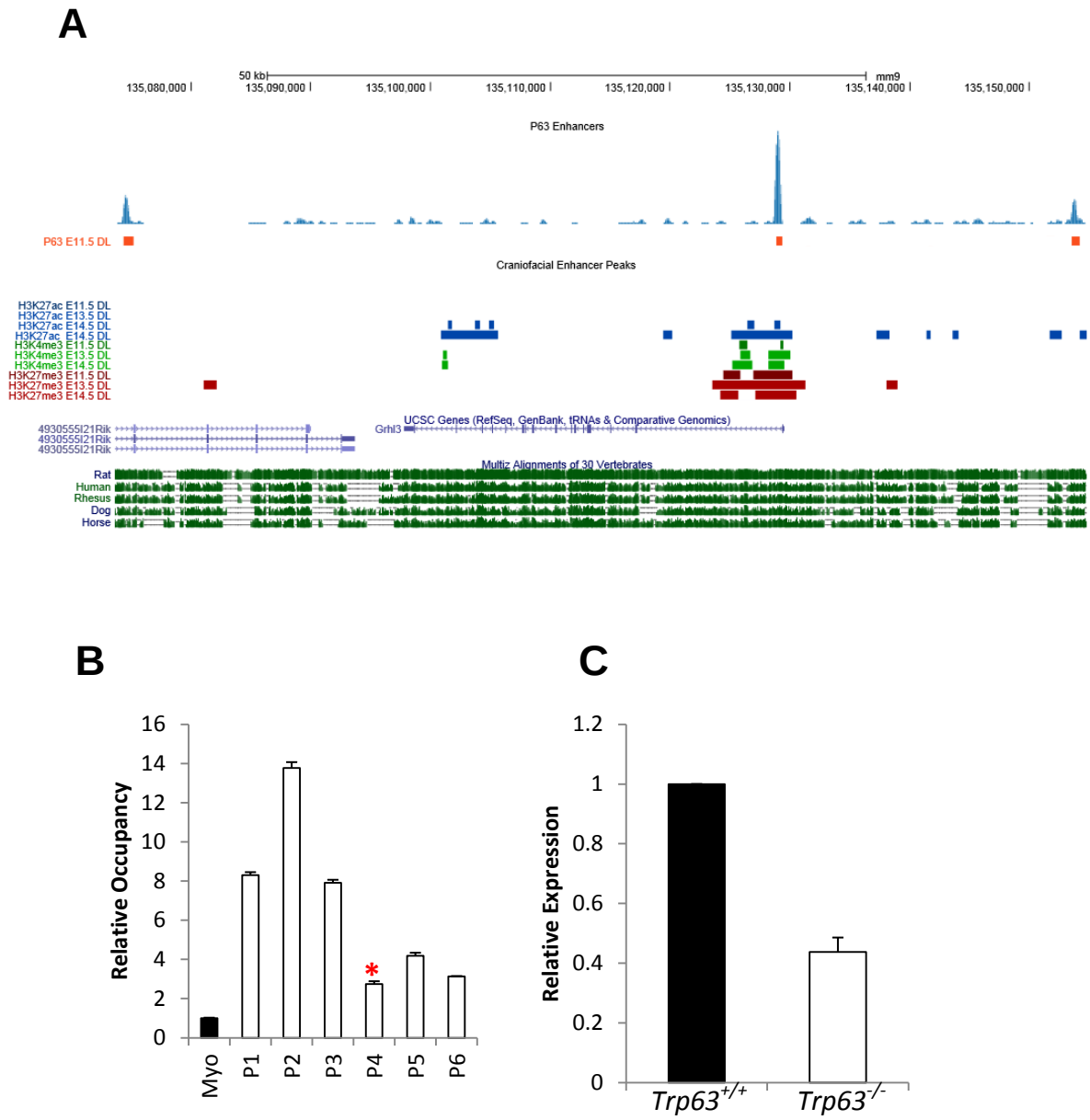

Figure 4.11 *Grhl3* is a target of P63 signalling. (**A**) ChIP-Seq/microarray intersection identified six putative P63 binding sites proximal to *Grhl3* (three not shown). Binding sites were shown to overlap with markers of active transcriptional regulation including H3k27ac and H3k27me3 sites identified in E11.5 facial and E13.5 and E14.5 palatal tissue. Mammalian conservation is shown. (**B**) ChIP-qPCR was conducted on six putative P63 binding sites proximal to *Grhl3*. Relative chromatin occupancy was calculated relative to the negative control *Myoglobin* (black). Five out of six binding sites displayed significant positive enrichment by P63 (p= 0.05), with *Grhl3* P4 (*) failing to display enrichment. (**C**) qPCR analysis between E11.5 *Trp63*$^{-/-}$ and WT facial processes identified a significant reduction in *Grhl3* expression relative to the house keeping gene *β-actin* (p= 0.05). Error bars display standard error of the mean.

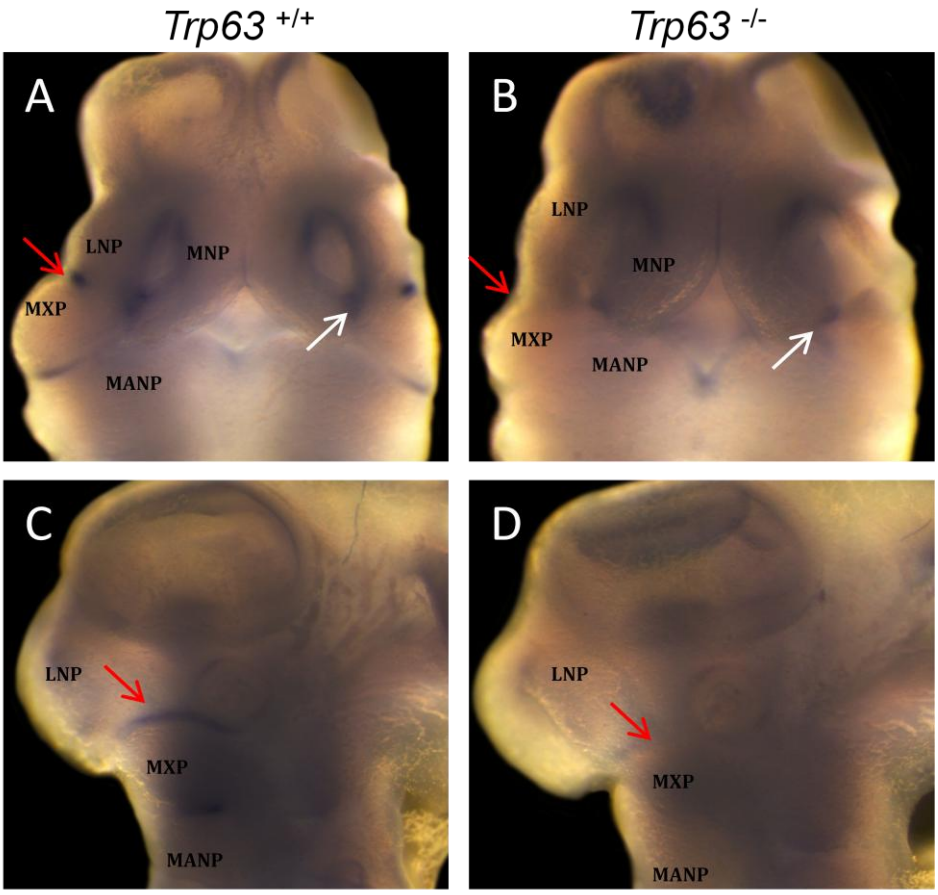

Figure 4.12 Whole mount *in situ* hybridisation analysis of *Grhl3*. (**A**-**D**) WISH analysis of *Grhl3* between *Trp63*$^{+/+}$ and *Trp63*$^{-/-}$ E11.5 embryos. (**A**&**C**) *Grhl3* expression was detected within the nasal epithelium of the medial nasal and lateral nasal processes. Further expression was detected throughout the oral epithelium of maxillary processes and within the lacrimal groove (arrowed - red) extending posteriorly towards the eye. Expression was detected within the epithelium of the lambdoidal junction (arrowed - white) (**B**&**D**) In *Trp63*$^{-/-}$ embryos, *Grhl3* expression was markedly reduced within the nasal epithelium of the medial nasal and lateral nasal processes. Expression within the lambdoidal junction was reduced (arrowed – white) and expression within the lacrimal groove was absent. Furthermore *Grhl3* expression was absent from the oral epithelium of the maxillary processes. LNP- lateral nasal processes, MNP – medial nasal processes, MXP- maxillary processes, MANP- mandibular processes.

4.3.9 P63 signalling is required for correct expression of *Lef1* during lip morphogenesis

ChIP-Seq analysis identified six potential binding sites ≤ 150 kb of the *Lef1* TSS and P63 scan identified P63 binding motifs at positions chr3: 130,639,639-130,639,661 (P1), 130,721,650-130,721,672 (P3), 130,846,288-130,846,310 (P4), 130,875,663-130,875,685 (P5) and 130,881,005-130,881,027 (P6) (mm9) (Figure 4.13A). P63 Scan identified five of the six peaks as being positive for the P63 binding motif, with the motif absent from *Lef1* P2 chr3: 130,675,646-130676467. Each binding site was assayed using ChIP-qPCR to determine if P63 binding was present in E11.5 wildtype facial processes. Due to the absence of the P63 binding motif at *Lef1* P2, this site was not assayed. Of the five binding sites assayed, four were found to be significantly enriched for P63 binding at E11.5 (p= 0.05) (Figure 4.13B). Binding sites P1, P3, P4, and P6 displayed occupancies ≥ 3 fold the negative control with occupancies of 12.73, 10.45, 17.10 and 5.25. Binding site *Lef1* P5 failed to display positive enrichment with an occupancy of 0.35. These results would suggest that P63 binds at multiple sites proximal to *Lef1* during upper lip morphogenesis. *Lef1* P1, P3 and P4 were found to overlap with previously identified E11.5 H3k27ac active enhancer sites, suggesting the peak is involved in transcriptional regulation. In addition *Lef1* P3 and P4 were also found to display an overlap with a H3k4me1site active at E11.5 providing further evidence that these sites are involved in transcriptional regulation during lip morphogenesis.

Having confirmed P63 binding proximal to *Lef1* in E11.5 facial processes, the expression levels of *Lef1* were quantified between *Trp63*$^{+/+}$ and *Trp63*$^{-/-}$ E11.5 facial processes. qPCR analysis identified a significant down-regulation in *Lef1* expression within *Trp63*$^{-/-}$ facial processes compared with wildtype littermates (Figure 4.13C), with relative expression of 0.34 compared to wildtype (p= 0.05).

Having identified a reduction in *Lef1* expression in *Trp63*$^{-/-}$ E11.5 facial processes, the expression profile of *Lef1* was characterised in *Trp63*$^{+/+}$ and *Trp63*$^{-/-}$ embryos. WISH analysis of *Lef1* expression in E11.5 *Trp63*$^{+/+}$ embryos identified weak expression within the nasal epithelium of the medial nasal and lateral nasal processes. Intense staining was observed within the maxillary processes. Further staining was observed throughout the limb buds (Figure 4.14A&C). In contrast to wildtype littermates, *Lef1* expression within *Trp63*$^{-/-}$ embryos appeared markedly reduced. Expression was detected within the medial nasal and lateral nasal processes surrounding the nasal pits, but appeared less intense. Strong expression previously observed in the anterior aspects of the lateral nasal processes of wildtype littermates was absent in *Trp63*$^{-/-}$ embryos (Figure 4.14B&D). The greatest reduction in expression was detected within the maxillary processes, with intensity markedly reduced. Furthermore the posterior boundary of expression appeared to have advanced posteriorly. *Lef1* expression within the limb buds was comparable between *Trp63*$^{-/-}$ and wildtype littermates, suggesting the loss of *Lef1* facial process expression to be tissue specific.

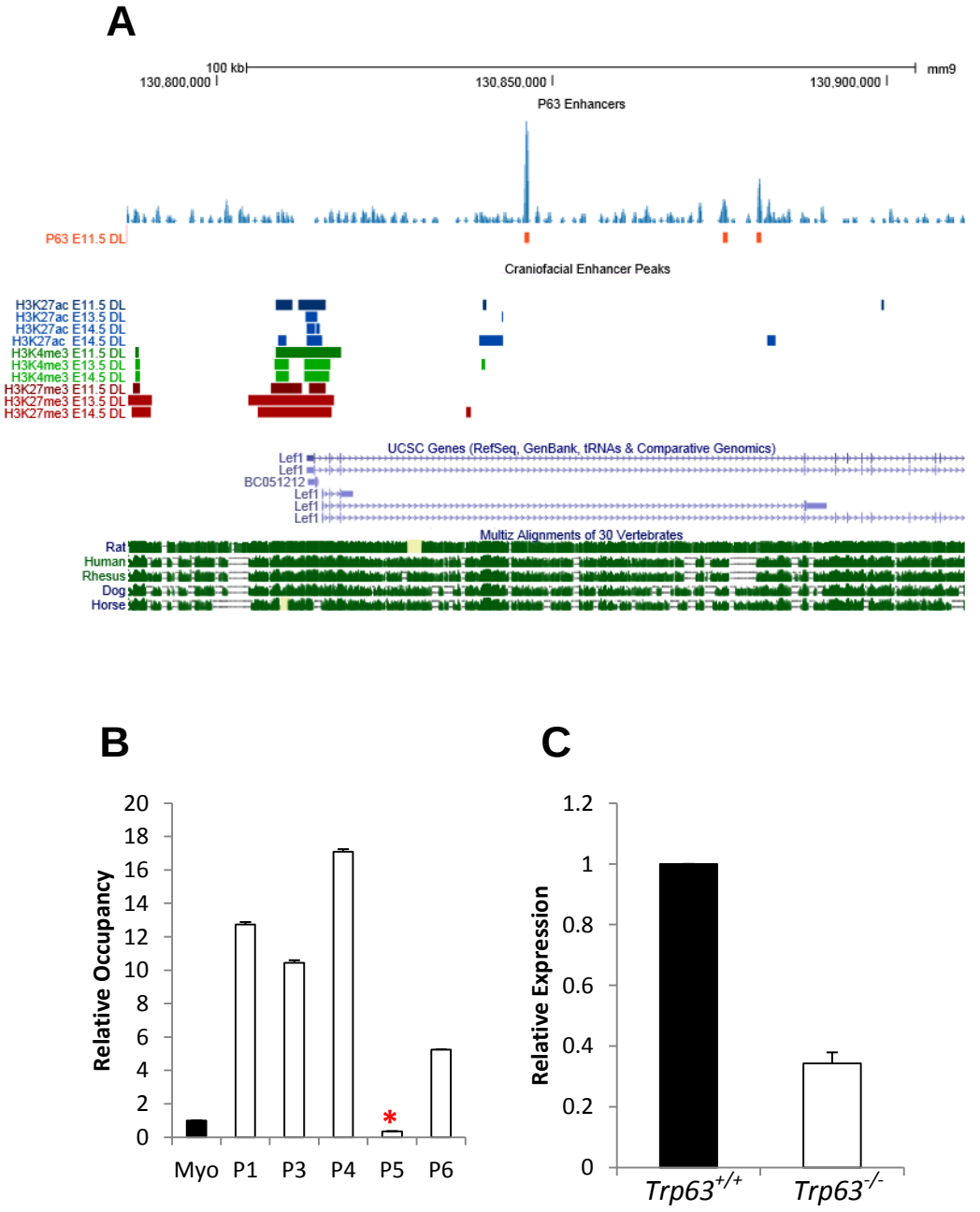

Figure 4.13 *Lef1* is a target of P63 signalling. (**A**) ChIP-Seq/microarray intersection identified six potential P63 binding sites proximal to *Lef1* (three not shown). Identified binding sites were shown to overlap with markers of active transcriptional regulation including H3k27ac and H3k4me1 sites identified in E11.5 facial tissue. Mammalian conservation is shown. (**B**) ChIP-qPCR was conducted on five putative P63 binding sites proximal to *Lef1*. Relative chromatin occupancy was calculated relative to the negative control *Myoglobin* (black). Four out of five binding sites displayed significant positive enrichment by P63 (p= 0.05), with *Lef1* P5 failing to display enrichment (*). (**B**) qPCR analysis between E11.5 *Trp63*$^{-/-}$ and WT facial processes identified a significant reduction in *Lef1* expression relative to the house keeping gene *β-actin* (p= 0.05). Error bars display standard error of the mean.

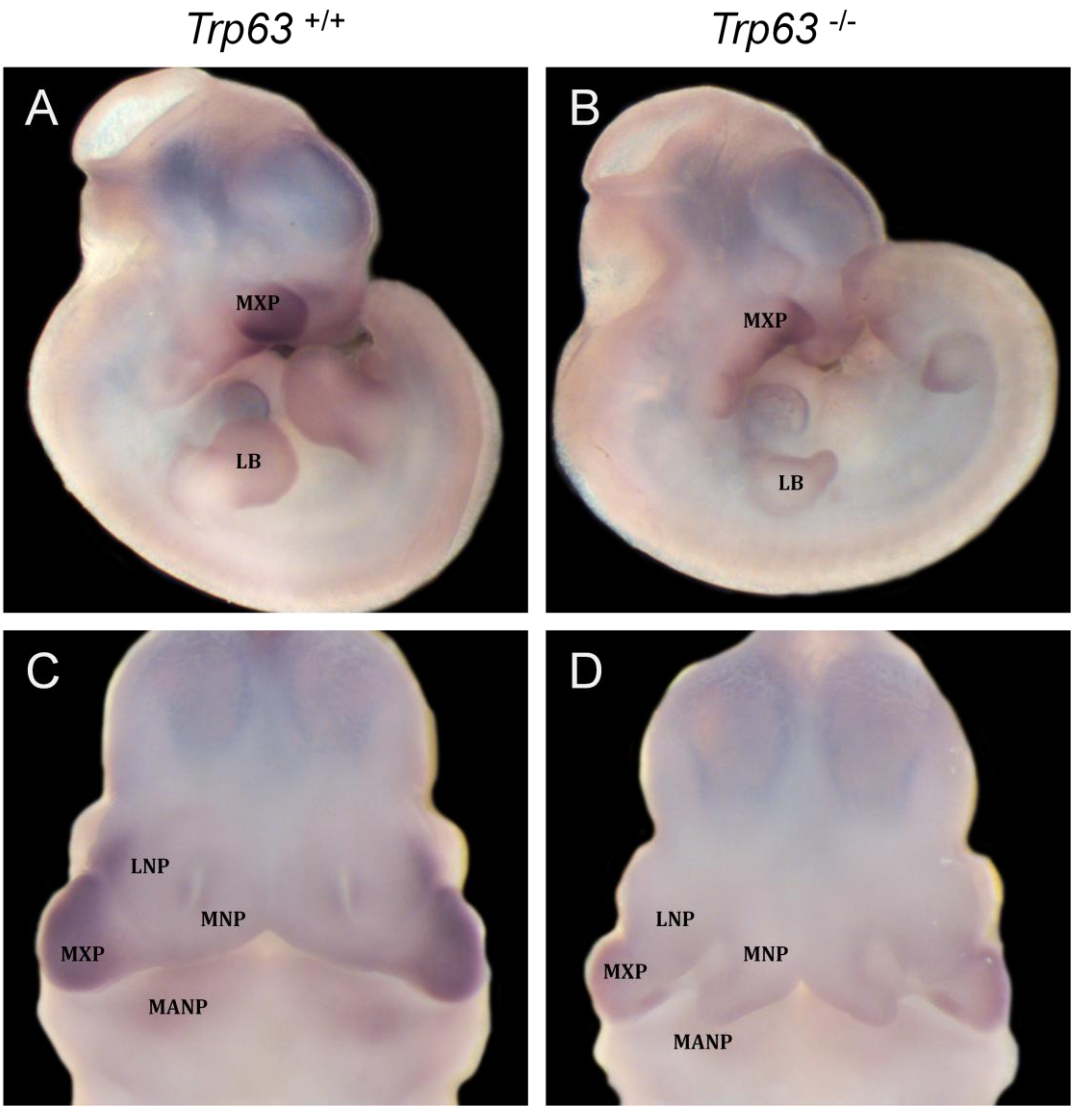

Figure 4.14 Whole mount *in situ* hybridisation analysis of *Lef1*. (**A**-**D**) WISH analysis of *Lef1* between *Trp63*$^{+/+}$ and *Trp63*$^{-/-}$ E11.5 embryos. (**A**&**C**) Weak *Lef1* expression was detected within the nasal epithelium of the medial nasal and lateral nasal processes, while strong expression was detected within the maxillary and mandibular processes. Further expression was detected within the limb buds. (**B**&**D**) In *Trp63*$^{-/-}$ embryos, *Lef1* expression was comparable in the nasal epithelium of the medial nasal and lateral nasal processes. In contrast, expression of *Lef1* within the maxillary and mandibular processes was markedly reduced compared with wildtype. Expression within the limb buds appeared comparable between WT and nulls. LNP- lateral nasal processes, MNP – medial nasal processes, MXP- maxillary processes, MANP- mandibular processes, LB- limb bud.

Taken together these findings would suggest that at E11.5 P63 binds proximal to *Lef1*, and a loss of P63 regulation results in a reduction in *Lef1* expression in a facial process specific manner. P63 is therefore required for *Lef1* expression at E11.5 and could suggest that *Lef1* is a direct target of P63 regulation during upper lip morphogenesis

4.3.10 P63 signalling is required for correct expression of *Pax6* during lip morphogenesis

Pax6 was identified as a potential target of P63 regulation during upper lip morphogenesis. ChIP-Seq analysis identified a potential P63 binding site proximal to *Pax6*. P63 scan identified a P63 binding motif at position Chr2: 105,556,346-105,556,365 (P1) (mm9) (Figure 4.15A). Analysis of mammalian conservation showed the P63 binding motif was conserved between mouse, rat, human, rhesus monkey, dog and horse. However no markers of active regulation were shown to overlap with *Pax6* P1. To determine if P63 binding was present in wildtype E11.5 facial processes, ChIP-qPCR analysis was conducted on *Pax6* P1. ChIP-qPCR analysis showed *Pax6* P1 displayed significant positive enrichment by P63 in wildtype E11.5 facial processes with a chromatin occupancy of 15.32 (p= 0.05) (Figure 4.15B).

Microarray and nCounter analyses indicated *Pax6* was significantly up-regulated in *Trp63*$^{-/-}$ facial processes at E11.5 and E12.5 against wildtype (p= 0.05) (Figure 4.15C). The expression profile of *Pax6* was therefore characterised in E11.5 *Trp63*$^{+/+}$ and *Trp63*$^{-/-}$ embryos using WISH analysis. In *Trp63*$^{+/+}$ embryos *Pax6* expression was weakly detected in the epithelium of the medial nasal and lateral nasal processes surrounding the nasal pit. Further strong expression was detected throughout the eyes and forebrain (Figure 4.16A&C). In comparison to wildtype littermates, expression of *Pax6* appeared up-regulated in *Trp63*$^{-/-}$ embryos. Increased expression was detected in the nasal epithelium of the medial nasal and lateral nasal processes. Additional expression was detected within the oral epithelium of the maxillary processes which was absent in wildtype (Figure 4.16B). Expression within the eyes and forebrain was comparable to wildtype littermates (Figure 4.16D).

Taken together these results suggested the P63 regulation is required for correct expression of *Pax6* during upper lip morphogenesis. P63 binds proximal to *Pax6* in E11.5 wildtype facial processes and the absence of P63 regulation resulted in the up-regulation of *Pax6*. Furthermore the overlapping expression patterns of *Trp63* and *Pax6* in the nasal epithelium coupled with the binding of P63 proximal to *Pax6* suggested that *Pax6* may be a bona fide target of direct P63 regulation during upper lip morphogenesis.

4.3.11 P63 signalling is required for correct expression of *Sox2* during lip morphogenesis

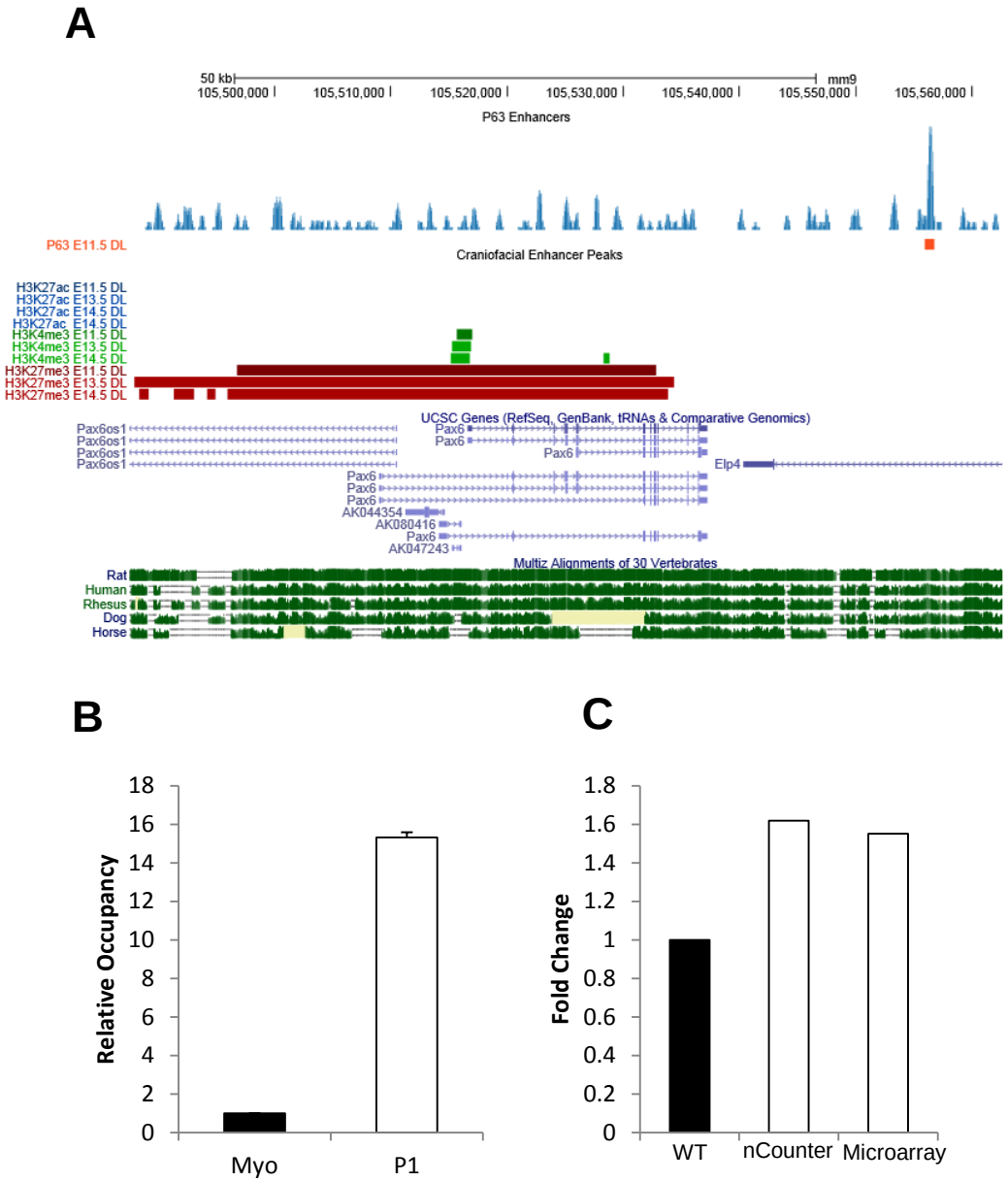

Figure 4.15 *Pax6* is a target of P63 signalling. (**A**) ChIP-Seq/microarray intersection identified a putative P63 binding site proximal to *Pax6*. *Pax6* P1 did not overlap with identified markers for active transcriptional regulation. The binding site was conserved between mouse, rat, human, rhesus monkey, dog and horse. (**B**) ChIP-qPCR was conducted on a putative P63 binding site proximal to *Pax6*. Relative chromatin occupancy was calculated relative to the negative control *Myoglobin* (black). *Pax6* P1 was shown to display significant positive enrichment by P63 (p= 0.05). (**C**) Expression analyses between E11.5 and E12.5 *Trp63*$^{-/-}$ and WT facial processes through nCounter and microarray analyses identified a significant up-regulation of *Pax6* expression compared to WT (p= 0.05). Error bars display standard error of the mean.

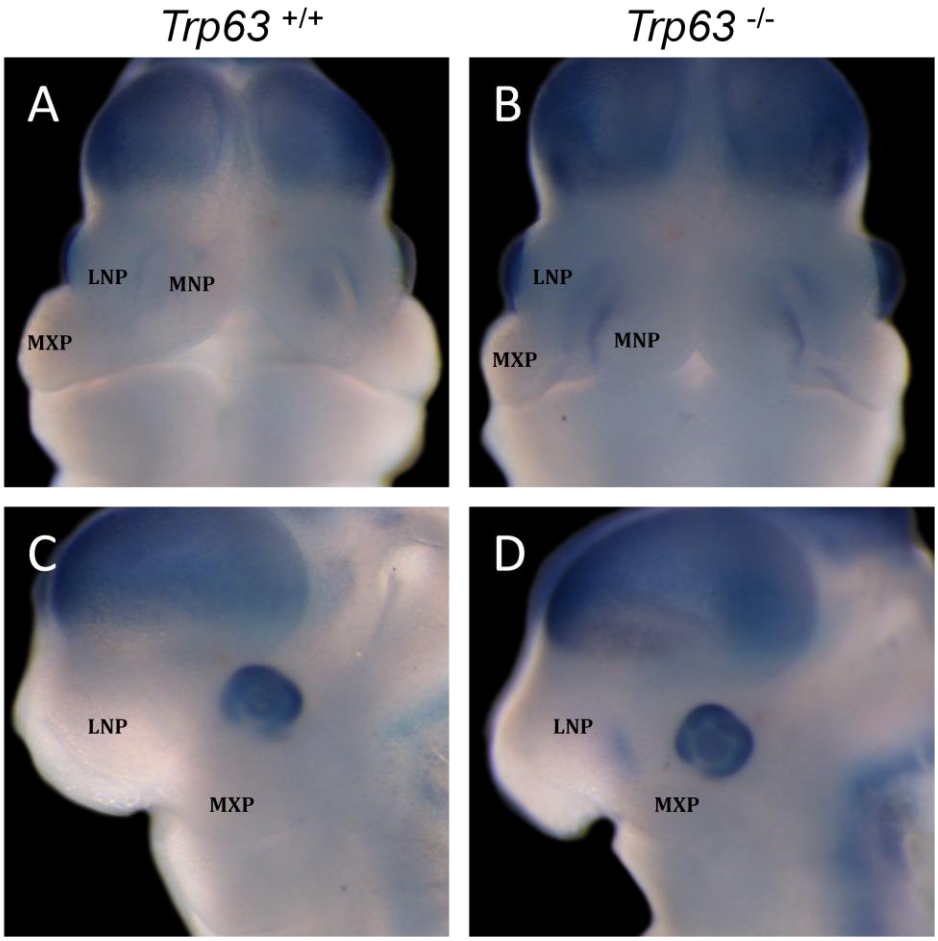

Figure 4.16 Whole mount *in situ* hybridisation analysis of *Pax6*. (**A**-**D**) WISH analysis of *Pax6* between *Trp63*$^{+/+}$ and *Trp63*$^{-/-}$ E11.5 embryos. (**A**&**C**) Weak *Pax6* expression was detected within the nasal epithelium of the medial nasal and lateral nasal processes, while strong expression was detected within the forebrain and eye (**B**&**D**) In *Trp63*$^{-/-}$ embryos, *Pax6* expression was markedly expanded within the nasal epithelium of the medial nasal and lateral nasal processes, with expression extending to the distal tips of the medial nasal processes. *Pax6* expression within the forebrain and eye was comparable to WT suggesting expansion within the facial processes was a tissue specific effect. LNP- lateral nasal processes, MNP – medial nasal processes, MXP- maxillary processes, MANP- mandibular processes.

Comparative analysis between the E12.5 microarray and E11.5 ChIP-Seq identified *Sox2* as a potential target of P63 gene regulation during upper lip morphogenesis. One P63 ChIP-Seq peak was identified ≤150 kb of the *Sox2* TSS with P63 scan identifying two P63 binding motifs at positions: chr3: 34,672,730-34,672,752 (P1) and 34,672,869-34,672,891 (P2) (mm9) (Figure 4.17A). Sequence analysis of P63 binding motifs showed *Sox2* P1 was conserved between mouse, rat, human, rhesus monkey, dog and horse while P2 was conserved between mouse, rat, rhesus monkey and human. Furthermore, *Sox2* P1 and P2 were shown to overlap with an H3k27ac enhancer site active in E11.5 facial tissue, while P2 overlapped with H3k27ac sites active in E13.5 and E14.5 palatal shelf tissue. To determine if the identified sites were bound by P63 during lip morphogenesis, ChIP-qPCR was conducted for each putative binding site using chromatin extracted from wildtype E11.5 facial processes. ChIP-qPCR analysis showed *Sox2* P2 displayed significant positive enrichment by P63 with an occupancy of 4.71 (p= 0.05), however *Sox2* P1 failed to display an occupancy greater than three-fold the negative control with an occupancy of 0.50 (Figure 4.17B). These results suggested that P63 does bind proximal to *Sox2* during upper lip morphogenesis. In addition, the overlap with active H3k27ac sites provided further evidence that P63 regulation is active at these sites.

Having confirmed P63 binding proximal to *Sox2*, the expression profile of *Sox2* was characterised in E11.5 *Trp63*$^{+/+}$ and *Trp63*$^{-/-}$ embryos. Microarray and nCounter analysis in RNA isolated from E11.5 and E12.5 facial processes showed a significant up-regulation of *Sox2* in *Trp63*$^{-/-}$ facial processes relative to wildtype (p= 0.05) (Figure 4.17C). WISH analysis using a riboprobe to *Sox2* identified that *Sox2* expression was detected within the nasal epithelium of the medial nasal processes in wildtype embryos. In addition expression was detected within the epithelium of the maxillary processes at the lambdoidal junction bordering the medial nasal and lateral nasal processes and the oral epithelium of the mandibular processes (Figure 4.18A). Furthermore, expression was detected within the neural tube and superior aspects of the optic cup (Figure 4.18C).

In contrast to wildtype embryos, expression of *Sox2* was markedly expanded in *Trp63*$^{-/-}$ embryos. Staining intensity was increased within the nasal epithelium of the medial nasal processes. In addition, the expression domain of *Sox2* was expanded to include the superior aspects of the medial nasal processes surrounding the nasal pit and was present within the lateral nasal processes. Expression was detected within the epithelium of the distal aspects of the medial nasal processes at the site of contact with the lateral nasal processes, the lambdoidal junction (Figure 4.18B). The maxillary expression detected in wildtype littermates was present, however appeared marginally reduced. Expression within the mandibular processes, neural tube and the optic cup was comparable to wildtype (Figure 4.18B&D).

Taken together these results suggested that correct expression of *Trp63* was required for *Sox2* expression during E11.5 upper lip morphogenesis. P63 binding has been confirmed proximal to *Sox2* and P63 binding sites were shown to overlap with H3k27ac sites active in

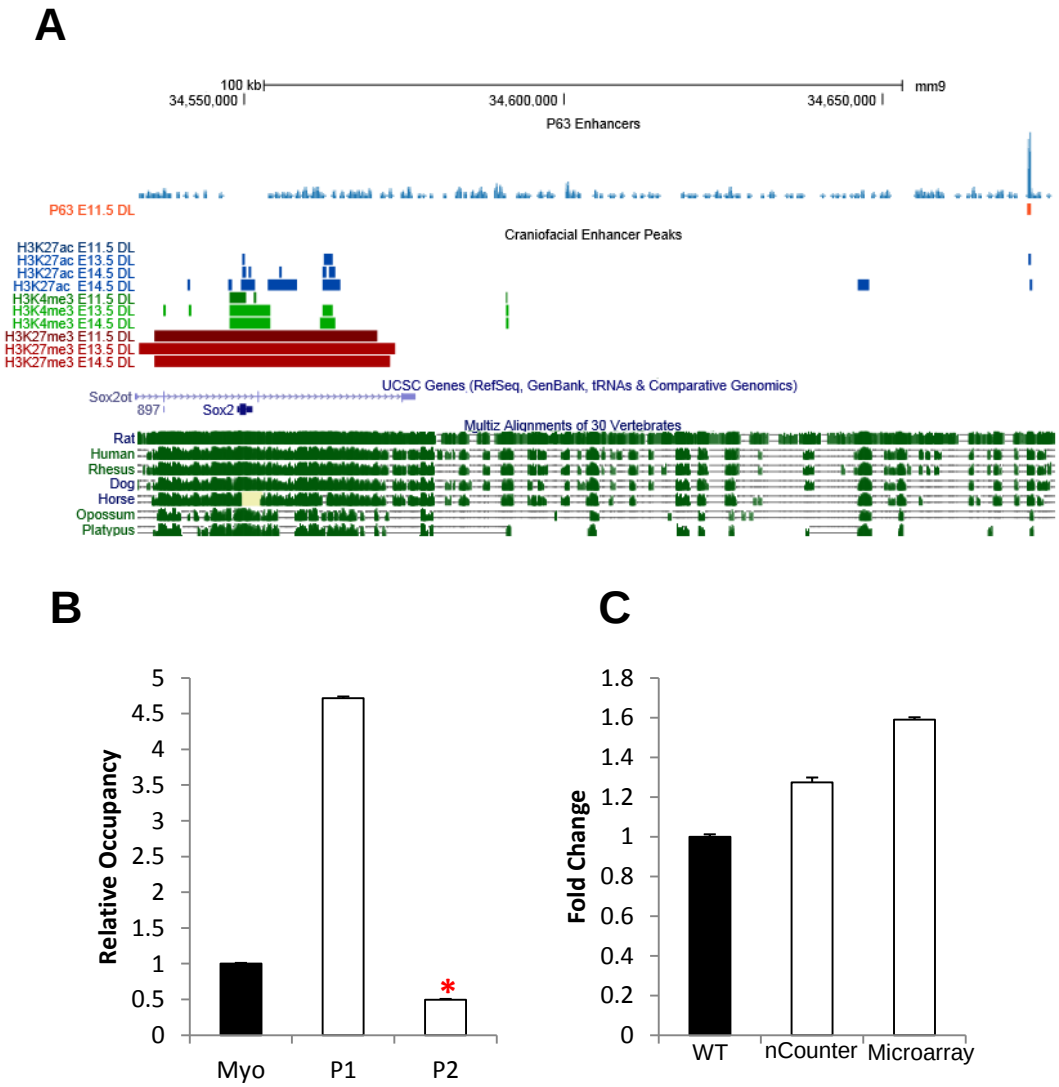

Figure 4.17 *Sox2* is a target of P63 signalling. (**A**) ChIP-Seq/microarray intersection identified a P63 peak proximal to *Sox2* which contained two putative P63 binding sites. The putative binding sites overlapped with H3k27ac sites, markers for active transcriptional regulation, identified in E11.5 facial and E14.5 palatal tissue. Sites were conserved between mouse, rat, human, rhesus monkey, dog and horse. (**B**) ChIP-qPCR was conducted on two putative P63 binding sites proximal to *Sox2*. Relative chromatin occupancy was calculated relative to the negative control *Myoglobin* (black). *Sox2* P1 was shown to display significant positive enrichment by P63 (p= 0.05), while *Sox2* P2 failed to display positive enrichment (*). (**B**) Expression analyses between E11.5 and E12.5 *Trp63*$^{-/-}$ and WT facial processes through nCounter and microarray analysis identified a significant up-regulation of *Sox2* expression compared to WT (p= 0.05). Error bars display standard error of the mean.

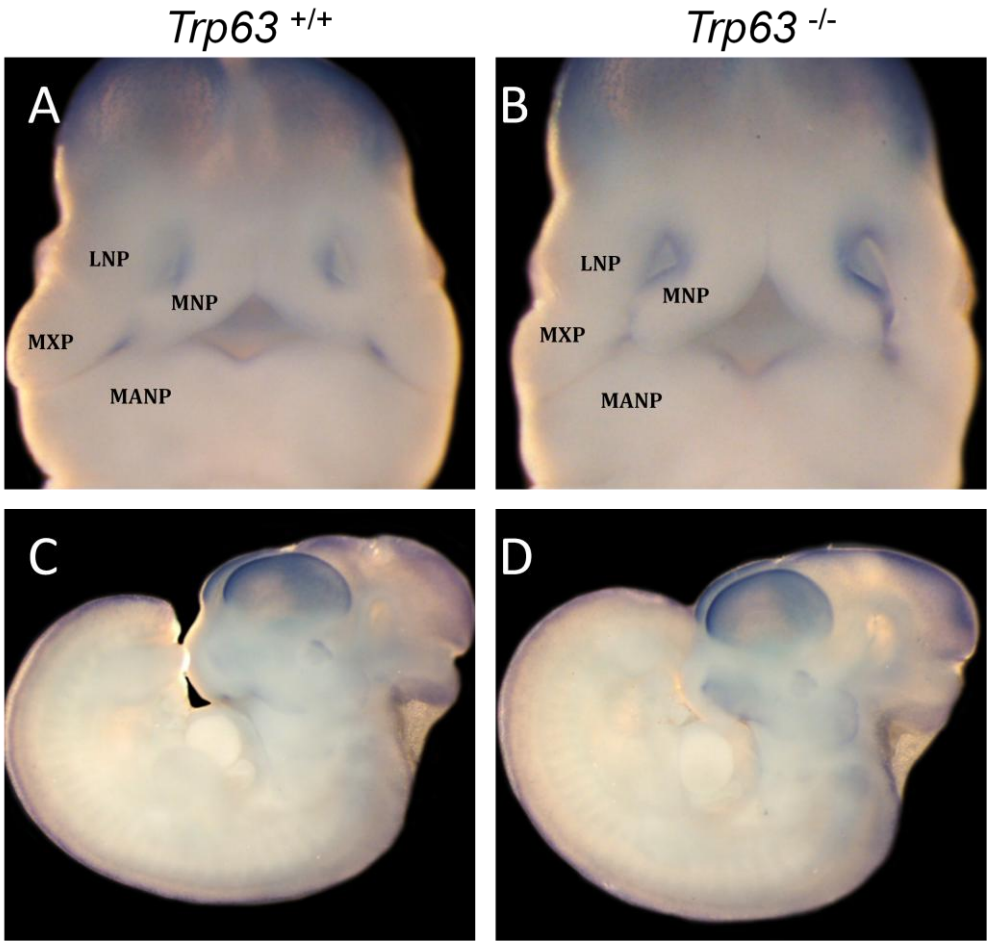

Figure 4.18 Whole mount *in situ* hybridisation analysis of *Sox2* (**A**-**D**) WISH analysis of *Sox2* in *Trp63*$^{+/+}$ and *Trp63*$^{-/-}$ E11.5 embryos. (**A**&**C**) Weak *Sox2* expression was detected within the nasal epithelium of the medial nasal processes, while strong expression was detected within the forebrain. Further expression was detected within the oral epithelium of the maxillary processes at the site of contact between the medial nasal and maxillary processes and the oral epithelium of the mandibular processes. Weak expression was detected throughout the neural tube and superior aspects of the optic cup. (**B**&**D**) In *Trp63*$^{-/-}$ embryos, *Sox2* expression was markedly expanded within the nasal epithelium of the medial nasal and lateral nasal processes, with expression extending to the distal tips of the medial nasal processes and into the maxillary processes. *Sox2* expression within the forebrain, mandibular processes, neural tube and optic cup was comparable to WT suggesting expansion within the facial processes was a tissue specific effect. LNP- lateral nasal processes, MNP – medial nasal processes, MXP- maxillary processes, MANP- mandibular processes.

facial and palatal shelf tissue. Expression analysis identified a significant up-regulation in cDNA from E11.5 and E12.5 *Trp63*$^{+/+}$ and null facial processes. Expansion in *Sox2* expression was confirmed using WISH. Furthermore, the presence of comparable *Sox2* expression patterns within the mandibular processes, neural tube and the optic cup suggested the change in upper lip *Sox2* expression was tissue specific. Together these results could suggest *Sox2* may be a direct target of P63 regulation.

4.3.12 Loss of P63 regulation results in misregulation of multiple members of the Wnt signalling network

In addition to the ligands *Wnt3*, *Wnt4* and *Wnt9b*, ChIP-Seq/microarray intersection identified a potential association between P63-regulation and the genes *Wnt2b*, *Wnt3a*, *Wnt7a*, *Wnt7b*, *Wnt10b*, *Wnt11*, *Krm2*, *Sfrp1* and *Fzd4*. A lack of *Trp63*$^{+/+}$ and *Trp63*$^{-/-}$ embryos, meant that it was not possible to assess the relative expression domains of these gene *in situ*, however the associated binding sites were assayed using ChIP-qPCR and their relative expression quantified in *Trp63*$^{+/+}$ and *Trp63*$^{-/-}$ E11.5 facial tissue.

4.3.12.1 *Wnt2b*

Two potential P63 binding sites were identified ≤150 kb of the *Wnt2b* TSS and P63 scan identified P63 binding motifs at positions: Chr3: 104,738,881-104,738,903 (P1) and 104,800,484-104,800,506 (P2) (mm9). Analysis of binding sites proximal to *Wnt2b*, showed both P1 and P2 were not conserved (outside of mice). Furthermore, P63 binding motifs were found to overlap with H3k27ac sites identified in E11.5 facial tissue. ChIP-qPCR analysis identified that *Wnt2b* P2 failed to display positive enrichment by P63 in wildtype E11.5 facial processes with an occupancy of 2.08 (Figure 4.19A). In contrast, *Wnt2b* P1 displayed significant positive enrichment by P63 (P= 0.05), with an occupancy of 12.25. The expression of *Wnt2b* was quantified in E11.5 *Trp63*$^{+/+}$ and *Trp63*$^{-/-}$ facial processes. qPCR analysis showed *Wnt2b* was up-regulated in the absence of P63, with a relative expression of 1.41 to wildtype (Figure 4.19B). However, the result failed to achieve significance with a p-value of 0.1. Previous expression analysis from the E12.5 microarray and E11.5 nCounter produced conflicting results, with microarray identifying a down-regulation in *Wnt2b* expression and nCounter identifying an up-regulation. It therefore remains unclear whether *Wnt2b* is a direct target of P63 signalling.

4.3.12.2 *Wnt3a*

ChIP-Seq/microarray analysis identified five potential P63 binding sites ≤150 kb of the *Wnt3a* TSS. P63 scan identified P63 binding motifs at positions: chr11: 59,097,826-59,097,848 (P1), 59,139,305-59,139,327 (P2), 59,219,646-59,219,668 (P3), 59,224,145-59,224,167 (P4) and 59,227,058-59,227,080 (P5) (mm9). Analysis of mammalian conservation found binding sites P2, P3, P4 and P5 were only conserved between mouse and rat. However *Wnt3a* P1 was shown to be conserved between mouse, rat, human and

rhesus monkey. Furthermore, *Wnt3a* P1 was found to overlap with an H3k27ac site identified in E13.5 palatal shelf tissue and an H3k27me3 site active in E11.5 (facial), E13.5 (palatal) and E14.5 (palatal). In addition, *Wnt3a* P4 and P5 were shown to overlap with an H3k27ac site identified in E11.5 (facial), E13.5 (palatal) and E13.5 (palatal) tissue. *Wnt3a* P3 was found to overlap with an H3k27ac site in E11.5 (facial) and E14.5 (palatal) tissue.

P63 binding at each potential binding site was analysed using ChIP-qPCR in chromatin from wildtype E11.5 facial processes. ChIP-qPCR analysis identified that P63 binding was significantly enriched (p= 0.05) at *Wnt3a* P1, P2, P3, P4 and P5 with occupancies of 18.47, 21.31, 14.26, 14.40 and 19.62 respectively (Figure 4.19A).

The expression of *Wnt3a* was therefore quantified in facial processes between E11.5 *Trp63*$^{+/+}$ and *Trp63*$^{-/-}$ embryos. qPCR analysis identified *Wnt3a* was significantly down-regulated in *Trp63*$^{-/-}$ facial processes with a relative expression of 0.19 compared to wildtype (p= 0.02) (Figure 4.19B). qPCR results agreed with the results of the E11.5 nCounter and E12.5 microarray, however previous work which characterised the expression of Wnt genes in upper lip morphogenesis, failed to demonstrate *Wnt3a* expression within the facial processes (Geetha-Loganathan *et al*. 2009). It is therefore unclear if *Wnt3a* is subject to P63 regulation.

4.3.12.3 *Wnt7a*

Five putative P63 binding sites were identified proximal to *Wnt7a*, with P63 scan identifying P63 binding motifs at positions: chr6: 91,314,308-91,314,330 (P1), 91,339,017-91,339,039 (P2), 91,402,311-91,402,333 (P4) and 91,517,496-91,517,518 (P5) (mm9). An additional binding site was identified at chr9: 91,385,921-91,386,495 (P3), however P63 scan failed to identify the presence of a P63 binding motif. Therefore no further analysis of this site was conducted. Analysis of mammalian conservation showed that *Wnt7a* P1, P4 and P5 were not conserved outside of mouse. In contrast, *Wnt7a* P2 was conserved between mouse, rat and human. ChIP-qPCR analysis of *Wnt7a* P1 and P4 identified significant P63 enrichment was present at P1 and P4 with chromatin occupancies of 3.64 and 3.49 (p= 0.05). *Wnt7a* P2 failed to achieve significant P63 enrichment with an occupancy of 0.71(Figure 4.19A). Due to a high GC content, it was not possible to design viable primers for *Wnt7a* P5.

Having confirmed P63 binding ≤150 kb of the *Wnt7a* TSS, the expression of *Wnt7a* was quantified between E11.5 *Trp63*$^{+/+}$ and *Trp63*$^{-/-}$ facial processes. qPCR analysis identified a significant down-regulation of *Wnt7a* expression in *Trp63*$^{-/-}$ facial processes compared with wildtype (p= 0.02). *Wnt7a* expression was shown to be down-regulated with a relative expression of 0.49 compared with wildtype (Figure 4.19B). Taken together these results show P63 binds proximal to *Wnt7a,* which is significantly down-regulated in *Trp63*$^{-/-}$ facial processes compared with wildtype. These results could suggest that during upper lip

morphogenesis, *Wnt7a* is a target of P63 regulation, however further work is required to characterise this relationship.

4.3.12.4 *Wnt7b*

In addition to *Wnt7a*, *Wnt7b* was identified as a potential target of P63 regulation. Two potential P63 binding sites were identified proximal to *Wnt7b*, with P63 scan identifying the presence of a P63 binding motifs at positions: Chr15: 85,311,633-85,311,655 (P1) and 85,408,613-85,408,635 (P2) (mm9). Analysis of mammalian conservation indicated that P1 was not conserved and did not overlap with identified enhancer sites. In contrast *Wnt7b* P2 was found to be conserved between mouse, rat, human, rhesus monkey, dog and horse. Furthermore, *Wnt7b* P2 overlapped with H3k4me3 and H3k27me3 sites identified in E11.5 (facial), E13.5 and E14.5 (palatal) tissue respectively. ChIP-qPCR analysis of E11.5 wildtype facial processes identified *Wnt7b* P1 displayed significant positive enrichment by P63 with an occupancy of 6.01 (p= 0.05) (Figure 4.19A). However, *Wnt7b* P2 failed to display positive enrichment with an occupancy of 1.85.

Having confirmed P63 binding proximal to *Wnt7b* in E11.5 upper lip morphogenesis, the expression of *Wnt7b* was quantified between *Trp63*$^{+/+}$ and *Trp63*$^{-/-}$ facial processes. qPCR analysis showed *Wnt7b* was significantly down-regulated in *Trp63*$^{-/-}$ facial processes compared to wildtype, with a fold-change of -6.57 (p= 0.05) (Figure 4.19B). The results indicated that P63 does bind proximal to *Wnt7b* during upper lip morphogenesis and *Wnt7b* is down-regulated in *Trp63*$^{-/-}$ facial processes which could indicate *Wnt7b* expression is regulated by P63 signalling. However further research will need to be conducted to characterise this relationship. In addition, it is interesting that *Wnt7b* P2, which displayed overlap with multiple markers of active gene regulation, failed to show positive enrichment by P63.

4.3.12.5 *Wnt10b*

Wnt10b expression was shown to be significantly down-regulated (p= 0.05) in E11.5 and E12.5 *Trp63*$^{-/-}$ facial processes using microarray and nCounter with a fold change of -1.80 and -4.90 respectively. ChIP-Seq analysis identified two potential P63 binding sites ≤150 kb of the *Wnt10b* TSS and P63 scan showed the P63 binding motif was present at positions: chr15: 98,574,911-98,574,933 and 98,607,838-98,607,860 (mm9). Analysis of mammalian conservation indicated *Wnt10b* P1 and P2 were conserved between mouse, rat and human with P2 showing additional conservation with rhesus monkey. *Wnt10b* P2 was found to overlap with multiple markers of transcriptional regulation including an H3k4me1 site identified in E11.5 facial tissue, H3k27ac in E14.5 palatal shelf tissue and an H3k27me3 site present in E11.5 (facial) and E13.5 and E14.5 (palatal) tissue.

ChIP-qPCR analysis of chromatin isolated from E11.5 wildtype facial processes, indicated *Wnt10b* P1 and P2 displayed significant positive enrichment by P63 with chromatin

occupancies of 3.60 and 3.14 (p= 0.05) (Figure 4.19A). Having established P63 binds proximal to *Wnt10b* in E11.5 facial processes, expression of *Wnt10b* was quantified in *Trp63*$^{+/+}$ and *Trp63*$^{-/-}$ facial processes. qPCR analysis demonstrated *Wnt10b* was significantly down-regulated in *Trp63*$^{-/-}$ facial processes with a relative expression of 0.08 compared to wildtype (p= 0.02) (Figure 4.19B). Taken together these results suggested that P63 binds proximal to *Wnt10b* during upper lip morphogenesis, and a loss of P63-regulation results in down-regulation of *Wnt10b*. Furthermore, the overlap with markers for transcriptional regulation could suggest P63 is active in gene regulation at these sites. Therefore *Wnt10b* may be a direct target of P63 regulation in upper lip morphogenesis.

4.3.12.6 *Wnt11*

ChIP-Seq/microarray intersection identified *Wnt11* as a putative target of P63 regulation during upper lip morphogenesis. Three potential P63 binding sites were identified ≤150 kb of *Wnt11* and P63 scan identified the P63 binding motif at positions: chr7: 105,878,357-105,878,379 (P1), 106,079,605-106,079,627 (P2) and 106,086,107-106,086,129 (P3) (mm9). Analysis of mammalian conservation indicated *Wnt11* P2 and P3 were conserved between mouse and rat while P1 was conserved between mouse, rat, human, rhesus monkey, dog and horse. Additionally *Wnt11* P2 and P3 overlapped with H3k27ac sites identified in E11.5 facial tissue, while P1 overlapped with an H3k4me1 site identified in E11.5 facial tissue.

ChIP-qPCR analysis indicated *Wnt11* P2 failed to display positive enrichment in chromatin isolated from E11.5 wildtype facial processes with a chromatin occupancy of 1.81. However, P63 binding was shown to be significantly positively enriched (p= 0.05) at *Wnt11* P1 and P3 with occupancies of 23.81 and 8.78 (Figure 4.19A).

The expression of *Wnt11* was quantified in facial processes isolated from *Trp63*$^{+/+}$ and *Trp63*$^{-/-}$ E11.5 embryos. qPCR analysis identified *Wnt11* was significantly up-regulated in *Trp63*$^{-/-}$ facial processes compared with wildtype, with a relative expression of 2.85 (p= 0.02) (Figure 4.19B). P63 binding was shown to be present at two sites proximal to *Wnt11* during E11.5 upper lip morphogenesis. Furthermore the significant up-regulation of *Wnt11* in the absence of P63 could suggest P63 is required for correct *Wnt11* expression, however further research will need to conducted to characterise this relationship.

4.3.12.7 *Sfrp1*

In addition to the Wnt genes, the Wnt antagonist *Secreted frizzled receptor protein 1* (*Sfrp1*) was identified as a potential P63 target gene. *Sfrp1* was shown to be up-regulated in E11.5 and E12.5 *Trp63*$^{-/-}$ facial processes using microarray and nCounter analyses, with fold changes of 1.21 and 1.20 respectively. ChIP-Seq analysis identified two potential P63 binding sites proximal to *Sfrp1* with P63 scan identifying P63 binding motifs at positions: chr8: 24,597,210-24,597,232 (P1) and 24,641,428-24,641,450 (P2) (mm9). Analysis of

mammalian conservation indicated that *Sfrp1* P1 and P2 were conserved across mouse and rat, with *Sfrp1* P1 showing additional conservation in dog and horse. ChIP-qPCR analysis showed *Sfrp1* P1 and P2 failed to display positive enrichment in chromatin extracted from E11.5 wildtype facial processes with occupancies of 2.82 and 1.99 (Figure 4.19A).

The expression of *Sfrp1* was quantified in *Trp63*$^{+/+}$ and *Trp63*$^{-/-}$ embryos. qPCR analysis identified *Sfrp1* was up-regulated in *Trp63*$^{-/-}$ facial processes with a relative expression of 1.19 compared to wildtype (Figure 4.19B). However the result failed to achieve significance with a p-value of 0.2. Taken together these results suggested that P63 does not bind proximal to *Sfrp1* in E11.5 wildtype facial processes. In addition, the failure of *Sfrp1* to display a significant fold-change between *Trp63*$^{+/+}$ and *Trp63*$^{-/-}$ facial processes would suggest that *Sfrp1* is not a direct target of P63-regulation in upper lip morphogenesis.

4.3.12.8 *Krm2*

Kremen2 (*Krm2*) encodes a transmembrane protein which functions as a negative regulator of Wnt signalling (Chu *et al*. 2004). *Krm2* was identified as a potential target of P63 regulation, with a P63 binding site identified ≤150 kb of the TSS. P63 scan identified a P63 binding motif at position: chr17: 23,883,781-23,884,412 (P1). Analysis of mammalian conservation showed *Krm2* P1 was conserved between mouse, rat, human and rhesus monkey. Furthermore *Krm2* P1 was found to overlap with H3k27me3 markers for transcriptional regulation active in E11.5 (facial), E13.5 and E14.5 (palatal) tissue. The overlap between *Krm2* P1 and markers of active transcriptional regulation provided further confidence that P63 binding at this site may be involved in gene regulation.

P63 binding at *Krm2* P1 was validated using ChIP-qPCR in chromatin extracted from E11.5 wildtype facial processes. ChIP-qPCR analysis indicated *Krm2* P1 displayed a significant positive enrichment (p= 0.05) with a chromatin occupancy of 3.49 (Figure 4.19A). Having confirmed P63 binding proximal to *Krm2*, expression was quantified in E11.5 *Trp63*$^{+/+}$ and *Trp63*$^{-/-}$ facial processes. qPCR analysis indicated *Krm2* displayed a significant down-regulation with a relative expression of 0.17 compared with wildtype (Figure 4.19B). P63 binding proximal to *Krm2*, coupled with the significant down-regulation in *Trp63*$^{-/-}$ embryos could suggest P63 regulates *Krm2*, however further characterisation is required.

4.3.12.9 *Fzd4*

In addition to Wnt ligands, the Wnt co-receptor *Fzd4* was identified as a putative P63 target. ChIP-Seq analysis identified three putative binding sites ≤150 kb of the *Fzd4* TSS. P63 scan identified a P63 binding motif at position: chr7: 96,612,704-96,612,726 (P3) (mm9). ChIP-Seq peaks at positions: chr7: 96,533,509-96,533,992 (P1) and 96,547,748-96,548,298 (P2) did not contain a P63 binding motif and so were not investigated further. *Fzd4* P3 was found to be conserved between mouse, rat, human, rhesus monkey, dog and horse. Furthermore, *Fzd4* P3 was found to overlap with the transcriptional regulation markers H3k4me1 and

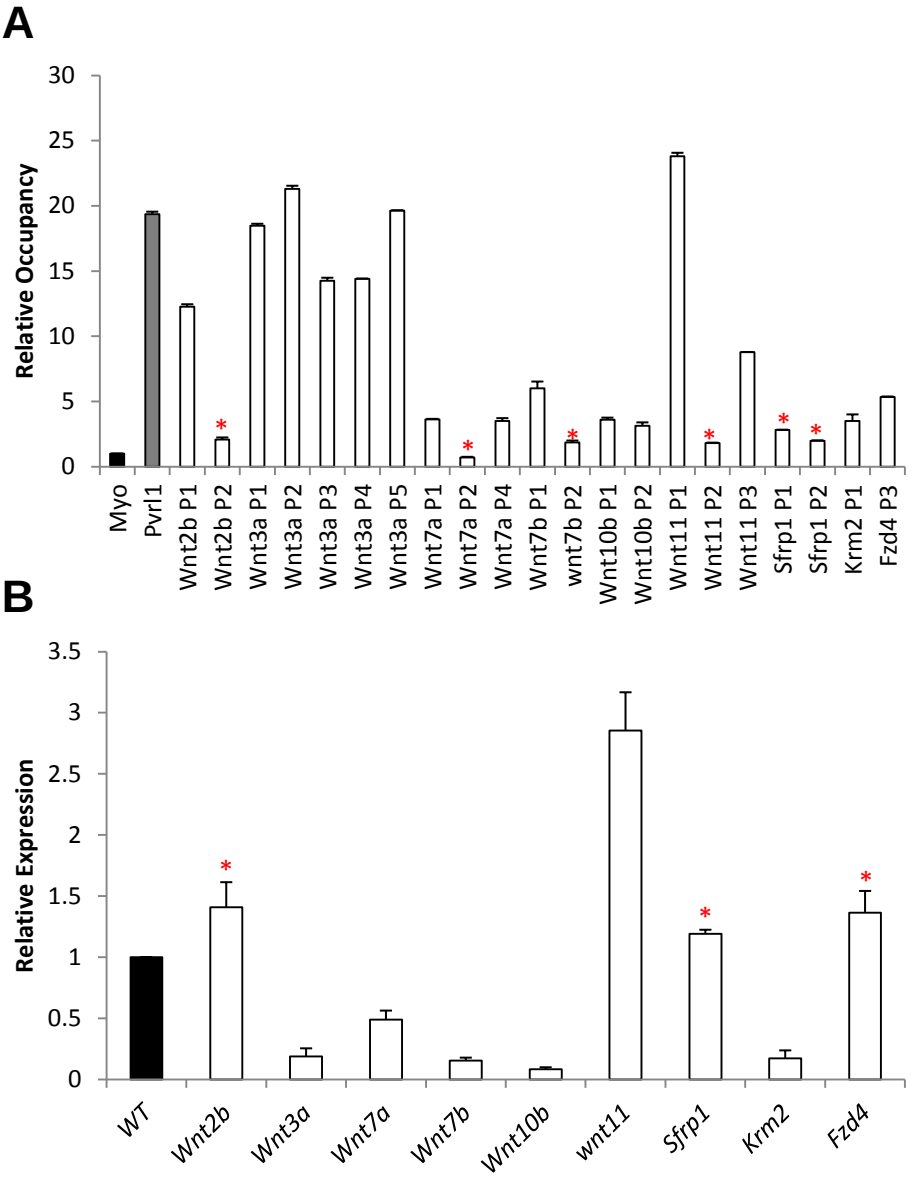

Figure 4.19 ChIP-qPCR and qPCR analysis of Wnt-related genes. (**A**) ChIP-qPCR was conducted on chromatin extracted from E11.5 WT embryos. For each binding site, a chromatin occupancy was calculated relative to the negative control *Myoglobin* (black) via the $2^{\Delta\Delta CT}$ method. Statistical significance was calculated using the student's T-test. A binding site within *Pvrl1* was used as a positive control (grey). Of the 21 binding sites assayed, 15 displayed significant positive enrichment by P63 with a calculated occupancy ≥ 3 fold the negative control (p= 0.05). Binding sites (*) *Wnt2b* P1, *Wnt7a* P2, *Wnt7b* P2, *Wnt11* P2 and Sfrp1 P1 and P2 failed to display positive enrichment. (**B**) qPCR was conducted on cDNA generated from *Trp63*$^{-/-}$ and *Trp63*$^{+/+}$ E11.5 facial processes. cDNA was normalised relative to the house keeping gene *β-actin* and differences in expression calculated by $2^{\Delta\Delta CT}$. Statistical significance was assayed using the Mann Whitney U test. *Wnt3a*, *Wnt7a*, *Wnt7b*, *Wnt10b*, *Wnt11* and *Krm2* displayed significant differential expression in *Trp63*$^{-/-}$ embryos compared with wildtype, with *Wnt7a*, *7a*, *7b*, *10b* and *Krm2* down-regulated and *Wnt11* up-regulated. *Wnt2b*, *Sfrp1* and *Fzd4* (*) were up-regulated in the absence of P63, but failed to display significant differential expression (p= 0.05). Error bars represent calculated standard error of the mean.

H3k27ac sites identified in E11.5 (facial), E13.5 and E14.5 (palatal) tissue. ChIP-qPCR analysis showed *Fzd4* P3 displayed significant positive enrichment with a chromatin occupancy of 5.35 (p= 0.05) (Figure 4.19A). The expression of *Fzd4* was therefore quantified in E11.5 *Trp63*$^{+/+}$ and *Trp63*$^{-/-}$ facial processes using qPCR. *Fzd4* was up-regulated in *Trp63*$^{-/-}$ facial process with a fold change of 1.36. However, the result failed to achieve significance with a p-value of 0.2 (Figure 4.19B). It is therefore unclear if *Fzd4* is a target of P63 regulation in upper lip morphogenesis. P63 binding was identified proximal to *Fzd4* however, the failure to display a significant expression change using qPCR in *Trp63*$^{-/-}$ facial processes could suggest *Fzd4* is not a direct target of P63 regulation. However without additional expression profile characterisation, it would be inappropriate to exclude *Fzd4* as a potential P63 transcriptional target.

4.3.13 Loss of P63 regulation does not affect expression of *Spry1*

Sprouty1 (*Spry1*) encodes a negative regulator Fgf signalling through the inhibition of receptor-tyrosine-kinase dependent signalling (Mason *et al*. 2006). ChIP-Seq microarray intersection identified *Spry1* as a potential target of P63 regulation. ChIP-Seq analysis identified five potential binding sites ≤ 150kb of the TSS. Furthermore P63 scan identified at least one P63 binding motif was present within all ChIP-Seq peaks. Binding sites were identified at positions: Chr3: 37,395,386-37,395,405 (P1), 37,401,995-37,402,014 (P2), 37,495,608-37,495,627 (P3), 37,552,869-37,552,888 (P4) and 37,614,849-37,614,868 (P5) (mm9) (Figure 4.20A). Analysis of mammalian conservation showed that *Spry1* P3 and P4 were conserved between mouse and rat. *Spry1* P5 showed conservation between mouse, rat, human and rhesus monkey. *Spry1* P1 and P2 showed the greatest degree of mammalian conservation with P1 conserved to opossum and P2 conserved to horse.

Analysis of transcriptional regulation markers identified overlap between *Spry1* P2, P3 and P4 with H3k27ac markers active in E11.5 facial and E14.5 palatal tissue. *Spry1* P4 displayed further overlap with an H3kme1 site active in E11.5 facial tissue. Having identified P63 motifs within all peaks, each binding site was interrogated using ChIP-qPCR to determine if P63 binding is present in E11.5 wildtype facial processes. ChIP-qPCR indicated *Spry1* P1 and P4 displayed significant positive enrichment greater than three-fold the negative control with occupancies of 32.27 and 15.90 (p= 0.05) (Figure 4.20B). *Spry1* P2, P3 and P5 failed to display positive enrichment with occupancies of 1.84, 2.02 and 1.91. These results suggested that sites were bona fide P63 binding sites active in E11.5 facial processes which overlapped with markers indicative of active transcriptional regulation.

Having confirmed P63 binding at sites proximal to *Spry1*, expression of *Spry1* was quantified in E11.5 facial processes of *Trp63*$^{+/+}$ and *Trp63*$^{-/-}$ embryos using qPCR. E12.5 microarray and E11.5 nCounter analyses suggested a loss of P63 regulation resulted in the up-regulation of *Spry1* with fold-changes of 1.21 and 1.20. qPCR analysis indicated *Spry1* expression was down-regulated between *Trp63*$^{-/-}$ and wildtype littermates, with a relative

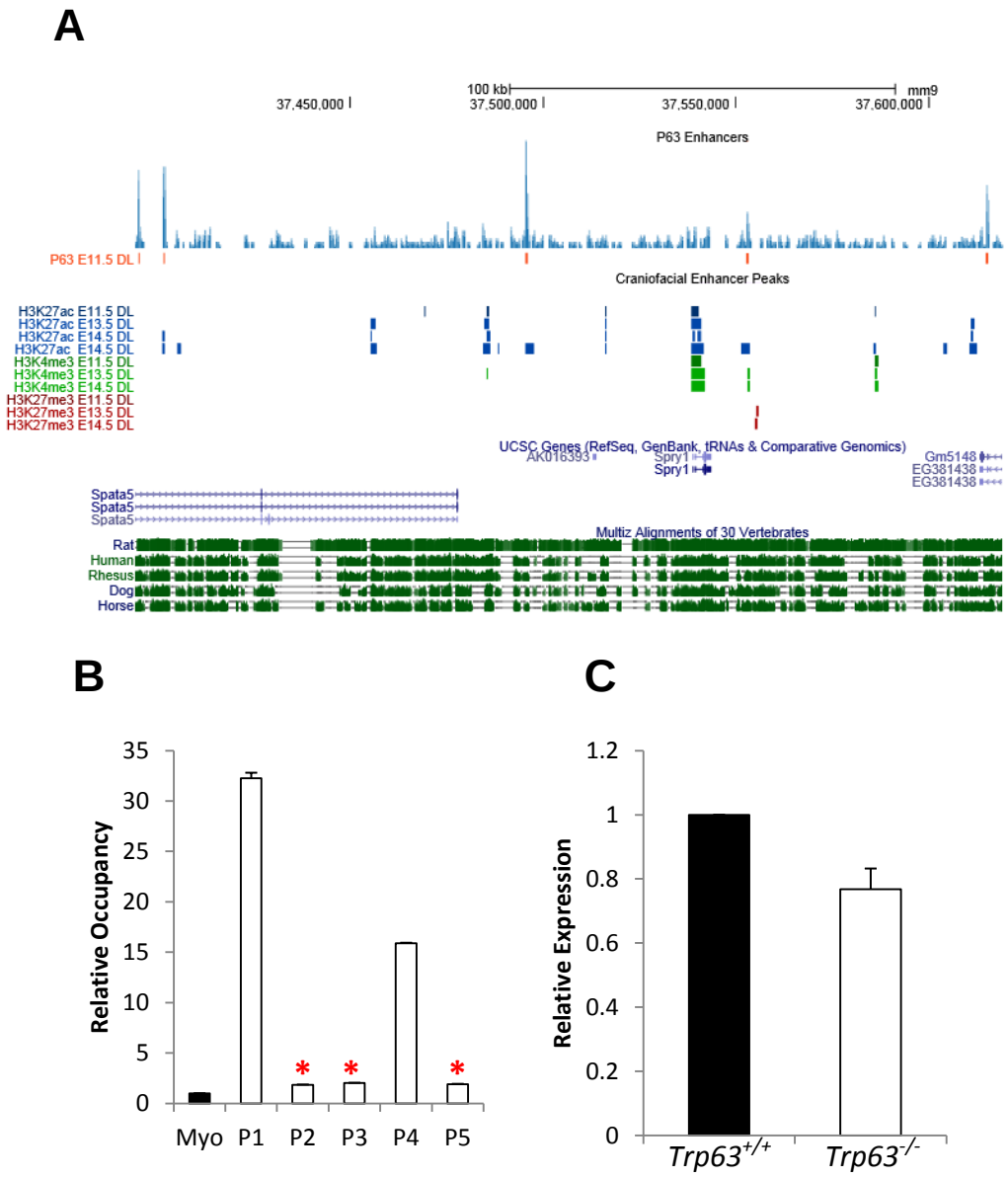

Figure 4.20 *Spry1* is not target of P63 signalling. (**A**) ChIP-Seq/microarray intersection identified five P63 binding sites proximal to *Spry1*. P63 binding sites overlapped with markers of active transcriptional regulation including H3k27ac and H3kme1 sites identified in E11.5 facial and E14.5 palatal tissue. Mammalian conservation is shown. (**B**) ChIP-qPCR was conducted on five putative P63 binding sites proximal to *Spry1*. Relative chromatin occupancy was calculated relative to the negative control *Myoglobin* (black). Two out of five binding sites displayed significant positive enrichment by P63 (p= 0.05), *with Spry1* P2, P3 and P5 failing to display enrichment (*). (**C**) qPCR analysis between E11.5 *Trp63*$^{-/-}$ and WT facial processes identified a reduction in *Spry1* expression relative to the house keeping gene *β-actin*, however the result was not significant. Error bars display standard error of the mean.

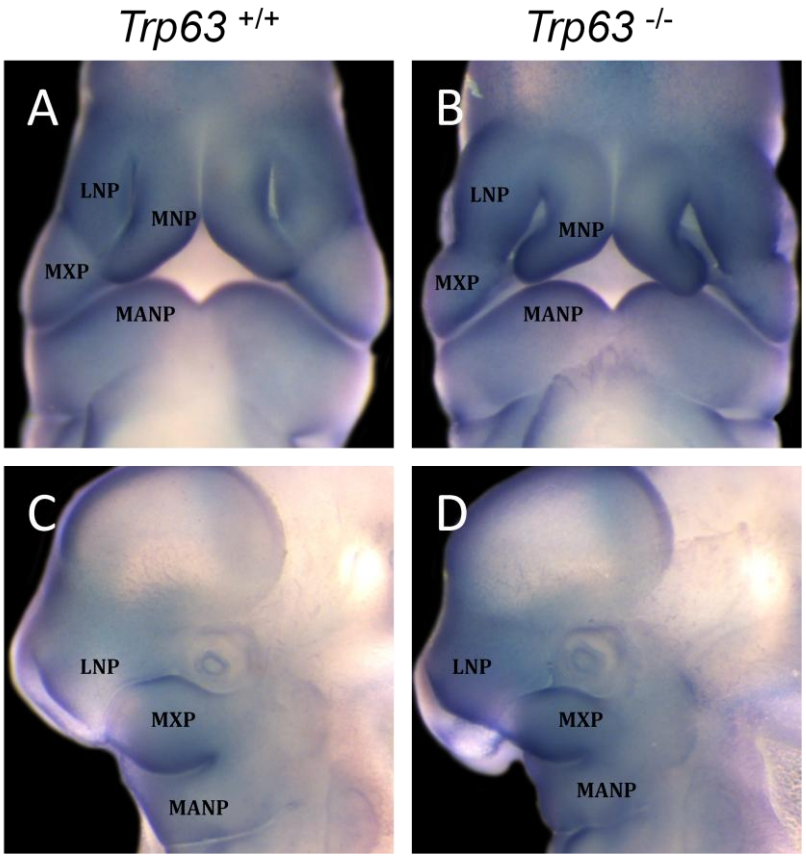

Figure 4.21 Whole mount *in situ* hybridisation analysis of *Spry1*. (**A**-**D**) WISH analysis of *Spry1* expression in *Trp63*$^{+/+}$ and *Trp63*$^{-/-}$ E11.5 embryos. (**A**&**C**) In *Trp63*$^{+/+}$ embryos, expression of *Spry1* was detected throughout the epithelium of the medial nasal, lateral nasal, maxillary and mandibular processes (**B**&**D**) in *Trp63*$^{-/-}$ embryos, expression of *Spry1* appeared comparable to WT embryos, with expression detected within the epithelium of the medial nasal, lateral nasal, maxillary and mandibular processes. It is therefore unlikely *Spry1* is a target of P63 regulation. LNP- lateral nasal processes, MNP – medial nasal processes, MXP- maxillary processes, MANP- mandibular processes.

expression of 0.77 compared to wildtype. However the result failed to achieve significance with a p-value of 2 (Figure 4.20C). Characterisation of *Spry1* expression using WISH within E11.5 *Trp63*$^{+/+}$ embryos indentified expression of *Spry1* throughout the epithelium of the medial nasal, lateral nasal and maxillary processes (Figure 4.21A). Further expression was detected in the lacrimal groove and within the epithelium of the mandibular processes (Figure 4.21B). Expression of *Spry1* in *Trp63*$^{-/-}$embryos appeared comparable to wildtype littermates with expression present throughout the facial processes (Figure 4.21B&D). Furthermore it was not possible to detect the up/down-regulation observed using quantification.

Based upon the data collected, it is unclear whether *Spry1* is a target of P63 regulation. P63 binding was detected proximal to *Spry1* and quantification of *Spry1* expression using nCounter and microarray between *Trp63*$^{+/+}$ and *Trp63*$^{-/-}$ facial processes at E11.5 and E12.5 identified significant up-regulation (p= 0.05). However, qPCR did not recapitulate these findings. Furthermore, the characterisation of *Spry1* expression in null embryos failed to produce an observable difference to wildtype. It is therefore unlikely that *Spry1* is a target of P63 regulation during upper lip morphogenesis.

4.3.14 Loss of P63 regulation results in the up-regulation of *Spry2*

In addition to *Spry1*, *Spry2* encodes a cytoplasmic protein which inhibits Fgf and other receptor-tyrosine-kinase dependent signalling networks (Mason *et al*. 2008). ChIP-Seq and microarray analysis identified *Spry2* as a potential target of P63 regulation. ChIP-Seq identified three peaks proximal to *Spry2* with P63 scan confirming all peaks contained at least one P63 binding motif. Binding sites were identified at positions chr14: 106,178,187-106,178,206 (P1), 106,243,190-106,243,209 (P2) and 106,290,387-106,290,406 (P3) (mm9) (Figure 4.22A). Analysis of mammalian conservation indicated that *Spry2* P1 and P2 were conserved between mouse and rat, with P1 showing additional conservation with human. Furthermore *Spry2* P3 displayed conservation between mouse, rat, human, rhesus monkey, dog and horse. *Spry2* P3 was shown to overlap with transcriptional regulation markers H3k4me1 and H3k27ac, shown to be active in E11.5 facial and E14.5 palatal tissue. To confirm if P63 binding is present at these sites in wildtype E11.5 facial processes, ChIP-qPCR was used to validate each potential binding site.

Analysis of identified P63 binding sites using ChIP-qPCR in E11.5 facial processes demonstrated *Spry2* P1 failed to display positive enrichment by P63 with an occupancy of 1.30. In contrast, *Spry2* P2 and P3 displayed significant positive enrichment (p= 0.05) greater than three-fold the negative control with chromatin occupancies of 8.34 and 27.87 (Figure 4.22B).

Microarray and nCounter analyses identified a significant up-regulation of *Spry2* in *Trp63*$^{-/-}$ embryos with fold-changes of 1.20 and 1.21 (p= 0.05). Therefore prior to further analysis,

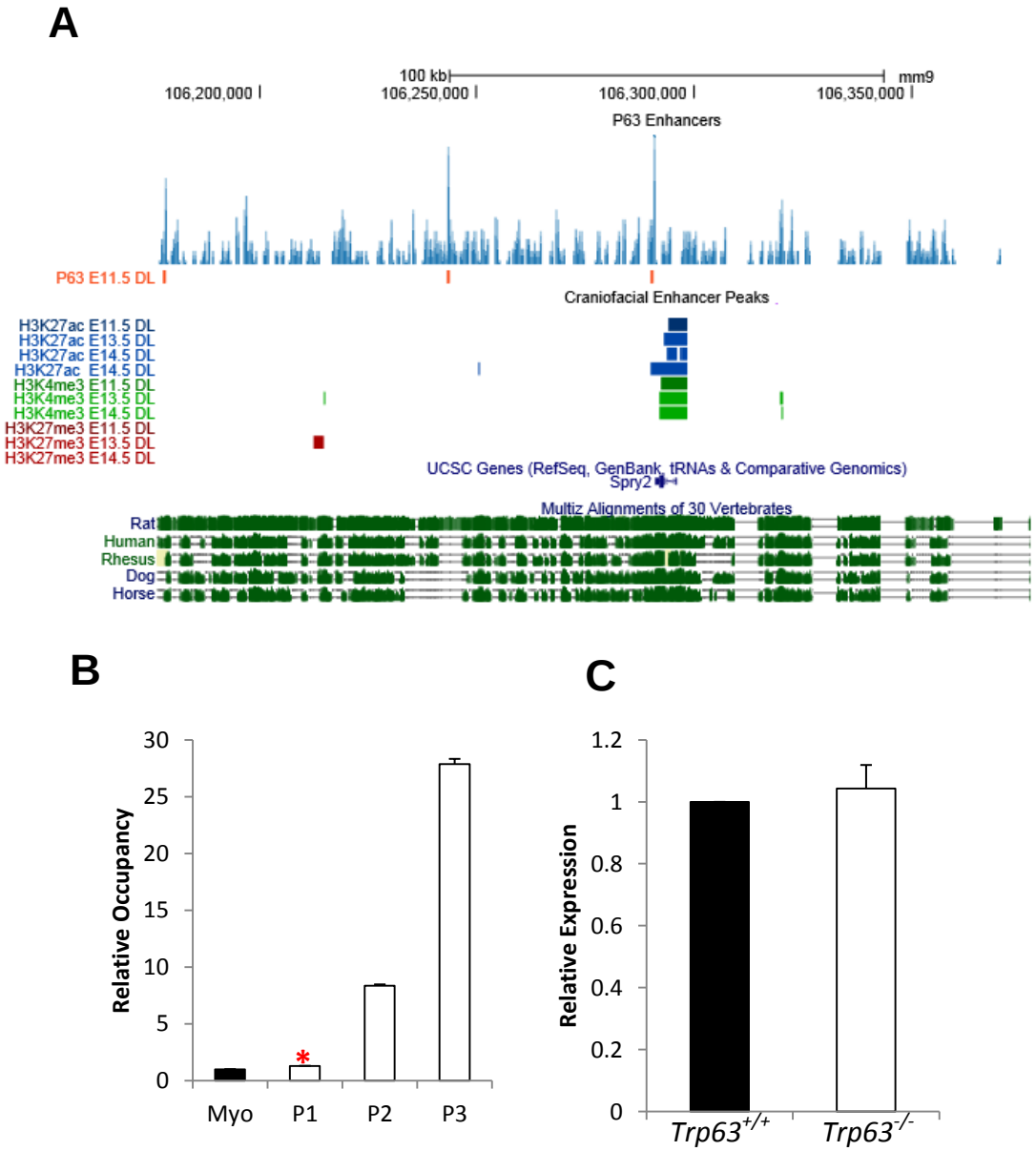

Figure 4.22 *Spry2* is a target of P63 signalling. (**A**) ChIP-Seq/microarray intersection identified three P63 binding sites proximal to *Spry2*. Putative binding sites overlapped with markers of active transcriptional regulation including Hek4me1 and H3k27ac sites identified in E11.5 facial and E14.5 palatal tissue. Mammalian conservation is shown. (**B**) ChIP-qPCR was conducted on three putative P63 binding sites proximal to *Spry2*. Relative chromatin occupancy was calculated relative to the negative control *Myoglobin* (black). Two out of three binding sites displayed positive enrichment by P63, with *Spry2* P1 (*) failing to display enrichment. (**C**) qPCR analysis between E11.5 *Trp63*$^{-/-}$ and WT facial processes identified a slight up-regulation in *Spry2* expression relative to the house keeping gene *β-actin*, however the result failed to achieve significance. Error bars display standard error of the mean.

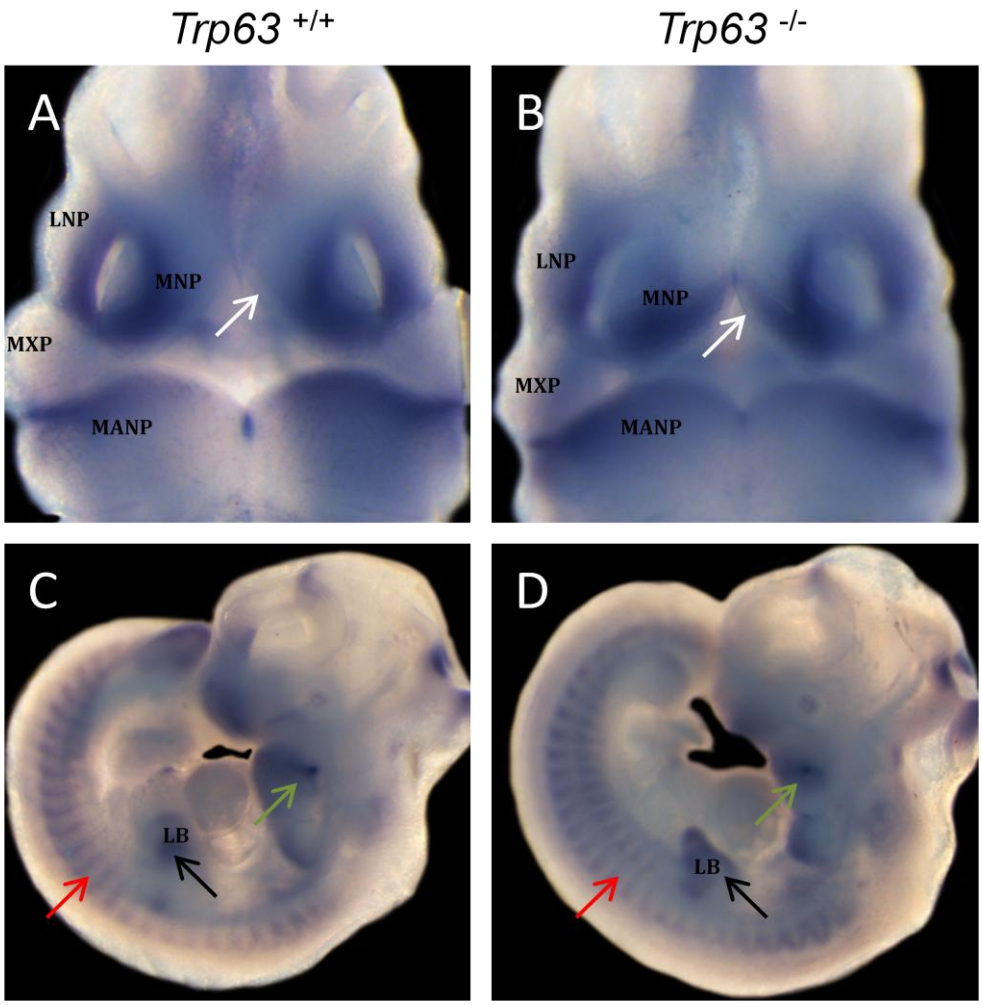

Figure 4.23 Whole mount *in situ* hybridisation analysis of *Spry2*. (**A**-**D**) WISH analysis of *Spry2* between *Trp63*$^{+/+}$ and *Trp63*$^{-/-}$ E11.5 embryos. (**A**&**C**) In *Trp63*$^{+/+}$ embryos, *Spry2* expression was detected within the mesenchyme of the medial nasal and maxillary processes surrounding the nasal slits and within the oral aspects of the mandibular processes. Expression appeared excluded from the maxillary processes and the oral epithelium of the medial nasal processes. Similar to *Lrp6*, a spot of intense staining was observed at the maxillary-mandibular boundary (arrowed – green). Additional expression was detected within the somites (arrowed – red) and the mesenchyme of the limb buds (arrowed - black). (**B**&**D**) in *Trp63*$^{-/-}$ embryos, *Spry2* expression within the facial processes appear largely comparable, however expanded medial expression was detected within the medial nasal processes (arrowed – white). Somite expression appeared comparable to WT, however limb expression appeared to have shifted distally (arrowed – black). Furthermore, the spot of intense staining at the maxillary-mandibular boundary was comparable to WT but was shifted anteriorly. The presence of comparable expression patterns within the somites and lateral nasal processes, suggested the medial expansion of *Spry2* expression within the medial nasal processes may be tissue specific. However the lack of epithelial expression could suggest *Spry2* is not a direct target of P63 regulation. LNP- lateral nasal processes, MNP – medial nasal processes, MXP- maxillary processes, MANP- mandibular processes, LB – limb bud.

the results of the microarrays and nCounter were validated using qPCR. Analysis at E11.5 between *Trp63*$^{+/+}$ and *Trp63*$^{-/-}$ embryos identified a minor up-regulation of *Spry2* in *Trp63*$^{-/-}$ facial processes compared to wildtype, with a relative expression of 1.04 (Figure 4.22C). However the result failed to achieve significance, with a p-value of 8.

Therefore the expression profile of *Spry2* was characterised between E11.5 *Trp63*$^{+/+}$ and *Trp63*$^{-/-}$ embryos using WISH. In *Trp63*$^{+/+}$ embryos *Spry2* expression was detected within the mesenchyme of the medial nasal and lateral nasal processes surrounding the nasal pits (Figure 4.23A). In addition expression was detected within the oral aspects of the mandibular processes with expression present at the maxillary to mandibular boundary. A small region of intense expression was detected at the posterior maxillary-mandibular boundary (Figure 4.23C). Furthermore *Spry2* expression was found to be expressed throughout the somites and within the limb buds. In contrast to wildtype littermates, *Spry2* expression in *Trp63*$^{-/-}$ embryos appeared expanded within the medial nasal processes (Figure 4.23B). Expression within the mandibular processes was comparable to wildtype littermates, with the region of intense expression present in *Trp63*$^{+/+}$ and *Trp63*$^{-/-}$ embryos, however it appeared to shifted anteriorly in null embryos. Somite expression was comparable between *Trp63*$^{-/-}$ and wildtype littermates, however expression within the limbs appeared to have shifted distally (Figure 4.23D). These results suggested that P63 is required for correct expression of *Spry2* within the medial nasal processes during upper lip morphogenesis. Furthermore the presence of comparable expression profiles suggests that the regulation is specific to the medial nasal processes.

Taken together these results would suggest that P63 is required for *Spry2* expression in E11.5 facial processes. P63 binding was identified at two sites proximal to *Spry2*, however qPCR analysis failed to show a significant change in *Spry2* expression in *Trp63*$^{-/-}$ facial processes. In addition WISH results were unclear, displaying subtle changes in *Spry2* expression between *Trp63*$^{-/-}$ and wildtype embryos. Furthermore, *Spry2* expression appeared mesenchymal and was absent from the oral epithelial of the medial nasal processes. As these analyses have provided conflicting results, it is therefore unclear if *Spry2* is a direct target of P63 regulation in upper lip morphogenesis.

4.3.15 Loss of P63 signalling results in misregulation of multiple members of the Fgf signalling network

In addition to the misregulation of *Spry1* and *Spry2*, *Fgfr2* and *Fgfr3* were found to be significantly down-regulated in the *Trp63*$^{-/-}$ E12.5 microarray (p= 0.05) with *Fgfr2* displaying a fold-change of -1.50 and *Fgfr3* a fold-change of -1.20. In addition *Fgfr3* was shown to be down-regulated in E11.5 *Trp63*$^{-/-}$ facial processes by nCounter with a fold-change of -1.33. Nine potential P63 binding sites were identified proximal to *Fgfr2* and one proximal to *Fgfr3*. A P63 binding motif was identified at position chr7: 136,809,750-136,809,772 (P1) proximal to *Fgfr2* and at position chr5: 34,039,233-34,039,255 (P1) proximal to *Fgfr3* (mm9). The

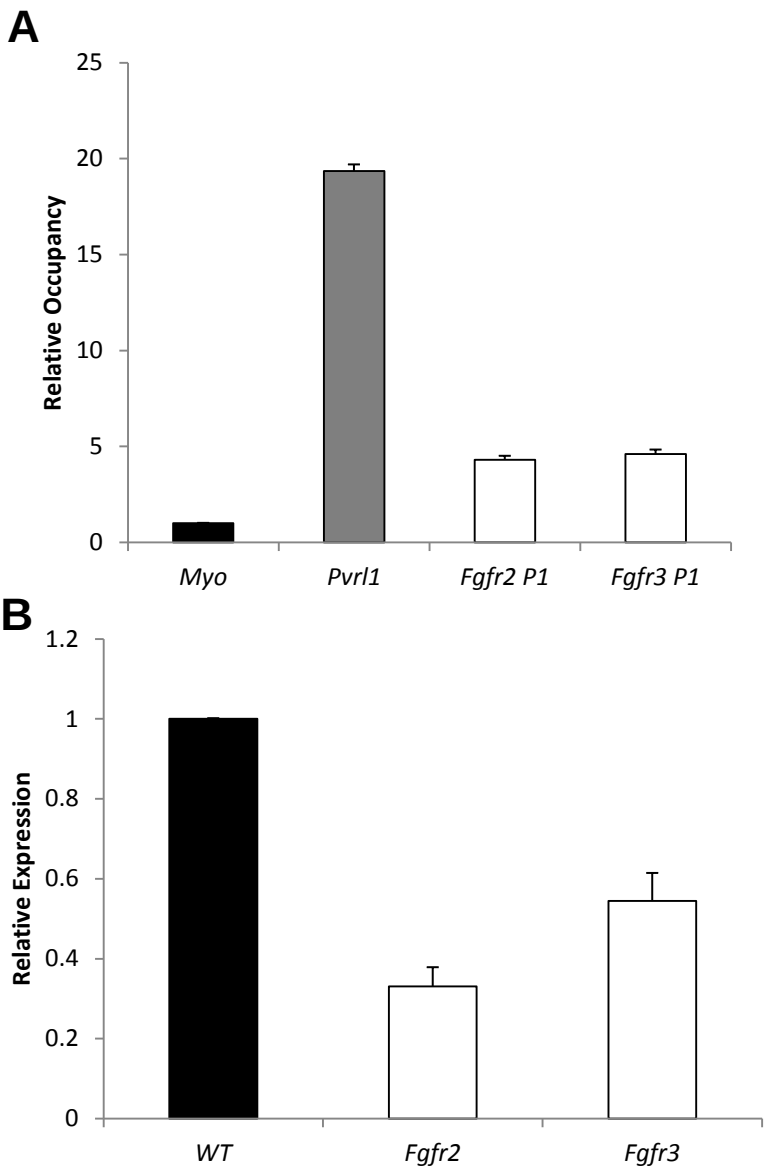

Figure 4.24 ChIP-qPCR and qPCR analysis of Fgf-related genes (**A**) ChIP-qPCR was conducted on chromatin extracted from E11.5 WT embryos. For each binding site, a chromatin occupancy was calculated relative to the negative control *Myoglobin* (black) via the $2^{\Delta\Delta CT}$ method. Statistical significance was calculated using the student's T-test. A binding site within *Pvrl1* was used as a positive control (grey). *Fgfr2* P1 and *Fgfr3* P1 both displayed significant positive enrichment (p= 0.05) by P63 with chromatin occupancies greater than three-fold the negative control. (**B**) qPCR was conducted on cDNA generated from *Trp63*$^{-/-}$ and *Trp63*$^{+/+}$ E11.5 facial processes. cDNA was normalised relative to the house keeping gene *β-actin* and differences in expression calculated by $2^{\Delta\Delta CT}$. Statistical significance was assayed using the Mann Whitney U test. *Fgfr2* and *Fgfr3* displayed significant down-regulation in the absence of P63 (p= 0.05). Error bars represent calculated standard error of the mean.

Fgfr2 (P1) binding site was shown to be conserved between mouse and rat and was found to overlap with an H3k27ac site active in E11.5 facial tissue. *Fgfr3* P1 was found to be conserved between mouse, rat and human. In addition *Fgfr3* P1 overlapped with a number of active enhancer sites. Overlaps with a H3k27ac site shown to be active in E11.5 (facial), E13.5 and E14.5 (palatal) tissue was seen, in addition to overlaps with E11.5 H3k4me1 (facial) and E13.5 H3k27me3 (palatal) tissue. Due to the presence of markers of active transcriptional regulation, it was decided to investigate P63 binding at these sites using ChIP-qPCR. ChIP-qPCR analysis of E11.5 wildtype facial processes indicated both *Fgfr2* P1 and *Fgfr3* P1 displayed significant positive enrichment by P63, with chromatin occupancies of 4.31 and 4.61 (p= 0.05) (Figure 4.24A).

Having confirmed P63 binding proximal to *Fgfr2* and *Fgfr3*, the expression of both genes was quantified in E11.5 *Trp63*$^{+/+}$ and *Trp63*$^{-/-}$ facial processes. The expression of *Fgfr2* had previously been quantified (Chapter 3.3.2.7) with a significant relative expression of 0.33 compared to wildtype (p= 0.05). qPCR analysis indicated *Fgfr3* was significantly down-regulated in *Trp63*$^{-/-}$ facial processes, with a relative expression of 0.54 compared to wildtype (p= 0.05) (Figure 4.24B). Taken together these results demonstrate that P63 binds to sites which may be involved in transcriptional regulation proximal to *Fgfr2* and *Fgfr3* during upper lip morphogenesis. Furthermore a loss of *Trp63* expression results in down-regulation of both genes. While functional WISH probes were generated for both *Fgfr2* and *Fgfr3* breeding of *Trp63*$^{+/-}$ mice failed to generate an adequate quantity of *Trp63*$^{-/-}$ and *Trp63*$^{+/+}$ embryos to fully characterise gene expression. Based upon the data gathered it could indicate that P63 regulates the expression of *Fgfr2* and *Fgfr3* in E11.5 upper lip morphogenesis, however the relationship would need to characterised in greater detail than was possible in this study.

4.3.16 P63 is required for correct canonical Wnt signalling during upper lip morphogenesis

Having identified the misregulation of multiple members of the Wnt signalling network, it was hypothesised the canonical Wnt signalling network would be perturbed in *Trp63*$^{-/-}$ facial processes. Therefore *Trp63*$^{+/-}$ and *Bat-Gal*$^{tg/+}$ mice were crossed to generate compound heterozygous reporter mice *Trp63*$^{+/+}$*; BAT-Gal*$^{tg/+}$ and *Trp63*$^{-/-}$*; BAT-Gal*$^{tg/+}$. *Trp63;BAT-Gal* mice were generated in collaboration with the Selleri lab (Weill Cornell Medical College, New York). *LacZ* expression was examined in whole embryos at E11.5. *Trp63*$^{+/+}$*/BAT-Gal*$^{tg/+}$ showed extensive staining within the medial nasal, lateral nasal and maxillary processes (Figure 4.25A). Intense LacZ activity was observed around the lambdoidal junction. Furthermore a clear boundary of expression could be seen with staining absent from the superior aspects of the medial nasal and lateral nasal processes (Figure 4.25C). Further *LacZ* expression was observed within the superior and medial aspects of the mandibular processes. In contrast to *Trp63*$^{+/+}$*; BAT-Gal*$^{tg/+}$, *Trp63*$^{-/-}$*; BAT-Gal*$^{tg/+}$ embryos showed a marked reduction in both the intensity and the expression domains of *LacZ* (Figure 4.25B).

LacZ expression was localised to the distal tips of the medial nasal processes, with expression absent from the superior regions. Within the lateral nasal processes expression was reduced with the expression boundary shifted distally (Figure 4.25D). In *Trp63*$^{+/+}$ and *Trp63*$^{-/-}$ maxillary processes, *LacZ* expression was highly localised anteriorly with expression reducing posteriorly. However the reduction in *LacZ* staining was more severe in the *Trp63*$^{-/-}$ embryos. In contrast to the facial processes, *LacZ* expression was increased within the mandibular processes, however expression was less diffuse. *LacZ* expression was present within the boundary of the optic cup of *Trp63*^{wt}*;BAT-Gal*$^{tg/+}$ but was absent within *Trp63*$^{-/-}$*; BAT-Gal*$^{tg/+}$. These results indicate that correct P63 regulation is required for canonical Wnt activity.

4.3.17 Induction of the Wnt canonical pathway fails to rescue the cleft phenotype of *Trp63*$^{-/-}$ embryos

Misregulation of canonical Wnt signalling in the facial processes of *Trp63*$^{-/-}$ embryos was identified. Previous studies have shown administration of LiCl was able to induce Wnt signalling (Clément-Lacroix *et al*. 2005). It was therefore hypothesised that should a loss of Wnt signalling contribute to the cleft lip phenotype of *Trp63*$^{-/-}$ embryos induction of Wnt signalling may affect a phenotypic rescue. Pregnant dams were injected with LiCl at E8.5 and E9.5 and embryos harvested at E14.5. Once isolated *Trp63*$^{+/+}$ and *Trp63*$^{-/-}$ embryos were incubated with Bouin's fixative and morphologically examined to determine if any phenotypic change was effected. Embryo genotyping showed *Trp63*$^{+/+}$ (n= 3), *Trp63*$^{-/+}$ (n= 6) and *Trp63*$^{-/-}$ (n= 3) were within the expected ratios. Administration of 120 µl LiCl (150 mM) failed to affect a phenotypic rescue. *Trp63*$^{+/+}$ and *Trp63*$^{-/-}$ embryos appeared unaffected. *Trp63*$^{+/+}$ embryos appeared phenotypically normal with no craniofacial abnormalities (Figure 4.26A&C). In contrast *Trp63*$^{-/-}$ embryos displayed a fully penetrant bilateral cleft lip with the null phenotype unchanged (Figure 4.26B&D). Previous studies have used varying concentrations of LiCl, it was therefore hypothesised that administering a higher concentration could induce a phenotypic effect. However due to a lack of *Trp63*$^{+/-}$ mice for breeding, further work on this hypothesis was not completed.

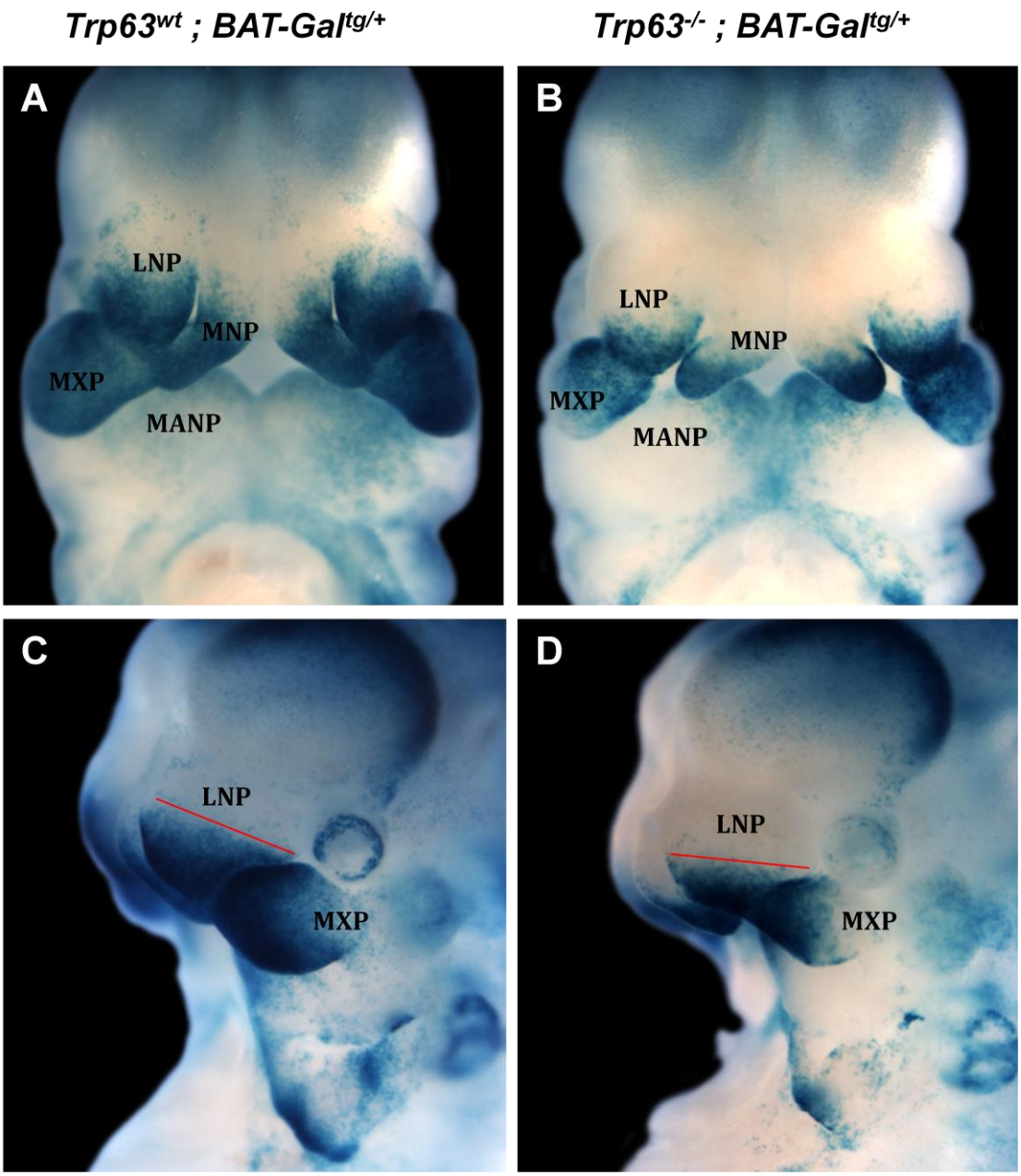

Figure 4.25 Canonical Wnt signalling is disrupted in *Trp63*$^{-/-}$ embryos. (**A**-**D**) *LacZ* staining for canonical Wnt signalling in whole E11.5 *Trp63*^{WT}*;BAT-Gal*$^{Tg/+}$ and *Trp63*$^{-/-}$*;BAT-Gal*$^{Tg/+}$ embryos. (**A**&**C**) In WT embryos strong canonical Wnt signalling was detected throughout the medial nasal, lateral nasal and maxillary processes. Weak signalling was detected within the mandibular processes. Further Wnt signalling was detected within the eye. (**B**&**D**) In contrast to WT embryos, canonical Wnt signalling in *Trp63*$^{-/-}$ embryos appeared markedly reduced within the medial nasal, lateral nasal and maxillary processes, however staining was still detected at the distal tips. Canonical Wnt signalling appeared expanded at the medial aspects of the mandibular processes. Furthermore staining within the posterior aspects of lateral nasal and maxillary processes appeared to be reduced (red). Ocular Wnt signalling also appeared reduced compared to WT. LNP – lateral nasal processes, MNP - medial nasal processes, MXP – maxillary processes, MANP – mandibular processes. Generation of *Trp63;BAT-Gal* mice was completed in collaboration with the Selleri group (Weill Cornell Medical College, New York).

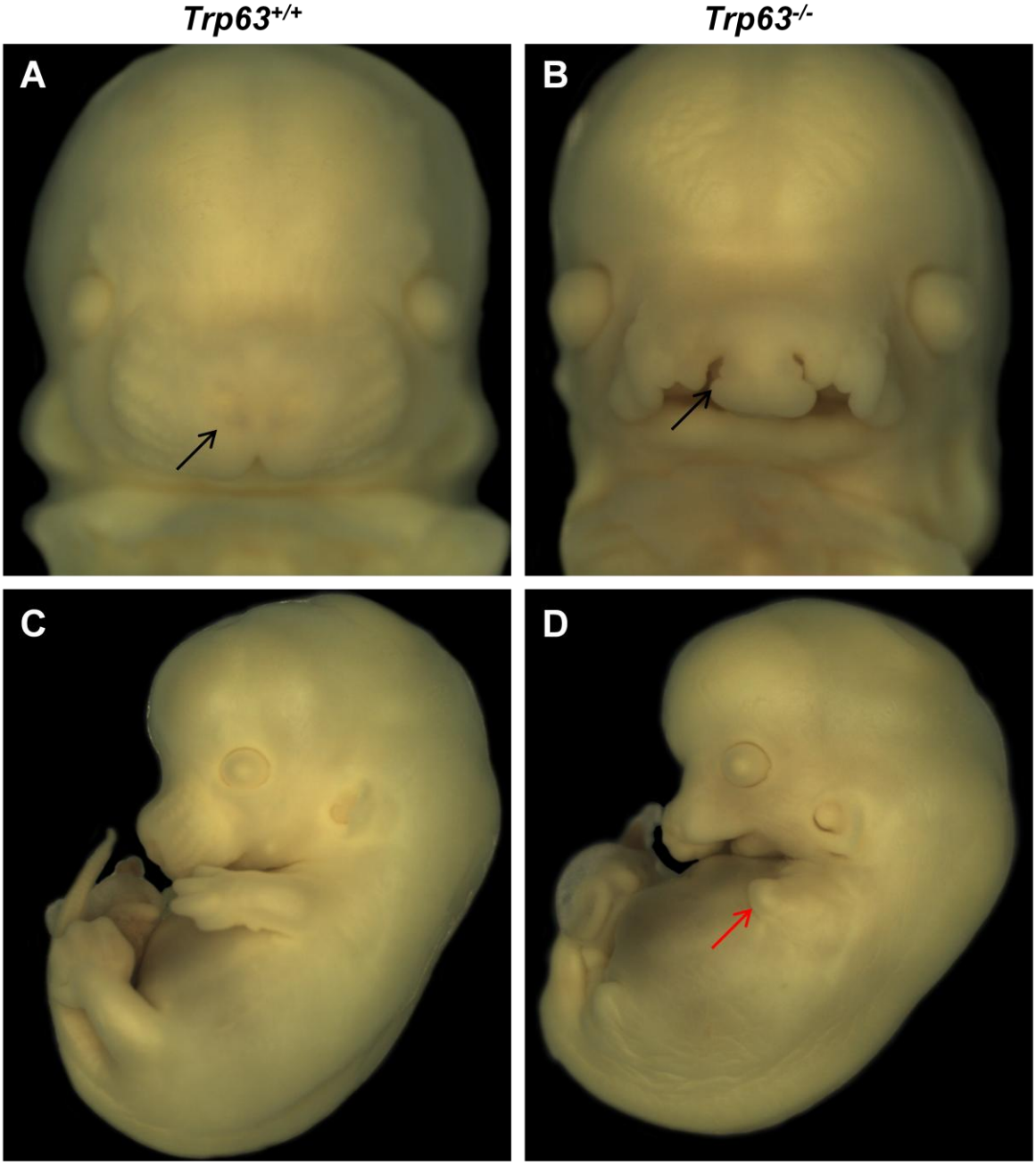

Figure 4.26 Induction of Wnt signalling via lithium chloride fails to induce a phenotypic change in *Trp63*$^{-/-}$ embryos. Embryos were treated with 120 µl 150 mM LiCl through intraperitoneal injection at E8.5 and E9.5. Embryos were dissected at E14.5 and incubated in Bouin's fixative. P63 genotyping identified the expected ratios of *Trp63*$^{+/+}$ (n= 3), *Trp63*$^{+/-}$ (n= 6) and *Trp63*$^{-/-}$ (n= 3) embryos were present. (**A**&**C**) *Trp63*$^{+/+}$ embryos appeared phenotypically normal, with expected upper lip and limb development. (**B**&**C**) The phenotype of *Trp63*$^{-/-}$ embryos appeared un-altered from the expected phenotype, with the presence of a fully penetrant bilateral cleft lip and palate (arrowed – black) and truncated limbs (arrowed – red). It is therefore unclear if induction of the Wnt signalling pathway through LiCl injection can affect a phenotypic rescue.

4.4 Discussion

4.4.1 Loss of P63 results in misregulation of Wnt and Fgf genes

Loss of P63 regulation resulted in the misregulation of multiple members of the Wnt and Fgf signalling networks, including Wnt receptors, ligands, antagonists, effectors and Fgf receptors and antagonists. nCounter analysis provided further evidence for the significant differential expression of Wnt- and Fgf-related genes in E11.5 *Trp63*$^{-/-}$ facial processes. The biological overlap between *Wnt3*, *Wnt10b*, *Wnt7b*, *Wnt3a*, *Fzd4* and *Lef1* with *Trp63* has previously been discussed (Chapter 3.4.6).

4.4.1.1 *Wnt2b*

Wnt2b was identified as a potential target of P63 regulation during upper lip morphogenesis, with three putative P63 binding sites identified ≤ 150 kb from the *Wnt2b* TSS. *WNT2B* encodes a Wnt ligand and has previously been shown to be expressed throughout the surface ectoderm of chick maxillary processes during facial development (Geetha-Loganathan *et al*. 2009). During chick facial development, in contrast to *WNT3* and *WNT9B* which were expressed within the surface ectoderm of the medial nasal and lateral nasal processes, expression of *WNT2B* was found to be absent from the frontonasal mass (Geetha-Loganathan *et al*. 2009). In addition to maxillary expression, *WNT2B* was shown to be expressed within the superior aspects of the optic cup (Geetha-Loganathan *et al*. 2009).

The structure and expression profile of *Wnt2b* in mouse was first characterised by Brûlet's group who showed *Wnt2b* was expressed within the superior aspects of the optic cup between E9.5-E10.5 (Zakin *et al*. 1998). No expression was observed within the developing facial processes, however, the group did not analyse expression post E10.5 (Zakin *et al*. 1998). Geetha-Loganathan and colleagues noted that *WNT2B* expression in chick began in the superior aspects of the optic cup, before extending into the ectoderm of the maxillary processes (Geetha-Loganathan *et al*. 2009). The lack of orofacial expression of *Wnt2b* by Brûlet's group may therefore be due to the developmental time chosen (Zakin *et al*. 1998).

In contrast to knockout models of Wnt-related genes such as *Lrp6*, *Wnt2b* conditional knockouts are comparable to wildtype, only displaying a short olfactory bulb phenotype (Song *et al*. 2009; Tsukiyama & Yamaguchi, 2012). Due to the overlapping expression patterns of *Wnt3*, *Wnt3a* and *Wnt8a* with *Wnt2b* during formation of the primitive streak, and the failure of *Wnt2b*$^{-/-}$ embryos to display a distinct phenotype, it has been suggested that *Wnt2b* displays a redundant function during development (Tsukiyama & Yamaguchi, 2012). Furthermore, it has been suggested that *Wnt2b* functions as a member of the canonical Wnt signalling pathway, with ectopic expression of *WNT2B* in chick facial prominences inducing expression of the canonical Wnt signalling target *MSX1* (Song *et al*. 2009; Medio *et al*. 2012).

Three potential P63 binding sites were identified proximal to *Wnt2b* in E11.5 facial processes, with two displaying significant positive enrichment using ChIP-qPCR. However expression analysis was inconclusive with the E12.5 microarray identifying a significant down-regulation of *Wnt2b*, while nCounter and qPCR identified up-regulation. The epithelial expression of *Wnt2b* within the optic cup and maxillary processes displays an overlap with P63 expression (Zakin *et al*. 1998; Thomason *et al*. 2008; Geetha-Loganathan *et al*. 2009). Due to the lack of a distinct *Wnt2b*$^{-/-}$, orofacial, limb or skin defect and a failure to generate a significant fold-change using qPCR between E11.5 *Trp63*$^{-/-}$ and *Trp63*$^{+/+}$ facial processes, coupled with the restricted availability of *Trp63*$^{+/-}$ mice, *Wnt2b* was not prioritised for WISH. As such it remains unclear if *Wnt2b* is a direct target of P63 regulation.

4.4.1.2 *Wnt11*

Three potential binding sites were identified proximal to *Wnt11* with two binding sites displaying positive enrichment by P63 in chromatin extracted from E11.5 wildtype facial processes. qPCR indicated *Wnt11* was up-regulated in the absence of P63 regulation. Previous studies have identified a significant association between single-nucleotide polymorphisms within *WNT11* and the incidence of non-syndromic cleft lip and palate (Chiquet *et al*. 2008; Mostowska *et al*. 2012). Furthermore, *Wnt11* has been demonstrated to be involved in upper lip and primary palate development and secondary palate development (Geetha-Loganathan *et al*. 2014).

Analysis of *Wnt11* expression in mouse secondary palate development identified an expression pattern highly similar to that of *Trp63* (Lee *et al*. 2008). Prior to palatal shelf elevation no *Wnt11* expression was detected within the palatal shelves. However once elevated, expression was detected throughout the medial edge epithelia localised to the future site of palatal contact. In a similar manner to *Trp63* expression, following palatal shelf adhesion, strong expression was detected within the MES (Lee *et al*. 2008; Thomason *et al*. 2010). Down-regulation of *Wnt11* and *Trp63* within the MES is immediately followed by palatal shelf fusion (Lee *et al*. 2008; Thomason *et al*. 2010).

Ectopic expression of *Wnt11* within developing palatal shelves resulted in significantly increased levels of apoptosis within the MEE. In contrast, siRNA *Wnt11*-knockdown assays indicated that reductions in *Wnt11* expression resulted in a lack of apoptosis and a persistent MES resulting in cleft palate (Lee *et al*. 2008). Expression of *Fgfr1b* was demonstrated to be inversely proportional to *Wnt11* expression with a reduction in *Wnt11* elevating *Fgfr1b* expression and over expression resulting in *Fgfr1b* down-regulation (Lee *et al*. 2008). It was therefore suggested that *Wnt11* was required for correct palatogenesis, and that *Wnt11* inhibition of *Fgfr1b* was required for correct apoptosis within the MES (Lee *et al*. 2008).

In the present study, a loss of *Trp63*$^{-/-}$ resulted in the up-regulation of the pro-apoptotic factor *Wnt11,* suggesting P63 inhibits *Wnt11* expression during lip morphogenesis. During normal upper lip and secondary palate development, the down-regulation of ΔNp63α is followed by apoptosis within the epithelial seams of the upper lip and the MES of the secondary palate (Jugessur & Murray, 2005; Thomason *et al*. 2008). Furthermore, increased levels of apoptosis have been observed within the epithelium of the medial nasal, lateral nasal and maxillary processes within *Trp63*$^{-/-}$ embryos (Thomason *et al*. 2008). The up-regulation of *Wnt11* within the facial processes of *Trp63*$^{-/-}$ embryos could provide a mechanism to explain the abnormal levels of apoptosis observed by Thomason and colleagues. Furthermore the presence of two P63 binding sites displaying positive enrichment by P63 in E11.5 facial processes could provide evidence for the direct transcriptional regulation of *Wnt11* by P63. In secondary palate development, *Wnt11* expression was shown to be exclusively epithelial and overlaps with *Trp63* expression (Lee *et al*. 2008; Thomason *et al.* 2010). However analysis of *WNT11* expression in chick facial processes produced conflicting data suggesting *WNT11* expression was excluded from the epithelium and was exclusively mesenchymal (Geetha-Loganathan *et al*. 2009). The presence of P63 binding proximal to *Wnt11* coupled with the significant down-regulation in *Trp63*$^{-/-}$ embryos compared with wildtype, suggests it would be prudent to further characterise *Wnt11* expression in wildtype and null embryos.

4.4.1.3 *Wnt4*

Wnt4 was identified as a potential target of P63 regulation, with ChIP-Seq identifying five potential P63 binding sites ≤ 150 kb of the *Wnt4* TSS. Identified binding sites were found to be highly conserved across mammals with four binding sites displaying significant positive enrichment by P63 in chromatin isolated from E11.5 facial processes. Furthermore qPCR showed *Wnt4* was significantly down-regulated in E11.5 *Trp63*$^{-/-}$ facial processes compared with wildtype. Epithelial expression of *Wnt4* was detected within the nasal aspects of the medial nasal and lateral nasal processes. Expression was found to be markedly reduced within the facial processes of *Trp63*$^{-/-}$ embryos compared with wildtype. *Trp63* has previously been shown to be expressed within the epithelium of the medial nasal, lateral nasal and maxillary processes at E11.5, which would display a clear overlap with *Wnt4* expression (Thomason *et al*. 2008). Furthermore, *Wnt4* expression within the neural tube was comparable between *Trp63*$^{-/-}$ and *Trp63*$^{+/+}$ embryos, suggesting the loss of *Wnt4* expression within the facial processes was tissue specific. Taken together these results provide evidence that *Wnt4* may a direct target of P63 regulation, however further characterisation will be required.

Analysis of *WNT4* expression in chick upper lip morphogenesis identified a similar pattern of expression to the one presented here (Geetha-Loganathan *et al*. 2009). Epithelial expression of *WNT4* was detected throughout the oral epithelium of the entire head in chick. However In contrast to the data presented here, expression of *WNT4* was absent from the

nasal pits or nasal slits at stages 20 and 25 (Geetha-Loganathan *et al*. 2009). The authors note that the nasal slit epithelium was not comprehensively characterised in their study and this may account for the absence of *WNT4* expression. Furthermore, the authors encountered difficulties in detecting *WNT4* expression using WISH, suggesting the abundance of *WNT4* transcript was too low (Geetha-Loganathan *et al*. 2009).

Wnt4 is required for correct sex assignment during embryogenesis, with female mice carrying *Wnt4* mutations displaying male attributes due to induction of testosterone biosynthesis (Vainio *et al*. 1999). Furthermore *Wnt4* has been shown to be required for kidney development, with *Wnt4*$^{-/-}$ mice displaying neonatal lethality due to kidney failure (Stark *et al*. 1994). Human mutations in *WNT4* cause conditions characterised by sexual reversal. As such the role of *WNT4* in sexual development is well characterised, however the role *WNT4* plays in orofacial development remains poorly characterised (Bernard & Harley, 2007). *WNT4* mutations in humans induce SERKAL syndrome, which is characterised by female to male sex reversal and renal, adrenal and lung dysgenesis (Mandel *et al*. 2008). In addition the presence of cleft lip and palate in patients with SERKAL syndrome has been reported, suggesting *WNT4* may also play a role in orofacial development (Mandel *et al*. 2008). Analysis of three co-sanguineous individuals identified a c.C341T mutation as the cause of SERKAL syndrome. Analysis of foetal tissue homozygous for the C341T mutation showed a complete absence of *WNT4* mRNA, it was therefore suggested that the C341T mutation results in the destabilisation of *WNT4* RNA, in effect producing a human *WNT4* knockout (Mandel *et al*. 2008). The potential role of *WNT4* in facial development was not further investigated within the study, and remains uncharacterised. However the presence of a cleft lip and palate phenotype associated with *WNT4* mutation, coupled with the expression data presented in this data set could indicate a role of *WNT4* in facial development.

4.4.1.4 *Wnt7a*

A P63 binding site was identified proximal to Wnt7a and was shown to display positive enrichment by P63 in E11.5 facial processes. Additionally, *Wnt7a* expression was significantly down-regulated in *Trp63*$^{-/-}$ E11.5 facial processes, however no expression profile characterisation was completed. From the data presented here, it remains unclear if *Wnt7a* is a direct target of P63 regulation during upper lip morphogenesis. Analysis of *WNT7A* expression within chick facial development failed to identify any expression within the developing facial processes (Geetha-Loganathan *et al*. 2009). However expression has been characterised within the developing limb bud (Dealy *et al*. 1993). In chick, *WNT7A* was found to be exclusively expressed within the dorsal ectoderm of the developing limb bud. It is important to note that P63 regulation is required for correct limb formation, with expression localised to the dorsal ectoderm in developing mouse embryos (Dealy *et al*. 1993; Yang *et al*. 1999). While a lack of identified *WNT7A* expression within the facial regions undermines the possibility of P63 regulation in the face, the presence of expressional overlap within the

limbs could suggest a possible association in limb development (Dealy *et al*. 1993; Yang *et al*. 1999; Geetha-Loganathan *et al*. 2009).

Interestingly while a lack of *WNT7A* expression was detected in chick facial development, human SNPs within *WNT7A* have been shown to display a significant association with the incidence of NSCLP within American and European populations (Chiquet *et al*. 2008). In addition, human mutations within *WNT7A* result in conditions characterised by limb defects (Woods *et al*. 2006). Woods and colleagues investigated two families who presented with Fuhrmann syndrome and Al-Awadi/Raas-Rothschild/Schinzel Phocomelia syndrome (AARRS). Patients exhibit a number of phenotypes including severe fore and hindlimb malformations and truncations, defects in the ectoderm derived nails, limb hypoplasia and fusion of the knees (Woods *et al*. 2006). Mutations within *WNT7A* were identified as the cause of Fuhrmann syndrome and AARRS within the patients with two mutations, Ala109Thr and Arg293Cys, identified. Furthermore functional analysis of *WNT7A* carrying the identified mutations in chick, showed $WNT7A^{A109T}$ retained partial wildtype function, while $WNT7A^{R292C}$was equivalent to a null mutation (Woods *et al*. 2006). These results suggested *WNT7A* mutations displayed a genotype to phenotype correlation, with patients carrying the Arg293Cys mutation displaying more severe limb truncations compared with patients presenting Ala109Thr mutations (Woods *et al*. 2006).

It is important to note that while no patients within Woods' study presented with cleft lip or palate, a subsequent case study of AARRS-affected individuals identified the presence of cleft palate associated with the disorder, however no patient genotyping was completed (Lonardo *et al*. 2007). *TP63*-related conditions commonly feature malformed and truncated limbs as well as defects within the ectoderm derived tissues as a phenotype, providing a clear phenotypic overlap with *WNT7A*-related conditions (Woods *et al*. 2006; Rinne *et al*. 2007). The role of *Wnt7a* in limb development was further characterised using the presence of limb defects within $Wnt7a^{-/-}$ mouse models, however no orofacial phenotype was observed (Parr & McMahon, 1995). It remains unclear if P63 regulates *Wnt7a* expression within the facial processes. Furthermore, due to the profound limb defects caused by *WNT7A* mutations in humans and the $Wnt7a^{-/-}$ mouse phenotype, it may prove prudent to investigate the possibility of P63-*Wnt7a* regulation during limb morphogenesis

4.4.1.5 *Wnt9b*

A P63 binding site was identified between *Wnt3* and *Wnt9b* and was shown to be significantly positively enriched by P63 in chromatin isolated from E11.5 wildtype facial processes. Quantification of *Wnt9b* expression in $Trp63^{-/-}$ facial processes failed to display significant differential expression to wildtype, by both qPCR and microarray analyses. However WISH showed a marked reduction in *Wnt9b* expression within the oral epithelium of the maxillary processes and within the nasal epithelium of the lateral nasal processes at the site of the lambdoidal junction. As an expansion of *Wnt9b* expression was observed

within the oral epithelium of the medial nasal processes, it may therefore be the case that the medial nasal expansion would counteract any quantifiable reduction of *Wnt9b* within the maxillary processes and could explain the failure to achieve significance using either qPCR or microarray. It is important to note that P63 expression during upper lip morphogenesis overlaps with that of *Wnt9b* and an association between *Wnt3* and *Wnt9b*, and *Trp63* expression has previously been discussed, with *Trp63* expression down-regulated in *Pbx*-knockout mice via Wnt signalling. In addition, *Trp63* expression is down-regulated in *Wnt9b*$^{-/-}$ embryos (Ferretti *et al*. 2009) (Chapter 1.4.5). The presence of a P63 binding site proximal to *Wnt9b* during upper lip morphogenesis and the subsequent reduction in *Wnt9b* expression in the absence of P63 could indicate a potential transcriptional feedback regulation system, however this will be discussed in further detail in the following chapter.

4.4.1.6 *Krm2*

A P63 binding site was identified proximal to *Krm2* which displayed positive enrichment by P63 in chromatin extracted from E11.5 wildtype facial processes. *Krm2* expression was significantly down-regulated in the absence of P63, which coupled with the presence of proximal P63 binding could indicate direct regulation. However extensive further characterisation would be required. It was not possible within this study to complete characterisation of *Krm2* expression between *Trp63*$^{-/-}$ and *Trp63*$^{+/+}$ embryos. *Krm2* expression has previously been shown to be epithelial and has been identified within the medial nasal, lateral nasal and maxillary processes of E11.5 embryos. Furthermore expression was detected throughout the epithelium of the limb buds (Chu *et al*. 2004). The potential overlap in the expression profiles of *Trp63* and *Krm2* in E11.5 embryos, coupled with the down-regulation of *Krm2* expression in *Trp63*$^{-/-}$ embryos could provide further evidence for P63 regulation, however *Krm2* expression would need to be characterised in *Trp63*$^{-/-}$ embryos.

It is interesting to note Krm2 has previously been shown to be a negative regulator of Wnt signalling (Moa & Niehrs, 2003; Chu *et al*. 2004). Therefore with the identified reduction in canonical Wnt signalling in E11.5 *Trp63*$^{-/-}$ embryos compared with wildtype, it would be expected that *Krm2* expression would be up-regulated rather that the down-regulation identified within this study. *Krm2* encodes a transmembrane protein which has been shown to modulate Wnt signalling via Dkk1 and Dkk2 binding (Mao *et al*. 2002; Mao *et al*. 2003). The roles of Dkk1 and Dkk2 in Wnt signalling have been characterised, with Dkk1 always acting as a Wnt antagonist, while Dkk2 functions as both an agonist and antagonist (Wu *et al*. 2000). Using the *TOP-FLASH* Luciferase reporter construct in human 293T keratinocytes, Mao and Niehrs investigated the ability of Dkk1, Dkk2 and Krm2 to regulate Wnt signalling via Lrp6 (Mao & Niehrs, 2003). Transfection of Krm2 alone was unable to down-regulate Wnt signalling, while Dkk1 weakly inhibited Wnt signalling. Transfection of Dkk2 activated Wnt signalling. In contrast, co-transfection of Dkk1 or Dkk2 with Krm2 resulted in a significant reduction in Wnt signalling (Mao & Niehrs, 2003).

It was therefore suggested that Dkk1 and Dkk2 inhibit Wnt signalling via binding to Lrp6 and Krm2 (Mao & Niehrs, 2003). Co-binding of Dkk1 or Dkk2 to Krm2 and Lrp6 resulted in the internalisation of the binding complex and removal of Lrp6 from the cell surface, preventing Lrp6-mediated Wnt signalling (Mao & Niehrs, 2001). As Lrp6 has been identified as a key mediator of canonical Wnt signalling during facial development, P63 regulation of Krm2 could provide a mechanism explaining the loss of canonical signalling observed in *Trp63*$^{-/-}$ embryos (Song *et al*. 2009). The down-regulation of *Krm2,* in isolation, should induce an expansion of canonical Wnt signalling. It is important to note that multiple members of the Wnt signalling network have been shown to be misregulated in *Trp63*$^{-/-}$ facial processes and the reduction in Wnt signalling is likely to be a compound effect of Wnt misregulation. To further clarify the relationship between P63 and *Krm2* the expression profile of *Krm2* will need to be analysed using WISH in *Trp63*$^{-/-}$ and *Trp63*$^{+/+}$ E11.5 embryos. Furthermore it would be prudent to characterise Krm2 protein distribution using immunohistochemistry within the epithelium of medial nasal, lateral nasal and maxillary processes in *Trp63*$^{-/-}$ and *Trp63*$^{+/+}$ embryos during upper lip morphogenesis.

4.4.1.7 *Pax6*

A P63 binding site was identified proximal to *Pax6* and shown to be positively enriched by P63 in E11.5 facial processes. Expression of *Pax6* was found to be expanded within the epithelium of the medial nasal and lateral nasal processes surrounding the nasal pit in the absence of P63. In contrast, expression within the eyes and forebrain was comparable between *Trp63*$^{-/-}$ and *Trp63*$^{+/+}$ embryos, suggesting expansion of *Pax6* expression was specific to facial development. *Pax6* encodes a transcription factor known be involved in ocular development, with human mutations in *PAX6* causing aniridia and Peter's anomaly which are characterised by ocular defects (Prosser & van Heyningen, 1998; Li *et al*. 2008). Aniridia is characterised by corneal opacification, cataract, lens dislocation, ciliary body hypoplasia, optic nerve hypoplasia and nystagmus (Prosser & van Heyningen, 1998). While mutations within *PAX6* are commonly linked to an ocular phenotype, some studies have identified an association between *PAX6* SNPs and the incidence of NSCLP (Sull *et al*. 2009). Sull and colleagues identified five SNPs within *PAX6* associated with the incidence of maternal parent-of-origin NSCLP, however the mechanism of parent-of-origin NSCLP remains unknown (Sull *et al*. 2009).

In addition to a link to NSCLP, *Pax6* has previously been associated with abnormal facial development in animal models (Hill *et al*. 1991; Kriangkrai *et al*. 2006). Mutations in *Pax6* were shown to underlie the phenotype of *Small eye* mice which are characterised by lack of eyes and failure to develop nasal cavities (Hill *et al*. 1991). Furthermore the *Pax6* mutant rat model *rSey*^{2}/*rSey*^{2} display a fully penetrant bilateral cleft lip between the medial nasal and maxillary processes (Kriangkrai *et al*. 2006). How *Pax6* mutation induces cleft lip in *rSey*^{2}/*rSey*^{2} rats is currently unknown (Kriangkrai *et al*. 2006). However studies into the

function of *Pax6* in ocular development and homeostatsis suggest *Pax6* functions to inhibit differentiation (Li *et al*. 2008; Ouyang *et al*. 2014).

Li and colleagues investigated the role of *PAX6* in maintaining epithelial homeostasis (Li *et al*. 2008). A loss of *PAX6* expression in epithelial cells isolated from human cornea and other ocular surface epithelia resulted in abnormal differentiation and squamous metaplasia (Li *et al*. 2008). In contrast over-expression of *Pax6* in rabbit corneal epithelial resulted in reduced levels of proliferation (Ouyang *et al*. 2006). In the context of upper lip morphogenesis, these findings are of great relevance. During normal orofacial development, *Trp63* is expressed within the epithelium of the medial nasal, lateral nasal and maxillary processes during facial process outgrowth (Thomason *et al*. 2008). Following facial process contact and adhesion, *Trp63* expression within the epithelial seam at the site of process contact is reduced and is immediately followed by apoptosis and differentiation (Thomason *et al*. 2008). Furthermore, the cleft lip phenotype of *Trp63*$^{-/-}$ embryos has been attributed in part to a loss of proliferation within the lateral nasal, medial nasal and maxillary processes (Thomason *et al*. 2008).

Within the present data set, *Pax6* expression was shown to be expanded within the medial nasal, lateral nasal and maxillary processes, suggesting during normal development *Pax6* is inhibited by P63. The over-expression of *Pax6* could therefore contribute to the reduced proliferation observed within *Trp63*$^{-/-}$ facial processes (Ouyang *et al*. 2006). To date a comprehensive characterisation of *Pax6* expression during upper lip morphogenesis has not been completed. However, the weak expression of *Pax6* detected in *Trp63*$^{+/+}$ facial processes, a time-point at which the epithelial seams of the facial processes are beginning to undergo apoptosis and differentiation, could suggest a role for *Pax6* in normal P63-mediated upper lip morphogenesis (Jiang *et al*. 2006). Extensive characterisation of *Pax6* and *Trp63* expression would need to be completed throughout upper lip morphogenesis. However, it may be that P63 represses *Pax6* expression during outgrowth of the facial processes to maintain proliferation. Following process contact and adhesion, the down-regulation of P63 could result in up-regulation of *Pax6* which would contribute to subsequent epithelial differentiation, in a similar manner to which P63 and *Irf6* interact during facial development.

4.4.1.8 *Fzd10*

Fzd10 was identified as a potential target of P63 regulation with four putative P63 binding sites identified ≤ 150 kb of the *Fzd10* TSS and displaying positive enrichment by P63 in E11.5 facial processes. *Fzd10* expression was shown to be significantly reduced within the facial processes of *Trp63*$^{-/-}$ embryos at E11.5, with WISH identifying a reduction in *Fzd10* expression within the nasal epithelium of the medial nasal and lateral nasal processes. A further reduction in expression was observed at the boundary of the maxillary and mandibular processes, where a region of intense staining was observed in wildtype controls. The reduction of expression in *Trp63*$^{-/-}$ embryos coupled with the identification of proximal

P63 binding to *Fzd10*, could suggest *Fzd10* is a direct target of P63 regulation during upper lip morphogenesis. Furthermore P63 expression is present within the nasal epithelium of the medial nasal and lateral nasal epithelium, suggesting their expression patterns overlap *in vivo* (Thomason *et al*. 2008).

FZD10 was originally characterised by the Katoh group in 1999, however the functions of *FZD10* and its roles in development remain relatively uncharacterised (Koike *et al*. 1999). Previous studies in chick have identified *FZD10* expression within the maxillary processes, however to date *Fzd10* has not been associated with a cleft lip and palate phenotype within humans or animal models (Geetha-Loganathan *et al*. 2009). It has previously been suggested Fzd10 mediates Wnt signalling through interactions with Wnt1, Wnt3a, Wnt7a and Wnt7b (Wang *et al*. 2005; Kawakami *et al*. 2000b; Galli *et al*. 2014). It is interesting to note that the expression pattern of *Fzd10* is highly similar to that of *Lrp6*, with a spot of intense expression detected at the boundary of the maxillary and mandibular processes.

While Fzd10 function within facial development has not been characterised, it has been suggested that *FZD10* expression is required for proliferation within the development of the dorsal spinal cord in chick and developing limb bud (Kawakami *et al*. 2000a; Kawakami *et al*. 2000b; Galli *et al*. 2014). *FZD10* was found to be expressed throughout the epithelium of the developing spinal cord, with expression overlapping with that of *Wnt1* and *Wnt3a* (Galli *et al*. 2014). Binding of Wnt1 or Wnt3a to Fzd10 and Lrp6 was shown to induce canonical Wnt signalling-dependent proliferation, with Fzd10 knockdown via morpholino resulting in a significant reduction in proliferation (Galli *et al*. 2014). During chick limb development, *Fzd10* expression was identified in the dorsal ectoderm and the posterior-distal limb mesenchyme (Kawakami *et al*. 2000b). Furthermore, it was shown that removal of the distal ectoderm resulted in down-regulation of *FZD10* expression. Due to the overlapping expression patterns of *SHH* and *FZD10* within the developing limb bud, it was suggested that epithelial expression of *SHH* induced *FZD10* expression (Kawakami *et al*. 2000b). In light of the data presented within this study, it is important to note that *Trp63* expression is detected within the dorsal epithelium of mouse limb buds, suggesting *Trp63* and *Fzd10* expression may overlap during limb development (Yang *et al*. 1999; Mills *et al*. 1999).

The overlapping expression patters of *Trp63* and *Fzd10* together with the expression changes of *Fzd10* between *Trp63*$^{-/-}$ and *Trp63*$^{+/+}$ embryos could suggest P63 may regulate *Fzd10* expression, however further characterisation is required. Furthermore, the previous association with Fzd10 mediated canonical Wnt signalling-dependent proliferation could suggest loss of *Fzd10* expression in *Trp63*$^{-/-}$ facial processes, could contribute to the hypoproliferative phenotype observed in *Trp63*$^{-/-}$ embryos and the reduction in canonical Wnt signalling observed within this study (Thomason *et al*. 2008; Galli *et al*. 2014).

4.4.1.9 *Sfrp1* and *Shh*

Sfrp1 was identified as a potential target of P63 regulation with two P63 binding sites identified ≤ 150 kb of the TSS. ChIP-qPCR failed to display significant positive enrichment for both sites, and qPCR analysis failed to generate a significant change in expression between *Trp63*$^{+/+}$ and *Trp63*$^{-/-}$ facial processes. Due to the lack of supporting evidence for P63 regulation of *Sfrp1* during lip morphogenesis, *Sfrp1* was not prioritised for analysis using WISH. As such these data would suggest *Sfrp1* is not a target of direct P63 regulation during E11.5 upper lip morphogenesis. Previous studies have shown Shh signalling negatively regulates the Wnt signalling pathway through the induction of *Sfrp1* and *Sfrp2* expression (Kurosaka *et al*. 2014). In light of this, *Shh* expression was characterised in *Trp63*$^{+/+}$ and *Trp63*$^{-/-}$ E11.5 embryos using WISH.

In keeping with the work of Thomason and colleagues, *Shh* was down-regulated in *Trp63*$^{-/-}$ facial processes compared with wildtype, with expression within the lambdoidal junction markedly reduced (Thomason *et al*. 2008). In addition, the analysis of canonical Wnt signalling using BAT-Gal mice showed a marked reduction in Wnt signalling throughout the facial processes of *Trp63*$^{-/-}$ embryos compared with wildtype. In light of the findings of Kurosaka and colleagues, it would be expected that a loss of *Shh* expression, an inhibitor of Wnt signalling, in *Trp63*$^{-/-}$ facial processes would result in expansion of Wnt signalling (Kurosaka *et al*. 2014). The reduction therefore, could suggest that in addition to *Shh*-negative regulation of Wnt signalling, P63 functions independently in the up-regulation of multiple members of the Wnt signalling pathway during upper lip morphogenesis. Further characterisation of the relationship between Wnt and P63 signalling will need to be completed and will be discussed further in the following chapter. These results, together with those of Kurosaka and colleagues, could suggest that correct modulation of Wnt signalling during upper lip morphogenesis is achieved through the integration of multiple signalling networks and further underpins the complex signalling networks active in orofacial development.

4.4.1.10 *Sox2*

The previous association between *Sox2* and *Trp63* and the role of *Sox2* in orofacial development have previously been discussed in Chapter 3.4.2. *Sox2* was identified as a putative P63 target gene with the identification of a P63 binding site proximal to *Sox2* which was significantly enriched by P63 in chromatin isolated from wildtype E11.5 facial processes. Expression of *Sox2* was found to be up-regulated within the nasal epithelia of the medial nasal and lateral nasal processes, with expression extending into the lambdoidal junction. Expression within the superior regions of the optic cup was found to be comparable between *Trp63*$^{+/+}$ and *Trp63*$^{-/-}$ embryos, suggesting expression expansion within the facial processes was tissue specific.

Mouse models of *Sox2* haploinsufficiency displayed a cleft palate but did not display defects of the upper lip and primary palate (Langer *et al*. 2014). Furthermore how loss of Sox2 induced orofacial clefting remains unknown (Langer *et al*. 2014). In contrast, conditional mouse knockouts for *Sox2* showed a reduction in *Sox2* expression resulted in defective frontonasal process formation (Mandalos *et al*. 2014). Mandalos and colleagues suggested that a loss of *Sox2* expression resulted in a lack of EMT of cranial neural crest cells which contribute to the formation of the facial primordia and this was the cause of orofacial defects in *Sox2*$^{-/-}$ embryos (Mandalos *et al*. 2014). Additionally a study in *Sox2* function in lung development showed over-expression of *Sox2* in lung epithelial cells resulted in premature differentiation (Gontan *et al*. 2008). As previous discussed in reference to *Pax6* (Section 4.4.1.7), P63 regulation of differentiation within facial development is well-documented (Thomason *et al*. 2008).

In a similar manner to *Pax6*, the over-expression of *Sox2* in *Trp63*$^{-/-}$ facial processes could indicate that in wildtype embryos, P63 inhibits *Sox2* expression. Furthermore *Sox2* may play a functional role in wildtype upper lip morphogenesis, through up-regulation following P63 down-regulation within the epithelial seams at the sites of facial process contact (Thomason *et al*. 2008). Substantial characterisation of *Sox2* expression throughout upper lip morphogenesis of *Trp63*$^{+/+}$ and *Trp63*$^{-/-}$ embryos would be required to determine if *Sox2* is required for upper lip morphogenesis. Furthermore the direct relationship between P63 and *Sox2* regulation will need to be further investigated and this will be further discussed in chapter 5.

4.4.1.11 Fgf-related genes

The likelihood of the Fgf-related genes, *Fgfr2*, *Fgfr3*, *Spry1* and *Spry2*, as potential P63 targets in E11.5 upper lip development has previously been discussed (Chapter 3.4.7). Both *Fgfr2* and *Fgfr3* have previously been shown to be targets of P63 regulation, with a loss of P63 regulation in primary mouse keratinocytes and embryonic skin resulting in their down-regulation (Ferone *et al*. 2012). Furthermore, studies in cells derived from human bladder cancers showed both TA and ∆Np63 isoforms were able to induce *FGFR3* expression with a loss of ∆Np63 isoforms resulting in down-regulation of *FGFR3* (Sayan *et al*. 2010). Within the present study, a loss of P63 regulation within E11.5 facial processes resulted in the significant down-regulation of both *Fgfr2* and *Fgfr3* which is in line with previous studies (Sayan *et al*. 2010; Ferone *et al*. 2012). Furthermore, it has previously been shown that during embryogenesis, ∆Np63α is the predominantly expressed isoform of P63 (Yang *et al*. 1999; Laurikkala *et al*. 2006). As such, presented data provided further evidence that *Fgfr3* is positively regulated by ∆Np63 isoforms. In addition, two P63 binding sites have been identified and shown to be significantly positively enriched by P63 in E11.5 facial processes ≤ 150 kb to *Fgfr2* and *Fgfr3* transcriptional start sites. Binding of P63 proximal to *Fgfr2* and *Fgfr3* could provide evidence of direct transcriptional regulation by P63, however further characterisation is required. Due to limitations in the access to *Trp63*$^{-/-}$ and *Trp63*$^{+/+}$

embryos, it was not possible to complete WISH for *Fgfr2* or *Fgfr3*, to further characterise their expression in E11.5 *Trp63*$^{-/-}$ facial processes.

Analysis of *Spry1*$^{-/-}$ and *Spry2*$^{-/-}$ embryos has shown both genes are required for correct upper lip morphogenesis, with knockout models commonly exhibiting a cleft lip and palate (Welsh *et al*. 2007; Matsumura *et al*. 2010; Yang *et al*. 2010). Within the present study expression analysis using qPCR showed *Spry1* was down-regulated and *Spry2* was up-regulated in *Trp63*$^{-/-}$ E11.5 facial processes compared to wildtype. However neither result achieved significance. Characterisation of *Spry1* expression using WISH failed to generate an observable difference between *Trp63*$^{-/-}$ and *Trp63*$^{+/+}$ E11.5 embryos, while *Spry2* expression displayed a subtle expansion within the medial aspects of the medial nasal processes. A loss of *Spry2* expression has previously been demonstrated to induce cleft lip and palate, with increased levels of mesenchymal proliferation identified as a contributory factor (Welsh *et al*. 2007; Matsumura *et al*. 2010). These results would suggest that Spry2 functions to inhibit proliferation. The apparent expansion of *Spry2* expression was therefore biologically relevant in *Trp63*$^{-/-}$ facial processes, where reduced proliferation has been suggested as a contributory factor to the cleft lip and palate phenotype observed (Thomason *et al*. 2008). In addition, ectopic expression of *SPRY1* in human ovarian cancer cells was shown to significantly reduce the number of proliferating cells, suggesting functional similarity to *Spry2* as a negative regulator of proliferation (Masoumi-Moghaddam *et al*. 2014). It has been suggested that Spry1 and Spry2 function as negative regulators of proliferation via repression of the p44/p42-MAPK signalling pathway (Hanafusa *et al*. 2002). The apparent down-regulation of *Spry1* expression is therefore puzzling as it could be expected that a loss of Spry1 inhibition would function in opposition to the loss of proliferation observed in *Trp63*$^{-/-}$ facial processes (Thomason *et al*. 2008; Hanafusa *et al*. 2002).

Two P63 binding sites proximal to *Spry1* and *Spry2* respectively were identified and shown to be significantly positively enriched by P63 during E11.5 upper lip morphogenesis. The presence of P63 binding sites proximal to *Spry1* and *Spry2* could provide evidence of direct P63 transcriptional regulation, however the mechanism of regulation has not been identified.

4.4.2 Human mutations of *LRP6* cause tooth agenesis and orofacial clefting

Studies have shown Lrp6 is a key mediator of canonical Wnt signalling during upper lip morphogenesis (Song *et al*. 2009). In Wnt signalling *Lrp6* encodes a cell surface receptor protein, which acts as a co-receptor with the Fzd family of receptors to mediate Wnt signalling (Arkell *et al*. 2013). Lrp6$^{-/-}$ embryos display multiple developmental defects including: spina bifida, no tail, malformations of the fore and hindlimbs, retinal coloboma, defects of the urogenital system, truncation of the axial skeleton and loss of the distal limb structures (Pinson *et al*. 2000). In addition, morphological analysis at E13.5 identified bilateral cleft lips and hypoplasia of the upper lip (Song *et al*. 2009). Further analysis at

E16.5 identified an absence of the primary palate and a fully penetrant bilateral cleft lip and palate (Song *et al*. 2009).

Previous further characterisation of *Lrp6*$^{-/-}$ embryos using BrdU analysis identified a reduction in the number of mesenchymal cells undergoing proliferation within the medial nasal, lateral nasal and maxillary processes. Furthermore, TUNEL assays identified a reduction in the number of epithelial cells undergoing apoptosis within the epithelial seam at the site of contact between the facial processes (Song *et al*. 2009). *Msx1* and *Msx2* were found to be down-regulated in *Lrp6*$^{-/-}$ facial processes, compared with wildtype littermates and Tcf/Lef-binding sites were identified within the promoter regions of both genes (Song *et al*. 2009). Induction of canonical Wnt signalling using lithium chloride resulted in elevated *Msx1* and *Msx2* expression. It was therefore suggested that *Msx1* and *Msx2* are targets of Lrp6 mediated Wnt signalling and the loss of *Msx1* and *Msx2* expression was a direct cause of the hypoproliferative phenotype and cleft lip and palate (Song *et al*. 2009).

Over the course of this project, a collaboration was established with the Hoischen (Radboud University Medical Center, Department of Human Genetics, Nijmegen, The Netherlands) and Carels (Radboud Univeristy Medical Center, Department of Dentistry, Nijmegen, The Netherlands) groups who identified human mutations in LRP6 as a cause of tooth agenesis (TA) and orofacial clefting (Ockeleon *et al*. 2015). Whole exome sequencing of two unrelated patients with TA and severe TA and bilateral cleft lip and palate identified two novel mutations in *LRP6*. The deleterious frameshift mutation c.4594delG was predicted to induce a premature stop codon, 15 codons down-stream, while the c.3395-2A>C mutation was shown to occur within the final exon of *LRP6* and was predicted to result in the formation of a truncated protein lacking all terminal phosphorylation domains (Ockeleon *et al*. 2015).

LRP6 re-sequencing of 67 patients displaying TA and 1,073 patients with orofacial clefting identified a significant enrichment for *LRP6* mutations within patients displaying severe TA, including mutations within canonical splice sites and three predicted missense mutations (Ockeleon *et al*. 2015). Mutations within *LRP6* failed to display significant enrichment within patients with orofacial clefting against the control population. The authors however suggest that common forms of TA may be present within controls who were not screened for this feature which would reduce the significance of any association identified (Ockeleon *et al*. 2015). Due to the phenotypic overlap between human *TP63*-related conditions which commonly feature dental defects and *LRP6*-TA, and the presence of phenotypic overlaps between *Trp63*$^{-/-}$ and *Lrp6*$^{-/-}$ mice, which both display bilateral cleft lip and palate and defects in limb development, *Lrp6* was investigated as a potential target of P63 regulation (Yang *et al*. 1999; Mills *et al*. 1999; Rinne *et al*. 2007; Ockeleon *et al*. 2015).

ChIP-Seq analysis identified a P63 binding motif within intron 7 of *Lrp6* which was shown to be significantly positively enriched by P63 in chromatin isolated from wildtype E11.5 facial processes. *Lrp6* expression was shown to be down-regulated in E11.5 *Trp63*$^{-/-}$ facial

processes compared with wildtype, however the change was not significant (p-value = 5). Furthermore, WISH analysis of early E11.5 and late E11.5 embryos showed *Lrp6* expression was largely comparable within the medial nasal, lateral nasal and maxillary processes, with late E11.5 embryos displaying a subtle expansion of *Lrp6* expression within the lateral nasal processes and a reduction at the boundary between the maxillary and mandibular processes. It is important to note however that *Lrp6* expression appeared mesenchymal, with expression absent from the epithelia; however this would need to be confirmed using sectioning of stained WISH embryos. These results would suggest that a loss of P63 may affect *Lrp6* expression, however the interaction is indirect as P63 is exclusively expressed epithelially within the facial processes (Thomason *et al*. 2008).

4.4.3 Canonical Wnt signalling is disrupted in *Trp63*$^{-/-}$ facial processes

Functional annotation identified the enrichment of multiple members of the Wnt signalling family as being differentially regulated in E11.5 *Trp63*$^{-/-}$ facial processes. Multiple members of the Wnt signalling family were found to be misregulated including: the Wnt ligands *Wnt3*, *Wnt3a*, *Wnt9b*, *Wnt10b* and *Wnt11*; Wnt co-receptors *Fzd4*, *Fzd10* and *Lrp6* and the Wnt transcriptional effector *Lef1*. With the exception of *Wnt11*, the majority of *Wnt* genes were found to be down-regulated in the absence of P63 which suggested an inhibition of Wnt signalling. Identified Wnt genes including *Wnt10b* and *Wnt3a* have been shown to induce Wnt signalling via the canonical Wnt pathway (Paik *et al*. 2015; Selvaraj *et al*. 2015). It was therefore hypothesised that the canonical Wnt signalling pathway was attenuated in *Trp63*$^{-/-}$ embryos, and may contribute to the cleft lip and palate phenotype observed.

The Wnt canonical pathway functions via the cytoplasmic regulation of active β-catenin (Bengoa-Vergniory & Kypta, 2015). In unstimulated cells, the Wnt co-receptors Lrp5/6 and Fzd proteins are unbound by Wnt ligand (Arkell *et al*. 2013). Ligand-receptor binding can be further attenuated via the presence of Wnt antagonists. Sfrp proteins bind Wnt ligands extracellularly and thus prevent them from binding receptors, while Dkk proteins act as direct competitors to Wnt ligands, binding to Lrp/Fzd receptors and causing their internalisation (Pannone *et al*. 2010). With a lack of Wnt activation, intracellular β-catenin is marked for proteasomal degradation by phosphorylation by the Ck1/Axin/Gsk3/APC complex and polyubiquitylation by the Scf/β-Trcp complex (Lu *et al*. 2015). In the absence of active cytoplasmic β-catenin, transcriptional activation by the Wnt effectors Lef1 and Tcf proteins is inhibited by Tcf7l1 and currently uncharacterised transcriptional co-repressors (Arkell *et al*. 2013; Kuwahara *et al*. 2014). Tcf7l1 has been shown to competitively bind to Wcf1/Lef1 sites and thus prevent transcriptional activation (Kuwahara *et al*. 2014).

Binding of Wnt ligand to Lrp5/6 and Fzd co-receptors results in recruitment and phosphorylation of the cytoplasmic protein Dishevelled (Dsh) and the β-catenin-inhibitors Axin and Gsk3β (Krasnow *et al*. 1995; Tamai *et al*. 2004; Zhang *et al*. 2012). Recruitment of Dsh, Axin and Gsk3β relieves inhibition of β-catenin by prevention of phosphorylation and

polyubiquination (Arkell *et al*. 2013). Increased levels of cytoplasmic β-catenin results in nucleus translocation, and binding to and phosphorylation of Tcf7l1 (Kuwahara *et al*. 2014). Tcf7l1 phosphorylation prevents DNA binding and relieves inhibition of Tcf/Lef sites allowing the transcription of Wnt down-stream targets (Hikasa *et al*. 2010).

Due to the misregulation of genes associated with canonical signalling, modification of canonical Wnt signalling was assayed using BAT-Gal reporter mice. s-catenin activated transgene (BAT) driving the expression of nuclear beta-galactosidase (Gal), BAT-Gal reporter mice were originally generated by the Piccolo group to visualise Wnt/β-catenin signalling during mouse development and in colorectal tumours (Maretto *et al*. 2003). BAT-Gal mice were generated via the fusion of seven Tcf/Lef-binding sites upstream of a 0.13 kb fragment containing the minimal promoter of the gene *siamois* and *LacZ* (Maretto *et al*. 2003).

To analyse canonical Wnt activity in E11.5 *Trp63*$^{-/-}$ embryos, Bat-Gal mice were crossed with *Trp63*$^{+/-}$ BalbC mice to generate a compound mouse strain modelling *Trp63*$^{-/-}$ and Bat-Gal reporter function. Crossings were kindly provided by the Selleri lab (Weill Cornell Medical College, New York). Subtle variations in mouse phenotypes and molecular expression have been identified between inbred mouse strains (Crawley *et al*. 1997). As such prior to *Trp63*$^{+/-}$ crosses BAT-Gal mice were crossed onto the BalbC background for six generations. Analysis of *Trp63*$^{+/+}$;*BAT-Gal*$^{tg/+}$ and *Trp63*$^{-/-}$;*BAT-Gal*$^{tg/+}$ identified a distinct reduction of LacZ reporter activity within the facial processes of *Trp63*$^{-/-}$ embryos compared with wildtype littermates. In *Trp63*$^{-/-}$;*BAT-Gal*$^{tg/+}$ embryos posterior *LacZ* expression was absent within the medial nasal, lateral nasal and maxillary processes. Furthermore remaining *LacZ* staining intensity was markedly reduced compared with controls. These results suggested that loss of P63 regulation causes down-regulation of the canonical Wnt signalling pathway.

A loss of β-catenin has previously been linked to the induction of cleft lip and palate in chick models (Kawakami *et al*. 2014). Interestingly the expression of *Ctnnb1* (β-catenin) was not significantly changed on either the E11.5 or E12.5 microarrays with fold changes of 1.01 (p= 0.9) and -1.05 (p= 0.4). The significant down-regulation of the Wnt ligands including *Wnt2b*, *Wnt3*, *Wnt4*, *Wnt9b* and *Wnt10b* could explain the reduction in canonical Wnt signalling. Furthermore as the effector of canonical Wnt signalling, the down-regulation of *Lef1* in *Trp63*$^{-/-}$ embryos could further provide a direct cause of canonical signal reduction (Arkell *et al*. 2013).

It has previously been suggested that a disruption of epithelial to mesenchymal signalling contributed the phenotype of *Trp63*$^{-/-}$ embryos (Mills *et al*. 1999; Yang *et al*. 1999). Furthermore, a study by Thomason and colleagues showed cell counts within the medial nasal, lateral nasal and maxillary processes in *Trp63*$^{-/-}$ embryos were significantly lower than wildtype controls with BrdU proliferation assays showing a significant reduction in proliferation at E11.5 (Thomason *et al*. 2008). Studies have shown that a reduction in

canonical Wnt signalling can result in a reduction of proliferation (He *et al*. 2015; Kahlert *et al*. 2015). Reduction of canonical Wnt signalling in chick embryos resulted in the down-regulation of the proliferation-associated genes *Msx1*, *Msx2* and *Lhx8* (Kawakami *et al*. 2014).

Msx1 and *Msx2* were down-regulated in the E12.5 microarray, however both failed to achieve significance. These findings conflict with those of Thomason and colleagues who showed *Msx1* was up-regulated in *Trp63*$^{-/-}$ medial nasal and maxillary processes (Thomason *et al*. 2008). However, the apparent conflict could be a result of the restrictions of microarray analysis. As has previously been discussed, (See Chapter 3.4.4) the conducted microarray analysis could introduce false positive or negatives into the data set. Furthermore, as has been shown with *Wnt9b*, which failed to display significant differential expression between *Trp63*$^{-/-}$ and *Trp63*$^{+/+}$ embryos by microarray but displayed marked spatial-expression differences, quantification of gene expression does not provide a definitive measure of gene expression differences.

The regulation of canonical Wnt signalling, and the expression of diffusible Wnt ligands could provide a mechanism by which P63 regulates epithelial to mesenchymal signalling. Furthermore, the previous associations between a loss of canonical Wnt signalling and a reduction in proliferation could contribute to the phenotype of *Trp63*$^{-/-}$ embryos (Thomason *et al*. 2008; Kawakami *et al*. 2014; He *et al*. 2015; Kahlert *et al*. 2015). However to confirm such a mechanism would require substantial further work, which was not possible within the boundaries of this project.

Previous studies of β-catenin mediated Wnt canonical signalling loss and cleft lip and palate, demonstrated addition of lithium chloride (LiCl) was able to induce canonical signalling and thus induce a phenotypic effect (Song *et al*. 2009; Kawakami *et al*. 2014). Clément-Lacroix and colleagues showed that LiCl was able to induce canonical Wnt signalling through inhibition of Gsk-3β which inhibits β-catenin via phosphorylation (Clément-Lacroix *et al*. 2005). Furthermore induction of Wnt signalling via LiCl was able to affect a phenotypic rescue of *Lrp5*$^{-/-}$ adult mice which display reduced bone density. Oral administration of LiCl resulted in a significant increase in osteoblast cell counts and bone density compared with controls (Clément-Lacroix *et al*. 2005).

Kawakami and colleagues, disrupted canonical Wnt signalling in chick facial processes through mesenchymal implantation of beads soaked in the Wnt inhibitor, Dkk1 (Kawakami *et al*. 2014). Down-regulation of canonical Wnt signalling resulted in abnormal craniofacial bone structure and cleft lip and palate. The group was able to affect a phenotypic rescue of the Dkk1-induced clefting using addition of LiCl (Kawakami *et al*. 2014). Activation of Wnt canonical signalling by LiCl has been further demonstrated in mouse embryos (Song *et al*. 2009). *Lrp6*$^{-/-}$ embryos display cleft lip via a disruption of canonical Wnt signalling, as measured by the TOP-Gal reporter system (Song *et al*. 2009).

Song and colleagues identified down-regulation of the cleft lip and palate-associated genes *Msx1* and *Msx2* within the facial processes of *Lrp6*$^{-/-}$ embryos (Song *et al*. 2009). Furthermore, *Raldh3*, a member of the retinoic acid pathway, which is associated with lip development (See Chapter 1.4.6) was shown to be significantly up-regulated in the epithelium of the medial nasal, lateral nasal and maxillary processes surrounding the nasal pits and the lambdoidal junction (Song *et al*. 2009). Intraperitoneal injections of 30 µl 600 mM LiCl at E8.5 and E9.5 significantly up-regulated the expression of *Msx1* and *Msx2* and restricted the expression of *Ralh3* (Song *et al*. 2009).

Having identified the misregulation of canonical Wnt signalling in *Trp63*$^{-/-}$ facial processes, it was hypothesised, administration of LiCl and induction of Wnt signalling may induce a phenotypic effect. Due to restricted *Trp63*$^{+/-}$ mouse numbers, only an initial experiment was completed using the intraperitoneal injection of 120 µl 150 mM LiCl. The pregnant dam was injected at E8.5 and E9.5 as described previously (Song *et al*. 2009). Embryos were collected at E14.5 in order that any phenotypic rescue would be more pronounced. Genotyping of collected embryos revealed both *Trp63*$^{+/+}$ and *Trp63*$^{-/-}$ embryos were present, and they did not vary from the expected phenotype. No phenotypic rescue was observed. As only a single experiment was completed it is not clear if LiCl administration can affect a phenotypic rescue. A number of variables within the experimental design would need to be addressed in any future work.

LiCl injections were completed as previously described by Song and colleagues, however the aim of their work was to identify gene expression changes at E10.5 and so embryos were collected prior to completion of upper lip morphogenesis (Song *et al*. 2009). In the present study embryos were collected post-lip morphogenesis. It is therefore plausible that administered LiCl dosage was too low to effect a phenotypic change over the course of facial process fusion which occurs from E9.5-E12.5 (Jiang *et al*. 2006). Any further research conducted should involve variation in LiCl dosage, in addition to a revised injection protocol. Furthermore, the generation of the *Trp63*$^{+/-}$*;BAT-Gal*$^{tg/+}$ could provide an excellent tool for dosage modulation in determining the dosage of LiCl required to restore wildtype levels of canonical signalling.

From the data produced it is clear that a loss of P63 regulation during upper lip morphogenesis results in a reduction in canonical Wnt signalling which may contribute to the hypoproliferative phenotype observed within *Trp63*$^{-/-}$ facial processes. Multiple members of the Wnt signalling network including ligands, receptors, effectors and antagonists were found to be misregulated in the absence of P63. Furthermore attenuation of canonical Wnt signalling was confirmed using generation of a compound *Trp63*$^{+/-}$*;BAT-Gal*$^{Tg/+}$ reporter mouse showing a distinct reduction in active Wnt signalling compared with wildtype littermates. An initial experiment into induction of Wnt signalling using LiCl injection failed to generate a phenotypic effect. It is clear that further characterisation of the interaction

between P63 and Wnt signalling is necessary and potential further work will be described in chapter 5.

4.5 Conclusions and Summary

To identify potential targets of P63 regulation during upper lip morphogenesis, ChIP-Seq was conducted on chromatin isolated from E11.5 wildtype facial processes and the results obtained intersected against am E12.5 expression data set generated by microarray analysis of *Trp63*$^{+/+}$ and *Trp63*$^{-/-}$ facial processes. The resultant data set was interrogated using gene ontology analyses and identified enrichment for genes related to biological adhesion, Wnt signalling and Fgf signalling which was in keeping with previous studies (Kouwenhoven *et al*. 2010; McDade *et al*. 2012; Mitchell *et al*. manuscript in preparation). A resultant target gene list of 72 genes was generated for further characterisation (Chapter 3). Within the current chapter target genes were prioritised and further analyses conducted.

To prioritise genes for further investigation, a cross section of 52 Wnt, Fgf and adhesion related genes were analysed using the high throughput expression analysis technique nCounter. nCounter of E11.5 *Trp63*$^{-/-}$ and *Trp63*$^{+/+}$ facial processes showed 31 of the 52 genes assayed displayed significant differential expression (p= 0.05), with 17 genes shown to be down-regulated and 14 up-regulated in the absence of P63. Comparisons between the fold changes identified in the E12.5 microarray and the E11.5 nCounter identified 14 discrepancies where identified fold changes varied. It was therefore decided that each target gene would be further characterised using qPCR. Wnt and Fgf genes were shown to be significantly differentially expressed between *Trp63*$^{-/-}$ and wildtype facial processes and so these genes were selected for further analysis.

For each prospective P63 target gene, putative P63 binding sites within 150 kb of the TSS were analysed using P63 scan for the presence of a P63 specific binding motif. Across the 22 target genes interrogated, 64 potential binding sites were identified ≤ 150 kb from the TSS of target genes, with P63 scan identifying the P63 binding motif within 62 of the putative binding sites. qPCR analysis showed 45 (73%) of identified P63 motif-positive sites displayed significant positive enrichment by P63 within E11.5 facial processes. Furthermore, of the 22 genes investigated, only *Sfrp1* failed to display positive enrichment at a P63 binding site proximal to its TSS. Taken together these results provided further evidence that the generated P63 ChIP-Seq data set is reproducible and accurate.

Further expression analysis of each gene using qPCR in E11.5 *Trp63*$^{-/-}$ and E11.5 *Trp63*$^{+/+}$ facial processes showed of the 20 genes interrogated by qPCR, 13 displayed significant differential expression in the absence of P63. 15 genes were shown to be down-regulated and 5 genes up-regulated. The expression profiles of 12 genes were further investigated using WISH, with 11 genes including: *Lef1*, *Wnt4*, *Wnt3*, *Wnt9b*, *Shh*, *Fzd10*, *Grhl3*, *Pax6*, *Sox2*, *Spry1* and *Spry2* displaying an epithelial expression overlap with the characterised

expression pattern of P63 in E11.5 embryos (Mills *et al*. 1999; Yang *et al*. 1999; Thomason *et al*. 2008). Expression profiles of *Lef1*, *Wnt4*, *Wnt3*, *Wnt9b*, *Shh*, *Lrp6*, *Fzd10* and *Grhl3* displaying a marked reduction in expression, while no discernible change could be detected in *Spry1* expression and *Spry2*, *Pax6* and *Sox2* appeared up-regulated in the absence of P63.

Over-expression of *Pax6* and *Sox2* has previously been shown to induce abnormal epithelial differentiation and animal models of *Pax6* and *Sox2* knockout display orofacial clefting (Kriangkrai *et al.* 2006; Gontan *et al*. 2008; Ouyang *et al*. 2014; Mandalos *et al*. 2014). Up-regulation of *Pax6* and *Sox2* in the absence of P63 signalling suggested P63 acts to inhibit their expression during E11.5 upper lip morphogenesis. Furthermore the presence of P63 binding ≤ 150 kb from their TSSs in E11.5 facial processes could provide further evidence of direct regulation by P63. In addition the biological function of each gene is highly relevant to P63-mediated upper lip morphogenesis, where P63 down-regulation within the epithelial seams at the site of facial process contact, is followed by apoptosis and differentiation to facilitate fusion of the facial processes (Thomason *et al*. 2008). The results presented here, could suggest a mechanism by which P63 inhibits expression of *Pax6* and *Sox2* during facial process outgrowth, and following P63 down-regulation within the epithelial seams, up-regulation of *Pax6* and *Sox2* contributes to the epithelial differentiation observed (Thomason *et al*. 2008; Ouyang *et al*. 2014; Gontan *et al*. 2008). However, extensive further characterisation of *Pax6* and *Sox2* expression in upper lip development will need to be completed to investigate this hypothesis.

A loss of P63 signalling was found to result in the significant down-regulation of multiple members of the Wnt signalling network. In addition, use of the BAT-Gal reporter for canonical Wnt signalling, showed a marked reduction in the activity of Tcf/Lef signalling complexes throughout the lateral nasal, medial nasal and maxillary processes of E11.5 *Trp63*$^{-/-}$ embryos compared with wildtype (Maretto *et al*. 2003). The presence of P63 binding ≤ 150 kb coupled with the expression changes observed and the overlap in Wnt-related expression patterns with *Trp63* suggests that P63 may regulate the expression of multiple Wnt ligands, receptors, co-factors and effectors during upper-lip morphogenesis. Furthermore characterisation of the Wnt-inhibition associated gene, *Shh*, showed a reduction in *Shh* expression at the site of the lambdoidal junction in *Trp63*$^{-/-}$ embryos (Kurosaka *et al*. 2014). Reduction of *Shh* expression should lead to an increase in Wnt signalling activity, however as a reduction was observed, it provides further evidence that P63 may provide a *Shh*-independent mechanism during upper lip morphogenesis. However this relationship will need to be further characterised and will this will be discussed in the following chapter.

If P63-mediated reduction of Wnt signalling does contribute to the phenotype of *Trp63*$^{-/-}$ embryos, induction of Wnt signalling could affect a partial-phenotypic rescue. As such a pregnant dam was injected with LiCl, an inducer of canonical Wnt signalling (Clément-

Lacroix *et al*. 2005; Song *et al*. 2009). Embryos collected at E14.5 failed to display any phenotypic change from expected. However due to limited numbers of *Trp63*$^{+/-}$ mice available for breeding, the experiment could only be completed once, and additional investigation of higher concentrations of LiCl and injection protocols is required.

In addition to Wnt signalling, the expression of Fgf receptors, *Fgfr2* and *Fgfr3*, were found to be down-regulated in the absence of P63. Furthermore expression of the Fgf inhibitor *Spry2* was expanded within the medial nasal processes. Loss of *Spry2* expression has previously been shown to result in increased levels of mesenchymal proliferation (Welsh *et al*. 2007; Matsumura *et al*. 2010). These results could suggest that a loss of P63 regulation may induce a reduction in the expression of the proliferation-positive *Fgfr2* and *Fgfr3* and expansion of the proliferative-inhibitor *Spry2* (Matsumura *et al*. 2010; Sayan *et al*. 2010; Ferone *et al*. 2012). The association between P63-mediated Fgf signalling and proliferation within the facial processes has previously been proposed by Thomason and colleagues, who suggested a loss of *Fgf8* expression contributed to the loss of proliferation observed in *Trp63*$^{-/-}$ medial nasal, lateral nasal and maxillary processes (Thomason *et al*. 2008). Together these results could suggest a mechanism by which P63 regulated facial process proliferation via the regulation of multiple members of the Fgf signalling network.

The work described within this chapter would suggest that P63 functions to regulate the expression of multiple members of the Wnt and Fgf signalling networks and provides further evidence to the complexity of transcriptional regulation and signalling network cross talk present during facial embryogenesis. Further characterisation of the P63 interactions presented here will be required and will be further discussed in the following chapter.

5.0 Discussion and further work

The aim of this project was to identify novel targets of P63 regulation during upper lip morphogenesis. Human mutations in *TP63* cause conditions such as ectrodactyly-ectodermal dysplasia clefting and ankyloblepharon-ectodermal dysplasia clefting, which are characterised by cleft lip and palate, malformed and truncated limbs and defects of the ectoderm derived tissues (Rinne *et al*. 2007). As such the role of P63 in secondary palate development has been extensively characterised, however the role of P63 in primary palate development is largely unknown (Thomason *et al*. 2008; Thomason *et al*. 2010; McDade *et al*. 2012). During upper lip morphogenesis, *Trp63* has been shown to be expressed throughout the epithelium of the developing facial processes and is required for correct regulation of proliferation and apoptosis (Thomason *et al*. 2008). A loss of P63 regulation in mouse models results in a fully penetrant cleft lip and palate, however the direct molecular mechanisms of P63 regulation remain unknown (Yang *et al*. 1999; Mills *et al*. 1999). Within the present study a two-tiered research approach was adopted to allow the high throughput identification of P63 binding sites in E11.5 facial processes and genes differentially regulated between *Trp63*$^{-/-}$ and *Trp63*$^{+/+}$ facial processes. While a similar research approach has been utilised by other groups in *Trp63* characterisation, P63 has been shown to function in a tissue specific manner (Kouwenhoven *et al*. 2010; McDade *et al*. 2012; Mitchell *et al*. manuscript in preparation). As such this study presents the first high throughput characterisation of P63 target genes in upper lip development using stage appropriate tissue. Identified potential target genes were characterised using ChIP-qPCR, qPCR and WISH. Using the described methods, potential P63-related regulation of Wnt and Fgf signalling was identified during upper lip morphogenesis.

5.1 A data set of P63 binding sites and putative target genes was generated

To identify targets of P63 regulation, ChIP-Seq was conducted on chromatin isolated from E11.5 wildtype facial processes. 41 randomly selected peaks were chosen and assayed using ChIP-qPCR to generation a minimum validation score for peak calling. Using MACS, 10,209 potential P63 binding sites were identified, with 83.9% containing the P63 specific binding motif. As has previously been discussed (Chapter 3.4.2), the number of binding sites negative for the P63 binding motif was within the expected range, in keeping with previous studies (Kouwenhoven *et al*. 2010; McDade *et al*. 2012; Kouwenhoven *et al*. 2015). Furthermore, ChIP-Seq functional annotation using GREAT analysis identified enrichment for genes related to cellular adhesion, Fgf signalling and Wnt signalling as well as identifying an enrichment for previously validated targets of TAp63 regulation. It is important to note that previous studies such as those by Kouwenhoven, McDade and Mitchell and colleagues identified enrichments within the same functional groups within their P63 ChIP-Seq data sets (Kouwenhoven *et al*. 2010; McDade *et al*. 2012; Mitchell *et al*. manuscript in preparation). As

such the identification of common functional groups between the studies would suggest the generated ChIP-Seq data set is a reliable representation of P63 binding.

Furthermore, binding site overlaps were seen with markers of transcriptional regulation, with 1.6% of identified P63 binding sites overlapping with a recently identified database of P300 facial enhancer sites (Attanasio *et al*. 2013). In addition P63 sites were shown to overlap with markers for active transcriptional regulation including H3k27ac, H3k4me3 and H3k27me3 sites (Kuzmichev *et al*. 2002; Barski *et al*. 2007; Tie *et al*. 2009). The presence of active markers of gene regulation overlapping with the identified P63 binding sites suggested identified P63 sites were involved in the regulation of target genes during upper lip morphogenesis. While the overlap between identified P63 sites and active markers of regulation, as well as enrichment for P63-related functions suggested the data set was accurate and reliable, ChIP-qPCR analysis of prospective binding sites showed that of the 62 binding sites assayed using ChIP-qPCR, 45 displayed significant positive enrichment by P63 ($p= 0.05$). This would suggest that 30% of binding sites assayed were not bound by P63 during upper lip morphogenesis.

It is important to remember that the ≥ 3 fold occupancy of the negative control *Myoglobin* was an arbitrary benchmark imposed upon the data. However as the minimum validation score was generated using this benchmark, it would be expected that all subsequent analysis of binding sites would meet it. The failure of all binding sites to meet this benchmark could therefore be indicative of two things. In contrast to primers for qPCR, ChIP-qPCR primers were not pre-screened with the same stringency. As qPCR primers were used to generate a quantification of cDNA levels of standardised samples, prior to use primer efficiencies were calculated and only primers exhibiting an efficiency of ≥ 95% were used. In contrast ChIP-qPCR primers were used to generate an approximation of chromatin occupancy relative to the negative control of samples which had not been standardised. As such primer efficiencies may impact upon the reliability of results obtained (Tong *et al*. 2015).

The apparent discrepancy between the numbers of binding sites displaying positive enrichment by P63 within the data set could also be attributed to the methodology adopted. As previously described (Chapter 3.4.4), while MACS peak calling software includes the ability to generate a minimum validation score which can limit the number of false positive results, it has been suggested that the use of input DNA for a comparative ChIP-Seq provides a more stringent method for peak calling (Zhang *et al*. 2008; Diaz *et al*. 2012). In addition previous studies have made use of multiple P63 antibodies in the generation of P63 binding site databases (McDade *et al*. 2012). While the chosen H129 antibody, which is specific to the α tail of P63α isoforms, was specific to the predominant P63 isoform expressed during embryogenesis, ΔNp63α, the comparative use of an additional antibody could improve the accuracy and reproducibility of the data set. Therefore further work including this data set should repeat the E11.5 H129 ChIP-Seq to include the input sample

and comparison between the generated data sets is likely to generate a more stringent data set. Furthermore it may prove additionally helpful to complete a second ChIP-Seq using a second P63-specific antibody such as the 4A4 pan-P63 antibody used by Kouwenhoven and colleagues to provide additional stringency to the data set (Kouwenhoven *et al*. 2010).

Throughout the analysis pipeline, attempts have been made to identify and limit possible sources of error. As such a potential source of error was identified in the intersection protocol. The E11.5 ChIP-Seq and E12.5 microarrays were intersected to identify the nearest significantly differentially expressed gene to each potential P63 binding site, at a maximum distance of 150 kb. As such genes which exceeded the 150 kb distance would be discarded, furthermore, if two differentially expressed genes were present within 150 kb, only the closest gene would be associated with the peak. Additionally as exemplified by *Wnt9b*, microarray analysis is a quantitative measure, as such spatial expression changes would not be detected. *Wnt9b* failed to show significant differential expression between E11.5 and E12.5 *Trp63*$^{+/+}$ and *Trp63*$^{-/-}$ by microarray and qPCR analyses. However analysis using WISH identified down-regulation of *Wnt9b* within the epithelium of the maxillary processes and the lambdoidal junction (Chapter 4.3.4). In contrast an expansion of *Wnt9b* expression was seen within the oral epithelium of the medial nasal processes. It was therefore suggested that *Wnt9b* was not identified as a significantly differentially expressed gene due to the medial nasal expansion compensating for the maxillary reduction.

In addition to *Wnt9b*, expression of *Lrp6* and *Lef1* was shown to be modified in *Trp63*$^{-/-}$ embryos within only one of the facial processes, with *Lef1* expression down-regulated in the maxillary processes and *Lrp6* expression expanded within the lateral nasal processes, compared to wildtype. It has previously been shown that P63 may function in a tissue specific manner, with the P63 binding site SHFM-BS1 regulating *DLX5*/*DLX6* expression during limb development but not in orofacial development (Lacono *et al*. 2008; Kouwenhoven *et al*. 2010). As such these results would suggest two important areas for further work. Firstly, within the current data set, facial processes were dissected in full, so that the medial nasal, lateral nasal and maxillary processes were all removed and subsequently, RNA or chromatin was isolated. It could however prove highly informative to dissect the individual facial processes and conduct microarray and ChIP-Seq analysis on them separately. This method would enhance the accuracy of the data in predicting process specific gene expression changes and would allow the process-specific characterisation of P63 regulation.

Secondly the current model of analysis presented in this study relies upon the assumption that the closest differentially expressed gene to each peak is likely the regulatory target. As such, peak to gene interactions are inferred by proximal binding and differential expression, but are not molecularly characterised relative to chromatin state. Further characterisation of potential target genes will require the confirmation of binding site to gene interaction. To do this it would be appropriate to employ chromatin conformation capture. Chromatin

conformation capture (3C) was originally developed by the Kleckner group to identify the frequency of interactions between two genomic loci (Dekker *et al*. 2002). The basic principles of 3C are as follows (Figure 5.1): DNA protein complexes are cross-linked by the addition of formaldehyde; cross-linked DNA is then digested with restriction enzymes to generate fragments of the required length; digested fragments are subjected to ligation at a very low concentration to encourage ligation of cross-linked fragments over random ligation; cross-linking can then be reversed and individual ligation products are detected and quantified by PCR using locus-specific products (Dekker *et al*. 2002).

Due to the requirement of two primer sets, one for each suspected interacting loci, 3C can only be used when the sequence of both loci are known (Dekker *et al*. 2002). Subsequent research has resulted in the development of the circularised chromosome conformation capture (4C) protocol which makes use of the basic protocol of 3C using cross-linking of DNA, restriction digestion, fragment ligation and reversal of cross-linking (Dekker *et al*. 2002). Following the reversal of cross-linking, fragments are further digested with an additional restriction enzyme to produce smaller fragments (Zhao *et al*. 2006; Simonis *et al*. 2006). When incubated with high concentrations of DNA ligase for extended periods, fragments will circularise, as such a single primer pair for a loci, for example an individual P63 binding site, can be used to amplify all interacting loci, therefore allowing the identification of multiple interactions at a single genomic loci (Zhao *et al*. 2006; Simonis *et al*. 2006). Sequencing can then be used for the identification of interacting chromatin loci (Zhao *et al*. 2006; Simonis *et al*. 2006). In addition to 4C, carbon-copy chromosome conformation capture (5C) can be used for the high throughput sequencing of multiple genetic loci interactions (Dostie & Dekker, 2007).

In 5C, the initial stages of 3C are completed followed by ligation-mediated amplification using primers designed to be specific to the 3' end of predicted restriction fragments. Primers are designed to contain the T7/T3 promoter sequences and are ligated to the 3C fragments. Subsequently, T7/T3 promoter sequences are used as templates for the universal amplification of fragments using PCR (Dostie & Dekker, 2007). The resultant 5C library can then be interrogated using custom microarray or deep sequencing allowing the simultaneous analysis of millions of genomic interactions (Dostie & Dekker, 2007).

A recent modification of the 3C protocol known as ChIP-Loop Assay, combines the principles of 3C chromatin conformation analysis with the specificity of ChIP (Horike *et al*. 2005). In this modified protocol, chromatin is cross-linked and digested as according to 3C protocols, unbound proteins are removed and a standard ChIP protocol is completed to isolate fragments bound by the protein of interest. Subsequently fragments are ligated and analysed as according to 3C protocols (Horike *et al*. 2005). The use of this methodology

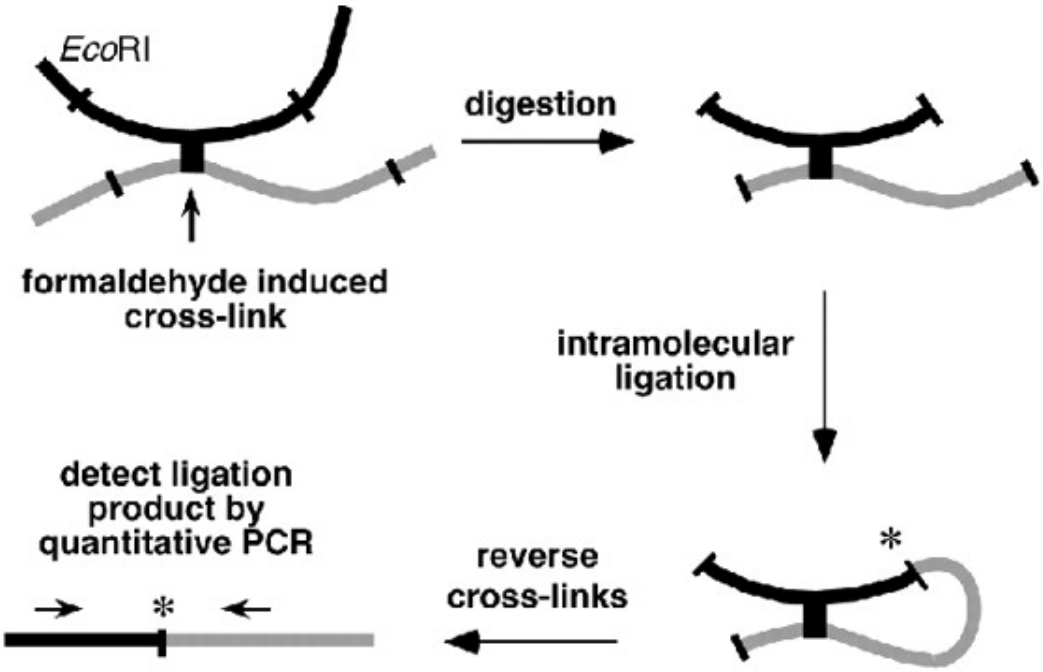

Figure 5.1 Chromatin conformation capture (3C). Chromatin conformation capture allows the identification of direct chromatin interactions. Isolated DNA is cross-linked using formaldehyde and subsequently digested using a frequently cutting restriction enzyme such as *Eco*RI. At a very low concentration, fragments are incubated with DNA ligase to encourage the ligation of cross-linked fragments. Cross-linking is reversed through high temperature incubation and fragments are subsequently detected using quantitative PCR (Adapted from Dekker *et al*. 2002).

would allow the analysis of P63-site-specific chromatin interactions and aid in the determination of binding site/gene interactions (Horike *et al*. 2005).

5.2 P63 regulates Wnt signalling during upper lip morphogenesis

Microarray/ChIP-Seq intersection identified the misregulation of multiple members of the Wnt signalling pathway, with P63 binding sites proximal to differentially expressed genes. 16 Wnt-related genes were further investigated using ChIP-qPCR, qPCR and WISH. In addition, the generation of *Trp63*$^{+/-}$*;BAT-Gal*$^{Tg/+}$ was used to identify a reduction in canonical Wnt signalling activity during E11.5 upper lip morphogenesis. It is therefore apparent that during normal facial development P63 up-regulates the expression of Wnt-related genes during upper lip morphogenesis.

Canonical Wnt signalling involves the cytoplasmic regulation of active β-catenin, meditated by the binding of secreted Wnt ligands to the cell surface receptors (Archbold *et al*. 2012). Active Wnt signalling results in the activation of Wnt transcription factor activity (Archbold *et al*. 2012). Within the present study Wnt ligands *Sfrp1*, *Wnt2b*, *Wnt3*, *Wnt3a*, *Wnt4*, *Wnt7a*, *Wnt7b*, *Wnt9b*, *Wnt10* and *Wnt11* were identified as potential target of P63 regulation. In addition, Wnt co-receptors *Lrp6*, *Fzd4* and *Fzd10* and the Wnt antagonist *Krm2* and effector *Lef1* were identified as putative P63 targets. ChIP-qPCR analysis showed P63 binding was present at sites proximal to the identified Wnt genes, excluding *Sfrp1* which did not display positive enrichment. Furthermore qPCR analysis showed *Lef1*, *Wnt3*, *Wnt4*, *Wnt3a*, *Wnt7a*, *Wnt7b*, *Wnt10b*, *Fzd10* and *Krm2* were significantly differentially expressed between *Trp63*$^{-/-}$ and *Trp63*$^{+/+}$ E11.5 facial processes. WISH analysis of *Wnt3*, *Wnt4*, *Lef1* and *Fzd10* identified epithelial expression throughout the facial processes with a loss of P63 regulation resulting in the down-regulation of Wnt genes, surrounding the nasal pits and lambdoidal junction.

Due to a limited availability of *Trp63*$^{-/-}$ and *Trp63*$^{+/+}$ embryos it was not possible to characterise the expression profile of all implicated Wnt genes. As such this would be the initial priority, to characterise each potential target gene's expression at E11.5. Subsequently, it would prove highly informative to characterise the expression profile of all potential target genes throughout upper lip development from E9.5 to E13.5 using WISH in both *Trp63*$^{+/+}$ and *Trp63*$^{-/-}$ embryos. Additionally post WISH, embryos can be fixed and sectioned to provide greater detail of tissue expression. It is hypothesised that P63 regulation of the diffusible Wnt ligands provides a mechanism of epithelial to mesenchymal signalling, as such it is important to characterise the tissue localisation of Wnt proteins between *Trp63*$^{+/+}$ and *Trp63*$^{-/-}$ facial processes using immunohistochemistry. Finally the proposed model of P63 up-regulation of Wnt-related proteins is inferred from the down-regulation of Wnt proteins in the absence of P63 and the presence of a P63 binding motif proximal to each target gene. P63 regulation of target binding sites will need to be

interrogated using Luciferase reporter assays to confirm if P63 regulation is active at each site and if P63 up or down-regulates expression at each site.

Luciferase reporter assays involve the insertion of a target sequence, in this case identified P63 binding sites, upstream of the luciferase reporter construct. Additionally a constitutively active expression vector containing *TP63* is added to cells containing the luciferase reporter construct. For the purpose of this study, these experiments would be conducted using human osteosarcoma Saos-2 cells which have been shown to be P53 null and express low levels of endogenous *TP63* (Kubbutat *et al*. 1998). Luciferase reporter activity is then measured via the addition of the luciferase substrate, luciferin, producing a quantifiable light (Thorne *et al*. 2010). This method would further confirm P63's capability to bind at identified sites and determine if P63 regulation is present. Furthermore as previously utilised by other studies into P63 function, functional residues within the P63 binding site can be modified using site directed mutagenesis to provide further verification that P63 binding is specific (Kouwenhoven *et al*. 2010; Thomason *et al*. 2010). Additionally previous studies have introduced common human mutations into *TP63* expression vectors using site directed mutagenesis (Ferone *et al*. 2011). Use of modified *TP63* expression vectors would allow the further characterisation of P63 regulation of target sites as well as providing data relevant to the molecular mechanisms of human *TP63*-related conditions

5.3 A putative P63/Wnt feedback regulatory loop

The work of Ferretti and colleagues has previously been discussed in detail (Chapter 1.4.5). The group identified the down-regulation of *Wnt3* and *Wnt9*b within the facial processes of *Pbx1*$^{-/-}$;*Pbx2*$^{+/-}$ embryos and identified Pbx-Prep (Meis) binding sites within the intergenic region between *Wnt3* and *Wnt9b* (Ferretti *et al*. 2011). Furthermore *Trp63* expression was shown to be attenuated in *Pbx1/2* compound mutants and *Wnt9b* knockout embryos. A Tcf/Lef binding site was identified within the *Trp63* promoter and shown to be active in *Trp63* up-regulation, suggesting Wnt signalling directly regulated *Trp63* expression during upper lip morphogenesis (Ferretti *et al*. 2011). Within the present study P63 binding sites have been identified within 150 kb of multiple Wnt-related genes including those implicated in the Ferretti study, *Wnt3*, *Wnt9b* and *Lef1* (Ferretti *et al*. 2011). Furthermore the epithelial expression of *Wnt3* and *Wnt9b* within the facial processes, at the lambdoidal junction, was shown to be down-regulated in *Trp63*$^{-/-}$ embryos compared with wildtype. Taken together these results could suggest that P63 and Wnt signalling may function in a positive feedback regulation loop, by which P63 up-regulates expression of *Wnt3*, *Wnt9b* and *Lef1* which subsequently up-regulate *Trp63* expression. The further characterisation of Wnt expression during upper lip morphogenesis of *Trp63*$^{+/+}$ and *Trp63*$^{-/-}$ embryos previously suggested (Section 5.2) would further elucidate if such a mechanism is present.

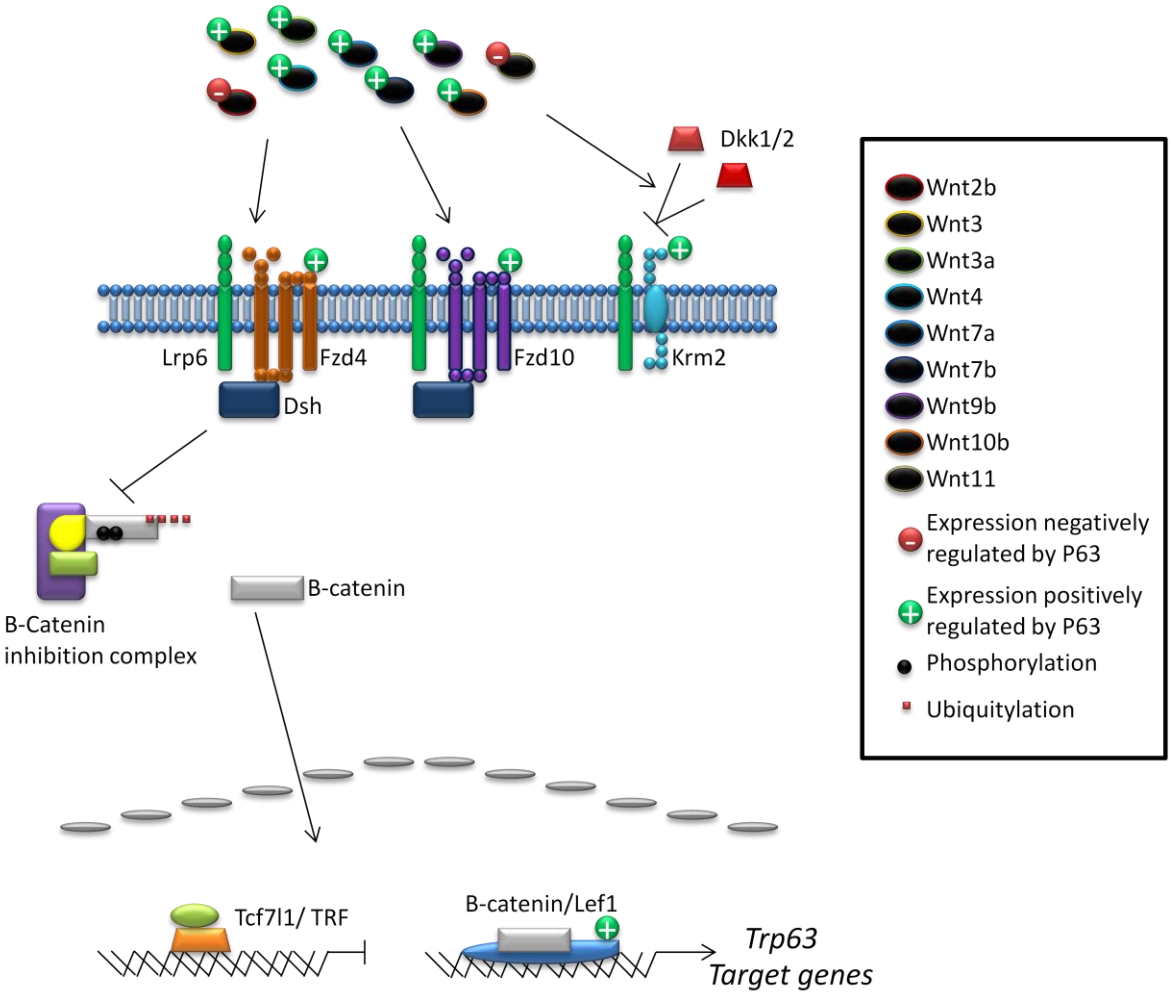

Figure 6.2 P63 regulates multiple members of the Wnt signalling pathway. Schematic representation of the canonical Wnt signalling network. Wnt signalling is activated by the binding of Wnt ligands to co-receptors Lrp6 and Fzd4/10. Wnt/receptor binding can be inhibited by Dkk1/2 binding to Krm2/Lrp6 causing internalisation of Lrp6 receptors. Wnt/receptor binding phsosphorylates the cytoplasmic protein Dishevelled (Dsh) which relieves β-catenin inhibition, allowing cytoplasmic accumulation of β-catenin. β-catenin translocates to the nucleus and relieves transcriptional repression by Tcf7l1/transcriptional repression factors (TRF) allowing Lef1 mediated transcription of target genes including *Trp63*. Multiple members of the Wnt signalling pathway were identified as prospective target of P63 signalling. (Krasnow *et al*. 1995; Tamai *et al*. 2004; Ferretti *et al*. 2011; Zhang *et al*. 2012; Arkell *et al*. 2013).

.

5.4 Canonical Wnt signalling is attenuated in E11.5 *Trp63*$^{-/-}$ facial processes

Due to the down-regulation of multiple members of the Wnt signalling network, *Trp63*$^{+/-}$*;BAT-Gal*$^{Tg/+}$ reporter mice were generated to examine canonical Wnt signalling activity in *Trp63*$^{-/-}$ embryos. Comparative analysis at E11.5 showed a marked reduction in canonical Wnt signalling activity within the medial nasal, lateral nasal and maxillary processes, suggesting P63 regulation is required to canonical Wnt activity. In addition, induction of the canonical Wnt signalling was attempted using intraperitoneal injection of lithium chloride at E11.5 to determine if induction of Wnt signalling could affect a phenotypic rescue. Due to a lack of *Trp63*$^{-/+}$ mice, only an initial experiment could be completed, which failed to generate any phenotypic effect.

Within the present study, *BAT-Gal* reporter mice were used to visualise canonical Wnt activity, however it is important to note that other reporter strains are available (Alam *et al*. 2011). Importantly, comparative analysis between three reporter mice, *BAT-Gal*, *TOP-Gal* and *Axin2*^{LacZ} mouse lines identified subtle differences in the identified domains of Wnt activity (Alam *et al*. 2011). In E11.5 and E13.5 whole embryos the *BAT-Gal* reporter mouse appeared to identify the broadest regions of canonical Wnt activity, with *TOP-Gal* and *Axin2*^{LacZ} strains presenting more subtle expression patterns. Due to the variation in reporter mouse specificity, it may prove prudent to assay the impact of *Trp63*$^{-/-}$ on a second reporter strain (Alam *et al*. 2011).

Lithium chloride injections were completed as previously published by Song and colleagues, however no phenotypic effect was apparent (Song *et al*. 2009). It is important to note that Song and colleagues used lithium chloride injections to modify the expression patterns of *Lrp6*-mediated canonical Wnt targets, as such for the purpose of this study a higher dosage of lithium chloride may be required (Song *et al*. 2009). It remains possible that if attenuation of Wnt signalling does contribute to the *Trp63*-cleft phenotype, sufficient Wnt induction may induce a phenotypic effect. As such subsequent experiments should include a range of lithium chloride dosages. In addition, within the present study two injections were administered at E8.5 and E9.5 in line with previous studies (Song *et al*. 2009). However it may prove prudent to administer injections daily for the entirety of upper lip morphogenesis from E8.5 to E11.5 to ensure sufficient Wnt induction. Use of the generated *Trp63;BAT-Gal* reporter mice could be used to identify the optimal lithium chloride dose to return wildtype levels of canonical Wnt activity, if possible. Subsequently, should wildtype canonical Wnt activity be restored, but no phenotypic effect is observed, this would discount a reduction of Wnt signalling as a major cause of the *Trp63*-clefting phenotype. However should lithium chloride induction induce a phenotypic effect, subsequent follow-up research could be conducted on mouse models of human mutations including the *Trp63*^{R279H} mouse and could provide further insights into the pathology of human *TP63* mutations (Lindahl *et al*. 2013).

5.5 P63 inhibits the expression of differentiation factors during upper lip morphogenesis

Identification of Wnt-related genes, showed *Pax6* and *Sox2* were up-regulated in the absence of P63. Previous studies indicate that a loss of Pax6 or Sox2 regulation results in abnormal differentiation (Gontan *et al*. 2008; Li *et al*. 2008; Ouyang *et al*. 2014). In addition the pro-differentiation factor *Irf6* has been shown to be a target of P63 regulation in both the secondary palate and primary palate (Thomason *et al*. 2010; Ferretti *et al*. 2011). During secondary palate development *Trp63* expression is highly similar to that of upper lip and primary palate development, with *Trp63* expressed within the medial edge epithelia of the palatal shelves, during palatal shelf outgrowth. Following shelf contact and adhesion *Trp63* expression is detected within the medial epithelial seam, where it up-regulates *Irf6* expression (Thomason *et al*. 2010). Increased expression of *Irf6* results in the proteasome-dependent degradation of P63, reducing proliferation and allowing differentiation (Moretti *et al*. 2010).

There is a clear functional overlap between *Sox2*, *Pax6* and *Irf6*. As such, in light of the up-regulation of *Sox2* and *Pax6* in the absence of P63, it could be suggested that during normal facial process development, *Trp63* expression in the facial processes epithelium inhibits expression of *Sox2* and *Pax6* during process outgrowth to maintain proliferation and prevent differentiation. Following up-regulation of *Irf6*, and the subsequent contact between facial processes, the proteasome dependent degradation of P63 would relieve inhibition of *Sox2* and *Pax6* and thus induce differentiation. It is interesting to note that Pax6 and Sox2 appear to display opposing roles in the regulation of differentiation, with Sox2 inducing differentiation, while Pax6 inhibits differentiation (Ouyang *et al*. 2014; Gontan *et al*. 2008). It could therefore be suggested P63-regulation of both genes modulates epithelial differentiation during upper lip morphogenesis. Further characterisation of *Sox2* and *Pax6* expression and protein concentration and localisations throughout upper lip morphogenesis would need to be conducted as previously described in reference to the Wnt genes (Section 5.2).

5.6 P63 regulates multiple members of the Fgf signalling pathway during upper lip morphogenesis

ChIP-Seq and microarray analyses identified the misregulation of four members of the Fgf signalling network, *Fgfr2*, *Fgfr3*, *Spry1* and *Spry2*. Previous studies have identified Fgf signalling as a target of P63 regulation during embryogenesis, with *Fgfr2* and *Fgfr3* targets of P63 regulation in embryonic skin and *Fgf8* down-regulated in *Trp63*$^{-/-}$ facial processes (Thomason *et al*. 2008; Ferone *et al*. 2012). Loss of *Fgf8* regulation in upper lip morphogenesis was suggested to directly contribute to the cleft lip and palate phenotype observed (Thomason *et al*. 2008). Fgfr2 and Fgfr3 receptors act as mediators of Fgf signalling through binding of ligands such as Fgf8 (Dorey & Amaya, 2010). Previous studies

have shown that Fgf signalling, mediated by Fgfr2 and Fgfr3 is involved in the regulation of differentiation and proliferation (Iseki *et al*. 1999; Zhang *et al*. 2015).

Within the present study down-regulation of *Fgfr2* and *Fgfr3* expression was observed in the absence of P63 during lip development, suggesting in normal development P63 up-regulates the expression of the Fgf receptors *Fgfr2* and *Fgfr3* and the Fgf ligand *Fgf8* (Thomason *et al*. 2008). However it was not possible within this study to complete WISH analysis of *Fgfr2* and *Fgfr3* expression in *Trp63*$^{-/-}$ and *Trp63*$^{+/+}$ E11.5 embryos. In addition expression of Fgf inhibitors, *Spry1* and *Spry2*, was altered in *Trp63*$^{-/-}$ facial processes. WISH analysis of *Spry1* failed to display observable differences between wildtype and null embryos. However *Spry2* expression appeared expanded within the medial nasal processes. Therefore it could be suggested P63 inhibits *Spry2* expression during upper lip morphogenesis to maintain the proliferative potential of facial processes, and the loss of inhibition in *Trp63*$^{-/-}$ embryos may contribute to the hypoproliferative phenotype observed (Thomason *et al*. 2008; Welsh *et al*. 2007; Matsumura *et al*. 2010).

Characterisation of Wnt signalling molecules was prioritised during this study, as such expression of Fgf-related genes in *Trp63*$^{-/-}$ embryos remains uncharacterised. Therefore as previously described in reference to Wnt signalling (Section 5.2) extensive further investigation of Fgf genes will be required.

5.7 Further characterisation of identified P63 binding sites

P63 scan analysis of identified P63 binding sites showed 17.1% of identified binding sites did not contain the characterised P63 binding motif (Chapter 3.4.2). The presence of P63 binding sites lacking the P63 binding motif could be indicative of a number of factors: It could suggest that P63 binds in the presence of a transcriptional co-factor; that P63 is binding at a half-site not recognised by P63 scan; or that P63 is binding at a currently uncharacterised binding site. Therefore further investigation of this subset of binding sites could be highly informative of P63 function. As previously discussed, the P63 scan programme was modified from the P53 scan programme and detects P63 binding sites based on the presence of two P63 half-sites with no medial spacer element (Smeenk *et al*. 2008; Kouwenhoven *et al*. 2010). P63 has previously been shown to be able to bind to a singular half site (Chen *et al*. 2011). Therefore, scanning of P63 motif-negative peaks for the presence of a single P63 half-site could reveal if there is an enrichment of these sites within the data and could characterise an inherent weakness in the design of P63 scan.

P63 has also been shown to associate directly with a number of binding partners including P300, Sox2 and AP2α (Avantaggiati *et al*. 1997; McDade *et al*. 2012; Watanabe *et al*. 2014). It could therefore prove highly informative to conduct motif discovery using a programme such as MEME Suite, to determine if there is an enrichment for additional transcription factor

binding sites (Bailey *et al*. 2009). Motif discovery could identify the enrichment of a known P63-co-factor or could identify novel co-factors of P63 regulation.

5.8 Summary

Potential P63 regulation of Wnt and Fgf signalling has been identified. It is suggested P63 signals via the Wnt and Fgf signalling network to regulate epithelial to mesenchymal interactions and to maintain the proliferative and differential potential of developing facial processes. While P63 binding sites have been identified proximal to differentially expressed genes, further characterisation is required. Proposed further work includes the full characterisation of target gene expression during upper lip morphogenesis, ChIP loop assay, luciferase reporter assays, further characterisation of canonical Wnt activity, and expansion of the LiCl experiments and further interrogation of the ChIP-Seq data set.

6.0 Summary and Conclusions

6.1 P63 regulates Wnt and Fgf signalling during upper lip morphogenesis

Human mutations in *TP63* result in conditions characterised by cleft lip and palate, malformation of the limbs and defects of the ectoderm derived tissues (Rinne *et al*. 2007). Due to the severe phenotype of *TP63*-related conditions, multiple animal models have been generated to investigate P63 function during development (Mills *et al*. 1999; Yang *et al*. 1999; Romano *et al*. 2012; Lindahl *et al*. 2013). Using the *Trp63*$^{-/-}$ mouse model, the role of P63 signalling in secondary palate development has been characterised, however the molecular targets of P63 in upper lip development remain largely uncharacterised (Thomason *et al*. 2008; Thomason *et al*. 2010). The aim of this project was to identify novel targets of P63 regulation during upper lip morphogenesis. Towards this aim, a two-tiered research strategy was adopted. Sites of P63 binding were identified using ChIP-Seq of E11.5 wildtype facial processes and genes differentially regulated by P63 were identified by microarray analysis of E11.5 and E12.5 *Trp63*$^{+/+}$ and *Trp63*$^{-/-}$ facial processes. Subsequently identified genes were further interrogated using ChIP-qPCR, qPCR and WISH. This study has identified a potential misregulation of Wnt and Fgf signalling during E11.5 upper lip morphogenesis, providing a mechanism by which P63 regulates epithelial to mesenchymal signalling.

Previous characterisation of *Trp63* expression has shown it is expressed throughout the epithelia of the medial nasal, lateral nasal and maxillary processes at E11.5, with expression detected at the lambdoidal junction (Thomason *et al*. 2008; Kurosaka *et al*. 2014). E11.5 is a key developmental time point in upper lip morphogenesis, at which the epithelia of the medial nasal, lateral nasal and maxillary processes have contacted and are beginning to undergo fusion (Jiang *et al*. 2006). At the site of epithelial contact between the facial processes known as the lambdoidal junction, a double epithelial seam is formed at each contact region which must be degenerated to allow successful upper lip fusion (Som & Naidich, 2013a). Furthermore at this stage of development, *Trp63*$^{-/-}$ embryos display a fully penetrant bilateral cleft lip and palate suggesting comparative expression analysis between WT and null facial processes would identify targets of P63-regulation (Mills *et al*. 1999; Yang *et al*. 1999; Thomason *et al*. 2008).

ChIP-Seq analysis using chromatin isolated from E11.5 wildtype facial processes identified 10,209 potential P63 binding sites, with 83.1% of binding sites containing the characterised P63 binding motif. Previous studies have identified targets of P63-regulation using high throughput methods including microarray and ChIP-Seq analyses (Kouwenhoven *et al*. 2010; McDade *et al*. 2012; Kouwenhoven *et al*. 2015). The studies by Kouwenhoven and McDade and colleagues identified in excess of 11,000 and 7000 potential P63 binding sites respectively (Kouwenhoven *et al*. 2010; McDade *et al*. 2012). Kouwenhoven and colleagues identified a P63 binding site, SHFM1-BS1 suggested to regulate the expression of

DLX1/*DLX2* in human primary keratinocytes taken from patients suffering from SHFM (Kouwenhoven *et al*. 2010). Luciferase reporter assays showed P63-regulation of *DLX1*/*DLX2* expression via SHFM1-BS1 was active during limb development, however failed to display activity in craniofacial tissue (Kouwenhoven *et al*. 2010). These results would suggest P63 functions in a tissue specific manner, underpinning the requirement of context and stage appropriate tissue, in the identification of P63 regulation. This finding was further confirmed via the intersection of the E11.5 ChIP-Seq data generated in this study against a previously published E14.5 palatal shelf data set (Mitchell *et al*. manuscript in preparation). ChIP-Seq intersection 25% of P63 binding sites identified at E11.5 were present within the E14.5, with 75% appearing to be specific to upper lip development (Mitchell *et al*. manuscript in preparation). As such this study presents the first whole-genome, high throughput analysis of P63 function in upper lip development using stage appropriate tissue.

Generated microarray and ChIP-Seq data sets were analysed using multiple parameters including multiple measurements of significance and variable ChIP-Seq/microarray intersection distances. DAVID and GREAT functional annotations tools were used in the prioritisation of potential target genes throughout the analysis process. Analysis of the data sets, in isolation and combined identified an enrichment for genes associated with biological adhesion, Wnt and Fgf signalling (Chapter 3). Previous studies have identified similar functional enrichments, which provided further evidence that the generated data sets were both accurate and reliable (Kouwenhoven *et al*. 2010; McDade *et al*. 2012; Kouwenhoven *et al*. 2015; Mitchell *et al*. manuscript in preparation). Furthermore, the presence of enrichment for these functions throughout all stages of analysis suggested these were valid functional targets of P63-regulation. Therefore, based on gene ontology and nCounter analyses a target gene list of 21 Wnt- and Fgf-associated genes was generated for further analysis (Chapter 4.3.1).

It has previously been suggested that the presence of abnormalities within the ectoderm-derived tissues such as teeth and hair follicles in *Trp63*$^{-/-}$ mice, which are formed through epithelial to mesenchymal interactions, implicate P63 function in epithelial to mesenchymal regulation (Mills *et al*. 1999; Yang *et al*. 1999). *Trp63* is expressed within the epithelia (Mills *et al*. 1999; Yang *et al*. 1999; Laurikkala *et al*. 2006; Thomason *et al*. 2008; Thomason *et al*. 2010). In *Trp63*$^{-/-}$ embryos, the cleft lip and palate phenotype was attributed to inappropriate apoptosis within the epithelia and a lack of mesenchymal proliferation (Thomason *et al*. 2008). Wnt signalling consists of secreted, diffusible Wnt ligands which bind to cell surface receptors which mediate down-stream signalling pathways implicated in the regulation of proliferation and differentiation (Arkell *et al*. 2013). It was therefore hypothesised that P63-regulation of Wnt signalling could function as the mechanism of P63 epithelial-mesenchymal regulation.

Binding of P63 was identified proximal to multiple Wnt-related genes including *Wnt3*, *Wnt4*, *Wnt9b*, *Fzd4*, *Fzd10*, *Krm2* and *Lef1* (Chapter 3). P63 binding proximal to identified Wnt

genes was validated using ChIP-qPCR and showed all identified Wnt-associated genes, excluding *Sfrp1*, displayed significant positive enrichment between by P63 (Chapter 4). Additionally binding sites were found to overlap with markers of active transcriptional regulation including H3k4me1, H3k27ac and H3k27me3 sites identified in mouse facial and palatal shelf tissue (Kuzmichev *et al*. 2002; Barski *et al*. 2007; Tie *et al*. 2009). qPCR analyses of target gene expression between E11.5 *Trp63*$^{-/-}$ and *Trp63*$^{+/+}$ facial processes identified the significant differential expression of 11 Wnt-associated genes, with *Wnt11* displaying significant up-regulation and *Wnt3*, *Wnt3a*, *Wnt4*, *Wnt7a*, *Wnt7b*, *Wnt10b, Fzd10*, *Grhl3*, *Krm2* and *Lef1* displaying significant down-regulation (Chapter 4).

Further characterisation of putative target genes was limited due to a lack of *Trp63*$^{-/-}$ and *Trp63*$^{+/+}$ embryos. However the expression patterns of *Wnt3*, *Wnt4*, *Wnt9b*, *Fzd10*, *Grhl3*, *Lef1*, *Pax6* and *Sox2* were shown to putatively overlap with *Trp63* expression in E11.5 facial processes, with expression detected within the epithelium of the facial processes and within the lacrimal groove and lambdoidal junction (Chapter 4). While further characterisation is required, the presence of P63 binding sites proximal to each gene, coupled with the expression differences observed between WT and null embryos could suggest P63 directly regulates multiple members of the Wnt signalling network during upper lip morphogenesis. Additionally it has been shown that Shh and Wnt signalling interact, with Wnt signalling negatively regulated via Shh signalling (Kurosaka *et al*. 2014). Expression of *Shh* was therefore investigated within *Trp63*$^{-/-}$ facial processes and found to be down-regulated within the epithelium of the lambdoidal junction (Chapter 4.3.5). A loss of *Shh* signalling should induce up-regulation of Wnt signalling, therefore the overall down-regulation of Wnt signalling within the presented data set gives further credence to the hypothesis that P63 directly regulates Wnt expression during upper lip morphogenesis in a Shh-independent manner (Kurosaka *et al*. 2014).

Wnt signalling functions via a number of pathways including canonical Wnt signalling which involves the cytoplasmic regulation of levels of active β-catenin (Arkell *et al*. 2013). Disruption of canonical Wnt signalling has previously been shown to result in a cleft lip and palate phenotype due to reduced levels of proliferation and so was characterised in *Trp63*$^{-/-}$ embryos using the BAT-gal reporter mouse (Kawakami *et al*. 2014). Wnt canonical signalling was shown to be attenuated throughout the medial nasal, lateral nasal and maxillary processes. Furthermore, the previous association between regulation of proliferation and canonical Wnt signalling provides further support for the hypothesis that Wnt signalling may mediate P63 epithelial to mesenchymal regulation of proliferation. Additionally LiCl has been shown to be a potent inducer of canonical signalling, with LiCl induction rescuing the orofacial phenotype of chicks in which canonical Wnt signalling was disrupted (Kawakami *et al*. 2014). It was hypothesised induction of canonical Wnt signalling in *Trp63*$^{-/-}$ embryos could induce a phenotypic effect, however the experiment could not be fully completed.

In addition to regulating proliferation, Wnt-associated genes *Pax6* and *Sox2* were identified as down-regulated in *Trp63*$^{-/-}$ embryos. Both *Pax6* and *Sox2* have been shown to regulate epithelial differentiation, with over-expression of *Pax6* or *Sox2* resulting in abnormal differentiation (Ouyang *et al*. 2014; Gontan *et al*. 2008). *Pax6* and *Sox2* display opposing functions, with loss of *Pax6* resulting in premature differentiation, while loss of *Sox2* results in a loss of differentiation (Ouyang *et al*. 2014; Gontan *et al*. 2008). It is therefore suggested that P63-regulation of *Sox2* and *Pax6* may function to modulate the epithelial differentiation observed in upper lip morphogenesis.

It has previously been suggested that P63 is a direct target of Wnt3/Wnt9b mediated signalling with a Lef1/Tcf site, active in upper lip morphogenesis, identified within the *Trp63* promoter region (Ferretti *et al*. 2011). The down-regulation of the genes *Wnt3*, *Wnt9b* and *Lef1* within the present study could suggest that a positive feedback-regulation loop is active during upper lip morphogenesis. It is therefore suggested that P63 expression up-regulates the expression of *Wnt3*, *Wnt9b* and *Lef1* during upper lip morphogenesis, which subsequently up-regulates *Trp63* expression. However it is currently unclear whether P63 or Wnt signalling initiates this system.

In addition to Wnt signalling, Fgf signalling was investigated. A loss of *Fgf8* expression in *Trp63*$^{-/-}$ embryos within the epithelium of the lambdoidal junction was suggested a contributory factor to the loss of mesenchymal proliferation in *Trp63*$^{-/-}$ embryos (Thomason *et al*. 2008). Within the present study additional members of the Fgf signalling network were identified as potential P63 target genes, including *Fgfr2*, *Fgfr3*, *Spry1* and *Spry2*. Expression of the Fgf receptors *Fgfr2* and *Fgfr3* was shown to be down-regulated in *Trp63*$^{-/-}$ E11.5 facial processes and P63 binding was confirmed proximal to these genes (Chapter 4). Both *Fgfr2* and *Fgfr3* have been identified as targets of P63 signalling in embryonic skin (Ferone *et al*. 2012). It was not possible to further characterise *Fgfr2* and *Fgfr3* expression within *Trp63*$^{-/-}$ and *Trp63*$^{+/+}$ embryos, however their previous association with regulation of differentiation and proliferation provides a biological relevance to P63-mediated upper lip development (Iseki *et al*. 1999; Zhang *et al*. 2015). *Spry1* and *Spry2* have been shown to be negative regulators of proliferation and so the over-expression in *Trp63*$^{-/-}$ embryos could provide a further mechanism for the hypoproliferative phenotype observed (Welsh *et al*. 2007; Thomason *et al*. 2008; Matsumura *et al*. 2010). While *Spry2* expression was shown to be expanded within *Trp63*$^{-/-}$ E11.5 facial processes, *Spry1* expression appeared unchanged. Expansion of *Spry2* expression provides further evidence to the hypothesis that misregulation of Fgf signalling contributes to the loss of proliferation in *Trp63*$^{-/-}$ facial processes (Chapter 4.3.14).

This project has provided further evidence that a loss of Wnt and Fgf signalling may contribute to the cleft lip and palate phenotype observed in *Trp63*$^{-/-}$ embryos. However further characterisation of P63/target gene interactions will be required. It is suggested further characterisation of target genes expression and protein distributions will need to be

conducted on WT and null embryos throughout upper lip morphogenesis. P63 binding site mediated regulation of target genes will need to be further confirmed using luciferase reporter assays and ChIP loop assay. The disruption of canonical Wnt signalling will need to be further characterised, LiCl experiments expanded and microarray analysis expanded to include analyses of individual facial processes. Finally identified P63 binding sites require further interrogation to identify potential P63 co-factors or motifs.

6.2 Conclusion

This project has produced a reliable and reproducible data set of potential P63 target genes. Using high throughput whole genome analyses, multiple genes of the Wnt and Fgf signalling networks have been identified as potential targets of P63-regulation during upper lip morphogenesis. Regulation of Wnt and Fgf signalling has been suggested as a potential mechanism of P63, epithelial to mesenchymal regulation and a potential P63/Wnt regulatory feedback mechanism has been proposed. This project has succeeded in the stated aim of expanding the P63 signalling network.

7.0 References

Abu-Issa. R, Smyth. G, Smoak. I, Yamamura. K & Meyers. E (2002) *Fgf8* is required for pharyngeal arch and cardiovascular development in the mouse *Development* 129 pp 4613-4625

Agochukwu. N, Soloman. B, Doherty. B, Doherty. E & Muenke. M (2012) The palatal and oral manifestations of Muenke Syndrome (FGFR3 related craniosyntosis) *Journal of Craniofacial Surgery* 23 (3) pp 664-668

Alam. D, Green. M, Irani. R, Parsa. S, Danopoulos. S, Sala. F, Branch. J, Agha. E, Tiozzo. C, Voswinckel. R, Jesudason. E, Warburton. D & Bellusci. S (2011) Contrasting expression of canonical Wnt signalling reporters *TOPGAL*, *BATGAL*, and *Axin2*^{LacZ} during murine lung development and repair *PLoS* DOI: 10.1371/journal.pone.0023139

Albert. I, Mavrich. T, Tomsho. L, Qi. J, Zanton. S, Schuster. S & Pugh. F (2007) Translational and rotational settings of H2A.Z nucleaosome across the *Saccharomycescerevisiae* genome *Nature* 446 pp 572-576

Aldhorae. K, Böhmer. A, Ludwig. K, Esmail. A, Al-Hebshi. N, Lippke. B, Gölz. L, Nöthen. M, Daratsianos. N, Knapp. M, Jäger. A & Mangold. E (2014) Nonsyndromic cleft lip with or without cleft palate in arab populations: Genetic analysis of 15 risk loci in a novel case-control sample recruited in Yemen *Birth Defects Research Part A*: *Clinical and Molecular Teratology* 100 (4) pp 307-313

Alkire. B, Hughes. C, Nash. K, Vincent. J & Meara. J (2011) Potential Economic Benefit of Cleft Lip and Palate Repair in Sub-Saharan Africa *World Journal of Surgery* 35 pp1194-1201

Aoto. K, Nishimura. T, Eto. K & Motoyama. J (2002) Mouse GLI3 regulates *Fgf8* expression and apoptosis in the developing neural tube, face, and limb bud *Developmental Biology* 251 pp 320-332

Archbold. H, Yang. Y, Chen. L & Cadigan. K (2012) How do they do Wnt they do? Regulation of transcription by the wnt/β-catenin pathway *Acta Pysiologica* 204 (1) pp 74-109

Arkell. R, Fossat. N & Tam. P (2013) Wnt signalling in mouse gastrulation and anterior development: new players in the pathway and signal output *Current opinion in genetics and development* 23 pp 454-460

Ashique. A, Fu. K & Richman. J (2002) Endogenous bone morphogenetic proteins regulate outgrowth and epithelial survival during avian lip fusion *Development* (129) pp 4647-4660

Attanasio. C, Nord. A, Zhu. Y, Blow. M, Li. Z, Liberton. D, Morrison. H, Plajzer-Frick. I, Holt. A, Hosseini. R, Phouanenavong. S, Akiyama. J, Shoukry. M, Afzal. V, Rubin. E, FitzPatrick. D, Ren. B, Hallgrímsson. B, Pennacchio. L & Visel. A (2013) Fine tuning of craniofacial morphology by distant-acting developmental enhancers *Science* 342 (6157) DOI: 10.1126/science.1241006

Aubert. J, Bar-Hen. A, Daudin. J & Robin. S (2004) Determination of the differentially expressed genes in microarray experiments using local FDR *BMC Bioinformatics* 5 pp 125

Auden. A, Caddy. J, Wilanowski. T, Ting. S, Cunningham. J & Jane. S (2006) Spatial and temporal expression of the *Grainyhead*-like transcription factor family during murine development *Gene Expression Patterns* 6 (8) pp 964-970

Avantaggiati. M, Ogryzko. V, Gardner. K, Giordano. A, Levine. A & Kelly. K (1997) Recruitment of p300/CBP in p53-dependent signal pathways *Cell* 89 (7) pp 1175-1184

Avilion. A, Nicolis. S, Pevny. L, Perez. L, Vivian. N & Lovell-Badge. R (2003) Multipotent cell lineages in early mouse development depend on SOX2 function *Genes and Development* 17 (1) pp 126-140

Bachler. M & Neubüser. A (2001) Expression of members of the Fgf family and their receptors during midfacial development *Mechanisms of development* 100 (2) pp 313-316

Bahuau. M, Houdayer. C, Tredano. M, Soupre. V, Couderc. R & Vazquez. M (2002) FOXC2 truncating mutation in distichiasis, lymphedema, and cleft palate *Clinical Genetics* 62 (6) pp 470-473

Bailey. T, Bodén. M, Buske. F, Frith. M, Grant. C, Clementi. L, Ren. J, Li. W & Noble. W (2009) MEME SUITE: tools for motif discovery and searching *Nucleic Acids Research* 37 pp 202-208

Bailey. T, Krajewski. P, Ladunga. I, Lefebvre. C, Li. Q, Liu. T, Madrigal. P, Taslim. C & Zhang. J (2013) Practical guidelines for the comprehensive analysis of ChIP-Seq Data *PLOS Computational biology* DOI: 10.1371/journal.pcbi.1003326

Barbieri. C, Perez. C, Johnson. K, Ely. K, Billheimer. D & Pietenpol. J (2005) IGFBP-3 is a direct target of transcriptional regulation by ΔNp63α in squamous epithelium *Cancer Research* 65 pp 2314-2320

Barlow. A & Francis-West. P (1997) Ectopic application of recombinant BMP-2 and BMP-4 can change patterning of developing chick facial primordia *Development* (124) pp 391-398

Barski. A, Cuddapah. S, Cui. K, Roh. T, Schones. D, Wang. Z, Wei. G, Chepelev. I & Zhao. K (2007) High-resolution profiling of histone methylations in the human genome *Cell* 129 (4) pp 823-837

Basson. A, Akbulut. S, Watson-Johnson. J, Simon. R, Carroll. T, Shakya. R, Gross. I, Martin. G, Lufkin. T, McMahon. A, Wilson. P, Costantini. F, Mason. I & Licht. J (2005) Sprouty1 is a critical regulator of GDNF/RET-mediated kidney induction *Developmental Cell* 8 (2) pp 229-239

Beaty. T, Murray. J, Marazita. M, Munger. R, Ruczinski. I, Hetmanski. J, Liang. K, Wu. T, Murray. T, Fallin. M, Redett. R, Raymond. G, Schwender. H, Jin. S, Cooper. M, Dunnwald. M, Mansilla. M, Leslie. E, Bullard. S, Lidral. A, Moreno. L, Menezes. R, Vieira. A, Petrin. A, Wilcox. A, Lie. R, Jabs. E, Wu-Chou. Y, Chen. P, Wang. H, Ye. X, Huang. S, Yeow. V, Chong. S, Jee. S, Shi. B, Christensen. K, Kimberly. D, Elizabeth. W, Hua. L, Eduardo. E, Czeizel. A, Ma. L, Field. L, Brody. L, Pangilinan. F, Mills. J, Molloy. A, Kirke. P, Scott. J, Arcos-Burgos. M & Scott. A (2010) A genome-wide association study of cleft lip with and without cleft palate identifies risk variants near *MAFB* and *ABCA4 Nature Genetics* 42 (6) pp 525-529

Beaty. T, Taub. M, Scott. A, Murray. J, Marazita. M, Schwender. H, Parker. M, Hetmanski. J, Balakrishnan. P, Mansilla. M, Mangold. E, Ludwig. K, Noethen. M, Rubini. M, Elcioglu. N & Ruczinski. I (2013) Confirming genes influencing risk to cleft lip with/without cleft palate in a case-parent trio study *Human Genetics* 132 (7) pp 771-781

Bell. S, Schreiner. C, Waclaw. R, Campbell. K, Potter. S & Scott. W (2003) *Sp8* is crucial for limb outgrowth and neuropore closure *PNAS* 100 (21) pp 12195-12200

Belloni. E, Muenke. M, Roessler. E, Traverso. G, Siegel-Bartelt. J, Frumkin. A, Mitchell. H, Donis-Keller. H, Helms. C, Hing. A, Heng. H, Koop. B, Martindale. D, Rommens. J, Tsui. L & Scherer. S (1996) Identification of *Sonic hedgehog* as a candidate gene responisible for holoprosencephaly *Nature Genetics* (14) pp 353-356

Belton. J, McCord. R, Gibcus. J, Naumova. N. Zhan. Y & Dekker. J (2012) Hi-C: a comprehensive technique to capture the conformation of genomes *Methods* 58 (3) pp 268-276

Bengoa-Vergniory. N & Kypta. R (2015) Canonical and noncanonical Wnt signalling in neural stem/progenitor cells *Cellular and Molecular Life Sciences* doi:10.1007/s00018-015-2028-6

Benko. S, Fantes. J, Amiel. J, Kleinjan. D, Thomas. S, Ramsay. J, Jamshidi. N, Essafi. A, Heaney. S, Gordon. C, McBride. D, Golzio. C, Fisher. M, Perry. P, Abadie. V, Ayuso. C, Holder-Espinasse. M, Kilpatrick. N, Lees. M, Picard. A, Temple. I, Thomas. P, Vazques. M, Vekemans. M, Roest Crollius. H, Hastie. N, Munnich. A, Etchevers. H, Pelet. A, Farlie. P, Fitzpatrick. D & Lyonnet. S (2009) Highly conserved non-coding elements on either side of SOX9 associated with Pierre Robin sequence *Nature Genetics* 41 (3) pp 359-364

Berdón-Zapata. V, Granillo-Álvarez. M, Valdés-Flores, García-Ortiz. J, Kofman-Alfaro. S & Zenteno. J (2004) *p63* gene analysis in Mexican patients with syndromic and non-syndromic ectrodactyly *Journal of Orthopaedic Research* 22 pp 1-5

Bernard. P & Harley. V (2007) Wnt4 action in gonadal development and sex determination *The international journal of biochemistry & cell biology* 39 (1) pp 31-43

Bertolancini. C, Ribeiro-Bicudo. L, Petrin. A, Richieri-Costa. A & Murray. J (2012) Clinical findings in patients with GLI2 mutations – phenotypic variability *Clinical Genetics* 81 (1) pp 70-75

Beverdam. A, Brouwer. A, Reijnen. M, Korving. J & Meijlink. F (2001) Severe nasal clefting and abnormal embryonic apoptosis in Alx3/Alx4 double mutant mice *Development* 128 pp 3975-3986

Bieging. K, Mello. S & Attardi. L (2012) Unravelling mechanisms of p53-mediated tumour suppression *Nature Reviews Cancer* 14 (5) pp 359-370

Bille. C, Winther. J, Bautz. A, Murray. J, Olsen. J, Christensen. K (2005) Cancer risk in persons with oral cleft—a population-based study of 8,039 cases. *American Journal of Epidemiology* 161 (11) pp 1047-1055

Birnbaum. S, Ludwig. K, Reutter. H, Herms. S, Steffens. M, Rubini. M, Baluardo. C, Ferrian. M, Almeida de Assis. N, Alblas. M, Barth. S, Freudenberg. J, Lauster. C, Schmidt. G, Scheer. M, Braumann. B, Bergé. S, Reich. R, Schiefke. F, Hemprich. A, Pötzch. S, Steegers-Theunissen. R, Pötzch. B, Moebus. S, Horsthemke.

B, Kramer. F, Wienker. T, Mossey. P, Propping. P, Cichon. S, Hoffmann. P, Knapp. M, Nöthen. M & Mangold. E (2009) Key susceptibility locus for nonsyndromic cleft lip with or without cleft palate on chromosome 8q24 *Nature Genetics* 41 pp 473-477

Blanco-Dávila. F & Olveda-Rodriguez. J (2001) Cleft palate in a patient with William's syndrome *Journal of Craniofacial Surgery* 12 pp 145-147

Blanton. S, Cortez. A, Stal. S, Mulliken. J, Finnell. R & Hecht. J (2005) Variation in IRF6 Contributes to Nonsyndromic Cleft Lip and Palate *American Journal of Medical Genetics* 137A pp 259-262

Blow. M, McCulley. D, Li. Z, Zhang. T, Akiyama. J, Holt. A, Plajzer-Frick. I, Shoukry. M, Wright. C, Chen. F, Afzal. V, Bristow. J, Ren. B, Black. B, Rubin. E, Visel. A & Pennacchio. L (2010) ChIP-Seq identification of weakly conserved heart enhancers *Nature Genetics* 42 (9) pp 806-810

Bokhoven. H. V & Brunner. H. G (2002) Splitting p63 *American Journal of Genetics* 71 pp 1-13

Bokhoven. H. V, Melino. G, Candi. E & Declercq. W (2011) P63, a story of Mice and Men *Journal of Investigative Dermatology* doi:10.1038/jid.2011.84

Borralleras. C, Sahun. I, Pérez-Jurado. L & Campuzano. V (2015) Intracisternal *Gtf2i* gene therapy ameliorates deficits in cognition an synaptic plasticity of a mouse model of Williams-Beuren syndrome *Molecular Therapy* doi: 10.1038/mt.2012.130

Boyles. A, Wilcox. A, Taylor. J, Meyer. K, Fredriksen. A, Ueland. P, Drevon. C, Vollset. S & Lie. R (2008) Folate and One-Carbon Metabolism Gene Polymorphisms and Their Associations With Oral Facial Clefts *American Journal of Medical Genetics Part A* 146A (4) pp 440-449

Browne. G, Cipollone. R, Lena. A, Serra. V, Zhou. H, Bokhoven. H, Dötsch. V, Merico. D, Mantovani. R, Terrinoni. A, Knight. R, Candi. E & Melino. G (2011) Differential altered stability and transcriptional activity of ΔNp63 mutants in distinct ectodermal dysplasias *Journal of Cell Science* 124 pp 2200-2207

Brunner. H, Hamel. B & Bokhoven. H. V (2002) *P63* Gene Mutations and Human Developmental Syndromes *American Journal of Medical Genetics* 112 pp 284-290

Brunner. H, Hamel. B & Bokhoven. H. V (2002b) The *p63* gene in EEC and other syndromes *Journal of Medical Genetics* 39 pp 377-381

Brydon. C, Conway. J, Kling. R, Mehta. L, Jabs. E & Taub. P (2014) Cleft Lip and/or Palate: One organization's experience with more than a quarter million surgeries during the past decade *The Journal of Craniofacial Surgery* 25 (5) pp 1601- 1609

Burgeson RE (1993) Type VII collagen, anchoring fibrils, and epidermolysis bullosa. *J Invest Dermatol.* Doi: 1993;101(3):252-255

Bush. J, Lan. Y & Jiang. R (2004) The cleft lip and palate defects in *Dancer* mutant mice result from gain of function of the *Tbx10* gene *PNAS* 101 (18) pp 7022-7027

Butali. A, Mossey. P, Adeyemo. W, Eshete. M, Gaines. L, Even. D, Braimah. R, Aregbesola. B, Rigdon. J, Emeka. C, James. O, Ogunlewe. M, Ladeinde. A, Abate. F, Hailu. T, Mohammed. I, Gravem. P, Deribew. M, Gesses. M, Adeyemo. A & Murray. J (2014) Novel IRF6 mutations in families with Van Der Woude syndrome and popliteal pterygium syndrome from sub-Saharan Africa *Molecular genetics & genomic medicine* 2 (3) pp 254-260

Cadigan. K & Peifer. M (2009) Wnt signalling from development to diease: insights from model systems Cold spring harbour perspectives in biology 1 (2) doi: 10.1101/cshperspect.a002881

Cambiaghi. S, Tadini. G, Barbareschi. M, Menni. S & Caputo. R (1994) Rapp-Hodgkin syndrome and AEC syndrome: are they the same entity? *British Journal of Dermatology* 130 pp 97-101

Candi. E, Rufini. A, Terrinoni. A, Giamboi-Miraglia. A, Lena. A, Mantovani. R, Knight. R & Melino. G (2007) ΔNp63 regulates thymic development through enhanced expression of FgfR2 and Jag2 *PNAS* 104 (29) pp 11999-12004

Carette. M & Ferguson. M (1992) The fate of medial edge epithelial cells during palatal fusion *in vitro*: an analysis by Dil labelling and confocal microscopy *Development* 114 (2) pp 379-388

Carroll. D, Carroll. J, Leong. C, Cheng. F, Brown. M, Mills. A, Brugge. J & Ellisen. L (2006) p63 regulated an adhesion programme and cell survival in epithelial cells *Nature Cell Biology* 8 (6) pp 551-561

Carroll. T, Park. J. Hayashi. S, Majumdar. A & McMahon. A (2005) Wnt9b plays a central role in the regulation of mesenchymal to epithelial transitions underlying organogenesis of the mammalian urogenital system *Developmental Cell* 9 (2) pp 283-292

Caserta. T, Kommagani. R, Yuan. Z, Robbins. D, Mercer. C & Kadakia. M (2006) p63 Overexpression Induces the Expression of Sonic Hedgehog *Molecular Cancer Research* 4 (10) pp 759-768

Celli. J, Duijf. P, Hamel. B, Bamshad. M, Kramer. B, Smits. A, Newbury-Ecob. R, Hennekam. R, Buggenhout. G, Haeringen. A, Woods. G, Essen. A, Waal. R, Vriend. G, Haber. D, Yang. A, Mckeon. F, Brunner. H & Bokhoven. H (1999) Heterozygous Germline mutations in the p53 homolog p63 are the Cause of EEC Syndrome *Cell* 99 (2) pp 143-153

Chan. D, Schrijver. I & Chang. K (2010) Connexin-26-associated deafness: Phenotypic variability and progression of hearing loss *Genetics in Medicine* 12 pp 174-181

Chan. H & Thangue. L (2001) p300/CBP proteins: HATs for transcriptional bridges and scaffolds *Journal of Cell Science* 114 (13) pp 2363-2373

Chen. C, Gorlatova. N, Kelman. Z & Herberg. O (2011) Structures of p63 DNA binding domain in complexes with half-site and with spacer-containing full response elements *PNAS* 108 (16) pp 6456-6461

Chi. S, Ayed. A & Arrowsmith. C (1999) Solution structure of a conserved C-terminal domain of p73 with structural homology to the SAM domain *The EMBO Journal* 18 (16) pp 4438-4445

Chiang. C, Litingtung. Y, Lee. E, Young. K, Corden. J, Westphal. H & Beachy. P (1996) Cyclopia and defective axial patterning in mice lacking *Sonic hedgehog* gene function *Nature* (383) pp 407-413

Chiquet. B, Blanton. S, Burt. A, Ma. D, Stal. S, Muliken. J & Hecht. J (2008) Variation in WNT genes is associated with non-syndromic cleft lip with or without cleft palate *Human Molecular Genetics* 17 (14) pp 2212-2218

Chishti. M, Muhammad. D, Haider. M & Ahmad. W (2006) A novel missense mutation in *MSX1* underlies autosomal recessive oligodontia with associated dental anomalies in Pakistani families *Journal of Human Genetics* 51 pp 872-878

Chiu. Y, Drolet. B, Duffy. K & Holland. K (2011) A Case of Ankyloblepharon, Ectodermal Dysplasia, and Cleft Lip/Palate Syndrome with Ectrodactyly: Are the p63 Syndromes Distinct After all? *Pediatric Dermatology* 28 (1) pp 15-19

Cho. Y, Gorina. S, Jeffery. P & Pavletich. N (1994) Crystal structure of a p53 tumour suppressor –DNA complex: understanding tumorigenic mutations *Science* 265 (5170) pp 346-355

Christensen. K & Mortensen. P (2002) Facial Clefting and Psychiatric Diseases: A Follow-Up of the Danish 1936-1987 Facial Cleft Cohort *Cleft Palate-Craniofacial Journal* 39 (4) pp 392-396

Christensen. K, Juel. K, Herskind. A & Murray. J (2004) Long term follow up study of survival associated with cleft lip and palate at birth *The British Medical Journal* 328 (7453) pp 1405

Chu. E, Hens. J, Andl. T, Kairo. A, Yamaguchi. T, Brisken. C, Glick. A, Wysolmerski. J & Millar. S (2004) Canonical WNT signalling promotes mammary placode development and is essential for initiation of mammary gland morphogenesis *Development* 131 pp 4819-4829

Chung. J, Grant. I, Kaplan. D & Irwin. M (2011) Special AT-rich binding protein-2 (SATB2) differentially affects disease-causing *p63* mutants *Journal of Biological Chemistry* doi: 10.1074/jbc.M111.271189

Clément-Lacroix. P, Ai. M, Morvan. F, Roman-Roman. S, Vayssiére. B, Belleville. C, Estrera. K, Warman. M, Baron. R & Rawadi. G (2005) Lrp5-independent activation of Wnt signaling by lithium chloride increases bone formation and bone mass in mice *PNAS* 102 (48) pp 17406-17411

Cohen. E, Ihda-Stansbury. K, Lu. M, Panettieri. R, Jones. P & Morrisey. E (2009) Wnt signalling regulates smooth muscle precursor development in the mouse lung via a tenascin C/PDGFR pathway *Journal of Clinical investigation* 119 (9) pp 2538-2549

Couly. G, Coltey. P & Le Douarin. N (1992) The developmental fate of the cephalic mesoderm in quail-chick chimeras *Development* 114 (1) pp 1-15

Crawley. J, Belknap. J, Collins. A, Crabbe. J, Frankel. W, Henderson. N, Hitzemann. R, Maxson. S, Miner. L, Solva. A, Wehner. J, Wynshaw-Boris. A & Paylor. R (1997) Behavioural phenotypes of inbred mouse strains: implications and recommendations for molecular studies *Psychopharmacology* 132 (2) pp 107-124

Cuervo. R & Covarrubias. L (2004) Death is the major fate of medial edge epithelial cells and the cause of basal lamina degradation during palatogenesis *Development* 131 pp 15-24

Dang. N & Murrell. D (2008) Mutation analysis and characterisation of *COL7A1* mutations in dystrophic epidermolysis bullosa *Experimental Dermatology* 17 (7) pp 553-568

Darnell. D, Stanislaw. S, Kaur. S & Antin. P (2010) Whole mount in situ hybridization detection of mRNAs using short LNA containing DNA oligonucleotide probes *RNA* 16 (3) pp 632-637

Dealy. C, Roth. A, Ferrari. D, Brown. A & Kosher. R (1993) *Wnt-5a* and *Wnt-7a* are expressed in the developing chick limb bud in a manner suggesting roles in pattern formation along the proximodistal and dorsoventral axes *Mechanisms of Development* 43 pp 175-186

Dekker. J, Rippe. K, Dekker. M & Kleckner. N (2002) Capturing chromosome conformation *Science* 295 (5558) pp 1306-1311

Deol. M & Lane. P (1966) A new gene affecting the morphogenesis of the vestibular part of the inner ear in the mouse *Journal of embryology and experimental morphology* 16 (3) pp 543-558

De-Regil. L, Fernández-Gaxiola. A, Dowswell. T & Peña-Rosas. J (2010) Effects and safety of periconceptional folate supplementation for preventing birth defects *Cochrane library* (10)

Diaz. A, Nellore. A & Song. J (2012) CHANCE: comprehensive software for quality control and validation of ChIP-Seq data *Genome Biology* 13 (10) doi: 10.1186/gb-2012-13-10-r98

Diewert. V (1983) A morphometric analysis of craniofacial growth and changes in spatial relations during secondary palatal development in human embryos and fetuses *The American Journal of Anatomy* 167 pp 495-522

Diewert. V & Wang. K-Y (1992) Recent Advances in Primary Palate and Midface Morphogenesis Research *Critical Reviews in Oral Biology and Medicine* 4 (1) pp 111-130

Ding. H, Wu. X, Boström. H, Kim. I, Wong. N, Tsoi. B, O'Rourke. M, Koh. G, Soriano. P, Betsholtz. C, Hart. T, Marazita. M, Field. L, Tam. P & Nagy. A (2004) A specific requirement for PDGF-C in palate formation and PDGFR-α signalling *Nature Genetics* 36 pp 1111-1116

Dixon. M, Marazita. M, Beaty. T & Murray. J (2011) Cleft lip and palate: understanding genetic and enviromental influences *Nature Reviews Genetics* 12 (3) pp 167-178

Dollé. P (2009) Developmental expression of retinoic acid receptors (RARs) Nuclear Receptor Signalling doi: 10.1621/nrs.07006

Dollé. P, Ruberte. E, Leroy. P, Morriss-Kay. G & Chambon. P (1990) Retinoic acid receptors and cellular retinoid binding proteins *Development* 110 pp 1133-1151

Domenico. S, Orlando. C, Graziana. F, Papi. P & Giulia. A (2013) Cleft palate in Williams syndrome *Annals of Maxillofacial surgery* 3 (1) pp 84-86

Dorey. K & Amaya. E (2010) FGF signalling: diverse roles during early vertebrate embryogenesis *Development* 137 (22) pp 3731-3742

Dostie. J & Dekker. J (2007) Mapping networks of physical interactions between genomic elements using 5C technology *Nature Protocols* 2 pp 988-1002

Dötsch. V, Bernassola. F, Coutandin. D, Candi. E & Melino. G (2011) p63 and p73, the Ancestors of p53 *Cold Spring Harbor Perspectives in Biology* doi: 10.1101/cshperspect.a004887

Drakopoulou. E, Outram. S, Rowbotham. N, Ross. S, Furmanski. A, Saldana. J, Hager-Theodorides. A & Crompton. T (2010) Non-redundant role for the transcription factor Gli1 at multiple stages of thymocyte development *Cell Cycle* 9 (20) pp 4144-4152

Dudas. M, Sridurongrit. S, Nagy. A, Okazaki. K & Kaartinen. V (2004) Craniofacial defects in mice lacking BMP type I receptor Alk2 in neural crest cells *Mechanisms of Development* 121 (2) pp 173-182

Eckner. R, Ewen. M, Newsome. D, Gerdes. M, DeCaprio. J, Lawrence. J & Livingston. D (1994) Molecular cloning and functional analysis of the adenovirus E1A-assocaited 300-kD protein (p300) reveals a protein with properties of a transcriptional adaptor *Genes and Development* 8 pp 869-884

Eckner. R, Yao. T, Oldread. E & Livingston. D (1996) Interaction and functional collaboration of p300/CBP and bHLH proteins in muscle and B-cell differentiation *Genes and Development* 10 pp 2478-2490

El-Deiry. W, Kern. S, Pietenpol. J, Kinzler. K & Vogelstein. B (1992) Definition of a consensus binding site for p53 *nature genetics* 1 pp 45-49

Elsahy. N (1973) The modified striped Y—a systematic classification for cleft lip and palate *The Cleft palate journal* (10) pp 247-50

Ferone. G, Thomason. H, Antonini. D, Rosa. L, Hu. B, Gemei. M, Zhou. H, Ambrosio. R, Rice. D, Acampora. D, Bokhoven. H, Vecchio. L, Koster. M, Tadini. G, Spencer-Dene. B, Dixon. M, Dixon. J & Missero. C (2012) Mutant p63 causes defective expansión of ectodermal progenitor cells and impaired FGF signalling in AEC síndrome *EMBO Molecular Medicine* 4 pp 192-205

Ferretti. E, Li. B, Zewdu. R, Wells. V, Hebert. J, Kamer. C, Anderson. M, Williams. T, Dixon. J, Dixon. M, Depew. M & Selleri. L (2011) A Conserved Pbc-Wnt-p63-Irf6 regulatory module controls face morphogenesis by promoting epithelial apoptosis *Developmental Cell* 21 pp 627-641

Fessing. M, Mardaryev. A, Gdula. M, Sharov. A, Sharova. T, Raspisarda. V, Gordon. K, Smorodchenko. A, Poterlowicz. K, Ferone. G, Kohwi. Y, Missero. C, Shigematsu. T & Botchkarev. V (2011) p63 regulates *Satb1* to control tissue-specific chromatin remodelling during development of the epidermis *Journal of Cell Biology* 194 (6) pp 825-839

Firnberg. N & Neubüser. A (2002) FGF signalling regulates expression of Tbx2, Erm, Pea3 and Pax3 in the early nasal region *Developmental Biology* 247 (2) pp 237-250

Fishwick. K, Neiderer. T, Jhingory. S, Bronner. M & Taneyhill. L (2012) The tight junction protein claudin-1 influences cranial neural crest cell emigration *Mechanisms of development* 129 (9-12) pp 275-283

Fitchett. J & Hay. E (1989) Medial edge epithelium transforms to mesenchyme after embryonic palatal shelves fuse *Developmental Biology* 131 (2) pp 455-474

FitzPatrick. D, Carr. I, McLaren. L, Leek. J, Wightman. P, Williamson. K, Gautier. P, McGill. N, Hayward. C, Firth. H, Markham. A, Fantes. J & Bonthron. D (2003) Identification of SATB2 as the cleft palate gene on 2q32-q33 *Human Molecular Genetics* 12 (19) pp 2491-2501

Francis-West. P, Tatla. T & Brickell. P (1994) Expression patterns of the bone morphogenetic protein genes Bmp-4 and Bmp-2 in the developing chick face suggest a role in outgrowth of the primordial *Developmental dynamics* 201 (2) pp 168-178

Frebourg. T, Oliveira. C, Hochain. P, Karam. R, Manouvrier. S, Graziadio. C, Vekemans. M, Hartmann. A, Baert-Desurmont. S, Alexandre. C, Dumoulin. L, Marroni. C, Martin. C, Castedo. S, Lovett. M, Winston. J, Machado. J, Attié. T, Jabs. E, Cai. J, Pellerin. P, Triboulet. J, Scotte. M, Pessot. F, Hedouin. A, Carneiro. F, Blayau. M & Seruca. R (2006) cleft lip/palate and *CDH1/E-cadherin* mutations in familes with hereditary diffuse gastric cancer *Journal of medical genetics* 43 (2) pp 198-142

Fruttinger. M, Karlsson. L, Hall. A, Abramsson. A, Calver. A, Boström. H, Willetts. K, Bertold. C, Heath. J, Betsholtz. C & Richardson. W (1999) Defective oligodendrocyte development and severe hypomyelination in PDGF-A knockout mice *Development* 126 pp 457-467

Furuse. M, Hata. M, Furuse. K, Yoshida. Y, Haratake. A, Sugitani. Y, Noda. T, Kubo. A & Tsukita. S (2002) Claudin-based tight junctions are crucial for the mammalian epidermal barrier: a lessonfrom claudin-1-deficient mice *Journal of Cell Biology* 156 (6) pp 1099-1111

Gaare. J & Langman. J (1977) Fusion of nasal swellings in the mouse embryo: regression of the nasal fin *American Journal of Anatomy* 150 (3) pp 477-499

Galli. L, Muniji. R, Chapman. S, Easton. A, Li. L, Onguka. O, Ramahi. J, Suriben. S, Szabo. L, Teng. C, Tran. B, Hannoush. R & Burrus. L (2014) Frizzled10 mediates WNT1 and WNT3A signalling in the dorsal spinal cord of the developing chick embryo *Developmental Dynamics* doi: 10.1002/dvdy.24123 Epub 2014 Apr1

Geetha-Loganathan. P, Nimmagadda. S, Antoni. L, Fu. K, Whiting. C, Francis-West. P & Richman. J (2009) Expression of WNT signalling pathway genes during chicken craniofacial development *Developmental Dynamics* 238 (5) pp 1150-1165

Geetha-Loganathan. P, Nimmagadda. S, Fu. K & Richman. J (2014) Avian facial morphogenesis is regulated by JNK/PCP wingless-related (WNT) signalling *Journal of Biological Chemistry* 289 pp 24153-24167

Ghioni. P, Bolognese. F, Duijf. P, Bokhoven. H, Mantovani. R & Guerrini. L (2002) Complex transcriptional effects of p63 isoforms: Identification of novel activation and repression domains *Molecular and Cellular Biology* 22 (24) pp 8659-8668

Gnessi. L, Emidi. A, Scarpa. S, Palleschi. S, Ragano-Caracciolo. M, Silvestroni. L, Modesti. A & Spera. G (1993) Platelet-derived growth factor effects on purified testicular peritubular myoid cells: binding, cytosolic Ca^{2+} increase, mitogenic activity, and extracellular matrix production enhancement *Endocrinology* 133 (4) pp 1880-1890

Gong. S & Guo. C (2003) Bmp4 gene is expressed at the putative site of fusion in the midfacial region *Differentiation* 71 (3) pp 228-236

Gong. S, White. N & Sakasegawa. A (2000) The Twirler mouse, a model for the study of cleft lip and palate *Archives of oral biology* (45) pp 87-94

Gontan. C, Munck. A, Vermeij. M, Grosveld. F, Tobboel. D & Rottier. R (2008) Sox2 is important for two crucial processes in lung development: Branching morphogenesis and epithelial cell differentiation *Developmental Biology* 317 (1) pp 296-309

Goodman. R & Smolik. S (2000) CBP/P300 in cell growth, transformation, and development *Genes and Development* 14 pp 1553-1577

Goodnough. H, Brugmann. S, Hu. D & Helms. J (2007) Stage-dependent craniofacial defects resulting from Sprouty2 overexpression *Developmental Dynamics* 236 (7) pp1918-1928

Goodrich. L, Milenkovic. L, Higgins. K & Scott. M (1997) Altered neural cell fates and medulloblastoma in mouse *patched* mutants *Science* 277 (5329) pp 1109-1113

Gottfried. I, Landau. M, Glaser. F, Di. W, Ophir. J, Mevorah. B, Ben-Tal. N, Kelsell. D & Avraham. K (2002) A mutation in *GJB3* is associated with recessive erythrokeratodermia variabilis (EKV) and leads to defective trafficking of the connexion 31 protein *Human Molecular Genetics* 11 (11) pp 1311-1316

Grant. S, Wang. K, Zhang. H, Glaberson. W, Annaiah. K, Kim. C, Bradfield. J, Glessner. J, Thomas. K, Garris. M, Frackelton. E, Otieno. G, Chiavacci. R, Nah. H, Kirschner. R & Hakonarson. H (2009) A genome-wide association study identifies a locus for nonsyndromic cleft lip with or without cleft palate on 8q24 *The journal of Pediatrics* 155 (6) pp 909-913

Green. R, Feng. W, Phang. T, Fish. J, Li. H, Spritz. R, Marcucio. R, Hooper. J, Jamniczky. H, Hallgrímsson. B & Williams. T (2015) *Tfap2a*-dependent changes in mouse facial morphology result in clefting that can be ameliorated by a reduction in *Fgf8* gene dosage *Disease Models & Mechanisms* 8 (1) pp 31-43

Griffin. J, Compagnucci. C, Hu. D, Fish. J, Klein. O, Marcucio. R & Depew. M (2013) *Fgf8* dosage determines midfacial integration and polarity within the Nasal and Optic Capsules *Developmental Biology* 374 (1) pp 185-197

Griffith. M & Hay. E (1992) Epithelial-mesenchymal transformation during palatal fusion: carboxylfluorescein traces at light and electron microscopic levels *Development* 116 pp 1087-1099

Gritli-Linde. A (2007) Molecular control of secondary palate development *Developmental Biology* 301 pp 309-326

Gritli-Linde. A (2008) The pathogenesis of cleft lip and cleft palate: usefulness and caveats of mouse models *Current Topics in Developmental Biology* 84 pp 37-138

Gritli-Linde. A (2010) p63 and IRF6: brothers in arms against cleft palate *Journal of Clincal Investigation* 120 (5) pp 1386-1389

Grossman. S, Perez. M, Kung. A, Joseph. M, Mansur. C, Xiao. Z, Kumar. S, Howley. P & Livingston. D (1998) p300/MDM2 complexes participate in MDM2-mediated p53 degradation *Molecular Cell* 2 (4) pp 405-415

Grosen. D, Bille. C, Petersen. I, Skytthe. A, Hjelmborg. J, Pedersen. J, Murray. J & Christensen. K (2011) Risk of oral clefts in twins *Epidemiology* 22 (3) pp 313-319

Grüneberg. H & Truslove. G (1960) Two closely linked genes in the mouse *Genetic Research Cambridge* 1 pp 69-90

Gu. W & Roeder. R (1997) Activation of p53 Sequence-Specific DNA binding by acetylation of the p53 C-terminal domain *Cell* 90 (4) pp 595-606

Guerrini. L, Costanzo. A & Merlo. G (2011) A symphony of Regulations Centered on p63 to control Development of Ectoderm-Derived Structures *Journal of Biomedicine and Biotechnology* doi:10.1155/2011/864904

Gundlach. K & Maus. C (2006) Epidemiological studies on the frequency of clefts in Europe and world-wide *Journal of Cranio-Maxillofacial Surgery* (34) Sup 2 pp 1-2

Guo. X, Keyes. W, Papazoglu. C, Zuber. J, Li. W, Lowe. S, Vogel. H & Mills. A (2009) TAp63 induces senescence and suppresses tumorigenesis *in vivo Nature cell biology* 11 (12) pp 1451-1457

Gustavsson. P, Greene. N, Lad. D, Pauws. E, Castro. S, Stanier. P & Copp. A (2007) Increased expression of *Grainyhead-like-3* rescues spina bifida in a folate-resistant mouse model *Human Molecular Genetics* 16 (21) pp 2640-2646

Hackshaw. A, Rodeck. C & Boniface. S (2011) Maternal smoking in pregnancy and birth defects: a systematic review based on 173 687 malformed cases and 11.7 million controls *Human Reproduction Update* 17 (5) pp 589-604

Hanafusa. H, Torii. S, Yasunaga. T & Nishida. E (2002) Sprouty1 and Sprouty2 provide a control mechanism for the Ras/MAPK signalling pathway *Nature Cell Biology* 4 (11) pp 850-858

Han. J, Xiao. Y, Lin. J & Li. Yong (2006) PDGF-C controls proliferation and is down-regulated by retinoic acid in mouse embryonic palatal mesenchymal cells *Birth Defects Research Part B: Developmental and Reproductive Toxicology* 77 (5) pp 438-444

Hau. P, Yip. Y, Huen. M & Tsao. S (2011) Loss of ΔNp63α promotes mitotic exit in epithelial cells *Federation of European Biochemical Societies* doi:10.1016/j.febslet.2011.07.030

He. F & Soriano. P (2013) A critical role for PDGFRα signalling in medial nasal process development Plos Genetics 9 doi: 10.1371/journal.pgen.1003851

He. J, Huang. Y, Weng. J, Xiao. L, Weng. K & Ma. X (2015) Specific inhibition of β-Catenin in Jeko-1 mantle cell lymphoma cell line decreases proliferation and induces apoptosis *Medical science monitor: international medical journal of experimental and clinical research* 21 pp 2218-2224

He. L, Naik. K, Meng. S, Cao. J, Sidhaye. A, Ma. A, Radovick. S & Wondisford. F (2012) Transcriptional co-activator p300 maintains basal hepatic gluconeogenesis *Journal of Biological Chemistry* 287 (38) pp 32069-32077

Hennekam. R & Van Doorne. J (1990) Oral aspects of Rubinstein-Taybi syndrome *American Journal of medical genetics, supplement* 6 pp 42-47

Heldin. C & Westermark. B (1999) Mechanism of Action and in vivo role of platelet-derived growth factor *American Physiological Society* 79 (4) pp 1283-1316

Helton. E, Zhu. J & Chen. X (2005) The unique NH2-terminally deleted (DeltaN) residues, the PXXP motif, and the PPXY motif are required for the transcriptional activity of the DeltaN variant of p63 *The Journal of Biological Chemistry* 3281 (5) pp 2533-2542

Hikasa. H, Ezan. J, Itoh. K, Li. X, Klymkowsky. M & Sokol. S (2010) Regulation of TCF3 by Wnt-dependent phosphorylation during vertebrate axis specification *Developmental Cell* 19 (4) pp 521-532

Hill. R, Favor. J, Hogan. B, Ton. C, Saunders. G, Hanson. I, Prosser. J, Jordan. T, Hastie. N & van Heyningen. V (1991) Mouse small eye results from mutations in a paired-like homeobox-containing gene *Nature* 354 (6354) pp 522-525

Hinrichsen. K (1985) The early development of morphology and patterns of the face in the human embryo *Advances in anatomy, embryology, and cell biology* 98 pp 1-79

Hoch. R & Soriano. P (2003) Roles of PDGF in animal development *Development* 130 (20) pp 4769-4784

Honein. M, Rasmussen. S, Reefhuis. J, Romitti. P, Lammer. E, Sun. L & Correa. A (2007) Maternal smoking and environmental tobacco smoke exposure and the risk of orofacial clefts. *Epidemiology* 18 (2) pp 226-233

Horike. S, Cai. S, Miyano. M, Cheng. J, Kohwi-Shigematsu. T (2005) Loss of silent-chromatin looping and impaired imprinting of DLX5 in Rett syndrome *Nature genetics* 37 (1) pp 31-40

Hozyasz. K, Mostowska. A, Wójcicki. P, Lasota. A, Offert. B, Balcerek. A, Dunin-Wilczyńska. I & Jagodziński (2014) Nucleotide variants of the cancer predisposing gene *CDH1* and the risk of non-syndromic cleft lip with or without cleft palate *Familial Cancer* 13 (3) pp 415-421

Hu. D & Helms. A (1999) The role of Sonic hedgehog in normal and abnormal craniofacial morphogenesis *Development* (126) pp 4873-4884

Huang. X, Goudy. S, Ketova. T, Litingtung. Y & Chiang. C (2008) Gli-3deficient mice exhibit cleft palate associated with abnormal tongue development *Developmental dynamics* 237 (10) pp 3079-3087

Huang. D, Sherma. B & Lempicki. R (2009a) Systematic and integrative analysis of large gene lists using DAVID Bioinformatics Resources *Nature Protocols* 4 (1) pp 44-57

Huang. D, Sherma. B & Lempicki. R (2009b) Bioinformatics enrichment tools: paths toward the comprehensive functional analysis of large gene lists *Nucleic Acids Research* 37 (1) pp 1-13

Ihrie. R, Marques. M, Nguyen. B, Horner. J, Papazpglu. C, Bronson. R, Mills. A & Attardi. L (2005) *Perp* is a p63-regulated gene essential for epithelial integrity *Cell* 120 pp 843-856

Iizuka. T (1973) Stage of the formation of the human upper lip *Okajimas Folia Anatomica Japonica* 50 (5) pp 307-315

Ingham. P & McMahon. A (2001) Hedgehog signalling in animal development: paradigms and principles *Genes and Development* (15) pp 3059-3087

Iorio. E, Kaye. S, Ponzin. D, Barbaro. V, Ferrari. S, Böhm. E, Nardiello. P, Castaldo. G, McGrath. J & Willoughby. C (2011) Limbal Stem Cell Deficiency and Ocular Phenotype in Ectrodactyly- Ectodermal Dysplasia- Clefting Syndrome Caused by *p63* mutations *Opthalmology* doi:10.1016/j.opyja.2011.06.044

Iseki. S, Wilkie. A, Morriss-Kay. G (1999) Fgfr1 and Fgfr2 have distinct differentiation- and proliferation-related roles in the developing mouse skull vault *Development* 126 (24) pp 5611-5620

Ito. Y, Yeo. J, Chytil. A, Han. J, Bringas. P, Nakajima. A, Shuler. C, Moses. H & Chai. Y (2003) Conditional inactivation of *Tgfbr2* in cranial neural crest causes cleft palate and calvaria defects *Development* 130 pp 5269-5280

Jeong. J, Mao. J, Tenzen. T, Kottmann. A & McMahon. A (2004) Hedgehog signalling in the neural crest regulates the patterning and growth of facial primordia *Genes and Development* (18) pp 937-951

Jezewski. P, Vieira. A, Nishimura. C, Ludwig. B, Johnson. M, O'Brien. S, Daack-Hirsh. S, Schultz. R, Weber. A, Nepomucena. B, Romitti. P, Christensen. K, Orioli. I, Machida. J, Natsume. N & Murray. J (2003) Complete sequencing shows a role for *MSX1* in non-syndromic cleft lip and palate *Journal of Medical Genetics* 40 pp 399-407

Jiang. R, Bush. J & Lidral. A (2006) Development of the Upper Lip: Morphogenetic and Molecular Mechanisms *Developmental Dynamics* 235 pp1152-1166

Jin. J & Ding. J (2006) Analysis of cell migration, transdifferentiation and apoptosis during mouse secondary palate fusion *Development* 133 pp 3341-3347

Jin. Y, Han. X, Taketo. M & Yoon. J (2012) Wnt9b-dependent FGF signalling is crucial for outgrowth of the nasal and maxillary processes during upper jaw and lip development *Development* 139 (10) pp 1821-1830

Jochumsen. U, Werner. R, Miura. N, Richter-Unruh. A, Hiort. O & Holterhus. P (2008) Mutation analysis of FOXF2 in patients with disorders of sex development (DSD) in combination with cleft palate *Sexual development: genetics, molecular biology, evolution, endocrinology, embryology, and pathology of sex determination and differentiation* 2 (6) pp 302-308

Johnson. D (1969) Brachyphalangy, an allele of extra-toes in the mouse *Genetical Research Cambridge* 13 (3) pp 275-280

Johnson. D, Lu. J, Chen. H, Werner. S & Williams. L (1991) The human fibroblast growth factor receptor genes: a common structural arrangement underlies the mechanisms for generating receptor forms that differ in their third immunological domain *Molecular and Cellular Biology* 11 (9) pp 4627-4634

Johnson. R, Rothman. A, Xie. J, Goodrich. L, Bare. J, Bonifas. J, Quinn. A, Myers. R, Cox. D, Epstein. E & Scott. M (1996) Human homolog of *patched*, a candidate gene for the basal cell nevus syndrome *Science* (272) pp 1668-1671

Johnston. J, Sapp. J, Turner. T, Amor. D, Aftimos. S, Aleck. K, Bocian. M, Bodurtha. J, Cox. G, Curry. C, Day. R, Donnai. D, Field. M, Fujiwara. I, Gabbett. M, Gal. M, Graham. J, Hedera. P, Hennekam. R, Hersh. J, Hopkin. R, Kayserili. H, Kidd. A, Kimonis. V, Lin. A, Lynch. S, Maisenbacher. M, Mansour. S, McGaughran. J, Mehta. L, Murphy. H, Raygada. M, Robin. N, Rope. A, Rosenbaum. K, Schaefer. G, Shealy. A, Smith. W, Soller. M, Sommer. A, Stalker. H, Steiner. B, Stephan. M, Tilstra. D, Tomkins. S, Trapane. P, Tsai. A, Van Allen. M, Vasudevan. P, Zabel. B, Zunish. J, Black. G & Biesecker. L (2010) Molecular analysis expands the spectrum of phenotypes associated with GLI3 mutations *Human Mutation* 31 (10) pp 1142-1154

Johnston. M & Bronsky (1995) Prenatal Craniofacial Development: New Insights on Normal and Abnormal Mechanisms *Critical Reviews in Oral Biology & Medicine* 6 (4) pp 368-422

Jugessur. A & Murray. J (2005) Orofacial clefting: recent insights into a complex trait *Current opinion in Genetics and Development* 15 (3) pp 270-278
Jugessur. A, Farlie. P & Kilpatrick. N (2009) The genetics of isolated orofacial clefts: from genotypes to subphenotypes *Oral Diseases* (15) pp 437-453

Juriloff. D & Harris. M (2004) A digenic cause of cleft lip in A-strain mice and definition of candidate genes for the two loci *Birth Defects Research Part A*: *Clinical Molecular Teratology* 70 (8) pp 509-518

Juriloff. D, Harris. M & Brown. C (2001) Unravelling the complex genetics of cleft lip in the mouse model *Mammalian Genome* (12) pp 426-435

Juriloff. D, Harris. M, McMahon. A, Carroll. T & Lidral. A (2006) *Wnt9b* is the mutated gene involved in multifactorial nonsyndromic cleft lip with or without cleft palate in A/WySn mice, as confirmed by a genetic complementation test *Clinical and Molecular Teratology* 76 (8) pp 574-579

Kaghad. M, Bonnet. H, Yang. A, Creancier. L, Biscan. J, Valent. A, Minty. A, Chalon. P, Lelias. J, Durmont. X, Ferrara. P, McKeon. F & Caput. D (1997) Monoallelically expressed gene related to p53 at 1p36, a region frequently deleted in neuroblastoma and other human cancers *Cell* 90 (4) pp 809-819

Kahlert. U, Suwala. A, Koch. K, Natsumeda. M, Orr. B, Hayashi. M, Maciaczyk. J & Eberhart. C (2015) Pharmacologic Wnt inhibition reduces proliferation, survival and clonogenicity of glioblastoma cells *Journal of neuropathology and experimental neurology* 74 (9) pp 889-900

Kang. P & Svoboda. K (2005) Epithelial-Mesenchymal Transformation during Craniofacial Development *Journal of Dental Research* 84 (8) pp 678-690

Kantaputra. P, Malaivijitnond, Vieira. A, Heering. J, Dötsch. V, Khankasikum. T & Sripathomsawat. W (2011) Mutation in SAM domain of *TP63* is Associated With Nonsyndromic Cleft Lip and Palate and Cleft Palate *American Journal of Medical Genetics* doi: 10.1002/ajmg.a.34011

Kasberg. A, Brunskill. E & Potter .S (2013) SP8 regulated signalling centers during craniofacial development *Developmental Biology* 381 (2) pp 312-323

Katoh. Y & Katoh. M (2005) Comparative genomics on Sonic hedgehog orthologs *Oncology Reports* 14 (4) pp 1087-1090

Kawakami. M, Okuda. H, Tatsumi. K, Kirta. T, Wanaka. A (2014) Inhibition of *Wnt/* β-catenin pathway by Dikkopf-1 affects midfacial morphogenesis in chick embryo *Journal of Bioscience and Bioengineering* 117 (6) pp 664-669

Kawakami. Y, Wada. N, Nishimatsu. S, Komaguchi. C, Noji. S & Nohno. T (2000a) Indentification of chick frizzled-10 expressed in the developing limb and the central nervous system *Mechanisms of Development* 91 (1-2) pp 375-378

Kawakami. Y, Wada. N, Nishimatsu. S & Nohno. T (2000b) Involvement of frizzled-10 in Wnt-7a signalling during chick limb development *Development, growth & differentiation* 42 (6) pp 561-569

Kelly. D, O'Dowd. T & Reulbach. U (2012) Use of folic acid supplements and risk of cleft lip and palate in infants: a population-based cohort study *The British Journal of General Practice* 62 (600) pp 466-472

Kemp. C, Thiele. H, Dankof. A, Schmidt. G, Lauster. C, Fernahl. G & Lauster. R (2009) Cleft Lip and/or Palate with monogenic autosomal recessive transmission in Pyrenees shepherd dogs *Cleft Palate-Craniofacial Journal* 46 (1) pp 81-88

Khan. S, Basit. S, Zimri. F, Ali. G, Ansar. M & Ahmad. W (2012) A novel homozygous mutation in *WNT10B* in familial split-hand/foot malformation *Clinical Genetics* pp 48-55

Kharchenko. P, Tolstorukov. M & Park. P (2008) Design and analysis of ChIP-Seq experiements for DNA-binding proteins *Nature Biotechnology* 26 (12) pp 1351-1359

Kim. H, Herrick. S, Lemyre. E, Kishikawa. S, Salisz. J, Seminara. S, MacDonald. M, Bruns. G, Morton. C, Quade. B & Gusella. J (2005) Hypogonadotropic hypogonadism and cleft lip and palate caused by a balanced translocation producing haploinsufficiency for FGFR1 *Journal of Medical Genetics* 42 (8) pp 666-672

Kimani. J, Yoshiura. K, Shi. M, Jugessur. A, Moretti-Ferreira, Christensen. K & Murray. J (2009) Search for genomic alterations in monozygotic twins discordant for cleft lip and /or palate *Twin Research and Human Genetics* 12 (5) pp 462-468

Kling. R, Taub. P, Ye. X & Jabs. E (2014) Oral clefting in china over the last decade: 205,679 patients *Plastic and reconstructive surgery, Global open* 2 (10)

Kohli .s & Kohli. V (2012) A comprehensive review of the genetic basis of cleft lip and palate *Journal of oral and maxillofacial pathology* 16 (1) pp 64-72

Koike. J, Takagi. A, Miwa. T, Hirai. M, Terada. M & Katoh. M (1999) Molecular cloning of *Frizzled-10*, a novel member of the *Frizzled* gene family *Biochemical and Biophysical research communications* 262 (1) pp 39-43

Kondo. S, Schutte. B, Richardson. R, Bjork. B, Knight. A, Watanabe. Y, Howard.E, Derreira de Lima. R, Daack-Hirsch. S, Sander. A, McDonald-McGinn. D, Zackai. E, Lammer. E, Aylsworth. A, Ardinger. H, Lidral. A, Pober. B, Moreno. L, Arcos-Burgos. M, Valencia. C, Houdayer. C, Bahuau. M, Moretti-Ferreira. D, Richieri-Costa. A, Dixon. M & Murray. J (2002) Mutations in *IRF6* cause Van der Woude and popliteal pterygium syndromes *Nature Genetics* 32 (2) pp 285-289

Kondo. H, Hayashi. H, Oshima. K, Tahira. T & Hayashi. K (2003) Frizzled 4 gene (*FZD4*) mutations in patients with familial exudative vitreoretinopathy with variable expressivity *British Journal of Ophthalmology* 87 (10) pp 1291-1295

Koressaar. T & Remm. M (2007) Enhancements and modifications of primer design program Primer3 *Bioinformatics* 23 (10) pp 1289-1291

Koster. M (2010) p63 in skin development and ectodermal dysplasias *Journal of Investigative Dermatology* 130 (10) pp 2352-2358

Kouwenhoven. E, Heeringen. S, Tena. J, Oti. M, Dutilh. B, Alonso. M, Calle-Mustienes. E, Smeenk. L, Rinne. T, Parsaulian. L, Bolat. E, Jurgelenaite. R, Huynen. M, Hoischen. A, Veltman. J, Brunner. H, Roscioli. T, Oates. E, Wilson. M, Manzanares. M, Gómez-Skarmeta. J, Stunnenberg. H, Lohrum. M, Bokhoven. H. V & Zhou. H (2010) Genome-Wide Profiling of p63 DNA-Binding Sites Identifies an Element that Regulates Gene Expression during Limb Development in the 7q21 SHFM1 Locus *PLos Genetics* 6 (8) doi:10.1371/journal.pgen.1001065

Kouwenhoven. E, Oti. M, Niehues. H, Van Heeringen. S, Schalkwijk. J, Stunnenberg. H, Van Bokhoven. H & Zhou. H (2015) Transcription factor p63 bookmarks and regulates dynamic enhancers during epidermal differentiation *EMBO reports* 16 (7) pp 863-878

Krasnow. R, Wong. L & Adler. P (1995) Dishevelled is a component of the frizzled signalling pathway in Drosophila *Development* 121 (12) pp 4095-4102

Krejci. P, Prochazkova. J, Bryja. V, Kozubik. A & Wilcox. W (2009) Molecular pathology of the fibroblast growth factor family *Human Mutation variation, informatics, and disease* 30 (9) pp 1245-1255

Kriangkrai. R, Chareonvit. S, Yahagi. K, Fujiwara. M, Eto. K, Iseki. S (2006) Study of Pax6 mutant rat revealed the association between upper incisor formation and midface formation *Developmental Dynamics* 235 (8) pp 2134-2143

Kubbutat. M, Ludwig. R, Ashcroft. M & Vousden. K (1998) Regulation of Mdm2-Directed degradation by the C Terminus of p53 *Molecular and Cellular Biology* 18 (10) pp 5690-5698

Kubo. T, Sugimoto. K, Kojima. T, Sawada. N, Sato. N & Ichimiya. S (2014) Tight junction protein claudin-4 is modulated via ΔNp63 in human keratinocytes *Biochemical and Biophysical Research communications* 455 (3-4) pp 205-211

Kulkarni. M (2011) Digital multiplexed gene expression analysis using the NanoString nCounter system *Current protocols in molecular biology* Chapter 25: Unit25B doi: 10.1002/0471142727

Kurima. K, Hertzano. R, Gavrilova. O, Monahan. K, Shpargel. K, Nadaraja. G, Kawashima. Y, Lee. K, Ito. T, Higashi. Y, Eisenman. D, Strome. S & Griffith. A (2011) A noncoding point mutation of Zeb1 causes multiple developmental malformations and obesity in twirler mice Plos Genetics 7 (9) doi: 10.1371/journal.pgen.1002307

Kurosaka. H, Iulianella. A, Williams. T & Trainor. P (2014) Disrupting hedgehog and WNT signalling interactions promotes cleft lip pathogenesis *Journal of Clinical Investigation* 124 (4) pp 1660-1671

Kuwahara. A, Sakai. H, Xu. Y, Itoh. Y, Hirabayashi. Y & Gotoh. Y (2014) Tcf3 represses Wnt-β-catenin signalling and maintains neural stem cell population during neocortical development *PloS One* 15 (9) doi: 10.1371/journal.pone.0094408.eCollection 2014

Kuzmichev. A, Nishioka. K, Erdjument-Bromage. H, Tempst. P & Reinberg. D (2002) Histone methyltransferase activity associated with a human multiprotein complex containing the enhancer of Zeste protein *Genes & Development* 16 (22) pp 2893-2905

Lacono. N, Mantero. S, Chiarelli. A, Garcia. E, Mills. A, Morasso. M, Costanzo. A, Levi. G, Guerrini. L & Merlo. G (2008) Regulation of *Dlx5* and *Dlx6* gene expression by p63 is involved in EEC and SHFM congenital limb defects *Development* 135 pp 1377-1388

Lammer. E, Chen. D, Hoar. R, Agnish. N, Benke. J, Curry. C, Fernhoff. P, Grix. A, Lott. I, Richard. J & Sun. S (1985) Retinoic acid embryopathy *New England journal of medicine* 313 (14) pp 837-841

Lan. Y, Ryan. R, Zhang. Z, Bullard. S, Bush. J, Maltby. K, Lidral. A & Jiang. R (2006) Expression of *Wnt9b* and activation of canonical Wnt signalling during midfacial morphogenesis in mice *Developmental Dynamics* 235 (5) pp 1448-1454

Langer. L, Sulik. K & Pevny. L (2014) Cleft palate in a mouse model of *SOX2* haploinsufficiency *Cleft palatal craniofacial journal* 51 (1) pp 110-114

Laumonnier. F, Holbert. S, Ronce. N, Faravelli. F, Lenzer. S, Schwartz. C, Lespinasse. J, Van. Esch. H, Lacombe. D, Goizet. C, Phan-Dinh Tuy. F, Van Bokhoven. H, Fryns. J, Chelly. J, Ropers. H, Moraine. C, Hamel & B, Briault. S (2005) Mutations in PHF8 are associated with X-linked mental retardation and cleft lip/palate *Journal of Medical Genetics* 42 (10) pp 780-786

Laurikkala. J, Mikkola. M, James. M, Tummers. M, Mills. A & Thesleff. I (2006) p63 regulated multiple signalling pathways required for ectodermal organogenesis and differentiation *Development* 133 pp 1533-1563

Lee. J, Kim. J, Cho. K, Lee. M, Cho. S, Kwak. S, Cai. J & Jung. H (2008) *Wnt11*/*Fgfr2b* cross-talk modulates the fate of cells in palate development *Developmental Biology* 314 (2) pp 341-350

Leoyklang. P, Siriwan. P & Shotelsersuk. V (2006) A mutation of the p63 gene in non-syndromic cleft lip *Journal of medical genetics* 43 (6) pp 28

Leslie. E & Marazita. M (2014) Genetics of Cleft Lip and Cleft Palate *American Journal of Medical Genetics Part C: Seminars in Medical Genetics* 163 (4) pp 246-258

Letra. A, Fakhouri. W, Fonseca. R, Menezes. R, Kempa. I, Prasad. J, McHenry. T, Lidral. A, Moreno. L, Murray. J, Daack-Hirsch. S, Marazita. M, Castilla. E, Lace. B, Orioli. L, Granjeiro. J, Schutte. B, Vieira. A (2012) Interaction between *IRF6* and *TGFA* Genes Contribute to the Risk of Nonsyndromic Cleft Lip/Palate *PLoS one* v.7 (9) http://dx.doi.org/10.1371%2Fjournal.pone.0045441

Letra. A, Menezes. R, Granjeiro. J & Vieira. A (2009) *AXIN2* AND *CDH1* polymorphisms, tooth agenesis and oral clefts *Birth defects research part A clinical and molecular teratology* 85 (2) pp 169-173

Levéen. P, Pekny. M, Gebre-Medhin. S, Swolin. B, Larsson. E & Betsholtz. C (1994) Mice deficient for PDGF B show renal, cardiovascular, and haematological abnormalities *Genes and Development* 8 pp 1875-1887

Léveillé. N, Melo. C, Rooijers. K, Diaz-Lagares. A, Melo. S, Korkmaz. G, Lopes. Rui. Moqadam. F, Maia. A, Wijchers. P, Geeven. G, Den Boer. M, Kalluri. R, De Laat. W, Esteller. M & Agami. R (2015) Genome-wide profiling of p53-regulated enhancer RNAs uncovers a subset of enhancers controlled by a lncRNA *Nature Communications* doi: 10.1038/ncomms7520

Li. P, Zhang. H, Huff. S, Nimmakayalu. M, Qumsiyeh. M, Yu. J, Szekely. A, Xu. T & Pober. B (2006) Karyotype-phenotype insights from 11q14.1-q23.2 interstitial deletions: FZD4 haploinsufficiency and exudative vitreoretinopathy in a patient with a complex chromosome rearrangement *American Journal of Medical Genetics* 140 (24) pp 2721-2729

Li. S, Chao. A, Li. Z, Moore. C, Liu. Y, Zhu. J, Erickson. J, Hao. L & Berry. R (2012) Folic acid use and nonsyndromic orofacial clefts in China: a prospective cohort study *Epidemiology* 23 (3) pp423-432

Li. W, Chen. Y, Hayashida. Y, Blanco. G, Kheirkah. A, He. H, Chen. S, Liu. C & Tseng. S (2008) Down-regulation of *Pax6* is associated with abnormal differentiation of corneal epithelial cells in severe ocular surface diseases *Journal of Pathology* 214 (1) pp 114-122

Lidral. A, Romitti. P, Basart. A, Doetschman. T, Leysens. N, Daack-Hirsh. S, Semina. E, Johnson. L, Machida. J, Burds. A, Parnell. T, Rubenstein. J & Murray. J (1998) Association of MSX1 and TGFB3 with Nonsyndromic Clefting in Humans *American Journal of Human Genetics* (63) pp 557-568

Lindahl. E, Garcia.E & Mills. A (2013) An Allelic series of *Trp63* mutations defines Tap63 as a modifier of EEC syndrome *American Journal of Medical Genetics* 0 (8) pp 1961-1971

Little. J, Cardy. A & Munger. R (2004b) Tabacco smoking and oral clefts: a meta-analysis *Bulletin of the World Health Organization* 82 (3) pp 213-218

Little. J, Cardy. A, Arslan. M, Gilmour. M & Mossey. P (2004a) Smoking and Orofacial Clefts: A United Kingdom-Based Case-Control Study *The Cleft Palate-Craniofacial Journal* 41 (4) pp 381-386

Liu. P, Wakamiya. M, Shea. M, Albrecht. U, Behringer. R & Bradley. A (1999) Requirement for *Wnt3* in vertebrate axis formation *Nature Genetics* 22 pp 361-365

Liu. W, Selever. J, Wang. D, Lu. M, Moses. K, Schwartz. R & Martin. J (2004) Bmp4 signalling is required for outflow-tract septation and branchial-arch artery remodelling *PNAS* 101 (10) pp 4489-4494

Liu. W, Sun. X, Braut. A, Mishina. Y, Behringer. B, Mina. M & Martin. J (2005) Distinct functions for BMP signalling in lip and palate fusion in mice *Development (*132) pp 1453-1461

Livak. K & Schmittgen. T (2001) Analysis of relative gene expression data using real-time quantitative PCR and the 2(-Delta Delta C(T)) method *Methods* 25 (4) pp 402-408

Lohnes. D, Mark. M, Mendelsohn. C, Dollé. P, Dierich. A, Gorry. P, Gansmuller. A & Chambon. P (1994) Function of the retinoic acid receptors (RARs) during development *Development* 120 pp 2723-2748

Lonardo. F, Sabba. G, Luquetti. D, Monica. M & Scarano. G (2007) Al-Awadi/Raas-Rothschild syndrome: Two new cases and review *American Journal of medical genetics* 143A (24) pp 3169-3174

Lopardo. T, Iacono. N, Marinari. B, Giustizieri. M, Cyr. D, Merlo. G, Crosti. F, Costanzo. A & Guerrini. L (2008) Claudin-1 is a p63 target gene with a crucial role in epithelial development *PLoS ONE* 3 (7) doi: 10.1371/journal.pone.0002715

Lovén. J, Orlando. D, Sigova. A, Lin. C, Rhal. P, Burge. C, Levens. D, Lee. T & Young. R (2012) Revisiting global gene expression analysis *Cell* 151 (3) pp 476-482

Ludwig. K, Mangold. E, Herms. S, Nowak. S, Reutter. H, Paul. A, Becker. J, Herberz. R, AlChawa. T, Nasser. E, Böhmer. A, Mattheisen. M, Alblas. M, Barth. S, Kluck. N, Lauster. C, Brumann. B, Reich. R, Hemprich. A, Pötzsch. S, Blaumeiser. B, Daratsianos. N, Kreusch. T, Murray. J, Marazita. M, Ruczinski. I, Scott. A, Beaty. T, Kramer. F, Wienker. T, Steegers-Theunissen. R, Rubini. M, Mossey. P, Hoffmann. P, Lange. C, Cichon. S, Propping. P, Knapp. M & Nöthen. M (2012) Genome-wide meta-analyses of nonsyndromic cleft lip with or without cleft palate identify six new risk loci *Nature Genetics* 44 (9) pp 968-971

Lu. W, Chua. M, Wei. W & So. S (2015) NDRG1 promotes growth of hepatocellular carcinoma cells by directly interacting with GSK-3β and Nur77 to prevent β-catenin degradation *Oncotarget* PMID: 26359353

Lyon. M (1958) Twirler: a mutant affecting the inner ear of the house mouse *Journal of embryology and experimental morphology* 6 (1) pp 105-116

MacPartlin. M, Zeng. S, Lee. H, Stauffer. D, Jin. Y, Thayer. M & Lu. H (2005) P300 regulates p63 transcriptional activity *The Journal of Biological Chemistry* 280 pp 30604-30610

Magdaleno. S, Jensen. P, Brumwell. C, Seal. A, Lehman. K, Asbury. A, Cheung. T, Cornelius. T, Batten. D, Eden. C, Norland. S, Rice. D, Dosooye. N, Shakya. S, Mehta. P & Curran. T (2006) BGEM: An In Situ Hybridization database of gene expression in the embryonic and adult mouse nervous system *PLOS Biology* Doi: 10.1371/journal.pbio.0040086

Mailleux. A, Spencer-Dene. B, Dillon. C, Ndiaye. D, Savona-Baron. C, Itoh. N, Kato. S, Dickson. C, Theiry. J & Bellusci. S (2002) Role of FGF10/FGFR2b signalling during mammary gland development in the mouse embryo *Development* 129 pp 53-60

Mandalos. N, Rhinn. M, Granchi.Z, Karampelas. I, Mitsiadis. T, Economides. A, Dollé. P & Remboutsika. E (2014) Sox2 acts as a rheostat of epithelial to mesenchymal transition during neural crest development *Frontiers in Physiology* 5 (345) doi: 10.3389/fphys.2014.00345

Mandel. H, Shemer. R, Borochowitz. Z, Okopnik. M, Knopf. C, Indelman. M, Drugan. A, Tiosano. D, Gershoni-Baruch. R, Choder. M & Sprecher. E (2008) SERKAL syndrome: An autosomal-recessive disorder caused by a loss-of-function mutation in *WNT4 American Journal of Human Genetics* 82 (1) pp 39-47

Mangiulli. M, Valletti. A, Caratozzolo. M. F, Tullo. A, Sbisà, Pesole. G & D'Erchia. A. M (2009) Identification and functional characterization of two new transcriptional variants of the human p63 gene *Nucleic Acids Research* 37 (18) pp6092-6104

Mangold. E, Ludwig. E, Birnbaum. S, Baluardo. C, Ferrian. M, Herms. S, Reutter. H, de Assis. N, Chawa. T, Mattheisen. M, Steffens. M, Barth. S, Kluck. N, Paul. A, Becker. J, Lauster. C, Schmidt. G, Braumann. B, Scheer. M, Reich. R, Hemprich. A, Pötzsch. S, Blaumeiser. B, Moebus. S, Krawczak. M, Schreiber. S, Meitinger. T, Wichmann. H, Steegers-Theunissen. R, Kramer. F, Cichon. S, Propping. P, Wienker. T, Knapp. M, Rubini. M, Mossey. P, Hoffmann. P & Nöthen. M (2010) Genome-wide association study identifies two susceptibility loci for nonsyndromic cleft lip with or without cleft palate *Nature Genetics* 42 (1) pp 42-26

Mansilla. M, Cooper. M, Goldstein. T, Castilla. E, Camelo. J, Marazita. M & Murray. J (2007) Contributions of PTCH gene variants to isolated cleft lip and palate *Cleft Palate Craniofacial Journal* 43 (1) pp 21-29

Mao. B & Niehrs. C (2003) Kremen2 modulates dickkopf2 activity during Wnt/LRP6 signalling *Gene* 302 (1-2) pp 179-183

Mao. B, Wu. W, Davidson. G, Marhold. J, Li. M, Mechler. B, Delius. H, Hoppe. D, Stannek. P, Walter. C, Glinka. A & Niehrs. C (2002) Kremen proteins are Dickkopf receptors that regulate Wnt/β-catenin signalling *Nature* 417 pp 664-667

Mao. B, Wu. W, Li. Y, Hoppe. D, Stannek. P, Glinka. A & Niehrs. C (2001) LDL-receptor-related protein 6 is a receptor for Dickkopf proteins *nature* 411 (6835) pp 321-325

Marazita. M (2012) The Evolution of Human Genetic Studies of Cleft Lip and Cleft Palate *Annual Review of Genomics and Human Genetics* DOI: 10.1146/annurev-genom-090711-163729

Mardaryev. A, Gdula. M, Yarker. J, Emelianov. V, Poterlowic. K, Sharov. A, Sharova. T, Scarpa. J, Chambon. P, Botchkarev. V & Fessing. M (2014) p63 and Brg1 control developmentally regulated higher-order chromatin remodelling at the epidermal differentiation complex locus in epidermal progenitor cells *Development* 141 (1) pp 101-111

Maretto. S, Cordenonsi. M, Dupont. S, Braghetta. P, Broccoli. V, Hassan. A, Volpin. D, Bressan. G & Piccolo. S (2003) Mapping Wnt/Beta-catenin signalling during mouse development and in colorectal tumours *Proceedings of the National Academy of Sciences of the United States of America* 100 (6) pp 3299-304

Martelli-Junior. H, Chaves. M, Swerts. M, Teixeira de Miranda. R, Bonan. P & Coletta. R (2007) Clinical and Genetic Features of Van der Woude Syndrome in Two Large Families in Brazil *The Cleft Palate-Craniofacial Journal* 44 (3) pp 239-243

Martínez-Álvarez. C, Tudela. C, Perez-Miguelsanz. J, O'Kane. S, Puerta. J & Ferguson. M (2000) Medial edge

epithelial cell fate during palatal fusion *Developmental Biology* 220 pp 343-357

Mason. J, Morrison. D, Basson. A & Licht. J (2006) Sprouty proteins: multifaceted negative-feedback regulators of receptor tyrosine kinase signalling *Trends in Cell Biology* 16 (1) pp 45-54

Masoumi-Moghaddam. S, Amini. A, Ehteda. A, Wei. A & Morris. D (2014) The expression of the Sprouty1 protein inversely correlated with growth, proliferation, migration and invasion of ovarian cancer cells *Journal of Ovarian Research* 7: 61

Matovinovic. E & Richman. J (1997) Epithelium is required for maintaining FGFR-2 expression levels in facial mesenchyme of the developing chick embryo *Developmental Dynamics* 210 pp 407-416

Matsumura. K, Taketomi. T, Yoshizaki. K, Yoshiga. D, Maehara. T, Sanui. T, Yoshimura. A & Nakamura. S (2010) Spry2 deficient mice exhibit cleft palate *IADR General Session conference paper 2010 https://www.researchgate.net/publication/266770951_Spry2_Deficient_Mice_Exhibit_Cleft_Palate*

Matthews. J, Oddone-Paolucci. E & Harrop. R (2014) The Epidemiology of Cleft Lip and Palate in Canada, 1998 to 2007 *The Cleft palate-craniofacial journal: official publication of the American Cleft Palate-Craniofacial Association* http://dx.doi.org/10.1597/14-047

McCabe. M, Gaston-Massuet. C, Tziaferi. V, Gregory. L, Alatzoglou. K, Signore. M, Puelles. E, Gerrelli. D, Farooqi. S, Raza. J, Walker. J, Kavanaugh. S, Tsai. P, Pitteloud. N, Martinez-Barbera. J & Dattani. M (2011) Novel *FGF8* mutations associated with recessive holoprosencephaly, craniofacial defects, and hypothalamo-pituitary dysfunction *Journal of Clinical endocrinology and metabolism* 96 (10) pp 1709-1718

McDade. S, Henry. A, Pivato. G, Kozarewa. Mitsopoulos. C, Fenwick. K, Assiotis. I, Hakas. J, Zvelebil. M, Orr. N, Lord. C, Patel. D, Ashworth. A & McCance. D (2012) Genome-wide analysis of p63 binding sites identifies AP-2 factors as co-regulators of epidermal differentiation *Nucleic Acids research* doi: 10.1093/nar/gks389

McGrath. J, Duijf. P, Doetsch. V, Irvine. A, De Waal. R, Vanmolkot. K, Wessagowit. V, Kelly. A, Atherton. D, Griffiths. W, Orlow. S, Van Haeringen. A, Ausems. M, Yang. A, McKeon. F, Bamshad. M, Brunner. H, Hamel. B & Van Bokhoven. H (2001) Hay-Wells syndrome is caused by heterozygous missense mutations in the SAM domain of p63 *Human molecular genetics* 10 (3) pp 221-229

McLean. C, Bristor. D, Hiller. M, Clarke. S, Schaar. B, Lowe. C, Wenger. A & Bejerano. G (2010) GREAT improves functional interpretation of cis-regulatory regions. *Nature Biotechnology* 28 (5) pp 495-501

McNeish. J, Scott. W & Potter. S (1988) Legless a novel mutation found in PHT1-1 Transgenic mice *Science* 241 (4867) pp 837-839

Medio. M, Yeh. E, Popelut. A, Babajko. S, Berdal. A & Helms. J (2012) Wnt/β-catenin signalling and Msx1 promote outgrowth of the maxillary prominences *Frontiers in Physiology* 3 pp 375

Melo. C, Drost. J, Wijchers. P, Van De Werken. H, De Wit. E, Oude Vrielink. J, Elkon. R, Melo. S, Léveillé. N, Kalluri. R, Laat. W & Agami. R (2013) eRNAs are required for p53-dependent enhancer activity and gene transcription *Molecular Cell* 49 (3) pp 524-535

Menezes. R, Marazita. M, McHenry. T, Cooper. M, Bardi. K, Brandon. C, Letra. A, Martin. R & Vieira. A (2009) *AXIN2*, Orofacial clefts and Positive Family History for Cancer *Journal of the American Dental Association* 140 (1) pp 80- 84

Merika. M, Williams. A, Chen. G, Collins. T & Thanos. D (1998) Recruitment of CBP/p300 by the IFNβ enhanceosome is required for synergistic activation of transcription *Molecular Cell* 1 (2) pp 277-287

Metzis. V, Courtney. A, Kerr. M, Ferguson. C, Rondón Galeano. M, Parton. R, Wainwright. B & Wicking. C (2013) Patched1 is required in neural crest cells for the prevention of orofacial clefts *Human Molecular Genetics* 22 (24) pp 5026-5035

Millicovsky. G & Johnston. M (1981) Hyperoxia and hypoxia in pregnancy: Simple experimental manipulation alters the incidence of cleft lip and palate in CL/Fr mice *Developmental Biology* 78 (9) pp 5722-5723

Mills. A, Zheng. B, Wang. X-J, Vogel. H, Roop. D & Bradley. A (1999) p63 is a p53 homologue required for limb and epidermal morphogenesis *Nature* 398 pp 708- 713

Mills. J, Molloy. A, Parle-McDermott. A, Troendle. J, Brody. L, Conley. M, Cox. C, Pangilinan. F, Orr. D, Earley. M, McKiernan. E, Lynn. E, Doyle. A, Scott. J and Kirke. P (2009) Folate-Related Gene Polymorphisms as Risk

Factors for Cleft Lip and Cleft Palate *Birth Defects Research Part A: Clinical and Molecular Teratology* 82 (9) pp 636-643

Mitchell. K, O'Sullivan. J, Missero. C, Blair. E, Richardson. R, Anderson. B, Antonini. D, Murray. J, Shanske. A, Schutte. B, Romano. R, Sinha. S, Bhaskar. S, Black. G, Dixon. J & Dixon. M (2012) Exome sequence identifies RIPK4 as the bartsocas-Papas syndrome locus *American Journal of Human Genetics* 90 (1) pp 69-75

Mitchell. K, Rosario. M, Zhou. H, Kouwenhoven. E, Donaldson. I, Zeef. L, Burgiss. T, Blance. R, Heeringen. S, Stunnenberg. H, Missero. C, Dixon. M & Dixon. J (manuscript in preparation) p63 is a master regulator of epithelial adhesion during palatal development

Mo. R, Freer. A, Zinyk. D, Crackower. M, Michaud. J, Heng. H, Wai Chik. K, Shi. X, Tsui. L, Cheng. S, Joyner. A & Hui. C (1997) Specific and redundant functions of Gli2 and Gli3 zinc finger genes in skeletal patterning and development *Development* 124 pp 113-123

Mollo. M, Antonini. D, Mitchell. K, Fortugno. P, Costanzo. A, Dixon. J, Brancati. F & Missero. C (2015) p63-dependent and independent mechanisms of nectin-1 and nectin-4 regulation in the epidermis *Experimental Dermatology* 24 (2) pp 114-119

Moreno. L, Mansilla. M, Bullard. S, Cooper. M, Busch. T, Machida. J, Johnson. M, Brauer. D, Krahn. K, Daack-Hirsch. S, L'Heureux. J, Valencia-Ramirez. C, Rivera. D, López. A, Moreno. M, Hing. A, Lammer. E, Jones. M, Christensen. K, Lie. R, Jugessur. A, Wilcox. A, Chines. P, Pugh. E, Doheny. K, Arcos-Burgos. M, Marazita. M, Murray. J & Lidral. A (2009) *FOXE1* association with both isolated cleft lip with or without cleft palate, and isolated cleft palate *Human Molecular Genetics* 18 (24) pp 4879-4896

Moretti. F, Marinari. B, Iancono. N, Botti. E, Giunta. A, Spallone. G, Garaffo. G, Vernersson-Lindahl. E, Merlo. G, Mills. A, Ballarò. C, Alemà, Chimenti. S, Guerrini. L & Costanzo. A (2010) A regulatory feedback loop involving p63 and IRF6 links the pathogenesis of 2 genetically different human ectodermal dysplasias *Journal of Clincal Investigation* 120 (5) pp1570-1577

Mossey. P & Modell. B (2012) Epidemiology of oral clefts 2012: an international perspecitve *Frontiers of Oral Biology* 16 pp 1-18

Mossey. P, Davies, Little. J (2007) Prevention of Orofacial Clefts: Does Pregnancy Planning Have a Role? *The Cleft Palate-Craniofacial Journal* 44 (3) pp 244-250

Mossey. P, Little. J, Munger. R, Dixon. M & Shaw. W (2009) Cleft lip and Palate *The Lancet* 374 (9703) pp 1773-1785

Mostowska. A, Hozyasz. K, Biedziak. B, Wojcicka. P, Lianeri. M & Jagodzinski. P (2012) Genotype and haplotype analysis of *WNT* genes in non-syndromic cleft lip with or without cleft palate *European Journal of Oral Sciences* 120 pp 1-8

Motoyama. J, Liu. J, Mo. R, Ding. Q, Post. M & Hui. C (1998) Essential function of *Gli2* and *Gli3* in the formation of lunch, trachea and oesophagus *Nature Genetics* 20 pp 54-57

Moxham. B (2003) The development of the palate- a brief review *European Journal of Anatomy* 7 pp53-74

Mukhopadhyay. M, Shtrom. S, Rodriguez-Esteban. C, Chen. L, Tsukui. T, Gomer. L, Dorward. D, Glinka. A, Grinberg. A, Guang. S, Niehrs. C, Belmonte. J & Westphal. H (2001) *Dickkopf1* is required for embryonic head induction and limb morphogenesis in the mouse *Developmental Cell* 1 (3) pp 423-434

Murray. J (2002) Gene/environment causes of cleft lip and/or palate *Clinical Genetics* 61 (4) pp 248-256

Nakazawa. M, Matsunaga. K, Asamura. S, Kusuhara. H, Isogai. N & Muragaki. Y (2008) Molecular mechanisms of cleft lip formation in CL/Fr mice *Scandinavian journal of plastic and reconstructive surgery and hand surgery* 42 (5) pp 225-232

Nanni. L, Ming. J, Bocian. M, Steinhaus. K, Bianchi. D, Die-Smulders. C, Giannotti. A, Imaizumi. K, Jones. K, Campo. M, Martin. R, Meinecke. P, Pierpont. M, Robin. N, Young. I, Roessler. E & Muenke. M (1999) The mutational spectrum of the *Sonic Hedgehog* gene in holoprosencephaly: *SHH* mutations cause a significant proportion of autosomal dominant holoprosencrephaly *Human Molecular genetics* 8 (13) pp 2479-2488

Neilson. D, Brunger. J, Heeger. S, Bamshad. M & Robin. N (2002) Mixed clefting type in Rapp-Hodgkin

syndrome *American Journal of Medical Genetics* 108 (4) pp 281-284

Ng. S, Buckingham. K, Lee. C, Bigham. A, Tabor. H, Dent. K, Huff. C, Shannon. P, Jabs. E, Nickerson. D, Shendure. J & Bamshad. M (2010) Exome sequencing identified the cause of a mendelian disorder *Nature Genetics* 42 (1) pp 30-35

Nickel. R & Forge. A (2010) Gap junctions and connexions: the molecular genetics of deafness *eLS* doi: 10.1002/9780470015902.a0021441

Nie. X, Luukko. K & Kettunen. P (2006) BMP signalling in craniofacial development *The international journal of developmental biology* 50 (6) pp 511-521

Niemann. S, Zhao. C, Pascu. F, Stahl. U, Aulepp. U, Niswander. L, Weber. J & Müller. U (2004) Homozygous *WNT3* mutation causes tetra-amelia in a large consanguineous family *American Journal of human genetics* 74 (3) pp 558-563

Nieto. M, Patel. K & Wilkinson. D (1996) In situ hybridization of chick embryos in whole mount and tissue sections *Methods in Cell biology* 51 pp 219-235

Northcott. P, Shih. D, Remke. M, Cho. Y, Kool. M, Hawkins. C, Eberhart. C, Dubuc. A, Guettouche. T, Cardentey. Y, Bouffet. E, Pomeroy. S, Marra. M, Malkin. D, Rutka. J, Korshunov. A, Pfister S & Taylor. M (2012) Rapid, reliable, and reproducible molecular sub-grouping of clinical medulloblastoma samples *Acta Neuropathologica* 123 (4) pp 615-626

Nopoulos. P, Langbehn. D, Canady. J, Magnotta. V & Richman. L (2007) Abnormal brain structure in children with isolated clefts of the lip or palate *Archives of paediatrics & adolescent medicine* 161 (8) pp 753-758

Ockeleon. C, Khandelwal. K, Dreesen. K, Ludwig. K, Sullivan. R, van Rooij. I, Thonissen. M, Swinnen. S, Phan. M, Conte. F, Ishorst. N, Gilissen. C, RoaFuentes. L, van de Vorst. M, Henkes. A, Steehouwer. M, Beusekom. E, Bloeman. M, Vankeirsbilck. B, Bergé. S, Hens. G, Schoenaers. J, Poorten. V, Roosenboom. J, Verdonck. A, Devriendt. K, Roeleveldt. N, Jhangiani. S, Vissers. A, Lupski. J, Ligt. J, Von den Hoff. J, Pfundt. R, Brunner. H, Zhou. H, Dixon. J, Mangold. E, Bokhoven. H, Dixon. M, Kleefstra. T, Hoischen. A, Carels. C (2015) Novel mutations in *LRP6* highlight the role of WNT signalling in tooth agenesis *In submission*

Ornitz. D (2000) FGFs, heparan sulphate and FGFRs: complex interactions essential for development *Bioassays* 22 pp 108-112

Orr-Urtreger. A, Bedford. M, Do. M, Eisenbach. L & Lonai. P (1992) Developmental expression of the α receptor for platelet-derived growth factor, which is deleted in the embryonic lethal *Patch* mutation *Development* 115 pp 289-303

Ortt. K & Sinha. S (2008) Derivation of the consensus DNA-binding sequence for p63 reveals unique requirements that are distinct from p53 *FEBS Letters* 580 (7) pp 4544-4550

Ouyang. J, Shen. Y, Yeh. L, Li. W, Coyle. B, Liu. C & Fini. M (2006) Pax6 overexpression suppresses cell proliferation and retards the cell cycle in corneal epithelial cells *Investigative ophthalmology & visual science* 47 (6) pp 2397-2407

Ouyang. H, Xue. Y, Lin. Y, Zhang. X, Xi. L, Patel. S, Cai. H, Luo. J, Zhang. M, Zhang. M, Yang. Y, Li. G, Jiang. W, Yeh. E, Lin. J, Pei. M, Zhu. J, Cao. G, Zhang. L, Yu. B, Chen. S, Fu. X, Liu. Y & Zhang. K (2014) WNT7A and PAX6 define corneal epithelium homeostasis and pathogenesis *Nature* 511 (7509) pp 358-361

Packman. E & Brook. J (2003) T-box genes in human disorders *Human Molecular Genetics* 12 (1) pp 37-44

Paik. D, Rai. M, Ryzhov. S, Sanders. L, Aisagbonhi. O, Funke. M, Feoktistov. I and Hatzopoulos. A (2015) Wnt10b gain of function improves cardiac repair by arteriole formation and attenuation of fibrosis *Circulation research* pii: CIRCRESAHA. 115.306886

Pankau. R, Gosch. A, Simeoni. E & Wessel. A (1993) Williams-Beuren syndrome in monozygotic twins with variable expression *American Journal of Medical Genetics* 47 (4) pp 475-477

Pannone. G, Bufo. P, Santoro. A, Franco. R, Aquino. G, Longo. F, Botti. G, Serpico. R, Cafarelli. B, Abbruzzese. A, Caraglia. M, Papagerakis. S & Muzio. L (2010) WNT pathway in oral cancer: epigenetic inactivation of WNT-inhibitors *Oncology Reports* 24 pp 1035-1041

Paperna. T, Peoples. R, Wang. Y, Kaplan. P & Francke. U (1998) Genes for the CPE receptor (*CPETR1*) and the human homolog of RVP1 (*CPETR2*) are localized within the Williams-Beuren syndrome deletion *Genomics* 54 (3) pp 453-459

Parada. C & Chai. Y (2013) Roles of BMP signalling pathway in lip and palate development *Frontiers of oral biology* (16) pp 60-70

Park. H, Platt. K, Matise. M, Beeghly. A, Hui. C, Nakashima. M & Joyner. A (2000) Mouse Gli1 mutants are viable but have defects in SHH signalling in combination with a Gli2 mutation *Development* 127 (8) pp 1593-1605

Parr. B & McMahon. A Dorsalizing signal *Wnt-7a* required for normal polarity of D-V and A-P axes of mouse limb *Letters to Nature* 374 pp 350-353

Patel. R, Tripathi. F, Singh. S, Rani. A, Bhattacharya. V & Ali. A (2014) A novel *GLI3*c.750delC truncation mutation in a multiplex Greig cephalopolysyndactyly syndrome family with an unusual phenotypic combination in a patient *Meta Gene* 2 pp 880-887

Pérez Jurado. L (2003) Williams-Beuren Syndrome: A model of Recurrent Genomic Mutation *Hormone Research* 59 (1) pp 106-113

Petiot. A, Conti. F, Grose. R, Revest. J, Hadovala-Dilke. K & Dickson. C (2003) A crucial role for Fgfr2-IIIb signalling in epidermal development and hair follicle patterning *Development* 130 pp 5493-5501

Peyrard-Janvid. M, Leslie. E, Kousa. Y, Smith. T, Dunnwald. M, Magnusson. M, Lentz. B, Unneberg. P, Fransson. I, Koillinen. H, Rautio. J, Pegelow. M, Karsten. A, Basel-Vanagaite. L, Gordon. W, Andersen. B, Svensson. T, Murray. J, Cornell. R, Kere. J & Schutte. B (2014) Dominant mutations in *GRHL3* cause Van der Woude Syndrome and disrupt oral periderm development *American Journal of Human Genetics* 94 (1) pp 23-32

Pinson. K, Brennan. J, Monkley. S, Avery. B & Skarnes. W (2000) An LDL-receptor-related protein mediates Wnt signalling in mice *Nature* 407 pp 535-538

Prosser. J & van Heyningen. V (1998) PAX6 mutations reviewed *Human mutation* 11 (2) pp 93-108

Quaderi. N, Schweiger. K, Gaudenz. K, Franco. B, Rugarli. E, Berger. W, Feldman. G, Volta. M, Andolfi. G, Gilgenkrantz. S, Marion. R, Hennekarn. R, Opitz. J, Muenke. M, Ropers. H & Ballabio. A (1997) Opitz G/BBB syndrome, a defect of midline development, is due to mutations in a new RNG finger gene on Xp22 *Nature genetics* 17 pp 285-291

Rahimov. F, Marazita. M, Visel. A, Cooper. M, Hitchler. M, Rubini. M, Domann. F, Govil. M, Christensen. K, Bille. C, Melbye. M, Jugessur. A, Lie. R, Wilcox. A, Fitzpatrick. D, Green. E, NISC Comparative sequencing Programme, Mossey. P, Little. J, Steegers-Theunissen. R, Pennacchio. L, Schutte. B & Murray. J (2008) Disruption of an AP-2α binding site in an *IRF6* enhancer is strongly associated with cleft lip *Nature Genetics* 40 (11) pp 1341-1347

Richard. A, Lyons. P, Peters. J, Biasci. D, Flint. S, Lee. J, McKinney. E, Siegel. R & Smith. K (2014) Comparison of gene expression microarray data with count-based RNA measurements informs microarray interpretation *BMC Genomics* 15 pp 649

Richard. G, Smith. L, Bailey. R, Itin. P, Hohl. D, Epstein. E, DiGiovanna. J, Compton. J & Bale. S (1998) Mutations in the human connexion gene GJB3 cause erythrokeratodermia variabilis *Nature Genetics* 20 (4) pp 366-369

Richarte. A, Mead. H & Tallquist. M (2007) Cooperation between PDGF receptors in cardiac neural crest cell migration *Developmental biology* 306 (2) pp 785-796

Richman. J & Crosby. Z Differential growth of facial primordial in chick embryos: responses of facial mesenchyme to basic fibroblast growth factor (bFGF) and serum in micromass culture *Development* (109) pp 341-348

Rijsewijk. F, Schuermann. M, Wagenaar. E, Parren. P, Weigel. D & Nusse. R (1987) The drosophila homolog of the mouse mammary oncogene int-1 is identical to the segment polarity gene wingless *Cell* 50 (4) pp 649-657

Riley. B, Mansilla. A, Ma. J, Daack-Hirsch. S, Maher. B, Raffensperger. L, Russo. E, Vieira. A, Dodé. C, Mohammadi. M, Marazita. M & Murray. J (2007) Impaired FGF signalling contributes to cleft lip and palate *PNAS* 104 (11) pp 4512-4517

Rinne. T, Brunner. H & Bokhoven. H. V (2007) p63-Associated Disorders *Cell Cycle* 6 (3) pp 262-268

Robbins. J, McGuire. P, Wehrle-Haller. B, Rogers. S (1999) Diminished Matrix Metalloproteinase 2 (MMP-2) in Ectomesenchyme-Derived Tissues of the *Patch* mutant mouse: Regulation of MMP-2 by PDGF and Effects on Mesenchymal Cell migration *Developmental Biology* 212 (2) pp 255-263

Robitaille. J, MacDonald. M, Kaykas. A, Sheldahl. L, Zeisler. J, Dubé. M, Zhang. L, Singaraja. R, Guernsey. R, Zheng. B, Siebert. L, Hoskin-Mott. A, Trese. M, Pimstone. S, Shastry. B, Moon. R, Hayden. M, Goldbery. Y & Samuels. M (2002) Mutant frizzled-4 disrupts retinal angiogenesis in familial exudative vitreoretinopathy *Nature Genetics* 32 (2) pp 326-330

Rocco. J, Leong. C, Kuperwasser. N, DeYoung. M & Ellisen. L (2006) p63 mediated survival in squamous cell carcinoma by suppression of p73-dependent apoptosis *Cancer Cell* 9 (1) pp 45-56

Roelfsema. J, White. S, Ariyürek. Y, Bartholdi. D, Niedrist. D, Papadia. F, Bacino. C, den Dunnen. J, van Ommen. G, Breuning. M, Hennekam. R & Peters. D (2005) Genetic heterogeneity in Rubinstein-Taybi syndrome: mutations in both the CBP and EP300 genes cause disease *American Journal of Human Genetics* 76 (4) pp 572-580

Roelfsema. N & Cobben. J (1996) The EEC syndrome: a literature study *Clinical Dysmorphology* (5) pp 115-127

Roessler. E, Belloni. E, Gaudenz. K, Jay. P, Berta. P, Scherer. W, Tsui. L & Muenke. M (1996) Mutations in the human sonic hedgehog gene cause holoprosencephaly *Nature Genetics* (14) pp 357- 360

Romano. R, Birkaya. B & Sinha. S (2006) A functional enhancer of keratin 14 is a direct transcriptional target of deltaNp63 *Journal of Investigative Dermatology* 127 (5) pp 1175-1186
Romano. R-A, Smalley. K, Liu. S & Sinha. S (2010) Abnormal hair follicle development and altered cell fate of follicular keratinocytes in transgenic mice expressing ΔNp63α *Development* 137 pp 1431-1439

Romano. R-A, Smalley. K, Magraw. C, Serna. V, Kurita. T, Raghavan. S & Sinha. S (2012) ΔNp63 knockout mice reveal its indispensable role as a master regulator of epithelial development and differentiation *Development* 139 (4) pp 772-782

Rosenfeld. J, Ballif. B, Martin. D, Aylsworth. A, Bejjani. B, Torchia. B & Shaffer. L (2010) Clinical characterisation of individuals with deletions of genes in holoprosencephaly pathways by aCGH refines the phenotypic spectrum of HPE *Human Genetics* 127 (4) pp 421-440

Ross. R, Glomset. J, Kariya. B & Harker. L (1974) A Platelet-dependent serum factor that stimulates the proliferation of arterial smooth muscle cells *in vitro PNAS* 71 (4) pp 1207-1210

Sangwa. C, Mukuku. O, Tshisuz. C, Panda. J, Kakinga. M, Kitembo. M, Mutomb. J & Obimba. B (2014) Cleft lip palate in the Katanga Province of the Democratic Republic of Congo: epidemiological clinicopathological and therapeutic aspects *The Pan African medical journal* (17) pp 319

Sathyamurthy. A, Freund. S, Johnson. C, Allen. M & Bycroft. M (2011) Structural basis of p63α SAM domain mutants involved in AEC syndrome *FEBS Journal* 278 pp 2680-2688

Sayan. E, D'Angelo. B, Sayan. B, Tucci. P, Cimini. A, Cerù. M, Knight. R & Melino. G (2010) p73 and p63 regulate the expression of fibroblast growth factor receptor 3 *Biochemical and Biophysical Research Communications* 394 (3) pp 824-828

Scapoli. L, Palmieri. A, Marinelli. M, Vaccari. C, Marchesini. J, Pezzetti. F, Baciliero. U, Padula. E, Carinci. P & Carinci. F (2006) Study of the PVRL1 gene in Italian nonsyndrome cleft lip patients with or without cleft palate *Annals of Human Genetics* 70 (3) pp 410-413

Selvaraj. P, Huang. J, Chen. A, Skalka. N, Rosin-Arbesfeld R & Loh. Y (2015) Neurotrophic factor-α1 modulates NGF-induced neurite outgrowth through interaction with Wnt-3a and Wnt-5a in PC12 cells and cortical neurons *Molecular and cellular neurosciences* doi: 10.1016/j.mcn.2015.08.005

Serber. Z, Lai. H, Yang. A, Ou. H, Sigal. M, Kelly. A, Darimont. B, Duijf. P, Bokhoven. H, Mckeon. F & Dötsch. V (2002) A C-terminal Inhibitory Domain Controls the Activity of p63 by an intramolecular mechanism *Molecular Cellular Biology* 22 (24) pp 8601-8611

Sethi. I, Sinha. S & Buck. M (2014) Role of chromatin and transcriptional co-regulators in mediating p63-genome interactions in keratinocytes *BMC Genomics* 15 (1) pp 1042

Setó-Salvia. N & Stanier. P (2014) Genetics of cleft lip and/or cleft palate: Association with common anomalies *European Journal of Medical Genetics* 57 pp 381-393

Shkoukani. M, Lawrence. L, Liebertz. D& Svider. P (2014) Cleft palate: A clinical review *Birth Defects Research Part C: Embryo Today: Reviews* 102 (4) pp 333-342

Shuler. C, Halpern. D, Guo. Y & Sank. A (1992) Medial edge epithelium fate traced by cell lineage analysis during epithelial-mesenchymal transformation in vivo *Dev. Biol.* 154 pp 318-330

Sieber. C, Kopf. J, Hiepen. C & Knaus. P (2009) Recent advances in BMP receptor signaling *Cytokine & Growth Factor Reviews* 20 (5-6) pp 343-355

Simonis. M, Klous. P, Splinter. E, Moshkin. Y, Willemsen. R, Wit. E, Steensel. B, Laat. W (2006) Nuclear organisation of active and inactive chromatin domains uncovered by chromosome conformation capture-on-chip (4C) *Nature Genetics* 38 pp 1348-1354

Singh. G, Supp. D, Schreiner. C, McNeish J, Merker. H, Copeland. N, Jenkins. N, Potter. S & Scott (1991) Legless insertional mutation: morphological, molecular, and genetic characterisation *Genes & Development* 5 (12A) pp 2245-2255

Smeenk. L, Van Heeringen. S, Koeppel. M, Van Driel. M, Bartels. S, Akkers. R, Denissov. S, Stunnenberg. H & Lohrum. M (2008) Characterization of genome-wide p53 binding sites upon stress response *Nucleic Acids Research* 36 (11) pp 3639-3654

Smith. C & Tallquist. M (2010) PDGF function in diverse neural crest cell populations *Cell Adhesion & Migration* 4 (4) pp 561-566

Som. P & Naidich. T (2013a) Illustrated review of the embryology and development of the facial region, part1: Early face and lateral nasal cavities *American journal of neuroradiology* (34) pp 2233-2240

Som. P & Naidich. T (2013b) Illustrated review of the embryology and development of the fetal face and changes in the face from the newborn to adulthood *American journal of neuroradiology* (35) pp 10-18

Song. L, Li. Y, Wang. K, Wang. Y-Z, Molotkov. A, Gao. L, Zhao. T, Yamagami. T, Wang. Y, G. Q, Pleasure. D & Zhou. C (2009) Lrp6-mediated canonical Wnt signalling is required for lip formation and fusion *Development* 136 pp 3161-3171

Soriano. P (1997) The PDGFα receptor is required for neural crest cell development and for normal patterning of the somites *Development* 124 pp 2691-2700

Sowińska-Seidler. A, Socha. M & Jamsheer. A (2014) Split-hand/foot malformation – molecular cause and implications in genetic counseling *Journal of Applied Genetics* 55 (1) pp 105-115

Sözen. M, Suzuki. K, Tolarova. M, Bustos. T, Fernández Iglesias. J & Spritz. R (2001) Mutation of PVRL1 is associated with sporadic, non-syndromic cleft lip/palate in northern Venezuela *Nature Genetics* 29 (2) pp 141-142

Stark. K, Vainio. S, Vassileva. G & McMahon. A (1994) Epithelial transformation of metanephric mesenchyme in the developing kidney regulated by Wnt-4 *Nature* 372 (6507) pp 679-683

Steele. J, Hansen. H, Arn. P & Kwong. P (2005) Spectrum of Phenotypic Manifestations from a Single Point Mutation of the *p63* Gene, Including New Cutaneous and Immunologic Findings *Pediatric Dermatology* 22 (5) pp 415-419

Storey. J & Tibshirani. R (2003) Statistical significance for genomewide studies *PNAS* 100 (16) pp 9440-9445

Sull. J, Liang. K, Hetmanski. J, Fallin. M, Ingersoll. R, Park. J, Wu-Chou. Y, Chen. P, Chong. S, Cheah. F, Yeow. V, Park. B, Jee. S, Jabs. E, Redett. R, Scott. A & Beaty. T (2009) Maternal transmission effects of the *PAX* genes among cleft case-parent trios from four populations *European Journal of Human Genetics* 17 (6) pp 831-839

Summerhurst. K, Stark. M, Sharpe. J, Davidson. D & Murphy. P (2008) 3D representation of Wnt and Frizzled gene expression patterns in the mouse embryo at embryonic day 11.5 (Ts19) *Gene Expression Patterns* 8 (5) pp 331-348

Sun. D, Baur. S & Hay. E (2000) Epithelial-Mesenchymal transformation is the mechanism for fusion of the

craniofacial primordial involved in morphogenesis of the chicken lip *Developmental Biology* 228 pp 337-349

Sun. X, Meyers. E, Lewandoski. M & Martin. G (1999) Targeted disruption of *Fgf8* causes failure of cell migration in the gastrulating mouse embryo *Genes and Development* 13 pp 1834-1846

Sun. Y, Huang. Y, Yin. A, Wang. Y, Wang. C, Du. Y, Wang. M, Lan. F, Wang. G, Jiang. M, Ma. J, Zhang. X, Ma. H, Ma. J, Zhang. W, Huang. Q, Zhou. Z, Ma. L, Li. Y, Jiang. H, Xie. L, Jiang. Y, Shi. B, Cheng. J, Shen. H, Wang. L & Yang. Y (2015) Genome-wide association study identifies a new susceptibility locus for cleft lip with or without cleft palate *Nature Communications* 6 (6414)

Suzuki. K, Hu. D, Bustos. T, Zlotogora. J, Richieri-Costa. A, Helms. J & Spritz. R (2000) Mutations of *PVRL1*, encoding a cell-cell adhesion molecule/herpesvirus receptor, in cleft lip/palate-ectodermal dysplasia *Nature Genetics* 25 pp 427-430

Szabo-Rogers. H, Geetha-Loganathan. P, Nimmagadda. S, Fu. K & Richman. J (2008) FGF signals from the nasal pit are nexessary for normal facial morphogenesis *Developmental Biology* 318 (2) pp 289-302

Tachibana. K, Nakanishi. H, Mandai. K, Ozaki. K, Ikeda. W, Yamamoto. Y, Nagafuchi. A, Tsukita. S & Takai. Y (2000) Two cell adhesion molecules, nectin and cadherin, interact through their cytoplasmic domain-associated proteins *Journal of Cell Biology* 150 (5) pp 1161-1176

Taipale. J, Cooper. M, Maiti. T & Beachy. P (2002) Patched acts catalytically to suppress the activity of Smoothened *Nature* (418) pp 892-896

Takagi. T, Moribe. H, Kondoh. H & Higashi. Y (1998) deltaEF1, a zinc finger homeodomain transcription factor, is required for skeleton patterning in multiple lineages *Development* 125 (1) pp 21-31

Takahara. S, Takigawa. T & Shiota. K (2004) Programmed cell death is not a necessary prerequisite for fusion of the fetal mouse palate *The International journal of developmental biology* 48 (1) pp 39-46

Tamai. K, Zeng. X, Liu. C, Zhang. X, Harada. Y, Chang. Z & He. X (2004) A mechanism for Wnt coreceptor activation *Molecular Cell* 13 (1) pp 149-156

Tanaka. S, Mahabir. R, Jupiter. D & Menezes. J (2012) Updating the Epidemiology of Cleft Lip with or without Cleft Palate *Plastic and Reconstructive Surgery* 129 (3) pp 511e-518e

The Treacher Collins Syndrome Collaborative Group (1996) Positional cloning of a gene involved in the pathogenesis of Treacher Collins syndrome. The Treacher Collins Syndrome Collaborative Group *Nature Genetics* 12 (2) pp 130-136

Thomas. P, Kim. J, Nunez. S, Glogauer. M & Kaartinen. V (2010) Neural crest cell-specific deletion of *Rac1* results in defective cell-matrix interactions and severe craniofacial and cardiovascular malformations *Developmental Biology* 340 (2) pp 613-625

Thomason. H, Dixon. M & Dixon. J (2008) Facial clefting in Tp63 deficient mice results from altered Bmp4, Fgf8 and Shh signalling *Developmental biology* 321 pp 273-282

Thomason. H, Zhou. H, Kouwenhoven. E, Dotto. G-P, Restivo. G, Nguyen. B-C, Little. H, Dixon. M, Bokhoven. H. V & Dixon. J (2010) Cooperation between the transcription factors p63 and IRF6 is essential to prevent cleft palate in mice *The Journal of Clinical Investigation* 120 (5) pp 1561-1569

Thorne. N, Inglese. J & Auld. D (2010) Illuminating insights into firefly luciferase and other bioluminescent reporters used in chemical biology *Chemistry & Biology* 17 (6) pp 646-657

Tie. F, Banerjiee. R, Stratton. C, Prasad-Sinha. J, Stepanik. V, Zlobin. A, Diaz. M, Scacheri. P & Harte. P (2009) CBP-mediated acetylation of histone H3 lysine 27 antagonizes Drosophila Polycomb silencing. *Development* 136 (18) pp 3131-3141

Tong. L, Xue. H, Xiong. L, Xiao. J & Zhou. Y (2015) Improved RT-PCR assay to quantitate the Pri-, Pre- and mature microRNAs with higher efficiency and accurary *Molecular biotechnology* 57 (10) pp 939-946

Trumpp. A, Depew. M, Rubenstein. J, Bishop. M & Martin. G (1999) Cre-mediated gene inactivation demonstrates that FGF8 is required for cell survival and patterning of the first branchial arch *Genes and Development* 13 (23) pp 3136-3148

Tsukita. S & Furuse. M (2000) Claudins constitute tight junction strands contain aqueous pores *Journal of Cell Biology* 149 (1) pp 13-16

Tsukiyama. T & Yamaguchi. T (2012) Mice lacking *Wnt2b* are viable and display a postnatal olfactory bulb phenotype *Neuroscience Letters* 512 (1) pp 48-52

Untergrasser. A, Cutcutache. I, Koressaar. T, Ye. J, Faircloth. B, Remm. M & Rozen. S (2012) Primer3 – new capabilities and interfaces *Nucleic Acids Research* 40 (15):e115
Vainio. S, Heikkilä. M, Kispert. A, Chin. N & McMahon. A (1999) Female development in mammals is regulated by Wnt-4 signalling *Nature* 397 (6718) pp 405-409

Van Der Woude. A (1954) Fistula labii inferioris congenital and its association with cleft lip and palate *American Journal of Human Genetics* 6 (2) pp 244-256

Vasudevan. H, Mazot. P, He. F & Soriano. P (2015) Receptor tyrosine kinases modulate distinct transcriptional programs by differential usage of intracellular pathways *eLife* 4 doi: 10.7554/eLife.07186

Vaziri Sani. F, Hallberg. K, Harfe. B, McMahon. A, Linde. A & Gritli-Linde. A (2005) Fate-mapping of epithelial seam during palatal fusion rules out epithelial-mesenchymal transformation *Developmental Biology* 285 (2) pp 490-495

Venkatesh. R (2009) Syndromes and anomalies associated with cleft *Indian Journal of Plastic Surgery* (42) pp 51-55

Vertino. A, Taylor-Jones. J, Longo. K, Bearden. E, Lane. T, McGehee. R, MacDougald & Peterson. C (2005) Wnt10B deficiency promotes coexpression of myogenic and adipogenic programs in myoblasts *Molecular Biology of the Cell* 16 (4) pp 2039-2048

Vieira. A (2008) Unraveling Human Cleft Lip and Palate Research *Journal of Dental Research* 87 (2) pp 119-125

Vieira. A, Avilla. J, Daack-Hirsch. S, Dragan. E, Félix. T, Rahimov. F, Harrington. J, Schultz. R, Watanabe. Y, Johnson. M, Fang. J, O'Brien. S, Orioli. I, Castilla. E, FitzPatrick. D, Jiang. R, Marazita. M & Murray. J (2005) Medical Sequencing of Candidate Genes for Nonsyndromic Cleft Lip and Palate *Plos Genetics* 1 (6) pp 0651-0659

Vortkamp. A, Franz. T, Gessler. M & Grzeshik. K (1992) Deletion of *GLI3* supports the homology of the human Greig cephalopolysyndactyly syndrome (GCPS) and the mouse mutant extratoes (Xt) *Mammalian Genome* 3 pp 461-463

Wågsäter. D, Zhu. C, Björck. H & Eriksson. P (2009) Effects of PDGF-C and PDGF-D on monocyte migration and MMP-2 and MMP-9 expression *Atherosclerosis* 202 (2) pp 415-423

Wang. B, Fallon. J & Beachy. P (2000) Hedgehog-related processing of Gli3 produced an anterior/posterior repressor gradient in the developing vertebrate limb *Cell* 100 (4) pp 423-434

Wang. K, Heike. C, Clarkson. M, Mejino. J, Brinkley. J, Tse. R, Birgfeld. C, Fitzsimons. D & Cox. T (2014) Evaluation and integration of disparate classification systems for clefts of the lip *Frontiers in physiology* (5) pp163

Wang. Z, Shu. W, Lu. M & Morrisey. E (2005) Wnt7b activates canonical signalling in epithelial and vascular smooth muscle cells through interactions with Fzd1, Fzd10, and LRP5 *Molecular and Cellular Biology* 25 (12) pp 5022-5030

Warbrick. J (1960) The early development of the nasal cavity and upper lip in the human embryo *Journal of Anatomy* (94 Pt3) pp 351-362

Warner. D, Smith. H, Webb. C, Greene. R & Pisano. M (2009) Expression of Wnts in the developing murine secondary palate *International Journal of Developmental Biology* 53 (7) pp 1105-1112

Watanabe. H, Ma. Q, Peng. S, Adelmant. G, Swain. D, Song. W, Fox. C, Francis. J, Pedamallu. S, Deluca. D, Brooks. A, Que. J, Rustgi. A, Wong. K, Ligon. K, Liu. S, Marto. J, Meyerson. M & Bass. A (2014) SOX2-p63 interaction and genomic co-localization in squamous cell carcinomas *Cancer Research* 74 doi: 10.1158/1538-7445.AM2014-1391

Wehby. G & Cassell. C (2010) The impact of orofacial clefts on quality of life and healthcare use and costs *Oral Diseases* 16 (1) pp 3-10

Welsh. I, Hagge-Greenberg. A & O'Brien. T (2007) A dosage-dependent role for Spry2 in growth and patterning during palate development *Mechanisms of development* 124 (9-10) pp 746-761

Wend. P, Wend. K, Krum. S & Miranda-Carboni. G (2011) The role of WNT10B in physiology and disease *ACTA Physiologica* 204 (1) pp 34-51

Widelitz. R (2005) Wnt signalling through canonical and non-canonical pathways: recent progress *Growth factors* 23 (2) pp 111-116

Wilke. T, Gubbels. S, Schwartz. J & Richman. J (1997) Expression of fibroblast growth factor receptors (FGFR1, FGFR2, FGFR3) in the developing head and face *Developmental Dynamics* 210 pp 41-52

Wilkie. A & Morriss-Kay (2001) Genetics of craniofacial development and malformation *Nature Reviews Genetics* 2 pp 458-468

Wolff. S, Talos. F, Palacios. G, Beyer. U, Dobbelstein. M & Moll. U (2009) The alpha/beta carboxyterminal domains of p63 are required for skin and limb development. New insights from the Brdm2 mouse which is not a complete p63 knockout but expresses p63 gamma-like proteins *Cell Death & Differentiation* 16 (8) pp 1108-1117

Woods. C, Stricker. S, Seemann. P, Stern. R, Cox. J, Sherridan. E, Roberts. E, Springell. K, Scott. S, Karbani. G, Sharif. S, Toomes. C, Bond. J, Kumar. D, Al-Gazali. L & Mundlos. S (2006) Mutations in *WNT7A* cause a range of limb malformations, including Fuhrmann Syndrome and Al-Awadi/Raas-Rothschild/Schinzel Phocomelia Syndrome *American Journal of Human Genetics* 79 (2) pp 402-408

Wu. D, Wang. M, Wang. X, Yin. N, Song. T, Li. H, Zhang. F, Zhang. Y, Ye. Z, Yu. J, Wang. D & Zhao. Z (2012) Maternal transmission effect of a PDGF-C SNP on nonsyndromic cleft lip with or without palate from a Chinese population PLos One 7 (9) doi: 10.1371/journal.pone.0046477

Wu. G, Osada. M, Guo. Z, Fomenkov. A, Begum. S, Zhao. M, Upadhyay. S, Xing. M, Wu. F, Moon. C, Westra. W, Koch. W, Mantovani. R, Califano. J, Ratovitski. E, Sidransky. D & Tink. B (2005) ΔNp63α Up-Regulates the *Hsp70* Gene in Human Cancer *Cancer Research* 65 (3) pp 758-766

Wu. W, Glinka. A, Delius. H & Niehrs. C (2000) Mutual antagonism between dickkopf1 and dickkopf2 regulates Wnt/β-catenin signalling *Current Biology* 10 pp 1611-1614

Xin. Y, Ma. L, Zhai. K, Zhou. Z, Yang. X, Ma. J, Wang. Y, Zhu. J, Jiang. M, Huang. Y (2013) Association between single nucleotide polymorphism in Wnt3 and nonsyndromic cleft lip with or without cleft palate in Hui and Han population of Ningxia autonomous region *West China Journal of stomatology* 31 (4) pp 379-402

Xu. X, Bringas. P, Soriano. P & Chai. Y (2005) PDGFR-alpha signalling is critical for tooth cusp and palate morphogenesis *Developmental dynamics* 232 (1) pp 75-84

Yamaguchi. M, Nakamoto. M, Honda. H, Nakagawa. T, Fujita. H, Nakamura. T, Hirai. H, Narumiya. S & Kakizuka. A (1998) Retardation of skeletal development and cervical abnormalities in transgenic mice expressing a dominant-negative retinoic acid receptor in chondrogenic cells *PNAS* 95 (13) pp 7491-7496

Yang. A, Kaghad. M, Wang. Y, Gillet. E, Fleming. M, Dötsch. V, Andrews. N, Caput. D & McKeon. F (1998) *p63* a *p53* Homolog at 3q27-29, Encodes Multiple Products with Transactivating, Death-Inducing, and Dominant-Negative Activities *Molecular Cell* 2 (3) pp 305-316

Yang. A, Schweitzer. R, Sun. D, Kaghad. M, Walkers. N, Bronson. R, Tabin. C, Sharpe. A, Caput. D, Crum. C & McKeon. F (1999) p63 is essential for regenerative proliferation in limb, craniofacial and epithelial development *Nature* 398 pp 714-718

Yang. X, Kilgallen. S, Andreeva. V, Spicer. D, Pinz. I & Friesel. R (2010) Conditional expression of Spry1 in neural crest causes craniofacial and cardiac defects *BMC Developmental Biology* 10 (48) doi:10.1186/1471-213X-10-48

Yao. T, Oh. S, Fuchs. M, Zhou. N, Ch'ng. L, Newsome. D, Bronson. R, Li. E, Livingston. D & Eckner. R (1998) Gene dosage-dependent embryonic development and proliferation defects in mice lacking the transcriptional integrator p300 *Cell* 93 (3) pp 361-372

Yao. T, Yang. L, Li. P, Wu. H, Xie. H, Shen. X, Xie. X (2011) Association of Wnt3A gene variants with non-syndromic cleft lip with or without cleft palate in Chinese population *Archives of Oral Biology* 56 (1) pp 73-78

Yee. W & Abbott. U (1978) Facial Development in Normal and Mutant Chick Embryos *Journal of Experimental*

Zoology 206 pp 307-322

Yoon. H, Chung. I, Seol. E, Park. B & Park. H (2000) Development of the lip and palate in staged human embryos and early foetuses *Yonsei medical Journal* 41 (4) pp 477-484

Yoshida. K, Hayashi. R, Fijita. H, Kubota. M, Kondo. M, Shimomura. Y & Niizeki. H (2015) Novel homozygous mutation c.400C>T (p.Arg134*), in the PVRL1 gene underlies cleft lip/palate-ectodermal dysplasia syndrome in an Asian patient *Journal of Dermatology* 42 (7) pp 715-719

Yu. J, Jin. L, Xiao. L & Jin. L (2014) Prevalence of birth defects in the Tongzhou District of Beijing between 2006 and 2012 *Chinese Journal of Contemporary Pediatrics* (11) pp 1133-1137

Zakin. L, Mazan. S, Maury. M, Martin. N, Guénet. J & Brûlet. P (1998) Structure and expression of *Wnt13*, a novel mouse *Wnt2* related gene *Mechanisms of Development* 73 (1) pp 107-116

Zhang. J, Upadhya. D, Lu. L & Reneker. L (2015) Fibroblast growth factor receptor 2 (FGFR2) is required for corneal epithelial cell proliferation and differentiation during embryonic development *PLos One* DOI: 10.1371/journal.pone.0117089

Zhang. K, Zhang. J, Han. L, Pu. P & Kang. C (2012) Wnt/beta-catenin signalling in glioma *Journal of Neuroimmune Pharmacology* 7 (4) pp 740-749

Zhang. Y, Gorry. M, Post. C & Ehrlich. G (1999) Genomic organisation of the human fibroblast growth factor receptor (*FGFR2*) gene and comparative analysis of the human *FGFR* gene family *Gene* 230 (1) pp 69-79

Zhang. Y, Liu. T, Meyer. C, Eeckhoute. J, Johnson. D, Bernstein. B, Nusbaum. C, Myers. R, Brown. M, Li. W & Liu. S (2008) Model-based analysis of ChIP-Seq (MACS) *Genome Biology* 9 (9) doi: 10.1186/gb-2008-9-9-r137

Zhang. Z, Song. Y, Zhoa. X, Zhang. X, Fermin. C & Chen. Y (2002) Rescue of cleft palate in Msx1-deficient mice by transgenic Bmp4 reveals a network of BMP and Shh signalling in the regulation of mammalian palatogenesis (2002) *Development* (129) pp 4135-4146

Zhao. Z, Tavoosidana. G, Sjölinder. M, Göndör. A, Mariano. P, Wang. S, Kanduri. C, Lezcano. M, Sandhu. K, Singh. U, Pant. V, Tiwari. V, Kurukuti. S & Ohlsson. R (2006) Circular chromosome conformation capture (4C) uncovers extensive networks of epigenetically regulated intra- and interchromosomal interactions *Nature Genetics* 38 pp 1341-1347

Zhu. X, Ozturk. F, Liu. C, Oakley. G & Nawshad. A (2012) Transforming growth factor-β activates c-Myc to promote palatal growth *Journal of Cellular Biochemistry* Accepted article doi: 10.1002/jcb.24184

Zucchero. T, Cooper. M, Maher. B, Daack-Hirsh. S, Nepomuceno. B, Ribeiro. L, Caprau. D, Christensen. K, Suzuki. Y, Machida. J, Natsume. N, Yoshiura. K, Vieira. A, Orioli. I, Castilla. E, Moreno. L, Arcos-Burgos. M, Lidral. A, Field. L, Liu. Y, Ray. A, Goldstein. T, Schultz. R, Shi. M, Johnson. M, Kondo. S, Schutte. B, Marazita. M & Murray. J (2004) Interferon regulatory factor 6 (IRF6) gene variants and the risk of isolated cleft lip or palate *New England journal of medicine* 351 (8) pp769-780

Appendix 1 ChIP-qPCR primers

Primer	Primer Sequence	Primer	Primer Sequence
1600029D21Rik_F	CAGTCACTTCCTGGGAGAGG	**Pdgfa_F**	CTGGAGCTCACCTCAGGAAC
1600029D21Rik_R	TGCAGAGGAGAGGTCCTGAT	**Pdgfa_R**	CAGGGCCTGTCTACAAGGAG
Afap1/1_F	GTGGATGGCATTTGAGGAAT	**Pdgfc F**	CCAGGCTTGACTTCCAACAC
Afap1/1_R	GAGTTTGCCCGAGCATGT	**Pdgfc R**	AGGACCTCATCCAGCAAATG
Arid 5B R	TGAAGAGAGCCGTTTCCAGT	**Pvrl1_F**	GCGAGGCTCCTGATAGACTC
Arid 5B F	CAGCCAGTCACGAAGATCAA	**Pvrl1_R**	AGCAGCGTCACAGTTTCAAG
Cdh3 FP F	CAAGCAGAGTGGGTGTTTGA	**Serpinb5_F**	TCCACCAACAGAACCTTCCT
Cdh3 SP R	CAGGAAGCAGAACACAACCA	**Serpinb5_R**	AGACATGATTCAGGCCCAAC
Cdh3_SP_F	CTGGAAACCCTGGGAAAAGT	**Sfn_F**	TGGGGAGCTTTCCCTTATTT
Cdh3_SP_R	CTGTTGGTGACTGTGGATGG	**Sfn_R**	GGTCACGTCAAGTGCTCAGA
Chst11_F	CATGCCTTCAAGCCTTTGAT	**Sfrp1 P1 F**	ACGGATCTCCGAGTCCTTCT
Chst11_R	CCCAGCAGCTGTAAGACCTC	**Sfrp1 P1 R**	CGTGCTCTCCTCTAGCCTTT
Col17a1_F	GAAGATCTGGCTTTCCCACA	**Sfrp1 P2 F**	TTCCCAGGACTGAAACAGGT
Col17a1_R	AAACTCCAGGACCCAAAAGG	**Sfrp1 P2 R**	TCAATGCCACTTCCACTTCA
Egfr (36 peak) F	AAGCCAAATTCCCTCAAAGG	**Sh3rf2_p1**	AAACTCCTAAGAGCCGCACA
Egfr (36 peak) R	CTCCTGCTCCAACACATTCA	**Sh3rf2_p1**	CAATCCCAGGCTACATGCTT
Egfr2_F	TGATTCCCAGTGTGGAGAAA	**Slc7a10_p1**	TGATGAATGCCTCTGAGCTG
Egfr2_R	TGCTGCAATGAAATCCATGT	**Slc7a10_p1**	CCAAGGAAACAAATGCCTGT
Elf3_F	GCCTAATGCAGGCAGAGAAG	**Sox2 P1 F**	TGGGTTGTTCTCACCATGAA
Elf3_R	GGGCCTTCAGAAGATGTGAG	**Sox2 P1 R**	AGGAAAGCTCGCTTCCTCTC
Eya1_F	TCATCCCTGCTGTGTGGTTA	**Sox2 P2 F**	TGCCTTCCTCACATTCTTCC
Eya1_R	GGCGCTCACAAGTCTACACA	**Sox2 P2 R**	ACCTGGGTGAGAGACGCTAA
Fgf20_F	CCAATAGGGTCAGCCTGGTA	**Spry1 P1 F**	AGGTGTGGAAGAGGAGCATG
Fgf20_R	TCTGTTTTCTGCCTTGCTCA	**Spry1 P1 R**	GCTCTCATATTTTACTGGTGGGC
Fgfr2 (peak 15) R	ACGGCACCCATTATGTGTTT	**Spry1 P2 F**	GAATGAACCTTGGCGCTGTC
Fgfr2 (peak 54) F	TGCAGATGATAGGCACCTTG	**Spry1 P2 R**	GCCATCAATGCCACTTCCAC
Fgfr2 (peak 54) R	GGCGATTAGCTGTCATCCAT	**Spry1 P3 F**	CACCAGCCACAAGGTGACTA
Fgfr2 (peak15) F	AAAATGAGTCCAGGCTGGTG	**Spry1 P3 R**	GCAGTATGCCAAACCATCAG
Fgfr2 F	TGCAGATGATAGGCACCTTG	**Spry1 P4 F**	GCTGTCCTTTGTGTGGATTG
Fgfr2 P1 F	CAGTCCAGAGTGCAGGTGAA	**Spry1 P4 R**	TCCAGGGCAAATACTTTGAA
Fgfr2 P1 R	TGTAAGTATGGGCAGGTACAGG	**Spry1 P5 F**	TAACTGCTCTCCTGTAGCATGTG
Fgfr2 R	GGCGATTAGCTGTCATCCAT	**Spry1 P5 R**	GGATGAGGGCAGAGCTATTG
Fgfr3 P1 F	AGTGGAGGCAGCCTGAAAG	**Spry2 P1 F**	GCTGAGGACCATAGGCAACT
Fgfr3 P1 R	ACTCGGAGCTGCAGGTGT	**Spry2 P1 R**	GATGCAGTTTGGAGGGGTTA
Frem2 F	GCCTTTCTCCCCACATGTTA	**Spry2 P2 F**	TGGCCTCTCTCTAGCTGGTT
Frem2 R	TGCTTGCAGTCCAGAAAGTG	**Spry2 P2 R**	TGAAAGGAAGGCAGAGGAGA
Fzd10 P1 F	GAGTCCTCAGTGCCTGGTGT	**Spry2 P3 F**	CACCAGCCACAAGGTGACTA
Fzd10 P1 R	TTGGGGTAGCAGCTTTAGAGA	**Spry2 P3 R**	GCAGTATGCCAAACCATCAG

Fzd10 P2 F	AGGCCACTGGGAAGTTCTG	**Srd5a1_F**	GCTGCTTCCTTAACCGTGTC
Fzd10 P2 R	AGGGAAAGACTCTGGGCACT	**Srd5a1_R**	CATTCCTCGATGCCAGATTT
Fzd10 P3 F	GATTGAATTTCCCCAGCAGA	**Tcfap2a_p1**	TTCTTGCCACTTGCTCATTG
Fzd10 P3 R	TGTGCGGACTCAGTTTTTCA	**Tcfap2a_p1**	AGGGACTTTGGGTACGTGTG
Fzd10 P4 F	ACACTGTCACTTCTGGGGAG	**Tcfap2a_p2**	GCCTGTAAGGACATGCTTGG
Fzd10 P4 R	TGCCTACAATTTGCCTGTCG	**Tcfap2a_p2**	TCCTTTTGTTGCAGCACGTA
Fzd10 P5 F	TTGTGACACATGGGAGCAGT	**Tmc7_F**	GCCTGTAGAGTCTGCACCAA
Fzd10 P5 R	CCTGGAGGTTCACGGTCTC	**Tmc7_R**	CTGGCTGCCCAGAGAGTAAA
Fzd4 P3 F	ACTTCATCCTGGCAGCAAAT	**Trim32_F**	GCTCTTTGAAGGGAGTGTGC
Fzd4 P3 R	CAGGAGGATCCAACTGAATGA	**Trim32_R**	CTAGGCCATTGCAGCTTTCT
Fzd6_F	GAGCAATCAGGACCCTTCAA	**Trp73_F**	ACCGCAAATACCGTTAACCA
Fzd6_R	AAGTCCTCCAAAGGCCAAAT	**Trp73_R**	TTTAAAAAGCCCCCACCAC
Galntl4 F	AAGAAAAGGGTGGGATGACC	**Wnt10b P1 F**	ACGCACCTCTGAAACAGTCA
Galntl4 R	CCAGGATTAGGCACGTTCTG	**Wnt10b P1 R**	GTGTCGCTGGTTTCCAGACT
Gjb2_F	ACCCAAAGCTGTGAAGTGCT	**Wnt10b P2 F**	AGCAATTAGGGGAGCAGGTT
Gjb2_R	TTGGAAGCCTAGGCCAAGTA	**Wnt10b P2 R**	CCAACCCAAGAAGCTTCAAA
Gli2(1)_F	TTAGGGAGAATCCCCCATTC	**Wnt11 P1 F**	AGGCAAGCTCCAGCTAGAAA
Gli2(1)_R	GGTGTGGATGATGCTTTGTG	**Wnt11 P1 R**	AGGGCATGTAGCAGCTTGTT
Grhl3 P1 F	AAAATGTGACGCCAGGAAAG	**Wnt11 P2 F**	ACTGCAGAAGGCAGGAAAAA
Grhl3 P1 R	AGGGCTCAATCTTGGGAAAT	**Wnt11 P2 R**	GCTCACCACTGTGTGGCTTC
Grhl3 P2 F	CCAGGGAAACAGTCAGCTCT	**Wnt11 P3 F**	TGTCATTTCCTCCACCAGAA
Grhl3 P2 R	TCACACGGCAATTTGTAAGG	**Wnt11 P3 R**	GATGAAAGTGCTGGCATGTG
Grhl3 P3 F	GGGTCTGAGCTGAGAACTGG	**Wnt2b P1 F**	AAATGTGCAGGTGGTGTCTG
Grhl3 P3 R	CAGGTGCTTCTGAGCTTCCT	**Wnt2b P1 R**	TCACATGAGAGTCAGCAAAGT
Grhl3 P4 F	CTCACAAAAGCCCCCTCTCT	**Wnt2b P2 F**	TCTCAAGTGGCTGCTTCCTT
Grhl3 P4 R	CTGACATCACCGTCCTACCC	**Wnt2b P2 R**	CCCTCAAACAACAGGTTTCC
Grhl3 P5 F	AACATCCCAGTCCCTTTGTG	**Wnt3 P1 F**	AACCTTGGTTCATGGGTCTG
Grhl3 P5 R	CTCTCTGGTCCAGCATCTGT	**Wnt3 P1 R**	TGTGTGTGTGTGTGTGTGCTT
Grhl3 P6 F	AGGCAGAGCAGGAGAGACTG	**Wnt3 P2 F**	GGAAGCGGAAAGGGAGTATC
Grhl3 P6 R	TCCCAGTCTAGGATGGAGGA	**Wnt3 P2 R**	CTGTGGGCAGCCTTCTTTAG
Jag2 F	CTGAACCAGGCAGAGAGCAT	**Wnt3 P3 F**	CATCCCAACTTTAGTGGTAGTTCC
Jag2 R	CCTCTGTCCACCCCTCTGTA	**Wnt3 P3 R**	GAATCGGGCTAAAGAACAAGC
Kcnh1_FP_F	TTTGGCAGACATGAAACAGC	**Wnt3 P4 F**	CCAGAACACTCAGGGCTTGT
Kcnh1_FP_R	GGGAGGCAAAAACACAAAGA	**Wnt3 P4 R**	GCTGCCCTGCTCTTCTCTAA
Krm2 P1 F	GTTCCTGCCACAAGTTCCAG	**Wnt3a P1 F**	GGTGAGACATGTTTGCCCAA
Krm2 P1 R	GAATGCTGGGGAAGTGTGTG	**Wnt3a P1 R**	AGTGTGTAGCTTCCCCTGAT
Krt14_F	AACTGCTCCCAGAAAGGACA	**Wnt3a P2 F**	AGCAAGGCAGTAGTCGAGG
Krt14_R	GTTTTTAAGCCCTGGTGTGG	**Wnt3a P2 R**	ACTGAAGACAAAGTGCCCCT
Krt5_F	TCAGCAGGAACATGTTGAGAA	**Wnt3a P3 F**	TGGCAGTTCACTGTGCTCTT
Krt5_R	TGGGCCAGAGATAGAGGAAA	**Wnt3a P3 R**	GTGTGCAGTGATGGGATCAG
Lef1 P1 F	CCAGAGAACCAGGCCTTTCT	**Wnt3a P4 F**	CAGACAAGTGGAGTCCATGC
Lef1 P1 R	CTGTAAGGGTGCTGGTCAAA	**Wnt3a P4 R**	AGTAATGAAATCCAGCCCACA
Lef1 P3 F	ACCCAGTCAAAGGCTTCAGA	**Wnt3a P5 F**	TGCAACTGTGAACTGTTCTTCC
Lef1 P3 R	GCCCTAAAGTCTGCCATTGT	**Wnt3a P5 R**	GGGTGGTCTGTGAGCTCTGT
Lef1 P4 F	CGCGGAGCAATTACCTACAC	**Wnt4 P1 F**	GGTGCAGGTAGAGAGTAGTCC

Lef1 P4 R	GGGAGTAAGCCTGCTGAGTG	**Wnt4 P1 R**	TGGTGTGTGTGAGTTAGAGCA
Lef1 P5 F	GGTGACTCAAGTTGGCTACAAA	**Wnt4 P2 F**	CATTTAAGTGGGCCATGTCA
Lef1 P5 R	CAGAATGGCCCACAGTCC	**Wnt4 P2 R**	TCAACCTGCCCACTGTGTAA
Lef1 P6 F	TCTGTGTTCAAAAGGGCTCA	**Wnt4 P3 F**	ACAGAAACAGCCCCTCTCCT
Lef1 P6 R	CCAGAGAGGAGCCAATGAGT	**Wnt4 P3 R**	CCTGGGGGTTTAGCCTAATTT
Lrp6 P1 F	CGGTGTTCACATTCTGAGGC	**Wnt4 P4 F**	GACAGGTCTCCGAGGGAAAG
Lrp6 P1 R	AACTGGATGTGATGTCTATGGG	**Wnt4 P4 R**	CTTCTATGTTTGGCTCCCGC
LRP6_CHIP1_F	CCAGCCAACTACCCAAACTG	**Wnt4 P5 F**	CAAGACAGTGCTCCCCAAAC
LRP6_CHIP1_R	TGGAACTCAATAGCTTCACCAC	**Wnt4 P5 R**	CCTGGTTGGTTCAGCTTGAG
Mapk1 F	CCAGCTGTCTCAGCACATTC	**Wnt7a P1 F**	TGTGCTTACATGCACACAGG
Mapk1 R	CCGGGAGGTCTATCTTCACA	**Wnt7a P1 R**	CTCAGCAGCAGAGACACAGC
Mapkapk2 F	AAACACCCTCGCCACACTAC	**Wnt7a P2 F**	ATGAGCTGGAGAAGGCAAGA
Mapkapk2 R	GTTGAGCCTCAGTCCTTTGC	**Wnt7a P2 R**	TCAAAGGACCAGGAGGGTTT
Myo_F	GGGTCTCTTCCTCTTACCCGAT	**Wnt7a P4 F**	TTGTCCCTCCCTTAAGAGTTCA
Myo_R	ACCTTGCTGGCCATGGAC	**Wnt7a P4 R**	CGGGCCTTAGGGGATAAATA
Notch1_F	CGCTGAGACTTGTTGTCCTG	**Wnt7b P1 F**	CCATCCCTTTGCTAAAGCTG
Notch1_R	GTTTGGCCCGTGTTACAACT	**Wnt7b P1 R**	CGAGGCGATGGAAAGTTAAG
P2ry5 F	ACTGGGTTGAAGCCTTCCTT	**Wnt7b P2 F**	AACCTTTGGCGAGAAACACC
P2ry5 R	TGTGAGATGGGCTGTCTCTG	**Wnt7b P2 R**	ACCATCCCTAACCAAGCTCC
Pax6 P1 F	AGCAAGCTGATTTCCTGGAG	**Zfhx3 _NR**	GCCTCACCTACTCCCAATCA
Pax6 P1 R	GCAATGCACATTGAACTGGT	**Zfhx3_FP_F**	ATCCCTGCTACATCCCTTCC
		Zfp64_F	ATCACCTCACGACACACTGC
		Zfp64_R	ACAGACTAGGCTGCCTGTGG

Appendix 2 qPCR primers

Primer	Primer Sequence	Primer	Primer Sequence
B-Actin F	CTAAGGCCAACCGTGAAAAGAT	**Perp F**	GGCGAAGAACGAGAGAATGA
B-Actin R	GCCTGGATGGCTACGTACATG	**Perp R**	TGCCAGAGCCTCATGGAGTA
Col17a1 F	TCTCGCTTGCTTTTCTTGGT	**Serpinb5 F**	CAGACACCAAACCCGTACAA
Col17a1 R	GAGAGGGTGTCTGCCTGAAG	**Serpinb5 R**	GGACACTCCCTTGGTCTCTG
Egfr F	ATCCTCTGCAGGCTCAGAAA	**Sfrp1 F**	AAGCGAGTTTGCACTGAGGA
Egfr R	GGCGTTGGAGGAAAAGAAAG	**Sfrp1 R**	CCCCAGCTTCAAGGGTTTCT
Fermt1 F	TTCGCCAATATGAAGCAGTG	**Sh3rf2 F**	CCTCTGTAGTTGCACAAGGC
Fermt1 R	TGCACTTAGGCAGGTGAATG	**Sh3rf2 R**	AGCAGCCCCAGAAGTCTACA
Fgfr2 F	TGGGCTGCCCTACCTCAAG	**Slc7a1 F**	ACCCTTGGGTGAGATGAAGA
Fgfr2 R	GCACTTCTGCATTGGAGCTATTT	**Slc7a1 R**	GGGTGGCACTCAAGAAAGAG
Fgfr3 F	GCGACAGGTGTCCTTGGAAT	**Spry1 F**	CTCAGCACGCAGGGGTTT
Fgfr3 R	ACATTGGCCAGAACAGGACC	**Spry1 R**	CACGCCGGCTAGTGCAG
Fzd4 F	AGAACCTCGGCTACAACGTG	**Spry2 F**	TCCACCGATTGCTTGGAAGT
Fzd4 R	ACCGAACAAAGGAAGAACTGC	**Spry2 R**	CACATCTGAACTCCGTGATCG
Fzd10 F	CCTTCCTCATCGACCCATCG	**Tcfap2a F**	ATTGACCTACAGTGCCCAGC
Fzd10 R	GCGGATGATATAGCCCACCG	**Tcfap2a R**	ATGCTTTGGAAACTGACGGA
Galantl4 F	AGTGTGCAAACAGGGAGGAG	**Wnt10b F**	TGTGGATCCTGCACCTGAAC

Galantl4 R	GCTGGACCACTTGGAGAATG	**Wnt10b R**	TAGAGCCCGACTGAACAAAGC
Gjb2 F	CTTGTCCTCTGGATGGTTGG	**Wnt11 F**	CAACCTCGCAGGCGGC
Gjb2 R	CGCTTCAGACCTGCTCCTTA	**Wnt11 R**	AAAGAGCAGAGCCTCGCAG
Grhl3 F	GCCTGAGGAATGCGATCTCT	**Wnt2b F**	GTCCTGGTGGTACATAGGGG
Grhl3 R	CCACGTGGTTGCTGTAGTGT	**Wnt2b R**	GTAGCGTTGACACAACTGCC
Itgb4 F	AGGCTGGCACTCAGCATT	**Wnt3 F**	CGTCGCTCCCCCTCTTCAT
Itgb4 R	GCCCAAGTCCGAGGTAGTCT	**Wnt3 R**	GGCCAGGGACCACCAAAT
Jag2 F	CGACACCCGCTCAATCAG	**Wnt3a F**	ATCTGGTGGTCCTTGGCTGT
Jag2 R	CGTCGTCATTCCCTTTCAGT	**Wnt3a R**	GGGCATGATCTCCACGTAGT
Krm2 F	GATTCCGGGAAAATGTCACCTG	**Wnt4 F**	CGAGCAATTGGCTGTACCTG
Krm2 R	TGGTGTCCCCATCTTCCCTA	**Wnt4 R**	CCTCAAGGTTCCGTTTGCAC
Krt14 F	GAGGTGAAGATTCGGGACTG	**Wnt7a F**	GGGACTATGACCCGGAAAGC
Krt14 R	GTCGATCTGCAGGAGGACAT	**Wnt7a R**	CGAAGAGAAGCCACCGATCC
Krt5 F	CAGAGCTGAGGAACATGCAG	**Wnt7b F**	TAGGAAGGCCAGTGACCAGA
Krt5 R	CACAAACTCATTCTCAGCCG	**Wnt7b R**	ACAATGCTCTGTAAGATGGCG
Lef1 F	GTCGACTTCAGGTGGTAAGAGA	**Wnt9b F**	CCAGAGAGGCTTTAAGGAGACG
Lef1 R	TGCTGTCAGTGTTCCTTGGG	**Wnt9b R**	GGGGAGTCGTCACAAGTACAG
Lrp6 F	CTTCTGCGTGCTGCTGAG	**Zfhx3 F**	CTTCCATGGTAAGGCCTGCT
Lrp6 R	CCTCCAAGCCTCCAACTACA	**Zfhx3 R**	CCTCCTTCCTCCTGAGGTGT

Appendix 3 Whole mount *in situ* hybridisation primers

Primer	Primer Sequence	Amplification
Fgfr2 F	AATTAACCCTCACTAAAGGGGCTGCTACCCAAGGAATCG	PCR
Fgfr2 R	TAATACGACTCACTATAGGTTTGGTTGGTGGCTCTTCTGG	
Fgfr3 F	AATTAACCCTCACTAAAGGGCGACAGGTGTCCTTGGAAT	PCR
Fgfr3 R	TAATACGACTCACTATAGGGCCCCCAGCAGGTTAATGAT	
Fzd4 F	AATTAACCCTCACTAAAGGGGGCTCCGGACGTCTGATA	PCR
Fzd4 R	TAATACGACTCACTATAGGACCGAACAAAGGAAGAACTGC	
Fzd10 F	AATTAACCCTCACTAAAGGGGCTTTGCTGCCTGTGCATAA	PCR
Fzd10 R	TAATACGACTCACTATAGGGTTTTGCTAGGGAGAGGGGGA	
Fzd4 F	AATTAACCCTCACTAAAGGGGGGCTCCGGACGTCTGATA	PCR
Fzd4 R	TAATACGACTCACTATAGGGACCGAACAAAGGAAGAACTGC	
Grhl3 F	AATTAACCCTCACTAAAGGACAATGCAGGAATCAAGGGCT	PCR
Grhl3 R	TAATACGACTCACTATAGGCAGGATGCCTCGCTTGCATT	
Krm2 F	TATGAAGTGTCTGTGGGCTCCT	PCR
Krm2 R	TAATACGACTCACTATAGGGTTGGCTTCAGTCATCTGGACC	
Lef1 F	CCGGATCCCTTCTCTGTCCCGATGGCAG	PCR
Lef1 R	CATCCCTCGAGGGAGACAGGGGGTAGAAGGT	
Lrp6 F	AATTAACCCTCACTAAAGGTGCAAACAGACGGGACTTGA	PCR
Lrp6 R	TAATACGACTCACTATAGGTGTCCAGTACATGAACCCACTT	
Pax6 F	Courtesy of I. Takayoshi (Division of Biochemistry and Cellular Biology, National Institute of Neuroscience, National Center of Neurology and Psychology, Tokyo, Japan)	Bacterial cloning
Pax6 R		
Sfrp1 F	AATTAACCCTCACTAAAGGAAGCGAGTTTGCACTGAGGA	PCR

Sfrp1 R	TAATACGACTCACTATAGGGAGCCAGGTGCAATGCAAAA	
Shh F	Courtesy of D. Headon (Roslin Institute and Royal School of Veterinary Studies, University of Edinburgh, Edinburgh, United Kingdom)	Bacterial cloning
Shh R		
Sox2 F	Courtesy of E. Robertson (Oxford Univsersity, Oxford, UK)	Bacterial cloning
Sox2 R		
Spry1 F	Courtesy of D. Martin (Department of Internal Medicine (Renal division), Washing Univsersity School of Medicine, St. Louis, USA)	Bacterial cloning
Spry1 R		
Spry2 F	AATTAACCCTCACTAAAGGCCGCGATCACGGAGTTCAG	PCR
Spry2 R	TAATACGACTCACTATAGGTTGTACTGCTCCGAGACCCT	
Wnt10b F	AATTAACCCTCACTAAAGGGGTTCAGTCGGGCTCTAAGCAA	PCR
Wnt10b R	TAATACGACTCACTATAGGGCACTACCCTTCCATCCGCAG	
Wnt11 F	AATTAACCCTCACTAAAGGCTGAGCTGCGTCTGGAAGAA	PCR
Wnt11 R	TAATACGACTCACTATAGGGACAGTGCCAGCCACTTGAT	
Wnt2b F	AATTAACCCTCACTAAAGGTAGCCCTAGGGACGTGTTGA	PCR
Wnt2b R	TAATACGACTCACTATAGGGTAGGTGGAAAGGGAGGCAC	
Wnt3 F	Courtesy of Prof. A. McMahon (Keck School of Medicine, University of South California, Los Angeles, USA)	Bacterial cloning
Wnt3 R		
Wnt3a F	AATTAACCCTCACTAAAGGATGATAGCCTGCATCCGCTC	PCR
Wnt3a R	TAATACGACTCACTATAGGGAACGCAAAGTTCCAGGCAG	
Wnt4 F	AATTAACCCTCACTAAAGGAAGGTGGTGACACAAGGGAC	PCR
Wnt4 R	TAATACGACTCACTATAGGGGCTTGAACTGTGCATTCCG	
Wnt7a F	AATTAACCCTCACTAAAGGGGAGCTCAAAGTGGGGAGTC	PCR
Wnt7a R	TAATACGACTCACTATAGGGTGTGGTCCAGCACGTCTTA	
Wnt7b F	AATTAACCCTCACTAAAGGGAGCCGCGATCTCCTTTAGAC	PCR
Wnt7b R	TAATACGACTCACTATAGGGGACAATGCTCTGTAAGATGGCG	
Wnt9b F	Dr. A. Lidral (Department of Orthodontics, College of Dentitry & Dental Clinics, The University of Iowa, Iowa, USA)	Bacterial cloning
Wnt9b R		